

# Gas Phase Chemical Physics Program

DOE Principal Investigators'  
Abstracts

May, 2017

Chemical Sciences, Geosciences, and Biosciences Division  
Office of Basic Energy Sciences  
Office of Science  
U.S. Department of Energy

The research grants and contracts described in this document are supported by the U.S. DOE Office of Science, Office of Basic Energy Sciences, Chemical Sciences, Geosciences and Biosciences Division.

## Foreword

This collection of active research abstracts illustrates the breadth and depth of basic research supported by the Department of Energy's Office of Basic Energy Sciences (BES) and, in large measure, by the chemical physics program that contributes to a better understanding of chemistry and physics of fundamental gas phase processes and reactions. The overall goal of this program is to understand energy flow and reaction mechanisms in complex, non-equilibrium, gas phase environments in which the coupling of chemical and transport processes is poorly understood, such as those encountered in combustion.

We appreciate the privilege of serving in the management of this research program. In carrying out these tasks, we learn from the achievements and share the excitement of the research of the many sponsored scientists and students whose work is summarized in the abstracts published on the following pages.

We thank all of the researchers whose dedication and innovation have advanced DOE BES research. We look forward to our assembly in 2018 for our 38th annual meeting.

Jeff Krause  
Mark Pederson  
Wade Sisk



# *Table of Contents*



# Table of Contents

<b>Foreword</b> .....	iii
<b>Table of Contents</b> .....	v
<b>Abstracts</b> .....	1
<b><u>Principal Investigators' Abstracts</u></b>	
Musahid Ahmed – The Chemical Dynamics Beamline.....	3
Millard H. Alexander and Paul J. Dagdigian – Theoretical Investigation of Kinetics Processes in Small Radicals .....	7
Robert S. Barlow - Turbulence-Chemistry Interactions in Reacting Flows.....	11
Josette Bellan - Predictive Large-Eddy Simulation of Supercritical-Pressure Reactive Flows in the Cold Ignition Regime .....	15
Laurie J. Butler - Dynamics of Product Branching from Radical Intermediates in Elementary Combustion Reactions.....	19
David W. Chandler – Chemical Dynamics Methods and Applications.....	23
Jacqueline H. Chen - Petascale Direct Numerical Simulation and Modeling of Turbulent Combustion.....	27
Robert E. Continetti - Dynamics and Energetics of Elementary Combustion Reactions and Transient Species.....	31
F.F. Crim - Vibrational Dynamics and Dissociation of Ground- and Excited-State Cluster.....	35
Rainer N. Dahms - Theory and Modeling of Multiphase Reacting Flow Dynamics in Simulations and Experiments.....	39
H. Floyd Davis - Bimolecular Dynamics of Combustion Reactions.....	43
Michael J. Davis - Exploration of chemical-kinetic mechanisms, chemical reactivity, and thermochemistry using novel numerical analysis.....	47
Gary Douberly - Vibrational Spectroscopy of Transient Combustion Intermediates Trapped in Helium Nanodroplets.....	51
Robert W. Field - Spectroscopic and Dynamical Studies of Highly Energized Small Polyatomic Molecules.....	55
Jonathan H. Frank - Quantitative Imaging Diagnostics for Reacting Flows.....	59
William H. Green - Computer-Aided Construction of Chemical Kinetic Models.....	63
Gregory E. Hall - Gas-Phase Molecular Dynamics: High Resolution Spectroscopy and Collision Dynamics of Transient Species.....	67
Nils Hansen - Flame Chemistry and Diagnostics.....	71
Lawrence B. Harding - Theoretical Studies of Potential Energy Surfaces.....	75
Martin Head-Gordon – Theory of Electronic Structure and Chemical Dynamics.....	79
Ahren W. Jasper - Theoretical Methods for Pressure Dependent Kinetics and Electronically Nonadiabatic Chemistry .....	83

Ralf I. Kaiser - Probing the Reaction Dynamics of Hydrogen-Deficient Hydrocarbon Molecules and Radical Intermediates via Crossed Molecular Beams.....	87
Christopher J. Kliewer - Time-Resolved Non-linear Optical Diagnostics.....	91
Stephen J. Klippenstein - Theoretical Chemical Kinetics.....	95
Stephen J. Klippenstein and Leonid Sheps et. al - Argonne-Sandia Consortium on High-Pressure Combustion Chemistry.....	99
Stephen R. Leone and Daniel M. Neumark– Spectroscopy and Dynamics of Free Radicals...	103
Marsha I. Lester – Spectroscopy and Dynamics of Reaction Intermediates in Combustion Chemistry.....	107
Robert P. Lucht - Advanced Nonlinear Optical Methods for Quantitative Measurements in Flames.....	111
H. A. Michelsen - Particle Chemistry and Diagnostics Development.....	115
William H. Miller - Reaction Dynamics in Polyatomic Molecular Systems.....	119
Habib N. Najm - Reacting Flow Modeling with Detailed Chemical Kinetics.....	123
David J. Nesbitt - Spectroscopy, Kinetics and Dynamics of Combustion Radicals.....	127
Joseph C. Oefelein - Large Eddy Simulation of Reacting Flow Physics.....	131
David L. Osborn – Kinetics, Dynamics, and Spectroscopy Gas Phase Chemistry.....	135
William J. Pitz and Charles K. Westbrook – Chemical Kinetic Modeling of Combustion Chemistry.....	139
Stephen B. Pope - Investigation of Non-Premixed Turbulent Combustion.....	143
Stephen T. Pratt - Optical Probes of Atomic and Molecular Decay Processes.....	147
Kirill Prozument – Chirped-Pulse Fourier Transform Millimeter-Wave Spectroscopy for Dynamics and Kinetics Studies of Combustion-Related Reactions.....	151
Krupa Ramasesha – Spectroscopic Probes of Dynamics on Multiple Potential Energy Wells.....	155
Hanna Reisler - Photoinitiated Reactions of Radicals and Diradicals in Molecular Beams.....	159
Branko Ruscic - Active Thermochemical Tables.....	163
Trevor Sears - Gas-Phase Molecular Dynamics: High Resolution Spectroscopy and Collision Dynamics of Transient Species.....	167
Ron Shepard - Theoretical Studies of Potential Energy Surfaces and Computational Methods.....	171
Raghu Sivaramakrishnan - Mechanisms and Models for Combustion Simulations.....	175
John F. Stanton - Quantum Chemistry of Radicals and Reactive Intermediates.....	179
Arthur G. Suits - Universal and State-Resolved Imaging Studies of Chemical Dynamics.....	183
James Sutherland - An Update on the Implementation of a Novel Multiscale Simulation Strategy.....	187
Craig A. Taatjes - Elementary Reaction Kinetics of Combustion Species.....	191
Robert S. Tranter - Elementary Reactions of PAH Formation.....	195
Albert Wagner – High Pressure Dependence of Combustion Reactions and Semiclassical Bimolecular Tunneling Approaches.....	199



Hua-Gen Yu - Gas-Phase Molecular Dynamics: Theoretical Studies in Spectroscopy and Chemical Dynamics.....	203
Judit Zádor - Chemical Kinetics of Elementary Reactions.....	207
Timothy S. Zwier - Isomer-specific Spectroscopy and Pyrolysis of Model Aromatic Fuels and Their Radical Intermediates.....	211
<b>Participant List</b> .....	<b>215</b>
<b>Critical Issues</b> .....	<b>218</b>

*Abstracts  
of  
Principal Investigator  
Awards*



## The Chemical Dynamics Beamline

Musahid Ahmed, Kevin Wilson & Oleg Kostko

Chemical Sciences Division, Lawrence Berkeley National Laboratory  
MS 6R2100, 1 Cyclotron Road, Berkeley, CA-94720, [mahmed@lbl.gov](mailto:mahmed@lbl.gov)

**Program Scope:** The Chemical Dynamics Beamline, located in the Advanced Light Source (ALS) at Lawrence Berkeley National Laboratory (LBNL), provides state-of-the-art experimental resources to undertake studies in chemical physics, energy production and utilization via combustion, environmental science and chemical reactions on interfaces. A vigorous user program exemplified in the works of Kaiser, Tranter, Osborn, Taatjes, Hansen, Michelsen & Sheps are reported in their respective abstracts at this meeting. A soft X-ray terminal has been commissioned at the beamline, and is being coupled to new instrumentation to allow access to probing heterogeneous chemistry and nanoparticle physics of relevance to the DOE-BES program.

### Recent Progress and Future Plans:

#### **Molecular growth processes in hydrocarbon chemistry and unimolecular decomposition in Jet Fuel-**

The formation mechanisms of polycyclic aromatic hydrocarbons (PAHs) with indene and naphthalene cores in hydrocarbon-based combustion processes are being examined in collaboration with Ralf Kaiser (Hawaii) and Alex Mebel (Florida International). This is achieved by simulating the combustion relevant conditions (pressure, temperature, reactant molecules) in a high temperature ‘chemical reactor’. The reactions of the phenyl radical with acetylene<sup>40</sup>, oxygen<sup>35</sup> and the reactions of benzyl<sup>24</sup>, and naphthyl<sup>27</sup> radicals with acetylene, shed light on molecular growth mechanisms relevant to soot formation. For instance, the phenyl radical with acetylene study provided first experimental evidence of the HACA (hydrogen abstraction followed by acetylene addition) mechanism, postulated over three decades ago, to be operative leading to PAH formation (naphthalene) under combustion relevant conditions. However, subsequently it was shown, formation of the third aromatic ring (anthracene or phenanthrene) was not so facile when the naphthyl radical was reacted with acetylene. Recently, the reactions of the styrenyl (C<sub>8</sub>H<sub>7</sub>) and the *ortho*-vinylphenyl radicals (C<sub>8</sub>H<sub>7</sub>)—key transient species of the HACA mechanism—with C<sub>2</sub>H<sub>2</sub> did lead to the formation of naphthalene,<sup>5</sup> and the reaction of *ortho*-biphenyl radical (C<sub>12</sub>H<sub>9</sub>) with C<sub>2</sub>H<sub>2</sub>, also led to the synthesis of phenanthrene,<sup>1</sup> but not to anthracene. In future, these studies are being extended to larger radicals which should provide a comprehensive understanding of the ring formation pathways to 4 and higher. In parallel, in collaboration with the same group, the unimolecular decomposition pathways of jet fuel (decane, dodecane, and *exo*-Tetrahydrodicyclopentadiene) decomposition have been completed.<sup>3-4</sup> New radical pathways have been elucidated experimentally and confirmed via theoretical calculations and simulations.

#### **Fundamental Processes in Unimolecular Decomposition of Biofuel Surrogates-**

We, in collaboration with Barney Ellison (Colorado), John Daily (Colorado) & John Stanton (Texas) have focused on a molecule that has proven to be a ubiquitous biomass cracking and combustion intermediate – cyclopentadienone (C<sub>5</sub>H<sub>4</sub>=O),<sup>3</sup> as well as 2,5-dimethylfuran. C<sub>5</sub>H<sub>4</sub>=O yields acetylene and vinylacetylene upon thermolysis. This work was extended to the furanic ether, 2-methoxyfuran, and a pressure-dependent kinetic model developed to model the decomposition.<sup>21</sup> A comprehensive pyrolytic and photoionization study on the benzyl radical, C<sub>6</sub>H<sub>5</sub>CH<sub>2</sub> was completed.<sup>8,34</sup> The power of tunable synchrotron radiation, which can resolve isomers based upon ionization energy, was demonstrated during the pyrolysis of cyclohexanone,<sup>14</sup> the simplest ketone, which can isomerize to its enol form under thermal conditions. Finally, a successful effort to understand the thermal decomposition of the simplest carbohydrate, glycolaldehyde, and glyoxal leads us to believe that the pyrolysis of complex sugars can be understood as well.<sup>12</sup>

**Molecular Growth and confinement in hydrocarbons-** In collaboration with Martin Head Gordon (LBNL), we use molecular beams coupled with photoionization to elucidate the pathways to molecular growth processes.<sup>10</sup> This has led to the discovery of a novel pathway to covalently bound ring formation

(benzene cation) that arises from van der Waals bound acetylene clusters. Future work seeks to understand how water interacts with polycyclic aromatic hydrocarbons to provide a first principle understanding of water-carbon interactions, and how water behaves under confinement.

**Multiphase Chemistry** - The overall goal of this work is to better elucidate interfacial reaction mechanisms and rates and to determine how surface reactions might differ from analogous processes in isolated gas phase molecules. Current work is focused on understanding the chemistry of Criegee intermediates (CI) formed by the heterogeneous reaction of Ozone (O<sub>3</sub>) with aerosol comprised of squalene; a long chain alkene whose six double bonds are highly reactive to O<sub>3</sub> attack. The key question that is addressed, using this model reaction, is exactly how elementary reaction pathways of the condensed phase CI's ultimately control molecular weight growth or decomposition. To do this, we employ aerosol mass spectrometry as well as a new endstation to enable sensitive measurements of X-ray and ultraviolet photoelectron spectra (XPS, UPS) of nanoparticle beams at the Advanced Light Source. Nanoparticle XPS spectra were collected during the reaction of O<sub>3</sub> with squalene aerosol. From analysis of the XPS, UPS and X-ray absorption spectra we determined the O<sub>3</sub> reaction probability per double bond is  $\sim 3 \times 10^{-4}$  and that 1.6 double bonds were consumed per reactive collision, indicating that the underlying reaction mechanism involves the production and subsequent evaporation of gas phase reaction products containing a least 1 C=C bond. The XPS spectrum revealed the presence of two main reaction products, secondary ozonides and carbonyls, which account for 16% and 84% of the reaction products, respectively. Aerosol mass spectrometry, using sized selected aerosol streams, revealed that although the overall O<sub>3</sub> reaction rate is independent of gas phase [H<sub>2</sub>O], the particles undergo substantial chemical erosion at high relative humidity. This result suggests a facile competition between the formation of higher molecular weight secondary ozonides and small carbonyl reactions products, which ultimately evaporate from the aerosol. Ongoing experimental work focuses on obtaining a complete set of both gas and particle phase reaction products. In collaboration with A. Goldstein's group (UC Berkeley) detailed measurements of gas phase products produced by the heterogeneous reaction are underway using Proton Transfer Reaction – Mass Spectrometry. In collaboration with Frances Houle (LBNL) we are developing a predictive model of the heterogeneous reaction mechanism using stochastic reaction diffusion simulations in an effort to quantitatively understand how a few key elementary reaction steps of CI's can alter the physical size and properties of the aerosol.

Future work will build on the results described above and focus on understanding how gas phase SO<sub>2</sub> alters the multiphase reaction mechanism of CI's produced heterogeneously by ozonolysis. Understanding these multiphase reaction pathways is greatly enhanced by recent work from Sandia (Taatjes and Osborn) and others in the GPCP program, which have provided new mechanistic insights and rate coefficients for reactions of CI's in the gas phase.

**Development of new capabilities** - The undulator servicing the beamline, has appreciable photon flux up to 1500 eV. This provides a rich source of soft X-rays and expands the beamline capabilities from VUV to soft X-rays. The beamline was commissioned in December 2016, with soft-X-ray photons delivered to the exit port. X-ray photoelectron spectroscopy of nanoparticles, aerosols and interfaces, X-ray absorption spectroscopy of size selected clusters, correlated multimodal probing of chemical reactions in solution with X-rays and mass spectrometry, and time-resolved pump probe dynamics on gas phase, liquids, interfaces and surfaces will be enabled at this terminal. A new versatile photoelectron spectroscopy apparatus has been recently commissioned. The apparatus was designed for UPS, XPS, and NEXAFS types of measurements on gas-phase molecular, aerosol and nano-particle samples. It will be utilized to probe the electronic properties of solvated species, surface chemistry and solid-liquid interfaces on nanoparticles and aerosols.

1. T. Yang, R. I. Kaiser, T. P. Troy, B. Xu, O. Kostko, M. Ahmed, A. M. Mebel, M. V. Zagidullin, V. N. Azyazov. *HACA's Heritage: A Free Radical Pathway to Phenanthrene in Circumstellar Envelopes of Asymptotic Giant Branch Stars*. *Angew. Chem.* (accepted) DOI: 10.1002/anie.201701259

2. B. Xu, M.I. Jacobs, O. Kostko, M. Ahmed, "Guanidinium group is protonated in a strongly basic arginine solution," Chem. Phys. Chem., DOI 10.1002/cphc.201700197 (2017)
3. L. Zhao, T. Yang, R.I. Kaiser, T.P. Troy, M. Ahmed, J.M. Ribeiro, D. Belisario-Lara, A.M. Mebel, "A Combined Experimental and Computational Study on the Unimolecular Decomposition of JP-8 Jet Fuel Surrogates II: n-Dodecane ( $n\text{-C}_{12}\text{H}_{26}$ )," J. Phys. Chem. A, 121, 1281, DOI: 10.1021/acs.jpca.6b11817 (2017)
4. L. Zhao, T. Yang, R.I. Kaiser, T.P. Troy, M. Ahmed, D. Belisario-Lara, J.M. Ribeiro, A.M. Mebel, "A Combined Experimental and Computational Study on the Unimolecular Decomposition of JP-8 Jet Fuel Surrogates I: n-Decane ( $n\text{-C}_{10}\text{H}_{22}$ )," J. Phys. Chem. A, 121, 1261, DOI: 10.1021/acs.jpca.6b11472 (2017)
5. T. Yang, T.P. Troy, B. Xu, O. Kostko, M. Ahmed, A.M. Mebel and R.I. Kaiser, "Hydrogen-Abstraction/Acetylene-Addition Exposed," Angew. Chem. Int. Ed., 55, 14983, DOI: 10.1002/anie.201607509 (2016)
6. M.I. Jacobs, B. Xu, O. Kostko, N. Heine, M. Ahmed, and K.R. Wilson, "Probing the Heterogeneous Ozonolysis of Squalene Nanoparticles by Photoemission," J. Phys. Chem. A, 120, 8645, DOI: 10.1021/acs.jpca.6b09061 (2016)
7. O. Kostko, T. P. Troy, B. Bandyopadhyay, and M. Ahmed, "Proton transfer in acetaldehyde-water clusters mediated by a single water molecule," Phys. Chem. Chem. Phys., 18, 25569, DOI: 10.1039/C6CP04916H (2016)
8. G.T. Buckingham, J. P. Porterfield, O. Kostko, T. P. Troy, M. Ahmed, D. J. Robichaud, M. R. Nimlos, J. W. Daily, G. B. Ellison, "The thermal decomposition of the benzyl radical in a heated micro-reactor. II. Pyrolysis of the tropyli radical," J. Chem. Phys., 145, 14305, DOI: 10.1063/1.4954895 (2016)
9. K. O. Johansson, T. Dillstrom, M. Monti, F. El Gabaly, M. F. Campbell, P. E. Schrader, D. M. Popolan-Vaida, N. K. Richards-Henderson, K. R. Wilson, A. Violi, and H. A. Michelsen, "Formation and emission of large furans and oxygenated hydrocarbons from flames," PNAS, 113, 8374, DOI: 10.1073/pnas.1604772113 (2016)
10. B. Bandyopadhyay, T. Stein, Y. Fang, O. Kostko, A. White, M. Head-Gordon, and M. Ahmed, "Probing Ionic Complexes of Ethylene and Acetylene with Vacuum Ultraviolet Radiation," J. Phys. Chem. A., 120, 5053, DOI: 10.1021/acs.jpca.6b00107, (2016)
11. O. Kostko, B. Bandyopadhyay, and M. Ahmed, "Vacuum Ultraviolet Photoionization of complex chemical systems," Ann. Rev. Phys. Chem., Vol. 67, 19, DOI: 10.1146/annurev-physchem-040215-112553 (2016)
12. J. P. Porterfield, J. H. Baraban, T. P. Troy, M. Ahmed, M. C. McCarthy, K. M. Morgan, J. W. Daily, T. L. Nguyen, J. F. Stanton, and G. B. Ellison, "Pyrolysis of the Simplest Carbohydrate, Glycolaldehyde ( $\text{CHO-CH}_2\text{OH}$ ), and Glyoxal in a Heated Micro-Reactor," J. Phys. Chem. A., 120, 2161, DOI: 10.1021/acs.jpca.6b00652 (2016)
13. N. K. Richards-Henderson, A. H. Goldstein, and K. R. Wilson, "Sulfur Dioxide Accelerates the Heterogeneous Oxidation Rate of Organic Aerosol by Hydroxyl Radicals," Environ. Sci. Technol., 50, 3554, DOI: 10.1021/acs.est.5b05369 (2016)
14. J. P. Porterfield, T. L. Nguyen, J. H. Baraban, G. T. Buckingham, T. P. Troy, O. Kostko, M. Ahmed, J. F. Stanton, J. W. Dailey, and G. B. Ellison, "Isomerization and Fragmentation of Cyclohexanone in a Heated Micro-Reactor," J. Phys. Chem. A., 119, 12635, DOI: 10.1021/acs.jpca.5b10984 (2015)
15. D. S. N. Parker, R. I. Kaiser, O. Kostko, T. Troy, M. Ahmed, B. J. Sun, S. H. Chen, and A. H. Chang, "On the Formation of Pyridine in the Interstellar Medium," Phys. Chem. Chem. Phys., 17, 32000, DOI: 10.1039/C5CP02960K (2015)
16. N. K. Richards-Henderson, A. H. Goldstein, and K. R. Wilson, "Large Enhancement in the Heterogeneous Oxidation Rate of Organic Aerosols by Hydroxyl Radicals in the Presence of Nitric Oxide," J. Phys. Chem. Lett., 6, 4451, DOI: 10.1021/acs.jpclett.5b02121 (2015)
17. D. R. Worton, H. Zhang, G. Isaacman-VanWertz, A. W. H. Chan, K. R. Wilson, and A. H. Goldstein, "Comprehensive chemical characterization of hydrocarbons in NIST standard reference material 2779 Gulf of Mexico crude oil," Environ. Sci. Technol., 49, 13130, DOI: 10.1021/acs.est.5b03472 (2015)
18. K. R. Kolesar, Z. Li, K. R. Wilson, C. D. Cappa, "Heating-Induced Evaporation of Nine Different Secondary Organic Aerosol Types," Environ. Sci. Technol., 49, 12242, DOI: 10.1021/acs.est.5b03038 (2015)
19. D. M. Popolan-Vaida, C.-L. Liu, T. Nah, K. R. Wilson, and S. R. Leone, "Reaction of chlorine molecules with unsaturated submicron organic particles," Z. Phys. Chem, 229, 1521, DOI: 10.1515/zpch-2015-0662 (2015)
20. J. H. Kroll, C. Y. Lim, S. H. Kessler, and K. R. Wilson, "Heterogeneous Oxidation of Atmospheric Organic Aerosol: Kinetics of Changes to the Amount and Oxidation State of Particle-Phase Organic Carbon," J. Phys. Chem. A., 119, 10767, DOI: 10.1021/acs.jpca.5b06946 (2015)
21. K. N. Urness, Q. Guan, T. P. Troy, M. Ahmed, J. W. Dailey, G. B. Ellison, and J. M. Simmie, "Pyrolysis Pathways of the Furanic Ether 2-Methoxyfuran," J. Phys. Chem. A., 119, 9962, DOI: 10.1021/acs.jpca.5b06779 (2015)
22. H. Zhang, D. R. Worton, S. Shen, T. Nah, G. Isaacman-VanWertz, K. R. Wilson, and A. H. Goldstein, "Fundamental Timescales Governing Organic Aerosol Multiphase Partitioning and Oxidative Aging," Environ. Sci. Technol. Lett., 49, 9768, DOI: 10.1021/acs.est.5b02115 (2015)
23. B. B. Kirk, J. D. Savee, A. Trevitt, D. L. Osborn and K. R. Wilson, "Molecular weight growth in Titan's atmosphere: branching pathways for the reaction of 1-propynyl radical ( $\text{H}_3\text{CC}=\text{C}\cdot$ ) with small alkenes and alkynes," Phys. Chem. Chem. Phys., 17, 20754, DOI: 10.1039/C5CP02589C (2015)

24. D. S. N. Parker, R. I. Kaiser, O. Kostko, and M. Ahmed, "Selective Formation of Indene via the Reaction of Benzyl Radicals with Acetylene," *Chem. Phys. Chem.*, **16**, 2091, DOI: 10.1002/cphc.201500313 (2015)
25. B. Bandyopadhyay, O. Kostko, Y. Fang, and M. Ahmed, "Probing Methanol Cluster Growth by Vacuum Ultraviolet Ionization," *J. Phys. Chem. A*, **119**, 4083, DOI: 10.1021/acs.jpca.5b00912 (2015)
26. T. K. Ormond, P. Hemberger, T. P. Troy, M. Ahmed, J. F. Stanton, and G. B. Ellison, "The Ionisation Energy of Cyclopentadienone: A Photoelectron-Photoion Coincidence Study," *Mol. Phys.*, **113**, 2350, DOI: 10.1080/00268976.2015.1042936 (2015)
27. D. S. N. Parker, R. I. Kaiser, B. Bandyopadhyay, O. Kostko, T. P. Troy, and M. Ahmed, "Unexpected Chemistry from the Reaction of Naphthyl and Acetylene at Combustion-Like Temperatures," *Angew. Chem. Int. Ed.*, **127**, 5511, DOI: 10.1002/anie.201411987 (2015)
28. T. P. Troy, and M. Ahmed, "Rings of fire: Carbon combustion from soot to stars," *Phys. Today*, **68**, 62, DOI: 10.1063/PT.3.2729 (2015)
29. D. S. N. Parker, R. I. Kaiser, O. Kostko, T. P. Troy, M. Ahmed, A. M. Mebel, and A. G. G. M. Tielens, "Gas Phase Synthesis of (Iso)Quinoline and Its Role in the Formation of Nucleobases in the Interstellar Medium," *Astrophys. J.*, **803**, 53, DOI: 10.1088/0004-637X/803/2/53 (2015)
30. E. C. Browne, J. P. Franklin, M. R. Canagaratna, P. Massoli, T. W. Kirchstetter, D. R. Worsnop, K. R. Wilson, and J. H. Kroll, "Changes to the Chemical Composition of Soot from Heterogeneous Oxidation Reactions," *J. Phys. Chem. A*, **119**, 7222, DOI: 10.1021/jp511390f (2015)
31. T. K. Ormond, A. M. Scheer, M. R. Nimlos, D. J. Robichaud, T. P. Troy, M. Ahmed, J. W. Daily, T. L. Nguyen, J. F. Stanton, and G. B. Ellison, "Pyrolysis of Cyclopentadienone: Mechanistic Insights From a Direct Measurement of Product Branching Ratios," *J. Phys. Chem. A*, **119**, 7222, DOI: 10.1021/jp511390f (2015)
32. P. T. Lynch, T. P. Troy, M. Ahmed, and R.S. Tranter, "Probing Combustion Chemistry in a Miniature Shock Tube with Synchrotron VUV Photo Ionization Mass Spectrometry," *Anal. Chem.*, **87**, 2345, DOI: 10.1021/ac5041633 (2015)
33. M. R. Canagaratna, P. Massoli, E. C. Browne, J. P. Franklin, K. R. Wilson, T. B. Onasch, T. W. Kirchstetter, E. C. Fortner, C. E. Kolb, J. T. Jayne, J. H. Kroll, and D. R. Worsnop, "Chemical Compositions of Black Carbon Particle Cores and Coatings via Soot Particle Aerosol Mass Spectrometry with Photoionization and Electron Ionization," *J. Phys. Chem. A.*, **119**, 4589, DOI: 10.1021/jp510711u (2015)
34. G. T. Buckingham, T. K. Ormond, J. P. Porterfield, P. Hemberger, O. Kostko, M. Ahmed, D. J. Robichaud, M. R. Nimlos, J. W. Daily, and G. B. Ellison, "The thermal decomposition of the benzyl radical in a heated micro-reactor: I. Experimental findings," *J. Chem. Phys.*, **142**, 044307, DOI: 10.1063/1.4906156 (2015)
35. D. S. N. Parker, R. I. Kaiser, T. P. Troy, O. Kostko, M. Ahmed, and A. M. Mebel, "Toward the Oxidation of the Phenyl Radical and Prevention of PAH Formation in Combustion Systems," *J. Phys. Chem. A.*, **119**, 7145, DOI: 10.1021/jp509170x (2015)
36. K. O. Johansson, J. Y. W. Lai, S. A. Skeen, K. R. Wilson, N. Hansen, A. Violi, and H. A. Michelsen, "Soot Precursor Formation and Limitations of the Stabilomer Grid," *Proc. Combust. Inst.*, **35**, 1819, DOI: 10.1016/j.proci.2014.05.033 (2015)
37. T. Nah, H. Zhang, D. R. Worton, C. Ruehl, B. B. Kirk, A. Goldstein, S. R. Leone, and K. R. Wilson, "Isomeric Product Detection in the Heterogeneous Reaction of Hydroxyl Radicals with Aerosol Composed of Branched and Linear Unsaturated Organic Molecules," *J. Phys. Chem. A*, **118**, 11555, DOI: 10.1021/jp508378z (2014)
38. D. M. Popolan-Vaida, S. R. Leone, and K. R. Wilson, "Reaction of Iodine Atoms with Submicrometer Squalane and Squalene Droplets: Mechanistic Insights into Heterogeneous Reactions," *J. Phys. Chem. A*, **118**, 10688, DOI: 10.1021/jp5085247 (2014)
39. M. R. Canagaratna, J. L. Jimenez, J. H. Kroll, Q. Chen, S. H. Kessler, P. Massoli, L. Hildebrandt Ruiz, E. Fortner, L. R. Williams, K. R. Wilson, J. D. Surratt, N. M. Donahue, J. T. Jayne, and D. R. Worsnop, "Elemental ratio measurements of organic compounds using aerosol mass spectrometry: characterization, improved calibration, and implications," *Atmos. Chem. Phys. Discuss*, **14**, 19791, DOI: 10.5194/acpd-14-19791-2014 (2014)
40. D. S. N. Parker, R. I. Kaiser, T. P. Troy, and M. Ahmed, "Hydrogen Abstraction-Acetylene Addition Revealed," *Angew. Chem. Int. Ed.*, **53**, 7740, DOI: 10.1002/anie.201404537 (2014)
41. T. Nah, S. H. Kessler, K. E. Daumit, J. H. Kroll, S. R. Leone, and K. R. Wilson, "The influence of molecular structure and chemical functionality on the heterogeneous OH-initiated oxidation of unsaturated organic particles," *J. Phys. Chem. A*, **118**, 4106, DOI: 10.1021/jp502666g (2014)
42. D. R. Worton, G. Isaacman, D. R. Gentner, T. R. Dallmann, A. W. H. Chan, C. Ruehl, T. W. Kirchstetter, K. R. Wilson, R. A. Harley, and A. H. Goldstein, "Lubricating oil dominates primary organic aerosol emissions from motor vehicles," *Environ. Sci. Technol.*, **48**, 3698, DOI: 10.1021/es405375j (2014)
43. N. Hansen, S. A. Skeen, H. A. Michelsen, K. R. Wilson, and K. Kohse-Höinghaus, "Flame Experiments at the Advanced Light Source: New Insights into Soot Formation Processes," *J. Vis. Exp.* **87**, doi:10.3791/51369 (2014)
44. K. R. Kolesar, G. Buffaloe, K. R. Wilson, and C. D. Cappa, "OH-Initiated Heterogeneous Oxidation of Internally-Mixed Squalane and Secondary Organic Aerosol," *Environ. Sci. Technol.*, **48**, 3196 (2014)

## Annual Progress Report on project entitled “Theoretical Investigation of Kinetic Processes in Small Radicals” (ER16100)

Paul J. Dagdigian (pjdagdigian@jhu.edu),  
Department of Chemistry, The Johns Hopkins University of Maryland, Baltimore, MD 21218-2685  
Millard H. Alexander (mha@umd.edu),  
Department of Chemistry and Biochemistry, University of Maryland, College Park, MD 20742-2021

### Program Scope

Our group studies inelastic and reactive collisions of small molecules, focusing on radicals important in combustion environments. The goal is the better understanding of kinetic processes that may be difficult to access experimentally. An essential component is the accurate determination and fitting of potential energy surfaces (PESs). We use time-independent (close-coupling) methods to treat the dynamics. We have studied inelastic energy transfer (rotational, vibrational, and/or electronic) in small hydrocarbon radicals ( $\text{CH}_2$  and  $\text{CH}_3$ ) and the CN radical. We have made a comparison with experimental measurements of relevant rate constants. Also, we are calculating accurate transport properties using state-of-the-art PESs and to investigate the sensitivity to these of 1-dimensional flame simulations. Of particular interest are collision pairs involving the light H atom.

### Personnel

Millard H. Alexander, University of Maryland, Principal Investigator  
Paul J. Dagdigian, The Johns Hopkins University, Principal Investigator  
Jacek Klos, University of Maryland, Research Assistant Professor  
Lifang Ma, University of Maryland, Graduate Research Assistant (Ph.D., 2014)  
Qianli Ma, The Johns Hopkins University, Graduate Research Assistant (Ph.D., 2014)  
Michael Warehime, University of Maryland, Graduate Research Assistant (Ph. D., 2015)

### Recent Progress and Future Work

#### *Collisional Relaxation*

We have studied extensively the collisional relaxation of methylene ( $\text{CH}_2$ ), to parallel the experimental investigation at Brookhaven by Hall and Sears. We determined potential energy surfaces (PES's) for the interaction of  $\text{CH}_2$  in both its ground  $X^3B_1$  and singlet excited  $a^1A_1$  electronic states with the He atom. We calculated state-to-state integral cross sections for inelastic transitions and rate constants for total removal of given rotational levels. The latter agreed well with the Brookhaven results. Vibrational relaxation of the bending mode of  $\text{CH}_2(X)$  in collisions with He is two orders of magnitude less efficient than rotational relaxation [1].

We also studied collision-induced internal conversion (CIIC) from the  $a$  to the  $X$  state of  $\text{CH}_2$ , a process mediated by the weak spin-orbit coupling. In the “gateway” model, CIIC is facilitated by coherent mixing of the scattering  $T$ -matrix elements for collisional transitions involving the few accidentally-degenerate pairs of rotational states. [2]. We then used our calculated CIIC and pure-rotational rate constants in a kinetic simulation of the collisional relaxation of  $\text{CH}_2(X,a)$  in collisions with He. Figure 1 presents snapshots, following the relaxation of the  $8_{18}$  mixed, nominal  $a$  state, studied at Brookhaven. Relaxation proceeds in three steps: (1) rapid equilibration of the two mixed-pair levels [ $a(0,0,0)8_{18}$  and  $X(0,2,0)9_{37}$ , in Fig. 1], (2) fast relaxation within the  $a$  state, and (3) slower relaxation among the  $X$ -state levels.

Stimulated by our earlier theoretical work, Orr-Ewing (Bristol, UK) applied molecular beam and velocity map imaging to the determination of differential cross sections for scattering of photolytically generated beam of  $\text{CD}_3$  with a number of collision partners (He,  $\text{H}_2$ , Ar, and  $\text{N}_2$ ). REMPI detection of the scattered  $\text{CD}_3$  allowed resolution of the rotational angular momentum  $n$ , but averaged over a subset of the projection quantum numbers. Our calculations, based on



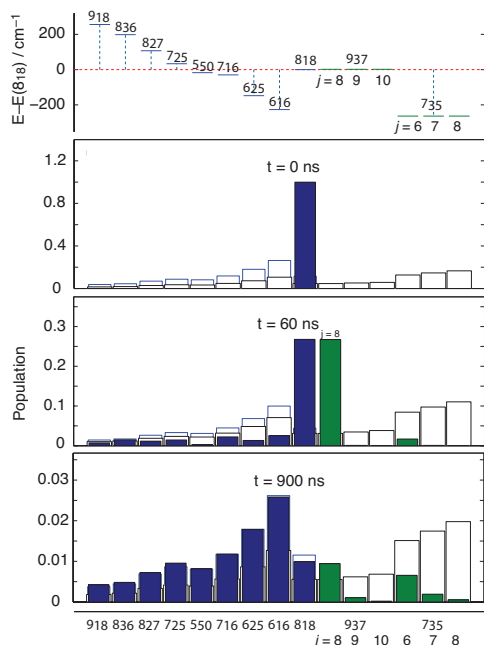


FIG. 1. Rotational distributions of selected singlet (blue) and triplet (green) levels at various times following initial population of the  $a(0,0,0)$   $8_{18}$  mixed level;  $p = 2$  Torr,  $T = 300$  K. The black rectangular empty boxes denote the relative  $T = 300$  K Boltzmann populations. The upper panel indicates the energies of the levels.

*ab initio* PES's agreed well with experiment [3-5]. The dynamics of collision of the symmetric top  $CD_3$  is richer than that of a diatomic. In collaborations with Orr-Ewing and van der Avoird (Nijmegen, Netherlands), [5] we compared the scattering of  $CD_3$  with that of  $ND_3$  [6].

Also with Hall and Sears we have studied rotational energy transfer (RET) of  $CN(X)$  in collisions with He and Ar. [7] These authors employed frequency modulated transient absorption in a double-resonance, depletion recovery experiment. We carried out quantum scattering calculations for RET of selected rotational levels. Our calculations agree well with measured thermal rate constants, as well as non-thermal Doppler-resolved rate constants. In the future we will investigate collisional depolarization of non-isotropic  $m$  distributions.

### Transport properties

Modeling combustion involves the prediction of the temporal and spatial dependence of the concentrations of all relevant species, as well as for the calculation of flame velocities. This requires knowledge of rate constants of all the relevant species, as well transport properties. Sensitivity analysis by several groups suggests that uncertainties in transport properties can be as significant as uncertainties in reaction rate constants. Present computational resources allow the accurate calculation of transport properties using state-of-the-art PESs. We have been computing accurate transport properties in quantum scattering calculations for collisions of various free radicals. [8-11] Based on our recent work, we found that: (a) Retention of just the isotropic part of the potential results in errors in transport properties of only a few percent. (The exceptions involve species with a low-lying LUMO, such as  $CH_2(a)$  and  $BH_3$ .) (b) Isotropic Lennard-Jones (LJ) 12-6 potentials yield diffusion coefficients with too steep a temperature dependence. This occurs because the repulsive walls of LJ 12-6 potentials are too steep. (c) Transport property calculations with LJ potentials for radical-radical systems disagree significantly with calculations using accurate potentials.

We have concentrated [9-11] on the calculation of transport properties for collision pairs involving the light H atom and have computed PESs when these are not available. We have also used these calculated properties to assess how a more accurate treatment of transport affects 1-dimensional laminar combustion simulations. In some cases accurate transport properties differ significantly from LJ estimates, as illustrated in Fig. 2 for the H-CO and H-CO<sub>2</sub> binary diffusion coefficients.

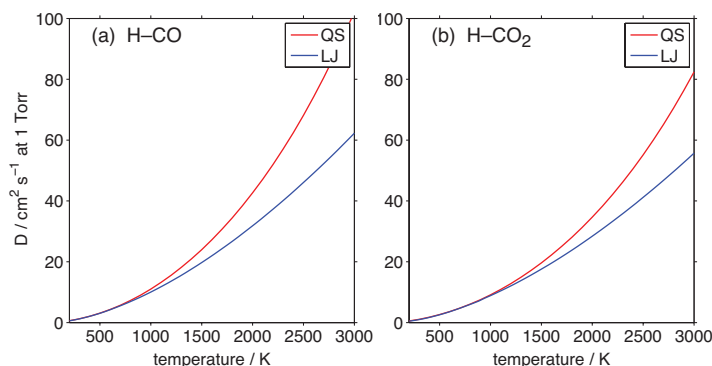


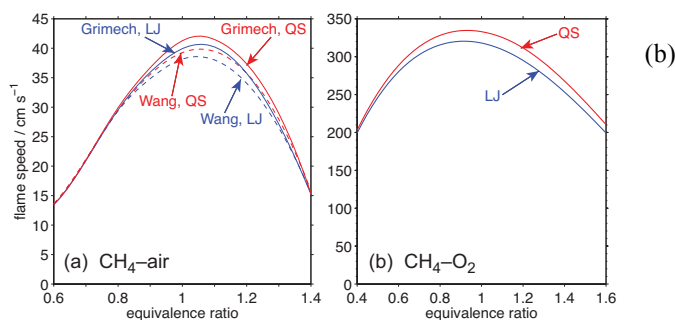
FIG. 2. Comparison of binary diffusion coefficients at 1 Torr for (a) H-CO and (b) H-CO<sub>2</sub>. QS and LJ denote quantum scattering calculations and conventional calculations with LJ (12-6) potentials, respectively.

Recently, [11] we have computed a new RCCSD(T) PES for H-N<sub>2</sub> and have computed transport properties for comparison with the previous calculations by Stallcop *et al.* [J. Chem. Phys. **97**, 3431 (1992)], who used a spherically averaged potential. We have also computed a PES for H-CH<sub>4</sub> and computed transport properties using both the full anisotropic and spherically averaged potentials.

### Flame Simulations

We have extended our 1-dimensional flame simulations to the combustion of methane in both air and in oxygen. Two sets of calculations were carried out: The first set was based on the conventional parameterized LJ 12-6 potentials, while the second set incorporated exact transport properties for the available collision pairs. The calculated flame speeds as a function of the equivalence ratio are presented in Fig. 3.

FIG. 3. Laminar flame speeds for (a) CH<sub>4</sub>-air and CH<sub>4</sub>-O<sub>2</sub> at 1 atm. The blue and red curves denote calculations with LJ and accurate transport properties, respectively. Chemistry models employed for CH<sub>4</sub>-air included Grimech 3.0 (solid lines) and USC Mech 3 (dashed lines). For CH<sub>4</sub>-O<sub>2</sub> Grimech 3.0 was employed as the chemistry model.



It can be seen from Fig. 3(a) that the differences in flame speeds computed with conventional LJ and accurate transport properties are comparable to differences in flame speeds computed with different chemistry models. A sensitivity analysis indicates that for the air flame the flame speed is most strongly affected by the transport properties for H-N<sub>2</sub>, while for the O<sub>2</sub> flame the most important transport properties are for the H-CO and H-CO<sub>2</sub> collision pairs. We are interested in collaborating with modelers simulating combustion in 2 or 3 dimensions.

### Outreach and Interactions

Dagdigian and Alexander have published several review articles [13,14] outlining theoretical methods used in the calculations carried out under this project.

### DOE Synergy

As mentioned above, Alexander and Dagdigian interact closely with Hall and Sears at Brookhaven. In addition to our collaborative work on the collisional relaxation of CH<sub>2</sub>, we have collaborated on the Doppler-resolved kinetics and pressure broadening of the CN radical. Alexander has collaborated with Chandler at Sandia Livermore on inelastic scattering of the NO radical. Development of Dagdigian's 1-dimensional combustion simulations were facilitated by Sivaramakrishnan at Argonne.

### Other groups

As discussed above, we collaborated with Orr-Ewing at Bristol UK on the determination of CD<sub>3</sub> differential cross sections in collisions with a number of species. We hope to compare recently-computed [15] pressure broadening calculations on the OH  $A - X$  transition with measurements from the group of Ritchie at Oxford. Oxford, UK.

Figure 1 (above) was based on solution of a kinetic master equation following a method first described by Alexander, Dagdigian and Hall. [15] This method has been recently used to interpret experiments carried out by Mullin supported by another grant. [16]

### Publications Supported by this Project (2014-2017)

1. L. Ma, P. J. Dagdigian, and M. H. Alexander, "Theoretical investigation of the relaxation of the bending mode of CH<sub>2</sub>(X) by collisions with helium," *J. Chem. Phys.* **141**, 214305 (4 pages) (2014).
2. L. Ma, M. H. Alexander, and P. J. Dagdigian, "Theoretical investigation of intersystem crossing between the  $a^1A_1$  and  $X^3B_1$  states induced by collisions with helium," *J. Chem. Phys.* **141**, 064312 (10 pages) (2014).
3. Ondrej Tkáč, A. J. Orr-Ewing, P. J. Dagdigian, M. H. Alexander, J. Onvlee, and A. van der Avoird, "Collision dynamics of symmetric top molecules: A comparison of the rotationally inelastic scattering of CD<sub>3</sub> and ND<sub>3</sub> with He," *J. Chem. Phys.* **140**, 134308 (10 pages) (2014).
4. Ondrej Tkáč, Q. Ma, C. A. Rusher, S. J. Greaves, A. J. Orr-Ewing, and P. J. Dagdigian, "Differential and integral cross sections for the rotationally inelastic scattering of methyl radicals with H<sub>2</sub> and D<sub>2</sub>," *J. Chem. Phys.* **140**, 204318 (12 pages) (2014).
5. Ondrej Tkáč, Q. Ma, M. Stei, A. J. Orr-Ewing, and P. J. Dagdigian, "Rotationally inelastic scattering of methyl radicals with Ar and N<sub>2</sub>," *J. Chem. Phys.* **142**, 014306 (10 pages) (2015).
6. Q. Ma, A. van der Avoird, J. Loreau, M. H. Alexander, S. Y. T. van de Meerakker, and P. J. Dagdigian, "Resonances in rotationally inelastic scattering of NH<sub>3</sub> and ND<sub>3</sub> with H<sub>2</sub>," *J. Chem. Phys.* **143**, 044312 (2015).
7. D. Forthomme, M. L. Hause, H.-G. Yu, P. J. Dagdigian, T. J. Sears, and G. E. Hall, "Doppler-resolved kinetics of saturation recovery," *J. Phys. Chem. A* **119**, 7439-7450 (2015).
8. P. J. Dagdigian and M. H. Alexander, "Transport cross sections for systems with deep potential wells," *J. Phys. Chem. A* **118**, 11935-11942 (2014).
9. P. J. Dagdigian, "Accurate transport properties for H-CO and H-CO<sub>2</sub>," *J. Chem. Phys.* **143**, 054303 (7 pages); erratum **143**, 159902 (1 page) (2015).
10. P. J. Dagdigian, J. Kłos, M. R. Warehime, and M. H. Alexander, "Accurate transport properties for O(<sup>3</sup>P)-H and O(<sup>3</sup>P)-H<sub>2</sub>," *J. Chem. Phys.* **145**, 164309 (9 pages) (2016).
11. P. J. Dagdigian, "Quantum Scattering Calculations of Transport Properties for the H-N<sub>2</sub> and H-CH<sub>4</sub> Collision Pairs," *J. Phys. Chem. A* **120**, 7793-7799 (2016).
12. P. J. Dagdigian, "Combustion simulations with accurate transport properties for reactive intermediates," *Comb. Flame* **162**, 2480-2486 (2015).
13. P. J. Dagdigian, "Theoretical investigation of collisional energy transfer in polyatomic intermediates," *Int. Rev. Phys. Chem.* **32**, 229-265 (2013).
14. P. J. Dagdigian and M. H. Alexander, "Application of Quantum Statistical Methods to the Treatment of Collisions," *Adv. Chem. Phys.* (in press).
15. P. J. Dagdigian, "Pressure Broadening Calculations for OH in Collisions with Argon: Rotational, Vibrational, and Electronic Transitions," *J. Quant. Spectrosc. Radiat. Transfer* **189**, 105-111 (2017).

### Other references

15. M. H. Alexander, G. Hall, and P. J. Dagdigian, "The Approach to Equilibrium: Detailed Balance and the Master Equation," *J. Chem. Educ.* **88**, 1538-1543 (2011).
16. M. J. Murray, H. M. Ogden, C. Toro, Q. N. Liu, D. A. Burns, M. H. Alexander, and A. S. Mullin, "State-Specific Collision Dynamics of Molecular Super Rotors with Oriented Angular Momentum," *J. Phys. Chem. A* **119**, 12471-12479 (2015)

## Turbulence-Chemistry Interactions in Reacting Flows

Robert S. Barlow  
Combustion Research Facility  
Sandia National Laboratories, MS 9051  
Livermore, California 94550  
barlow@sandia.gov

### Program Scope

This program is directed toward achieving a more complete and quantitative understanding of the coupled, multiscale interactions of chemistry, molecular diffusion, and turbulent mixing in gas-phase reacting flows. In the Turbulent Combustion Laboratory (TCL) simultaneous line imaging of spontaneous Raman scattering, Rayleigh scattering, and two-photon laser-induced fluorescence (LIF) of CO is applied to obtain spatially and temporally resolved measurements of temperature, the concentrations of all major species, mixture fraction, and reaction progress, as well as gradients in these quantities in hydrocarbon flames. The instantaneous three-dimensional orientation of the turbulent reaction zone is also measured by imaging of OH LIF or Rayleigh scattering at 355 nm in two crossed planes, which intersect along the laser axis for the multiscale measurements. These combined data characterize both the thermo-chemical state and the instantaneous flame structure, such that the influence of turbulent mixing and molecular transport on flame chemistry may be quantified. Our experimental work is closely coupled with international collaborative efforts to develop and validate predictive models for turbulent combustion. This is accomplished through our visitor program and through the TNF Workshop series. In recent years the workshop and this program have expanded their scope to address a range of combustion modes, including premixed, stratified, partially premixed, and nonpremixed flames. We are also working to extend our quantitative multiscale diagnostics to more complex hydrocarbon fuels, such as dimethyl ether. Entry into these new research areas has prompted developments in both hardware and methods of data analysis to achieve unprecedented spatial resolution and precision of multiscale measurements. Within the CRF we collaborate with Jonathan Frank, who applies advanced imaging diagnostics to turbulent flames, and with Joe Oefelein, who performs high fidelity large-eddy simulations (LES) in order to gain greater fundamental understanding of the dynamics of multi-scale flow-chemistry interactions.

### Recent Progress

#### *Piloted Partially-Premixed jet Flames with Multi-regime Combustion*

It is common in combustion systems to have in inhomogeneous fuel-air mixtures entering a turbulent flame zone, such that the instantaneous reaction zone may have premixed character, nonpremixed character, or something in between. This is referred to as multimode or multi-regime combustion. In collaboration with H. Cutcher and A. Masri (Sydney University), we are continuing to investigate multimode combustion a set of jet flames stabilized on a piloted burner that has a retractable center tube within the main jet tube. When the central tube delivers fuel and is recessed by an optimal distance, the flame exhibits stratified-premixed combustion close to the jet exit. The mode of combustion then transitions rapidly within the first several jet diameters, such that the measured characteristics ten diameters downstream ( $x/D=10$ ) resemble a

diffusion flame [Meares et al. *Proc. Combust. Inst.* 2015, 35, 1477–1484; Barlow et al. *Combust. Flame* 2015, 162, 3516–3540]. This transition region presents a challenge for combustion models, many of which assume a particular flame structure (either premixed or nonpremixed). Consequently, these experiments make an attractive and relevant target for simulations, and fifteen computational groups submitted results for initial comparisons at the TNF13 Workshop (July 2016, Seoul, Korea).

One important result from the experiments is that 1D measurements of mixture fraction dissipation were shown to be fully resolved for all measurements at elevated temperature, including measurements within the near-field region where the transition in combustion mode takes place [Cutcher et al. *Proc. Combust. Inst.* in press]. In recent work, the crossed-planar OH-LIF images, which were acquired in 2015 along with the line-imaged Raman/Rayleigh/CO-LIF measurements, have been analyzed to determine local 3D flame normal vectors and to estimate the full 3D mixture fraction dissipation from the measured 1D projection. The difference between the 1D and 3D conditional dissipation results tends to increase with downstream distance as the pdf of flame normal angles becomes broader.

Mixture fraction and reaction progress variable are both central concepts in theory and modeling of turbulent partially-premixed flames. However, there has been no consensus on a definition of progress variable. A progress variable,  $c_O$ , was defined, based on the mass fraction of oxygen bound in products  $\text{CO}_2$ ,  $\text{H}_2\text{O}$ , and  $\text{CO}$ , which can be easily calculated from Raman/Rayleigh experiments or from simulations and offers some advantages over alternative definitions [Barlow et al., *Combust. Flame*, accepted]. Analysis of the joint statistics of mixture fraction and progress variable in the Sydney piloted jet flames has shown that fluctuations in these quantities are highly correlated at most locations, with the exception of regions characterized by near-stoichiometric premixed combustion. This result contradicts the common modeling assumption of statistical independence.

#### *A Novel Method for Reaction Zone Characterization based on 1D Raman/Rayleigh Data*

In turbulent partially-premixed flames it is of great value to be able to identify local reaction zones and characterize them as having premixed or nonpremixed local structure. Several regime identifiers have been developed in the context of direct numerical simulation (DNS). However, these all rely on knowledge of 3D scalar gradients that are not experimentally accessible. In collaboration with S. Hartl and C. Hasse (Freiberg University) and D. Geyer and A. Dreizler (TU Darmstadt), we are developing a method of gradient-free regime identification (GFRI) based on 1D Raman/Rayleigh measurements of temperature and major species. As illustrated in Figure 1a, Raman/Rayleigh experimental data are taken as the initial conditions for a homogeneous batch reactor (HR) calculation. The HR calculation is terminated when it reaches a manifold, which approximates the full thermochemical state of the measured sample. The chemical explosive mode (CM) and heat release rate (HRR) are then calculated as flame markers along with mixture fraction,  $Z$ . This novel approach has been extensively tested using fully-resolved 1D and 2D flame simulations from which Raman/Rayleigh equivalent data are generated [Hartl et al., submitted]. We have also compared results from recent Raman/Rayleigh measurements in laminar opposed-jet flames with those derived from opposed flow (Chemkin) simulations at matched conditions, as shown in Figure 1b. The locations of CM zero crossings (premixed flame markers) are very consistent. HRR results show greater effects of experimental noise, but relative heat release rates in different parts of the flame can still be assessed.

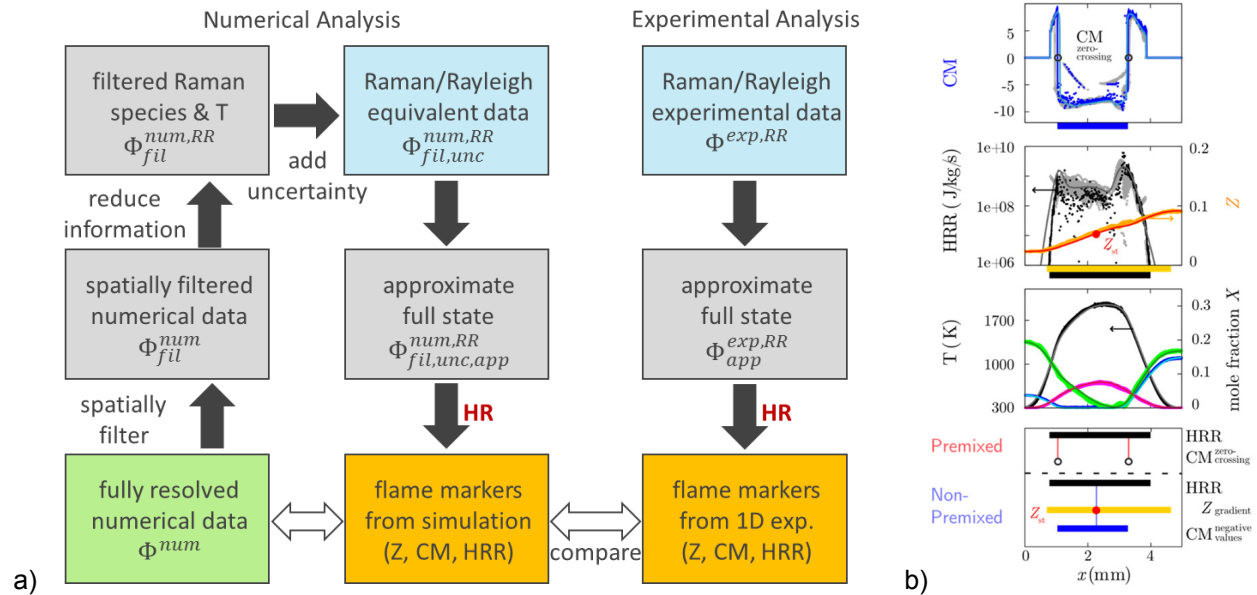


Figure 1. a) Procedures for generating flame markers from numerical simulations (left) or Raman-Rayleigh experiments (right). b) Example of measured profiles (300 separate shots) across a laminar counterflow triple flame, showing: T, O<sub>2</sub>, CH<sub>4</sub>, CO<sub>2</sub>, Z, CM and HRR; a Chemkin calculation at matching conditions; and the corresponding CM and HRR results from the fully resolved numerical data (light blue, dark gray lines), the Raman/Rayleigh equivalent data (dark blue, black scatter), and the experimental data (gray scatter). Lean and rich premixed flames are marked by the CM zero crossings.

### Other Progress

Papers were published during the past year on turbulent stratified combustion (Stahler et al. *Proc. Combust. Inst.* in press), dual-resolution Raman measurements of six hydrocarbon species and twelve species overall, including N<sub>2</sub>, O<sub>2</sub>, H<sub>2</sub>O, CO<sub>2</sub>, CO, H<sub>2</sub>, CH<sub>4</sub>, DME, CH<sub>2</sub>O, C<sub>2</sub>H<sub>2</sub>, C<sub>2</sub>H<sub>4</sub>, and C<sub>2</sub>H<sub>6</sub> (Magnotti et al. *Proc. Combust. Inst.* in press). Experiments on stratified CH<sub>4</sub>/H<sub>2</sub> flames were conducted in collaboration with S. Schneider, D. Geyer, and A. Dreizler (TU Darmstadt) and data are being analyzed. We are collaborating with Z. Chen and N. Swaminathan (Cambridge University) to compare measured and modeled joint statistics of progress variable and mixture fraction.

### **Future Plans**

Our ongoing analysis of the Sydney piloted flames is focused on multiply conditioning methods aimed at identifying metrics that can be used to quantitatively characterize local reaction structures within the spectrum between premixed and nonpremixed flames. Metrics of particular interest include mixture fraction, progress variable, the ratio of their spatial gradients, and CO conditioned on temperature and mixture fraction. These metrics will be analyzed in combination with the CM and HRR flame markers described above. Methods of reducing the effects of experimental noise on the HRR results will be investigated thoroughly because the benefit of deriving quantitatively useful HRR from instantaneous Raman/Rayleigh line measurements would be significant. Numerical tests indicate that HRR results can be improved by including OH concentration along with major species and temperature in the initial conditions for the homogeneous reactor calculation. Therefore, we will be adding the capability for quantitative line imaging of OH LIF. We are also planning to add capability for quantitative, line-imaged NO LIF measurements.

## **BES Supported Publications (2015 - present)**

Fuest, F.; Magnotti, G.; Barlow, R.S.; Sutton, J.A., Scalar structure of turbulent partially-premixed dimethyl ether/air jet flames, *Proc. Combust. Inst.* **2015**, *35*, 1235–1242.

Meares, S.; Prasad, V.N.; Magnotti, G.; Barlow, R.S.; Masri, A.R., Stabilization of piloted turbulent flames with inhomogeneous inlets, *Proc. Combust. Inst.* **2015**, *35*, 1477–1484.

Magnotti, G.; Geyer, D.; Barlow, R.S., Interference-free spontaneous Raman spectroscopy for measurements in rich hydrocarbon flames, *Proc. Combust. Inst.* **2015**, *35*, 3765–3772.

Magnotti, G.; Barlow, R.S., Effects of high shear on the structure and thickness of turbulent premixed methane/air flames stabilized on a bluff-body burner, *Combust. Flame* **2015**, *162*, 100–114.

Barlow, R.S.; Dunn, M.J.; Magnotti, G., Preferential transport effects in premixed bluff-body stabilized CH<sub>4</sub>/H<sub>2</sub> flames, *Combust. Flame* **2015**, *162*, 727–735.

Fuest, F.; Barlow, R.S.; Magnotti, G.; Dreizler, A.; Ekoto, I.W., Sutton, J.A., Quantitative acetylene measurements in laminar and turbulent flames using 1D Raman/Rayleigh scattering, *Combust. Flame* **2015**, *162* 2248–2255.

Magnotti, G.; KC, U.; Varghese, P.L.; Barlow, R.S., Raman spectra of methane, ethylene, ethane, dimethyl ether, formaldehyde and propane for combustion applications, *JQSRT* **2015** *163*, 80–101

Barlow, R.S.; Meares, S.; Magnotti, G.; Cutcher, H., A.R. Masri, Local extinction and near-field structure in piloted turbulent CH<sub>4</sub>/air jet flames with inhomogeneous inlets, *Combust. Flame* **2015**, *162*, 3516–3540.

Kamal, M.M.; Barlow, R.S.; Hochgreb, S., Conditional analysis of turbulent premixed and stratified flames on local equivalence ratio and progress of reaction, *Combust. Flame* **2015**, *162*, 3896–3913.

Kamal, M.M.; Barlow, R.S.; Hochgreb, S., Scalar structure of turbulent stratified swirl flames conditioned on local equivalence ratio, *Combust. Flame* **2016**, *166*, 76–79.

Cutcher, H.C.; Magnotti, G.; Barlow, R.S.; Masri, A.R., Turbulent Flames with Compositionally Inhomogeneous Inlets: Resolved Measurements of Scalar Dissipation Rates, *Proc. Combust. Inst.* **2016** (in press) <http://dx.doi.org/10.1016/j.proci.2016.07.093>.

Stahler, T.; Geyer, D.; Magnotti, G.; Trunk, P.; Barlow, R.S.; Dreizler, A., Multiple conditioned analysis of the Turbulent Stratified Flame A, *Proc. Combust. Inst.* **2016** (in press) <http://dx.doi.org/10.1016/j.proci.2016.08.070>

Magnotti, G.; Barlow, R.S., Dual-Resolution Raman Spectroscopy for Measurements of Temperature and Twelve Species in Hydrocarbon-Air Flames, *Proc. Combust. Inst.* **2016**, (in press) <http://dx.doi.org/10.1016/j.proci.2016.06.128>.

Barlow, R.S.; Magnotti, G.; Cutcher, H.C.; Masri, A.R., On defining progress variable for Raman/Rayleigh experiments in partially-premixed methane flames, *Combust. Flame* (in press).

Fuest, F.; Barlow, R.S.; Magnotti, G.; Sutton, J.A., Scalar dissipation rates in a turbulent partially-premixed dimethyl ether/air jet flame, *Combust. Flame* (submitted).

Hartl, S.; Geyer, D.; Dreizler, A.; Magnotti, G., Barlow, R.S.; Hasse, C., Reaction zone detection and characterization from Raman/Rayleigh line measurements in partially premixed flames, *Combust. Flame* (submitted).

**TNF Workshop Information:** <http://www.sandia.gov/tnf>

**TNF13 Workshop Proceedings:** <http://www.sandia.gov/TNF/13thWorkshop/TNF13.html>

# Predictive Large-Eddy Simulation of Supercritical-Pressure Reactive Flows in the Cold Ignition Regime

Josette Bellan

Mechanical and Civil Engineering Department, California Institute of Technology  
Pasadena, CA 91125

[Josette.Bellan@jpl.nasa.gov](mailto:Josette.Bellan@jpl.nasa.gov)

DOE Award Number: **02\_GR-ER16107-14-00**

STRIPES award number: **SC0002679/0009**

## I. Program Scope

This study addresses issues highlighted in the Basic Energy Needs for Clean and Efficient Combustion of 21st Century Transportation Fuels (DOE BES, 2006) under the topic of Combustion under Extreme Pressure. It is there noted that “the most basic concepts of thermal autoignition” are “based on experience and theory at near atmospheric pressures” and that “as pressure increases significantly..., many of these conceptual pictures begin to change or disappear”. It is also stated “A better description of the coupling and interaction of high pressure flow and molecular transport processes with chemistry is also necessary”, particularly because “Ignition and flame propagation of alternative and renewable fuels, as well as of the changing feed stocks of conventional fossil-based fuels, are very likely to be much different at very high pressures than under the more familiar, lower pressure conditions of current engines.” Recognizing that “Under such (*increasing pressure*) conditions distinctions between gas and liquid phases become moot, new equations of state must be used...”, it is immediately apparent that there must be “a re-examination of the basic assumptions that govern the physics and chemistry related to combustion; and the need for this type of re-examination increases as the combustion pressure increases.” This recognition is also stated under the topic of Multiscale Modeling since due to the new equations of state “The combination of unexplored thermodynamic environments and new physical and chemical fuel properties results in complex interactions among multiphase (*according to the above, the multiphase distinction becomes moot with increasing pressure*) fluid dynamics, thermodynamic properties, heat transfer, and chemical kinetics that are not understood even at a fundamental level.” From the theoretical viewpoint for “systems at high pressure, fluid dynamic time scales can be comparable to chemical time scales.” and therefore “completely diffusion-controlled reactions ... can become important”.

Thus, the objective of this study is the investigation of the coupling among thermodynamics, transport properties, intrinsic kinetics and turbulence under the high-pressure and the relatively (with respect to combustion) low-temperature conditions typical of the auto-ignition regime, with particular emphasis on the manifestation of this coupling on the effective kinetic rate. As planned, we established collaboration with Dr. Joseph Oefelein of the Combustion Research Facility at Sandia Livermore to work together towards implementing the models developed in this research into the high-pressure Large Eddy Simulation (LES) code (named RAPTOR) under development by him at Sandia.

## II. Recent Progress

This report contains results obtained during the previous year of funding. The focus of the research during that year was on spatial simulations rather than the temporal simulations of our previous studies. To this effect we conducted two types of simulations: **(1)** Large Eddy Simulations (LES) at supercritical pressure in order to evaluate our model with experimental



data [i] and understand the effect of a proposed subgrid-scale (SGS) model for unconventional terms in the momentum equation [ii], and (2) Direct Numerical Simulations (DNS) of a fluid jet injected into a chamber filled with a species different from that in the jet (these are the first jet-DNS ever conducted for a binary species system).

(1) For conducting LES the conservation equations were re-written in curvilinear coordinates to enable a natural progression to coarser grids away from the injection plane. Two LES were conducted at the jet Reynolds number of  $1.6 \times 10^5$ : in SLES the only SGS model is that for the

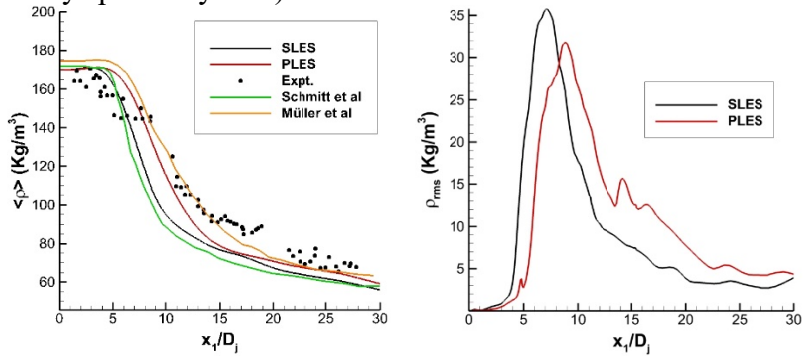


**Figure 1. Time-averaged statistics from LES of a N2 jet (at 137 K) injected into a N2-filled chamber (at 298 K and 39.7 bar).**

conventionally modeled terms whereas in PLES a model for the SGS pressure-gradient term was also added to the equations. In essence, this last term acted as a surface tension per unit area and its effect was to maintain the morphological features of the flow. Figure 1(left) shows that indeed, for the same initial conditions, PLES is closer to the data than SLES whereas Fig. 1(right) reveals that while both cases show the same trend, with very low fluctuations near injection leading to a steep rise near the jet breakup region, PLES predicts slightly smaller maximum fluctuations compared to SLES, a fact which is attributed to the larger PLES mean density in that region, meaning that it is more difficult to distort the fluid; however, both cases decay to approximately the same level far downstream where the mean density is similar. These results indicate that measurements to evaluate models should be conducted both near the jet breakup and closely downstream to address the variability of the models' predictions in these regions. Figure 2 indicates that not only is the potential core longer in PLES, but also that the temperature remains smaller further downstream in PLES compared to SLES and the small-T regions are more tapered.

Since density and temperature are two essential variables in combustion, it is clear that field-resolved experimental data will be most beneficial to determine whether the additional SGS model used in PLES provides higher-fidelity results compared to SLES. The results were described in a publication [7].

(2) The DNS of binary-fluid jet injection were performed to determine, in the spatial setting, the separate influence of the chamber pressure and of the density ratio between injected and chamber fluid. To this end N2 was injected into a CO2-filled chamber which was at several pressures: 1, 35, 60 and 80 atm. The temperatures of the jet and chamber were selected so that there were 4 simulations having an initial density ratio in the range 0.335-0.38, 1 simulation

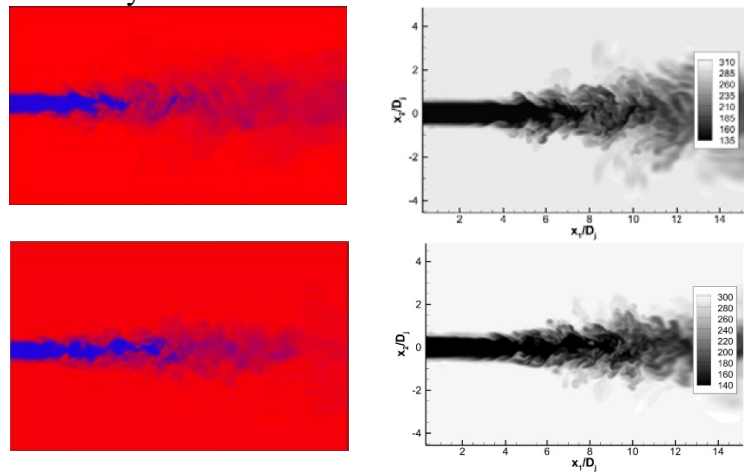


**Figure 2. Instantaneous ( $t^*=125$ ) visualizations of the density (left) and temperature (right) for SLES (top) and PLES (bottom).**

simulation having an initial density ratio in the range 0.335-0.38, 1 simulation

where the ratio was 0.5 and 1 simulation with the ratio of 0.98. For all simulations the Reynolds number of the jet was 2000. Some of the pertinent results are shown in Figs. 3-5 and a manuscript is in progress [iii]. The results of Figs. 3 and 4 show that as far as jet spreading and associated mixing, the pressure itself is not a strong parameter and only the initial density ratio matters. In particular, the results reveal that side jets (not shown) only

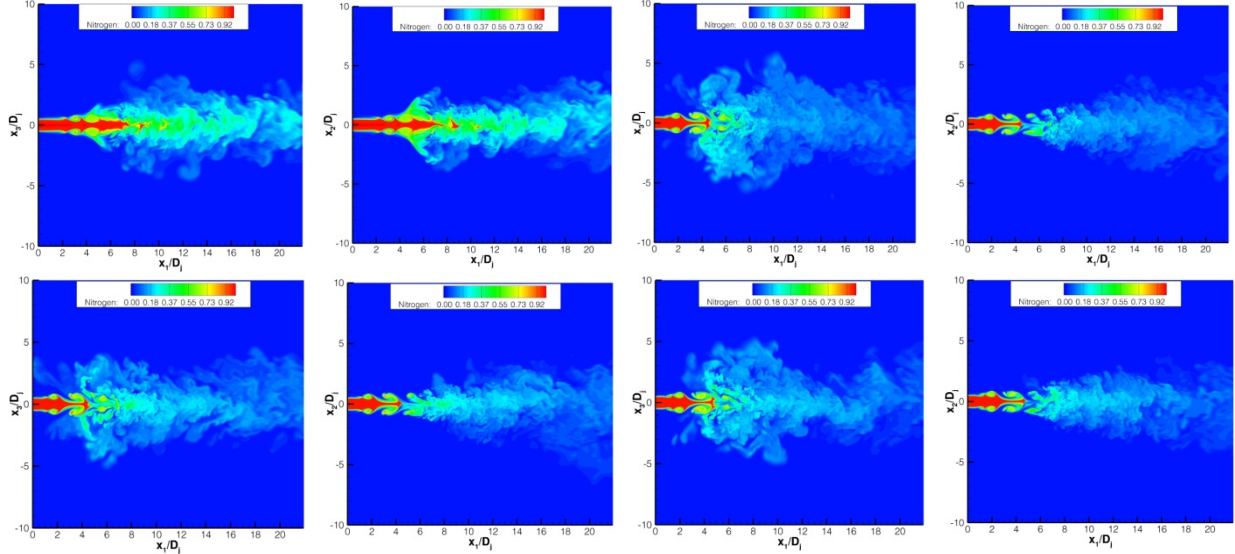


**Figure 3. Effect of density ratio (0.5, top; 0.3 bottom) on jet spreading at 35 atm. N<sub>2</sub> mass fraction visualization in the  $x_2=0$  plane (left) and the  $x_3=0$  plane (right).**

**Figure 4. Effect of pressure (60 atm, top; 80 atm, bottom) on jet spreading at density ratio of 0.3. N<sub>2</sub> mass fraction visualization in the  $x_2=0$  plane (left) and the  $x_3=0$  plane (right).**

occur for a density ratio smaller than 1, agreeing with information from experimental data at 1 bar and different density ratios [iv]. The results comparing the influence of the density ratio versus pressure provide insight regarding the influence of pressure in turbulent combustion. The density ratio, which is a function of both pressure and temperature, initially determines the spreading of the injected fluid and therefore jet penetration; the temperature field is determined by the jet penetration/spreading through the enthalpy transported by the species and through the mixture thermal-conductivity which is function of pressure. Both temperature and pressure influence ignition and combustion. The second invariant of the rate of deformation tensor,  $Q$ , is visualized in Fig. 5.  $Q$  is particularly apt to highlight regions of vortical activity for  $Q>0$  from those of stress for  $Q<0$ . Clearly, jet axial penetration is higher at the larger density ratio but jet radial spreading is larger at the smaller density ratio.

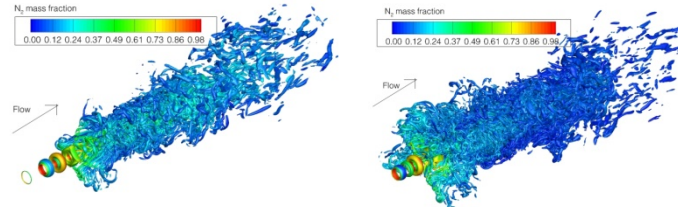


**Figure 5. Isosurfaces of  $Q=9 \times 10^7$  visualizing the vorticity field at 35 atm. The isosurfaces are colored by  $Y_{N_2}$ . Density ratio of 0.5 (left) and 0.3 (right).**

The PI has continued the collaboration with Dr. Oefelein who will modify RAPTOR once we have developed the methodology of LES for high- $p$  flows.

### III. Future Plans

The following activities are planned:

- Develop a model for the mixture fraction pdf in the presence of differential diffusion.
- Implement a mixture-fraction-based turbulent-reaction-rate model into the code and perform simulations.

#### IV. References

- i. Mayer, W.; Telaar, J.; Branam, R.; Schneider, G.; Hussong, J., *Heat Mass Trans.*, **2003** 39(8-9) 709
- ii. Taşkinoğlu, E.S.; Bellan, J., *J. Fluid Mech.* **2010** 645 211
- iii. Gnanskandan, A.; Bellan, J., DNS of a fluid jet mixing with another fluid at supercritical pressure, to be submitted
- iv. Monkewitz, P. A.; Bechert, D. W.; Basikow, B.; Lehman, B., *J. Fluid Mech.* **1990** 213 611

#### V. Publications, presentations, submitted articles supported by this project 2014- 2017

- [1] Borghesi, G.; Bellan, J., Models for the Large Eddy Simulation equations to describe multi-species mixing occurring at supercritical pressure, *Int. J. Energ. Mat. Chem. Prop.*, 13(5), 435-453, 2014
- [2] Borghesi, G.; Bellan, J., Irreversible entropy production rate in high-pressure turbulent reactive flows, *Proc. of the Comb. Inst.*, 35, 1537-1547, 2015
- [3] Borghesi, G.; Bellan, J., *A priori* and *a posteriori* analysis for developing Large Eddy simulations of multi-species turbulent mixing under high-pressure conditions, *Phys. Fluids.*, 27, 035117 (35 pages), 2015
- [4] Bellan, J., Direct Numerical Simulation of a high-pressure turbulent reacting mixing layer, *Combust. Flame*, 176, 245-262, 2017
- [5] Gnanaskandan, A.; Bellan, J., Numerical Simulation of jet injection and species mixing under high-pressure conditions, in print *Journal of Physics*, Institute of Physics Conference Series: Materials Science and Engineering, 2017
- [6] Bellan, J., Evaluation of mixture-fraction-based turbulent-reaction-rate model assumptions for high-pressure reactive flows, *Combust. Flame*, 179, 253-266, 2017
- [7] Gnanaskandan, A.; Bellan, J., Large Eddy Simulations of high pressure jets : Effect of subgrid scale modeling, submitted to the *AIAA Progress Series* book titled *High Pressure Flows for Propulsion Applications* (Ed. J. Bellan), 2017
- [8] Bellan, J., Possible phase formation during high-pressure multi-species jet disintegration, **Keynote Invited Lecture**, ILASS meeting, May 18-21, 2014, Portland, OR.
- [9] Bellan, J., Modeling and numerical simulations of multi-species high-pressure flows, **Invited Plenary Lecture**, 10<sup>th</sup> International Symposium on Special Topics in Chemical Propulsion, June 2-6, 2014, Poitiers, France
- [10] Bellan, J., Modeling and numerical simulations of multi-species high-pressure reactive flows, **Invited Plenary Lecture**, Summer Program of the SFBTRR40, Institute of Aerodynamics and Fluid Mechanics Technische Universität München, Garching, Germany, August 3, 2015
- [11] Bellan, J., Modeling and numerical simulations of multi-species high-pressure reactive flows, **Invited Seminar**, Purdue University, West Lafayette, IN., October 22, 2015
- [12] Bellan, J., Reduced models for the simulation of multi-scale problems in physics and chemistry, **Invited Seminar**, Cornell University, Ithaca, NY., November 17, 2015
- [13] Bellan, J., Modeling and Numerical Simulations of Multi-Species High-Pressure Turbulent Mixing and Combustion, **Invited Seminar**, SpaceX, Hawthorne, CA., 12/14/2016
- [14] Borghesi, G.; Bellan, J., Models for the LES equations to describe multi-species mixing occurring at supercritical pressure, paper 2014-0823 presented at the 52<sup>nd</sup> Aerospace Sciences Meeting, New Harbor, MD, January 13-17, 2014 Borghesi, G. and Bellan, J., Irreversible entropy production rate in high-pressure turbulent reactive flows, *Proc. of the Comb. Inst.*, 35, 1537-1547, 2015
- [15] Borghesi, G.; Bellan, J., *A priori* and *a posteriori* analyses of multi-species turbulent mixing layers at supercritical-*p* conditions, paper 2015-0162 presented at the 53rd Aerospace Sciences Meeting, Kissimmee, FL., January 5-9, 2015; also presented at the 9<sup>th</sup> US National Combustion Meeting, Cincinnati, OH., May 17-20, 2015
- [16] Bellan, J., The mixture fraction for high-pressure turbulent reactive flows, paper 2016-1686 presented at the 54<sup>th</sup> Aerospace Sciences Meeting, San Diego, CA, January 4-8, 2016
- [17] Gnanaskandan, A.; Bellan, J., Large Eddy Simulations of high pressure jets: Effect of subgrid scale modeling, paper 2017-1105 presented at the 55<sup>th</sup> Aerospace Sciences Meeting, Grapevine, TX, January 9-13, 2017

# Dynamics of Product Branching from Radical Intermediates in Elementary Combustion Reactions

Laurie J. Butler

The University of Chicago, The James Franck Institute

929 E 57<sup>th</sup> St, CIS E 211, Chicago, IL 60637

L-Butler@uchicago.edu

## I. Program Scope

While the total rate constant for many elementary reactions is well-characterized, understanding the product branching in complex reactions presents a formidable challenge. To gain an incisive probe of such reactions, our experiments investigate the dynamics of the product channels that arise from transient radical intermediates along the bimolecular reaction coordinates. Our recent published work<sup>1-6</sup> uses the methodology developed in my group in the last fifteen years, using both imaging and scattering apparatuses. The experiments generate a particular isomeric form of an unstable radical intermediate along a bimolecular reaction coordinate and study the branching between the ensuing product channels of the energized radical as a function of its internal rotational and vibrational energy under collision-less conditions.

The experiments use a combination of: 1) measurement of product velocity and angular distributions in a crossed laser-molecular beam apparatus, with electron bombardment detection in my lab in Chicago or 2) with tunable vacuum ultraviolet photoionization detection at Taiwan's National Synchrotron Radiation Research Center (NSRRC), and 3) velocity map imaging using state-selective REMPI and single photon VUV ionization of radical intermediates and reaction products. We also employ tunable VUV photoionization detection in our imaging apparatus, using difference frequency four-wave mixing to produce photoionization light tunable from 8 to 10.8 eV. This year of support funded our work to photolytically generate the radical intermediate important in the OH + propene reaction when OH adds to an end carbon. We describe our results on the product channels of the photolytic precursor and some of the dissociation channels of the radical intermediate in Section II.A below. Our other major result this past year was on the photoionization detection of vinoxy radicals. Our experiments at the NSRRC definitively show that vinoxy dissociatively ionizes to both  $\text{CH}_3^+$  and  $\text{HCO}^+$ , and establishes the absolute partial photoionization cross section of vinoxy to  $\text{CH}_3^+$  at 10.5 and 11.44 eV. This should allow experimentalists detecting vinoxy radicals produced in bimolecular reactions such as OH + propene to get good branching fractions to that product channel. Finally we initiated studies of the photodissociation of 1-bromo-2-chloroethane and 1,1-bromochloroethane at 193 nm at the NSRRC.

## II. Recent Progress

### A. OH + Propene: The $\text{CH}_3\text{CHCH}_2\text{OH}$ radical intermediate

The theoretically predicted product channels of the OH + propene reaction depend on whether the products are formed from direct H atom abstraction dynamics, or addition of the OH to the C=C double bond at either the end C atom or the center C atom. We sought to generate exclusively the radical intermediate formed from the addition of OH to an end carbon atom by photodissociating an isomerically pure precursor, 2-chloro-1-propanol. Our prior experiments on the OH + propene reaction produced a mixture of the two radical intermediates by photodissociating a 70/30 mixture of 1-bromo-2-propanol (producing the  $\text{C}_3\text{H}_6\text{OH}$  radical

intermediate from OH addition at the center carbon) and 2-bromo-1-propanol (producing the radical intermediate from OH addition at the end carbon). Although those experiments detected the methyl + acetaldehyde and ethyl + formaldehyde product channels from the addition intermediates, they were not able to confirm the radical intermediate responsible for each. Furthermore the enol product channels were not investigated nor was a possible roaming channel to produce H<sub>2</sub>O + allyl from the radical intermediate rather than from direct abstraction. Our March 2016 experiments at the NSRRC were able to selectively produce the CH<sub>3</sub>CHCH<sub>2</sub>OH radical intermediate and study its product channels. Our conclusions from analysis of the data follows.

We photodissociated 2-chloro-1-propanol at 157 nm to generate the CH<sub>3</sub>CHCH<sub>2</sub>OH intermediate of the OH + propene reaction without interference from the radical intermediate from OH addition to the center carbon atom. Selected predicted products from the addition of OH to the end C=C carbon atom are shown in Figure 1. The ethyl + H<sub>2</sub>CO product channel should result from this intermediate, but not CH<sub>3</sub>CHO + CH<sub>3</sub>. The figure shows the lowest barrier pathway giving an enol product from this intermediate, propenol + H.

Our study first detected three photodissociation channels of 2-chloro-1-propanol. They are C-Cl photofission to form the CH<sub>3</sub>CHCH<sub>2</sub>OH radical intermediate of interest, an HCl photoelimination channel, and a C-C bond photofission channel analogous to that observed in 2-chloroacetaldehyde. Figures 2-4 show that data.

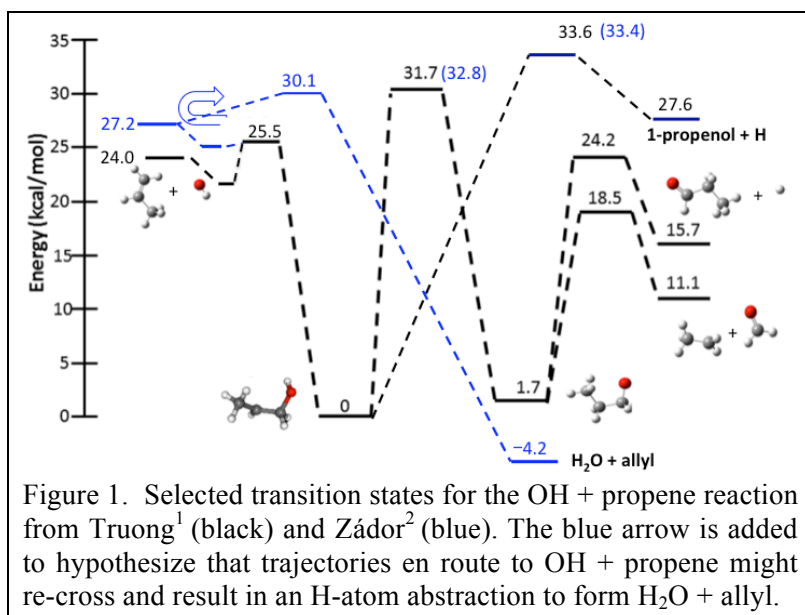


Figure 1. Selected transition states for the OH + propene reaction from Truong<sup>1</sup> (black) and Zádor<sup>2</sup> (blue). The blue arrow is added to hypothesize that trajectories en route to OH + propene might re-cross and result in an H-atom abstraction to form H<sub>2</sub>O + allyl.

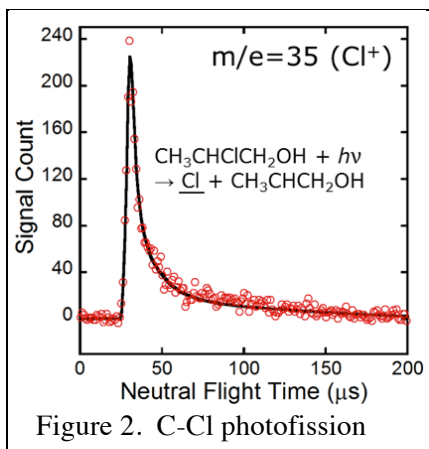


Figure 2. C-Cl photofission

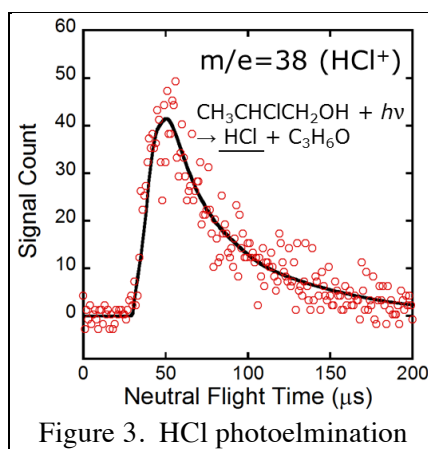


Figure 3. HCl photoelimination

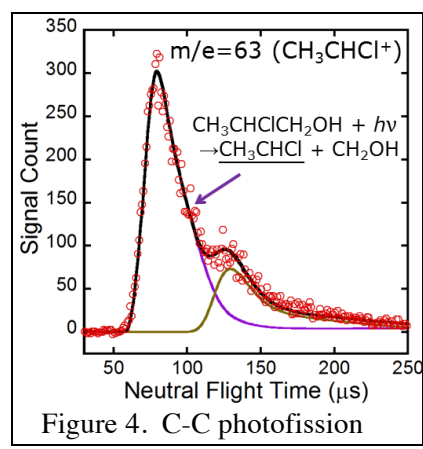


Figure 4. C-C photofission

We sought to detect not only the ethyl + H<sub>2</sub>CO product channel from the CH<sub>3</sub>CHCH<sub>2</sub>OH radical, but also the H + propenol channel predicted by theory and a possible dissociation channel

to  $\text{H}_2\text{O} + \text{allyl}$  resulting from a non-IRC pathway. (An analogous non-IRC channel occurred from the  $\text{CH}_2\text{CH}_2\text{OH}$  radical intermediate of the  $\text{OH} + \text{ethene}$  reaction.) No signal was detected at  $m/z = 18$  ( $\text{H}_2\text{O}^+$ ) upon integrating for one million laser shots, so we conclude that the non-IRC channel is not important from this  $\text{OH} + \text{propene}$  radical intermediate. We did detect the  $\text{H} + \text{propenol}$  product channel (the lowest barrier enol product channel in Figure 1). Our data is shown in Figure 5. Although propenol can also result as a co-fragment of  $\text{HCl}$  photoelimination, the  $\text{HCl}$  photoelimination channel leaves the propenol with so much internal energy that it undergoes unimolecular dissociation to  $\text{CH}_2\text{CHCH}_2 + \text{OH}$ . In contrast, propenol from the dissociation of the  $\text{CH}_3\text{CHCH}_2\text{OH}$  radical intermediate to  $\text{H} + \text{propenol}$  is formed stable to subsequent dissociation. We observed it at the  $m/z=41$   $\text{CH}_2\text{CHCH}_2^+$  daughter ion, as it undergoes efficient dissociative photoionization. The TOF of this product, shown by the green-line fit in Figure 5, is well predicted from the velocity of the  $\text{CH}_3\text{CHCH}_2\text{OH}$  radical intermediates that dissociate to  $\text{H} + \text{propenol}$  (the loss of an  $\text{H}$  atom does not change the velocity significantly).

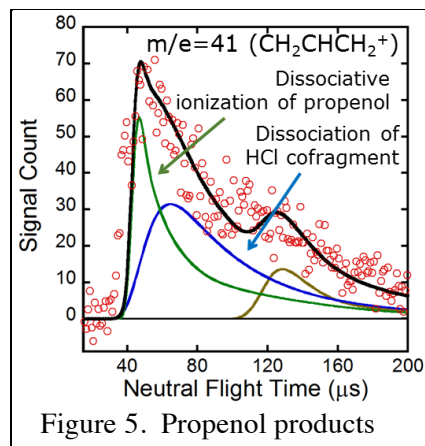


Figure 5. Propenol products

## B. Photoionization Detection of Vinyoxy Radicals at $m/z=15$ and $m/z=29$

Despite its importance in combustion, the photoionization detection of vinyoxy radicals has eluded high-resolution spectroscopists for decades. Two experiments on bimolecular reactions producing vinyoxy radicals (J. D. Savee et al, *Phys. Chem. Chem. Phys.* **2012**, *14*, 10410-10423 and S-H Lee et al, *Chem. Phys. Lett.* **2007**, *446*, 276-280) detected vinyoxy radicals with photoionization at  $m/z=15$ , though they were unable to determine the partial photoionization cross section. Recent work by Scrape et al. (*J. Phys. Chem. A*, 10.1021/acs.jpca.5b12669) detected the very small signal from vinyoxy radicals at parent ion, in addition to signal from its dissociative ionization to  $m/z=15$ .

In order to determine the partial photoionization cross section of vinyoxy radicals, our experiments in March 2016 at the NSRRC formed vinyoxy radicals from the photodissociation of 2-chloroacetaldehyde at 157 nm. Though the majority of the vinyoxy radicals are formed with enough energy to dissociate to  $\text{H} + \text{ketene}$  and  $\text{CH}_3 + \text{CO}$ , 21% of the  $\text{C-Cl}$  bond fission events form  $\text{Cl}$  in conjunction with stable vinyoxy radicals. This portion of the  $\text{C-Cl}$  bond fission  $P(E_T)$  is shown in grey dashed line in Figure 6. Any signal from dissociative ionization of vinyoxy radicals would then have a sharp TOF distribution that is easily predicted from this portion of the  $\text{C-Cl}$  fission  $P(E_T)$ . In contrast to velocity map imaging experiments, the scattering experiments at the NSRRC detect the velocity of the neutral stable vinyoxy products, with a precalibrated ion flight time, whether the vinyoxy is detected at parent ion or at  $\text{CH}_3^+$ . Figure 7 shows signal from dissociative photoionization of vinyoxy radicals appeared at  $\text{CH}_3^+$ , and, unexpectedly, at  $\text{HCO}^+$ . Calibrating with the signal from the momentum matched  $\text{Cl}$  product, our measured

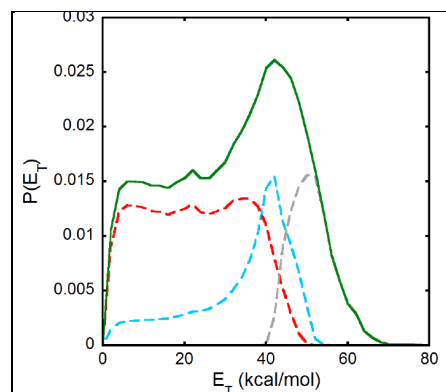
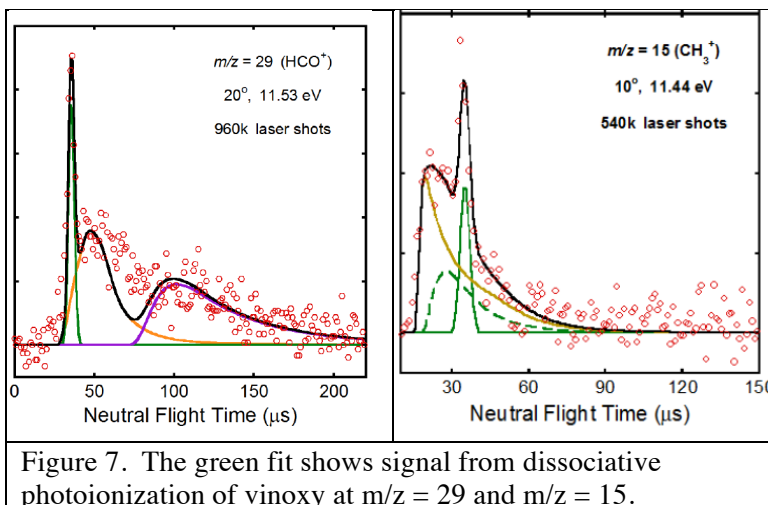


Figure 6. The portion of the  $\text{C-Cl}$  photofission  $P(E_T)$  producing stable vinyoxy is in grey dashed line.

partial photoionization cross section of vinoxy to form  $\text{CH}_3^+$  is 1.9 Mb at 10.5 eV and 2.2 Mb at 11.44 eV.

### III. Future Work

A manuscript reporting the dissociative ionization of vinoxy radicals is in preparation. We are analyzing data we took in Dec. 2016 on the photodissociation of 1-bromo-2-chloroethane and 1,1-bromochloroethane.



### III. Publications Acknowledging DE-FG02-92ER14305 (2014 to present)

1. Imaging and scattering studies of the unimolecular dissociation of the  $\text{BrCH}_2\text{CH}_2\text{O}$  radical from  $\text{BrCH}_2\text{CH}_2\text{ONO}$  photolysis at 351 nm, L. Wang, C. -S. Lam, R. Chhantyal-Pun, M. D. Brynteson, L. J. Butler, and T. A. Miller, *J. Phys. Chem. A*, **118**, 404-416 (2014).
2. Radical Intermediates in the Addition of OH to Propene: Photolytic Precursors and Angular Momentum Effects, M. D. Brynteson, C. C. Womack, R. S. Booth, S.-H. Lee, J. J. Lin, and L. J. Butler, *J. Phys. Chem. A* **118**, 3211-3229 (2014).
3. Predicting the effect of angular momentum on the dissociation dynamics of highly rotationally excited radical intermediates, M. D. Brynteson and L. J. Butler, *J. Chem. Phys.* **142**, 054301 (2015). (Joint funding with NSF.)
4. Two HCl-Elimination Channels and Two CO-Formation Channels Detected with Time-Resolved Infrared Emission upon Photolysis of Acryloyl Chloride [ $\text{CH}_2\text{CHC}(\text{O})\text{Cl}$ ] at 193 nm, P.-W. Lee, P. G. Scrape, L. J. Butler, and Y.-P. Lee, *J. Phys. Chem. A*, DOI 10.1021/jp512376a (2015).
5. Dissociation Pathways of the  $\text{CH}_2\text{CH}_2\text{ONO}$  Radical:  $\text{NO}_2 + \text{Ethene}$ ,  $\text{NO} + \text{Oxirane}$  and a non-Intrinsic Reaction Coordinate  $\text{HNO} + \text{Vinoxy}$  Pathway, P. G. Scrape, T. D. Roberts, S.-H. Lee and L. J. Butler, *J. Phys. Chem. A*, in press (2016).
6. The Onset of H + Ketene Products from Vinoxy Radicals Prepared by Photodissociation of Chloroacetaldehyde at 157, Chow-Shing Lam, Jonathan D. Adams, and Laurie J. Butler, *J. Phys. Chem. A*, 10.1021/acs.jpca.6b01256 (2016).

<sup>1</sup> Kinetics of Enol Formation from Reaction of OH with Propene, L. K. Huynh, H. R. Zhang, S. Zhang, E. Edding, A. Sarofim, M. E. Law, P. R. Westmoreland, and T. N. Truong, *J. Phys. Chem. A* **113**, 3177-3185 (2009).

<sup>2</sup> The Reaction between Propene and Hydroxyl, J. Zádor, A. W. Jasper and J. A. Miller, *Phys. Chem. Chem. Phys.* **11**, 11040-11053 (2009). Note that Fig. 1 in this reference accidentally reversed the labels on the  $\text{CH}_2\text{CH}_2\text{CH}_2\text{OH}$  and  $\text{CH}_3\text{CH}_2\text{CH}_2\text{O}$  wells at -20.9 and -24.9 kcal/mol. Also Zádor informed us that the H-atom abstraction barrier shown in Fig. 3 of the paper is incorrect while the barrier given in the text, 2.9 kcal/mol, is correct.

Chemical Dynamics Methods and Applications  
David W. Chandler  
Combustion Research Facility  
Sandia National Laboratory  
Livermore, CA 94551-0969  
Email: chand@sandia.gov

### Program Scope:

My research focuses on the field of chemical dynamics of gas phase molecular species. Chemical dynamics is the detailed study of the motion of molecules and atoms on inter- or intra- molecular potential energy surfaces in order to learn about the details of the surface as well as the dynamics of their interactions. We have tested simple bimolecular potential energy surfaces by the careful study of collisional energy transfer processes in crossed molecular beam arrangements utilizing Velocity Mapped Ion Imaging techniques. Two years ago we reported on our study of electronically excited state collisions of NO(A). This year we report on an extension of these studies: the study of rotational energy transfer of aligned NO(A). We use circularly polarized laser light to state-selectively excite the NO and detect the products of collisional energy transfer processes. We do this with high velocity resolution and with single quantum-state resolution of the product molecules. We have also been working on continuing our development of a multiplexed spectroscopic techniques for detection of multiple species with microsecond time resolution we call dual etalon frequency comb spectroscopy. Utilizing a new Velocity Mapped Ion Imaging (VMII) apparatus we have studied the alignment of hydrogen produced in a single quantum states of an electronically excited state. We have also demonstrated a new use of the VMII technique to perform multiplexed high resolution spectroscopy. All of these studies are geared to understand fundamental properties of molecules, molecule-light interactions and molecule molecular collision dynamics.

### Recent Progress:

**Alignment of  $H_2$  utilizing double resonance techniques:** We utilized the  $E,F$  electronic state to study alignment at relatively low laser intensities where we can better observe and quantify the photo-physics. The unusual shape of the  $E,F$  electronic potential curve has two minima resulting from the avoided crossing of the  $(1s\sigma_g)(2s\sigma_g)$ ,  $E$  state, and  $(2p\sigma_u)^2$ ,  $F$  state, potential energy curves. Here we describe new experiments that utilized the Velocity Mapped Ion Imaging technique to study the photophysics and photochemistry of  $H_2$   $E,F$  ( $v=0,J$ ).  $H_2$   $E,F$  is formed in a particular  $v, J$  state by 2- photon excitation from the ground state utilizing light near 201.5-nm. 532-nm light is used to provide non-resonant two-photon dissociation of  $H_2$   $E,F$  ( $v=0,J=0,1$ ) molecules and to ionize the fragment  $H(n=3)$  atoms formed in the dissociation process. Measurement of the velocity distribution of the  $H^+$  formed from photodissociation of  $H_2$   $E,F$  ( $v=0,J=0,1$ ) molecules at different laser intensities were recorded. An example of such an image is shown in Figure 1. A careful analysis of both photoelectron and photofragment images provides information about the dissociation processes observed in Figure 1.

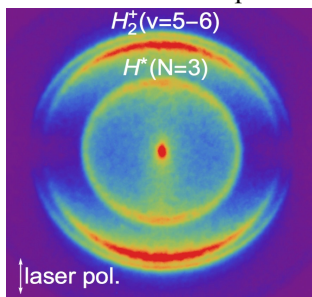


**Figure 1.** Image of  $H^+$  following 201-nm excitation of  $H_2$  to the  $J=0$  rotational level of the  $E,F$  electronic state, followed by 532-nm dissociation of  $H_2$  and ionization of  $H$  ( $n=3$ ) products (inner ring) as well as ionization of  $H_2$  followed by dissociation of  $H_2^+$  (outer ring).



By combining a new, 100 picosecond long, 532-nm Nd:YAG laser with a tunable 201-nm laser we are able to selectively populate a rotational state in the  $E,F$  electronic state, and align and dissociate that state. The tunable 201-nm dye-laser generated light that is resonant with a two-photon transition in  $H_2$  between the ground state and the excited  $E,F$  electronic state. The  $E,F$  state lives for about 200 ns. After approximately 100 ns an intense 532-nm laser beam is introduced and two processes that generate  $H^+$  are observed. The first is 2-photon dissociation of  $H_2$  to generate two neutral H atoms: one in the  $n=3$  Rydberg state and one in the ground state. The  $H(n=3)$  atom then absorbs two more 532-nm photons and ionizes, forming  $H^+$  (the inside of the image in Figure 1). The second process that is observed is the 2- or 3-photon ionization of  $H_2$  followed by one-photon dissociation of the  $H_2^+$ , forming  $H^+$  and a ground state H atom (the outside partial rings in the image in Figure 1 and 2). As the  $H_2$   $E,F$  state, in a strong static electric field, is calculated to have large delta polarizability,  $-9000$  au (difference in the polarizability along the internuclear axis and perpendicular to the internuclear axis)<sup>1</sup>. The presence of a static electric field mixes the  $E,F$  state with the nearby B and C states creating a very polarizable mixed state. With the velocity mapped ion imaging we are able to quantify the angular distribution of the two-photon dissociation channel as a function of 532-nm laser power and measure the alignment of the  $H_2$  ( $E,F$   $v=0$   $J=0$ ) state molecules. Our initial experiments indicate a delta polarizability of close to  $103 \pm 37$  au – much smaller than calculations indicate for the polarizability induced by a static electric field and of the opposite sign but much larger than either ground state or pure EF state hydrogen ( $\sim 0.7$  a.u.). This work was performed in collaboration with Dr. Peter Rakitzis of University of Crete and with the assistance of postdoctoral fellows Justin Jankunas, Martin Fournier and Gary Lopez

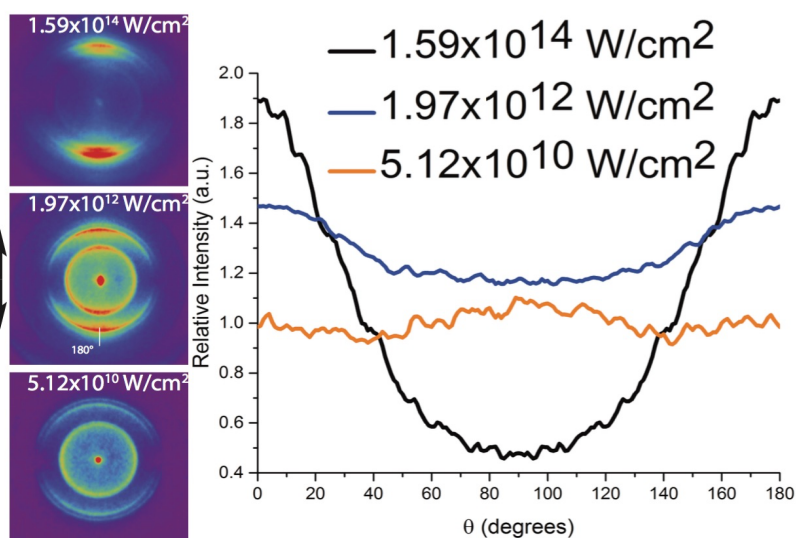


**Figure 2.** Angular distribution analysis of the inner ring feature in the photodissociation of  $H_2$  ( $E,F$  state)  $v=0$ ,  $J=0$  at different 532 nm laser intensities ( $1 \times 10^{11} \text{ W cm}^{-2}$  –  $2 \times 10^{14} \text{ W cm}^{-2}$ ). Black arrow indicates the laser polarization. A strong alignment effect is observed (see text).

state molecules. Our initial experiments indicate a delta polarizability of close to  $103 \pm 37$  au – much smaller than calculations indicate for the polarizability induced by a static electric field and of the opposite sign but much larger than either ground state or pure EF state hydrogen ( $\sim 0.7$  a.u.). This work was performed in collaboration with Dr. Peter Rakitzis of University of Crete and with the assistance of postdoctoral fellows Justin Jankunas, Martin Fournier and Gary Lopez

**Imaging spectroscopy: A novel use for Velocity Mapped Ion Imaging:** The development of intense, broadly tunable, Fourier transform limited laser light sources have made it possible to study in great detail the interaction of light with atoms and molecules. Processes such as Rabi cycling (the coherent movement of populations between two states of a molecule by a laser light field), and associated processes, such as power broadening and lifetime broadening, have been measured using high resolution lasers. Other processes that affect optical transitions, such as Zeeman, Stark and AC Stark<sup>2</sup> (Autler-Townes processes) effects, also change the nature of optical transitions, causing splittings and shifts. Here we describe a new technique for studying these and related processes. Traditionally, these effects are measured by tuning a high-resolution laser over a transition and measuring the line width as a function of power. In some cases two high-resolution lasers are required, one for creating a broadening or splitting and a second for interrogation of the broadening or splitting. The technique described here utilizes the capability of velocity mapped ion imaging (VMII) to measure the speed of the atoms or molecules that have been Doppler-shifted into resonance with the laser. This is a form of multiplexed spectroscopy where a single laser frequency is in resonance with many different spectroscopic features simultaneously as they have Doppler-shifted themselves into resonance, and we simultaneously measure the Doppler shifts by VMII. This technique

relies upon the creation of ions through a multi-step resonantly enhanced multi-photon ionization (REMPI) process where one of the laser sources is a narrow band laser that is either resonant or near resonant (within the thermal Doppler width of the transition) with one of the steps in the multi-photon process.

To demonstrate this technique, we use metastable Kr because the multi-step excitation process is sensitive to the narrow-band CW laser light. These transitions have been well studied and we can accurately test this technique against previous measurements of the line strengths and Zeeman behavior of this transition. We utilize the transition between the metastable  $4s^2 4p^5(^2P_{3/2})5s(3/2)_2^0$  state and the  $4s^2 4p^5(^2P_{3/2})5p(5/2)_3$  state at 811.5 nm as metastable and upper state have very different ionizations efficiency with 266-nm light. This enhancement allows us to monitor the excited state atoms and measure their velocity. By imaging and quantifying the fraction of the thermal Doppler width whose ionization is enhanced by the 811.5 nm laser light, we determine the frequency broadening induced in the transition.

We utilize the same scheme for the production of metastable Kr atoms and detection of metastable Kr atoms that was described previously.<sup>39</sup> A 214.7-nm laser beam is generated and excites the  $5p[3/2]_2$  state that efficiently fluoresces to the metastable  $5s[3/2]_2^0$  state at an energy  $79,971.74 \text{ cm}^{-1}$  above the ground state. Selection rules inhibit emission from this state, which lives for many seconds and can be one-photon ionized by a pulse of 266-nm light. In this study a 811.5-nm CW laser is added to the detection scheme and tuned to the atomic resonance of the  $5s[3/2]_2^0 \leftarrow 5p[5/2]_3$  transition. A tunable Coherent Titanium Sapphire laser at 811.5 nm is used to excite the atoms. Once resonant with this transition, the atoms undergo Rabi cycling between these respective levels. The beam is then retro-reflected through the Kr sample. The counter-propagating laser beams are observed as enhanced ionization on the image below, Fig. 3. The beam of 811.5 nm light is expanded into a 1-cm diameter and collimated, thus ensuring that the intensity distribution of the light is relatively uniform across the focused 214-nm light beam. Typically, 30 mW of laser power in a 1 cm diameter beam was used for the experiments but the power of the laser was varied to observe and quantify the broadening due to Rabi Cycling. We are also able to observe broadening due to lifetime shortening of the excited state due to ionization. Addition of a magnetic field Zeeman splits the levels and this splitting is observed on the images as well.

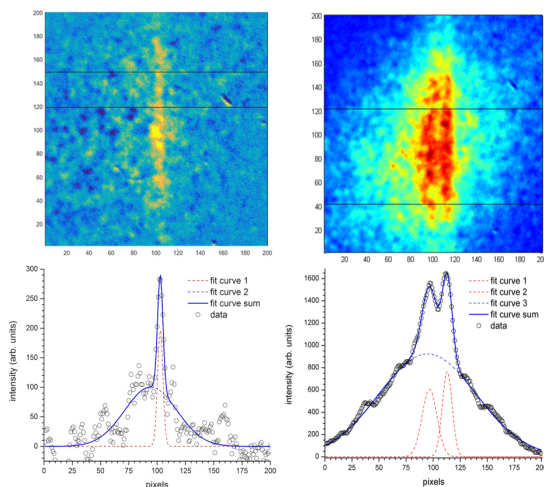


**Figure 3.** Top panel of the figure on the left is an image obtained at the laser power of the 811.5 nm laser of  $1.5 \text{ mW cm}^{-2}$  with 10 minutes of averaging.

**Dual Etalon Spectrometer:** Fourier Transform spectroscopy is a technique for monitoring multiple frequencies simultaneously by analyzing how they interfere with each other on a single detector. Frequency combs are light sources that have multiple frequencies that are equally spaced. We utilized this fact in the past to patent a new concept for a spectrometer where two transient frequency combs are formed by

confocal etalons outputs and interfered.<sup>3</sup> However, a new concept is being developed, and recently the first efforts realized, to simplify this spectrometer. The new concept involves placing an anti-reflection coated polarization rotator within a single etalon cavity. This optic breaks the linearly polarized photons entering the cavity into left- and right-handed circularly polarized light waves, and these travel at different speeds through the crystal depending on their alignment to the crystal axis. In this manner a single etalon cavity with a wave-plate within it can simultaneously contain two frequency combs with two free spectral ranges locked together. A simple polarizing cube before the detector will mix the left- and right-handed light on the detector creating an interference pattern that can be analyzed to extract the absorption spectra of a molecule within the cavity. This manifestation of the dual etalon spectrometer when developed will be more robust and offer the ability to perform transient absorption measurements with high signal-to-noise.

***Collisions with Aligned NO(A) molecules:*** The correlations among vector quantities in molecular collisions are sensitive reporters on the accuracy of theoretical descriptions of the collisional interactions, especially on the anisotropic part of the intermolecular potential.<sup>4</sup> Laser preparation of the NO(A) state to align the NO molecules angular momentum axis toward or against the collision vector; an arrangement that specifically focuses on anisotropic interactions was built. These experiments excited the NO to the A state using circularly polarized light creating an oriented NO (A, J=1.5) molecule, rotating clockwise or counterclockwise relative to the collision vector with a Ne atom depending upon the handedness of the light. The data for the measured differential cross sections for collisional energy transferred into the NO N=3 state. After the oriented NO(A) molecules undergo a collision their final quantum state and orientation was measured by 1+1' resonant ionization through the E state using circularly polarized light and VMII. From the data, one can see that the probability of transfer to NO(A, N=3) that is co-rotating with the original NO(A, N=1) molecule is much more probable. This work was done in collaboration with Dr. Matt Costen and Dr. Ken McKendrick at Heriot-Watt University in Scotland.

**References:**

- 1) J. Komasa, Adv. Quant. Chem. **48**, 151 (2005).
- 2) Autler, S. H.; Townes, C. H., Phys. Rev. 1955, 100, 703-722
- 3) Chandler, D. W.; Strecker, K. E., J. Chem. Phys. 2012, 136.
- 4) Steill, J. D.; Kay, J. J.; Paterson, G.; Sharples, T. R.; Klos, J.; Costen, M. L.; Strecker, K. E.; McKendrick, K. G.; Alexander, M. H.; Chandler, D. W., *J. Phys. Chem. A* **2013**, *117*, 8163-8174.

**Publications acknowledging BES support for DWC, 2015 –**

- 1) Determination of the Collisional Energy Transfer Distribution Responsible for the Collision Induced Dissociation of NO<sub>2</sub> with Ar. J. D. Steill, A. Jasper and D. W. Chandler, Frontier Article Chem. Phys. Lett. 636, 1-14 (2015). Cover Article.
- 2) Chemical Physics: Quantum Control of light-induced reactions. D. W. Chandler, Nature (2016) Vol 535 pages 42-44.
- 3) Editorial: The Future of Chemical Physics Conference 2016, A. Michaelides, D. E. Manolopoulos, (C. Vega, P. Hamm, D. W. Chandler, E. Brigham, M. I. Lester, J. of Chemical Physics (2016) Vol 145 # 220401
- 4) Alignment, Dissociation and Ionization of H<sub>2</sub> Molecule in Intense Laser Fields using Velocity Mapped Imaging, G. V. Lopez, M. Fournier, J. Jankunas, A. K. Spiliotis, T. P. Rankisis, D. W. Chandler, J. Chem. Phys., Submitted 2017.
- 5) Imaging Spectroscopy: A Novel Use for the Velocity Mapped Ion Imaging Technique, J. Guzman, L. Culberson, K. E. Strecker, J. D. Steill, C. Montcrieffe, and D. W. Chandler, J. chem. Phys. Submitted 2017.
- 6) Perspective: Advanced Particle Imaging, D. W. Chandler, D. H. Parker and P. H. Houston, J. Chem. Phys., Submitted 2017 for special Issue on Advanced Particle Imaging

## Petascale Direct Numerical Simulation and Modeling of Turbulent Combustion

Jacqueline H. Chen (PI) Aditya Konduri and Giulio Borghesi  
Sandia National Laboratories, Livermore, California 94551-0969  
Email: [jhchen@sandia.gov](mailto:jhchen@sandia.gov)

### Program Scope

In this research program we have developed and applied massively parallel three-dimensional direct numerical simulation (DNS) of building-block, laboratory scale flows that reveal fundamental turbulence-chemistry interactions in combustion. The simulation benchmarks are designed to expose and emphasize the role of particular phenomena in turbulent combustion. The simulations address fundamental issues associated with ‘chemistry-turbulence’ interactions that underly combustion in engines for power generation and transportation: high pressure multi-stage autoignition with negative temperature coefficient (NTC) chemistry, extinction and reignition of forced ignition kernels in turbulence, premixed and stratified flame propagation in intense shear-driven turbulence, lifted flame stabilization assisted by cool flame ignition, preferential diffusion effects on stabilization of reactive jets in crossflow, flashback of stratified premixed flames in boundary layers, and flame stabilization over cavities. In addition to the new understanding provided by these simulations, the DNS data are used to develop and validate predictive models required in Reynolds-Averaged Navier Stokes (RANS) and large-eddy (LES) simulations.

### Recent Progress

In the past year, we have investigated multi-regime combustion, *i.e.* flame propagation into (non)reactive mixtures, associated with 1) n-dodecane auto-ignition with NTC chemistry, and 2) turbulent flame propagation in premixed piloted methane-air flames subjected to intense turbulence in the broken reaction zones regime. Highlights from DNS of two-stage autoignition of a turbulent n-dodecane/air jet in the NTC regime are presented. This is followed by a discussion of future work on identifying the role of turbulent diffusion and autoignition on premixed flame structure and propagation in the broken reaction zones regime.

#### ***Two-stage autoignition of a turbulent n-dodecane /air jet in the NTC regime at 25 bar***

DNS of a 3D turbulent, auto-igniting temporal jet between partially premixed n-dodecane and diluted air was performed to understand the influence of low-temperature chemistry on the transient dynamics of two-stage ignition [1]. Chemical reactions were described by a 35-species reduced n-dodecane mechanism [2], including both low- and high-temperature oxidation pathways. Spatial inhomogeneities in the mixture composition due to the underlying sheared turbulence were found to strongly affect low-temperature chemical reactions in turbulent mixtures of air and n-dodecane undergoing spontaneous ignition. High values of scalar dissipation rate, a measure of the local turbulent mixing rate, redistribute some of the heat and ketohydroperoxide radicals generated at early times in lean mixtures toward richer regions, resulting in significant low-temperature reactions occurring across a wide range of mixture compositions. Ultimately, the faster propagation of low-temperature reactions in mixture fraction space by cool flame propagation and diffusional processes compensates for the higher heat and radical losses from the ignition kernels at high values of scalar dissipation rate. Consequently, ignition occurs sooner and at mixture conditions richer than the minimum homogeneous ignition delay. The conditional distributions of the ignition delay times of the reacted fluid elements in the DNS are plotted in Figure 1a conditioned on mixture fraction. Note that each of the distributions is normalized by its maximum value. The cyan line in the figure corresponds to the homogeneous ignition delay time of the cool flame as a function of mixture fraction. It is observed that, at low mixture fraction values, cool-flame ignition is generally delayed relative to the homogeneous reactor calculations, due to the dissipative effect of scalar fluctuations. However, at mixture fractions greater than 0.1, there is an increasing fraction of fluid that has undergone cool flame auto-ignition earlier than the corresponding homogeneous delay time, consistent with earlier observations by Krisman et al. [3] and Dahms [4]. Turbulence induced scalar dissipation rate in the jet redistributes heat generated in earlier ignited lean mixtures towards richer

regions, resulting in significant low-temperature reactions occurring at all mixture compositions. From the conditional temperature evolution shown in Figures 1b and 1c it is evident that first-stage ignition commences at lean conditions near the most reactive mixture fraction of 0.06 shown in Fig 1d, and cool flame propagation spreads towards richer mixtures. Note that first- (denoted in blue) and second-stage (denoted in red) ignition progress simultaneously in different regions of the jet as shown in Fig. 1e by the temperature isocontours. This is followed by second-stage ignition occurring at slightly richer conditions than the minimum homogeneous ignition delay. Once second-stage ignition occurs spontaneous ignition front propagation from fuel rich towards stoichiometric conditions occurs, as shown by the instantaneous heat release rate isocontours in Fig. 1f, establishing a high-temperature flame.

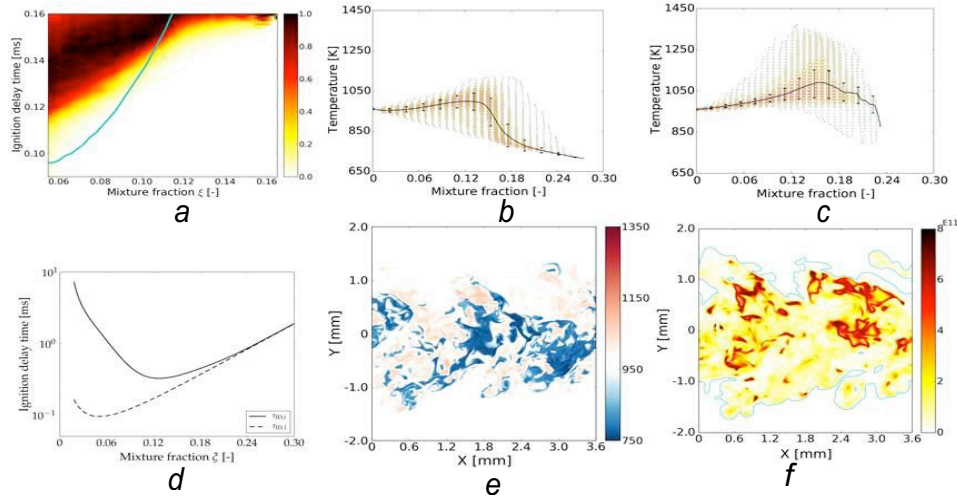


Figure 1. Turbulent auto-ignition of *n*-dodecane at 25 bar: a) normalized conditional distribution of the cool flame ignition delay time of reacted fluid elements, conditioned on mixture fraction. The cyan line corresponds to the corresponding homogeneous ignition delay (HIT); b and c) conditional temperature evolution at 0.62 HIT and 0.98 HIT, respectively where the condition mean (solid line) and standard deviation (bars) are superposed; colored symbols represent fraction of data in a given temperature/mixture fraction bin; second-stage ignition occurs for  $T > 1300\text{K}$ ; d) first and second ignition delay times for homogeneous mixtures of diluted air (15% O<sub>2</sub>) and *n*-dodecane as a function of mixture fraction at  $p = 25$  bar,  $T_{\text{amb}} = 960\text{K}$  and  $T_{\text{fuel}} = 450\text{K}$ ; e) spanwise slice of temperature isocontours at 0.67 HIT showing simultaneous first-stage (blue) and second-stage (red) ignition occurring; and f) spanwise slice of heat release rate isocontours at 0.98 HIT showing spontaneous ignition propagation (red iso-contours) from rich conditions towards the stoichiometric mixture fraction (cyan line) following high-temperature ignition.

## Future Work:

### ***The Role of Turbulent Diffusion and Autoignition in Turbulent Premixed Jet Flames in the Broken Reaction Zones Regime***

We plan to perform and analyze DNS of CH<sub>4</sub>/air piloted premixed jet flames [5] under intense turbulence to study turbulence-chemistry interactions affecting the structure of the reaction layers and the overall turbulent burning velocity. These interactions affect the local combustion regime, *i.e.* flame propagation assisted by ignition, autoignition or stratified flame propagation into an inert mixture.

To understand the downstream evolution of the flame structure we have performed a preliminary reaction flux analysis to identify the main elementary reactions contributing to the overall heat release rate. The results reveal that the chemical pathways for heat release generation evolve from reactions primarily involving methyl radical in the near field of the jet to CO/H<sub>2</sub> oxidation reactions together with hydroperoxy reactions in the far field. We will investigate the roles of turbulent strain rate on impeding reactions in the near field, and turbulent diffusion in transporting heat and intermediate species generated in the near field to downstream locations in the jet. We plan to also perform a chemical

explosive mode (CEMA) eigenanalysis in collaboration with Tianfeng Lu and Xinyu Zhao to investigate the influence of species diffusion on the chemical explosive mode, and especially the relative importance of chemistry and diffusion on the explosive behavior. The CEMA analysis will reveal whether diffusion has a role in promoting or inhibiting ignition.

#### References:

1. G. Borghesi and J. H. Chen, (2016) "A DNS investigation of turbulent n-dodecane/air mixing layer autoignition," *Western States Section of the Combustion Institute Spring 2016 Meeting*, March 21-22, 2016.
2. T. Lu, <http://www.engr.uconn.edu/~tlu/mechs/mechs.htm>. Accessed: 2010-09-30.
3. A. Krisman, E. R. Hawkes, M. Talei A. Bhagatwala, J. H. Chen, (2017) "A DNS of a cool-flame affected autoignition in diesel engine-relevant conditions," *Proc. Combust. Inst.*, **36**:3567-3575.
4. Dahms, R.N., Paczko, G.A., Skeen, S.A., and Pickett, L.M. (2017) Understanding the ignition mechanism of high-pressure spray flames. *Proc. Combust. Inst.*, **36**:2615-2623.
5. H. Wang, E. R. Hawkes, B. Zhou, J. H. Chen, Z. Li, M. Alden, (2017) "A comparison between DNS and experiment of the turbulent burning velocity-related statistics in a turbulent methane-air premixed jet flame at high Karlovitz number," *Proc. Combust. Inst.*, **36**:2045-2053.

#### BES Publications (2015-2017)

1. Y. Xin, C. S. Yoo, J. H. Chen, C. K. Law, "A DNS study of self-accelerating cylindrical hydrogen-air flames with detailed chemistry," *Proc. Combust. Inst.*, **35** (2015) 753-760.
2. A. Bhagatwala, T. Lu, H. Shen, J. Sutton, J. H. Chen, "Numerical and experimental investigation of turbulent DME jet flames," *Proc. Combust. Inst.*, **35** (2015) 1157-1166.
3. A. Krisman, E. R. Hawkes, M. Talei, A. Bhagatwala, J. H. Chen, "Tribrachial, tetrabrachial and pentabrachial structures in dimethyl ether edge-flames at NTC conditions," *Proc. Combust. Inst.* **35**, (2015) 999-1006.
4. A. Gruber, A. Kerstein, D. Valiev, H. Kolla, J. H. Chen, "Modelling of Mean Flame Shape During Premixed Flame Flashback in Turbulent Boundary Layers," *Proc. Combust. Inst.*, **35** (2015) 1485-1492.
5. R. A. C. Griffiths, J. H. Chen, H. Kolla, R. S. Cant, W. Kollmann, "Three-dimensional topology of turbulent premixed flame interaction," *Proc. Combust. Inst.*, **35** (2015) 1341-1348.
6. Bansal, G., Mascarenhas, A. and Chen, J. H., "Direct numerical simulation of autoignition in stratified dimethyl-ether (DME)/Air turbulent mixtures," *Combustion and Flame* (2015) **162**:688-702.
7. Lyra, S., Wilde, B., Kolla, H., Seitzman, J., Lieuwen T., Chen, J. H., "Structure and stabilization of hydrogen-rich transverse jets in a vitiated turbulent flow," *Combustion and Flame*, (2015) **162**:1234-1248.
8. Scholtissek, A., Chan, W. L. Xu, H., Hunger, F., Kolla, H., Chen, J. H., Ihme, M., Class, A., "A multi-scale asymptotic analysis of flamelet equations including tangential diffusion effects for laminar and turbulent flames," *Combustion and Flame* (2015) **162**:1507-1529.
9. S. Kim, M. B. Luong, J. H. Chen, C. S. Yoo, "A DNS study of the ignition of lean PRF/air mixtures with temperature inhomogeneities under high pressure and intermediate temperature," *Combustion and Flame*, (2015) **162**:717-726.
10. C. Bruno, V. Sankaran, H. Kolla and J. H. Chen, "Impact of multi-component diffusion in turbulent combustion using direct numerical simulations," *Combustion and Flame*, (2015) **162**(11):4313-4330.
11. R. Sankaran, E. R. Hawkes, C. S. Yoo, and J. H. Chen, "Response of flame thickness and propagation speed under intense turbulence in spatially developing lean premixed methane-air jet flames," *Combustion and Flame*, (2015), **162** (9): 3294-3306.
12. Y. Minamoto, H. Kolla, R. W. Grout, A. Gruber, and J. H. Chen, "Effect of fuel composition and differential diffusion on flame stabilization in reacting syngas jets in turbulent cross-flow," *Combustion and Flame*, (2015) **162**(10): 3569-3579.
13. Z. Jozefik, A. R. Kerstein, H. Schmidt, S. Lyra, H. Kolla, J. H. Chen, "One-dimensional turbulence modeling with comparison to DNS," *Combustion and Flame* (2015), **162**: 2999-2015.

14. S. Karami, E.R. Hawkes, M. Talei, and J. H. Chen, "Mechanisms of flame stabilization at low lifted height in a turbulent lifted slot-jet flame," *J. Fluid Mech.* (2015) **777**:633-689.
15. H. S. Bak, S. R. Lee, J. H. Chen, and C. S. Yoo, "A numerical study of the diffusive-thermal instability of opposed nonpremixed tubular flames," *Combustion and Flame* (2015), **162**:4612-4621.
16. Bhagatwala, A., Sankaran, R., Kokjohn, S., Chen, J. H., Numerical investigation of spontaneous flame propagation in RCCI conditions, *Combustion and Flame* (2015), **162**(9): 3412-3426.
17. Zhao, X., Bhagatwala, A., Chen, J. H., Haworth, D. C., Pope, S. B., "An a priori DNS study of the shadow-position mixing model," *Combustion and Flame* (2016) **165**:223-245.
18. Karami, S., Hawkes, E. R., Talei, M., Chen, J. H. "Edge flame structure in a turbulent lifted flame: a direct numerical simulation study," *Combustion and Flame* (2016), **169**:110-128.
19. Gao, Y., Shan, R., Lyra, S., Li, C., Wang, H., Chen, J. H., Lu, T., "A lumped-reduced reaction model for combustion of liquid fuels," *Combustion and Flame* (2016), **163**:437-446.
20. Y. Gao, H. Kolla, J. H. Chen, N. Swaminathan, and N. Chakraborty, "A comparison of scalar dissipation rate transport between simple and detailed chemistry based on direct numerical simulations," in press *Combustion Theory and Modeling* (2016).
21. Kolla, H., Zhao, X., Chen, J. H., Swaminathan N., "Velocity and Reactive Scalar Dissipation Spectra in Turbulent Premixed Flames," *Combustion Science and Technology* (2016), **188**:1424-1439.
22. Y. Minamoto and J. H. Chen, "DNS of a turbulent lifted di-methyl ether jet flame," *Combustion and Flame* (2016), **169**:38-50.
23. F. Salehi, M. Talei, E. Hawkes, A. Bhagatwala, J. H. Chen, S. Kook, "Doubly conditional moment closure modeling for HCCI with temperature inhomogeneities," *Proc. Combust. Inst.* (2017), **36**:3677-3685.
24. A. Krisman, E. R. Hawkes, M. Talei A. Bhagatwala, J. H. Chen, "A DNS of a cool-flame affected autoignition in diesel engine-relevant conditions," *Proc. Combust. Inst.* (2017), **36**:3567-3575.
25. H. Wang, E. R. Hawkes, B. Zhou, J. H. Chen, Z. Li, M. Alden, "A comparison between DNS and experiment of the turbulent burning velocity-related statistics in a turbulent methane-air premixed jet flame at high Karlovitz number," *Proc. Combust. Inst.* (2017), **36**:2045-2053.
26. S. Karami, M. Talei, E. R. Hawkes, and J. H. Chen, "Local extinction and reignition mechanism in a turbulent lifted flame: a DNS study," *Proc. Combust. Inst.* (2017), **36**:1685-1692.
27. E. S. Richardson and J. H. Chen, "Analysis of turbulent flame propagation in equivalence ratio-stratified flow," *Proc. Combust. Inst.* (2017), **36**:1729-1736.
28. H. Wang, E. R. Hawkes, J. H. Chen "Turbulence-Flame Interactions in DNS of a Laboratory High Karlovitz Premixed Turbulent Jet Flame," *Physics Fluids* (2016), **28**, 095107.
29. H. Wang, E. R. Hawkes, B. Zhou, J. H. Chen, Z. Li, M. Alden, "Petascale direct numerical simulations of a high Ka laboratory premixed jet flame," in press *J. Fluid Mech.*, (2017).
30. M. Kuron, Z. Ren, H. Zhou, E. Hawkes, J. Tang, J. H. Chen, and T. Lu, "Performance of transported PDF mixing models in a turbulent premixed flame," *Proc. Combust. Inst.* (2017), **36**:1987-1995.
31. M. Kuron, Z. Ren, E. R. Hawkes, H. Zhou, H. Kolla, J. H. Chen, T. Lu, "A mixing timescale model for TPDF simulations of turbulent premixed flames," *Combust. Flame* (2017), **177**:171-183.
32. A. Krisman, E. R. Hawkes, M. Talei A. Bhagatwala, J. H. Chen, "Characterisation of two-stage ignition in diesel engine-relevant thermochemical conditions using DNS," *Combust. Flame*, (2016), **172**:326-341.
33. A. Krisman, E. R. Hawkes, and J. H. Chen, "Autoignition and edge flames in a turbulent jet at diesel engine relevant thermochemical conditions," submitted to *J. Fluid Mech.* (2016).
34. C. Han, D.O. Lignell, E. R. Hawkes, J. H. Chen, H. Wang, "Examination of differential molecular diffusion in DNS of turbulent non-premixed flames, *International Journal of Hydrogen Energy* (2017), <http://dx.doi.org/10.1016/j.ijhydene.2017.01.094>.
35. S. Chaudhuri, H. Kolla, H. Dave, E.R. Hawkes, J. H. Chen, C.K. Law, "Flame thickness and conditional scalar dissipation rate in a premixed temporal turbulent reacting jet," in press *Combust. Flame* (2016).
36. H. Wang, E. R. Hawkes, J. H. Chen, "A direct numerical simulation study of flame structure and stabilisation of an experimental high Ka CH<sub>4</sub>/air premixed jet flame," in press *Combust. Flame*, (2017).
37. H. Pouransari, H. Kolla, J. H. Chen, A. Mani, "Spectral analysis of energy transfer in turbulent flows laden with heated particles," *J. Fluid Mech.* (2017), **813**:1156-1175.
38. Z. Ren, M. Kuron, X.Zhou, T. Lu, H. N. Kolla, and J. H. Chen, "Micromixing models for PDF simulations of premixed flames," review article submitted to *Combustion Science and Technology* (2017).

# Dynamics and Energetics of Elementary Combustion Reactions and Transient Species

## Grant DE-FG03-98ER14879

Robert E. Continetti (rcontinetti@ucsd.edu)

Department of Chemistry and Biochemistry, University of California San Diego  
9500 Gilman Drive, La Jolla, CA 92093-0340

### I. Program Scope

This research program continues to provide benchmark experimental results to underpin an important goal for combustion chemists: development of accurate methods for the calculation of potential energy surfaces (PESs) and the dynamics of molecular collisions. The research program involves the development and application of advanced experimental techniques that enable the use of photodetachment and dissociative photodetachment of anionic precursors to prepare energized radicals and collision complexes and study the subsequent lifetimes and dissociation dynamics of these species. Kinematically complete measurements of dissociative photodetachment (DPD) processes provide a novel measure of the dynamics of unimolecular and bimolecular reactions and allow the identification of long-lived reaction resonances. These measurements involve the detection of photoelectrons, stable photoneutrals and photofragments in coincidence, using photoelectron-photofragment coincidence (PPC) spectroscopy. Some significant recent contributions from this project include the identification and measurement of the electron affinities of the cis- and trans-HOCO radicals<sup>1</sup> as well as the critical role of deep-tunneling in the decay of cis-HOCO,<sup>2</sup> results that helped motivate the calculation of improved PESs<sup>3</sup> and multidimensional quantum dynamics.<sup>4,5</sup> These studies also led to a collaboration with Al Wagner and colleagues extending in a more quantitative fashion our earlier quasi-1D model<sup>2</sup> for deep tunneling and applying it to *ab initio* HOCO PESs (DOE Pub. 5).<sup>6</sup> The program has also developed an ongoing collaboration with Hua Guo examining benchmarks for multidimensional quantum dynamics, beginning with the experimental-theoretical study reported on the  $F + H_2O \rightarrow HF + OH$  reaction in Science in 2014 (DOE Pub. 2).<sup>7</sup> In the last year the apparatus has been functioning at a new level of sophistication following the commissioning of a

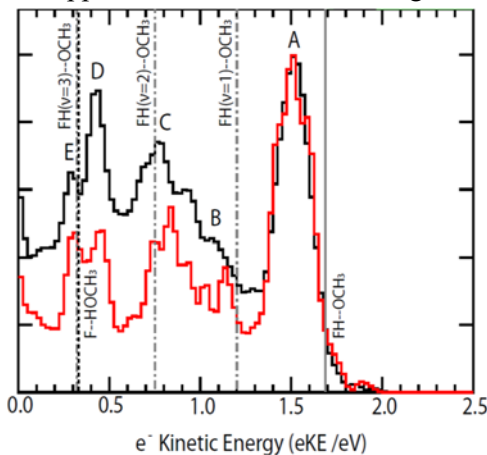


Figure 1. Beam-energy dependence of the ‘stable’ photoelectron spectrum for F-HOCH<sub>3</sub>. Red histogram, P(eKE) at a beam energy of 4.0 keV (11  $\mu$ s flight time). Black histogram, 7.0 keV (8.4  $\mu$ s flight time). Black dotted line corresponds to the zero-point corrected *ab initio* calculated eKE for production of the ground state F-HOCH<sub>3</sub> reactant complex. The solid gray vertical line corresponds to production of the ground state FH-OCH<sub>3</sub> H-bonded product channel complex and the grey dash-dot-dash lines represent estimated well-depths for metastable H-bonded resonances associated with excitation in HF.

cryogenic octupole accumulator trap (COAT) in the ion source to allow buffer gas cooling of polyatomic anions ultimately to temperatures < 10 K. A collaborative study of the energetics and dissociation dynamics of the F-HOCH<sub>3</sub> system with the Schaefer group appeared in 2016 (DOE Pub. 7).<sup>8</sup> This work is notable as photodetachment of F<sup>-</sup>(CH<sub>3</sub>OH) allows probing both the entrance and exit channel wells in addition to distinguishing long-lived resonances from direct dissociation processes. A study of the temperature dependence of the photodissociation of the ozonide anion, O<sub>3</sub><sup>-</sup>, at 3.2 eV is also complete as well as the collaborative effort with the Stanton group to examine the stability and dissociation dynamics of the low-lying electronic states of the propioly radical (HC≡C-CO<sub>2</sub>). A new hydroxyl radical reaction OH + CH<sub>4</sub> → H<sub>2</sub>O + CH<sub>3</sub> is now under study, using photodetachment of the OH<sup>-</sup>(CH<sub>4</sub>) anion. These results, as well as ongoing efforts to characterize the exotic ethylenedione molecule C<sub>2</sub>O<sub>2</sub>, will be discussed further below.

### II. Recent Progress

#### A. Transition State Dynamics of the F + HOCH<sub>3</sub> → HF + OCH<sub>3</sub> Reaction

Photodetachment of the F<sup>-</sup>(CH<sub>3</sub>OH) anion produces the F(CH<sub>3</sub>OH) complex in the vicinity of the submerged barrier on the F + CH<sub>3</sub>OH → HF + OCH<sub>3</sub> PES. This system, with



7 atoms and 15 degrees of freedom, remains beyond the limit of full-dimensionality quantum dynamics calculations, but is a tractable system for high accuracy electronic structure calculations, as illustrated by the recent work by Schaefer and co-workers.<sup>9</sup> As discussed in last year's report, PPC measurements on  $F^-(CH_3OH)$  at photon energies of 4.80 and 3.20 eV allowed studies of both stable and dissociative neutral complexes, and a full account of these results has been published in DOE pub. 7. A notable result is that complexes that are stable on the timescale of the flight time from the interaction region to the neutral particle detector, or dissociate with exceedingly small kinetic energy release, can be resolved in PPC spectra. The photoelectron spectra for these 'stable' complexes are shown in Figure 2 at a photon energy of 4.80 eV. It should be noted that the features observed with the exception of the truly stable product channel complex corresponding to peak A at  $eKE = 1.50$  eV represent  $\sim 5\text{-}10\%$  of the total (dissociative + 'stable') signal at any given  $eKE$ . These long-lived components of the photoelectron spectrum are significant – 16% of the overall signal, including the stable peak A. The new result here is the identification of peak E as corresponding to the reactant channel  $F\text{-HOCH}_3$  complex. In the presence of other long-lived complexes, this feature is identified as having a particularly long lifetime from the ion beam kinetic energy dependence shown in Figure 1, and it lies just below the maximum calculated  $eKE$  for photodetachment to the bottom of the shallow reactant complex well. The ability of PPC spectroscopy to identify minor stable or long-lived product channels in the presence of dominant dissociative channels is unique, and shows that this single measurement probes the dynamics on the  $F\text{-CH}_3OH$  PES across the reaction coordinate from reactant to product channel wells.

## B. Stability and Dissociation Dynamics of the Propioly Radical ( $HC\equiv C\text{-CO}_2$ )

This research program not only makes use of anionic precursors to prepare transient collision complexes, but also uses photodetachment to study the dynamics of oxygenated radicals. In particular this year we have completed our analysis of the propioly radical  $HC\equiv C\text{-CO}_2$ , an extension of our previous studies of the formyloxyl and acetyloxyl radicals,  $HCO_2$  and  $CH_3CO_2$ , respectively. In this system there are three low-lying electronic states,  ${}^2B_2$ ,  ${}^2A_1$  and  ${}^2A_2$ . Similar to the simpler carboxyl radicals, there are strong vibronic interactions between the  ${}^2B_2$  and  ${}^2A_1$  states, leading to a very congested photoelectron spectrum for the photodetachment of the propiolate anion  $HC\equiv C\text{-CO}_2^-$  at a photon energy of 4.80 eV. The higher-lying  ${}^2A_2$  state, however, has a vibrationally resolved photoelectron spectrum even at the modest resolution ( $\Delta eKE/eKE \sim 4\%$ ) obtainable on our apparatus. The strong vibronic interactions in this system require a high-level of theory, and to enable the assignment of the spectrum, we collaborated with Stanton and co-workers who carried out calculations of the vibronic interactions in the system, photodetachment cross-sections and Franck-Condon calculations. In spite of the complexity of the system, including the carboxyl moiety interacting with a carbon-carbon triple bond, these sophisticated calculations did an outstanding job of reproducing the measured spectrum as shown in Figure 2. Dissociative photodetachment spectra (not shown here) were found to derive from high-lying levels

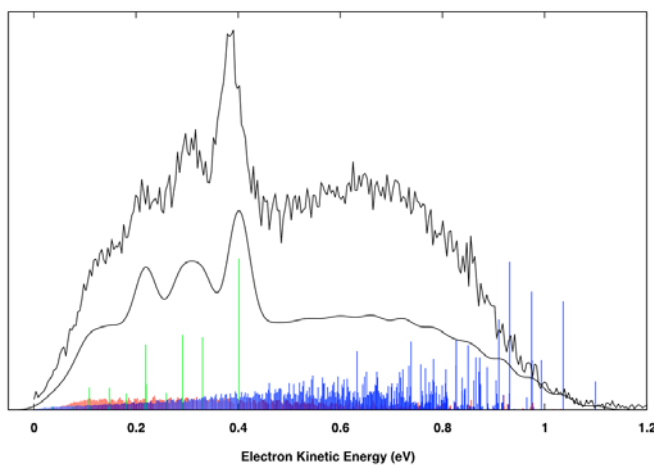


**Figure 2.** CCSD/EOMIP-CCSD/ANO0 Franck-Condon simulations for photodetachment of  $HCCO_2^-$  to the  ${}^2B_2$  (blue sticks),  ${}^2A_1$  (red sticks), and  ${}^2A_2$  (green sticks) electronic states and the summed fit compared to the experimental data  $P(eKE)$ .

in the  ${}^2A_1$  state that adiabatically correlate with the  $CCH({}^2\Sigma^+) + CO_2$  products, with a kinetic energy release peaking at  $\sim 0.4$  eV providing a measure of the dissociation barrier to products.

### C. Cryogenic Octupole Accumulator Trap (COAT) – Cooling of Ozonide Anion, $\text{O}_3^-$

The apparatus is now equipped with a cryogenic octupole accumulation trap (COAT) providing the ability to collisionally cool precursor anions, as well as the ability to heat them through energetic collisions with helium buffer gas. This has been demonstrated by studying the photochemistry of the  $\text{O}_3^-$  anion at a photon energy of 3.2 eV. This work, reported on last year, is now ready for publication, and on deeper analysis has revealed further details about the competing ionic photodissociation channels in the low-lying  $^2\text{A}_2$  excited state of  $\text{O}_3^-$  formed by photon absorption. Taking full advantage of the coincidence measurements, evidence for state-resolved predissociation of bend and asymmetric stretch excited levels in the  $^2\text{A}_2$  state to  $\text{O}_2^-(v=4) + \text{O}(^3\text{P})$  was observed. The experiments also showed the ability to collisionally heat the ions in the trap as well, providing an alternative approach to examining thermal effects in molecular anion photodissociation and photodetachment.

### D. Hydroxyl radical reactions: $\text{OH} + \text{CH}_4 \rightarrow \text{H}_2\text{O} + \text{CH}_3$

The  $\text{OH} + \text{CH}_4 \rightarrow \text{H}_2\text{O} + \text{CH}_3$  reaction is one of the elementary steps involved in the oxidation of methane. Because of the importance of this reaction in combustion, this system has been studied

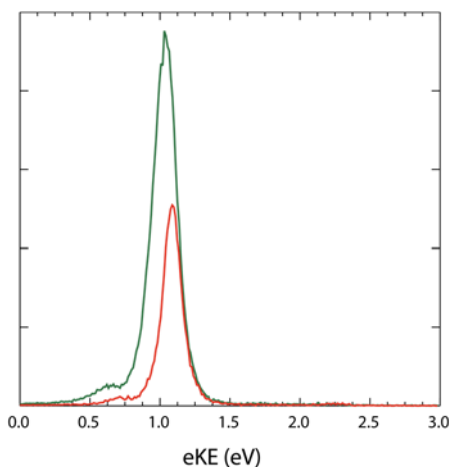


**Figure 3.** Photoelectron spectrum of both the stable and dissociative  $\text{OH-CH}_4$  complex at a photon energy of 3.20 eV. The intensities are  $P(e\text{KE})$  extracted from a single dataset.

experimentally<sup>10</sup> and at various levels of theory<sup>11, 12</sup> to understand the barrier to the reaction and rate coefficients. Recently, Li and Guo constructed a full-dimensional global PES for the  $\text{OH} + \text{CH}_4 \rightarrow \text{H}_2\text{O} + \text{CH}_3$  reaction.<sup>13</sup> Thus, this is an ideal system to pursue using the PPC technique. In the last year a dual pulsed valve ion source<sup>14</sup> was added to the PPC spectrometer, allowing the entrainment of a plasma generated in a side discharge into the high density region of the primary supersonic expansion. This type of source allows for the creation of cold anions and a rational approach to synthesizing anions of interest. This setup was key to creating the  $\text{OH}(\text{CH}_4)$  anion complex needed to study the dynamics of the  $\text{OH} + \text{CH}_4 \rightarrow \text{H}_2\text{O} + \text{CH}_3$  neutral reaction. PPC measurements were carried out on  $\text{OH}(\text{CH}_4)^-$  at a photon energy of 3.20 eV and the photoelectron spectra for stable ( $1 e^- + 1$  particle) and dissociative ( $1 e^- + 2$  momentum-matched fragments) complexes are seen in Figure 3. The stable spectrum peaks at 1.09 eV, suggesting that the entrance channel complex is being formed, with an expected eKE of 1.01 eV based on calculations of the AEA for  $\text{OH}(\text{CH}_4)$  at the MP2/6-311++G(3df, 2p) level of theory. In addition, the low eKE shoulder on both spectra are consistent with excitation of an asymmetric stretch of methane in the  $\text{OH} + \text{CH}_4$  reactant channel. This will be another ideal seven-atom benchmark system for hydroxyl radical reactions given the PES calculated by Li and Guo.<sup>13</sup>

### E. Dissociation Dynamics of $\text{C}_2\text{O}_2$ and the $\text{C}_2\text{O}_2^-$ Anion

The transient molecule ethylenedione,  $\text{C}_2\text{O}_2$ , was discovered only recently by Sanov and coworkers, who assigned a ground state triplet,  $T_0$ , as well as two higher energy singlet states that dissociate into  $\text{CO}(^1\Sigma^+) + \text{CO}(^1\Sigma^+)$  through photoelectron spectroscopy.<sup>15</sup> Vibrational structure observed in the  $T_0$  state of  $\text{C}_2\text{O}_2$  indicated a lifetime of neutral  $\text{C}_2\text{O}_2$  of  $\sim 0.5$  ns. Thus, this is an ideal system to examine using PPC spectroscopy, and characterization of exotic oxides of carbon is a fundamentally important question. We have examined the DPD of  $\text{C}_2\text{O}_2^-$  produced in a pulsed discharge both with and without buffer gas cooling in COAT. In the higher temperature source, the anion isomer studied by Sanov’s group was identified, however, in the COAT ion source a more stable anion is formed. One possible explanation is that the stable anion is the trans-bent  $^2\text{A}_u$  electronic state, while the higher-temperature measurements are observing the  $^2\text{B}_u$  configuration that relaxes to a linear

geometry. This remains an open question to be addressed by theory, as well as explanation of an ionic photodissociation pathway producing  $O^- + C_2O$  and possibly other anionic photochemistry.

## F. Future Work

In the coming months we will finalize studies of  $C_2O_2/C_2O_2^-$  and the  $OH(CH_4)/OH^-(CH_4)$  systems. Current experiments include characterization of the dissociation dynamics of the important reactive intermediate HONO by photodetachment of  $HONO^-$ . Following this we will work with the negative ion sources to synthesize new precursors including  $O^-(CH_4)$  for studies of the  $O + CH_4 \rightarrow OH + CH_3$  radical-radical reaction as well as other relevant hydroxyl radical systems including  $OH-C_2H_2$ ,  $OH-C_2H_4$  and  $OH + NH_3$ . Later, in 2018, we will return to the challenging measurements of vibrationally excited anions for control of product channels, starting with  $HCO_2^-$  and  $HOCO^-$  as well as finalizing the development of a high-temperature RF octupole accumulator trap.

## G. DOE-supported publications by this project 2014-2017

1. A.W. Ray, B.B. Shen, B.L.J. Poad and R.E. Continetti, *State-resolved predissociation dynamics of the formyl radical*, Chem. Phys. Lett. **592**, 30-35 (2014).
2. R. Otto, J. Ma, A.W. Ray, J.S. Daluz, J. Li, H. Guo and R.E. Continetti, *Imaging dynamics on the  $F + H_2O \rightarrow HF + OH$  potential energy surfaces from wells to barriers*, Science, **343**, 396-399 (2014).  
DOE BES Highlight <http://science.energy.gov/bes/highlights/2014/bes-2014-10-d/>
3. R. Otto, A.W. Ray, J.S. Daluz and R.E. Continetti, *Direct IR excitation in a fast ion beam: Application to  $NO^-$  photodetachment cross sections*, EPJ Techniques and Instrumentation **1**:3 (2014).
4. A.F. Wagner, R. Dawes, R.E. Continetti and H. Guo, *Theoretical/experimental comparison of deep tunneling decay of quasi-bound  $H(D)OCO$  to  $H(D)+CO_2$* , J. Chem. Phys. **141**, 054304 (2014).
5. C.J. Johnson, R. Otto and R.E. Continetti, *Spectroscopy and dynamics of the HOCO radical*, Phys. Chem. Chem. Phys. **16**, 19091-19105 (2014).
6. B.B. Shen, B.L.J. Poad and R.E. Continetti, *Photoelectron-photofragment coincidence studies of the tert-butoxide anion  $(CH_3)_3CO^-$ , the carbanion isomer  $(CH_3)_2CH_2COH^-$  and corresponding radicals*, J. Phys. Chem. A **118**, 10223-10232 (2014).
7. A.W. Ray, J. Agarwal, B.B. Shen, H.F. Schaefer, III and R.E. Continetti, *Energetics and transition-state dynamics of the  $F + HOCH_3 \rightarrow HF + OCH_3$  reaction*, Phys. Chem. Chem. Phys. **18**, 30612-30621 (2016),

## H. References

1. C. J. Johnson, M. E. Harding, B. L. J. Poad, J. F. Stanton and R. E. Continetti, J. Am. Chem. Soc. **133**, 19606-19609 (2011).
2. C. J. Johnson, B. L. J. Poad, B. B. Shen and R. E. Continetti, J. Chem. Phys. **134**, 171106 (2011).
3. J. Li, Y. Wang, B. Jiang, J. Ma, R. Dawes, D. Xie, J. M. Bowman and H. Guo, J. Chem. Phys. **136**, 041103 (2012).
4. J. Ma, J. Li and H. Guo, Phys. Rev. Lett. **109** (6), 063202 (2012).
5. X. Wang and J. M. Bowman, J. Phys. Chem. A **118**, 684-689 (2014).
6. A. F. Wagner, R. Dawes, R. E. Continetti and H. Guo, J. Chem. Phys. **141**, 054304 (2014).
7. R. Otto, J. Ma, A. W. Ray, J. S. Daluz, J. Li, H. Guo and R. E. Continetti, Science **343**, 396-399 (2014).
8. A. W. Ray, J. Agarwal, B. B. Shen, H. F. Schaefer and R. E. Continetti, Phys. Chem. Chem. Phys. **18**, 30612-30621 (2016).
9. H. Feng, K. R. Randall and H. F. Schaefer, J. Phys. Chem. A **119**, 1636-1641 (2015).
10. N. K. Srinivasan, M.-C. Su, J. W. Sutherland and J. V. Michael, J. Phys. Chem. A **109**, 1857-1863 (2005).
11. B. A. Ellingson, J. Pu, H. Lin, Y. Zhao and D. G. Truhlar, J. Phys. Chem. A **111**, 11706-11717 (2007).
12. A. Karton, A. Tarnopolsky, J.-F. Lamere, G. C. Schatz and J. M. L. Martin, J. Phys. Chem. A **112**, 12868-12886 (2008).
13. J. Li and H. Guo, J. Chem. Phys. **143**, 221103 (2015).
14. Y.-J. Lu, J. H. Lehman and W. C. Lineberger, J. Chem. Phys. **142**, 044201 (2015).
15. A. R. Dixon, T. Xue and A. Sanov, Angew. Chem. Int. Ed. **54**, 8764-8767 (2015).

## Vibrational Dynamics and Dissociation of Ground- and Excited-State Clusters

F.F. Crim  
Department of Chemistry  
University of Wisconsin–Madison  
Madison, Wisconsin 53706  
fcrim@chem.wisc.edu

Our research investigates the chemistry of vibrationally excited molecules. The properties and reactivity of vibrationally energized molecules are central to processes occurring in environments as diverse as combustion, atmospheric reactions, and plasmas and are at the heart of many chemical reactions. The goal of our work is to unravel the behavior of vibrationally excited molecules and to exploit the resulting understanding to determine molecular properties and to control chemical processes. A unifying theme is the preparation of a molecule in a specific vibrational state using one of several excitation techniques and the subsequent photodissociation of that prepared molecule. Because the initial vibrational excitation often alters the photodissociation process, we refer to our double-resonance photodissociation scheme as *vibrationally mediated photodissociation*. In the first step, fundamental or overtone excitation prepares a vibrationally excited molecule, and then a second photon, the photolysis photon, excites the molecule to an electronically excited state from which it dissociates. Vibrationally mediated photodissociation provides new vibrational spectroscopy, measures bond strengths with high accuracy, alters dissociation dynamics, and reveals the properties of and couplings among electronically excited states.

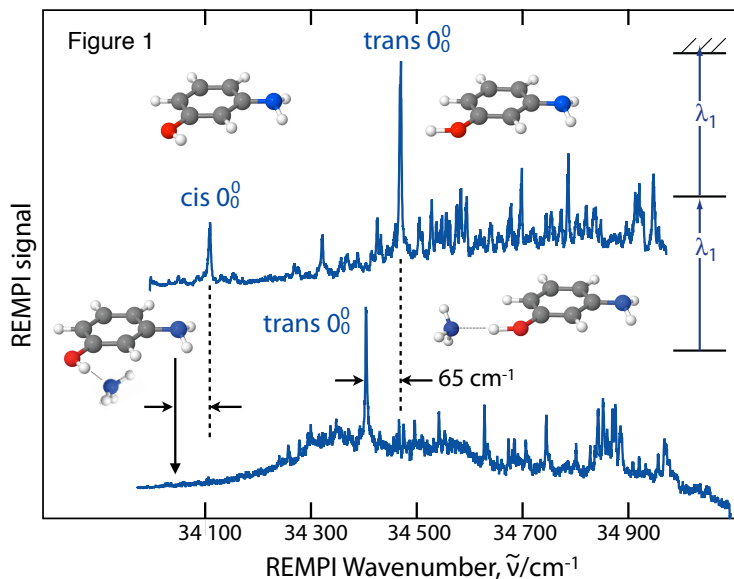
Our recent research on vibrational dynamics in clusters has produced new insights into ammonia clusters, one of the prototypical hydrogen-bonded systems. We have determined the dissociation energy of the dimer very precisely ( $660 \pm 20 \text{ cm}^{-1}$ ) and obtained an experimental estimate of the dissociation energy of the trimer ( $1600 \pm 100 \text{ cm}^{-1}$ ). The dynamics we probe show selective coupling of vibrational energy during the dissociation of the dimer. These studies have led us into new studies of ammonia-containing complexes that build on our previous investigations, and we have obtained intriguing results on vibrationally induced isomerization in the complex of ammonia with a substituted phenol. An extension of this research is now probing the excited-state dynamics of a halomethane,  $\text{CHBrCl}_2$ .

### Aminophenol-Ammonia Complexes

We studied the complex of 3-aminophenol with ammonia to understand its bond-strength and its vibrational predissociation as we move toward studying its excited-state dissociation. There are two conformers of 3-aminophenol corresponding to different orientations of the O-H bond. The structures in the top portion of Fig. 1 illustrate the slightly higher energy *cis* conformer and the lower energy *trans* conformer. The spectrum in the top of Fig. 1 is the (1+1) REMPI spectrum of 3-aminophenol with the *cis* and *trans* origins marked. [W. Y. Sohn, *et al.*, Phys. Chem. Chem. Phys. 13, 7006 (2011).] The spectrum in the bottom of the figure is that of the complex, in which the *trans* origin appears about  $65 \text{ cm}^{-1}$  below that of the bare 3-aminophenol, but the *cis* isomer does not appear, possibly because of interconversion between the two conformers during the formation of the complex.

We have recently observed the influence of vibrational excitation on the complex by obtaining the REMPI spectrum after exciting the ammonia cluster ( $3\text{-AP-NH}_3$ ) in the OH stretching and NH stretching

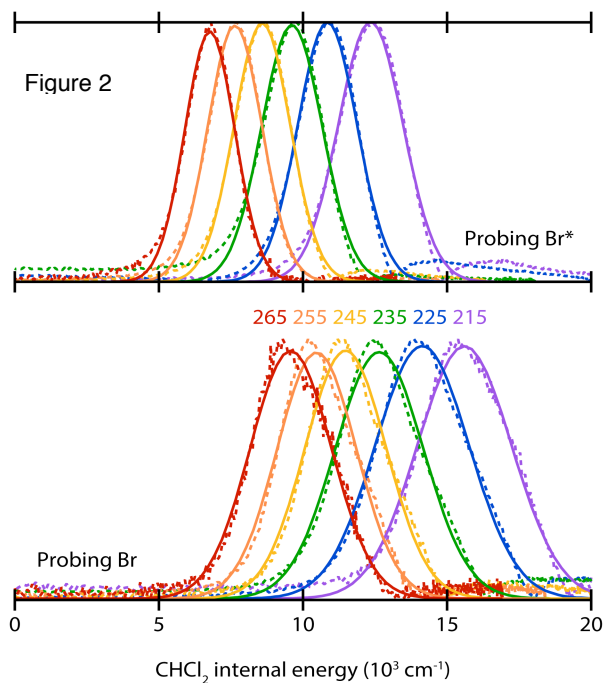
regions. The vibrational energy is sufficient to dissociate the cluster into its constituent 3-AP and  $\text{NH}_3$  monomers, and we detect the 3-AP fragments *via* (1+1) resonance-enhanced multiphoton ionization (REMPI). The distribution of vibrational-state population of the 3-AP fragment suggests the presence of two distinct dissociation pathways. The first dissociation channel produces a broad, unstructured predissociation feature in the REMPI action spectrum after excitation of any of the O-H or N-H stretching vibrations, suggesting a nearly statistical dissociation pathway with strong coupling of the vibrations in the cluster during the predissociation. The second dissociation channel produces sharp features on top of the broad predissociation features, but only following excitation of the OH stretch or the symmetric  $\text{NH}_3$  stretch in the cluster. This striking mode-specificity is consistent with strong coupling of these two modes to the dissociation coordinate (the O-H $\cdots$ N bond). The presence of clearly resolved transitions to the electronic origin and to the  $10a_0^2 + 10b_0^2$  state of the *cis*-3-AP isomer shows that vibrational excitation is driving the isomerization of the *trans*-isomer to the *cis*-isomer in the course of the dissociation of the cluster.



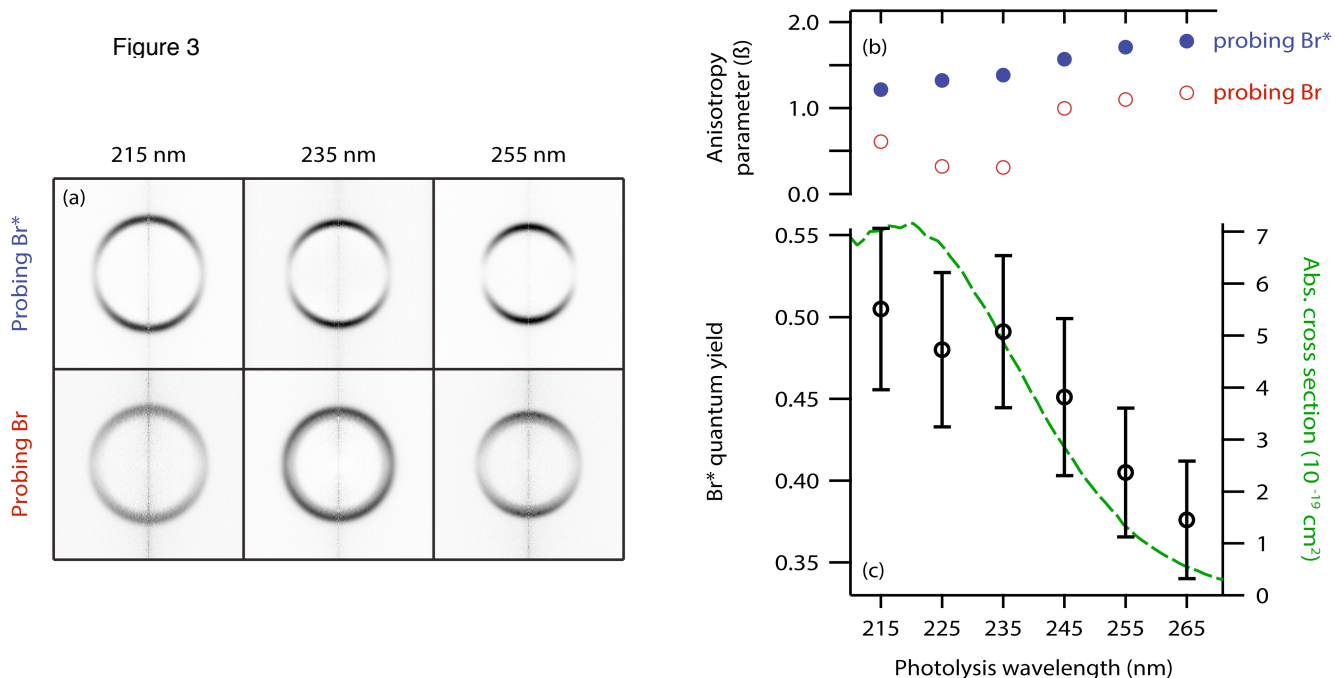
### Dissociation of a Halomethane, $\text{CHBrCl}_2$

We have returned to the velocity-mapped ion imaging technique of our earlier ammonia studies to investigate the recoil energies and relative product yields in the dissociation of  $\text{CHBrCl}_2$  in the range of 215 - 265 nm. The low symmetry of this molecule brings many close-lying electronic states in to play, and we are able to detect both the ground-state Br fragment and the spin-orbit excited-state  $\text{Br}^*$  fragment.

Following C-Br bond cleavage, resonance enhanced multiphoton ionization and time of flight mass spectrometry provide selective detection of the two product channels, from which we quantify the relative quantum yield of  $\text{Br}/\text{Br}^*$  production. As Fig. 2 shows, velocity-map imaging of the photofragments allows us to determine the energy partitioning as a function of the photolysis energy for the different exit channels. Figure 3 collects examples of the distributions from the reconstructed images, the anisotropy, and quantum yields for the various photolysis wavelengths. The anisotropy suggests that absorption to the  ${}^3Q_{0+}(A')$  state is important throughout the entire region we study, though competition with other excited states is evident.



The  ${}^3Q_{0+}(A')$  state forms an avoided crossing with the  ${}^1Q_1(A')$  state, and we find that the propensity for adiabatic passage through this crossing region dictates the Br quantum yield at longer wavelengths. At shorter wavelengths, Br production from excited states not subject to the crossing is more evident. While we find that spin-orbit excitation comes largely at the expense of the  $\text{CHCl}_2$  internal energy, both channels still produce highly excited  $\text{CHCl}_2$  photofragments. Impulsive modeling and comparison with similar halomethane dissociations suggests that a high degree of rotational excitation is present, dictated by the torque inherent in  $C_s$ -symmetry dissociation and the angular dependence of the potential.



### PUBLICATIONS SINCE 2013 SUPPORTED BY DOE

*Vibrational Predissociation and Vibrationally Induced Isomerization of 3-Aminophenol-Ammonia.* Cornelia Heid, Wyatt Merrill, Amanda Case, and F. Fleming Crim, *J. Chem. Phys.* **142**, 014310 (2015).

*Dynamics and Yields for  $\text{CHBrCl}_2$  Photodissociation from 215-265 nm.* Wyatt G. Merrill, F. Fleming Crim, and Amanda S. Case, *Phys. Chem. Chem. Phys.* **18**, 32999 (2016).



# Theory and Modeling of Multiphase Reacting Flow Dynamics in Simulations and Experiments

Rainer N. Dahms  
Combustion Research Facility, Sandia National Laboratories  
Livermore, CA 94551-0969  
[Rndahms@sandia.gov](mailto:Rndahms@sandia.gov)

## I. Program Scope

This theoretical and modeling effort on multiphase reacting flow dynamics is based on three primary objectives. The first is to establish a physically-based understanding of improved turbulent mixing and combustion models in multiphase flows. Many of the relevant fluid flow processes take place on time and length scales which are not feasible to resolve directly in simulations. Therefore, sophisticated sub-grid scale models have to be developed. This requires a comprehensive understanding of the fundamental processes of the underlying relevant phenomena. In this context, a major focus is the development of more general regimes that incorporate broader ranges of combustion modes and a more complete set of non-dimensional parameters. The second objective is to develop techniques and methods to understand data sets obtained from high-fidelity Large-Eddy simulations (Oefelein) and measurements performed in the Advanced Imaging Laboratory (Frank) and in the Turbulent Combustion Laboratory (Barlow) in a meaningful manner. The fundamental issues of comparing, validating, and understanding advanced combustion data sets will become even more important as we attempt to understand the dynamics of turbulence-flame interactions using data sets that capture the temporal evolution of turbulent flames. The third objective is to understand the implications of the conclusions obtained from well-controlled experiments in the context of advanced power and propulsion systems including gas turbines, automotive engines, and liquid rockets. This effort has to consider the poorly understood effect of elevated pressure on the fundamentals of multiphase combustion phenomena. It builds on the developed theoretical framework, which establishes a meaningful set of major scaling parameters. Combined with the identification of relevant ranges of combustion regimes and non-dimensional parameters in modern transportation and power systems, the framework will serve the general objective of this program to accelerate the development and validation of science-based, predictive computational models for turbulent combustion systems.

## II. Recent Progress

Understanding and quantifying multiphase reacting flow phenomena in fundamental experiments and modern transportation and energy systems is widely recognized as a critical research area for future combustion design. However, the scientific challenges addressed directly impact many fundamental and applied research areas such as 1) understanding and predicting high-pressure spray flame ignition which represents a cornerstone to the design of modern energy, transportation, and propulsion systems; 2) analysis of atmospheric chemical dynamics in which the coupling of low-temperature kinetics and molecular large-scale transport at large Reynolds numbers plays an essential role; and 3) understanding of detonation waves in supernovas and explosions where extreme heterogeneities in regions of chemical activity exist. In the context of combustion, the importance to develop a basic science foundation for predictive models has been consistently highlighted over many years in a variety of industry, government, and academic forums including recent DOE workshops such as the *Workshop to Identify Research Needs and Impacts in Predictive Simulations for Internal Combustion Engines (PreSICE)*,<sup>1</sup> and the *Workshop on*



*Clean and Efficient Combustion of 21<sup>st</sup> Century Transportation Fuels.*<sup>2</sup> Liquid injection processes largely determine the mixture preparation process which ultimately governs the detailed evolution of chemical kinetic processes and their interaction with the turbulent flow field.

Recently, Skeen *et al.*<sup>3</sup> provided time-resolved imaging showing how cool-flame dynamics play a significant role in high-pressure spray ignition. Simultaneous formaldehyde PLIF and high-speed schlieren imaging were applied to a spray flame ignition experiment. The measurements showed initiation of low-temperature reactions near the radial periphery of the spray, followed by rapid appearance of low-temperature reactions across the entire spray head at a position where high-temperature ignition finally occurs. Cool-flame chemistry was also found significant in fundamental droplet combustion studies mainly motivated by micro-gravity experiments performed on board the International Space Station<sup>4,5</sup> and in recent Direct Numerical Simulations (DNS) of a 2D turbulent stratified mixing layer using a reduced chemical mechanism for dimethyl ether.<sup>6</sup>

Most recently, studies aimed to develop a conceptual model for turbulent ignition in high-pressure spray flames.<sup>7</sup> The model is motivated by first-principle simulations and optical diagnostics applied to high-pressure n-dodecane spray flames. The Lagrangian flamelet equations are combined with full LLNL kinetics (2755 species; 11,173 reactions) to resolve all time and length scales and chemical pathways of the ignition process at engine-relevant pressures and turbulence intensities unattainable using classic DNS. The first-principle value of the flamelet equations is established by a spectral analysis of the fully-coupled chemical and turbulent time scales. Contrary to conventional wisdom, this analysis revealed that the high Damköhler number limit, a key requirement for the validity of the flamelet derivation from the reactive Navier-Stokes equations, applies during the entire ignition process.

The analysis demonstrates the significance of turbulence in the ignition mechanism of high-pressure stratified mixtures. Figure 1 compares the 1<sup>st</sup> and 2<sup>nd</sup> stage ignition delay using homogeneous reactor model (left) and from a turbulent high-pressure spray flame (right). Fundamental differences arise between both configurations due to the presence of turbulent cool and hot flame waves. Those waves largely result from the molecular diffusion of temperature and reactive species into yet unburnt regions in highly stratified mixtures and, hence, are naturally absent under homogeneous conditions.

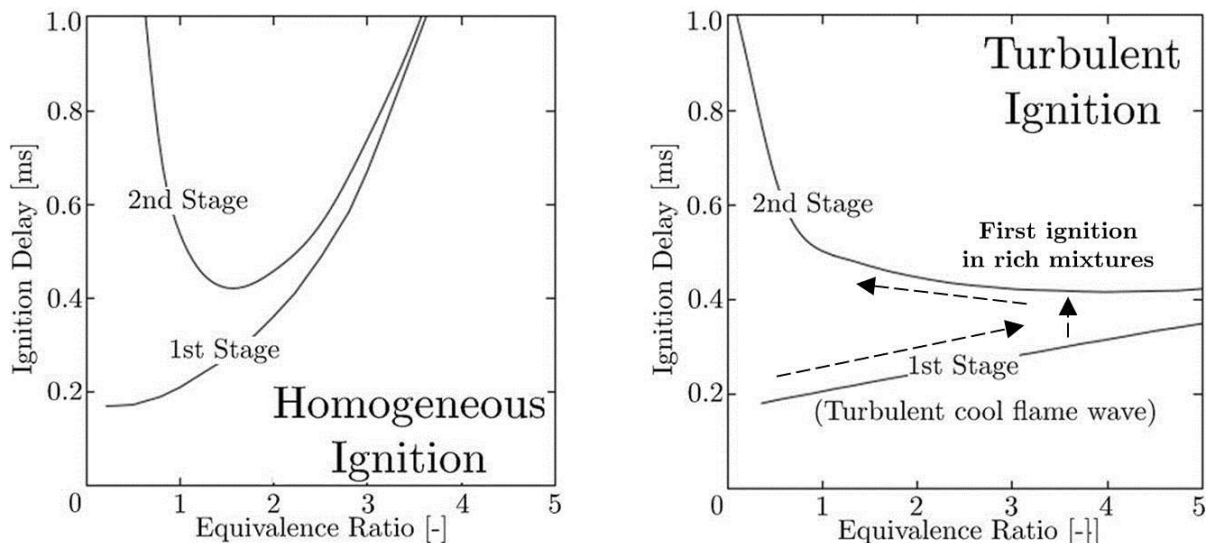


Figure 1: 1<sup>st</sup> and 2<sup>nd</sup> stage ignition delay using (left) homogeneous reactor model and (right) a turbulent high-pressure spray flame. Fundamental differences arise between homogeneous and stratified ignition delays due to the presence of turbulent cool (and hot) flame waves. Those waves are naturally absent under homogeneous conditions (see Dahms *et al.*<sup>7</sup>).

As an illustrative example, Fig. 1 (right) shows how a turbulent cool flame wave significantly shortens the 1<sup>st</sup>-stage ignition delay in rich mixture regions in comparison to its homogeneous counterpart. This finding answers the long standing question of why stratified turbulent ignition is typically observed in distinctively fuel-rich regions instead of in the “most reactive” mixture regions ( $\phi \approx 1.4$ ).

Those works discovered the existence of reaction wave fronts in stratified environments and established their fundamental significance in stratified ignition kinetics. However, the properties and internal dynamics of these fronts are still largely unknown. Their propagation speed, which represents one of their most basic quantities, directly determines the deviation of turbulent ignition dynamics from their homogeneous analog, compare Fig. 1. An initial inquiry into mesoscale science methods has uncovered a pathway for first-principle calculations of wave front structures at relevant pressures and heterogeneities caused by realistic scalar dissipation rates. An initial result of this effort is presented in Fig. 2.

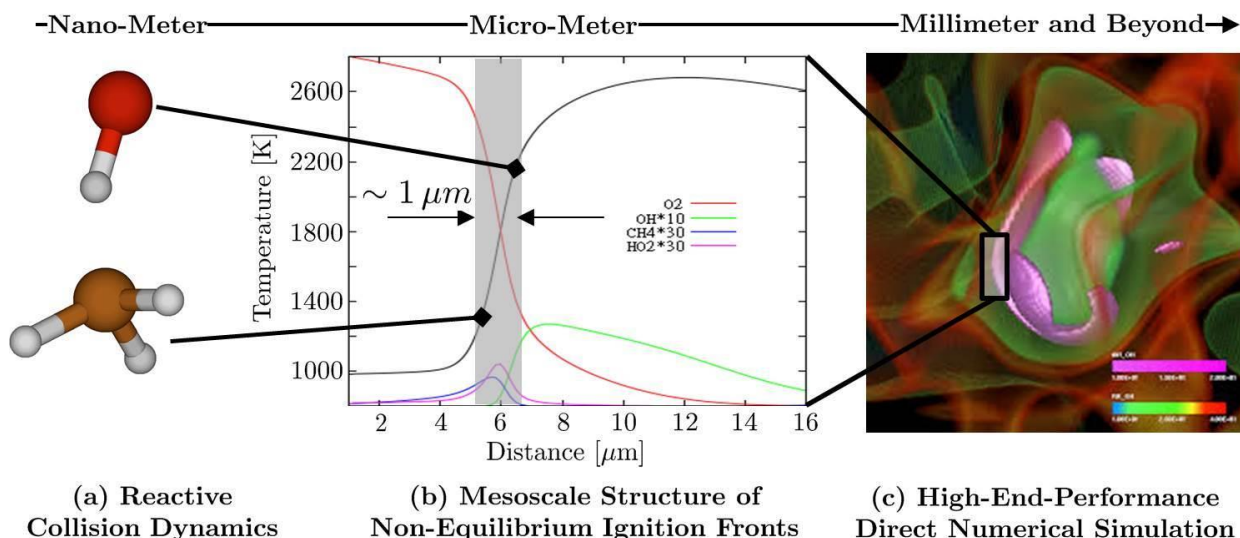


Figure 2: Mesoscale science framework to combine our fundamental research techniques over a wide range of spatial and temporal scales. (Left) Ab-initio molecular dynamics simulation of non-equilibrium reactive collisions. (Middle) Mesoscale simulation of a propagating reaction wave front structure during stratified turbulent ignition. (Right) High-end-performance DNS of an auto-igniting turbulent flow field.

The simulation suggests extreme internal thermal gradients across the ignition front structure. This information is then utilized to perform non-thermalized elementary reactive collision simulations using a quasi-classical trajectory approach. The simulation reflects a scenario in which both collision partners originate from different enthalpy pools due to the present heterogeneity. The purpose of these simulations is to obtain insights into the significance of non-thermalized elementary kinetics.

### III. Future Work

All developed chemical mechanisms and performed experiments utilize a homogeneous mixture configuration. They therefore entirely neglect the presence of cool flame and hot flame waves in turbulent mixtures which were discovered here. The presented fundamental finding could carry immense implications for the development of more accurate chemical mechanisms for turbulent flames since the inclusion of this discovered physical complexity in simulations promises to significantly improve their predictive capabilities. The fundamental approach described above will be further developed with an emphasis on interrelated areas of research. A close collaboration between the Large-Eddy simulation program and the experimental flow research program will be maintained. A significant effort on the validation and generalization of the proposed theory will be initiated. Such efforts include detailed

comparisons to Direct Numerical Simulations, improvements of model accuracy, and the investigation of turbulent combustion processes at extreme system pressures. The objective is to develop a predictive first-principle model framework suitable for high-fidelity and industry-type combustion simulations.

#### IV. Literature Cited

1. A Workshop to Identify Research Needs and Impacts in Predictive Simulation for Internal Combustion Engines. [http://science.energy.gov/~media/bes/pdf/reports/files/PreSICE\\_rpt.pdf](http://science.energy.gov/~media/bes/pdf/reports/files/PreSICE_rpt.pdf) , 2011; Sponsored by the Office of Basic Energy Sciences, Office of Science and the Vehicle Technologies Program, Office of Energy Efficiency and Renewable Energy, U.S. Department of Energy
2. Basic Research Needs for Clean and Efficient Combustion of 21<sup>st</sup> Century Transportation Fuels. <http://www.osti.gov/scitech/servlets/purl/935428>, 2006; Report of the Basic Energy Sciences Workshop on Clean and Efficient Combustion of 21<sup>st</sup> Century Transportation Fuels, U.S. Department of Energy.
3. S.A Skeen, J. Manin, and L.M. Pickett, “Simultaneous formaldehyde PLIF and high-speed schlieren imaging for ignition visualization in high-pressure spray flames,” *Proc. Combust. Inst.* **35**:3167-3174, 2015
4. T. Farouk and F. Dryer, “On the extinction characteristics of alcohol droplet combustion under microgravity conditions – a numerical study,” *Combust. Flame* **159**:3208-3223, 2012
5. V. Nayagam, D.L. Dietrich, P.V. Ferkul, M.C. Hicks, and F.A. Williams, “Can cool flames support quasi-steady alkane droplet burning?,” *Combust. Flame* **159**:3583-3588, 2012
6. A. Krisman, E.R. Hawkes, M. Talei, A. Bhagatwala, J.H. Chen, “A direct numerical simulation of cool-flame affected autoignition in diesel engine-relevant conditions,” *Proc. Combust. Inst.* **36**(3):3567-3575, 2017, doi: [10.1016/j.proci.2016.08.043](https://doi.org/10.1016/j.proci.2016.08.043)

#### V. BES Sponsored Publications (2015-2017)

7. R.N. Dahms, G.A. Paczko, S.A. Skeen, and L.M. Pickett, “Understanding the ignition mechanism of high-pressure spray flames,” *Proc. Combust. Inst.*, **36**(2):2615-2623, 2017, doi:10.1016/j.proci.2016.08.023
8. R.N. Dahms, “Understanding the breakdown of classic two-phase theory and spray atomization at engine-relevant conditions,” *Phys. Fluids*, **28**:042108, 2016, doi: 10.1063/1.4946000
9. R.N. Dahms and J.C. Oefelein, “The significance of drop non-sphericity in sprays,” *Int. J. Multiphase Flow* **86**:67-85, 2016, doi: 10.1016/j.ijmultiphaseflow.2016.07.010
10. R.N. Dahms. “Gradient Theory simulations of pure fluid interfaces using a generalized expression for influence parameters and a Helmholtz energy equation of state for fundamentally consistent two-phase calculations.” *J. Colloid Interface Sci.* **445**:48-59, 2015, doi: 10.1016/j.jcis.2014.12.069
11. R.N. Dahms and J.C. Oefelein, “Liquid jet breakup regimes at supercritical pressures,” *Combust. Flame*, **162**:3648-3657, 2015, doi:10.1016/j.combustflame.2015.07.004.
12. T.D. Fansler, D.L. Reuss, V. Sick, and R.N. Dahms, “Combustion instability in spray-guided stratified-charge engines: A review,” *Intl. J. Engines Res.*, Cyclic Dispersion Special Issue, **16**:260-305, 2015. doi:10.1177/1468087414565675.
13. R.N. Dahms and J.C. Oefelein. “Atomization and dense fluid breakup regimes in liquid rocket engines.” *J. Propulsion Power*, **31**:1221-1231, 2015. doi:10.2514/1.B35562
14. R.N. Dahms and J.C. Oefelein. “Non-equilibrium gas-liquid interface dynamics in high-pressure liquid injection systems.” *Proc. Combust. Inst.* **35**:1587-1594, 2015. doi: 10.1016/j.proci.2014.05.155

# Bimolecular Dynamics of Combustion Reactions

H. Floyd Davis  
Department of Chemistry and Chemical Biology, Cornell University  
Ithaca, NY 14853-1301

## I. Program Scope:

The goal of this project is to better understand the mechanisms, products, and product energy disposal in elementary bimolecular and unimolecular reactions fundamental to combustion chemistry. Using the crossed molecular beams method, the angular and velocity distributions of neutral products from decomposition of molecules formed from bimolecular reactive collisions or through electronic excitation are measured to gain insight into the reaction dynamics.

## II. Recent Progress:

Our DOE-supported experimental research program is conducted using a rotatable source crossed molecular beams machine with universal electron impact and single photon ionization detection using high intensity pulsed tabletop VUV light sources developed at Cornell.

We have developed a technique for producing pulsed radiation extending to 14.6 eV with higher conversion efficiencies than previously reported.<sup>1</sup> A description of this technique has appeared in *Rev. Sci. Instrum.*, involving noncollinear mixing of focused lasers in laser vaporized mercury (Hg) at room temperature. This approach facilitates windowless operation with the short wavelength radiation spatially isolated from the residual UV and visible beams without need for lossy optical elements such as windows, lenses, and gratings.

We have developed a windowless VUV beamline for use with our previously-reported high-intensity VUV light source employing 4-wave mixing of unfocussed nanosecond lasers.<sup>2-4</sup> This beamline provides access to line tunable photoionization energies ranging from 9.5 eV to 11.9 eV. This makes it possible to carry out “soft” single photon ionization of products from photodissociation or bimolecular reactions with ionization energies ranging from < 9.5 eV (e.g., CH<sub>2</sub>CHOH) to > 11.3 eV (e.g., HO<sub>2</sub>).

As part of the development of molecular beam sources of ethyl, propyl and butyl radicals, we have studied the UV photodissociation of several primary, secondary and tertiary iodoalkanes.<sup>5</sup> While the photodissociation of the simplest iodoalkane, methyl iodide (CH<sub>3</sub>I), has been studied very extensively<sup>6</sup> over many decades, there have been relatively few studies of larger systems. In contrast to methyl iodide where only C-I bond fission is operable at 266 nm, we have found that HI elimination

in secondary and tertiary compounds forming the corresponding alkenes plays an important role. In all previous studies except one,<sup>7</sup> HI elimination has not been considered in iodoalkane photochemistry.

Since the mass resolution of our detector is sufficiently high to discriminate between I ( $m/e = 127$ ) and HI ( $m/e = 128$ ), the competing channels were studied unambiguously using both electron impact and VUV ionization. For *primary* 3-, and 4- carbon iodoalkanes, C-I fission is the exclusive channel with dominant production of excited I ( $^2P_{1/2}$ ), hereafter denoted I\*, relative to ground state I ( $^2P_{3/2}$ ), hereafter denoted I. The highly anisotropic product angular distributions were similar to those for CH<sub>3</sub>I. Time-of-flight (TOF) spectra were recorded for the I, I\*, and C<sub>3</sub>H<sub>7</sub> products, making it possible to derive internal energy distributions of radicals correlated to each I atomic state. For secondary and tertiary iodoalkanes, the angular and velocity distributions for the HI molecular elimination products were found to be similar to those for I. Because the same velocity distributions are observed for HI products ionized using electron impact, 10 eV photons (only capable of ionizing HI ( $v > 3$ )), and 11.9 eV photons, the HI is clearly produced primarily in  $v > 3$ .

The availability of two complementary detection methods (electron impact and photoionization) makes it possible for us to cross-check the branching ratios for competing pathways. In the case of 1-iodopropane photodissociation, the C<sub>3</sub>H<sub>7</sub> and I products have very different translational energy distributions for the I and I\* channels, allowing us to calibrate our detection sensitivity for all channels using two independent detection methods. This made it possible to unambiguously unravel the dynamics for 2-iodopropane, where the kinetic energy distributions for all channels are very similar.<sup>5</sup>

Azoalkanes, having the molecular formula R-N=N-R, where R is an alkyl group, readily undergo thermal dissociation to N<sub>2</sub> + 2R. Previously, the simplest alkyl radical, CH<sub>3</sub>, has been produced by a number of groups via flash pyrolysis of azomethane in a pulsed nozzle. However, for production of ethyl and propyl radicals, it was not clear that C-H bond fission of the initially-produced alkyl radicals (producing the corresponding alkene) could be avoided. Our studies have been encouraging in this regard, and we have completed a set of experiments on the 248 nm photodissociation of 1- and 2-propyl radicals (C<sub>3</sub>H<sub>7</sub>).<sup>8</sup> The radicals were produced by pyrolysis of 1- and 2- azopropane, and, for comparison, by 266 nm photolysis of 1- and 2-iodopropane in a quartz tube. In previous work by others, it was shown that H atom elimination plays an important role in the UV photodissociation dynamics.<sup>9</sup> However, C-C bond fission producing CH<sub>3</sub> + C<sub>2</sub>H<sub>4</sub> is actually the thermodynamically more favorable channel but has never been detected in previous studies. Using soft VUV photoionization detection at 9.9 eV, we have, for the first time, clearly observed both of the

momentum-matched nascent products, *i.e.*,  $\text{CH}_3 + \text{C}_2\text{H}_4$ , from photolysis of both alkyl radical isomers.<sup>8</sup>

### III. Current and Future Plans:

For studies of the isomer-specific bimolecular reactions of alkyl radicals, our primary focus is on reactions of  $\text{C}_2\text{H}_5$ , and the two  $\text{C}_3\text{H}_7$  isomers, with  $\text{O}_2$ . To date, these  $\text{R} + \text{O}_2$  reactions have never been studied under single-collision crossed beam conditions. It is believed that this class of reactions involves initial addition forming  $\text{RO}_2$ , followed by isomerization to  $\text{QOOH}$  followed by decomposition producing  $\text{OH}$  or  $\text{HO}_2$ . For the reaction of  $\text{C}_3\text{H}_7$ , the thermodynamically-accessible product channels are  $\text{HO}_2 + \text{propene}$ , and  $\text{OH} + \text{C}_3\text{H}_6\text{O}$ , where  $\text{C}_3\text{H}_6\text{O}$  ( $m/e = 58$ ) includes several different isomers, *i.e.*, propanal, propylene oxide, trimethylene oxide, or the corresponding enol. These systems are difficult to study in crossed beams due to the difficulty in producing clean, intense radical beams, the relatively small reaction cross sections, and the difficulty in detecting all of the chemical products with high sensitivity. While we are able to produce  $\text{CH}_3$  and  $\text{C}_2\text{H}_5$  pyrolytic radical beams free of significant impurities, in the case of the  $\text{C}_3\text{H}_7$  isomers, nonreactive elastic scattering of trace impurities from  $\text{O}_2$  yields signals comparable to those from the bimolecular reactions. We have therefore devoting considerable effort to the purification of the azopropane samples.

The reactions of hydroxyl radicals,  $\text{OH}$ , with alkenes are of considerable interest in combustion chemistry and are presently under study in our laboratory. While it is known that enols are among the primary reaction products following H atom loss, the dynamics of the competing channels have not been unraveled under single-collision conditions. Over the past years we have developed and characterized a number of different intense  $\text{OH}$  radical beam sources, including 193 nm photodissociation of nitric acid ( $\text{HNO}_3$ ) or formic acid ( $\text{HCOOH}$ ), reactions of photolytically generated  $\text{O}(^1\text{D})$  with  $\text{H}_2$  and  $\text{H}_2\text{O}$ , and reactions of pyrolytically generated F atoms with  $\text{H}_2\text{O}$ . For studies of reactions with alkenes, the presence of O atom impurities in the  $\text{OH}$  beam is a significant complication. Recently, we have characterized the production of  $\text{OH}$  by flash pyrolysis of nitric acid. Although to our knowledge this technique has not been used previously for production of  $\text{OH}$  beams, because  $D_0(\text{HO-NO}_2)$  is only  $\sim 48$  kcal/mol, this method is quite efficient. Most importantly, we find that the yield of O atom impurity is much smaller than from the alternative methods described above. Our recent studies of  $\text{OH}$  reactions with alkenes in crossed beams have been very promising in this regard, and represent a second ongoing project.

#### IV. References (Numbers 1-4 are publications 2013-2017 citing DOE support):

1. High Intensity VUV and XUV Production by Noncollinear Mixing in Laser Vaporized Media, M.A. Todt, D.R. Albert and H. F. Davis, *Rev. Sci. Instrum.* **87**, 063106 (2016).
2. Experimental Studies of Bimolecular Reaction Dynamics Using Pulsed Tabletop VUV Photoionization Detection, invited perspective article, D.R. Albert and H.F. Davis *Phys. Chem. Chem. Phys.* **15**, 14566-14580 (2013).
3. High-Intensity Coherent Vacuum Ultraviolet Source Using Unfocussed Commercial Dye Lasers, D.R. Albert, D.L. Proctor, and H.F. Davis, *Rev. Sci Instrum.* **84**, 063104 (2013).
4. Crossed Molecular Beam Studies of Phenyl Radical Reactions with Propene and 2-Butene, D.R. Albert, M. A. Todt, and H.F. Davis, *J. Phys. Chem. A* **117**, 13967-13975 (2013).
5. Dynamics of HI elimination from the UV Photodissociation of Alkyl Iodides, M. A. Todt and H. F. Davis, in preparation.
6. Excited Fragments from Excited Molecules: Energy partitioning in the Photodissociation of Alkyl Iodides, S.J. Riley and K.R. Wilson, *Faraday Disc. Chem. Soc.* **53**, 132 (1972).
7. Excited State Photochemistry of Iodoalkanes, P.L. Ross and M.V. Johnston, *J. Phys. Chem.* **99**, 4078 (1995).
8. Photodissociation of the 1- and 2- propyl radicals at 248 nm: observation of the C-C bond fission channel, M.A. Todt, and H. F. Davis, in preparation.
9. Ultraviolet photodissociation dynamics of the n-propyl and i-propyl radicals, Y. Song, X. Zheng, W. Zhou, M. Lucas, and J. Zhang, *J. Chem. Phys.* **142**, 224306 (2015).

## Exploration of chemical-kinetic mechanisms, chemical reactivity, and thermochemistry using novel numerical analysis

Michael J. Davis

Chemical Sciences and Engineering Division  
Argonne National Laboratory  
Argonne, IL 60439  
Email: davis@tcg.anl.gov

The work involves exploration of chemically reactive systems using novel numerical analyses. One focus of the work is exploration and theoretical validation of chemical-kinetic mechanisms, combining global sensitivity analysis with the exploration of the characteristics of the sensitivity analysis over physical and chemical parameters. An effort on reaction pathway analysis has also been undertaken under this focus. An important aspect of this part of the work is the use of state of the art methods in numerical analysis, statistics, and signal processing for making the global sensitivity analysis efficient for large-scale chemical mechanisms. The global sensitivity and reaction pathway analysis is used to pinpoint chemical reactions that need to be studied accurately to improve the accuracy of chemical mechanisms. The expertise developed in that work has led to a second focus: the implementation of these techniques for studying problems in chemical reactivity, including isolated chemical kinetics and dynamics. Key features of this focus are regression analysis, intelligent sampling, power transformations, and subset selection. There is a major effort underway for using these techniques for fitting potential energy surfaces, where it is difficult to scale existing methods to larger molecular systems. Generating accurate potential surfaces is important for developing fundamental understanding of chemical reactivity. The regression analysis is also being used for thermochemical active tables.

### Recent Progress

Two areas have shown noticeable progress in the last year. The first area is the continued application of global sensitivity, including its application to engine simulations. The second area is broader and includes the accurate and efficient fitting of potential energy surfaces and has been a major focus of work in the preceding year, much of it developmental. The area is an outgrowth of the sensitivity analysis work, where state of the art numerical analysis has been used to make the calculation of sensitivity coefficients much more efficient. The research includes a collaboration with Ahren Jasper and involves fitting these potentials using basis functions and requires linear regression. An important aspect of the work is regression diagnostics, which also has applications for the analysis of thermochemical active tables. Upcoming realizations of active tables will include new regression diagnostics, as implemented by Bross and Ruscic.

Table 1: Group Sensitivities

Reaction Type	$T_0 = 825, P = 81.4$ $\phi_0 = 2.76$	$T_0 = 886, P = 82.7$ $\phi_0 = 1.2$	$T_0 = 935, P = 76.1$ $\phi_0 = 1.16$
RO <sub>2</sub> = QOOH	0.297	0.231	0.145
Formation of KHP	0.156	0.123	0.085
HO <sub>2</sub> Abstractions	0.016	0.095	0.138
OH Abstractions	0.045	0.010	0.000
$\beta$ -scissions	0.000	0.000	0.032
C <sub>0</sub> reactions	0.000	0.032	0.061
C <sub>4</sub> reactions	0.000	0.012	0.032
Abstraction by RO <sub>2</sub>	0.020	0.000	0.000



The most recent set of global sensitivity calculations were published in Ref. (11) for the ignition of a mixture of n-heptane, methylbutanoate, and air under constant pressure conditions, in collaboration with Raghu Sivaramakrishnan. The calculations reported in that publication lead to insightful analysis of the chemistry and the Table, which shows sums of sensitivity coefficients for classes of reactions at 3 different conditions, indicates that the sensitivity of the ignition delay is most dependent on the accuracy of a few classes of reactions, indicating which reactions need further and more accurate rate coefficients.

Global sensitivity coefficients are calculated by fitting of the two models:

$$\tau^{(1)}(\{u_i\}) = \sum_{i=1}^{n_r} \sum_{k=1}^p a_{ik} u_i^k \quad (1a)$$

$$\tau^{(2)}(\{u_i\}) = \sum_{i=1}^{n_r} \sum_{k=1}^p a_{ik} u_i^k + \sum_{j=1}^{n_r} \sum_{m=1}^{m_s} \{b_{jm}\}^s Q^{(s)}(u_{j_1}, u_{j_2}) \quad (1b)$$

The  $u$ 's refer to reaction uncertainties,  $\tau$  the ignition delay time,  $n_r$  the number of reactions, and  $p$  the order of the polynomial. Equation (1b) differs from Eq. (1a), by including cross terms in the second summation, which are referred to as ‘‘interaction terms’’. The fitting of these surfaces is accomplished with linear regression. A large number of simulations are run and the  $a$ 's and  $b$ 's are calculated using the following set of transformations:

$$\mathbf{Xc} = \mathbf{y} \quad (2a)$$

$$\mathbf{c} = (\mathbf{X}^T \mathbf{X})^{-1} \mathbf{X}^T \mathbf{y} \quad (2b)$$

where  $\mathbf{y}$  is a vector of ignition delay times,  $\mathbf{c}$  is a vector of coefficients [‘‘a’’ and ‘‘b’’ in Eqs. (1a) and (1b)], and the matrix  $\mathbf{X}$  summarizes the results of the simulations with the expansions shown in the equations above. Equation (2b) results from minimization of the least squares error. We use this error along with a leave-one-out error to fix which models and how many simulations are needed to calculate sensitivity coefficients.

The leave-one-out error is calculated using the following:

$$\hat{\mathbf{y}} = \mathbf{H}\mathbf{y} \quad (3a)$$

$$\mathbf{H} = \mathbf{X}(\mathbf{X}^T \mathbf{X})^{-1} \mathbf{X}^T \quad (3b)$$

$$y_i - \hat{y}_i^{(-i)} = \frac{y_i - \hat{y}_i}{1 - h_{ii}} \quad (3c)$$

$$E_{\text{loocv}}^2 = \sum_i^n \left( \frac{y_i - \hat{y}_i}{1 - h_{ii}} \right)^2, E_{\text{loocv}} = \sqrt{\frac{E_{\text{loocv}}^2}{n}}. \quad (3d)$$

Equation (3d) defines the leave one out error. The  $\hat{y}_i$ 's refer to the fitted value of the ignition delay time and  $\hat{y}_i^{(-i)}$ 's refer to the values of the fitted ignition delay if all simulations are used in the fit, except for the  $i^{\text{th}}$  simulation. The  $h_{ii}$ 's are the diagonal values of the matrix  $\mathbf{H}$  and are

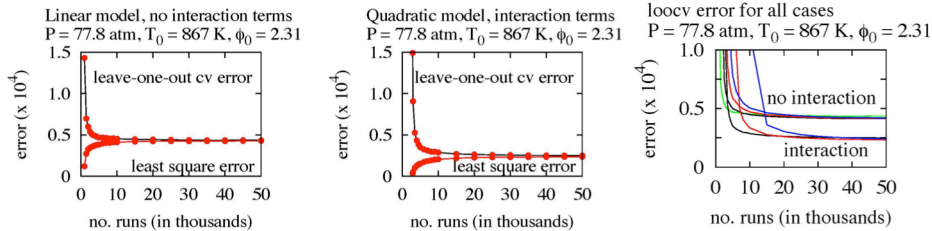


Fig. 1. Convergence plots are shown for two of the models in the left two panels and the rightmost panel shows loocv error for seven models.

commonly called the leverages. The  $h_{ii}$ 's have values between 0 and 1 and an average value of  $\frac{p}{n}$ , the ratio of the number of terms in the expansion ( $p$ ) and the number of simulations ( $n$ ).

The plots in the first two panels of Fig. 1 are used to determine the convergence of the fits in Eqs. (1a) and (1b) for each of the models. They also demonstrate that the more complex model, the quadratic with interaction terms has significantly lower error, but requires significantly more simulations to reach convergence. The plot on the far right compares 7 models, up to quartic fits with and without interaction terms. This plot once again indicates that models with cross terms give much better fits than ones without, but also indicates that there is little reason to use higher order polynomials as the errors do not change much with the order.

The results in Fig. 1 indicate that the simplest models with or without interaction terms should be used for global sensitivity and a more complete analysis is provided in Ref. 11, where the linear model is chosen based on the goal of obtaining accurate sensitivity coefficients for only the first 10-15 most sensitive reactions. These plots and Eqs. (3a) – (3d) indicate the importance of the leverages, the  $h_{ii}$ 's. When these leverages are near 1.0, the leave one out error may be very large. High leverage points are often referred to as “x-outliers”, as they are points that are relatively far from the mean of the independent variables. Because we are using random sampling and relatively low-order polynomials none of the points in our sample are high leverage, as demonstrated in the left plot of Fig. 2, where the distribution of leverages are shown.

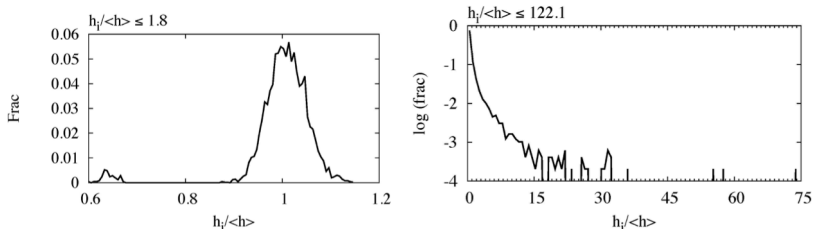


Fig. 2. The left and the panels show the distributions of the leverages for the sensitivity and potential fit potentials, respectively.

The general rule for efficient fitting is that no points should have leverages higher than twice the average value, which is not true for the results in the right panel of Fig. 2.

These results are from fitting a potential describing the collisions of He with  $\text{HO}_2$  at fixed geometry (3-D). In the example in the left panel, the leverages were used to calculate the leave one out error and do not play a role in guiding the sampling. However the situation can change when a more complex model is used in the fitting, as shown in the right panel.

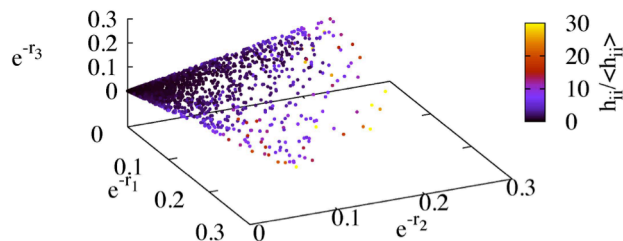


Fig. 3. Points used for the potential fit plotted in function space, along with the leverages (colors).

$r_i$ 's are between the He atom and the atoms of  $\text{HO}_2$ ). The plot shows that high leverage points are well separated from other points in the function space. Sampling adapted to the basis set will

Figure 3 demonstrates why the leverages are distributed the way they are in the right panel of Fig. 2. The sample of points used in the fitting of the potential surface are randomly sampled in the spherical coordinates, but are not randomly sampled in the space of the function of the internal coordinates (the

improve the fit and is being implemented in the collaboration with Jasper. Improving the accuracy of potential surfaces increases the accuracy of trajectory calculations, increasing the understanding of chemical reactivity and collisional energy transfer.

The leverages play a key role in adjusting the sampling, because high leverage values are reduced if additional points are included near them. This plays a key role in the accuracy of the surface fitting problem where the presence of high leverage points suggest additional calculations to improve accuracy and for active thermochemical tables, where the high leverage points suggest additional experiments and calculations to improve the accuracy of the fit.

### Future Plans

Figure 3 and the right panel of Fig 2 suggest that sampling should depend on the model used and in the next year we plan to implement model-based sampling inspired by work in the literature on the Design of Experiments and the Design and Analysis of Computer Experiments to improve the accuracy of potential energy surfaces. In addition we intend to try several ideas from the regression analysis literature, including power transformations of the potential and adaptive sampling. We also intend on using biased and robust estimators to move the convergence point in Fig. 1 to smaller sample sizes. Finally we intend on using multiple basis sets and best subset selection to improve the fitting in collaboration with Ahren Jasper and Maria Chan (CNM/ANL).

### Publications

1. Y. Pei, R. Shan, S. Som, T. Lu, D. E. Longman, and M. J. Davis, "Global Sensitivity Analysis of a Diesel Engine Simulation with Multi-Target Functions", Proceedings of the Society of Automotive Engineers (SAE) World Congress, 2014, SAE Paper 2014-01-1117.
2. S. Bai, D. Zhou, M. J. Davis, and R. T. Skodje, "Sum over Histories Representation for Chemical Kinetics", *J. Phys. Chem. Lett.*, 6, 183–188 (2015).
3. D. M. A. Karwat, M. S. Wooldridge, S. J. Klippenstein, and M. J. Davis, "Effects of New Ab Initio Rate Coefficients on Predictions of Species Formed during *n*-Butanol Ignition and Pyrolysis", *J. Phys. Chem. A* 119, 543-551 (2015).
4. Y. Pei, M. J. Davis, L. M. Pickett, S. Som, "Engine Combustion Network (ECN): Global sensitivity analysis of Spray A for different combustion vessels", *Combustion and Flame* 162, 2337-2347.
5. S. Som, Z. Wang, G. M. Magnotti, W. Liu, R. Sivaramakrishnan, and M. J. Davis, "Application of Sparse Sensitivity Analysis to Detailed Chemical Kinetics in High Fidelity Compression-Ignition Engine Simulations", Proceedings of the 9<sup>th</sup> US National Technical Meeting of the Combustion Institute (2015).
6. F. G. Sen, A. Kinaci, B. Narayanan, S. K. Gray, M. J. Davis, S. K. R. S. Sankaranarayanan, and M. K. Y. Chan, "Towards Accurate Prediction of Catalytic Activity in IrO<sub>2</sub> Nanoclusters Via First Principles-Based Variable Charge Force Field", *J. Mater. Chem A* 3, 18970-18982 (2015).
7. S. Bai, M. J. Davis, and R. T. Skodje, "The Sum Over Histories Representation for Kinetic Sensitivity Analysis: How Chemical Pathways Change When Reaction Rate Coefficients Are Varied", *J. Phys. Chem A* 119, 11039-11052 (2015).
8. B. Narayanan, A. Kinaci, F. G. Sen, M. J. Davis, S. K. Gray, M. K. Y. Chan, and S. K. R. S. Sankaranarayanan, "Describing the Diverse Geometries of Gold from Nanoclusters to Bulk—A First-Principles-Based Hybrid Bond-Order Potential", *J. Phys. Chem. C* 120, 13787-13800 (2016).
9. B. Narayanan, K. Sasikumar, Z.-G. Mei, A. Kinaci, F. G. Sen, M. J. Davis, S. K. Gray, M. Chan, and S. K. R. S. Sankaranarayanan, "Development of a Modified Embedded Atom Force Field for Zirconium Nitride Using Multi-Objective Evolutionary Optimization", *J. Phys. Chem. C* 120, 17475–17483 (2016).
10. A. Kinaci, B. Narayanan, F. G. Sen, M. J. Davis, S. K. Gray, M. Chan, and S. K. R. S. Sankaranarayanan, "Unraveling the Planar-Globular Transition in Gold Nanoclusters through Evolutionary Search", *Scientific Reports* 6, online in November, 2016.
11. M. J. Davis, W. Liu, and R. Sivaramakrishnan, "Global Sensitivity Analysis with Small Sample Sizes: Ordinary Least Squares Approach", *J. Phys. Chem. A* 121, 553-570 (2017).

# Vibrational Spectroscopy of Transient Combustion Intermediates Trapped in Helium Nanodroplets (DE-FG02-12ER16298)

Gary E. Douberly

University of Georgia, Department of Chemistry, 1001 Cedar St., Athens, GA 30602-1546

## **Program Scope**

The objective of this research is to isolate and stabilize transient intermediates and products of prototype combustion reactions. This will be accomplished by Helium nanodroplet isolation (HENDI) spectroscopy, a novel technique where liquid helium nanodroplets freeze out high energy metastable configurations of a reacting system, permitting infrared spectroscopic characterizations of products and intermediates that result from hydrocarbon radical reactions with molecular oxygen and other small molecules relevant to combustion environments. A major aim of this work is to directly observe the elusive hydroperoxyalkyl radical (QOOH) and its oxygen adducts (O<sub>2</sub>QOOH), which are important in low temperature hydrocarbon oxidation chemistry.

## **Recent Projects**

### **Two-center Three-electron Bonding in ClNH<sub>3</sub> Revealed via Helium Droplet Infrared Laser Stark Spectroscopy: Entrance Channel Complex along the Cl + NH<sub>3</sub> → ClNH<sub>2</sub> + H Reaction**

Pyrolytic dissociation of Cl<sub>2</sub> in a newly developed, continuous-wave, SiC pyrolysis furnace was employed to dope helium droplets with single Cl atoms. Sequential addition of NH<sub>3</sub> to Cl-doped droplets leads to the formation of a complex residing in the entry valley to the substitution reaction, Cl + NH<sub>3</sub> → ClNH<sub>2</sub> + H. Infrared Stark spectroscopy in the NH stretching region reveals symmetric and antisymmetric vibrations of a C<sub>3v</sub> symmetric top. Frequency shifts from NH<sub>3</sub> and dipole moment measurements are consistent with a ClNH<sub>3</sub> complex containing a relatively strong two-center three-electron (2c-3e) bond. The nature of the 2c-3e bonding in ClNH<sub>3</sub> was explored computationally and found to be consistent with the complexation-induced blue shifts observed experimentally. Computations of interconversion pathways reveal nearly barrierless routes to the formation of this complex, consistent with the absence in experimental

spectra of two other complexes,  $\text{NH}_3\text{Cl}$  and  $\text{Cl-HNH}_2$ , which are predicted in the entry valley to the hydrogen abstraction reaction,  $\text{Cl} + \text{NH}_3 \rightarrow \text{HCl} + \text{NH}_2$ .

### **Infrared Spectroscopy of the Tropyli Radical in Helium Droplets**

The infrared spectrum of the  $X^2E_2''$  tropyli radical was recorded in the range of the CH-stretch vibrational modes using the helium droplet isolation technique. Two bands are observed at 3053 and 3058  $\text{cm}^{-1}$ . The electronic degeneracy of the ground state results in a Jahn-Teller interaction for two of the CH-stretch modes, *i.e.* first-order interaction for  $E_3'$  symmetry modes and second-order interaction for  $E_2'$  symmetry modes. The experimentally observed bands are assigned to the  $E_1'$  and the  $E_3'$  CH-stretch modes. The  $E_1'$  mode is infrared active, whereas the  $E_3'$  mode is inactive in the absence of the Jahn-Teller interaction. The transition to the upper component of the Jahn-Teller split  $E_3'$  mode gains intensity *via* vibronic coupling, giving rise to the second experimentally observed band.

### **Infrared Stark and Zeeman Spectroscopy of OH-CO: The Entrance Channel Complex along the $\text{OH} + \text{CO} \rightarrow \textit{trans}\text{-HOCO}$ Reaction Pathway**

Sequential capture and solvation of OH and CO by helium droplets leads to the exclusive formation of the OH-CO linear complex, as confirmed by IR spectroscopy in the fundamental OH stretching region. A systematic spectroscopic study is reported for the OH-CO hydroxyl stretching band near 3551  $\text{cm}^{-1}$ . The ground state rotational constant is observed to be reduced by about a factor of two in comparison to the gas-phase value. Stark spectra reveal the vibrationally averaged dipole moments in the ground and excited vibrational states to be 1.852(5) and 1.885(6) D, respectively. The computed equilibrium dipole moment at the CCSD(T)/aug-cc-pVQZ level of theory is 0.333 D larger than the experimental ground state value. Nearly 80% of this difference can be accounted for by averaging the dipole moment over the OH intermolecular bending coordinate on the  $A'$  potential surface. Zeeman spectra reveal the magnitude of  $g$ -factors to be the same as those expected for the isolated OH system, thereby indicating that, within the experimental error, neither complexation with CO nor solvation in superfluid helium results in any quenching of the orbital angular momentum.

Strongly  $J$ -dependent inhomogeneous line broadening effects are observed in the zero-field rovibrational spectrum. We have attempted to simulate this broadening *via* the application of a

model that partially accounts for the coupling of translational and rotational motion that arises from the anisotropic nature of the molecule-helium interaction potential as the impurity is displaced from the droplet's center of mass. Qualitative broadening features are reproduced, although it is not yet clear if the parameters in the model are physically reasonable, the confirmation of which will require a calculation of the (OH-CO)-(He)<sub>N</sub> interaction potential averaged over both low-lying electronic states (*A'* and *A''*).

### **Infrared Laser Spectroscopy of the *n*-propyl and *i*-propyl Radicals: Stretch-bend Fermi Coupling in the Alkyl CH Stretch Region**

The *n*-propyl and *i*-propyl radicals were generated in the gas phase *via* pyrolysis of *n*-butyl nitrite [CH<sub>3</sub>(CH<sub>2</sub>)<sub>3</sub>ONO] and *i*-butyl nitrite [(CH<sub>3</sub>)<sub>2</sub>CHCH<sub>2</sub>ONO], respectively. Nascent radicals were promptly solvated by a beam of He nanodroplets, and the infrared spectra of the radicals were recorded in the CH stretching region. Several previously unreported bands are observed between 2800 and 3150 cm<sup>-1</sup>. The CH stretching modes observed above 3000 cm<sup>-1</sup> are in excellent agreement with CCSD(T) anharmonic frequencies computed using second-order vibrational perturbation theory. However, between 2800 and 3000 cm<sup>-1</sup>, the spectra of *n*- and *i*-propyl radicals become congested and difficult to assign due to the presence of multiple anharmonic resonance polyads. To model the spectrally congested region, Fermi and Darling-Dennison resonances are treated explicitly using “dressed” Hamiltonians and CCSD(T) quartic force fields in the normal mode representation, and the agreement with experiment is less than satisfactory. Computations employing local mode effective Hamiltonians reveal the origin of the spectral congestion to be strong coupling between the high frequency CH stretching modes and the lower frequency CH<sub>*n*</sub> bending/scissoring motions. The most significant coupling is between stretches and bends localized on the same CH<sub>2</sub>/CH<sub>3</sub> group. Spectral simulations using the local mode approach are in excellent agreement with experiment.

### **Ongoing Work and Future Plans**

We have spectra and theory for the ethyl peroxy radical, and a manuscript is being prepared. We have discovered an adiabatic funneling mechanism that leads to the exclusive production of a single peroxy radical rotamer upon sequential capture of ethyl and O<sub>2</sub> and subsequent cooling *via* He atom evaporation. Now that we have a complete assignment of the CH stretch region of the

propyl radical spectra, experiments are currently being carried out to study the outcome of the sequential pick-up and reaction between propyl and O<sub>2</sub> within helium droplets. While we expect to observe the formation of propylperoxy radicals, in principle, this is the first system we have studied in which the hydroperoxypropyl radical (QOOH) is accessible via a submerged barrier below the reactant asymptote.

### **Publications acknowledging DOE support (2014-present):**

1. Christopher M. Leavitt, Christopher P. Moradi, John F. Stanton and Gary E. Douberly “Communication: Helium Nanodroplet Isolation and Rovibrational Spectroscopy of Hydroxymethylene” *Journal of Chemical Physics*, **140**, 171102 (2014). Published: May 5, 2014.
2. Bernadette M. Broderick, Laura McCaslin, Christopher P. Moradi, John F. Stanton and Gary E. Douberly “Reactive Intermediates in <sup>4</sup>He Nanodroplets: Infrared Laser Stark Spectroscopy of Dihydroxycarbene” *Journal of Chemical Physics*, **142**, 144309 (2015). Published: April 14, 2015.
3. Christopher P. Moradi and Gary E. Douberly “On the Stark Effect in Open Shell Complexes Exhibiting Partially Quenched Electronic Angular Momentum: Infrared Laser Stark Spectroscopy of OH-C<sub>2</sub>H<sub>2</sub>, OH-C<sub>2</sub>H<sub>4</sub>, and OH-H<sub>2</sub>O” *Journal of Molecular Spectroscopy*, **314**, 54-62 (2015). Published: June 22, 2015.
4. Bernadette M. Broderick, Christopher P. Moradi and Gary E. Douberly “Infrared Laser Stark Spectroscopy of Hydroxymethoxycarbene in <sup>4</sup>He Nanodroplets” *Chemical Physics Letters*, **639**, 99-104 (2015). Published: September 7, 2015.
5. Christopher P. Moradi, Changjian Xie, Matin Kaufmann, Hua Guo and Gary E. Douberly “Two-center Three-electron Bonding in ClNH<sub>3</sub> Revealed via Helium Droplet Infrared Laser Stark Spectroscopy: Entrance Channel Complex along the Cl + NH<sub>3</sub> → ClNH<sub>2</sub> + H Reaction” *Journal of Chemical Physics*, **144**, 164301 (2016). Published: April 2016.
6. Matin Kaufmann, Daniel Leicht, Martina Havenith, Bernadette M. Broderick, Gary E. Douberly “Infrared Spectroscopy of the Tropylium Radical in Helium Droplets” *Journal of Physical Chemistry A*, **120**, 6768-6773 (2016). Published: August 16, 2016.
7. Joseph T. Brice, Tao Liang, Paul L. Raston, Anne B. McCoy, Gary E. Douberly “Infrared Stark and Zeeman spectroscopy of OH-CO: The Entrance Channel Complex along the OH + CO → *trans*-HOCO Reaction Pathway” *Journal of Chemical Physics*, **145**, 124310 (2016). Published: September 2016.
8. Peter R. Franke, Daniel Tabor, Christopher P. Moradi, Gary E. Douberly, Jay Agarwal, Henry F. Schaefer, Edwin L. Sibert “Infrared Laser Spectroscopy of the *n*-propyl and *i*-propyl Radicals: Stretch-Bend Fermi Coupling in the Alkyl CH Stretch Region” *Journal of Chemical Physics*, **145**, 224304 (2016). Published: December 2016.

# Spectroscopic and Dynamical Studies of Highly Energized Small Polyatomic Molecules

Robert W. Field  
Massachusetts Institute of Technology  
Cambridge, MA 02139  
[rwfield@mit.edu](mailto:rwfield@mit.edu)

## I. Introduction

The primary aim of this research program is to develop a thorough understanding of dynamic chemical processes including isomerization, predissociation, multi-photon dissociation, and vibronic coupling. These insights are gained through the development and use of new experimental techniques, spectrum-assignment strategies, quantitative and qualitative descriptions of physical systems, and the formation and refinement of effective Hamiltonian models that describe the underlying molecular physics. Current efforts are focused on atmospherically relevant sulfur-containing compounds, such as SO<sub>2</sub>, as well as dynamical processes in acetylene, prototypical of dynamics in other molecules.

## II. Recent Progress

### A. Multi-Photon Photodissociation of Acetylene

We have recently developed a new method to study vibrational levels of the first excited singlet (S<sub>1</sub>) state of acetylene at energies above the onset of both predissociation and *trans-cis* isomerization. These highly excited vibrational levels provide information about the mechanisms of predissociation and isomerization and, more importantly, provide an excitation pathway toward the rotationally resolved spectrum of vibrational levels that will reveal details of the acetylene-vinylidene transition state on the S<sub>0</sub> potential energy surface. What started out as an annoying background fluorescence signal has turned into the most sensitive known method for exploring the high energy levels of the HCCH S<sub>1</sub> state. A one-laser, three-photon, resonance-enhanced (at the HCCH S<sub>1</sub> level) photodissociation process generates electronically excited C<sub>2</sub>\* molecules. The C<sub>2</sub>\* fluorescence is more intense than any other detection scheme we have encountered in more than 30 years of study of the acetylene S<sub>1</sub>-S<sub>0</sub> electronic transition. This process – which we've termed Photofragment Fluorescence Action Spectroscopy, or PFAS – results in a sufficiently strong signal to facilitate study of many previously unobservable regions of the acetylene S<sub>1</sub>-S<sub>0</sub> spectrum. The full analysis of these newly discovered bands is ongoing. Additionally, we expect that this method will be applicable to unsaturated hydrocarbon systems other than S<sub>1</sub>←S<sub>0</sub> acetylene, as is further discussed in the Future Work section.

### B. Investigations of the Molecular Origins of the PFAS Signals

Fluorescence signals from the photofragments, excited via three selected intermediate S<sub>1</sub> levels ( $K = 1, J = 6, e$ -symmetry levels of *trans* 3<sup>4</sup>, *trans* 3<sup>5</sup>, and *cis* 3<sup>1</sup>6<sup>1</sup> vibrational levels), have been studied, in both a flow cell and under supersonic jet conditions. In the flow cell (~3 torr), dispersed fluorescence (DF) spectra of the photofragments were obtained. For all three S<sub>1</sub> levels, we observe the C<sub>2</sub> Swan band ( $d^3\Pi_g \rightarrow a^3\Pi_u$ ) and the C<sub>2</sub> Deslandres-d'Azambuja band ( $C^1\Pi_g \rightarrow A^1\Pi_u$ ) fluorescence (Fig. 1). Both *C* and *d* states were generated with high rotational excitation (i.e. the maximum in the rotational population is around  $J=30$ ) and moderate vibrational excitation (i.e. vibrational levels with  $v=5$  and above are observed). Under supersonic-jet conditions (collision-free), fluorescence time-traces at selected wavelength regions were analyzed. We confirmed the presence of the two C<sub>2</sub> emission band systems and their relative intensities in the DF spectra. We also observed a long-lifetime visible fluorescence signal (>3 μs lifetime), likely due to emission from C<sub>2</sub>H fragments. The population ratios among the three observed fluorescing photofragments is estimated to be C<sub>2</sub>H:C<sub>2</sub>(*d*):C<sub>2</sub>(*C*) = >40:4:1. Based on the analysis of the DF spectra and the fluorescence time-traces obtained under the supersonic jet conditions, we infer that the C<sub>2</sub>H fragment was generated from one-photon photodissociation of S<sub>1</sub> acetylene, and an additional photon photolyzes the C<sub>2</sub>H fragment, producing the C<sub>2</sub> *C* and *d* states.

### C. Two-state interaction model of the C<sub>2</sub> C<sup>1</sup>Π<sub>g</sub> state

The rotation and vibration structure of the state is modeled as the result of homogenous interactions between two electronic configurations (with common  $1\sigma_g^2 1\sigma_u^2 2\sigma_g^2 2\sigma_u^2$  inner core):  $1\pi_{ux}^2 1\pi_{uy}^1 3\sigma_g^2$  and  $1\pi_{ux}^1 1\pi_{uy}^1 3\sigma_g^1 1\pi_{gx}^1$ . By fitting to the experimental *C*-state term values of both <sup>12</sup>C<sub>2</sub> and <sup>13</sup>C<sub>2</sub> isotopologues



(specifically,  $J=1, 5, 10, 15,$  and  $20$  levels of the observed vibrational states), we obtain a fit model which reproduces all of the key  $C$ -state rotation and vibration features (i.e. rapid and early convergence in the vibrational energy spacings and rotational constants) with near-spectroscopic accuracy ( $rms=1.5\text{ cm}^{-1}$ ) (Fig. 2). The model Hamiltonian is constructed in both adiabatic and diabatic rovibronic basis sets. We show that the adiabatic basis is a better representation of the  $C_2\ C^1\Pi_g$  system. Our two-state interaction model provides a framework for accurate determinations of the transition probabilities between  $C^1\Pi_g$  and  $A^1\Pi_u$  rovibrational levels. A three-state interaction model (guided by *ab initio* calculations) will be used in future modeling to improve the quality of our fit.

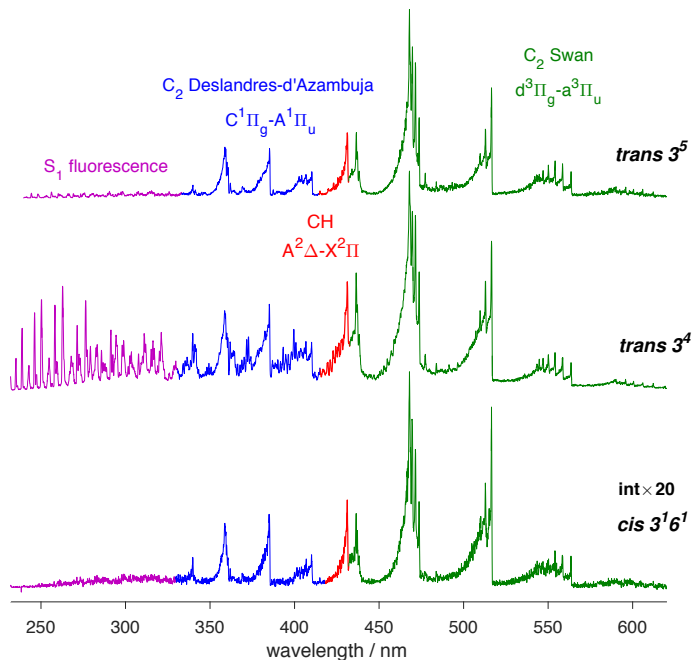


**Figure 1.** Dispersed fluorescence spectra of photodissociation products from  $K = 1, J = 6,$   $e$ -symmetry levels of  $\text{trans } 3^5$  (top),  $\text{trans } 3^4$  (middle), and  $\text{cis } 3^1 6^1$  (bottom) vibrational levels. The signal intensities are scaled to correct for the wavelength-dependent quantum yield of the PMT. The four main emission features are color-coded on each DF spectrum. The DF spectrum from the  $\text{cis } 3^1 6^1$  level is magnified  $20\times$  in order to be shown on the same intensity scale as the other two spectra.

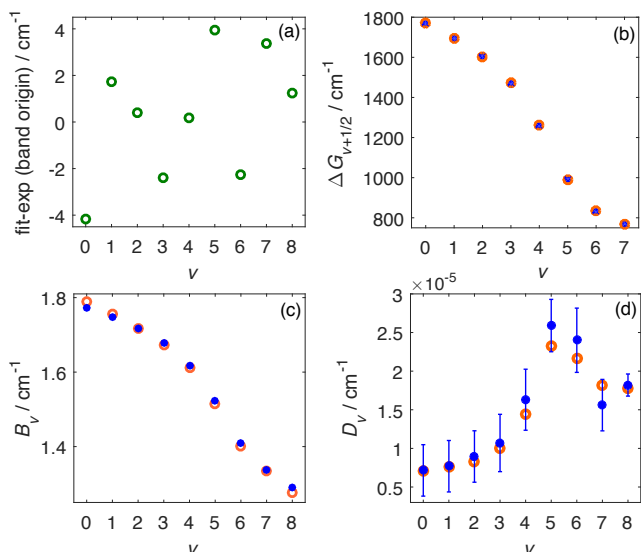


**Figure 2.** Comparison of the fit model (orange empty circles) and the experiments (blue filled circles). (a) Residuals in the band-origins. (b) Vibrational energy spacings. (c) Rotational constants. (d) Centrifugal distortion constants. Error bars in (d) are  $2\sigma$  uncertainties of the experimental values, and the error bars are too small to be visible in (b) and (c).

#### D. The Origins of Unequal S-O Bond Lengths in the $\text{SO}_2\ \tilde{C}^1B_2$ state

The  $\text{SO}_2\ \tilde{C}^1B_2$  state has a double-well structure along the antisymmetric stretch direction ( $\nu_3$ ) on the potential energy surface (PES), so it prefers non-equivalent bond lengths ( $C_s$  geometry). The double-well minimum leads to energy level-staggering along the  $\nu_3$  progression. The measured staggering pattern is consistent with a vibronic coupling model for the double-minimum, which involves direct coupling of the diabatic  $1^1B_2$  ( $\tilde{C}$ ) state to the bound  $2^1A_1$  state and indirect coupling with the repulsive  $3^1A_1$  state (Fig. 3). The

degree of staggering in the symmetry-breaking mode increases with quanta of bending excitation, consistent with the approach along the  $\tilde{C}$ -state PES to a conical intersection with the  $2^1A_1$  surface at a bond angle of  $\sim 145^\circ$ . Our work demonstrates the usefulness of low-lying vibrational level structure, where the character of the wavefunctions can be relatively easily understood, to extract information about the nature of dynamically important PES crossings that occur at much higher energy.

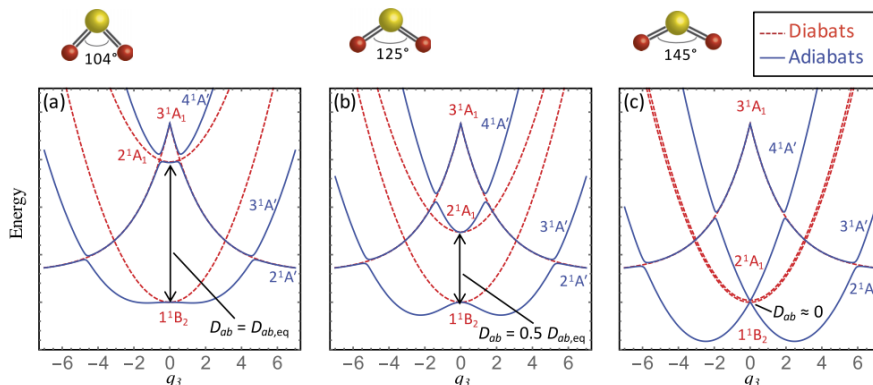


**Figure 3.** The  $q_3$ -mediated vibronic interaction between the  $1^1B_2(\tilde{C})$  state and the  $2^1A_1$  state at different bond angles. Interaction with the repulsive  $4^1A'$  state is also included. The two bound potential energy surfaces cross via a conical intersection that occurs at a bond angle of  $\sim 145^\circ$ , but the crossing is avoided at  $C_s$  geometries. Therefore, as the bond angle increases, the energy denominator for the vibronic interaction decreases and the effective barrier in the  $\tilde{C}$  state adiabatic potential energy surface (and thus the degree of staggering) increases.

### III. Future Work

We plan to demonstrate that PFAS can be applied to many molecules that contain a carbon-carbon triple bond. We have developed a spectroscopic technique, based on frequency-modulation spectroscopy, which distinguishes between lines in a spectrum that originate from upward vs. downward transitions, without any *a priori* knowledge of the spectral structure. Specifically, our current model for the mechanism that leads to strong  $C_2$  fluorescence indicates that the  $C_2$  photofragments that originate from resonant multiphoton dissociation of acetylene, cannot be initially produced in the electronic ground state of  $C_2$ . The electronically excited state of a molecule, which has a triply-bonded CC ground state, has a  $\pi^3\pi^*$  configuration, and the electronically excited states of  $C_2$  from which we observe PFAS fluorescence belong to  $\pi^3$  configurations. In contrast, the ground state of  $C_2$  has a  $\pi^4$  configuration. Our propensity rule for resonance enhanced multiphoton photodissociation of a hydrocarbon molecule requires that laser excitation from a  $\pi^3\pi^*$  parent molecule (like  $S_1$  HCCH) cannot produce a photofragment in a  $\pi^4$  configuration via -H or -H<sub>2</sub> photofragmentation. No  $C_2$  can be directly produced in its electronic ground state by resonance enhanced multiphoton dissociation of acetylene. Our frequency-modulation-based technique, then, will determine whether any  $C_2$  is directly produced in its  $\pi^4$  electronic ground state.

We are implementing a new method to gain spectroscopic access to high-lying vibrational levels of the  $S_0$  surface of acetylene, approaching energies where the onset of isomerization to vinylidene is expected to become observable. Previously, we have observed high-lying pure local-bender states with polyad number  $N_B=16$ , accessed via the  $B^4$  polyad of the  $S_1$  state. Unfortunately, transitions into higher local bender states on the  $S_0$  surface were unobservably weak from this intermediate state. Higher- $n$   $B^n$   $S_0$  polyads are predicted to have larger Franck-Condon factors for access via downward transitions out of higher energy  $S_1$  vibrational levels (e.g.  $B^6$  polyad), but are unsuitable to use as intermediates in fluorescence dip-detected SEP experiments, because predissociation significantly reduces the fluorescence quantum yield. The modified SEP scheme that we are currently exploring extends the viability of SEP to situations in which the fluorescence lifetime of the intermediate state is comparable to the duration of the DUMP pulse. The  $\sim 6$  ns duration PUMP and DUMP pulses arrive simultaneously at the sample. A significant fraction of the population transferred by

the PUMP into the intermediate level is transferred by the DUMP into the long-lived target level. When the intermediate level is short-lived (~10 ns), detectable fluorescence from that state will disappear quickly. A ~20 ns delayed PROBE pulse, at the same frequency as the DUMP pulse, transfers population from the long-lived target level back into the short-lived intermediate level, resulting in weak but detectable fluorescence against a dark background. With this method, the SEP method can be extended to reveal details of the dynamics of the transition between acetylene and vinylidene. Detailed information about the  $S_0$  acetylene-vinylidene isomerization transition state is encoded in the sequence of  $N_B=20, 22, 24$  local-bender polyads. The analysis method is similar to what we used to map the trans-cis isomerization transition state in the acetylene  $S_1$  state.

#### IV. Publications supported by this project 2015-2017

1. G. B. Park and R. W. Field, "Perspective: The first ten years of broadband chirped pulse Fourier transform microwave spectroscopy" *J. Chem. Phys.* **144**, 200901 (2016).
2. (a) G. B. Park, J. Jiang, C. A. Saladrigas and R. W. Field, "Observation of  $b_2$  symmetry vibrational levels of the  $SO_2$   $\tilde{C}^1B_2$  state: Vibrational level staggering, Coriolis interactions, and rotation-vibration constants" *J. Chem. Phys.* **144**, 144311 (2016).  
(b) J. Jiang, G. B. Park and R. W. Field, "The rotation-vibration structure of the  $SO_2$   $\tilde{C}^1B_2$  state explained by a new internal coordinate force field" *J. Chem. Phys.* **144**, 144312 (2016).  
(c) G. B. Park, J. Jiang and R. W. Field, "The origin of unequal bond lengths in the  $\tilde{C}^1B_2$  state of  $SO_2$ : Signatures of high-lying potential energy surface crossings in the low-lying vibrational structure" *J. Chem. Phys.* **144**, 144313 (2016).
3. G. Barratt Park, C. C. Womack, A. R. Whitehill, J. Jiang, S. Ono and R. W. Field, "Millimeter-wave optical double resonance schemes for rapid assignment of perturbed spectra, with applications to the  $\tilde{C}^1B_2$  state of  $SO_2$ " *J. Chem. Phys.* **142**, 144201-1 – 144201-12 (2015).
4. J. H. Baraban, P. Bryan Changala, G. C. Mellau, J. F. Stanton, A. J. Merer and R. W. Field, "Spectroscopic Characterization of Transition states" *Science* **350**, 1338-1342 (2015).
5. R. W. Field, "Spectra and Dynamics of Small Molecules, Alexander von Humboldt Lectures" Springer Heidelberg, 2015.
6. R. Fernando, C. Qu, J. Bowman, R. W. Field, and A. Suits, "Does Infrared Multiphoton Dissociation of Vinyl Chloride Yield Cold Vinylidene?" *J. Phys. Chem. Lett.* **6**(13), 2457 (2015).
7. A. H. Steeves, H. A. Bechtel, J. H. Baraban and R. W. Field, "Communication: Observation of local-bender eigenstates in acetylene," *J. Chem. Phys.* **143**, 071101 (2015).
8. G. B. Park and R. W. Field. "Edge effects in chirped-pulse Fourier transform microwave spectra", *J. Mol. Spectroscopy.* **312**, 54-57 (2015).
9. C. C. Womack, M.-A. Martin-Drumel, G. G. Brown, R. W. Field and M. C. McCarthy, "Observation of the smallest Criegee intermediate  $CH_2OO$  in the gas phase ozonolysis of ethylene", *Science Advances* **1**(2), e1400105 (2015).
10. P. B. Changala, J. H. Baraban, A. J. Merer and R. W. Field, "Probing *cis-trans* isomerization in the  $S_1$  state of  $C_2H_2$  via H-atom action and hot band-pumped IR-UV double resonance spectroscopies," *J. Chem. Phys.* **143**, 084310 (2015).
11. G. B. Park, J. H. Baraban, A. H. Steeves and R. W. Field "Simplified Cartesian basis model for intrapolyad emission intensities in the bent-to-linear electronic transition of acetylene." *Journal of Physical Chemistry A*, **2015**, 857 (2015).
12. K. Prozument, Y. V. Suleimanov, B. Buesser, J. M. Oldham, W. H. Green, A. G. Suits, R. W. Field, "A signature of roaming dynamics in the thermal decomposition of ethyl nitrite: Chirped pulse rotational spectroscopy and kinetic modeling" *J. Phys. Chem. Lett.* **5**(21), 3641-3648 (2015).
13. C. Abeysekera, L. Zack, G. B. Park, B. Joalland, J. Oldham, K. Prozument, N. Ariyasingha, I. Sims, R. Field, and A. Suits, A Chirped-Pulse Fourier-Transform Microwave /Pulsed Uniform Flow Spectrometer: II. Performance and applications for reaction dynamics," *J. Chem. Phys.* **141**(21), 214203 (2015).
14. C. Abeysekera, B. Joalland, N. Ariyasingha, L. N. Zack, I. R. Sims, R. W. Field and A. G. Suits, "Product branching in the low temperature reaction of CN with propyne by chirped-pulse microwave spectroscopy in uniform supersonic flows," *J. Phys. Chem. Lett.* **6**(9), 1599 (2015).

# Quantitative Imaging Diagnostics for Reacting Flows

Jonathan H. Frank  
Combustion Research Facility  
Sandia National Laboratories  
Livermore, CA 94551-0969  
jhfrank@sandia.gov

## Program Scope

The primary objective of this project is the development and application of quantitative laser-based imaging diagnostics for studying the interactions of fluid dynamics and chemical reactions in reacting flows. Imaging diagnostics provide temporally and spatially resolved measurements of species, temperature, and velocity distributions over a wide range of length scales. Multi-dimensional measurements are necessary to determine spatial correlations, scalar and velocity gradients, flame orientation, curvature, and connectivity. Current efforts in the Advanced Imaging Laboratory focus on studying the detailed structure of both isolated flow-flame interactions and turbulent flames. The investigation of flow-flame interactions is of fundamental importance in understanding the coupling between transport and chemistry in turbulent flames. These studies require the development of imaging diagnostic techniques to measure key species in the hydrocarbon-chemistry mechanism as well as mixture fraction, reaction rates, dissipation rates, and the velocity field. Diagnostic development includes efforts to extend measurement capabilities to a broader range of flame conditions and combustion modes and to perform three-dimensional measurements of the velocity field. A major thrust continues to be the development and application of diagnostic capabilities for measuring the temporal evolution and spatial structure of turbulent flames using high-repetition rate imaging techniques. Recent studies have focused on understanding the interaction between flames and the structure of turbulent flows using three-dimensional measurements of the velocity field.

## Recent Progress

### *Tomographic PIV measurements in turbulent flames*

We continue to develop capabilities for using tomographic particle image velocimetry (TPIV) measurements to understand the dynamics and structure of turbulence-chemistry interactions. The TPIV technique provides volumetric, three-component velocity measurements that enable determination of key fluid dynamic quantities such as vorticity and strain rate. Fluctuations in the fluid dynamic strain rate affect the progress of chemical reactions, which leads to variations in heat release rates and plays a central role in the dynamics of flame extinction and re-ignition. The heat release from chemical reactions in turn introduces changes in density, viscosity, and diffusivity that can have important effects on the turbulence. Our TPIV studies have thus far focused on the interaction of combustion with the local structure of the strain rate tensor and vorticity. Measurements of the magnitude and orientation of the eigenvectors of the strain rate tensor relative to the vorticity have provided insights into the effects of chemical heat release on vorticity production and suppression in turbulent jet flames. Studies in turbulent premixed Bunsen flames have measured the extent to which combustion heat release preferentially aligns the strain rate eigenvectors. We are currently extending investigations to other flow configurations to better understand the impact of flow shear and bulk strain on the coupling between combustion and turbulence.

### ***Piloted jet flames of dimethyl ether***

Studies of turbulent dimethyl ether (DME) flames provide insights into turbulence-chemistry interactions for an oxygenated fuel and may reveal enhanced effects of turbulent transport for intermediate species relative to methane flames. The relatively stable combustion intermediates that are formed in the rich-side chemistry during decomposition of DME could be subject to significant transport in highly turbulent flames. We have established a benchmark series of piloted partially-premixed DME/air jet flames for experiments and simulations, and recently published velocity, OH-LIF, and CH<sub>2</sub>O-LIF imaging measurements on the full series of flames. These flames form the basis of ongoing studies in our research program and that of R. Barlow. Our combined experimental capabilities provide a unique opportunity to understand turbulence-flame interactions for oxygenated fuels and to promote development of predictive models for these interactions within the framework of the TNF Workshop. Our research on DME jet flames includes collaborations with T.U. Darmstadt, U. Stuttgart, T.U. Freiberg, and Ohio State Univ. Comparisons with simulations have, so far, included large-eddy simulations (LES) that incorporated a conditional moment closure combustion model, and LES with a flamelet-progress variable approach. Overall, the LES/CMC simulations showed good agreement with the measured downstream evolution of the velocity, OH, and CH<sub>2</sub>O distributions. This result indicates that these computationally less expensive modelling approaches show promise for simulating aspects of turbulent partially-premixed DME flames. Experimentally observed intermittent gaps between the OH and CH<sub>2</sub>O distributions were captured by the LES-FPV calculations. The separation of these species varies as a function of strain rate, which is captured within the flamelet library. We continue to investigate this issue further. We plan to refine the formaldehyde LIF measurements and to further study dynamics of localized extinction and re-ignition using high-speed TPIV and LIF imaging measurements. R. Barlow has also extended Raman scattering measurement capabilities to enable direct measurement of the main hydrocarbon intermediates in DME flames.

### ***Application of large-eddy simulations to investigations of experimental uncertainty***

The growing use of imaging and high-speed diagnostics has created a need for the development of methods for coupling multi-dimensional measurements with simulations and capturing conditional statistics of turbulent flame structure and time-history effects. We are investigating methods for coupling large-eddy simulations and imaging measurements. Previously, we used companion Rayleigh scattering imaging measurements and LES calculations of passive scalar mixing in turbulent jet flows to investigate assumptions about sub-grid scale models and the combined effects of spatial and temporal averaging on the LES representation of the dissipation field at different grid cell sizes. We are currently collaborating with J. Oefelein to develop methods for quantification of uncertainties in tomographic particle image velocimetry measurements. The evaluation of TPIV measurement uncertainties in turbulent flames is particularly challenging because the 3D image reconstruction process involves solving an inherently underdetermined problem, which can result in reconstruction artifacts. The impact of these artifacts and other measurement uncertainties depend on locally fluctuating parameters, such as particle seed density, velocity gradients, and turbulence length scales. The use of data that are synthesized from LES calculations enables parametric studies of measurement uncertainties under a range of different conditions.

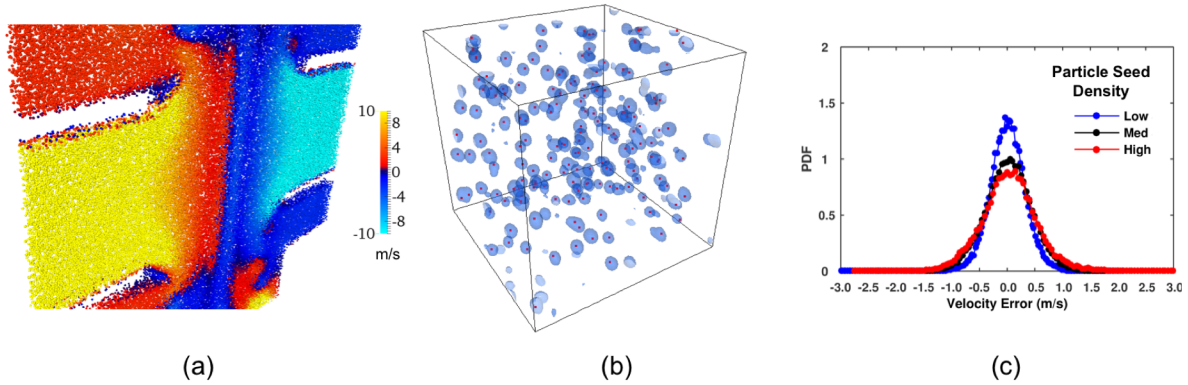


Figure 1: Synthetic TPIV experiment using LES solution of a turbulent counterflow seeded with particles (a) Synthetic particles color-coded by axial velocity. (b) Subset of 3D reconstruction of particle distribution (blue = reconstruction, red = actual particle positions), (c) PDFs of error in axial velocity as a function of particle seed density.

This approach is illustrated using LES calculations of the Yale turbulent counterflow burner to generate synthetic particle image data. The LES is performed using the RAPTOR code framework developed by J. Oefelein. The domain of the simulation is identical to the geometry of the actual counterflow burner, including the internal flow of the nozzles. The geometric details of the turbulence generating plate are fully resolved in the calculations, and boundary conditions precisely match the experimental operating conditions without the use of tuning parameters. The LES grid contains approximately 10 million cells for each nozzle with a grid spacing of  $450\ \mu\text{m}$ , which is slightly larger than the TPIV interrogation region used in the corresponding experimental configuration. To emulate the PIV methodology used in the experiment, we seed the LES calculations with particles using the Lagrangian-Eulerian approach of J. Oefelein. Figure 1a shows an example of the particles emerging from each of the counterflow nozzles with the particles color-coded by their axial velocities.

The TPIV measurements are simulated by constructing projections of synthetic particle images at the viewing angles of our four-camera TPIV experimental configuration. These synthetic TPIV data are analyzed using the same multiplicative algebraic reconstruction tomography algorithm and cross-correlation methods that are used for calculating the velocities in the experiments. A single-shot reconstructed particle distribution for a  $1.5 \times 1.5 \times 1.5\ \text{mm}^3$  subset of the domain is shown in Fig. 1b with the reconstruction in blue and the actual particle positions in red. Discrepancies between the positions of corresponding reconstructed and actual particles constitute an error in the measurement. Reconstruction artifacts are identified by instances of reconstructed particles that are not paired with a corresponding actual particle. These artifacts introduce uncertainties in the measured velocities, and their number density increases as the seed density increases. Figure 1c shows PDFs of the error in the axial velocity for simulated TPIV measurements using seed densities of 60, 120, and 180 particles per  $\text{mm}^3$ . The PDFs broaden as the seed density increases with the largest degradation occurring from the low to medium seed density. The root-mean squared (RMS) velocity error for the lowest seed density is approximately  $0.27\ \text{m/s}$ , corresponding to a displacement of approximately 0.27 voxels. We are using similar methods to analyze effects of other experimental parameters on uncertainties in velocity measurements. In general, synthetic experimental data from LES calculations of

turbulent reacting flows provide a powerful tool for systematic studies of measurement uncertainties as well as for developing new data analysis methods.

### Future Plans

The investigation of the structure and dynamics of flow-flame interactions in turbulent non-premixed, premixed, and stratified modes of combustion will remain a major thrust in our research program. In the near term, we plan to use our diagnostic capabilities to improve understanding of the interactions between combustion and the strain rate and vorticity fields. Our planned high-speed imaging effort includes optimization of TPIV analysis and further evaluation of uncertainties, methods for noise reduction, and efficient methods for analyzing large sets of imaging data in collaboration with J. Oefelein and H. Najm. These collaborations will include the development of a framework for comparing multi-dimensional measurements and simulations of turbulent flame dynamics, including analysis of time-history effects.

Diagnostics development plans include high-speed imaging with an order-of-magnitude increase in temporal resolution as well as 3D scalar imaging measurements using a custom burst-mode laser. We also plan to develop the capability for joint velocity and temperature measurements using PIV and 2-D CARS in collaboration with C. Klierer.

### BES-supported publications (2015-present)

B. Coriton, J.H. Frank, "High-speed tomographic PIV measurements of strain rate intermittency and clustering in turbulent partially premixed jet flames," *Proc. Combust. Inst.*, **35**, 1243-1250 (2015).

B. Coriton, M. Zendejdel, S. Ukai, A. Kronenburg, O.T. Stein, S-K Im, M. Gamba, J.H. Frank, "Imaging measurements and LES-CMC modeling of a partially-premixed turbulent dimethyl ether/air jet flame," *Proc. Combust. Inst.*, **35**, 1251-1258 (2015).

A.M. Steinberg, B. Coriton, J.H. Frank, "Influence of combustion on principal strain rate transport in turbulent premixed flames," *Proc. Combust. Inst.*, **35**, 1287-1294 (2015).

J. Weinkauff, P. Trunk, J. H. Frank, M.J. Dunn, A. Dreizler, B. Böhm, "Investigation of flame propagation in a partially premixed jet by high-speed stereo PIV and acetone PLIF," *Proc. Combust. Inst.*, **35**, 3773-3781 (2015).

S. Popp, F. Hunger, S. Hartl, D. Messig, B. Coriton, J. H. Frank, F. Fuest, C. Hasse, "LES flamelet-progress variable modelling and measurements of a turbulent partially-premixed dimethyl ether jet flame," *Combust. Flame*, **162**, 3016-3029 (2015).

B. Coriton, J.H. Frank, "Experimental study of vorticity-strain rate interaction in turbulent partially premixed jet flames using tomographic particle image velocimetry," *Phys. Fluids*, **28**, 025109 (2016).

B. Coriton, J.H. Frank, A. Gomez, "Interaction of turbulent premixed flames with combustion products: Role of stoichiometry," *Combust. Flame*, **170**, 37-52 (2016).

B. Coriton, J. H. Frank, "Impact of heat release on strain rate field in turbulent premixed Bunsen flames," *Proc. Combust. Inst.*, **36**, 1885-1892 (2017).

M. Kamal, B. Coriton, R. Zhou, J. H. Frank, S. Hochgreb, "Scalar dissipation rate and scales in swirling turbulent premixed flames," *Proc. Combust. Inst.*, **36**, 1957-1965 (2017).

B. Coriton, S.-K. Im, M. Gamba, J. H. Frank, "Flow Field and Scalar Measurements in a Series of Turbulent Partially-Premixed Dimethyl Ether/Air Jet Flames," *Combust. Flame*, **180** 40-52 (2017).

# Computer-Aided Construction of Chemical Kinetic Models

William H. Green  
Department of Chemical Engineering  
Massachusetts Institute of Technology  
Cambridge, MA 02139  
whgreen@mit.edu

## I. Program Scope

The combustion chemistry of even simple fuels can be extremely complex, involving hundreds or thousands of kinetically significant species. The most reasonable way to deal with this complexity is to use a computer not only to numerically solve the kinetic model, but also to construct the kinetic model in the first place. Because these large models contain so many numerical parameters (e.g. rate coefficients, thermochemistry) one never has sufficient data to uniquely determine them all experimentally. Instead one must work in “predictive” mode, using theoretical values for many of the numbers in the model, and as appropriate refining the most sensitive numbers through experiments. Predictive chemical kinetics is exactly what is needed for computer-aided design of combustion systems based on proposed alternative fuels, particularly for early assessment of the value and viability of proposed new fuels. It is also very helpful in other fuel chemistry problems, and in understanding emissions and environmental chemistry. Our research effort is aimed at making accurate predictive chemical kinetics practical; this is a challenging goal which necessarily includes a range of science advances. Our research spans a wide range from quantum chemical calculations on individual molecules and elementary-step reactions, through the development of improved rate/thermo calculation procedures, the creation of algorithms and software for constructing and solving kinetic simulations, the invention of methods for model-reduction while maintaining error control, and finally comparisons with experiment. Many of the parameters in the models are derived from quantum chemistry, and the models are compared with experimental data measured in our lab or in collaboration with others.

## II. Recent Progress

### A. Improved mechanism-construction software and algorithms

To construct an accurate chemical kinetic model, one needs:

- (1) a faithful computer representation of the chemical species
- (2) accurate values of the rate coefficients and other parameters
- (3) an efficient algorithm for identifying all the kinetically-significant species and reactions (ideally without including too many species and reactions which are *not* kinetically-significant)

All three of these requirements are quite challenging. During this past year, we focused on issues (1) and (3).

#### A.1. More flexible, higher fidelity representation of the chemical species

In the past, model-generation software could only handle the ordinary molecules where all the atoms are uncharged, the bond orders were all clearly integers or half integers, and it was obvious which of the rings were aromatic. When all these things are clear, it is relatively simple to write a faithful computer representation of all the species, and the rigidity of this framework makes it relatively straightforward to enumerate the possible chemical reactions. With this simple representation of molecules, our reaction



mechanism generator software was able to successfully model most aliphatic chemistry of CHO compounds and some organosulfur chemistry.

However, many of the reactive species formed in combustion have structures where these things are not so clear. For example, consider NO<sub>2</sub>: the resonance form where the odd electron is on an O atom has an obvious Lewis structure with all the atoms uncharged, but the form where the odd electron is on the N atom either violates the octet rule or requires including formal charges on the atoms. NO<sub>3</sub> poses similar problems, and in addition the resonance forms imply an N-O bond order that is not a half-integer. Many polycyclic aromatic and heterocyclic species pose similar challenges, and it can be difficult to identify which rings are aromatic. Molecules like SF<sub>6</sub> and SO<sub>3</sub> raise additional challenges.

To address this problem, we developed a new Reaction Mechanism Generator software package in Python (called RMG-Py) with a more flexible representation of molecules, which is aware that atoms can take on multiple valences, keeps track of formal charges and the locations of lone pairs, and allows resonance to move these electrons around. With this representation the software is able to handle most chemistry of the elements C, H, N, O, and S. The new open-source software package has been carefully documented [5], and it has been downloaded hundreds of times. In its first 10 months it has already been cited in 14 publications by other research groups.

## A.2. Fast memory-efficient algorithm for discovery of the kinetically-significant reactions

The number of possible reactions increases rapidly with average molecule size ( $N_{\text{atoms}}$ ) and the complexity of the reacting mixture ( $N_{\text{species}}$ ), scaling as  $N_{\text{species}}^2 N_{\text{atoms}}^2$ . Enumerating all of these reactions (so that they can then be tested for kinetic significance) is often very slow. We invented a method for pre-filtering the slowest bimolecular reactions and implemented it in RMG-Py.[5] Since typically most of the possible reactions are bimolecular reactions of between two low-concentration species, but these reactions are collision-rate limited, we can identify those guaranteed to be too slow to compete with the major pathways even before we work out details of their reaction mechanisms or compute their rate coefficients. We find pre-filtering reduces the CPU time required to construct our models by about an order of magnitude.

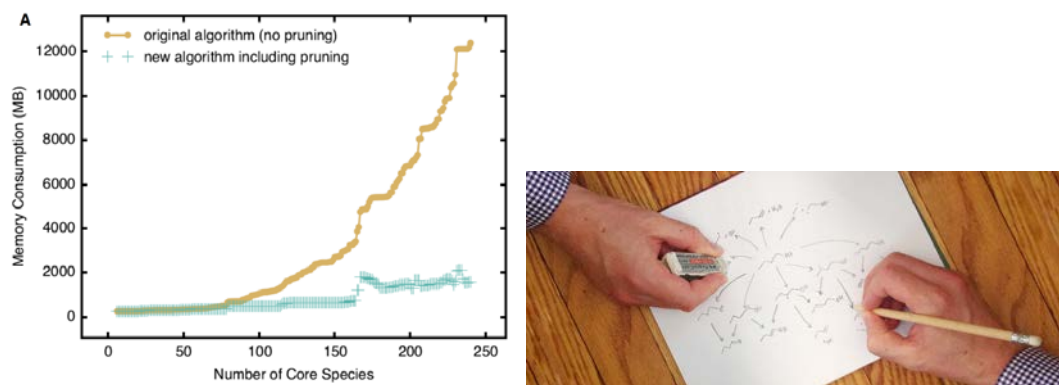


**Fig. 1** Memory consumption comparison with and without applying pruning. The algorithm erases negligible species and reaction pathways during the process of writing out the full reaction network.

However, with this CPU speed up, the rate-construction process now more quickly becomes memory-limited. Most of the memory is taken by storing the structures of the hundreds of thousands of byproduct species. To reduce this memory limitation, we developed a method [9] for rapidly identifying which byproducts are produced so slowly they can be safely pruned out of the reaction network without affecting the predictions for any of the kinetically significant species, and we apply this pruning during

the model construction process, Fig. 1. This new screen reduces memory requirements by about an order of magnitude, allowing us to build models containing about 3x more important species than was possible previously on the same hardware. This new capability opens the possibility of discovering unexplored reaction networks and modeling more complicated reacting systems. This is quite important for accurately modeling ignition chemistry and polycyclic aromatic chemistry, since in those situations there are a large number of kinetically-significant species.

## B. Organonitrogen in automatic reaction mechanism generation

Nitrogen chemistry is important in understanding the behavior of many combustion systems. Examples include nitrogenous fuel additives (e.g., cetane number improvers), fuel-bound nitrogen in biofuels, and  $\text{NO}_x$  formation and abatement. These recent enhancements to RMG-Py made it the first software to automatically generate mechanisms that describe nitrogen chemistry in combustion. The various enhancements made to RMG-Py in this perspective include: defining nitrogen atom type representation, adding ring strain thermodynamic corrections, adding new kinetic and thermodynamic libraries, improving reaction family rate rules, adding nitrogen-specific resonance structures, and adding group frequencies for pressure-dependent network generation. More specifically, atom types in RMG-Py are used while deriving kinetic rate rules and estimating thermodynamic data. The defined nitrogen atom types classify nitrogen atoms by valence and type of chemical bonds. A set of rules was defined for transitions between the different atom types while a reaction recipe ‘action’ is applied (e.g., adding a radical, breaking a bond, decreasing an electron lone pair, etc.).

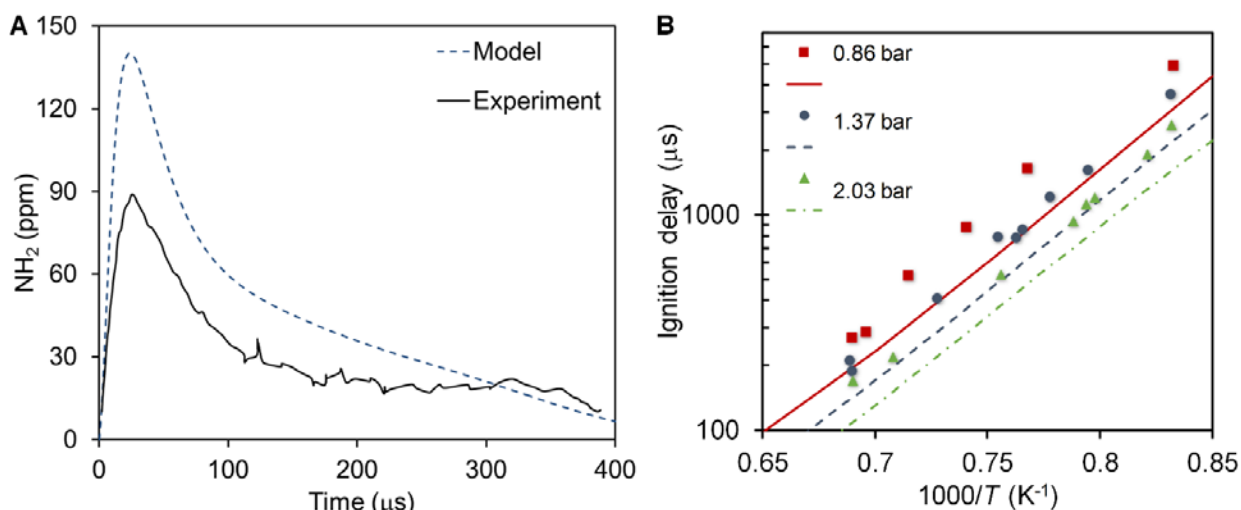


**Fig. 2** Experimental values (from Hanson group) and RMG-Py model predictions comparison for an ethylamine oxidation system. (A) concentration profiles of  $\text{NH}_2$  for 2000 ppm EA and 8000 ppm  $\text{O}_2$  in Ar at 1441 K and 2.13 bar, (B) ignition delay times for 1% EA and 4%  $\text{O}_2$  in Ar for three pressures. Symbols – experimental data, lines – simulated values.

This new version of RMG-Py has been tested by generating a detailed pyrolysis and oxidation mechanism for ethylamine ( $\text{CH}_3\text{CH}_2\text{NH}_2$ ), which is a model fuel-bound nitrogen biofuel molecule. Validation of the reaction network with recent experimental data showed that the generated model successfully reproduced the experimentally-observed species  $\text{NH}_2$  (Fig. 2 A) and OH (not shown), as well as ignition delay measurements at different pressures (Fig. 2 B).

### III. Future Plans

We are currently using this new capability to predict the chemistry of combustion systems containing both SO<sub>x</sub> and NO<sub>x</sub>; these two chemistries interact leading to the formation of sulfuric acid in some power plant exhaust systems. Our new capability to build detailed kinetic models for systems containing both N and S will be helpful in designing new CO<sub>2</sub> capture systems avoiding known problems due to SO<sub>x</sub> in the CO<sub>2</sub> stream, and also for predicting particulate emissions.

We are also developing better methods for handling molecules with fused cyclics, so that we can more accurately model the chemistry leading up to soot formation, and also handle jet fuels which contain these species.

Finally, we are developing improved methods for handling coupled hindered rotors, to more accurately compute the entropies and A factors of reactions for molecules containing several C-C or C-O single bonds.

### IV. Publications and submitted journal articles supported by BES 2015-2017

1. A. Fridlyand, S.S. Goldsborough, K. Brezinsky, S.S. Merchant, and W.H. Green, "Influence of the Double Bond Position on the Oxidation of Decene Isomers at High Pressures and Temperatures", *Proceedings of the Combustion Institute* **35**, 333-340 (2015).
2. Connie W. Gao, Aaron Vandeputte, Nathan W. Yee, William H. Green, Robin E. Bonomi, Gregory R. Magoon, Hsi-Wu Wong, Oluwayemisi O. Oluwole, David K. Lewis, Nick M. Vandewiele, and Kevin Van Geem, "JP-10 combustion studied with shock tube experiments and modeled with automatic reaction mechanism generation", *Combustion & Flame* **162**, 3115-3129 (2015).
3. Zachary J. Buras, Enoch E. Dames, Shamel S. Merchant, Guozhu Liu, Rehab M.I. Elsamra and William H. Green, "Kinetics and Products of Vinyl + 1,3-Butadiene, a Potential Route to Benzene" *Journal of Physical Chemistry A* **119**, 7325-7338 (2015).
4. Shamel S. Merchant, C. Franklin Goldsmith, Aaron G. Vandeputte, Michael P. Burke, Stephen J. Klippenstein, and William H. Green, "Understanding low-temperature first-stage ignition delay: Propane", *Combustion & Flame* **162**, 3658-3673 (2015).
5. Connie W. Gao, Joshua W. Allen, William H. Green, and Richard H. West, "Reaction Mechanism Generator: Automatic Construction of Chemical Kinetic Mechanisms", *Computer Physics Communications* **203**, 212-225 (2016). <http://dx.doi.org/10.1016/j.cpc.2016.02.013>
6. Rehab M.I. Elsamra, Amrit Jalan, Zachary J. Buras, Joshua E. Middaugh, and William H. Green, "Temperature and Pressure Dependent Kinetics of CH<sub>2</sub>OO + CH<sub>3</sub>COCH<sub>3</sub> and CH<sub>2</sub>OO + CH<sub>3</sub>CHO: Direct Measurements and Theoretical Analysis", *International Journal of Chemical Kinetics* **48**, 474-488 (2016).
7. Enoch E. Dames and William H. Green, "The effect of alcohol and carbonyl functional groups on the competition between unimolecular decomposition and isomerization in C<sub>4</sub> and C<sub>5</sub> alkoxy radicals", *Int. J. Chem. Kinet.* **48**, 544-555 (2016). <http://dx.doi.org/10.1002/kin.21015>
8. Alon Grinberg Dana, Soumya Gudiyella, William H. Green, Santosh J. Shanbhogue, Dan Michaels, Nadim W. Chakroun, and Ahmed Ghoniem. "Automated Generation of Chemical Mechanisms for Predicting Extinction Strain Rates with Applications in Flame Stabilization and Combustion Instabilities", 55th AIAA Aerospace Sciences Meeting, AIAA SciTech Forum, (AIAA 2017-0835) <http://dx.doi.org/10.2514/6.2017-0835>
9. Kehang Han, William H. Green, and Richard H. West, "On-the-Fly Pruning for Rate-Based Reaction Mechanism Generation", *Computers and Chemical Engineering* **100**, 1-8 (2017). <http://dx.doi.org/10.1016/j.compchemeng.2017.01.003>

# Gas-Phase Molecular Dynamics: High Resolution Spectroscopy and Collision Dynamics of Transient Species

Gregory E. Hall  
Chemistry Division, Brookhaven National Laboratory  
Upton, NY 11973-5000  
[gehall@bnl.gov](mailto:gehall@bnl.gov)

## Program Scope

This research is carried out as part of the Gas-Phase Molecular Dynamics program in the Chemistry Division at Brookhaven National Laboratory. Chemical intermediates in the elementary gas-phase reactions involved in combustion chemistry are investigated by high resolution spectroscopic tools. Production, reaction, and collisional energy transfer processes are investigated by transient, double resonance, polarization and saturation spectroscopies, with an emphasis on technique development and connections with theory.

## Recent Progress

### A. Single detector, dual-beam balanced detection for supercontinuum FTIR

In a project to explore applications of mode locked fiber lasers and the broadband supercontinuum sources derived from them, we have developed and demonstrated a method for combining commercial FTIR instrumentation with supercontinuum sources. The spatial coherence, brightness, and ease of focusing encourage the use of supercontinuum sources for a variety of illumination and spectroscopic applications. When used directly as a source for absorption spectroscopy, these advantages are tempered by some disadvantages to be overcome related to fluctuations, both in the total intensity and variations in spectral content. Fluctuation noise is particularly pernicious in Fourier Transform Spectrometry (FTS), leading to a multiplex disadvantage, where multiplicative source noise appears on all resolved spectral detection channels simultaneously, in contrast to additive detector noise that is effectively divided among all detection channels. Therefore, minimizing or correcting for source fluctuations should be given high priority.

We have demonstrated a method of combining a supercontinuum light source with a commercial Fourier transform spectrometer, using a novel approach to dual-beam balanced detection, implemented with phase-sensitive detection on a single light detector.<sup>1</sup> A 40 dB reduction in the relative intensity noise is achieved for broadband light, analogous to conventional balanced detection methods using two matched photodetectors. Unlike conventional balanced detection, however, this method exploits the time structure of the broadband source to interleave signal and reference pulse trains in the time domain, recording the broadband differential signal at the fundamental pulse repetition frequency of the supercontinuum. The method is capable of real-time correction for instability in the supercontinuum spectral structure over a broad range of wavelengths and is compatible with commercially designed spectrometers. A proof-of-principle experimental setup has been demonstrated for weak absorption in the 1500-1600 nm region. This method is a good match for sensitive measurement of weak signals such as those encountered in surface reflection/attenuation methods, where the baseline stability and

reproducibility limits the detectable signals, and when aggressive pathlength multiplication by multipass or cavity methods is less practical than for gas or liquid samples.

## **B. Photodissociation Dynamics in NO-Rare gas complexes**

The weakly bound complex of the free radical NO with rare gases undergoes a particularly simple type of molecular photodissociation, producing electronically excited NO (*A*) and an unbound rare gas atom when excited at energies slightly above the energy of the *A-X* transition in diatomic NO. The excitation to a repulsive region of the upper state leads to a direct dissociation with a mostly unstructured excitation spectrum with a width of a few hundred  $\text{cm}^{-1}$ . The apparent simplicity made it surprising to find dramatic energy-dependent variations in the fragment angular distributions as well as the rotational state distributions, when comparing NO-He, NO-Ne and NO-Ar in recent experiments by Australian colleagues at Flinders University.<sup>2</sup> Two-dimensional,  $J=0$ , time-dependent wavepacket calculations performed by BNL colleague H.-G. Yu account very well for the excitation spectra, including resonance structures close to the dissociation threshold, and experimental rotational state distributions, which display a rotational rainbow structure in the case of NO-Ar and NO-Ne, but not in the case of NO-He. The distinctive and unexpected energy-dependent variation in the NO angular distributions can be qualitatively explained with an approximate Franck-Condon model in an axial recoil limit.<sup>2</sup>

A rigorous quantum mechanical treatment requires methods that include the rotational coordinates, the electronic degeneracy of the floppy ground state complex, as well as a dynamical treatment that does not rely on the axial recoil approximation. The simplicity of a  $^1\text{S}$  atom and a  $^2\Sigma$  state of the vibrationally inactive diatomic co-fragment removes most other complexity from the problem. Substantial progress along these lines has been made in a continuing collaboration with Hua-Gen Yu, Gabriel Balint-Kurti (U. Bristol), and Tomás González Lezana (CSIC, Madrid).

## **Future Work**

### **A. Nonthermal kinetics in a vibronically mixed free radical: $\text{C}_2\text{H}$**

Reactions of the ethynyl radical,  $\text{C}_2\text{H}$ , contribute to the mechanisms of rich fuel oxidation, and have been extensively studied, often by kinetic spectroscopy following photolytic generation of  $\text{C}_2\text{H}$  from precursors  $\text{C}_2\text{H}_2$  or  $\text{CF}_3\text{C}_2\text{H}$ . In the presence of a large excess of inert gas, there is general agreement on the thermal rate constants for many reactions of  $\text{C}_2\text{H}$ . At reduced pressures of nonreactive gases, the reaction rates compete with thermalization and state-dependent kinetics can be observed.<sup>3</sup> As described by T. Sears in this abstract book, we have recently obtained spectra of  $\text{C}_2\text{H}$  in the  $7000\text{ cm}^{-1}$  region, some of the strongest bands in the spectrum, corresponding to nominally vertical transitions between the vibronically mixed *X* and *A* states of  $\text{C}_2\text{H}$ .<sup>3</sup> The region is rich with hot band transitions, some of which have been assigned, and more that we hope to assign in the near future, with the assistance of computational guidance,<sup>4</sup> previous LIF measurements,<sup>5</sup> and distinctive kinetic signatures for states of different internal energy.

The  $\text{C}_2\text{H} + \text{H}_2 \rightarrow \text{H} + \text{C}_2\text{H}_2$  reaction occurs in a region of the global  $\text{C}_2\text{H}_3$  potential surface(s), which has already received extensive theoretical study upon which our work can build.<sup>6, 7</sup> The temperature dependent thermal rate constant increases steeply at elevated temperatures, but with a non-Arrhenius behavior that has been fit to the expression:<sup>6</sup>

$$k(T) = 3.92 \times 10^{-19} T^{2.57 \pm 0.30} \exp[-(130 \pm 140)K/T] \text{ cm}^3 \text{ molec}^{-1} \text{ s}^{-1}$$

The degree to which the presence of the C<sub>2</sub>H A-state surface affects the behavior is an open question. The strong mixing of *A* and *X* character in the vibronic eigenstates may make it impossible in principle to treat the *A* and *X* states as kinetically distinct species, as discussed by Wittig and co-workers<sup>8</sup> in the context of infrared fluorescence quenching from excited C<sub>2</sub>H. Time dependent populations in a selection of vibronic levels during the collisional relaxation and reaction will provide an experimental record more complete and distinctive than our preliminary measurements with the ground state and an unassigned hot band transition, for the reaction of C<sub>2</sub>H with its precursor. Theoretical comparisons will require multiple surface reaction calculations for selected vibronic states of C<sub>2</sub>H, combined with master equation modeling of the evolving internal energy distributions.

## B. Velocity-changing collisions and sub-Doppler saturation in CN radicals

Combined effects of velocity-dependent collision rates and velocity-changing elastic collisions play a key role in pressure-dependent line shapes of linear absorption and sub-Doppler saturation spectra. We have combined experimental studies of pressure broadening and narrowing<sup>9</sup> and Doppler-resolved recovery kinetics following broadband saturation<sup>10</sup> with studies of sub-Doppler saturation spectra<sup>11</sup> and recovery kinetics, all on the CN(*X*) + Ar and CN(*A*) + Ar collision systems. Accurate potential energy surfaces are available and the relevant quantum scattering cross sections have been computed by P. Dagdigian for comparison with the experiments. Two-color saturation spectroscopy and the collisional recovery from sub-Doppler saturation provide incisive probes to untangle the collisional effects responsible for line shapes, with validation derived from Monte Carlo solutions of the Boltzmann equation, using realistic total and differential cross sections for elastic scattering and energy-dependent cross sections for total inelastic collisions.

For typical thermal energy Ar + CN collisions, the elastic scattering is very strongly peaked in the forward direction, with most likely center-of-mass deflection angles near 1 degree, and these collisions occur with a total probability 5-10 times higher than rotationally inelastic collisions, depending on the rotational state and (not so much) on the collision energy. With constant narrow-band pumping, a steady-state is achieved within the time required for a few inelastic collisions. The steady-state tagged molecules have not yet had their first hard, inelastic collision since their Doppler tagging, yet have suffered multiple soft collisions, collectively spreading their lab-frame Doppler distribution away from the initially selected sharp value, but still far from fully thermalized. The transient broadening of the time-resolved sub-Doppler saturation spectra reflects this limited velocity diffusion, occurring on the timescale of inelastic collisions. When the bleach laser is abruptly extinguished, the steady-state sub-Doppler line shape broadens further with continuing elastic velocity-changing collisions, while the integrated area of the saturation signal relaxes at the rate of inelastic collisions. This is seen as a faster saturation recovery rate at the peaks than the wings of the sub-Doppler spectra. Quantitative modeling of the observed spectra and kinetics will include this essentially exact numerical treatment of the evolution of the velocity-space ensembles, combined with a velocity-resolved relaxation rate, contributing a pressure-dependent, additional lifetime broadening of each Doppler component at increasing pressures, when the collision rate is fast enough to additionally broaden the tagged and evolving Doppler spectrum.

## Publications supported by this project since 2015

- Quadrupole splittings in the near-infrared spectrum of  $^{14}\text{NH}_3$ , S. Twagirayezu, G. E. Hall and T. J. Sears, *J. Chem. Phys.* **145**, 144302 (2016). <http://dx.doi.org/10.1063/1.4964484>
- Supercontinuum Fourier transform spectrometry with balanced detection on a single photodiode, V. V. Goncharov and G. E. Hall, *J. Chem. Phys.* **145**, 084201 (2016). <http://dx.doi.org/10.1063/1.4961655>
- The near-infrared spectrum of ethynyl radical, A. T. Le, G. E. Hall, and T. J. Sears, *J. Chem. Phys.* **145**, 074306 (2016). <http://dx.doi.org/10.1063/1.4961019>
- Rotational and angular distributions of NO products from NO-Rg (Rg = He, Ne, Ar) complex photodissociation, H. L. Holmes-Ross, R. J. Valenti, Hua-Gen Yu, G. E. Hall and W. D. Lawrance, *J. Chem. Phys.* **144**, 044309 (2016). <http://dx.doi.org/10.1063/1.4940690>
- Application of the Hartmann–Tran profile to precise experimental data sets of  $^{12}\text{C}_2\text{H}_2$ . Forthomme, M. J. Cich, S. Twagirayezu, G. E. Hall and T. J. Sears, *J. Quant. Spectrosc. Rad. Trans.* **165** 28-37 (2015). <http://dx.doi.org/10.1016/j.jqsrt.2015.06.013>
- Frequency-comb referenced spectroscopy of  $\nu_4$ - and  $\nu_5$ -excited hot bands in the 1.5  $\mu\text{m}$  spectrum of  $\text{C}_2\text{H}_2$  S. Twagirayezu, M. J. Cich, T. J. Sears, C. P. McRaven, G. E. Hall, *J. Molec. Spectrosc.* **316**, 64-71 (2015). <http://dx.doi.org/10.1016/j.jms.2015.06.010>
- Doppler-Resolved Kinetics of Saturation Recovery, D. Forthomme, M. L. Hause, H.-G. Yu, P. J. Dagdigian, T. J. Sears and G. E. Hall, *J. Phys. Chem. A* **119** 7439-7450 (2015). <http://dx.doi.org/10.1021/acs.jpca.5b00628>

## References cited

- [1] V. V. Goncharov, and G. E. Hall, *J. Chem. Phys.* **145**, 084201 (2016).
- [2] H. L. Holmes-Ross, R. J. Valenti, H.-G. Yu, G. E. Hall, and W. D. Lawrance, *J. Chem. Phys.* **144**, 044309 (2016).
- [3] A. T. Le, G. E. Hall, and T. J. Sears, *J. Chem. Phys.* **145**, 074306 (2016).
- [4] R. Tarroni, and S. Carter, *Mol. Phys.* **102**, 2167 (2004).
- [5] W.-Y. Chiang, and Y.-C. Hsu, *J. Chem. Phys.* **111**, 1454 (1999).
- [6] J. Peeters, B. Ceursters, H. M. T. Nguyen, and M. T. Nguyen, *J. Chem. Phys.* **116**, 3700 (2002).
- [7] L. Y. Chen, K. J. Shao, J. Chen, M. H. Yang, and D. H. Zhang, *J. Chem. Phys.* **144**, 194309 (2016).
- [8] F. Shokoohi, T. A. Watson, H. Reisler, F. Kong, A. M. Renlund, and C. Wittig, *J. Phys. Chem.* **90**, 5695 (1986).
- [9] D. Forthomme, C. P. McRaven, T. J. Sears, and G. E. Hall, *J. Phys. Chem. A* **117**, 50 (2013).
- [10] D. Forthomme, M. L. Hause, H. G. Yu, P. J. Dagdigian, T. J. Sears, and G. E. Hall, *J. Phys. Chem. A* **119**, 7439 (2015).
- [11] D. Forthomme, C. P. McRaven, T. J. Sears, and G. E. Hall, *J. Mol. Spectrosc.* **296**, 36 (2014).

# Flame Chemistry and Diagnostics

Nils Hansen

*Combustion Research Facility, Sandia National Laboratories, Livermore, CA 94551-0969*

Email: nhansen@sandia.gov

## SCOPE OF THE PROGRAM

In this program, we seek to understand the detailed chemistry of combustion through a unique scheme of diagnostics development and experimental studies of simple flames. Our goal is to provide reliable experimental data on the chemical composition of laboratory-scale model flames and reactors through state-of-the-art diagnostics. The experiments are designed to serve as benchmarks for the development and validation of detailed chemical kinetic models. In particular, we study the composition of laminar premixed flames, which are stabilized on a flat-flame burner under a reduced pressure of ~15-30 Torr, of laminar opposed-flow diffusion flames at low and atmospheric pressure, and of a jet-stirred reactor that is also operated near atmospheric pressure. We employ mass spectrometry and our experimental data in the form of species identification and quantification serve as stringent tests for the development and validation of any detailed chemical kinetic mechanisms. Over the past years, the overall objective of this program has been to elucidate the chemistry of soot precursors and the formation of unwanted byproducts in incomplete combustion in flames fueled by hydrocarbons and oxygenates. Studying this complex combustion chemistry with an unprecedented level of detail requires determining the chemical structures and concentrations of species sampled from sooting or nearly-sooting model flames. Using the jet-stirred reactor we study the low-temperature oxidation chemistry of selected hydrocarbon and oxygenated fuels.

## PROGRESS REPORT

**Dimethyl ether (DME) Low-Temperature Oxidation in a Jet-Stirred Reactor:** In collaboration with the groups of Jasper (Argonne), Sarathy (KAUST), Dagaut (Orleans), Taatjes (Sandia), and Kohse-Höinghaus (Bielefeld) we reported the quantification of the keto-hydroperoxide hydroperoxymethyl formate (HPMF) and other partially oxidized intermediate species arising from the low-temperature (540 K) oxidation of dimethyl ether (DME) and compared them to up-to-date kinetic modeling results. Special emphasis was paid towards the validation and application of a theoretical method for determining unknown photoionization cross sections for hydroperoxide species. This approach enabled a scientifically-based quantification of the keto-hydroperoxide  $\text{HOOCH}_2\text{OCH}_2\text{O}$  and revealed new opportunities for the development of a next-generation DME combustion chemistry model.

**Aromatic ring formation in opposed-flow diffusive 1,3-butadiene flames:** The chemical structures of two different 1,3- $\text{C}_4\text{H}_6/\text{Ar}-\text{O}_2/\text{Ar}$  flames were explored using flame-sampling molecular-beam mass



spectrometry with both electron and single-photon ionization. Mole fraction profiles of 47 components are reported as function of distance from the fuel outlet and compared to chemically detailed modeling results that were provided by the group of F. Mauss (University of Cottbus, Germany). In particular, benzene was found to be formed mainly via fulvene through the reactions of the  $C_4H_5$  isomers with  $C_2H_2$ . The *n*- $C_4H_5$  radical reacts with  $CH_3$  forming 1,3-pentadiene ( $C_5H_8$ ), which is subsequently oxidized to form the naphthalene precursor cyclopentadienyl ( $C_5H_5$ ). Oxidation of naphthalene is predicted to be a contributor to the formation of phenylacetylene ( $C_8H_6$ ), indicating that consumption reactions can be of similar importance as molecular growth reactions.

#### **The Influence of *iso*-Butanol Addition to the Chemistry of Premixed 1,3-Butadiene Flames:**

Chemical structures of three low-pressure premixed flames of 1,3-butadiene/*i*-butanol mixtures with different ratios of 1,3-butadiene and *i*-butanol were investigated experimentally with flame-sampling molecular-beam mass spectrometry and numerically by chemically detailed modeling provided by the DLR (Stuttgart, Germany). It is shown, by referring to both experimental and modeling results, that the concentration of benzene depends on the amount of 1,3-butadiene in the fuel mixture, indicating that *i*-butanol chemistry is not adding significantly towards aromatic ring formation. Trends in the concentration of other intermediates can also be largely predicted based on the established oxidation of 1,3-butadiene and *i*-butanol, thus revealing no detectible cross-linkages between the intermediate pools of the individual fuel components.

#### **2D-Imaging of Sampling-Probe Perturbations in Laminar Premixed Flames using Kr X-ray**

**Fluorescence:** In a collaborative effort with the groups of Tranter and Kastengren (both Argonne), the perturbation of the temperature field caused by a quartz sampling probe has been investigated in a fuel-rich low-pressure premixed ethylene/oxygen/argon/krypton flame using X-ray fluorescence. Distortions of up to 1000 K of the burner-probe centerline flame temperature were found with the tip of the probe in the preheat zone and distortions of up to 500 K were observed with it in the reaction and postflame zones. Furthermore, perturbations of the temperature field have been revealed that reach radially as far as 20 mm from the burner-probe centerline and about 3 mm in front of the probe tip. These results clearly reveal the limitations of one-dimensional models for predicting flame-sampling experiments.

## **OUTLOOK**

**Low-Temperature Oxidation in a Jet-Stirred Reactor:** We will continue to explore the reaction network of low-temperature oxidation processes by using the above mentioned jet-stirred reactor with molecular-beam sampling capabilities. Our work on DME will be complemented with efforts to provide new insights into the oxidation of tetrahydrofuran, *n*- and *neo*-pentane. New information in the form of species identification and mole fraction profiles is critically needed to improve their respective

combustion chemistry models. Preliminary mass spectra were recorded and the data reduction, *i.e.* species identification and quantification, is currently in progress.

**Experimental Studies on the Molecular-Growth Chemistry of Soot Precursors in Combustion Environments:** PAH formation chemistry will be studied by analyzing the detailed chemical structures of laminar, premixed or opposed-flow flames. The data is expected to provide guidance and benchmarks needed to improve and test theoretical models describing soot-formation chemistry with predictive capabilities. Work on flames fueled by the C<sub>5</sub> fuels *n*-pentane, 1-pentene, and 2-methyl-2-butene is currently in progress.

**2D-Imaging of Sampling-Probe Perturbations in Laminar Premixed Flames using Kr X-ray Fluorescence:** We will expand our efforts to quantify the probe effects varying the flame conditions and the probe design.

#### **PUBLICATIONS ACKNOWLEDGING BES SUPPORT 2015-PRESENT**

1. A. Nawdiyal, N. Hansen, T. Zeuch, L. Seidel, F. Mauß, “Experimental and Modelling Study of Speciation and Benzene Formation Pathways in Premixed 1-Hexene Flames”, *Proc. Combust. Inst.*, **2015**, 35(1), 325-332.
2. N. Hansen, M. Braun-Unkhoff, T. Kathrotia, A. Lucassen, B. Yang, “Understanding the Reaction Pathways in Premixed Flames Fueled by Blends of 1,3-Butadiene and n-Butanol”, *Proc. Combust. Inst.*, **2015**, 35(1), 771-778.
3. A. Lucassen, S. Park, N. Hansen, S.M. Sarathy, “Combustion Chemistry of Alcohols: Experimental and Modeled Structure of a Premixed 2-Methylbutanol Flame”, *Proc. Combust. Inst.*, **2015**, 35(1), 813-820.
4. M. Schenk, N. Hansen, H. Vieker, A. Beyer, A. Gölzhäuser, K. Kohse-Höinghaus, “PAH Formation and Soot Morphology in Flames of C<sub>4</sub> Fuels”, *Proc. Combust. Inst.*, **2015**, 35(2), 1761-1769.
5. D. Felsmann, K. Moshhammer, J. Krüger, A. Lackner, A. Brockhinke, T. Kasper, T. Bierkandt, E. Akyildiz, N. Hansen, A. Lucassen, P. Oßwald, M. Köhler, G.A. Garcia, L. Nahon, P. Hemberger, A. Bodi, T. Gerber, K. Kohse-Höinghaus, “Electron Ionization, Photoionization and Photoelectron/Photoion Coincidence Spectroscopy in Mass-Spectrometric Investigations of a Low-Pressure Ethylene/Oxygen Flame”, *Proc. Combust. Inst.*, **2015**, 35(1), 779-786.
6. K. O. Johansson, J. Y. W. Lai, S. A. Skeen, K. R. Wilson, N. Hansen, A. Violi, H. A. Michelsen, “Soot Precursor Formation and Limitations of the Stabilomer Grid”, *Proc. Combust. Inst.*, **2015**, 35(2), 1819-1826.
7. K. Moshhammer, A. Lucassen, C. Togbé, K. Kohse-Höinghaus, N. Hansen, “Formation of Oxygenated and Hydrocarbon Intermediates in Premixed Combustion of 2-Methylfuran”, *Z. Phys. Chem.*, **2015**, 229(4), 507-528.
8. H. Selim, S. Mohamed, A. Lucassen, N. Hansen, S. M. Sarathy, “Effect of the Methyl Substitution on the Combustion of Two Methylheptane Isomers: Flame Chemistry Using VUV Photoionization Mass Spectrometry”, *Energy Fuels*, **2015**, 29(4), 2696-2708.
9. O. P. Korobeinichev, I. E. Gerasimov, D. A. Knyazkov, A. G. Shmakov, T. A. Bolshova, N. Hansen, C. K. Westbrook, G. Dayma, B. Yang, “An Experimental and Kinetic Modeling Study of Premixed Laminar Flames of Methyl Pentanoate and Methyl Hexanoate”, *Z. Phys. Chem.*, **2015**, 229(5), 759-780.
10. K. Moshhammer, A. W. Jasper, D. M. Popolan-Vaida, A. Lucassen, P. Dievart, H. Selim, Hatem, A. J. Eskola, C. A. Taatjes, S. R. Leone, S. M. Sarathy, Y. Ju, P. Dagaut, K. Kohse-Höinghaus, N. Hansen, “Detection and Identification of the Keto-Hydroperoxide (HOCH<sub>2</sub>OCHO) and other Intermediates during Low-Temperature Oxidation of Dimethyl Ether”, *J. Phys. Chem. A*, **2015**, 119(28), 7361-7374.
11. I. W. Ekoto, S. A. Skeen, R. R. Steeper, N. Hansen, “Detailed Characterization of Negative Valve Overlap Chemistry by Photoionization Mass Spectrometry”, *SAE International Journal of Engines*, **2015**, 9 (2015-01-1804), 20159013.

12. W. Sun, N. Hansen, C. K. Westbrook, F. Zhang, G. Wang, K. Moshhammer, C. K. Law, B. Yang, "An Experimental and Kinetic Modeling Study on Dimethyl Carbonate (DMC) Pyrolysis and Combustion", *Combust. Flame*, **2016**, 164(2), 224-238.
13. Z. Wang, L. Zhang, K. Moshhammer, D. M. Popolan-Vaida, V. S. B. Shankar, A. Lucassen, C. Hemken, C. A. Taatjes, S. R. Leone, K. Kohse-Höinghaus, N. Hansen, P. Dagaut, S. M. Sarathy, "Additional Chain-Branching Pathways in the Low-Temperature Oxidation of Branched Alkanes", *Combust. Flame*, **2016**, 164(2), 386-396.
14. B. Wolk, I. Ekoto, W. F. Northrop, K. Moshhammer, N. Hansen, "Detailed Speciation and Reactivity Characterization of Fuel-Specific In-Cylinder Reforming Products and the Associated Impact on Engine Performance", *Fuel*, **2016**, 185, 348-361.
15. K. Moshhammer, A. W. Jasper, D. M. Popolan-Vaida, Z. Wang, V. S. B. Shankar, L. Ruwe, C. A. Taatjes, P. Dagaut, N. Hansen, "Quantification of the Keto-hydroperoxide (HOOCH<sub>2</sub>OCHO) and Other Elusive Intermediates in Low-Temperature Combustion of Dimethyl Ether", *J. Phys. Chem. A*, **2016**, 120(40), 7890-7901.
16. W. Sun, B. Yang, N. Hansen, K. Moshhammer, "The Influence of Dimethoxy Methane (DMM)/Dimethyl Carbonate (DMC) Addition on Premixed Ethane/Oxygen/Argon Flame", *Proc. Combust. Inst.*, **2017**, 36(1), 449-457.
17. K. Moshhammer, L. Seidel, Y. Wang, H. Selim, S. M. Sarathy, F. Mauss, N. Hansen, "Aromatic Ring Formation in Diffusive 1,3-Butadiene Flames", *Proc. Combust. Inst.*, **2017**, 36(1), 947-955.
18. Z. Wang, S. Y. Mohamed, L. Zhang, K. Moshhammer, D. M. Popolan-Vaida, V. S. B. Shankar, A. Lucassen, L. Ruwe, N. Hansen, P. Dagaut, S. M. Sarathy, "The Importance of Third O<sub>2</sub> Addition in 2-Methylhexane Auto-Oxidation", *Proc. Combust. Inst.*, **2017**, 36(1), 373-382.
19. I. Gerasimov, D. A. Knyazkov, N. Hansen, A. G. Shmakov, O. P. Korobeinichev, "Photoionization Mass Spectrometry and Modeling Study of a Low-Pressure Premixed Flame of Ethyl Pentanoate (Ethyl Valerate)", *Proc. Combust. Inst.*, **2017**, 36(1), 1185-1192.
20. T. Tao, W. Sun, B. Yang, N. Hansen, K. Moshhammer, C. K. Law, "Investigation of the Chemical Structures of Laminar Premixed Flames Fueled by Acetaldehyde", *Proc. Combust. Inst.*, **2017**, 36(1) 1287-1294.
21. M. Braun-Unkhoff, N. Hansen, T. Methling, K. Moshhammer, B. Yang, "The Influence of iso-Butanol Addition to the Chemistry of Premixed 1,3-Butadiene Flames", *Proc. Combust. Inst.*, **2017**, 36(1) 1311-1319.
22. L. Ruwe, K. Moshhammer, N. Hansen, K. Kohse-Höinghaus, "Consumption and Hydrocarbon Growth Processes in a 2-Methyl-2-Butene Flame", *Combust. Flame*, **2017**, 175, 34-46.
23. N. Hansen, M. Schenk, K. Moshhammer, K. Kohse-Höinghaus, "Investigating Repetitive Reaction Pathways for the Formation of Polycyclic Aromatic Hydrocarbons in Combustion Processes", *Combust. Flame*, **2017**, in press.
24. H. Selim, S. Y. Mohamed, N. Hansen, S. M. Sarathy, "Premixed Flame Chemistry of a Gasoline Primary Reference Fuel Surrogate", *Combust. Flame*, **2017**, in press
25. W. Sun, C. Huang, T. Tao, F. Zhang, W. Li, N. Hansen, B. Yang, "Exploring the High-Temperature Kinetics of Diethyl Carbonate (DEC) under Pyrolysis and Flame Conditions", *Combust. Flame*, **2017**, in press
26. N. Hansen, R. S. Tranter, K. Moshhammer, J. B. Randazzo, J. P. A. Lockhart, P. G. Fugazzi, T. Tao, A. L. Kastengren, "2D-Imaging of Sampling-Probe Perturbations in Laminar Premixed Flames using Kr X-ray Fluorescence", *Combust. Flame*, **2017**, in press.

# Theoretical Studies of Potential Energy Surfaces

Lawrence B. Harding  
Chemical Sciences and Engineering Division  
Argonne National Laboratory, Argonne, IL 60439  
harding@anl.gov

## Program Scope

The goal of this program is to calculate accurate potential energy surfaces for both reactive and non-reactive systems. Our approach is to use state-of-the-art electronic structure methods (CASPT2, MR-CI, CCSD(T), etc.) to characterize multi-dimensional potential energy surfaces. Depending on the nature of the problem, the calculations may focus on local regions of a potential surface or may cover the surface more globally. A second aspect of this program is the development of techniques to fit multi-dimensional potential surfaces to convenient, global, analytic functions suitable for use in dynamics calculations. A new part of this program is the use of diffusion Monte-Carlo calculations to obtain high accuracy, anharmonic zero point energies for molecules having multiple minima.

## Recent Progress

### Diffusion Monte-Carlo for High Accuracy Anharmonic Zero Point Energies

The accuracy of electronic structure calculations has now reached the point where a significant remaining source of error in calculated heats of formation is in the zero point energy. In the past, high accuracy predictions of thermochemical properties have typically employed spectroscopic perturbation theory or vibrational configuration interaction calculations to obtain estimates of

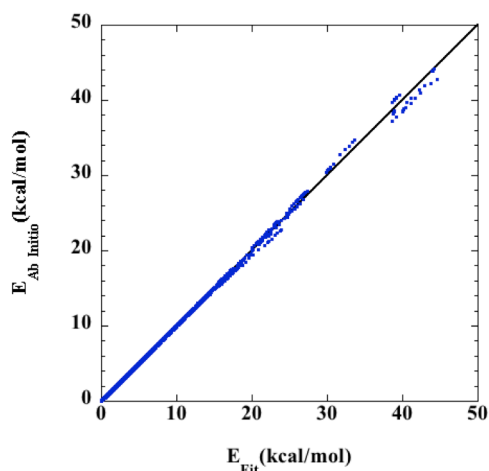


Figure 1. Scatter plot of the ab initio and fitted energies for methanol (see text).

anharmonic corrections to the zero point energy. Both of these methods rely on normal coordinate, force field expansions that are not appropriate for species in which the zero point wavefunction spans multiple minima, as is often the case for radicals relevant to combustion. Last year we embarked on a program to address this issue using diffusion Monte-Carlo methods<sup>1</sup> to obtain high accuracy predictions of anharmonic, zero point energies for combustion related species. This year we completed calculations on 48 combustion related species, ranging in size from H<sub>2</sub>O up to iso-propyl radical. Our calculations have demonstrated that a simple Taylor series expansion in the  $N_{\text{atom}}*(N_{\text{atom}}-1)/2$  internuclear distance coordinates can yield remarkably accurate fits. As an example, in Figure 1 we show a scatter plot comparing ab initio energies and fitted energies for methanol. For this case

the quartic Taylor series expansion involves 905 terms. These were least-squares fit using 50,000 randomly sampled ab initio points. We then evaluated energies at an additional 75,000 test points

used in Figure 1. The test points covered an energy range of  $15,000\text{ cm}^{-1}$ . For the whole set of test points the fit had an RMS error of  $20\text{ cm}^{-1}$ . For those test points within  $1000\text{ cm}^{-1}$  of the minimum the RMS error was just  $1\text{ cm}^{-1}$ .

In Figure 2 we show a two dimensional plot of the ethyl radical potential energy surface illustrating the complexity of these surface for small hydrocarbon radicals relevant to

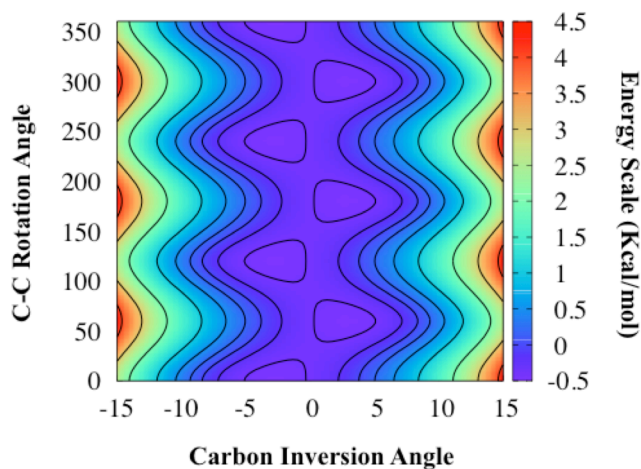


Figure 2. Contour plot of the internal rotation and inversion modes of the  $\text{CH}_3\text{CH}_2$  radical.

combustion. The two coordinates in this plot are rotation about the CC bond and inversion of the  $\text{CH}_2$  radical center. The plot shows six equivalent minima separated by six equivalent saddle points. The saddle points are predicted to lie only  $32\text{ cm}^{-1}$  above the minima. In this particular case, in spite of the fact that the ground, vibrational wavefunction will be spread over all six minima, we find surprisingly good agreement between the DMC result and second order vibrational perturbation theory (VPT2) using the same level of electronic structure theory, CCSD(T)/aug-cc-pVTZ. Indeed the anharmonic corrections from these two calculations agree to within 10%.

However we find many cases where VPT2 fails catastrophically. Most problematic for VPT2 are pseudo-linear and pseudo-planar molecules. For example, fulminic acid,  $\text{HCNO}$ , is a pseudo linear molecule having a barrier to linearity of  $42\text{ cm}^{-1}$ . DMC predicts an anharmonicity correction of  $-26\text{ cm}^{-1}$  while VPT2 predicts  $-385\text{ cm}^{-1}$ , more than an order of magnitude too large. Formamide is a pseudo planar molecule having a barrier to planarity of just  $5\text{ cm}^{-1}$ . In this case the predicted anharmonic corrections from DMC and VPT2 are  $-131$  and  $-209\text{ cm}^{-1}$  respectively.

For non-fluxional molecules the RMS deviation between DMC anharmonicity corrections and B3LYP (or MP2) based VPT2 is  $\sim 15\text{ cm}^{-1}$ . For fluxional molecules these RMS deviations increase to  $\sim 50\text{ cm}^{-1}$ . The much simpler G4 approach which relies on scaled B3LYP harmonic frequencies yields deviations relative to DMC of  $\sim 50\text{ cm}^{-1}$  for both sets of molecules.

One important conclusion from this study is that for non-fluxional molecules B3LYP based VPT2 yield remarkably accurate anharmonic corrections, more accurate in fact than much more expensive, MP2 based VPT2. Even CCSD(T) based VPT2 shows only a modest improvement in accuracy over the B3LYP based calculations. We conclude then that a reasonable approach to obtaining high accuracy anharmonic zero points for larger, non-fluxional molecules is to combine CCSD(T) harmonic zero points with B3LYP based VPT2 anharmonic corrections.

## Reactions of hydrogen atoms with Aromatic Alkynes

In a collaborative effort with Mebel, Klippenstein and Jasper we are studying the temperature and pressure dependence of the recombination reactions of hydrogen atoms with benzyne, naphthyne and several larger aromatic alkynes. The predicted rates exhibit strong non-Arrhenius behavior having negative temperature dependence at low temperatures becoming positive for temperatures above ~200 K.

### Future Plans

In a collaboration with Branko Ruscic, we plan to use some of the analytic potential energy surfaces from our diffusion Monte-Carlo studies to calculate anharmonic, partition functions for fluxional molecules. We also plan to extend our previous study of the O<sub>2</sub> plus vinyl radical reaction in an attempt to identify the mechanism by which CH<sub>3</sub>+CO<sub>2</sub> products are produced. One possibility under consideration involves a 'roaming' type mechanism. We are also planning to use Morokuma's global reaction route mapping strategy (GRRM)<sup>2</sup> to discover previously missed pathways. In a collaboration involving Klippenstein, Hase and Jasper we plan to use direct dynamics to model the decomposition of vibrationally excited Criegee intermediates formed in the ozonolysis of ethylene.

**Acknowledgement:** This work was performed under the auspices of the Office of Basic Energy Sciences, Division of Chemical Sciences, Geosciences and Biosciences, U.S. Department of Energy, under Contract DE-AC02-06CH11357.

### References:

- (1) A. B. McCoy, *Int. Rev. Phys. Chem.* **25**, 77-107 (2006).
- (2) S. Maeda, K. Ohno and K. Morokuma, *Phys. Chem. Chem. Phys.* **15**, 3683 (2013).

**PUBLICATIONS (2014 - Present):**

**Secondary Channels in the Thermal Decomposition of monomethylhydrazine (CH<sub>3</sub>NHNH<sub>2</sub>)**

P. Zheng, S. J. Klippenstein, L. B. Harding, H. Sun, C. K. Law  
RSC Advances **4**, 62951 (2014)

**Electronic States of the Quasilinear Molecule Propargylene (HCCCH) from Negative Ion Photoelectron Spectroscopy**

D. L. Osborn, K. M. Vogelhuber, S. W. Wren, E. M. Miller, Y.-J. Lu, A. S. Case, L. Sheps, R. J. McMahon, J. F. Stanton, L. B. Harding, B. Ruscic, W. C. Lineberger  
J. Amer. Chem. Soc. **136**, 10361 (2014)

**Predictive A Priori Pressure-Dependent Kinetics**

A.W. Jasper, K. M. Pelzer, J. A. Miller, E. Kamarchik, L. B. Harding, S. J. Klippenstein  
Science **346**, 1212 (2014)

**Resolving Some Paradoxes in the Thermal Decomposition Mechanism of Acetaldehyde**

R. Sivaramakrishnan, J. V. Michael, L. B. Harding, S. J. Klippenstein  
J. Phys. Chem. A **119**, 7724-7733 (2015)

**Thermal Dissociation and Roaming Isomerization of Nitromethane: Experiment and Theory**

C. Annesley, J. Randazzo, S. J. Klippenstein, L. B. Harding, A. Jasper, Y. Georgievski, B. Ruscic, R. S. Tranter, J. Phys. Chem. A **119**, 7872-7893 (2015)

**Comment on “A Novel and Facile Decay Path of Criegee Intermediates by Intramolecular Insertion Reactions Via Roaming Transition States” [J. Chem. Phys. **142**, 124312 (2015)]**

L. B. Harding and S. J. Klippenstein, J. Chem. Phys. **143**, 167101-1 / 167101-2 (2015)

**Accurate Anharmonic Zero Point Energies for some Combustion Related Species from Diffusion Monte Carlo**

L. B. Harding, Y. Georgievskii, and S. J. Klippenstein, J Phys. Chem. A (submitted)

## Theory of Electronic Structure and Chemical Dynamics

*Martin Head-Gordon, William H. Miller, and Eric Neuscamman*

Chemical Sciences Division, Lawrence Berkeley National Laboratory and  
Department of Chemistry, University of California, Berkeley, California 94720.

[mhg@cchem.berkeley.edu](mailto:mhg@cchem.berkeley.edu), [millerwh@berkeley.edu](mailto:millerwh@berkeley.edu), [neuscamman@berkeley.edu](mailto:neuscamman@berkeley.edu)

**Scope of the Project:** To expand knowledge of transient species such as radicals relevant to combustion chemistry and other areas including catalysis, new theoretical methods are needed for reliable computer-based prediction of their properties. The two main areas of relevant theory are electronic structure methods and techniques for chemical dynamics. Within electronic structure theory, focus centers on the development of new density functional theory methods and new wave function theories. Examples of current activity include the introduction of combinatorial design strategies for density functionals, and new quantum Monte Carlo approaches for excited states. In chemical dynamics, recent progress and planned activity centers on the development of tractable semi-classical dynamics approaches that can address non-adiabatic processes. The focus is on turning semi-classical theory into a practical way of adding quantum effects to classical molecular dynamics simulations of large, complex molecular systems. Newly developed theoretical methods, as well as existing approaches, are employed to study prototype radical reactions, often in collaboration with experimental efforts. These studies help to deepen understanding of the role of reactive intermediates in diverse areas of chemistry. They also sometimes reveal frontiers where new theoretical developments are needed in order to permit better calculations in the future.

### Recent Progress

Due to length limitations, only a selection of projects can be summarized here.

*High Accuracy Excited States and Novel Ansatzes.* Neuscamman and co-workers have used new techniques in quantum Monte Carlo to construct an excited state generalization of the quantum variational principle and two promising new wave function ansatzes. Variational treatment of excited states allows an approximate wave function ansatz to be fully optimized for an individual excited state, greatly increasing accuracy compared to traditional approaches that share elements of the wave function, such as the orbital basis, between different states. This method has been paired with a new variation-after-response ansatz in order to allow a wave function to fully relax itself within the presence of its own linear response, thus capturing important nonlinear effects that are absent in excited state descriptions such as configuration interaction singles and time-dependent density functional theory. Preliminary investigations have shown this approach to outperform even equation-of-motion coupled cluster in difficult excited state situations, including metal-oxide charge transfer and the low-lying spectrum of the carbon dimer. In addition to excited state methods, new QMC technology has also allowed for the development of a polynomial-cost, variational analogue to pairwise coupled cluster theory. As polynomial-cost variational coupled cluster has remained elusive, close analogues that may be evaluated efficiently by QMC methods offer a promising new direction in the search for methods with coupled-cluster-like accuracy and size consistency that remain viable even when molecules are stretched far from equilibrium, as commonly occurs in gas phase studies.

*Density functionals.* Head-Gordon and co-workers have been seeking the limit of transferable accuracy that can be achieved with generalized gradient approximations (GGA's), and meta-GGA's, which are the basis of semi-local functionals. To achieve high accuracy, non-local density-based corrections for long-range dispersion interactions are added, as well as the option of non-local range-separated hybrid (RSH) treatment of exact exchange. They introduced a novel "survival of the most transferable" (SOMT) procedure to achieve this goal. SOMT is a combinatorial design protocol that involves training a very large numbers of functionals using a fraction of the data, and then selecting the functional that performs best on the remaining data (with the fewest parameters). Between 2014 and the present, this approach has been used to create three new density functionals, each of which is most accurate in its class for target problems in chemistry, as measured by performance on test data.



The most recent, and most accurate density functional, is a RSH meta-GGA including the VV10 van der Waals correction. On a statistical basis, this functional,  $\omega$ B97M-V, provides substantially improved accuracy for thermochemistry, barrier heights, isomerization energies and non-covalent binding energies relative to existing functionals of the same class. It must be noted that like all broadly applicable density functionals, it performs increasingly poorly for problems that exhibit strong correlation effects and/or sensitivity to self-interaction errors, where wavefunction methods are still advisable. Nonetheless, for most chemical problems, this functional, and its hybrid GGA cousin,  $\omega$ B97X-V, and non-hybrid meta-GGA cousin, B97M-V, represent a very useful step forwards. Implementations of B97M-V for condensed matter codes have been recently completed. A variety of comparative benchmark tests and studies have been reported as follow-on tests of the functionals.

*Semi-classical dynamics.* It has been long established that semi-classical (SC) theory provides a very good description of essentially *all* quantum effects in molecular dynamics, and the outstanding challenge has been to what extent one can implement it efficiently enough to make it routinely useful. Recently, however, Miller and co-workers have been exploring how successful even simpler, *purely classical* MD approaches can be (with some judicious SC ideas incorporated), especially for the important case of *electronically non-adiabatic processes*, i.e., involving transitions between different electronic states. The two essential ingredients to the approach are, (a) how are the electronic degrees of freedom described within a classical mechanics framework (currently by the Meyer-Miller (MM) ‘electronic oscillator’ model), and (b) how one identifies specific electronic states (initially and finally) within a classical picture (where the ‘symmetrical quasi-classical’ (SQC) model is currently being used). Both approaches have a long history but have never been used in concert before in this way. They have given remarkably good results for a series of standard “strong coupling” non-adiabatic problems, even being able to describe ‘quantum coherence’ effects within a standard classical MD simulation. Recent developments and extensions of the SQC/MM approach have been (1) to show that it can treat very weak electronic coupling as well as it does strong coupling (by using a “triangular” modification of the ‘window functions’ of the SQC model), and (2) how off-diagonal elements of the electronic density matrix can be obtained within the same ensemble of trajectories that gives the diagonal elements (i.e., the populations).

*Computational studies of chemical properties and reactivity.* A joint study of the radical-neutral association reactions between ethylene radical cation and neutral ethylene, acetylene cation and acetylene, and mixed association, was finished in 2016, involving calculations from Head-Gordon’s group and experimental measurements from the Ahmed group at LBNL. A follow-on project, also in collaboration with the Ahmed group, identified novel pathways to the benzene radical cation from the ionization of cold acetylene clusters, and has just been accepted for publication. Both these studies employed the new density functionals described above.

**Future Plans:** (i) High Accuracy Targeting of Excited States: Current efforts focus on extending EVP-QMC to the variational optimization of an entire linear response function, rather than just an ansatz, in order both to improve accuracy and to make the method more black-box. Crucially, this approach has a cost very similar to optimizing the ansatz itself through a careful application of finite difference techniques. Formal analysis as well as preliminary results for this linear response form of EVP-QMC suggest an accuracy in single excitations on par with equation-of-motion coupled cluster (currently the gold standard), but with a lower cost-scaling and an algorithm that parallelizes more easily onto modern supercomputer architectures. (ii) Density functionals: Extensive comparative benchmarking of the new functionals against the full spectrum of existing functionals is an important pre-requisite for their broader use in the future. One more new class of functional, a so-called double hybrid functional that includes PT2 correlation is currently being completed. Whilst more computationally demanding, this may be the most accurate possible within the SOMT paradigm. (iii) Semiclassical dynamics: Since Miller’s SQC/MM model has proved quite reliable for describing electronically non-adiabatic dynamics in simple model problems, work is in progress to extend its application to more general and complex non-adiabatic processes. (iv) Computational studies of

chemical properties and reactivity: It is planned to continue the study of radical-neutral clustering reactions, possibly also including larger polycyclic aromatic hydrocarbon species. Suitable candidates for collaborative applications of the new EVP-QMC excited state methods will also be sought. (v) A new collaboration between the Head-Gordon and Leone groups on core-excited state calculations has been initiated.

### Recent Publications Citing DOE Support (2014-2017)

- Bandyopadhyay, B., T. Stein, Y. Fang, O. Kostko, A. White, M. Head-Gordon, and M. Ahmed, "Probing Ionic Complexes of Ethylene and Acetylene with Vacuum-Ultraviolet Radiation" *J. Phys. Chem. A* **2016**, 120, 5053–5064; DOI: 10.1021/acs.jpca.6b00107
- Cotton, S. J., Igumenshchev, K. and Miller, W. H., "Symmetrical Windowing for Quantum States in Quasi-Classical Trajectory Simulations: Application to Electron Transfer" *J. Chem. Phys.* **2014**, 141, 084104.1-14. DOI: 10.1063/1.4893345
- Cotton, S. J. and W. H. Miller, "A Symmetrical Quasi-Classical Spin-Mapping Model for the Electronic Degrees of Freedom in Non-Adiabatic Processes", *J. Phys. Chem. A* **2015**, 119, 12138-12145 (2015).
- Cotton, S. J. and W. H. Miller, "The Symmetrical Quasi-Classical Model for Electronically Non-Adiabatic Processes Applied to Energy Transfer Dynamics in Site-Exciton Models of Light-Harvesting Complexes", *J. Chem. Theory Comput.* **2016**, 12, 983-991; doi: 10.1021/acs.jctc.5b01178
- Cotton, S.J. and W. H. Miller, "A New Symmetrical Quasi-Classical Model for Electronically Non-Adiabatic Processes: Application to the Case of Weak Non-Adiabatic Coupling", *J. Chem. Phys.* **2016**, 145, 144108.1-16; doi: 10.1063/1.4963914
- Goldey, M. and M. Head-Gordon, "Separate Electronic Attenuation Allows a Spin-Component Scaled Second Order Møller-Plesset Theory to be Effective for Both Thermochemistry and Non-Covalent Interactions" *J. Phys. Chem. B*, **2014**, 118, 6519-6525. DOI: 10.1021/jp4126478
- Goldey, M. B. and M. Head-Gordon, "Convergence of Attenuated Second Order Møller-Plesset Perturbation Theory Towards the Complete Basis Set Limit" *Chem. Phys. Lett.*, **2014**, 608, 249-254. DOI: 10.1016/j.cplett.2014.05.092
- Goldey, M., R. A. DiStasio, Jr., Y. Shao, and M. Head-Gordon, "Shared Memory Multi Processing Implementation of Resolution-of-the-Identity Second Order Møller-Plesset Perturbation Theory with Attenuated and Unattenuated Results for Intermolecular Interactions between Larger Molecules" *Mol. Phys.*, **2014**, 112, 836-843. DOI: 10.1080/00268976.2013.869363
- Goldey, M.B., B. Belzunces, and M. Head-Gordon, "Attenuated MP2 with a long-range dispersion correction for treating non-bonded interactions", *J. Chem. Theory Comput.* **2015**, 11, 4159–4168; DOI: 10.1021/acs.jctc.5b00509
- Huang, Y.-H., M. Goldey, M. Head-Gordon, and G. J. O. Beran, "Achieving High Accuracy Intermolecular Interactions Through Coulomb-Attenuated Dispersion Corrected Second Order Møller-Plesset Theory" *J. Chem. Theory Comput.*, **2014**, 10, 2054-2063. DOI: 10.1021/ct5002329
- Lehtola, S., M. Head-Gordon, and H. Jónsson, "Complex orbitals, multiple local minima and symmetry breaking in Perdew-Zunger self-interaction corrected density-functional theory calculations", *J. Chem. Theory Comput.* **2016**, 12, 3195-3207 (2016); DOI: 10.1021/acs.jctc.6b00347
- Lehtola, S., J.A. Parkhill and M. Head-Gordon, "Cost-effective description of strong correlation: efficient implementations of the perfect quadruples and perfect hexuples models", *J. Chem. Phys.* **2016**, 145, 134110 (2016); doi: 10.1063/1.4964317
- Li, B., Miller, W. H., Levy, T. J., and Rabani, E., "Classical Mapping for Hubbard Operators: Application to the Double-Anderson Model" *J. Chem. Phys.* **2014**, 140, 204106.1-7. DOI: 10.1063/1.4878736
- Li, B., Wilner, E. Y., Thoss, M., Rabani, E., and Miller, W. H., "A Quasi-Classical Mapping Approach to Vibrationally Coupled Electron Transport in Molecular Junctions" *J. Chem. Phys.* **2014**, 140, 104110.1-7. DOI: 10.1063/1.4867789
- Mardirossian, N. and M. Head-Gordon, "ωB97X-V: A 10 Parameter Range Separated Hybrid Density Functional Including Non-Local Correlation, Designed by a Survival of the Fittest Strategy" *Phys. Chem. Chem. Phys.*, **2014**, 16, 9904-9924. DOI: 10.1039/c3cp54374a
- Mardirossian, N., and M. Head-Gordon, "Exploring the Limit of Accuracy for Density Functionals Based on the Generalized Gradient Approximation: Local, Global Hybrid and Range-Separated Hybrids With and Without Dispersion Corrections" *J. Chem. Phys.*, **2014**, 140, 18A527. DOI: 10.1063/1.4868117

- Mardirossian, N. and M. Head-Gordon, “Mapping the genome of meta-generalized gradient approximation density functionals: The search for B97M-V”, *J. Chem. Phys.* **2015**, 142, 074111; (32 pages) <http://dx.doi.org/10.1063/1.4907719>
- Mardirossian, N. and M. Head-Gordon, “ $\omega$ B97M-V: A combinatorially-optimized, range-separated hybrid, meta-GGA density functional with VV10 nonlocal correlation”, *J. Chem. Phys.* **2016**, 144, 214110 (2016); doi: 10.1063/1.4952647
- Mardirossian, N. and M. Head-Gordon, “How accurate are the Minnesota density functionals for thermochemistry, non-covalent interactions, isomerization energies and barrier heights of molecules containing main group elements?” *J. Chem. Theory Comput.* **2016**, 12, 4303–4325; DOI: 10.1021/acs.jctc.6b00637
- Mardirossian, N. and M. Head-Gordon, “Note: The performance of new density functionals for a recent blind test of non-covalent interactions”, *J. Chem. Phys.* **2016**, 145, 186101; DOI: 10.1063/1.4967424
- Miller, W. H., “A Journey Through Chemical Dynamics” *Annu. Rev. Phys. Chem.* **2014**, 65, 1- 19. DOI: 10.1146/annurev-physchem-040513-103720
- Miller, W.H. and S. J. Cotton, “Communication: Note on Detailed Balance in Symmetrical Quasi-Classical Models for Electronically Non-Adiabatic Dynamics”, *J. Chem. Phys.* **2015**, 142, 131103.1-3; doi: 10.1063/1.4916945
- Miller, W.H. and S. J. Cotton, “Communication: Wigner Functions in Action-Angle Variables, Bohr-Sommerfeld Quantization, the Heisenberg Correspondence Principle, and a Symmetrical Quasi-Classical Approach to the Full Electronic Density Matrix”, *J. Chem. Phys.* **2016**, 145, 081101.1-4; doi: 10.1063/1.4961551
- Miller, W.H. and S. J. Cotton, “Classical Molecular Dynamics Simulation of Electronically Non-Adiabatic Processes”, *Faraday Discuss.* **2016**, 195, 9-30; doi: 10.1039/c6fd00181e
- Neuscammann, E. “Communication: Variation After Response in Quantum Monte Carlo” *J. Chem. Phys.* **2016**, 145, 081103, <http://dx.doi.org/10.1063/1.4961686>
- Ruiz Pestana, L., N. Mardirossian, M. Head-Gordon, T. Head-Gordon, “Ab Initio Simulations of Liquid Water using High Quality Meta-GGA Functionals”, *Chem. Sci.* **2017**, (in press); doi: 10.1039/C6SC04711D
- Sharada, S.M, D. Stück, E.J. Sundstrom, A.T. Bell, and M. Head-Gordon, “Wavefunction stability analysis without analytical electronic Hessians: Application to orbital-optimized post-Hartree-Fock methods and VV10-containing density functionals,” *Mol. Phys.* **2015**, 113, 1802-1808. DOI:10.1080/00268976.2015.1014442CH
- Small, D. W., K. V. Lawler, and M. Head-Gordon, “Coupled Cluster Valence Bond Method: Efficient Implementation and Application to Extended Acene Oligomers” *J. Chem. Theor. Comput.*, **2014**, 10, 2027-2040. DOI: 10.1021/ct500112y
- Small, D.W., E.J. Sundstrom, and M. Head-Gordon, “A simple way to test for collinearity in spin symmetry broken wave functions: Theory and application to Generalized Hartree-Fock”, *J. Chem. Phys.* **2015**, 142, 094112 (9 pages). <http://dx.doi.org/10.1063/1.4913740>
- Stein, T., B. Bandyopadhyay, T. Troy, Y. Fang, O. Kostko, M. Ahmed, and M. Head-Gordon, “Ab initio dynamics and photoionization mass spectrometry reveal ion-molecule pathways from ionized acetylene clusters to benzene cation”, *Proc. Nat. Acad. Sci.* **2017**, (in press).
- Womack, J.C., N. Mardirossian, M. Head-Gordon, and C.-K. Skylaris, “Self-consistent implementation of meta-GGA functionals for the ONETEP linear-scaling electronic structure package”, *J. Chem. Phys.* **2016**, 145, 204114; doi: 10.1063/1.4967960
- Zhao, L. and Neuscammann, E. “An efficient variational principle for the direct optimization of excited states” *J. Chem. Theory Comput.* **2016**, 12, 3436, DOI: 10.1021/acs.jctc.6b00508
- Zhao, L. and Neuscammann, E. “Equation of motion theory for excited states in variational Monte Carlo and the Jastrow antisymmetric geminal power in Hilbert space” *J. Chem. Theory Comput.* **2016**, 12, 3719, DOI: 10.1021/acs.jctc.6b00480
- Zhao, L. and Neuscammann, E. “Amplitude determinant coupled cluster with pairwise doubles” *J. Chem. Theory Comput.* **2016**, 12, 5841, DOI: 10.1021/acs.jctc.6b00812

# Theoretical Methods for Pressure Dependent Kinetics and Electronically Nonadiabatic Chemistry

Ahren W. Jasper  
Chemical Sciences and Engineering Division  
Argonne National Laboratory  
ajasper@anl.gov

## Program Scope

The accuracy of a priori chemical kinetics calculations is improving and is broadly approaching so-called “kinetic accuracy,” defined as a factor of  $\sim 2$  in the calculated rate coefficient. This term may be compared with the 1990s realization of “chemical accuracy” ( $\sim 1$  kcal/mol) in thermochemistry, when calculated thermochemistry began to be accurate enough to be used alongside experimental values. A similar situation has emerged in chemical kinetics thanks to ongoing improvements in computational power and theoretical methods. One may now define a second accuracy milestone of  $\sim 20\%$ , which may be called the “semiclassical accuracy” limit and is intended to represent the accuracy of the best non-quantal dynamics and kinetics methods. The principal goal of this project is to develop and validate new theoretical methods for broadening the applicability and improving the accuracy of theoretical chemical kinetics and to aid in the realization of semiclassical and kinetic accuracy for applications throughout gas phase chemistry. The model developments we are presently focused on are: (1) predicting pressure dependence in elementary reactions using detailed master equation models of energy transfer informed by classical trajectories, (2) characterizing spin-forbidden kinetics using both multistate trajectory methods and statistical theories, and (3) predicting anharmonic vibrational properties for polyatomic molecules at high energies and temperatures via Monte Carlo phase space integration.

## Recent Progress

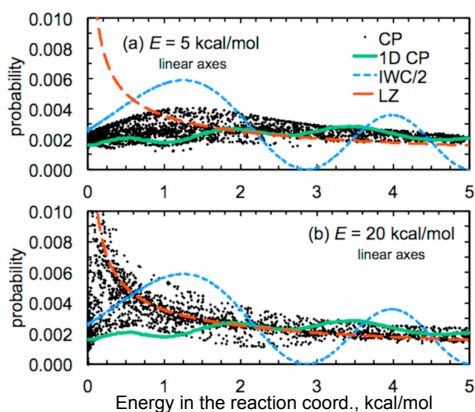


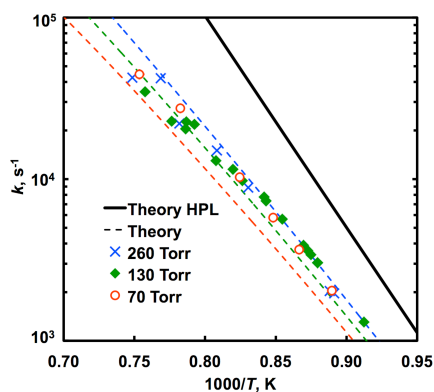
Fig. 1. Nonadiabatic transition probabilities for O + CO calculated using the 1D Landau-Zener (LZ), weak coupling (IWC), and classical path (CP) formulas, and the full-dimensional CP method.

The accuracy of one-nuclear-dimensional models (such as the Landau-Zener approximation) for nonadiabatic transition probabilities were tested against a full-dimensional semiclassical model for the spin-forbidden reaction  $^3\text{O} + \text{CO} \rightarrow \text{CO}_2$  (see Fig. 1). We identified and quantified several multidimensional effects, including those associated with sampling the crossing seam, with the energy distribution in degrees of freedom orthogonal to the reaction coordinate, and with the interference of the electronic phase at multiple seam crossings. Fast electronic decoherence was demonstrated to localize the nonadiabatic dynamics near the crossing seam. The one-dimensional models were found to have errors as large as a factor of two.

With Moshhammer and Hansen (Sandia), photoionization cross sections were calculated for twelve species using a readily applicable approach based on the frozen-core Hartree-Fock approximation, as made available by Lucchese in his ePolyScat code. First, this approach was validated against measured photoionization cross sections and found to have an average error of  $\sim 2\times$ , which likely

improves on the estimates commonly used to quantify species with unknown cross sections. Next, the ketohydroperoxide relevant to the low temperature oxidation of dimethyl ether was identified in a jet stirred reactor, and its mole fraction was quantified using the predicted cross section. This study demonstrated that theoretical cross sections can be useful for quantifying key intermediates, which in turn provide additional targets for testing chemical kinetic models.

With Klippenstein, Georgievskii (Argonne), and Mebel (FIU), the temperature- and pressure-dependent kinetics of several key steps in the HACA molecular growth mechanism were predicted. As part of this effort, the collision parameters (i.e., efficiencies,  $\alpha = \langle \Delta E_d \rangle$ , and effective Lennard-Jones rate parameters) required for predicting pressure dependence in the master equation were calculated using newly fitted potential energy surfaces for collisions involving small aromatic molecules and the colliders He, Ar, and N<sub>2</sub>. Similar to our previous work on saturated hydrocarbons, we found that, for a given collider, the collision parameters depended most sensitively on the chemical composition of the hydrocarbon and were relatively insensitive to the chemical arrangement. Furthermore, parameterizations of the separable pairwise functional form for the interaction potential were found to be transferable to larger aromatics. The present strategies are therefore readily applicable to the study of larger PAHs.



With Tranter (Argonne), the dissociation and the self-recombination of 2-methylallyl radicals were calculated using ab initio, transition state theory, classical trajectory, and master equation calculations. The predicted pressure- and temperature-dependent kinetics for both reactions were found to agree very well with the accompanying shock tube measurements, with, notably, no adjustments to the theory required (see Fig. 2). The observed quantitative agreement is likely somewhat fortuitous, as one might expect significant uncertainty in the partition function for the self-recombination adduct (2,5-dimethyl-1,5-hexadiene). Nonetheless, the comparisons provide yet another example of the good accuracy that can be achieved with fully a priori

kinetics calculations, including trajectory-based predictions of pressure dependence.

As part of the AITSTME project (PI: Klippenstein), the spin-forbidden and spin-allowed product branching of <sup>3</sup>O + C<sub>2</sub>H<sub>4</sub> was calculated using a combination of quantum chemistry, master equation, classical trajectory, and nonadiabatic statistical theory calculations. This reaction has been widely studied, and it is known that product branching is largely controlled via the fate of the initial triplet adduct OC<sub>2</sub>H<sub>4</sub>, where intersystem crossing (ISC) to the singlet surface competes with spin-allowed bimolecular channels on the triplet surface. Here we used a Landau-Zener statistical calculation for the ISC rate (sometimes called “nonadiabatic transition state theory”) alongside conventional TST to predict the temperature-dependent branching within a single master equation calculation. Product branching immediately following ISC was determined using short-time direct classical trajectories initiated at the crossing seam. Our predicted room temperature branching agreed well with available experimental results, as well as with a previous master equation study of Vereecken, Peeters, and co-workers, who used a more approximate treatment of ISC. The two master equation studies predict different product branching at elevated temperatures, however.

In other work,  $P(E, J; E' = 97\%$  of the dissociation threshold of NO<sub>2</sub>( $J' = 0$ ) for NO<sub>2</sub> + Ar was calculated as part of a joint theoretical/experimental study with Dave Chandler (Sandia). Both determinations of  $P$  showed biexponential (“long tail”) behavior, although the theoretical value

for the long tail range parameter ( $275\text{ cm}^{-1}$ ) was  $\sim 3\times$  larger than the experimental value. The source of this discrepancy is unclear and may be related to the role of excited electronic states.

We have used direct dynamics trajectories to study collisional energy transfer for  $\text{CH}_4 + \text{He}$ ,  $\text{Ne}$ , and  $\text{H}_2$ ,  $\text{C}_2\text{H}_5 + \text{He}$ , and  $\text{C}_2\text{H}_6 + \text{He}$ . These results were used to test the accuracy of the pairwise approximation for the interaction potential. We further tested the accuracy of using pairwise interaction potentials obtained for  $\text{CH}_4 + \text{M}$  for systems larger than methane, i.e., we tested the accuracy of using methane's interaction parameters as universal  $\text{C}_x\text{H}_y + \text{M}$  interaction parameters. For the saturated and lightly unsaturated systems we considered, results obtained using the universal  $\text{C}_x\text{H}_y + \text{M}$  potentials were found to agree with direct dynamics results within the statistical uncertainties of the calculations. The resulting universal potentials are very efficient relative to direct dynamics and may be used to study systems with dozens of C atoms.

We used the universal  $\text{C}_x\text{H}_y + \text{M}$  potentials to evaluate Troe's collision efficiency (and an approximation to it) for seven atomic and diatomic baths and for molecules and radicals as large as octane. In total, 266 systems were studied, including normal, branched, cyclic, and unsaturated hydrocarbon molecules, as well as hydrocarbon radicals interacting with the seven baths. These collision efficiencies are simple functions of the first moment of the energy transferred in deactivating collisions,  $\langle\Delta E_d\rangle$ . We also considered the *rotational* collision efficiency for several systems by calculating the first moment of the angular momentum transferred in deactivating collisions,  $\langle\Delta J_d\rangle$ . Trends in the collision efficiencies with respect to the bath gas, its temperature, and the size and chemical structure of the hydrocarbon target were quantified and discussed.

## Future Work

We will continue the development and application of predictive models for pressure-dependent chemical kinetics. We will extend the types of species considered to include those with halogen and oxygen atoms. Enhanced energy transfer for halogens and alcohols has been reported, and trajectory studies will be used to elucidate the dynamical mechanisms of these enhancements. Ongoing applications include  $\text{HO}_2 + \text{He}$ ,  $\text{Ar}$ , and  $\text{H}_2\text{O}$  as well as  $\text{C}_x\text{H}_{2x+1}\text{O}_n\text{H} + \text{M}$ , where  $n = 1$  and  $2$ .

An important limitation to broadly generating accurate trajectory-based collision parameters is the difficulty in obtaining high-quality analytic representations of the intermolecular potential. We are developing automated parameterization schemes for the intermolecular potential using both (1) class-based pairwise Buckingham representations (describing, e.g., the interaction of  $\text{Ar}$  with all monoalcohols), and (2) system-specific permutationally-invariant polynomials representations. In the latter application, we will explore with Davis (Argonne) efficiency and accuracy improvements related to the choice of sampling strategy and functional form optimization.

The MCPSI method for calculating vibrational anharmonicity will continue to be applied and developed. We will focus on systems where the accuracy of existing vibrational anharmonicity approaches is not known, such as those involving constrained torsions and rings. The MCPSI method is particularly well-suited for predicting high energy/temperature rovibrational properties. We will quantify the accuracy of "dual level" thermochemistry approaches, where the anharmonicity corrections are computed at a lower level of theory than the harmonic frequencies.

We will continue to apply our new theoretical methods in collaboration with experimentalists and modelers at Sandia (Hansen and Dahms) and Argonne (Tranter and Sivaramakrishnan). These studies include the characterization of nonthermal kinetics with Dahms and improved predictions of photoionization cross sections with Hansen.

## Publications supported by this project since 2015

1. Recombination and dissociation of 2-methyl allyl radicals: Experiment and theory. R. S. Tranter, A. W. Jasper, J. B. Randazzo, J. P. A. Lockhart, and J. P. Porterfield, *Proc. Combust. Inst.* 36, 211–218 (2017).
2. Theoretical kinetics of  $O + C_2H_4$ . X. Li, A. W. Jasper, J. Zádor, J. A. Miller, and S. J. Klippenstein, *Proc. Combust. Inst.* 36, 219–227 (2017).
3. Temperature- and pressure-dependent rate coefficients for the HACA pathways from benzene to naphthalene. A. M. Mebel, Y. Georgievskii, A. W. Jasper, and S. J. Klippenstein, *Proc. Combust. Inst.* 36, 919–926 (2017).
4. Quantification of the keto-hydroperoxide ( $HOOCH_2OCHO$ ) and other elusive intermediates during low-temperature oxidation of dimethyl ether, K. Moshhammer, A. W. Jasper, D. M. Popolan-Vaida, Z. Wang, V. S. B. Shankar, L. Ruwe, C. A. Taatjes, P. Dagaut, and N. Hansen, *J. Phys. Chem. A* 120, 7890–7901 (2016).
5. Pressure dependent rate constants for PAH growth: formation of indene and its conversion to naphthalene. A. M. Mebel, Y. Georgievskii, A. W. Jasper, and S. J. Klippenstein, *Faraday Discuss. Chem. Soc.* 195, 637–670 (2016).
6. Low temperature kinetics of the first steps of water cluster formation. V. Roussel, M. Capron, J. Bourgalais, A. Benidar, A. W. Jasper, S. J. Klippenstein, L. Biennier, and S. D. Le Picard, *Phys. Rev. Lett.* 116, 113401 (2016).
7. Comment on “When rate constants are not enough.” J. A. Miller, S. J. Klippenstein, S. H. Robertson, M. J. Pilling, R. Shannon, J. Zádor, A. W. Jasper, C. F. Goldsmith, and M. P. Burke, *J. Phys. Chem. A* 120, 306–312 (2016).
8. Determination of the collisional energy transfer distribution responsible for the collision-induced dissociation of  $NO_2$  with Ar. J. D. Steill, A. W. Jasper, and D. W. Chandler, *Chem. Phys. Lett.* 636, 1–14 (2015).
9. Multidimensional effects in nonadiabatic statistical theories of spin-forbidden kinetics: A case study of  $^3O + CO \rightarrow CO_2$ . A. W. Jasper, *J. Phys. Chem. A* 119, 7339–7351 (2015).
10. Kinetics of propargyl radical dissociation. S. J. Klippenstein, J. A. Miller, and A. W. Jasper, *J. Phys. Chem. A* 119, 7780–7791 (2015).
11. Thermal dissociation and roaming isomerization of nitromethane: Experiment and theory. C. J. Annesley, J. B. Randazzo, S. J. Klippenstein, L. B. Harding, A. W. Jasper, Y. Georgievskii, and R. S. Tranter, *J. Phys. Chem. A* 119, 7872–7893 (2015).
12. Detection and identification of the keto-hydroperoxide ( $HOOCH_2OCHO$ ) and other intermediates during low-temperature oxidation of dimethyl ether. K. Moshhammer, A. W. Jasper, S. M. Popolan-Vaida, A. Lucassen, P. Dievart, H. Selim, A. J. Eskola, C. A. Taatjes, S. R. Leone, S. M. Sarathy, Y. Ju, P. Dagaut, K. Kohse-Höinghaus, and N. Hansen, *J. Phys. Chem. A* 119, 7361–7374 (2015).
13. Ab initio variational transition state theory and master equation study of the reaction  $(OH)_3SiOCH_2 + CH_3 \rightarrow (OH)_3SiOC_2H_5$ . D. Nurkowski, S. J. Klippenstein, Y. Georgievskii, M. Verdicchio, A. W. Jasper, J. Akroyd, S. Mosbach, and M. Kraft, *Z. Phys. Chem.* 229, 691–708 (2015).
14. “Third-body” collision efficiencies for combustion modeling: Hydrocarbons in atomic and diatomic baths. A. W. Jasper, C. M. Oana, and J. A. Miller, *Proc. Combust. Inst.* 35, 197–204 (2015).

# Probing the Reaction Dynamics of Hydrogen-Deficient Hydrocarbon Molecules and Radical Intermediates via Crossed Molecular Beams

Ralf I. Kaiser

Department of Chemistry, University of Hawai'i at Manoa, Honolulu, HI 96822

[ralfk@hawaii.edu](mailto:ralfk@hawaii.edu)

## 1. Program Scope

The major goals of this project are to explore experimentally in crossed molecular beams experiments the reaction dynamics and potential energy surfaces (PESs) of hydrocarbon molecules and their corresponding radical species, which are relevant to combustion processes. The reactions are initiated under single collision conditions by crossing two supersonic reactant beams containing radicals and/or closed shell species under a well-defined collision energy and intersection angle. By recording angular-resolved time of flight (TOF) spectra, we obtain information on the reaction products, intermediates involved, branching ratios of competing reaction channels, reaction energetics, and on the underlying reaction mechanisms. These data are of crucial importance to comprehend the formation of two key classes of molecules in combustion processes: resonantly stabilized free radicals (RSFRs) and (substituted) polycyclic aromatic hydrocarbons (PAHs).

## 2. Recent Progress

### 2.1. Nitrogen-Substituted (Polycyclic) Aromatic Hydrocarbons

Having explored the formation of (polycyclic) aromatic hydrocarbons (PAHs) and their acyclic isomers, [P1-14, P16-P20, P26], our research program exposed that nitrogen-substituted aromatics [pyridine ( $C_5NH_5$ ), (iso)quinoline ( $C_9NH_7$ ) and dihydro(iso)quinoline ( $C_9NH_9$ )] can be formed via reactions involving, for example, pyridinyl radicals ( $C_5H_4N$ ) and closed shell C2 and C4 hydrocarbons (acetylene, 1,3-butadiene) under single collision conditions as provided in crossed beam experiments and within a pyrolytic reactor. The reaction dynamics and formation pathways were compared to the benzene and PAH counterparts (naphthalene, 1,4-dihydronaphthalene). These projects were conducted in collaboration with experimental and theoretical groups involved in DOE-BES sponsored research including Dr. Ahmed (Lawrence Berkeley National Laboratory) and Prof. Mebel (Florida International University) [P15, P21, P22, P25].

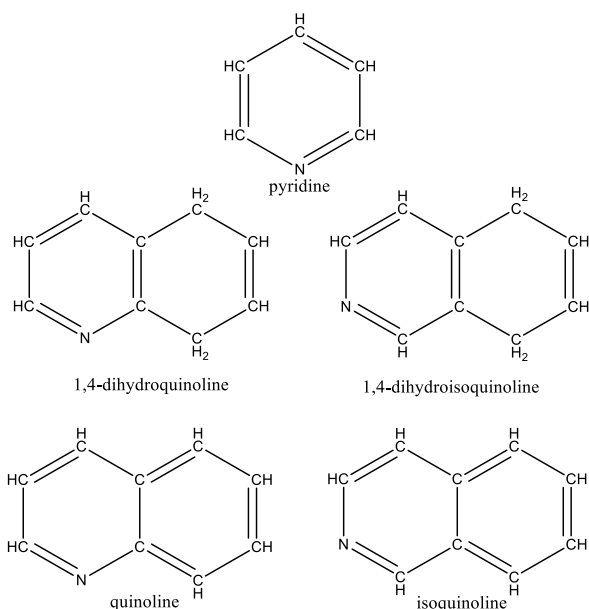


Fig. 1: Nitrogen-bearing aromatic hydrocarbons formed under single collision conditions and within a pyrolytic reactor: pyridine, 1,4-dihydro(iso)quinoline, and (iso)quinoline.



## 2.2. Acetylene Reactions Relevant to the Hydrogen Abstraction – Acetylene Addition Mechanism

Despite the popularity of the hydrogen abstraction – acetylene addition (HACA) mechanism, the underlying elementary reactions leading to PAH formation have not been verified experimentally to date under controlled experimental conditions. Exploiting our chemical reactor to simulate combustion conditions and interrogating the supersonically cooled product via tunable vacuum ultraviolet light (ALS), we exposed for the first time that HACA-type mechanisms can produce the prototype PAH naphthalene ( $C_{10}H_8$ ) via reactions of the styrenyl ( $C_8H_7$ ) and the *ortho*-vinylphenyl radicals ( $C_8H_7$ ) – key transient species of the HACA mechanism – with acetylene ( $C_2H_2$ ). This study highlights the importance of the HACA mechanism to the formation of the prototype PAH naphthalene. These studies have been expanded to unravel the formation of phenanthrene involving reactions of biphenyl radicals [P23, P27].

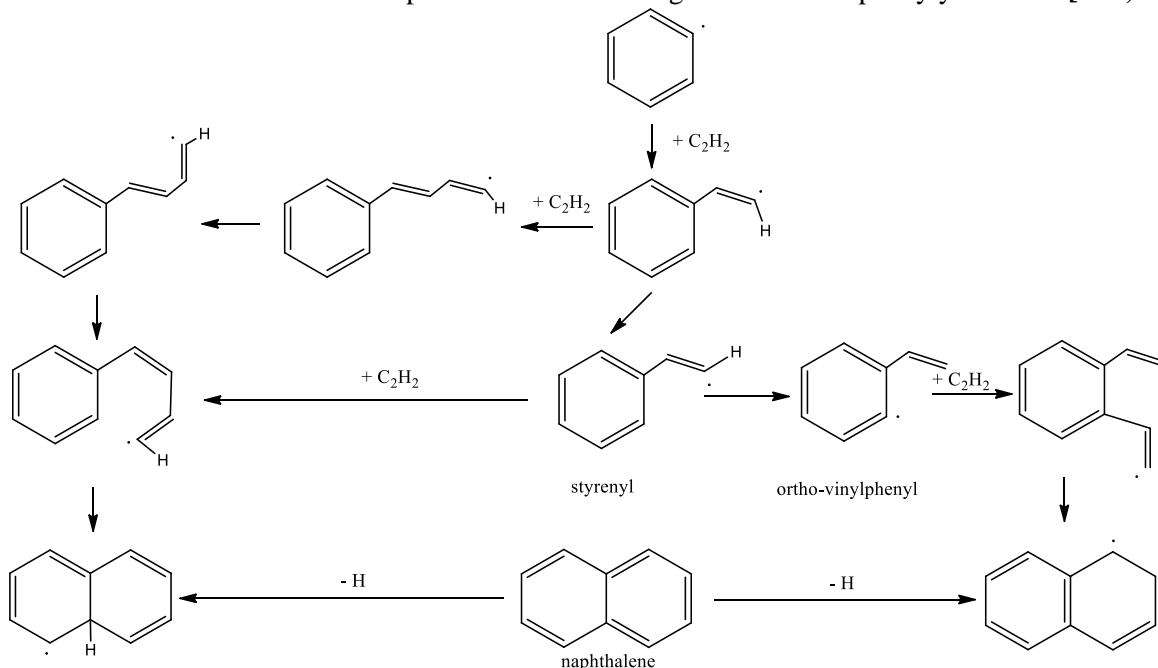


Fig. 2: Modified Bittner-Howard and Frenklach reaction sequences leading to the formation of naphthalene via styrenyl and *ortho*-vinylphenyl radicals, respectively. The reaction sequences in our experiments start with the reaction of the styrenyl and *ortho*-vinylphenyl radical.

## 2.3. Oxidation of Aromatic Radicals

Crossed molecular beam experiments were performed to elucidate the chemical dynamics of the *para*-tolyl radical reaction with molecular oxygen. Combined with theoretical calculations, the results show that *para*-tolyl is efficiently oxidized by molecular oxygen to *para*-toloxy plus ground state atomic via a complex forming, overall exoergic reaction (experimentally:  $-33 \pm 16 \text{ kJ mol}^{-1}$ ; computationally:  $-42 \pm 8 \text{ kJ mol}^{-1}$ ). Since the methyl group is distant from the radical site, it does not participate in the initial addition of molecular oxygen to *para*-tolyl. These results highlight an understanding of the reactivity of tolyl radicals and of the oxidation mechanism of aromatic precursors to polycyclic aromatic hydrocarbons (PAHs) in combustion systems [P18, P24].

## 3. Future Plans

We are planning to explore the formation of tri- and tetracyclic PAHs carrying six- membered rings such as anthracene/phenanthrene and triphenylene/pyrene under single collision conditions (Hawaii) and in the pyrolytic reactor (Advanced Light Source, Chemical Dynamics Beamline; collaboration with Musa Ahmed). Electronic structure calculations are conducted by Prof. Mebel (Florida International University).

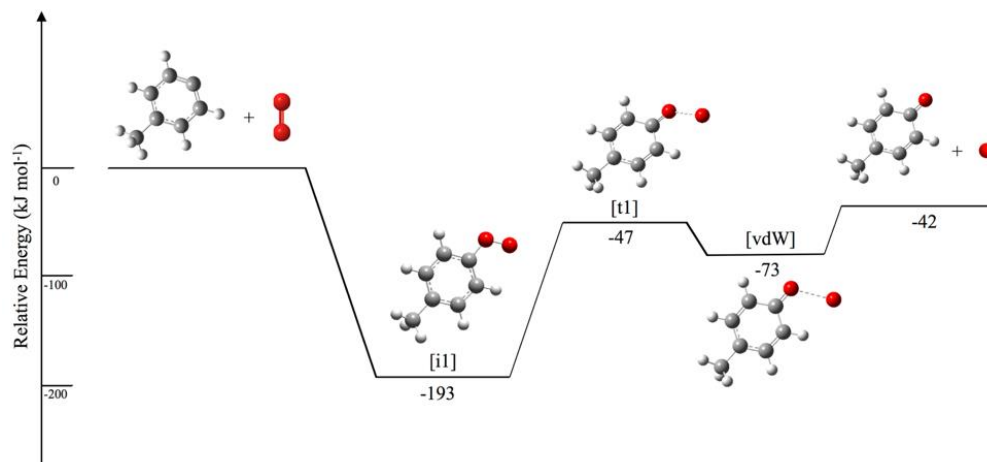


Fig. 3: Potential energy diagram for the reaction of *p*-tolyl ( $\text{H}_3\text{CC}_6\text{H}_4$ ,  $X^2A'$ ) with molecular oxygen ( $\text{O}_2$ ,  $X^3\Sigma_g^-$ ) forming the *p*-toloxyl ( $\text{H}_3\text{CC}_6\text{H}_4\text{O}$ ,  $X^2A'$ ) radical plus ground state atomic oxygen ( $\text{O}$ ,  $^3P_j$ ) calculated at the G3(MP2,CC)//B3LYP/6-311++G\*\* level of theory.

#### 4. Acknowledgements

This work was supported by US Department of Energy (Basic Energy Sciences; DE-FG02-03-ER15411).

#### 5. Publications Acknowledging DE-FG02-03ER15411 (1/2014 – now)

**P1** D.S.N. Parker, T. Yang, R. I. Kaiser, A. Landera, A. M. Mebel, *On the Formation of Ethynylbiphenyl ( $\text{C}_{14}\text{D}_5\text{H}_5$ ;  $\text{C}_6\text{D}_5\text{C}_6\text{H}_4\text{CCH}$ ) Isomers in the Reaction of D5-Phenyl Radicals ( $\text{C}_6\text{D}_5$ ;  $X^2A_1$ ) with Phenylacetylene ( $\text{C}_6\text{H}_5\text{C}_2\text{H}$ ;  $X^1A_1$ ) Under Single Collision Conditions.* CPL 595, 230-236 (2014).

**P2** D.S.N. Parker, B. B. Dangi, R.I. Kaiser, A. Jamal, M.N. Ryazantsev, K. Morokuma, A. Korte, W. Sander, *An Experimental and Theoretical Study on the Formation of 2-Methylnaphthalene ( $\text{C}_{11}\text{H}_{10}/\text{C}_{11}\text{H}_3\text{D}_7$ ) in the Reactions of the Para-Tolyl ( $\text{C}_7\text{H}_7$ ) and Para-Tolyl-d7 ( $\text{C}_7\text{D}_7$ ) with Vinylacetylene ( $\text{C}_4\text{H}_4$ ).* The Journal of Physical Chemistry A, 118, 2709-2718 (2014).

**P3** B.B. Dangi, D.S.N. Parker, T. Yang, R.I. Kaiser, A.M. Mebel, *Gas Phase Synthesis of the Benzyl Radical ( $\text{C}_6\text{H}_5\text{CH}_2$ ).* Angew. Chemie Int. Ed. 53, 4608-4613 (2014).

**P4** D.S.N. Parker, S. Maity, B.B. Dangi, R.I. Kaiser, T. Labrador, A. M. Mebel, *Understanding the Chemical Dynamics of the Reactions of Dicarbons with 1-Butyne, 2-Butyne, and 1,2-Butadiene – Toward the Formation of Resonantly Stabilized Free Radicals.* Physical Chemistry Chemical Physics 16, 12150-12163 (2014).

**P5** B. B. Dangi, D.S.N. Parker, R.I. Kaiser, A.M. Mebel, *An Experimental and Theoretical Investigation of the Formation of  $\text{C}_7\text{H}_7$  Isomers in the Bimolecular Reaction of Dicarbons with 1,3-Pentadiene.* Chem. Phys. Lett. 607 92-99 (2014).

**P6** T. Yang, D.S.N. Parker, B. Dangi, R.I. Kaiser, V.V. Kislov, A.M. Mebel, *Crossed Beam Reactions of the Reaction of Phenyl ( $\text{C}_6\text{H}_5$ ;  $X^2A_1$ ) and D5-Phenyl Radical ( $\text{C}_6\text{D}_5$ ;  $X^2A_1$ ) with 1,2-Butadiene ( $\text{H}_2\text{CCCHCH}_3$ ;  $X^1A'$ ).* The Journal of Physical Chemistry A 118, 4372–4381 (2014).

**P7** B.B. Dangi, T. Yang, R.I. Kaiser, A.M. Mebel, *Reaction Dynamics of the 4-Methylphenyl Radical ( $\text{C}_6\text{H}_4\text{CH}_3$ ; *p*-Tolyl) with Isoprene ( $\text{C}_5\text{H}_8$ ) - Formation of Dimethyldihydronaphthalenes.* Physical Chemistry Chemical Physics 16, 16805-16814 (2014).

**P8** D.S.N. Parker, R.I. Kaiser, T. Troy, M. Ahmed, *Hydrogen Abstraction Acetylene Addition Revealed!* Angew. Chemie Int. Edition 53, 7440-7444 (2014).

**P9** R.I. Kaiser, B.B. Dangi, T. Yang, D.S.N. Parker, A.M. Mebel, *Reaction Dynamics of the 4-Methylphenyl Radical (*p*-Tolyl) with 1,2-Butadiene (1-Methylallene) – Are Methyl Groups purely Spectators?* The Journal of Physical Chemistry A 118, 6181-6190 (2014).

- P10** D.S.N. Parker, B. B. Dangi, R.I. Kaiser, A. Jamal, K. Morokuma, *Formation of 6-Methyl-1,4-Dihydronaphthalene in the Reaction of the Para-Tolyl Radical with 1,3-Butadiene under Single Collision Conditions*. The Journal of Physical Chemistry A 118, 12111-12119 (2014).
- P11** R.I. Kaiser, D.S.N. Parker, A.M. Mebel, *Reaction Dynamics in Astrochemistry: Low Temperature Pathways to Polycyclic Aromatic Hydrocarbons (PAHs) in the Interstellar Medium (ISM)*. Annu. Rev. Physical Chemistry 66, 43-67 (2015).
- P12** T. Yang, L. Muzangwa, D.S.N. Parker, R. I. Kaiser, A.M. Mebel, *Synthesis of 2- and 1-Methyl-1,4-Dihydronaphthalene Isomers studied via the Crossed Beam Reactions of Phenyl Radicals ( $C_6H_5$ ) with 1,3-Pentadiene ( $CH_2CHCHCHCH_3$ ) and Isoprene ( $CH_2C(CH_3)CHCH_2$ )*. Physical Chemistry Chemical Physics, 17, 530-540 (2015).
- P13** L.G. Muzangwa, R.I. Kaiser, T. Yang, D.S.N. Parker, A.M. Mebel, A. Jamal, K. Morokuma, *A Crossed Molecular Beam and Ab Initio Study on the Formation of 5- and 6-Methyl-1,4-Dihydronaphthalene ( $C_{11}H_{12}$ ) via the Reaction of Meta-Tolyl ( $C_7H_7$ ) with 1,3-Butadiene ( $C_4H_6$ )*. Physical Chemistry Chemical Physics 17, 7699-7706 (2015).
- P14** T. Yang, D.S.N. Parker, B. B. Dangi, R. I. Kaiser, A.M. Mebel, *Formation of 5- and 6-Methyl-1H-Indene ( $C_{10}H_{10}$ ) via the Reactions of the Para-Tolyl Radical ( $C_6H_4CH_3$ ) with Allene ( $H_2CCCH_2$ ) and Methylacetylene ( $HCCCH_3$ ) under Single Collision Conditions*. Physical Chemistry Chemical Physics 17, 10510-10519 (2015).
- P15** D.S.N. Parker, R.I. Kaiser, O. Kostko, T.P. Troy, M. Ahmed, A.M. Mebel, A.G.G.M. Tielens, *On the Synthesis of (Iso)Quinoline in Circumstellar Envelopes and Its Role in the Formation of Nucleobases in the Interstellar Medium*. The Astrophysical Journal 803-812, 53 (2015).
- P16** D.S.N. Parker, R.I. Kaiser, O. Kostko, T.P. Troy, M. Ahmed, *Unexpected Chemistry from the Reaction of Naphthyl plus Acetylene Molecules*. Angewandte Chemie – International Edition 54, 5421-5424 (2015).
- P17** D.S.N. Parker, R.I. Kaiser, O. Kostko, M. Ahmed, *Selective Formation of Indene via the Reaction of Benzyl Radicals with Acetylene* Chem. Phys. Chem. 16, 2091-2093 (2015).
- P18** D.S.N. Parker, R.I. Kaiser, T. P. Troy, O. Kostko, M. Ahmed, A.M. Mebel, *Toward the Oxidation of the Phenyl Radical and Prevention of PAH Formation in Combustion Systems*. The Journal of Physical Chemistry A 119, 7145-7150 (2015).
- P19** T. Yang, L. Muzangwa, R.I. Kaiser, A. Jamal, K. Morokuma, *A Combined Crossed Molecular Beam and Theoretical Investigation of the Reaction of the Meta-Tolyl Radical with Vinylacetylene - Toward the Formation of Methyl-naphthalenes*. Physical Chemistry Chemical Physics 17, 21564 - 21575 (2015).
- P20** A.M. Mebel, R.I. Kaiser, *Formation of Resonantly Stabilized Free Radicals via the Reactions of Atomic Carbon, Dicarbon, and Tricarbon with Unsaturated Hydrocarbons: Theory and Crossed Molecular Beams Experiments*. Int. Rev. Phys. Chem. 34, 461-514 (2015).
- P21** D.S.N. Parker, R.I. Kaiser, O. Kostko, T.P. Troy, M. Ahmed, A.H.H. Chang, *On the Formation of Pyridine in the Interstellar Medium*. Physical Chemistry Chemical Physics 17, 32000 – 32008 (2015).
- P22** D.S.N. Parker, T. Yang, B.B. Dangi, R.I. Kaiser, P.Bera, T.J. Lee, *Low Temperature Formation of Nitrogen-Substituted Polycyclic Aromatic Hydrocarbons (NPAHs) - Barrierless Routes to Dihydro(iso)quinolines*, 815, 115 The Astrophysical Journal (2015).
- P23** T. Yang, R.I. Kaiser, A.M. Mebel, T. P. Troy, M. Ahmed, *Hydrogen Abstraction – Acetylene Addition Exposed* Angewandte Chemie – International Edition 55, 14983-14987 (2016).
- P24** A.M. Thomas, T. Yang, B.B. Dangi, R.I. Kaiser, A.M. Mebel, *Oxidation of the Para-Tolyl Radical by Molecular Oxygen Under Single Collision Conditions - Formation of the Para-Toloxyl Radical*. J. Phys. Chem. Lett 7, 5121-5127 (2016).
- P25** D.S.N. Parker, R.I. Kaiser, *On the Formation of Nitrogen-Substituted Polycyclic Aromatic Hydrocarbons (NPAHs) in Circumstellar and Interstellar Environments*. Chem. Soc. Rev 46, 452 - 463 (2017).
- P26** A.M. Mebel, A.Landera, R.I. Kaiser, *Formation Mechanisms of Naphthalene and Indene: From the Interstellar Medium to Combustion Flames*. The Journal of Physical Chemistry A 121, 901–926 (2017).
- P27** T. Yang, R.I. Kaiser, A.M. Mebel, T. P. Troy, M. Ahmed, *On the Formation of Phenanthrene in Extreme Environments and Implications for the Hydrogen-Abstraction/Acetylene-Addition (HACA) Mechanism* (submitted 2017).

# Time-Resolved Nonlinear Optical Diagnostics

Christopher J. Kliewer (PI)  
Combustion Research Facility, Sandia National Laboratories  
P.O. Box 969, MS 9055  
Livermore, CA 94551-0969  
cjkliew@sandia.gov

## Program Scope

This program focuses on the development of innovative laser-based techniques for measuring temperature and concentrations of important combustion species as well as the investigation of fundamental physical and chemical processes that directly affect quantitative application of these techniques. Our development efforts focus on crossed-beam approaches such as time-resolved nonlinear wave-mixing. A critical aspect of our research includes the study of fundamental spectroscopy, energy transfer, molecular dynamics, and photochemical processes. This aspect of the research is essential to the development of accurate models and quantitative application of techniques to the complex environments encountered in combustion systems. These investigations use custom-built tunable picosecond (ps) and commercial femtosecond lasers, which enable efficient nonlinear excitation, provide high temporal resolution for pump/probe studies of collisional processes, and are amenable to detailed physical models of laser-molecule interactions.

## Recent Progress

**Development and validation of a time-domain  $H_2$  pure-rotational CARS model enabled by ultrabroadband CARS.** Our recent development of two-beam ultrabroadband CARS has allowed for the first measurement of the full pure-rotational coherent anti-Stokes Raman spectrum (RCARS) of the  $H_2$  molecule (Fig. 1). At flame temperatures, the  $H_2$  RCARS spectrum spans from 0-2200  $cm^{-1}$ . Although  $H_2$  is of interest given its prevalence as a reactant and product in many gas-phase reactions, laser bandwidth limitations have precluded the extension of CARS thermometry to the full  $H_2$  S-branch. As a low mass molecule with wide energy level spacings,  $H_2$  is also important in the validation of common assumptions in collisional energy transfer thermal equilibration, and thus the ability to measure instantaneously the mode-specific temperature could provide insight into the process of thermalization and the validity of the equipartition theorem. Thus, we have recently studied the viability of utilizing S-branch  $H_2$  RCARS for mode-specific thermometry and combustion diagnostics. RCARS thermometry is generally regarded as more accurate than its vibrational counterpart (VCARS) at lower temperatures because of the absence of a significantly populated hot vibrational band. However, once temperatures are high enough, a significant fractional population exists in the first vibrational excited state, and VCARS is regarded as the more accurate technique. For the  $N_2$  molecule, this temperature threshold is around  $\sim 1200$  K, at

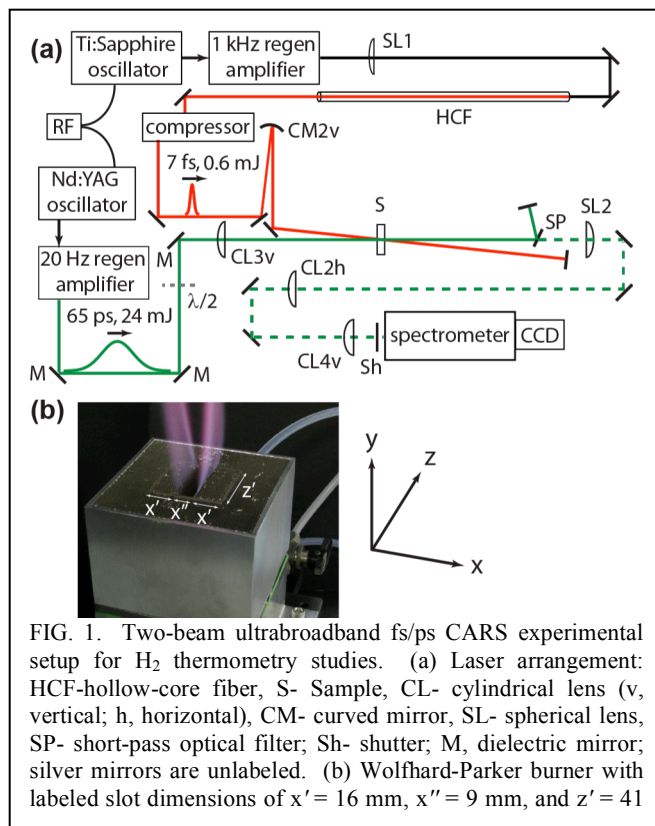


FIG. 1. Two-beam ultrabroadband fs/ps CARS experimental setup for  $H_2$  thermometry studies. (a) Laser arrangement: HCF-hollow-core fiber, S- Sample, CL- cylindrical lens (v, vertical; h, horizontal), CM- curved mirror, SL- spherical lens, SP- short-pass optical filter; Sh- shutter; M, dielectric mirror; silver mirrors are unlabeled. (b) Wolfhard-Parker burner with labeled slot dimensions of  $x' = 16$  mm,  $x'' = 9$  mm, and  $z' = 41$

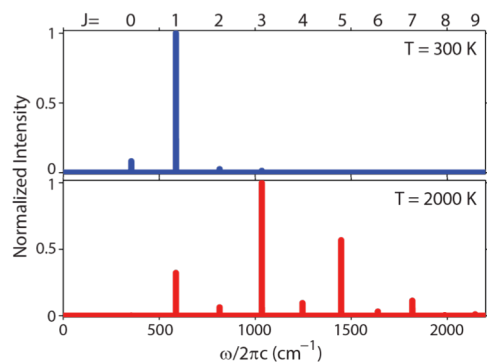


FIG. 2. The height-normalized set of pure-rotational H<sub>2</sub> CARS transitions out of initial states  $J = [0, 9]$  are simulated for two temperatures: 300 K (top panel, blue) and 2000 K (bottom panel, red) using our new time-domain H<sub>2</sub> CARS model.

which point a Boltzmann analysis shows  $\sim 6\%$  of the vibrational population resides in the  $v = 1$  initial state. The H<sub>2</sub> molecule has a larger vibrational transition energy, and a temperature of  $\sim 2140$  K is required to achieve the same 6% population of  $v = 1$ . Thus, the accuracy advantage of RCARS over VCARS for H<sub>2</sub> thermometry may conceivably exist at even higher temperatures than for N<sub>2</sub> thermometry. N<sub>2</sub> is a dominant species in air-fed combustion reactions, and its linewidth, line-broadening, and other spectroscopic parameters are better known than those of H<sub>2</sub>. Thus, developing a fitting model for H<sub>2</sub> spectra requires careful calibration and testing of the various parts of the model, such as the Herman-Wallis factors which account for the vibration-rotation interaction, and the collisional linewidths. We performed ultrabroadband CARS measurements of H<sub>2</sub> in both a heated flow up to 700 K, and in a standard Wolfhard-Parker burner to access temperatures up to 1700 K. We composed a time-domain coherent Raman model similar to our previous N<sub>2</sub> pure-rotational CARS code. Fig. 2 displays the evolution of the calculated spectral line intensities with elevated temperature from our model. Because the supercontinuum source drives transitions across the entire range from 0-4000 cm<sup>-1</sup>, we simultaneously monitor the CARS signal from H<sub>2</sub> and N<sub>2</sub>, and the N<sub>2</sub> provided an excellent internal standard for evaluating our ability to accurately fit the H<sub>2</sub> spectra. From 300–650 K in the heated flow, the H<sub>2</sub> and N<sub>2</sub> CARS extracted temperatures were, on average, within 2% of the set temperature. For flame measurements, the fitted H<sub>2</sub> and N<sub>2</sub> temperatures were, on average, within 5% of each other from 300–1600K. Our results confirmed the viability of pure-rotational H<sub>2</sub> CARS thermometry for probing combustion reactions.

**Dispersive Fourier Transformation for Megahertz Detection of Coherent Raman Spectra.** While much recent effort has been devoted to the development of high-rate Raman-based techniques and new high repetition rate laser sources, far less focus has been placed on our ability to detect coherent Raman signals at equivalently high scan rates. However, to follow time-correlated dynamics of a system which is evolving on the time scale of  $\mu\text{s}$ , the spectral detection strategy must also be capable of a very high refresh rate, in the megahertz regime. Cutting-edge CMOS camera technologies are now capable of 1 MHz detection frame rates when operated in a cropped array mode with  $\sim 128$  active pixels across the chip for spectral detection. Such systems are however limited to 12-bit depth, while the squared dependence on molecular density for coherent Raman spectroscopy often requires 14- or 16-bit depth for sufficient dynamic range. Line-scan CCD cameras have been demonstrated for continuous spectral measurements at 100-kHz, for example, in transient absorption spectroscopy experiments. Faster CCD detection rates may be possible with multi-frame CCD options, but such technologies are limited by the physical framing built into the camera to  $\sim 10$ 's of frames and also suffer from blooming effects as the charge is transferred through the storage array, reducing the quantitative accuracy of stored data. As a possible solution, we have explored the possibility of frequency-resolved spectral detection performed in the time-domain by the technique of dispersive Fourier transformation (DFT) [A]. The basic idea, depicted in Fig. 3, is to send the pulsed

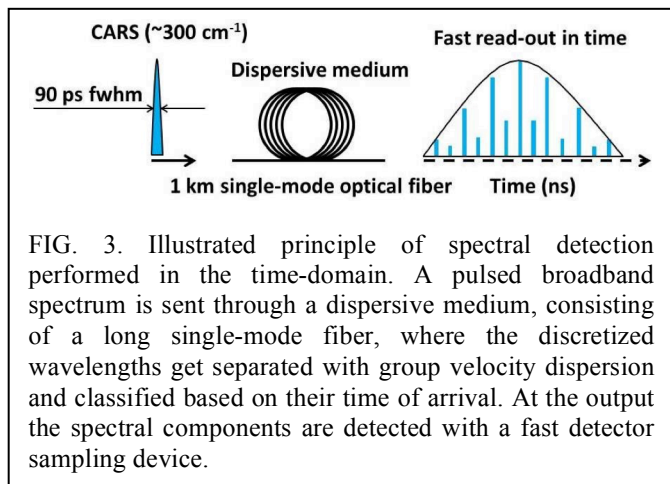


FIG. 3. Illustrated principle of spectral detection performed in the time-domain. A pulsed broadband spectrum is sent through a dispersive medium, consisting of a long single-mode fiber, where the discretized wavelengths get separated with group velocity dispersion and classified based on their time of arrival. At the output the spectral components are detected with a fast detector sampling device.

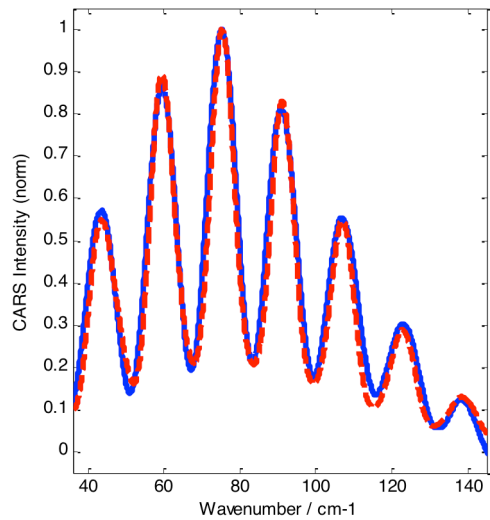


FIG. 4. (Blue) Measured CARS spectrum of  $N_2$  at 295 K, as detected through the DFT detector. The time axis has been converted to Raman shift by accounting for the dispersion of the fiber. The total detection time is 20 nanoseconds (50 MHz). (Red) The simulated CARS spectrum of  $N_2$  at 295 K, convolved with the instrument response function of the current DFT spectrometer. Quantitative spectral agreement is demonstrated.

Alternatively, the same spectral resolution could be achieved with far less fiber length, with a corresponding linear gain in signal count.

## Future Work

**High-pressure diagnostics development.** We have recently completed the construction of an optical high pressure cell capable of up to 100 atm pressure and up to 1000 K temperature, and incorporated an active pulse-shaper into our femtosecond laser setup to correct for higher order chirp in the cell windows. Thus, we plan to continue development of high pressure nonlinear mixing strategies, and tailored probe arrangements for multiplex coherent imaging of temperature and species concentrations at high pressure. Nonlinear optical strategies benefit from the squared number density dependence at high pressure, but fast dephasing requires the use of tailored probe pulses. We plan to develop molecular phase mask pulse shaping for excitation of only the species of interest, while eliminating the broad signal from neighboring transitions of other species which are collisionally broadened.

**Multiplexing 2D-CARS with particle imaging velocimetry (PIV).** With the recent development of the first 2D-CARS measurements in our lab, our plan is to begin multiplexing the diagnostic with other techniques to gain access to joint statistics not previously attainable, such as the instantaneous thermal field and flow field obtained by combining 2D-CARS with PIV, respectively. Initial experiments will be conducted to determine if the particle scattering will interfere with the interpretation of the 2D-CARS signals, since the temperature is extracted by retrieving intensity spectra. However, since the signal is Raman shifted from the scattering frequency, it is expected that the PIV measurement will not interfere with the 2D-CARS assessment. Once this is determined, in collaboration with Dr. Jonathan Frank (CRF,

broadband CARS signal through a long fiber where the intrinsic group velocity dispersion (GVD) of the medium acts to spectrally separate the different wavelengths of the signal. Then, at the output of the fiber, a fast single-pixel detector (fast photodiode) and high bandwidth oscilloscope are used to detect the arriving highly dispersed photons, akin to a time-of-flight instrument. Using this technique, we were able to detect frequency-resolved CARS spectra within a 20 nanosecond detection window, at which point the photodiode and oscilloscope are ready for the next wave form, indicating an upper detection scan rate of 50 MHz, faster than any other coherent Raman detection strategy reported to date. In Fig. 4, a spectrum of  $N_2$  collected at 295 K is fitted by convolving the simulated CARS spectrum with the instrument response function and modeling the frequency-to-time conversion as,  $\Delta\tau = |D|z\Delta\omega$ , where  $D$  is the GVD of the dispersive element, which was measured to be  $D = 496 \text{ ps nm}^{-1} \text{ km}^{-1}$ ,  $\Delta\omega$  is the bandwidth of the signal pulse and  $z$  is the propagation distance in the fiber. As can be seen, quantitative fits are achieved. In the next step for the DFT spectrometer, we plan to explore simultaneous stimulated Raman pumping within the fiber element to fully compensate for signal loss encountered by propagation through the single-mode fiber. Further, our current oscilloscope bandwidth (6 GHz) is the limiting factor in the achievable resolution with the setup, and we plan to purchase a higher bandwidth oscilloscope which will improve the spectral resolution by several fold.

Sandia), we will perform joint PIV and 2D-CARS in turbulent DME flames of current interest in Jonathan's lab. Planar CARS measurements before and after the addition of the PIV seeding particles at increasing densities will ensure the negligible effects of the seeding density on the combustion itself, or, at least, set an upper limit on the seeding density before perturbations to the evaluated 2D-CARS temperatures are observed.

**Single-shot correction for laser chaos.** The 7 femtosecond supercontinuum pulse used in our ultrabroadband CARS experiments is generated by focusing the femtosecond laser output through a hollow core fiber filled with noble gas. The fiber acts as a waveguide to keep the intensity high enough for significant self-phase modulation to occur on the pulse, which has the effect of adding significant bandwidth. This bandwidth is then compressed after the fiber, allowing the generation of ultrashort pulses. Unfortunately, highly nonlinear processes occurring in the fiber are chaotic, and result in a pulse spectrum that varies substantially from shot to shot. This ultimately limits the single-laser-shot precision attainable in the multiple species measurement capability the technique enables. However, by detecting the nonresonant signal separate from the resonant signal of interest, a single-laser-shot measurement of the effective excitation profile of the laser could be achieved. This would dramatically increase the precision of ultrabroadband CARS measurements by enabling on-the-fly correction for the fluctuating excitation profile. We plan to achieve this by one of two methods: 1) polarization based separation of the resonant and nonresonant signals detected through separate spectrometer channels, or 2) using a portion of the beam to mix in a high pressure cell of argon and detect the resulting signal on a separate camera.

**Direct measurement of  $N_2$ -Fuel and  $N_2$ - $H_2O$  broadening coefficients.** With the successful development of the time-domain technique for acquiring high-accuracy S-branch broadening coefficients, demonstrated thus far for the  $N_2$ - $N_2$  and  $N_2$ - $H_2$  collisional systems, we propose to continue the collaboration with Per-Erik Bengtsson of Lund University, Sweden, to tackle the relative paucity of broadening coefficient data in the literature for air-fuel collisional systems. Initial studies will focus on the collisional broadening of  $N_2$  and  $O_2$  when perturbed by DME, ethane, ethylene, propane, and propylene. Accurate broadening models must be developed for these collisional environments, especially at elevated pressures. We will alter our current time-domain CARS code to implement these new linewidth libraries and test the validity of the model in our newly constructed high-pressure, high-temperature cell.

## References

- A. K. Goda and B. Jalali, "Dispersive Fourier transformation for fast continuous single-shot measurements," *Nat Photon* 7, 102-112 (2013).

## Journal publications supported by this BES project (2015-2017)

1. A. Bohlin, M. Mann, B.D. Patterson, A. Dreizler, C. J. Kliewer, "Development of two-beam femtosecond/picosecond one-dimensional rotational coherent anti-Stokes Raman spectroscopy: time-resolved probing of flame wall interactions," *Proc. Combust. Inst.* **35**, 3723-3730 (2015).
2. A. Bohlin and C. J. Kliewer, "Direct Coherent Raman Temperature Imaging and Wideband Chemical Detection in a Hydrocarbon Flat Flame," *J. Phys. Chem. Lett.* **6**, 643-649 (2015)
3. M. Campbell, A. Bohlin, P. Schrader, R. Bambha, C. J. Kliewer, K. Johansson, and H. Michelsen, "Design and characterization of a linear Hencken-type burner," *Rev. Sci. Instrum.* **87**, 115114 (2016)
4. A. Bohlin, C. Jainski, B.D. Patterson, A. Dreizler, and C.J. Kliewer, "Multiparameter spatio-thermochemical probing of flame-wall interactions advanced with coherent Raman imaging," *Proc. Combust. Inst.* **36**, 4557-4564 (2017)
5. T.L. Courtney, A. Bohlin, B.D. Patterson, C.J. Kliewer, "Pure-Rotational  $H_2$  Thermometry by Ultrabroadband Coherent Anti-Stokes Raman Spectroscopy," *J. Chem. Phys.* (2017) *submitted*
6. A. Bohlin, B.D. Patterson, C.J. Kliewer, "Dispersive Fourier Transformation for Megahertz Detection of Coherent Raman Spectra," *Optica* (2017) *submitted*

## THEORETICAL CHEMICAL KINETICS

Stephen J. Klippenstein  
Chemical Sciences and Engineering Division  
Argonne National Laboratory  
Argonne, IL, 60439  
[sjk@anl.gov](mailto:sjk@anl.gov)

### Program Scope

The focus of this program is the development and application of theoretical methods for exploring gas phase chemical kinetics. The research involves a combination of *ab initio* electronic structure calculations, variational transition state theory (TST), classical trajectory simulations, and master equation (ME) calculations. Detailed applications, including careful comparisons with experiment as feasible, are used to (i) develop a deeper understanding of the applicability of various foundational principles of gas phase chemical kinetics, (ii) motivate improvements in theoretical chemical kinetics methodologies, and (iii) enhance our understanding of various aspects of combustion chemistry. The specific reactions studied are generally motivated by our interactions with combustion modeling efforts and include studies of (i) polycyclic aromatic hydrocarbon (PAH) formation, (ii) hydrocarbon oxidation, and (iii) NO<sub>x</sub> chemistry.

### Recent Progress

*Chemically Termolecular Transformations in Combustion:* Ephemeral collision complexes, formed from two molecules colliding, are generally not thought to react chemically with a third molecule in the gas-phase systems of combustion and planetary atmospheres. Such “chemically termolecular” reactions, involving three chemically participating molecules, were hypothesized long ago in studies establishing radical chain branching mechanisms, but were later concluded to be unimportant. In collaboration with Burke (Columbia) we have used a combination of *ab initio* ME and kinetic-transport simulations to reveal that reactions of H + O<sub>2</sub> collision complexes with other radicals (i.e., H, OH, and O) constitute major kinetic pathways under common combustion situations. These reactions are also found to influence flame propagation speeds, a common measure of global reactivity. Notably, these reactions tend to reduce the flame speed, which compensates to some extent for the increase in the flame speed that arises from the consideration of the direct decomposition of HCO. Analogous chemically termolecular reactions mediated by ephemeral collision complexes are likely of significance in various combustion and planetary environments.

*Accurate Anharmonic Zero Point Energies:* Currently, the effect of vibrational anharmonicities is often the greatest uncertainty in high-level theoretical predictions of the 0 K heat of formation. Harding, whose abstract contains a more detailed discussion of this work, performed diffusion Monte Carlo calculations with CCSD(T)/cc-pVTZ based analytic potential energy surfaces for 48 small combustion relevant species. A comparison of these high-accuracy predictions of the anharmonic zero-point energies with related vibrational perturbation theory (VPT2) based evaluations illustrates the limitations of VPT2 for different classes of molecules.

*Decomposition Kinetics of Criegee Intermediates (CI):* Lester (Penn) has recently developed a vibrational activation based method for directly observing the microcanonical dissociation rates for CIs. Her observations for CH<sub>3</sub>CHOO, (CH<sub>3</sub>)<sub>2</sub>COO, and CH<sub>3</sub>CH<sub>2</sub>CHOO



provide critical tests for statistical theories of the decomposition process. In prior work, we collaborated with Lester in predicting the decomposition rates with RRKM theory based on high-level electronic structure methods. Recently, Lester and coworkers have extended the observations for  $\text{CH}_3\text{CHOO}$  and  $(\text{CH}_3)_2\text{COO}$  to lower energies, where the decomposition is clearly dominated by tunneling. For  $\text{CH}_3\text{CHOO}$ , the observed rates appear to fluctuate about the RRKM predictions, which is perhaps due to the sparsity of the vibrational density of states for this small molecule at low energies or to some form of mode specific behaviour. Overall though, the *a priori* RRKM theory predictions retain their remarkably good agreement with the experimental data, with maximum deviations on the order of 30%. This agreement allows for the quantitative prediction of the thermal high-pressure decomposition rates, which are of utility for both atmospheric and combustion modeling, where these species are prevalent.

*Chemical Kinetic Modeling of Methyl Trans-3-Hexenoate Epoxidation by  $\text{HO}_2$* : In collaboration with Nicolle and de Bruin (both at IFPEN), a bottom-up methodology, involving post-Hartree-Fock electronic structure calculations, RRKM-ME kinetic modeling, and macrokinetic reactor modeling was used to explore the epoxidation of methyl trans-3-hexenoate, a realistic biodiesel surrogate, by hydroperoxy radicals. The obtained rate constants are in good agreement with experimental data for alkenes epoxidation by  $\text{HO}_2$ . Incorporating the predicted rate constants into a detailed combustion mechanism resulted in fairly good agreement with engine experiments.

*Formation of Indene and its Conversion to Naphthalene*: In collaboration with Mebel (FIU), we continue to explore the kinetics of reactions of relevance to the expansion from one to two aromatic rings. To this end, we recently used our MESS code to obtain ab initio TST based ME predictions of the temperature and pressure dependent kinetics for a number of reactions on the  $\text{C}_9\text{H}_9$  and  $\text{C}_9\text{H}_{11}$  potential energy surfaces. These predictions contribute to a mapping of the pathways for formation of indene and for the conversion of indene to naphthalene.

## Future Directions

We continue to be interested in exploring the foundations of kinetic modeling, through careful analysis of the dynamics and kinetics of combustion relevant reactions. Currently, we are particularly interested in developing formalisms for treating the instability of radicals that commonly arises in the 1000 - 2000 K temperature range. Within the ME, this instability is evidenced by the corresponding chemically significant eigenvalue becoming similar in magnitude to those for internal energy relaxation. In effect, chemical transformations happen as rapidly as collisional thermalization and the species ceases to exist as a chemical species that can be trapped in a thermal environment. One consequence of this instability is that the corresponding phenomenological rate coefficients for the isomerization and decomposition of this species also cease to exist. The chemically significant eigenvalue approach, as implemented in our MESS program, properly produces rate coefficients for all the species that exist at a given temperature and pressure, merging species together as their eigenvalues enter the continuum and then producing rate constants for the merged species. However, there is still a conundrum for chemical modeling: as currently formulated, rate descriptions must be provided for all species at all temperatures of relevance to the simulation. In other words, there is no possibility for a species to disappear with temperature. We plan to explore possible solutions to this conundrum.

We continue to collaborate with Jasper on the development of effective procedures for coupling trajectory simulations of energy transfer with the two-dimensional ME in order to accurately predict the pressure dependence of chemical reaction kinetics. The key next step in

this effort will involve improved procedures for obtaining simplified yet kinetically accurate descriptions of the energy and angular momentum transition kernels.

Further collaborations with Lester and Hase (Texas Tech) are planned for the analysis of the kinetics of CIs. Work with Lester is now exploring the effects of isotopic substitution, which provides severe constraints on the models and often illuminates unexpected shortcomings. A collaboration with Hase, Harding, and Jasper is using a combination of direct dynamics and ME modeling to explore the role of direct decomposition of the incipient CI arising from ozonolysis. We are also planning a ME analysis of the secondary decomposition of the vinyl hydroperoxide formed from the isomerization of the CI.

### DOE Supported Publications, 2015-Present

1. **Pressure-Dependent Branching in the Reaction of  $^1\text{CH}_2$  with  $\text{C}_2\text{H}_4$  and other Reactions on the  $\text{C}_3\text{H}_6$  Potential Energy Surface**, L. Ye, Y. Georgievskii, S. J. Klippenstein, *Proc. Comb. Inst.* **35**, 223-230 (2015).
2. **The Role of Prompt Reactions in Ethanol and Methylformate Low-Pressure Flames**, N. J. Labbe, R. Sivaramakrishnan, S. J. Klippenstein, *Proc. Comb. Inst.* **35**, 447-455 (2015).
3. **Effects of New *Ab Initio* Rate Coefficients on Predictions of Species Formed During *n*-Butanol Ignition**, D. M. A. Karwat, M. S. Wooldridge, S. J. Klippenstein, M. J. Davis, *J. Phys. Chem. A* **119**, 543-551 (2015).
4. **Hydrolysis of Ketene Catalyzed by Formic Acid: Modification of Reaction Mechanism, Energetics, and Kinetics with Organic Acid Catalysis**, M. K. Louie, J. S. Francisco, M. Verdicchio, S. J. Klippenstein, A. Sinha, *J. Phys. Chem. A* **119**, 4347-4357 (2015).
5. ***Ab Initio* Variational Transition State Theory and Master Equation Study of the Reaction  $(\text{OH})_3\text{SiOCH}_2 + \text{CH}_3 = (\text{OH})_3\text{SiOC}_2\text{H}_5$** , D. Nurkowski, S. J. Klippenstein, Y. Georgievskii, M. Verdicchio, A. W. Jasper, J. Akroyd, S. Mosbach, M. Kraft, *Zeit. Phys. Chem.*, **229**, 691-708 (2015).
6. **The 2014 KIDA Network for Interstellar Chemistry**, V. Wakelam, J.-C. Loison, E. Herbst, B. Pavone, A. Bergeat, K. Beroff, M. Chabot, A. Faure, W. D. Geppert, D. Gerlich, P. Gratier, N. Harada, K. M. Hickson, P. Honvault, S. J. Klippenstein, S. D. LePicard, G. Nyman, M. Ruaud, S. Schlemmer, I. R. Sims, D. Talbi, J. Tennyson, R. Wester, *Astrophys. J. Supp.*, **217**, 20 (2015).
7. **Resolving Some Paradoxes in the Thermal Decomposition Mechanism of Acetaldehyde**, R. Sivaramakrishnan, J. V. Michael, L. B. Harding, S. J. Klippenstein, *J. Phys. Chem. A*, **119**, 7724-7733 (2015).
8. **Kinetics of Propargyl Radical Dissociation**, S. J. Klippenstein, J. A. Miller, A. W. Jasper, *J. Phys. Chem. A* **119**, 7780-7791 (2015).
9. **Global Uncertainty Analysis for RRKM/Master Equation Based Kinetic Predictions: A Case Study of Ethanol Decomposition**, L. Xing, S. Li, Z. Wang, B. Yang, S. J. Klippenstein, F. Zhang, *Comb. Flame* **162**, 3427-3436 (2015).
10. **Comment on "A Novel and Facile Decay Path of Criegee Intermediates by Intramolecular Insertion Reactions via Roaming Mechanisms"**, L. B. Harding, S. J. Klippenstein, *J. Chem. Phys.* **143**, 167101 (2016).
11. **Dimethylamine Addition to Formaldehyde Catalyzed by a Single Water Molecule: A Facile Route for Carbinolamine Formation and Potential Promoter of Aerosol Growth**, M. K. Louie, J. S. Francisco, M. Verdicchio, S. J. Klippenstein, A. Sinha, *J. Phys. Chem. A* **120**, 1358-1368 (2016).

12. **Low Temperature Kinetics of the First Steps of Water Cluster Formation**, J. Bourgalais, V. Roussel, M. Capron, A. Benidar, S. J. Klippenstein, L. Biennier, S. D. Le Picard, *Phys. Rev. Lett.* **116**, 113401 (2016).
13. **Communication: Real Time Observation of Unimolecular Decay of Criegee Intermediates to OH Radical Products**, Y. Fang, F. Liu, V. P. Barber, S. J. Klippenstein, A. B. McCoy, M. I. Lester, *J. Chem. Phys.* **144**, 061102 (2016).
14. **Pressure Dependent Low Temperature Kinetics for CN + CH<sub>3</sub>CN: Competition Between Chemical Reaction and van der Waals Complex Formation**, C. Sleiman, S. Gonzalez Rubio, S. J. Klippenstein, D. Talbi, G. El Dib, A. Canosa, *Phys. Chem. Chem. Phys.* **18**, 15118-15132 (2016).
15. **Direct Observation of Unimolecular Decay of CH<sub>3</sub>CH<sub>2</sub>CHOO Criegee Intermediates to OH Radical Products**, Y. Fang, F. Liu, S. J. Klippenstein, M. I. Lester, *J. Chem. Phys.*, **145**, 044312:1-9 (2016).
16. **Pressure Dependent Rate Constants for PAH Growth: Formation of Indene and its Conversion to Naphthalene**, A. M. Mebel, Y. Georgievskii, A. W. Jasper, S. J. Klippenstein, *Faraday Disc.* **195**, 637-670 (2016).
17. **Deep Tunneling in the Unimolecular Decay of CH<sub>3</sub>CHOO Criegee Intermediates to OH Radical Products**, Y. Fang, F. Liu, V. P. Barber, S. J. Klippenstein, A. B. McCoy, M. I. Lester, *J. Chem. Phys.*, **145**, 234308 (2016).
18. **From Theoretical Reaction Dynamics to Chemical Modeling of Combustion**, S. J. Klippenstein, *Proc. Combust. Inst.*, **36**, 77-111 (2017).
19. **Recombination of Aromatic Radicals with Molecular Oxygen**, F. Zhang, A. Nicolle, L. Xing, S. J. Klippenstein, *Proc. Combust. Inst.* **36**, 169-177 (2017).
20. **Theoretical Kinetics of O + C<sub>2</sub>H<sub>4</sub>**, X. Li, A. W. Jasper, J. Zádor, J. A. Miller, S. J. Klippenstein. *Proc. Combust. Inst.* **36**, 219-227 (2017).
21. **Temperature- and Pressure-Dependent Rate Coefficients for the HACA Pathways from Benzene to Naphthalene**, A. M. Mebel, Y. Georgievskii, A. W. Jasper, S. J. Klippenstein, *Proc. Combust. Inst.* **36**, 919-926 (2017).
22. **First-Principles Chemical Kinetic Modeling of Methyl Trans-3-Hexenoate Epoxidation by HO<sub>2</sub>**, S. Cagnina, A. Nicolle, T. de Bruin, Y. Georgievskii, S. J. Klippenstein, *J. Phys. Chem. A*, **121**, 1909-1915 (2017).
23. **Tunneling Effects in the Unimolecular Decay of (CH<sub>3</sub>)<sub>2</sub>COO Criegee Intermediates to OH Radical Products**, Y. Fang, V. P. Barber, S. J. Klippenstein, A. B. McCoy, M. I. Lester, *J. Chem. Phys.*, in press (2017).

## ARGONNE-SANDIA CONSORTIUM ON HIGH-PRESSURE COMBUSTION CHEMISTRY

Stephen J. Klippenstein (PI), Raghu Sivaramakrishnan, Robert S. Tranter  
*Chemical Sciences and Engineering Division, Argonne National Laboratory, Argonne, IL, 60439*  
[sjk@anl.gov](mailto:sjk@anl.gov)

Leonid Sheps, Craig A. Taatjes (PI)  
*Combustion Research Facility, Mail Stop 9055, Sandia National Laboratories*  
*Livermore, CA 94551-0969*  
[cataatj@sandia.gov](mailto:cataatj@sandia.gov)

**Program Scope:** The goal of this project is to explore the fundamental effects of high pressure (P) on the chemical kinetics of combustion and to use that knowledge in the development of accurate models for combustion chemistry at the high pressures of current and future combustion devices. We design and implement novel experiments, theory, and modeling to probe high-pressure combustion kinetics from elementary reactions, to submechanisms, to flames. The work focuses on integrating modeling, experiment, and theory (MET) through feedback loops at all levels of chemical complexity. We are currently developing and testing the methodology for small alkanes, alcohols, and ethers as key prototype fuels. The consortium expands and enhances collaborations between Argonne's Chemical Dynamics in the Gas Phase Group and the Combustion Chemistry Group in Sandia's Combustion Research Facility.

### Recent Progress:

#### *Experimental method development*

We have continued to invest in the development of sensitive time-resolved experimental methods that enable direct high-pressure studies of chemical systems of interest to HPCC. Our experimental facilities now include a miniature high-repetition rate shock tube (HRRST) and two high-pressure flow reactors. These setups span a wide range of conditions (300 – 2500 K, 0.5 – 100 bar) and exploit complementary probe techniques: laser-induced fluorescence (LIF), electron impact mass spectrometry, and photoionization mass spectrometry (PIMS). We also constructed a novel high-pressure mass spectrometer (HP-PIMS), which provides 100 times greater sensitivity than the previous PIMS apparatus, enabling studies at much greater dilution. This increase in sensitivity is achieved by creating ions in the high density region of the supersonic sampling expansion, followed by a sophisticated ion extraction scheme. The HP-PIMS was used in three successful campaigns at the ALS, where we assessed and refined its performance and began studies of chemical reactivity. The feasibility of HP-PIMS experiments at engine-relevant source pressures of 1 – 50 bar was demonstrated with excellent mass resolution ( $m/\Delta m \sim 1800$ ), which allows for pure hydrocarbons to be separated from oxygenated compounds at the same nominal mass.

All the apparatuses have been used in VUV-PIMS studies at the Chemical Dynamics Beamline of the Advanced Light Source (ALS); most recently, experiments up to  $P = 50$  bar and 700 K were conducted with the latest version of the photolysis flow reactor coupled to the HP-PIMS. The flow reactor was completely re-designed and includes key performance upgrades, allowing studies of reactive fuels which were previously plagued by wall interactions.

High P and T HRRST/VUV-PIMS experiments resulted in 3D datasets (ion signal vs.  $m/z$ , ionization energy, time) similar to those obtained from other PIMS experiments but impossible to acquire with conventional shock tubes. These datasets are composed of 7000-10000 shocks and produce high-quality PI spectra which are in excellent agreement with literature. Recent tests with the HRRST have generated shock conditions of 40 bar and 2000 K indicating that shock pressures up to 100 bar will be easily accessible at engine-relevant temperatures. In the near future we will couple the HRRST and HP-PIMS to take advantage of unique features of both devices.

#### *Autoignition chemistry of hydrocarbon and oxygenated fuels*

*Tetrahydrofuran (THF):* We completed a study of the autoignition chemistry of tetrahydrofuran, a cyclic ether that demonstrates the effects of ring strain and O atom substitution in the molecular structure on oxidation behavior. Using synchrotron-based tunable PIMS probing ( $P = 10 - 2000$  Torr,  $T = 400 - 700$  K), experiments on partially deuterated THF, and calculated potential energy surfaces, we elucidated the chemical mechanism for the first- and second- $O_2$  addition reactions in THF oxidation, as shown in Fig. 1. Our measurements provide a direct experimental probe of the key pressure-dependent competition between radical chain-inhibiting, chain-propagating, and chain-branching reactions. Notably, the second- $O_2$  addition products show strong positive pressure-dependence owing to the collisional stabilization of OOQOOH, whereas the products of competing reactions have either weakly negative P-dependence or none at all. Our results also highlight the complexity of chain-branching in THF by identifying competing OOQOOH decomposition channels to  $OH +$  ketohydroperoxide (KHP) and  $HO_2 +$  unsaturated

hydroperoxide. The former is an accepted general pathway, while the latter has not been observed in autoignition studies before and maybe more important than previously thought.

**Diethyl ketone (DEK):** We investigated another aspect of the relationship between molecular structure and reactivity, the role of resonance stabilization, in a low-temperature oxidation study of a prototypical compound, diethyl ketone. Resonance enables the delocalization of the unpaired electron in some isomers of the initial fuel radicals and QOOH, which can dramatically influence the relative stability and reactivity of these intermediates and ultimately the product branching. This effect was highlighted recently by detection for the first time of a resonantly stabilized, relatively long-lived QOOH in 1,3-cycloheptatriene oxidation. In DEK, previous low-pressure work showed that resonance stabilization led to temperature-dependent competition among the available OH + cyclic ether channels of QOOH decomposition. Our latest study at pressures up to 2 bar revealed preferential formation of one out of four possible ketohydroperoxide isomers *via* a pathway favored by resonance stabilization of the initial 3-oxopent-2-yl radical and QOOH.

**Dimethyl Ether (DME) Related Theory:** As the first step in our efforts to develop a high fidelity mechanism for DME we studied its reaction with OH radical. Abstraction reactions are particularly simple reactions to treat theoretically, and *a priori* rate predictions are routinely performed in conjunction with combustion modeling efforts. However, for biofuels, the presence of hydrogen bonding interactions between the fuel and the abstractor, coupled with the low, or even submerged (below one of the bimolecular asymptotes), barriers leads to various scientifically intriguing complexities in the analysis. The abstraction of an H-atom from dimethyl ether by OH is particularly well studied experimentally and so provides a useful test for theoretical methodologies. Our high level theoretical analysis, which incorporated ANL0 energies, variational and 2-dimensional hindered rotor effects, and asymmetric Eckart tunneling corrections yielded rate predictions that are in quantitative agreement with the available experimental data from 300 to 1400 K.

In collaboration with Pitsch and Leonhard (Aachen) we have been exploring the kinetics of DME radical oxidation with high-level theoretical calculations. To begin we mapped the potential energy surfaces for the  $\text{CH}_3\text{OCH}_2 + \text{O}_2$ ,  $\text{CH}_2\text{OCH}_2\text{OOH} + \text{O}_2$ , and  $\text{OCHOCH}_2\text{OOH}$  systems. Preliminary kinetic predictions have been obtained from master equation calculations employing VRC-TST (variable reaction coordinate transition state theory) analyses for the barrierless channels, a variety of two- and three-dimensional quantized hindered rotor treatments, Eckart corrections for tunneling, and simple empirical treatments of energy transfer.

As noted by Suzaki et al., some of the key TSs in DME radical oxidation are highly multireference in nature. These TSs involve an electron transfer to form a zwitterionic state, which creates severe difficulties even for standard multireference methods, due to low overlap of the reference states. In prior work, we explored the role of such TSs for alcohol radical oxidation. We are currently exploring the degree to which we can predict the properties of such TSs for DME radical oxidation. Comparison with experimental data obtained in the experimental part of the program is planned.

### Core Mechanism

**Methane and Ethane High Pressure Mechanisms:** Glarborg (DTU) and coworkers have recently examined the oxidations of methane and ethane at high pressures in a laminar flow reactor (700-900 K, 100 bar) and in a rapid compression machine (800-1250 K, 15-80 bar). We collaborated with Glarborg in the modeling of this experimental data. For methane, high sensitivities and uncertainties were noted to the  $\text{CH}_3\text{OO} + \text{CH}_4 = \text{CH}_3\text{OOH} + \text{CH}_3$  and  $\text{CH}_3\text{OH} + \text{CH}_3 = \text{CH}_3\text{O} + \text{CH}_4$  reactions. Thus, we performed high level *ab initio* TST calculations for these reactions. The final model performed well, aside from an underprediction of the methanol yield under reducing conditions. For ethane, Glarborg posed the question of a possible role for stabilization of the  $\text{CH}_2\text{CH}_2\text{OOH}$  complex near 100 bar. We used this opportunity to reexamine the full kinetics of the prototypical  $\text{C}_2\text{H}_5 + \text{O}_2$  system at a high level of theory. The resulting rate predictions were in good agreement with microscopic rate data, but suggest that stabilization of  $\text{CH}_2\text{CH}_2\text{OOH}$  is not a significant factor in the kinetics.

### Prompt Dissociation

**Prompt Dissociations of Oxygenated Radicals:** Prompt dissociations are a general feature for all weakly-bound radicals. Prompt dissociation probabilities for a variety of small weakly bound oxygenated radicals ( $\text{CH}_3\text{O}$ ,  $\text{CH}_2\text{OH}$ ,

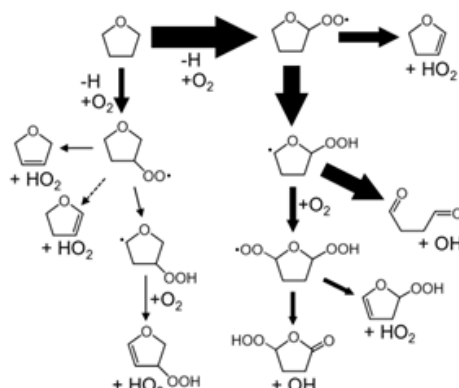


**Figure 1.** Primary low-T THF oxidation mechanism. Arrow widths qualitatively represent the relative importance of each reaction channel.

CH<sub>3</sub>CO, CH<sub>3</sub>CH<sub>2</sub>O, CH<sub>3</sub>CHOH, and CH<sub>3</sub>OCO) were calculated to characterize their potential relevance to combustion modeling. A rough estimate of the prompt dissociation probabilities ( $P_{diss}$ ) can be obtained by calculating  $f_{ne}(T)$  for these radicals. The trends in  $f_{ne}(T)$  illustrated in Fig. 2 for six small oxygenated radicals predominantly reflect trends in bond energies and density of states; i.e., higher bond energies correlate with  $f_{ne}$  values closer to unity, while larger molecules correlate with smaller  $f_{ne}$  values.

It is not immediately clear how the observed trends in Fig. 2 will affect the role of these non-equilibrium effects in combustion modeling. Although the CH<sub>3</sub>CO and CH<sub>3</sub>CH<sub>2</sub>O have severe deviations in  $f_{ne}$  from 1 and consequently large  $P_{diss}$  even at temperatures relevant to low-temperature combustion, the dissociations of these radicals may be so fast under these conditions that prompt dissociations may be irrelevant. Recasting the  $f_{ne}(T)$  plots in Fig. 2 in terms of the thermal unimolecular dissociation rate constants ( $k_{uni}$ ) at 1 atm as in Fig. 3, provides some indication of the relevancy of prompt dissociations in these radicals. From these plots it is clear that while very weakly-bound radicals such as CH<sub>3</sub>CO and CH<sub>3</sub>CH<sub>2</sub>O have severe deviations in  $f_{ne}$  from 1 at low temperatures, these onsets in  $f_{ne}$  deviations from 1 occur only when  $k_{uni} > 10^7$  s<sup>-1</sup>. Under such conditions *thermal* dissociations are so fast that they occur almost "instantaneously" regardless of whether or not non-equilibrium effects are included. Preliminary simulations of the relevance of CH<sub>2</sub>OH and CH<sub>3</sub>O prompt dissociations to flame speed simulations have been performed using these  $f_{ne}$  values and the C<sub>0</sub>-C<sub>3</sub> mechanism from this work. Figure 4 is a summary of simulations performed for CH<sub>3</sub>OH-air flames at P = 1 bar and T<sub>u</sub> = 343 K. While the inclusion of HCO prompt dissociation in the simulations leads to ~13% increase in flame speeds, including CH<sub>2</sub>OH prompt dissociation increases flame speeds by ~3%. The smaller magnitude of the effect for this radical may be primarily due to the  $f_{ne}(T)$  values being closer to 1 for CH<sub>2</sub>OH relative to HCO (at all temperatures). But interestingly, CH<sub>3</sub>O with an earlier temperature onset (and similar  $k_{uni}$  onset) for  $f_{ne}$  values deviating from 1 has a negligible effect on the simulated flame speeds. This may be due to the lower populations of CH<sub>3</sub>O (relative to CH<sub>2</sub>OH) within these flames.

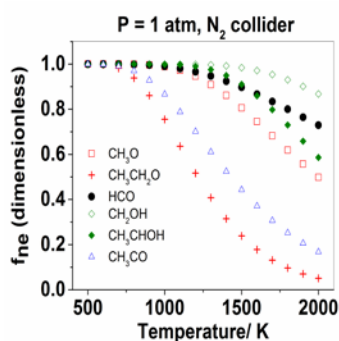


Figure 2:  $f_{ne}(T) (= 1 - P_{diss})$ .

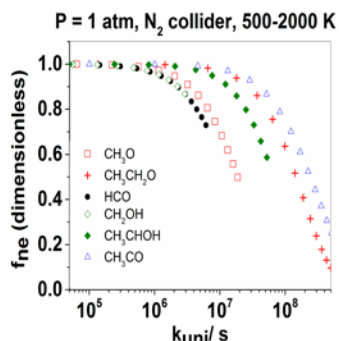


Figure 3:  $f_{ne}(k_{1atm})$

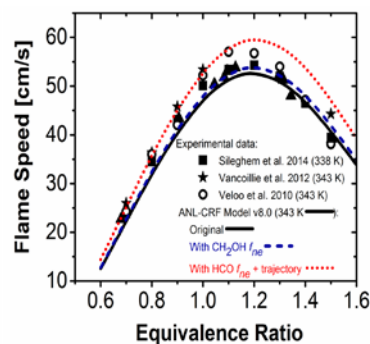


Figure 4: CH<sub>3</sub>OH-air, 1 atm, 343 K.

### Future Directions:

We plan to exploit the new instruments developed as part of this project to explore scientific challenges of importance to the HPCC goals: a rigorous description of non-Boltzmann effects, a comprehensive C<sub>0</sub>-C<sub>3</sub> combustion mechanism, and a fundamental understanding of diverse traditional and bio-derived fuels.

More specifically, we plan to conduct high-pressure autoignition studies of alkanes and ethers with a general goal of linking molecular structure with reactivity trends, using flow reactors coupled to PIMS probing or to OH radical detection by LIF. New high-pressure experiments on propyl oxidation will leverage our earlier low-pressure studies and the considerable theoretical and modeling framework built by the HPCC team to validate a comprehensive propane combustion mechanism. We will pay special attention to the pressure-dependence of the initial R + O<sub>2</sub> reaction for small alkyl radicals such as ethyl and propyl and compare them to theoretical predictions, performed in parallel. Neopentyl and cyclopentyl radical oxidation will extend this work to larger, more complex systems. Cyclopentane oxidation will be compared with the similarly-sized cyclic ether, THF, and both systems will be the focus of model development in collaboration with Zádor. We also plan to extend our ongoing studies of low-T DME oxidation to diethyl ether to explore general features of the combustion behavior of ethers.

At the same time, we plan to investigate the decomposition of the small oxygenated radicals formed in the combustion of ethanol and methyl formate, using PIMS measurements in the absence of O<sub>2</sub>. This work closely aligns with a major thrust of our modeling efforts: accurate description of bond scission reactions that includes the effects of non-statistical energy distributions. It is also complementary to proposed fuel pyrolysis measurements in the HRRST.

Dynamical simulations of the energy deposition in the primary CH<sub>2</sub>OH formation pathways in flames (OH and H + CH<sub>3</sub>OH) may exacerbate prompt dissociation effects in simulations such as in Figure 4. Such efforts are now in progress, in addition to our continued studies on the relevance of prompt dissociations of small combustion relevant

radicals. Preliminary simulations are also being performed using our core mechanism to design PIMS experiments to probe thermal decompositions (and potentially prompt dissociations) of radicals generated with Cl abstractions from ethanol and methylformate.

We plan to continue our effort to map out the key reactions of relevance to DME oxidation with high-level theoretical analyses. These analyses will include a treatment of the non-thermal effects in the multistep chain branching process. We will also analyze the thermal decomposition of DME, which occurs in competition with the chain branching process. We will also continue our efforts to obtain high accuracy theoretical predictions for the reactions of importance to the core mechanism.

#### DOE-BES Supported Publications, 2015-Present

1. **High Temperature Rate Constants for H/D + n-C<sub>4</sub>H<sub>10</sub> and i-C<sub>4</sub>H<sub>10</sub>**, S. L. Peukert, R. Sivaramakrishnan, J. V. Michael, *Proc. Comb. Inst.* **35**, 171-179 (2015).
2. **Adventures on the C<sub>3</sub>H<sub>5</sub>O Potential Energy Surface: OH + Propyne, OH + Allene and Related Reactions**, J. Zádor, J.A. Miller, *Proc. Comb. Inst.* **35**, 181-188 (2015).
3. **“Third-body” Collision Efficiencies for Combustion Modeling: Hydrocarbons in Atomic and Diatomic Baths**, A. W. Jasper, C. M. Oana, J. A. Miller, *Proc. Comb. Inst.* **35**, 197-204 (2015).
4. **Toward a Quantitative Understanding of the Role of Non-Boltzmann Reactant Distributions in Low-Temperature Oxidation**, M. P. Burke, C. F. Goldsmith, Y. Georgievskii, S. J. Klippenstein, *Proc. Comb. Inst.* **35**, 205-213 (2015).
5. **Effect of Non-Thermal Product Energy Distributions on Ketohydroperoxide Decomposition Kinetics**, C. F. Goldsmith, M. P. Burke, Y. Georgievskii, S. J. Klippenstein, *Proc. Comb. Inst.* **35**, 283-290 (2015).
6. **Probing the Low-Temperature Chain-Branching Mechanism for n-Butane Autoignition Chemistry via Time Resolved Measurements of Ketohydroperoxide Formation in Photolytically Initiated n-C<sub>4</sub>H<sub>10</sub> Oxidation**, A. J. Eskola, O. Welz, J. Zádor, I. O. Antonov, L. Sheps, J. D. Savee, D. L. Osborn, C. A. Taatjes, *Proc. Comb. Inst.* **35**, 291-298 (2015).
7. **Direct Observation and Kinetics of a Hydroperoxyalkyl Radical (QOOH)**, J. D. Savee, E. Papajak, B. Rotavera, H. Huang, A. J. Eskola, O. Welz, L. Sheps, C. A. Taatjes, J. Zádor, D. L. Osborn, *Science* **347**, 643-646 (2015).
8. **Probing Combustion Chemistry in a Miniature Shock Tube with Synchrotron VUV-Photoionization Mass Spectrometry**, P. T. Lynch, M. Ahmed, T. P. Troy, R. S. Tranter, *Anal. Chem.* **87**, 2345-2352 (2015).
9. **Multi-Scale Informatics for Low-Temperature Propane Oxidation: Further Complexities in Studies of Complex Reactions**, M. P. Burke, C. F. Goldsmith, S. J. Klippenstein, O. Welz, H. Huang, I. O. Antonov, J. D. Savee, D. L. Osborn, J. Zádor, C. A. Taatjes, L. Sheps, *J. Phys. Chem. A* **119**, 7095-7115 (2015).
10. **New Insights into Low-Temperature Oxidation of Propane from Synchrotron Photoionization Mass Spectrometry and Multi-Scale Informatics Modeling**, O. Welz, M. P. Burke, I. O. Antonov, C. F. Goldsmith, J. D. Savee, D. L. Osborn, C. A. Taatjes, S. J. Klippenstein, L. Sheps, *J. Phys. Chem. A* **119**, 7116-7129 (2015).
11. **OH + 2-butene: A Combined Experimental and Theoretical Study in the 400-800 K Temperature Range**, I. O. Antonov, J. Kwok, J. Zádor, L. Sheps, *J. Phys. Chem. A* **119**, 7742-7752 (2015).
12. **Temperature and Pressure-Dependent Rate Coefficients for the Reaction of Vinyl Radical with Molecular Oxygen**, C. F. Goldsmith, L. B. Harding, J. A. Miller, S. J. Klippenstein, *J. Phys. Chem. A* **119**, 7766-7779 (2015).
13. **Direct Observation and Kinetics of a Critical Reactive Intermediate in Hydrocarbon Oxidation**, J. D. Savee, E. Papajak, B. Rotavera, H. Huang, A. J. Eskola, O. Welz, L. Sheps, C. A. Taatjes, J. Zádor, D. L. Osborn, *Science* **347**, 643-646 (2015).
14. **Understanding Low Temperature First State Ignition Delay: Propane**, S. S. Merchant, C. F. Goldsmith, M. P. Burke, S. J. Klippenstein, W. H. Green, *Comb. Flame* **162**, 3658-3673 (2015).
15. **Comment on “When Rate Constants are Not Enough” by John R. Barker, Michael Frenklach, and David R. Golden**, J. A. Miller, S. J. Klippenstein, S. H. Robertson, M. J. Pilling, R. Shannon, J. Zádor, A. W. Jasper, C. F. Goldsmith, M. P. Burke, *J. Phys. Chem. A* **120**, 306-312 (2016).
16. **Weakly Bound Free Radicals In Combustion: “Prompt” Dissociation of Formyl Radicals and Its Effect on Laminar Flame Speeds**, N. J. Labbe, R. Sivaramakrishnan, C. F. Goldsmith, Y. Georgievskii, J. A. Miller, S. J. Klippenstein, *J. Phys. Chem. Lett.* **7**, 85-89 (2016).
17. **High Pressure Oxidation of Methane**, H. Hashemi, J. M. Christensen, S. Gersen, H. Levinsky, S. J. Klippenstein, P. Glarborg, *Combust. Flame*, **172**, 349-364 (2016).
18. **Pressure-Dependent Competition among Reaction Pathways From First- and Second- O<sub>2</sub> Additions In The Low-Temperature Oxidation Of Tetrahydrofuran**, I. O. Antonov, J. Zádor, B. Rotavera, E. Papajak, D. L. Osborn, C. A. Taatjes, L. Sheps, *J. Phys. Chem. A*, **120**, 6582-6595 (2016).
19. **Resonance Stabilization Effects on Ketone Autoxidation: Isomer-Specific Cyclic Ether and Ketohydroperoxide Formation in the Low-Temperature (400–625 K) Oxidation of Diethyl Ketone**, A. M. Scheer, A. J. Eskola, D. L. Osborn, L. Sheps, C. A. Taatjes, *J. Phys. Chem. A*, **120**, 8625-8636 (2016).
20. **From Theoretical Reaction Dynamics to Chemical Modeling of Combustion**, S. J. Klippenstein, *Proc. Comb. Inst.* **36**, 219-227 (2017).
21. **Ramifications of Including Non-equilibrium Effects for HCO in Flame Chemistry**, N. J. Labbe, R. Sivaramakrishnan, C. F. Goldsmith, Y. Georgievskii, J. A. Miller, S. J. Klippenstein, *Proc. Comb. Inst.* **36**, 525-532 (2017).
22. **High Pressure Oxidation of Ethane**, H. Hashemi, J. G. Jacobsen, C. T. Rasmussen, J. M. Christensen, P. Glarborg, S. Gersen, M. van Essen, H. B. Levinsky, S. J. Klippenstein, *Combust. Flame*, *in press* (2017).

## Spectroscopy and Dynamics of Free Radicals

*Stephen R. Leone and Daniel M. Neumark*

Lawrence Berkeley National Laboratory and Departments of Chemistry and Physics, University of California, Berkeley, California 94720 (510) 643-5467 [srl@berkeley.edu](mailto:srl@berkeley.edu), 510-642-3502  
[dmneumark@berkeley.edu](mailto:dmneumark@berkeley.edu)

**Scope of the Project:** In this experimental program, novel methods are used to study radical spectroscopy and dynamics with a focus on important species in combustion. The characterization of key properties of free radicals includes bond dissociation energies, orbital energetics, electron affinities, spectroscopy of low-lying electronic states, primary photochemistry, transition state regions, and reaction dynamics. The studies facilitate a detailed understanding of the role of free radicals in reaction mechanisms that govern diverse processes such as low-temperature autoignition, the oxidation of aromatic hydrocarbons, and the growth of complex molecules such as PAH's in flames. A jet-stirred reactor at the Advanced Light Source provides information about combustion oxidation reactions. Ultrafast x-ray transient absorption spectroscopy investigates transition states and products. Slow Electron Velocity-Map Imaging of cryogenically cooled anions (cryo-SEVI) yields precise electron affinities, vibrational frequencies, and term values of low-lying states for radicals that are generated by negative ion photodetachment. Negative ion photodetachment forms the basis of another fast radical beam (FRBM) instrument, in which neutral free radicals generated in this manner are photodissociated, with the kinetic energy and angular distributions of the various photofragment channels analyzed using sophisticated coincidence detection techniques. The photodissociation processes of radicals generated by flash pyrolysis are investigated using a molecular beam instrument with a rotating mass spectrometer as a detector.

### **Recent Progress:**

#### ***Jet Stirred Reactor experiments***

A high temperature (500-1100 K) jet-stirred reactor is used to investigate the mechanisms of n-butane, dimethyl ether, cyclohexane, 2-methylhexane and 2,5-dimethylhexane low temperature oxidation reactions. Ketohydroperoxide species are corroborated in the oxidation of butane, and the use of partially deuterated butane provides evidence for the Korcek mechanism of decomposition of the intermediate ketohydroperoxide species into acid, ketone and aldehyde pairs, through the observation of the partially deuterated acetone and formic acid Korcek pair. The Korcek decomposition mechanism of  $\gamma$ -ketohydroperoxide is a substantial fraction of the organic acid production, but it is not likely to be a significant contributor to autoignition processes. Highly oxygenated species with four and five oxygen atoms were identified in the low temperature oxidation of nine non-oxygenated (i.e., normal alkanes, branched alkanes, cycloalkanes, and aromatics) and five oxygenated organic compounds. The elemental composition of the multifunctional peroxides formed during the oxidation reactions are identified by means of temperature-dependent speciation profiles, H/D exchange reactions, and by using isotopically labelled oxygen ( $^{18}\text{O}$ ). The detection of these species suggests that a third  $\text{O}_2$  addition process might exist at combustion-relevant conditions, indicating the presence of previously unrevealed radical chain-branching pathways.

#### ***Femtosecond Soft X-ray Transient Absorption Experiments***

A unique femtosecond soft x-ray transient absorption spectroscopy apparatus with x-ray probe energies up to 310 eV is used to characterize the electronic structure of transient intermediates of chemical reactions. The ultrafast photoinduced ring-opening reaction of 1,3-cyclohexadiene, a fundamental prototype of photochemical pericyclic reactions, is investigated. Following ultraviolet photoexcitation to the 1B excited state via a  $\pi \rightarrow \pi^*$  transition at 266 nm, the key step in this reaction is the ultrafast relaxation through a transient 2A excited-state intermediate known as the pericyclic minimum, which leads to isomerization via non-adiabatic decay onto the ground state of the photoproduct. With the capability of femtosecond soft x-ray transient absorption spectroscopy near the carbon K-edge (284 eV), the electronic structure of this transient intermediate state is obtained.



The ultrafast excited state non-adiabatic dynamics of acetylacetone (pentane-2,4-dione) is directly probed up to 150 ps after excitation at 266 nm using time-resolved x-ray absorption spectroscopy near the carbon K-edge (284 eV). At this wavelength, the enolic tautomer of the molecule is excited to the  $S_2$  ( $^1\pi\pi^*$ ) electronic state from which it undergoes internal conversion to the lower-lying singlet states and intersystem crossing to the triplet states. In the experiment, rapid internal conversion leads to changes in the electronic structure within 2 ps after excitation, characterized by significant changes in the near-edge x-ray absorption fine-structure spectrum. Four distinct core-to-valence transitions are observed by 10 ps, which represent the ultrafast cascade of the excited wavepacket via the singlet-states manifold. Assignment of these new core-to-valence resonances to specific electronic states is being pursued with the aid of density functional theory.

The photodissociation dynamics of dimethyldisulfide at 266 nm is studied using broadband soft x-ray probe pulses covering the sulfur  $L_{2/3}$  edge (160 eV), the sulfur  $L_1$  edge (225 eV) and the carbon K-edge (284 eV). The element-sensitivity of the probe determines the propensity for C-C versus C-S bond cleavage to form the corresponding alkyl or thiyl radicals. Depletions of both the carbon  $1s \rightarrow \sigma^*$  and sulfur  $2p \rightarrow \sigma^*$  ground-state resonances are observed. A new feature at 223 eV, possibly arising from the radical species, is identified. Calculations by Head-Gordon are underway to identify the x-ray spectral features of the radicals to specifically determine the branching ratios for the C-C and C-S bond dissociation channels.

The photodissociation of halogenated hydrocarbons represents an important class of benchmark reactions in chemical reaction dynamics. In ongoing experiments, the frontier molecular orbitals in substituted methyl radicals ( $\cdot\text{CH}_2\text{Cl}$ ,  $\cdot\text{CH}_2\text{Br}$ ,  $\cdot\text{CH}_2\text{I}$ ) are being studied through the photodissociation of dihalogenated methanes at 266 nm, and the possible stabilizing effect of the halogen atom partially bonding with the carbon 2p orbital is being interrogated through the core-to-SOMO resonances in the radicals. These studies address the possibility of multichannel dissociation in the dihalogen-substituted methanes at 266 nm and the corresponding branching ratios as well as the reactivity of the halogenated methyl radicals.

### ***Cryo-SEVI Spectroscopy of Radicals***

The electronic and vibrational structure of the  $\alpha$ - and  $\beta$ -furanil radicals is probed using slow photoelectron velocity-map imaging of cryogenically-cooled anions (cryo-SEVI). Use of a trimethylsilyl-substituted molecular precursor facilitated acquisition of isomer-specific spectra, resulting in the first observation of the  $\beta$ -furanide photoelectron spectrum and yielding an electron affinity (EA) of 1.6566(4) eV for the  $\beta$ -furanil radical. Cryo-SEVI is also used to characterize the *tert*-butyl peroxy radical (tBuOO), yielding vibrationally-resolved detachment to the two lowest electronic states of the neutral, an EA of 1.1962(20) eV for tBuOO, and a term energy of 0.9602(24) eV for the first radical excited state. The improved resolution of these spectra reveal underlying vibrational structure not resolved in previous work.

### ***Fast Radical Beam Spectroscopy***

The photodissociation dynamics of the *tert*-butyl peroxy radical ( $(\text{CH}_3)_3\text{OO}\cdot$ ) are investigated on the fast radical beam (FRBM) instrument. *Tert*-butyl peroxy radicals are produced by photodetachment of the  $(\text{CH}_3)_3\text{OO}^-$  anion followed by photodissociation at 248 nm (5.0 eV). Photofragment mass distributions and translational energy distributions are measured for both two- and three-fragment coincident events at 248 nm. Experimental results show that three-body dissociation to acetone, methyl radical and oxygen atom products is the dominant channel at 248 nm. An anisotropic distribution of the photofragments and a translational energy that peaks away from zero kinetic energy indicate that the dissociation occurs rapidly along a repulsive excited state. A small shoulder in the translational energy distribution suggests that a separate dissociation mechanism may govern dissociation events that result in small kinetic energy release and is interpreted as a sequential dissociation mechanism, in which the O-O bond breaks first, followed by the fragmentation of the *tert*-butoxy radical counterfragment. Two-fragment dissociation to  $\text{O}_2$  + *tert*-butyl radical and  $\text{HO}_2$  + isobutene is also observed. Translational energy distributions and RRKM calculations suggest that two-fragment dissociation occurs statistically

on the ground electronic state, with dissociation to HO<sub>2</sub> + isobutene proceeding directly from the peroxy radical (RO<sub>2</sub>) rather than via isomerization to the QOOH radical.

### ***Molecular Beam Radical Photodissociation***

The photodissociation of fulvenallene, C<sub>7</sub>H<sub>6</sub>, and the fulvenallenyl radical, C<sub>7</sub>H<sub>5</sub>, is studied using photofragment translational spectroscopy at 248 nm and 193 nm. Fulvenallene was synthesized using vacuum flash thermolysis and its identity was confirmed by NMR. A single photodissociation channel was observed for fulvenallene, H atom loss to form the fulvenallenyl radical. The translational energy distribution determined for this channel suggests that the dissociation occurs via internal conversion to the ground state followed by intramolecular vibrational redistribution and dissociation. At higher laser power, the subsequent photodissociation of the fulvenallenyl radical was observed. Two photodissociation pathways were measured, C<sub>5</sub>H<sub>3</sub> + C<sub>2</sub>H<sub>2</sub> and C<sub>4</sub>H<sub>2</sub> + C<sub>3</sub>H<sub>3</sub>. Translational energy distributions are determined for both channels and each suggests ground state statistical dissociation over a barrier. The branching ratio between these two channels is found to be C<sub>5</sub>H<sub>3</sub> + C<sub>2</sub>H<sub>2</sub> : C<sub>4</sub>H<sub>2</sub> + C<sub>3</sub>H<sub>3</sub> = 0.27 ± 0.14 at 248 nm and 0.33 ± 0.21 at 193 nm. The dominance of the C<sub>4</sub>H<sub>2</sub> + C<sub>3</sub>H<sub>3</sub> channel is corroborated by the branching ratio calculated using Rice-Ramsperger-Kassel-Marcus theory.

### **Future Plans:**

The newly constructed UV-pump, soft x-ray-probe apparatus will be used to spectroscopically investigate hydrocarbon radicals including methyl, allyl, vinyl, and phenyl and fundamental hydrocarbon photochemical processes including internal conversion, predissociation, and ring-opening/closing reactions. The current spectral resolution (330 meV) of the apparatus will be improved to enable the study of vibrational excitation in the radicals born with high internal energy upon UV photodissociation and the effect of the hot-band character in the core-to-SOMO x-ray resonances. The fourth harmonic (200 nm) of the fundamental 800 nm amplified output will be generated to provide access to small straight-chain and cyclic hydrocarbon molecules as well as those containing heteroatoms (such as oxygen and nitrogen) that are ubiquitous in combustion chemistry. Future efforts will involve improving the high-harmonic flux and stability to extend the soft x-ray probe to obtain energy-tuneable pulses covering the nitrogen K-edge (410 eV) and the oxygen K-edge (550 eV).

The three instruments available to the second part of the effort will provide an integrated experimental platform for the study of free radical spectroscopy and dissociation experiments. The cryo-SEVI and FRBM instruments are highly complementary since both are based on negative ion photodetachment. Investigations of the RO<sub>2</sub> radicals on these two instruments will be expanded, given the unexpected observation that excitation of tBuOO at 248 nm results in both excited state and ground state dissociation. In addition, a tuneable infrared laser source based on difference frequency generation is now available on the cryo-SEVI instrument; this will enable studies of hydrocarbon radicals for which the electron affinities are typically well below 0.5 eV. The molecular beam experiments will focus on photodissociation of the cyclopentadienyl radical, a resonance-stabilized species that has been successfully generated in our flash pyrolysis source.

### **Recent Publications Citing DOE Support (2014-2017):**

- A. R. Attar, A. Bhattacharjee, C. D. Pemmaraju, Kirsten Schnorr, Kristina D. Closser, David Prendergast, and S. R. Leone, "Femtosecond x-ray spectroscopy of an electrocyclic ring-opening reaction", *Science*, **in press**.
- B. Nichols, E. N. Sullivan, M. Ryazanov, D. M. Neumark, "Photodissociation Dynamics of the *i*-Methylvinoxy Radical at 308, 248, and 225 nm Using Fast Beam Photofragment Translational Spectroscopy" *J. Phys. Chem. A* **121**, 579 (2017).
- J. A. DeVine, M. L. Weichman, S. J. Lyle, D. M. Neumark, "High-resolution photoelectron imaging of cryogenically cooled  $\alpha$ - and  $\beta$ -furanil anions" *J. Mol. Spec.* **332**, 16 (2017).
- S. D. Chambreau, C. J. Koh, D. M. Popolan-Vaida, C. J. Gallegos, J. B. Hooper, D. Bedrov, G. L. Vaghjiani, and S. R. Leone, "Flow-Tube Investigations of Hypersonic Reactions of a Dicyanamide

- Ionic Liquid Via Tunable Vacuum Ultraviolet Aerosol Mass Spectrometry*", J. Phys. Chem. A, **120**, 8011 (2016).
- A. W. Harrison, M. Ryazanov, E. N. Sullivan, D. M. Neumark, "Photodissociation dynamics of the methyl perthiyl radical at 248 and 193 nm using fast-beam photofragment translational spectroscopy" J. Chem. Phys. **145**, 024305 (2016).
  - Z. Wang, L. Zhang, K. Moshhammer, D. M Popolan-Vaida, V. S. Bhavani Shankar, A. Lucassen, C. Hemken, C. A Taatjes, S. R Leone, K. Kohse-Höinghaus, N. Hansen, P. Dagaut, S Mani Sarathy, "Additional chain-branching pathways in the low-temperature oxidation of branched alkanes", Combustion and Flame, **164**, 386 (2016).
  - N. C. Cole-Filipiak, M. Shapero, C. Haibach-Morris, and D. M. Neumark, "Production and Photodissociation of the Methyl Perthiyl Radical", J. Phys. Chem. A, **120**, 4818 (2016).
  - M. L. Weichman, J. A. DeVine, D. S. Levine, J. B. Kim, and D. M. Neumark, "Isomer-specific vibronic structure of the 9-, 1-, and 2-anthracenyl radicals via slow photoelectron velocity-map imaging" PNAS, **113**, 1698 (2016).
  - A. Bhattacharjee, A. R. Attar, and S. R. Leone, "Transition-state region in the A-band photodissociation of Allyl Iodide – A femtosecond extreme ultraviolet transient absorption study", J. Chem. Phys. **144m** 124311 (2016).
  - M. Shapero, N. C. Cole-Filipiak, C. Haibach-Morris, and D. M. Neumark, "Benzyl Radical Photodissociation Dynamics at 248 nm" J. Phys. Chem. A **119**, 12349 (2015).
  - A. R. Attar, A. Bhattacharjee, and S. R. Leone, "Direct observation of the Transition-State Region in the Photodissociation of CH<sub>3</sub>I by Femtosecond Extreme Ultraviolet Transient Absorption Spectroscopy", J. Phys. Chem. Lett., **6**, 5072 (2015).
  - D. M. Popolan-Vaida, C.-L. Liu, T. Nah, K. R. Wilson, and S. R. Leone, "Reaction of chlorine molecules with unsaturated submicron organic particles", Z. Phys. Chem. **229**, 1521 (2015).
  - K. Moshhammer, A. W. Jasper, D. M. Popolan-Vaida, A. Lucassen, P. Diévar, H. Selim, A. J. Eskola, C. A. Taatjes, S. R. Leone, S. M. Sarathy, Y. Ju, P. Dagaut, K. Kohse-Höinghaus, and Nils Hansen, "Detection and Identification of the Keto-Hydroperoxide (HOOCH<sub>2</sub>OCHO) and Other Intermediates during Low-Temperature Oxidation of Dimethyl Ether", J. Phys. Chem. A, **119**, 7361 (2015).
  - M. L. Weichman, J. B. Kim and D. M. Neumark, "Slow Photoelectron Velocity-Map Imaging Spectroscopy of the ortho-Hydroxyphenoxide Anion", J. Phys. Chem. A, DOI: 10.1021/acs.jpca.5b00768, (2015).
  - M. L. Weichman, J. B. Kim, J. A. DeVine, D. S. Levine and D. M. Neumark, "Vibrational and Electronic Structure of the  $\alpha$ - and  $\beta$ -naphthyl Radicals via Slow Photoelectron Velocity-Map Imaging", J. Am. Chem. Soc., **137**, 1420, (2015).
  - A. R. Attar, L. Piticco, and S. R. Leone, "Core-to-valence spectroscopic detection of the CH<sub>2</sub>Br radical and element-specific photodissociation dynamics of CH<sub>2</sub>IBr", J. Chem. Phys., **141**, 164308 (2014).
  - J. F. Lockyear, M. Fournier, I. R. Sims, J.-C. Guillemin, C. A. Taatjes, D. L. Osborn and S. R. Leone, "Formation of fulvene in the reaction of C<sub>2</sub>H with 1,3-butadiene", Int. J. Mass. Spectrom., in press (2014).
  - T. Nah, S. H. Kessler, K. E. Daumit, J. H. Kroll, S. R. Leone, and K. R. Wilson, "Influence of molecular structure and chemical functionality on the heterogeneous OH-initiated oxidation of unsaturated organic particles", J. Phys. Chem. A, **118**, 4106 (2014).
  - D. M. Popolan-Vaida, K. R. Wilson, and S. R. Leone, "Reaction of I atoms with sub-micron squalene and squalene droplets: mechanistic insights into heterogeneous reactions", J Phys. Chem. A, **118**, 10688 (2014).
  - N. Cole-Filipiak, M. Shapero, B. Negru and D. M. Neumark, "Revisiting the Photodissociation Dynamics of the Phenyl Radical", J. Chem. Phys., **141**, 104307, (2014).
  - M. Ryazanov, A. Harrison, G. Wang, P. Crider and D. M. Neumark, "Investigation of 3-fragment Photodissociation of O<sub>3</sub> at 193.4 and 157.6 nm by Coincident Measurements", J. Chem. Phys., **140**, 234304, (2014).

# SPECTROSCOPY AND DYNAMICS OF REACTION INTERMEDIATES IN COMBUSTION CHEMISTRY

Marsha I. Lester  
Department of Chemistry  
University of Pennsylvania  
Philadelphia, PA 19104-6323  
milester@sas.upenn.edu

## I. Program Scope

The hydroxyl radical, a key oxidant in combustion, is generally detected by laser-induced fluorescence on the  $A^2\Sigma^+ - X^2\Pi$  band system. Sensitive, state-selective ionization detection of OH radicals offers additional advantages, and thus this laboratory is expanding its efforts to develop and apply a robust  $1+1'$  ionization scheme that combines OH A-X excitation with VUV ionization via autoionizing Rydberg states. Carbonyl oxides (Criegee intermediates), important intermediates in tropospheric hydrocarbon oxidation and some combustion reactions, and related isomeric species are being examined to determine their intrinsic stability and explore dynamical pathways.

## II. Recent Progress

### A. State-selective ionization of OH radicals

This laboratory has demonstrated a new  $1+1'$  resonance enhanced multiphoton ionization (REMPI) scheme for sensitive and state-selective detection of OH  $X^2\Pi$  radicals,<sup>1,2</sup> which is readily implemented using typical laboratory laser setups. UV excitation on the  $A^2\Sigma^+ - X^2\Pi$  transition is used to prepare a range of intermediate  $A^2\Sigma^+$  ( $v'=1, 2$ ) levels. Subsequent fixed-frequency VUV excitation at 118 nm (10.5 eV), generated by frequency-tripling the third harmonic of a Nd:YAG laser in Xe, accesses autoionizing OH [ $A^3\Pi, 3d$ ],  $v=0$  Rydberg states. The OH  $1+1'$  REMPI scheme is now routinely utilized in this laboratory for velocity map imaging studies of OH radicals, as discussed below.

Recently, the underlying mechanism for the  $1+1'$  REMPI scheme was examined by using tunable VUV generated via two-photon resonant four-wave mixing ( $\omega_{\text{VUV}}=2\omega_1-\omega_2$ ) in Kr.<sup>3</sup> VUV scans revealed distinct rotational and fine structure associated with two newly identified OH  $^2\Pi$  Rydberg states (with an  $A^3\Pi$  core and  $3d$  electron) accessed from the  $A^2\Sigma^+$  ( $v'=1$ ) state. The broadened linewidths of the VUV transitions indicated that autoionization occurs on a picosecond timescale. Most importantly, this study demonstrated that the OH  $1+1'$  REMPI scheme is enhanced by accidental overlap of the fixed VUV radiation at 118 nm (10.5 eV) with distinct  $^2\Pi$  Rydberg -  $A^2\Sigma^+$  transitions, followed by ionization.

### B. Velocity map imaging studies

We have now utilized the  $1+1'$  REMPI ionization scheme for state-selective detection of OH  $X^2\Pi$  radicals in velocity map imaging (VMI) studies. The initial VMI studies examined the angular and velocity distributions of OH products arising from unimolecular decay of vibrationally activated  $\text{CH}_3\text{CHOO}$  and  $(\text{CH}_3)_2\text{COO}$  Criegee intermediates.<sup>4,5</sup> The VMI studies reveal the release of excess energy to internal and translational degrees of freedom as a means of elucidating the dynamical pathway(s) to products. IR excitation in the CH stretch overtone

region was used to access the transition state (TS) barrier region leading to OH products. The reaction pathway involves intramolecular 1,4 hydrogen atom transfer that results in isomerization to vinyl (or methylethenyl) hydroperoxide. This is followed by O-O bond cleavage to form OH + vinyloxy (or 1-methyl vinyloxy) products, although not via a simple barrierless O-O bond breaking process due to the presence of exit channel barriers and associated product minima. The VMI experiments on CH<sub>3</sub>CHOO were complemented by quasi-classical trajectory (QCT) calculations from the TS to products by Wang and Bowman.<sup>4</sup>

The angular distributions of the OH products obtained using VMI are isotropic, indicating that CH<sub>3</sub>CHOO and (CH<sub>3</sub>)<sub>2</sub>COO undergo rotation prior to unimolecular decay.<sup>4,5</sup> This is consistent with the nanosecond timescales observed in recent direct time domain measurements as well as statistical RRKM evaluation of their microcanonical dissociation rates.<sup>6</sup> In both systems, the total kinetic energy release distributions derived from the 2D images are broad and unstructured, and account for ~20% of the energy released on average. The OH products are released with minimal excitation, indicating that most of available energy flows into internal excitation of the vinyloxy (or 1-methyl vinyloxy) products. For CH<sub>3</sub>CHOO, the release of the excess energy to product internal and translational degrees of freedom differs considerably from a statistical distribution, but is captured in QCT calculations initiated at critical configurations along the reaction pathway.<sup>4</sup> The best agreement comes from trajectories starting at a submerged saddle point in the exit channel. For (CH<sub>3</sub>)<sub>2</sub>COO, the release of excess energy to translation is well represented by a statistical distribution. In both systems, the OH X<sup>2</sup>Π (v=0) product rotational distributions differ from statistical models.

Most recently, we utilized velocity map imaging to demonstrate the prompt release of O <sup>1</sup>D products upon UV excitation of the CH<sub>2</sub>OO Criegee intermediate in the long wavelength tail region (364 to 417 nm) of the B<sup>1</sup>A' - X<sup>1</sup>A' spectrum.<sup>7</sup> The VMI images exhibit anisotropic distributions indicating that dissociation to H<sub>2</sub>CO X<sup>1</sup>A<sub>1</sub> + O <sup>1</sup>D products is rapid compared to the rotational period of CH<sub>2</sub>OO and occurs on a picosecond or faster timescale. As a result, the broad oscillatory structure reported previously by several groups<sup>8-10</sup> in the long wavelength tail region of the UV absorption spectrum is attributed to short-lived resonances associated with the excited B<sup>1</sup>A' state of CH<sub>2</sub>OO, in accord with theoretical predictions.<sup>11</sup>

The total kinetic energy release distributions show that the available energy is nearly equally partitioned, on average, between product translational energy and internal excitation of the H<sub>2</sub>CO co-fragments. The anisotropy and energy partitioning are unchanged with excitation wavelength, and consistent with previously reported experimental and theoretical findings of the CH<sub>2</sub>OO B-X transition moment and dissociation energy to H<sub>2</sub>CO X<sup>1</sup>A<sub>1</sub> + O <sup>1</sup>D products.<sup>12,13</sup> Thus, the strong UV absorption spectrum over the entire wavelength range (308 to 417 nm)<sup>8-10,14</sup> arises from electronic excitation of CH<sub>2</sub>OO from its ground X<sup>1</sup>A' state to a single excited electronic state, namely the B<sup>1</sup>A' state, which couples to repulsive singlet states and results in rapid O-O bond breakage and dissociation.

### C. Photoionization mass spectrometry studies

In collaboration with Taatjes and coworkers, we have also carried out experiments on hydroxyacetone (CH<sub>3</sub>C(O)CH<sub>2</sub>OH) formation using the multiplexed photoionization mass spectrometer at the Chemical Dynamics Beamline with tunable VUV radiation from the Advanced Light Source.<sup>15</sup> Hydroxyacetone was identified as a stable product from reactions of the (CH<sub>3</sub>)<sub>2</sub>COO Criegee intermediate in a flow tube. In the experiment, the two isomers at

$m/z = 74$  are distinguished by their different photoionization spectra and reaction times. Hydroxyacetone was observed as a persistent signal at  $m/z$  74 at longer ( $\geq 5$  ms) reaction times and higher photoionization energies starting at ca. 9.7 eV. Complementary electronic structure calculations by Kumar and Thompson have revealed multiple reaction pathways for hydroxyacetone formation including a unimolecular isomerization mechanism involving hydrogen atom transfer and -OH group migration as well as self-reaction of the Criegee intermediates. Varying the concentration of Criegee intermediates suggests contributions from both unimolecular and self-reaction pathways to hydroxyacetone. The unimolecular mechanism is more likely to occur for alkene ozonolysis reactions, where hydroxyacetone can potentially be monitored as a stable end product.

### III. Future Work

Future studies will expand our investigation of the 1+1' REMPI detection scheme for OH  $X^2\Pi$  ( $v, N$ ) radicals. We also plan to utilize this novel OH detection scheme in VMI studies of photochemical and unimolecular reactions. A new line of research is being pursued to generate hydroperoxyalkyl radicals in a pulsed supersonic expansion, and characterize them spectroscopically.

### IV. References

1. J. M. Beames, F. Liu, M. I. Lester and C. Murray, *J. Chem. Phys.* 134, 241102 (2011).
2. J. M. Beames, F. Liu, and M. I. Lester, *Mol. Phys.* 112, 897 (2014).
3. A. M. Green, F. Liu, and M. I. Lester, *J. Chem. Phys.* 144, 184311 (2016).
4. N. M. Kidwell, H. Li, X. Wang, J. M. Bowman, and M. I. Lester, *Nat. Chem.* 8, 509-14 (2016).
5. H. Li, N. M. Kidwell, X. Wang, J. M. Bowman, and M. I. Lester, *J. Chem. Phys.* 145 104307 (2016).
6. Y. Fang, F. Liu, V. P. Barber, S. J. Klippenstein, A. B. McCoy, and M. I. Lester, *J. Chem. Phys.* 144, 061102 (2016).
7. M. F. Vansco, H. Li and M. I. Lester, *J. Chem. Phys.* 147, 013907 (2017).
8. L. Sheps, *J. Phys. Chem. Lett.* 4, 4201 (2013).
9. W.-L. Ting, Y.-H. Chen, W. Chao, M. C. Smith and J. J.-M. Lin, *Phys. Chem. Chem. Phys.* 16, 10438 (2014).
10. E. S. Foreman, K. M. Kapnas, Y. Jou, J. Kalinowski, D. Feng, R. B. Gerber and C. Murray, *Phys. Chem. Chem. Phys.* 17, 32539 (2015).
11. R. Dawes, B. Jiang and H. Guo, *J. Am. Chem. Soc.* 137, 50 (2015).
12. J. H. Lehman, H. Li, J. M. Beames and M. I. Lester, *J. Chem. Phys.* 139, 141103 (2013).
13. H. Li, Y. Fang, J. M. Beames and M. I. Lester, *J. Chem. Phys.* 142, 214312 (2015).
14. J. M. Beames, F. Liu, L. Lu, and M. I. Lester, *J. Am. Chem. Soc.* 134, 20045-48 (2012).
15. C. A. Taatjes, F. Liu, B. Rotavera, M. Kumar, R. Caravan, D. L. Osborn, W. H. Thompson, and M. I. Lester, *J. Phys. Chem. A* 121, 16-23 (2017).

### V. Publications supported by this DOE project (2014-2017)

1. M. F. Vansco, H. Li, and M. I. Lester, "Prompt release of O  $^1D$  products upon UV excitation of CH<sub>2</sub>OO Criegee intermediates", [J. Chem. Phys. 147, 013907 \(2017\)](#).

2. C. A. Taatjes, F. Liu, B. Rotavera, M. Kumar, R. Caravan, D. L. Osborn, W. H. Thompson, and M. I. Lester, "Hydroxyacetone production from C<sub>3</sub> Criegee intermediates", *J. Phys. Chem. A* **121**, 16-23 (2017).
3. H. Li, N. M. Kidwell, X. Wang, J. M. Bowman, and M. I. Lester, "Velocity map imaging of OH radical products from IR activated (CH<sub>3</sub>)<sub>2</sub>COO Criegee intermediates", *J. Chem. Phys.* **145** 104307 (2016).
4. A. M. Green, F. Liu, and M. I. Lester, "UV + VUV double-resonance studies of autoionizing Rydberg states of the hydroxyl radical", *J. Chem. Phys.* **144**, 184311 (2016).
5. N. M. Kidwell, H. Li, X. Wang, J. M. Bowman, and M. I. Lester, "Unimolecular dissociation dynamics of vibrationally activated CH<sub>3</sub>CHOO Criegee intermediates to OH radical products", *Nat. Chem.* **8**, 509-14 (2016).
6. H. Li, Y. Fang, N. M. Kidwell, J. M. Beames, and M. I. Lester, "UV photodissociation dynamics of the CH<sub>3</sub>CHOO Criegee intermediate: Action spectroscopy and velocity map imaging of O-atom products", *J. Phys. Chem. A* **119**, 8328-37 (2015).
7. H. Li, Y. Fang, J. M. Beames, and M. I. Lester, "Velocity map imaging of O-atom products from UV photodissociation of the CH<sub>2</sub>OO Criegee intermediate", *J. Chem. Phys.* **142**, 214312 (2015).
8. K. Samanta, J. M. Beames, M. I. Lester, and J. E. Subotnik, "Quantum dynamical investigation of the simplest Criegee intermediate CH<sub>2</sub>OO and its O-O photodissociation channels", *J. Chem. Phys.* **141**, 134303 (2014).
9. J. H. Lehman and M. I. Lester, "Dynamical outcomes of quenching: Reflections on a conical intersection", *Ann. Rev. Phys. Chem.* **65**, 537-55 (2014).
10. J. M. Beames, F. Liu, and M. I. Lester, "1+1' resonant ionization of OH radicals via the A<sup>2</sup>Σ<sup>+</sup> state: Insights from direct comparison with A-X fluorescence detection", *Mol. Phys.* **112**, 897-903 (2014).

# Advanced Nonlinear Optical Methods for Quantitative Measurements in Flames

Robert P. Lucht

School of Mechanical Engineering, Purdue University

West Lafayette, IN 47907-2088

Lucht@purdue.edu

## I. Program Scope

Nonlinear optical techniques such as laser-induced polarization spectroscopy (PS), resonant wave mixing (RWM), and ultrafast coherent anti-Stokes Raman scattering (CARS) are techniques that show great promise for sensitive measurements of transient gas-phase species, and diagnostic applications of these techniques are being pursued actively at laboratories throughout the world. The objective of this research program is to develop and test strategies for quantitative concentration and temperature measurements using nonlinear optical techniques in flames and plasmas. We have continued our fundamental theoretical and experimental investigations of these techniques. In recent years our theoretical and experimental efforts have been focused on investigating the potential of femtosecond (fs) laser systems for sensitive and accurate CARS measurements in gas-phase media. Our initial efforts have been focused on fs CARS, although the systems will be useful for a wide range of future diagnostic techniques involving two-photon transitions. In the last few years we have demonstrated the acquisition of single-shot temperature measurements at data rates of 5 kHz in highly turbulent, swirl-stabilized methane-air flames (these measurements are described in P1, P3, and P4) and now in pilot-stabilized jet flames with both gaseous and liquid fuels.

We have just completed an extensive set of measurements in jet flames in collaboration with Prof. Assaad Masri's group at the University of Sydney. Visiting PhD student Albyn Lowe from the University of Sydney brought over the Sydney Needle Spray Burner (SYNSBURN<sub>TM</sub>) experimental apparatus which was installed in our laboratory at Purdue University. Mr. Lowe and my PhD student Levi Thomas and postdoctoral research associate Dr. Aman Satija performed single-shot, 5 kHz fs CARS temperature measurements in jet flames stabilized on the SYNSBURN apparatus over a wide range of operating conditions. In particular, measurements were performed in jet flames in which liquid fuel was injected along the centerline using an injection tube placed different distances from the nozzle exit.

We are investigating the physics of both fs CARS and two-color PS by direct numerical integration (DNI) of the time-dependent density matrix equations for the resonant interaction. Significantly fewer restrictive assumptions are required using this DNI approach compared with the assumptions required to obtain analytical solutions. We are concentrating on the accurate simulation of two-photon processes, including Raman transitions, where numerous intermediate electronic levels contribute to the two-photon transition strength. Recent progress has been slow on our modeling efforts because of the computational time required for realistic simulation of these complicated physical processes. However, during the past year my PhD student Mingming Gu parallelized the time-dependent density matrix code with the assistance of my faculty colleague Prof. Carlo Scalo. The code was parallelized such that different computer nodes performed independent calculations for separate Q-branch transitions. The calculated electric field amplitude of the signal from each of these transitions was then added to give us the time-dependent CARS signal amplitude, and the spectrum was then calculated by Fourier transforming the time-dependent CARS signal amplitude. Using this parallelized computer code, we have investigated the effect of chirp in the pump and Stokes beams on the Raman excitation efficiency and on signal generation for chirped-probe-pulse (CPP) fs CARS. We have also started to explore the effects of collisional narrowing on the spectrum and intensity of CPP fs CARS. The study of collisional narrowing required communication between different computational nodes due to the transfer of coherence during rotational transfer collisions.

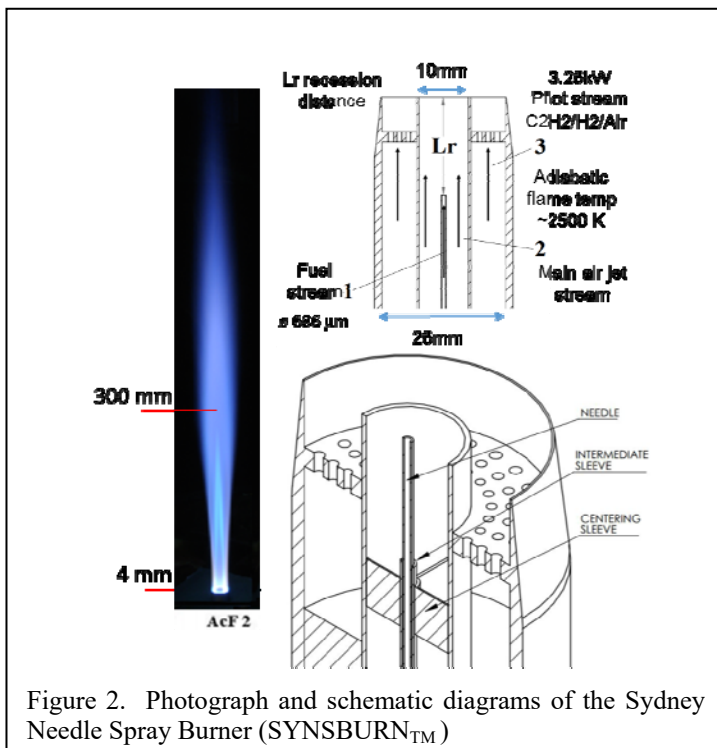
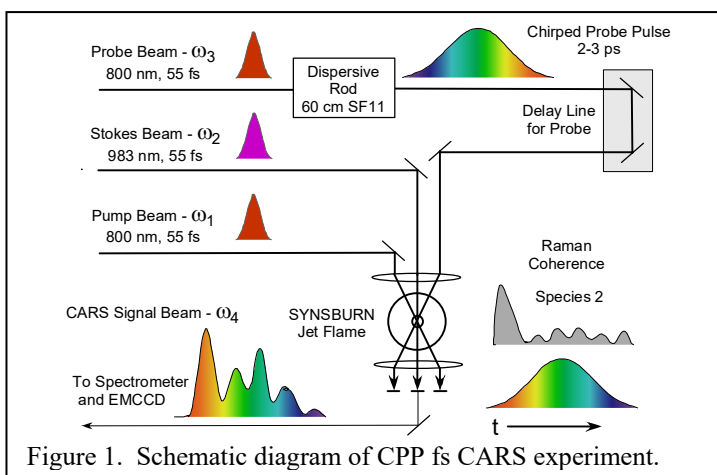


We also completed a theoretical analysis of two-photon line strengths of the nitric oxide molecule. The theoretical line strengths were compared with the results of high-resolution two-photon-absorption laser-induced fluorescence measurements of nitric oxide. The measurements were performed several years ago on this project.

## II. Recent Progress

### A. Femtosecond CARS Temperature Measurements in the SYNBSURN Jet Flames

The single-shot, chirped-pulse-probe (CPP) fs CARS system used for temperature measurements in the SYNBSURN jet flames is shown in Fig. 1. Fs CARS offers several major potential advantages compared with nanosecond (ns) CARS; i.e., CARS as usually performed with nanosecond pump and Stokes lasers. These potential advantages include an elimination of collisional effects in the signal generation and the capability of performing real-time temperature and species measurements at data rates of 1 kHz or greater as compared to 10-50 Hz for ns CARS. Our Coherent ultrafast laser system operates at 5 kHz with a fundamental pulse width of 55-60 fs and pulse energy of over 2 mJ. The fundamental 800-nm beam was used for the pump and probe beams for the SYNBSURN measurements. The Stokes beam at 983 nm was generated by frequency doubling the idler output of the OPA. The resulting CARS signal was generated at a center wavelength of 675 nm.



A photograph of a SYNBSURN jet flame and schematic diagrams of the jet burner apparatus are shown in Fig. 2. The jet flame is pilot stabilized and features a liquid fuel injector on the centerline in the inner tube. We investigated flames with liquid acetone and ethanol into surroundings main air jet stream. The fuel flow rate, the main air jet flow rate, and the distance of the liquid jet injection upstream of the jet nozzle exit plane were all parametrically varied. Premixed methane/air jet flames and nonpremixed ethylene/nitrogen jet flames were also investigated. CPP fs CARS data were acquired along the axial centerline and radial scans were performed at selected axial locations for over thirty flames. We are still in the early stages of the data analysis for these flames.

### B. Numerical Investigation of Pump and Stokes Chirp effects and Collisional Narrowing for Fs CARS

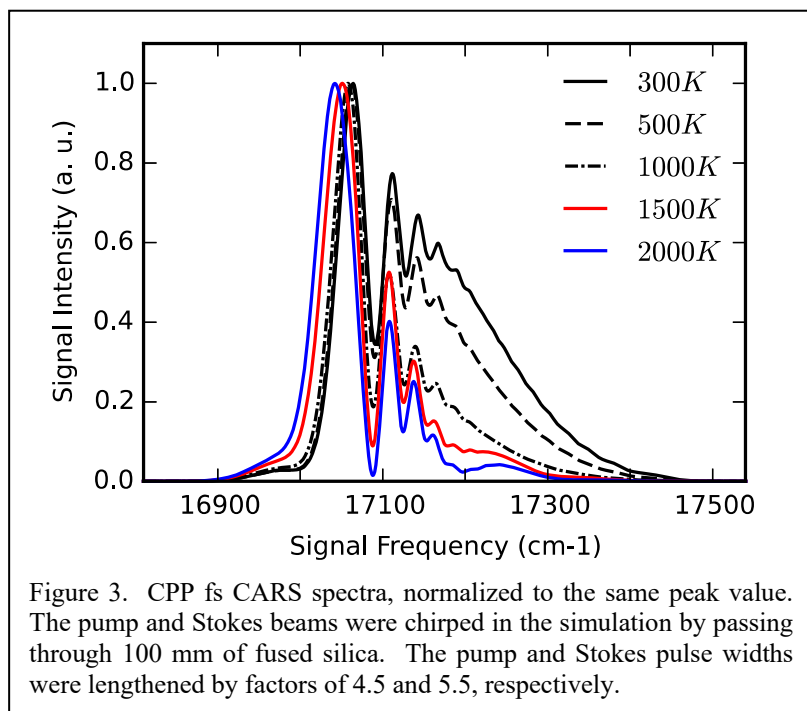
During the last year we parallelized our time-dependent

density matrix code for fs CARS. We were able to speed up the calculations by a factor of almost 100 by parallelizing and rewriting the code using the Python programming language. This in turn has allowed us to extract much more physical insight from our computer calculations because we can perform parametric variation studies much faster. We have investigated the effects of chirp in the pump and Stokes beams on the Raman excitation efficiency and signal generation for CPP fs CARS. The key result of our study of pump and Stokes chirp effects is that as long as the sign and magnitudes of the chirp are nearly equal for the pump and Stokes beams, the Raman excitation efficiency decreases only slightly, even when the pulses are lengthened by a factor of five. In addition, even with these very high levels of chirp, the temperature dependence of the CPP fs CARS spectra is preserved as shown in Fig. 3.

We have also incorporated the effects of collisional narrowing in the computer code and are investigating these effects for CPP fs CARS. The results of this study are important because for high pressure, eventually our assumption that CPP fs CARS is independent of collisions will not longer be valid. Our computational results show that by the CPP fs CARS spectrum is actually much less sensitive to increasing pressure than when we do not incorporate collisional narrowing. This is because the frequency-spread dephasing of the Raman coherence induced by impulsive pump-Stokes excitation is maintained due to the transfer of coherence during rotational transfer collisions.

### C. Two-Photon Absorption Line Strengths in Nitric Oxide

We discuss the results of high-resolution, sub-Doppler two-photon-absorption laser-induced fluorescence (TPALIF) spectroscopy of nitric oxide in Paper P5. The measurements were performed using the single-longitudinal mode output of a diode-laser-seeded optical parametric generator (OPG) system with a measured frequency bandwidth of 220 MHz. The measurements were performed using a counter-propagating pump beam geometry, resulting in sub-Doppler TPALIF spectra of NO for various rotational transitions in the (0,0) vibrational band of the  $A^2\Sigma^+-X^2\Pi$  electronic transition. The experimental results are compared with the results of a perturbative treatment of the rotational line strengths for the 20 different rotational branches of the  $X^2\Pi-A^2\Sigma$  two-photon absorption band. In the derivation of the expressions for the two-photon transition absorption strength, the closure relation is used for rotational states in the intermediate levels of the two-photon transition in analogy with the Placzek treatment of Raman transitions. The theoretical treatment of the effect of angular momentum



coupling on the two-photon rotational line strengths features the use of irreducible spherical tensors and  $3j$  symbols. The final results are expressed in terms the Hund's case (a) coupling coefficients  $a_J$  and  $b_J$  for the  $X^2\Pi$  rotational level wavefunctions, which are intermediate between Hund's case (a) and case (b). Considerable physical insight is provided by this final form of the equations for the rotational line strengths.

### III. Future Work

We will continue to perform fs CARS experiments in our laboratory using the Coherent ultrafast laser system.

Our studies of temperature measurements using CPP fs CARS will continue. We continue to investigate the effect of laser system parameters on the CPP fs CARS spectrum to improve the temperature accuracy of the technique. We will explore the potential for using CPP fs CARS for accurate concentration measurements for hydrocarbon species and other polyatomic molecules, very hard species to measure using ns CARS. We will make full use of the high-temperature, high-pressure gas cell that we have fabricated for fundamental studies of the effects of temperature and pressure on fs CARS measurements of temperature and species concentrations. We are also performing ns and CPP fs CARS measurements of the sooting, laminar jet flames studied for many years by the Yale group. We will explore further the effects of soot and droplets on the CPP fs CARS process.

Our theoretical studies of the physics of fs CARS will continue. The parallelization of our density matrix computer code will allow us to explore effects such as collisional narrowing that was simply not possible using the serial version of our code.

Our investigation of the physics of two-color PS for species such as NO will continue. We will explore collisional effects on the PS and 6WM processes in much more detail using the two-dye laser system that we are currently setting up. We will explore further the effects of buffer gas collisions on collision-induced resonances in single-photon, two-color PS of NO. We will continue to use the density matrix code to gain insight into the physics of the PS and 6WM processes; these codes will also be parallelized during next year so that we can incorporate Doppler broadening and velocity narrowing effects in model of two-color PS for atomic hydrogen.

#### **IV. Refereed publications and submitted journal articles supported by this project 2015-2017**

- P1. C. N. Dennis, C. D. Slabaugh, I. G. Boxx, W. Meier, R. P. Lucht, "Femtosecond Coherent Anti-Stokes Raman Scattering Thermometry at 5 kHz in a Gas Turbine Model Combustor," *Proceedings of the Combustion Institute* **35**, 3731-3738 (2015). DOI: 10.1016/j.proci.2014.06.063
- P2. C. N. Dennis, A. Satija, and R. P. Lucht, "High Dynamic Range Thermometry at 5 kHz in Hydrogen-Air Diffusion Flame using Chirped-Probe-Pulse Femtosecond Coherent Anti-Stokes Raman Scattering," *Journal of Raman Spectroscopy* **47**, 177-188 (2016). DOI: 10.1002/jrs.4773
- P3. C. N. Dennis, C. D. Slabaugh, I. G. Boxx, W. Meier, and R. P. Lucht, "5 kHz Thermometry in a Swirl-Stabilized Gas Turbine Model Combustor using Chirped Probe Pulse Femtosecond CARS. Part 1: Temporally Resolved Swirl-Flame Thermometry," *Combustion and Flame* **173**, 441-453 (2016). DOI: 10.1016/j.combustflame.2016.02.033
- P4. C. D. Slabaugh, C. N. Dennis, I. G. Boxx, W. Meier, and R. P. Lucht, "5 kHz Thermometry in a Swirl-Stabilized Gas Turbine Model Combustor using Chirped Probe Pulse Femtosecond CARS. Part 2: Analysis of Swirl Flame Dynamics," *Combustion and Flame* **173**, 454-467 (2016). DOI: 10.1016/j.combustflame.2016.02.032
- P5. W. D. Kulatilaka and R. P. Lucht, "Two-Photon-Absorption Line Strengths for Nitric Oxide: Comparison of Theory and Sub-Doppler, Laser-Induced Fluorescence Measurements," *Journal of Chemical Physics* **146**, 124311 (2017). DOI: 10.1063/1.4978921

# Particle Chemistry and Diagnostics Development

H. A. Michelsen

Sandia National Labs, MS 9055, P. O. Box 969, Livermore, CA 94551

hamiche@sandia.gov

## I. Program Scope

Combustion processes often produce solid carbon particles, i.e., soot. These particles may be oxidized to form gas-phase species or released into the exhaust stream, and they can be coated with semi-volatile coatings either in the exhaust stream or in the combustor. The research program described here focuses on the development and use of diagnostics for soot particles in combustion environments and combustion exhaust plumes and the use of these diagnostics to study soot formation, growth, chemical and physical evolution, oxidation, and other chemical processing. The work involves *in situ* measurements of volume fraction, size, composition, and morphology of combustion-generated particles with fast time response and high sensitivity for studies of particle chemistry coupled with complementary *ex situ*. Measurement techniques must be versatile enough to probe particles throughout their entire life cycle. Techniques are being developed for detection and characterization of particles in combustion environments from incipient particles that are <6 nm in diameter and composed of condensed large organic species to mature soot particles composed of aggregates of carbonaceous primary particles resembling polycrystalline turbostratic graphite. Studies are targeted at developing an understanding at a fundamental level of particle-light interactions and soot chemistry as a non-ideal material.

## II. Recent Progress

Our work has focused on developing a detailed understanding of the chemical and physical mechanisms that influence the applicability of laser-based, X-ray, and mass spectrometric techniques for soot detection and characterization under a wide range of conditions. In recent work, we have developed, refined, and applied a range of diagnostic methods to investigate the formation, evolution, and oxidation of soot in atmospheric premixed flat and laminar diffusion flames.

### A. Probing Soot Maturity Level Using Bulk- and Surface-Sensitive Diagnostics

We have studied the evolution of soot composition and fine structure, i.e., maturity level, in a partially premixed atmospheric ethylene-air diffusion flame. We used aerosol mass spectrometry using single-photon vacuum ultraviolet photoionization (VUV-AMS) to provide information about availability of gas-phase species to adsorb to the particle surface, laser-induced incandescence (LII) to provide information about soot volume fraction and maturity level of the bulk primary particle, and X-ray photoelectron spectroscopy (XPS) to provide complementary information about particle-surface maturity level.<sup>1</sup> XPS is sensitive to the chemical environment of atoms in a sample, is quantitative, and provides a measure of atomic composition, surface functional groups, and electronic structure, including carbon hybridization. At a photon energy of 1,253.6 eV, the mean electron escape depth in graphite is on the order of 1-2 nm, making XPS sensitive to only the surface layers of the particle. This surface sensitivity is a good complement to the bulk sensitivity of LII.

The equation for the absorption cross section can be written for a Rayleigh particle with diameter  $d$  as

$$\sigma_{abs} = \frac{\pi d^3}{6} \frac{\beta}{\lambda^\xi}, \quad (1)$$

where  $\lambda$  is the wavelength of light. The dispersion or Ångström exponent  $\xi$  decreases with increasing soot maturity level, and the scaling factor  $\beta$  increases with increasing soot maturity level.<sup>2</sup> We derived the dispersion exponent  $\xi$  using LII measured with two laser wavelengths.<sup>2-3</sup> Figure 1 shows the peak of the LII temporal profiles as a function of laser fluence measured using laser wavelengths of 532 and 1064 nm at different heights above the burner (HABs); these data were used to derive  $\xi$  and  $\beta$ .<sup>1</sup> The results are shown in Fig. 2a. The soot maturity level increases with HAB as the LII-derived soot volume fraction increases (Fig. 2b). The maturity level only slight decreases as the soot volume fraction decreases during oxidation in the upper part of the flame. The surface maturity level is probed using XPS to measure the  $sp^2$ /defect ratio (Fig. 2c), which increases with increasing maturity level. Comparison of Figs. 2a and 2c indicate that the surface maturity level increases more slowly than the bulk maturity level as the soot volume fraction is increasing between HABs of 4 and 6 mm. These changes occur while the hydrocarbon

concentration is high, as shown by the VUV-AMS ion signal (Fig. 2b), and we hypothesize that the particles grow by surface addition of hydrocarbons in this region of the flame. The soot surface maturity level decreases rapidly as the particles are oxidized at higher HABs, but the bulk maturity level remains relatively high, indicating that oxidation occurs on the surface of the particle. Oxidation tends to generate defects in the surface structure but does not lead to oxygen integration into the particle, as demonstrated by the low O/C ratio observed at high HABs (Fig. 2c).

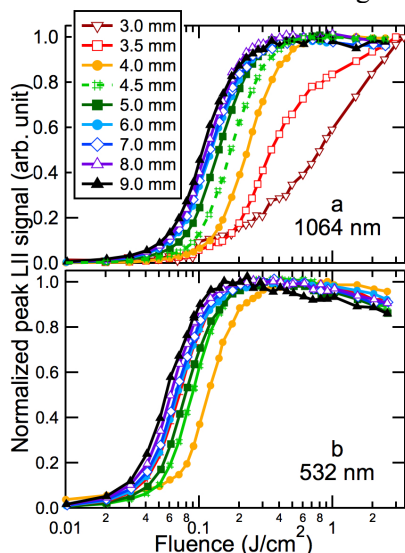


Figure 1. Normalized peak LII signal as a function of laser fluence. Measurements were made at different HABs (see legend) at laser wavelengths of (a) 1064 nm and (b) 532 nm. Each curve was normalized to unity at the maximum value. From Ref. 1.

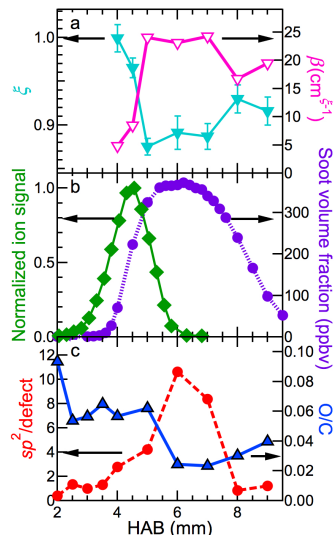


Figure 2. Optical properties, soot volume fraction, normalized heavy hydrocarbon distribution, and XPS C 1s  $sp^2$ /defect and O/C ratios. Results are shown as a function of HAB for (a) the dispersion exponent ( $\zeta$ ), absorption cross section scaling factor ( $\beta$ ), (b) normalized VUV-AMS ion signal, soot volume fraction, (c) the ratio between the signal from  $sp^2$ -hybridized carbon atoms and carbon atoms in defect locations at the surface, and the ratio of oxygen to carbon atoms at the surface. From Ref. 1.

## B. Gaining Insight into Soot Formation through Measurements and Simulations

Soot formation involves growth of hydrocarbon species to produce gas-phase precursors and nucleation of these precursors to generate condensed-phase particles, but there are large gaps in our understanding of the fundamental chemical physics of steps involved in this process. In addition to uncertainties about gas-phase precursor formation, incipient particle nucleation is even more poorly understood and is perhaps the least well understood step in soot formation.<sup>4</sup> Although large PAHs appear to be linked to soot formation, it is not known which species characteristics or species trigger particle inception and how this nucleation process occurs.

We are working on a SISGR project led by Prof. Angela Violi (University of Michigan) to develop a validated predictive multiscale model to describe the chemical composition of soot nanoparticles in premixed and diffusion flames. This project closely couples experimental investigations of soot precursors and incipient particle characteristics with the development of a predictive model for the chemical composition of soot nanoparticles. The co-investigators on the project are Prof. Angela Violi for model development and Dr. Hope Michelsen (Sandia) and Dr. Kevin Wilson (LBNL ALS) for aerosol mass spectrometry (AMS), coupled with other techniques for particle composition, size, and morphology measurements. This project uses *ab initio* and probabilistic computational techniques to identify low-barrier reaction mechanisms for the formation of soot precursors and online VUV-AMS and other techniques to confirm model predictions.

We recorded VUV-AMS spectra of particles sampled from premixed and diffusion flames. Figure 3 shows VUV-AMS spectra measured from particles extracted from a premixed flat flame at three different HABs. Based on mass, peaks shown in red were identified as entirely or partly stemming from species containing oxygen atoms at certain HABs.<sup>5</sup> The spatial distributions of the oxygenated species are very different from those of pure hydrocarbon species and are weighted very heavily toward regions of the flame that contain high concentrations of  $O_2$ ,  $O$ , and  $OH$  relative to pure hydrocarbon species. Thus,

peaks stemming entirely from oxygenated species, e.g., the peak at 160 u go away at high HABs in the premixed flame (Fig. 3), where there is no reactive oxygen available. Peaks that contain contributions from both oxygenated and non-oxygenated species, e.g., 194 u and 220 u tend to decrease in intensity and slightly shift their mass locations when moving away from the flame zone containing reactive oxygen, i.e., increasing HAB in the premixed flame (Fig. 3). A shift in mass location of a mass peak is consistent with a change in atomic constituents contributing to the signal. Hence, the mass shifts measured with increasing HAB for many of the peaks marked in red in Fig. 3 are attributable to a change in constituents contributing to a mass peak from predominantly oxygenated species to predominantly pure hydrocarbon species. The masses of the oxygenated species agree well with the atomic compositions predicted by the simulations. Both experiments and simulations demonstrate that ~50% of the mass peaks observed at some flame heights in the mass range 140 – 350 u contain signal from oxygenated species. The predicted structures for these species are predominantly alcohols or enols near the burner or fuel outlet (for a counter-flow flame) and are mainly furans or ethers far from the burner or fuel outlet (e.g., Fig. 4).

The mass spectra yield masses and some elemental information, but they do not provide functional group information. In order to identify functional groups, we measured XPS spectra at the oxygen *K* edge, as shown in Fig. 5. These results support the prediction of alcohols and enols lower in the flame and a preference for ethers and furans at larger HABs. The most probable pathway to furan formation is shown in Fig. 6 and starts with H-abstraction from a PAH edge site followed by addition of OH or O<sub>2</sub>. The most probable pathway for embedding oxygen into the hydrocarbon molecules is *via* ethers formed when H is abstracted from hydroxyl groups or OH/O is abstracted from peroxy acid/radical groups, followed by hydrocarbon addition to the oxyradical and furan-ring closure. Acetylene is the most frequently added hydrocarbon. We expect this scheme to be important to a wide range of hydrocarbon oxidation processes and hydrocarbon-combustion systems because of high acetylene concentrations and low reaction barriers.

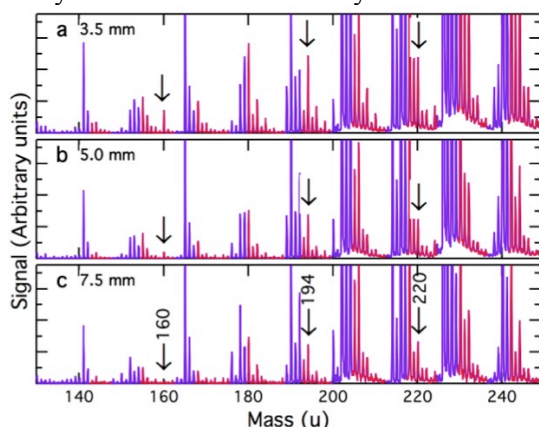


Figure 3. VUV-AMS spectra from a premixed flame. Mass spectra are shown for particles extracted from HABs of (a) 3.5, (b) 5.0, and (c) 7.5 mm. Red peaks contain signal from oxygenated species. From Ref. 5.

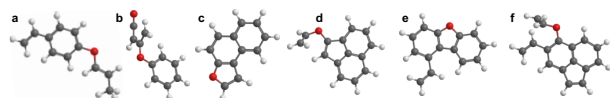


Figure 4. Frequently predicted oxygen-containing structures of selected masses low in a premixed flame. Red atoms: oxygen, gray: carbon, white: hydrogen. a-b, 160 u – ether, ether/ketene. c, 168 u – furan. d-e, 194 u – ether, furan. f, 220 u – ether. From Ref. 5.

### III. Future Work

Future work will refine and expand on the application of X-ray measurement techniques for studies of soot formation, evolution, and oxidation. We will continue to develop laser-based diagnostics that can be used to probe particle size, morphology, and composition and apply these *in situ* diagnostics to study soot evolution and oxidation in flames. These diagnostics will be complemented by *ex situ* diagnostics, such as AMS, transmission electron microscopy (TEM), scanning mobility particle sizing (SMPS), centrifugal

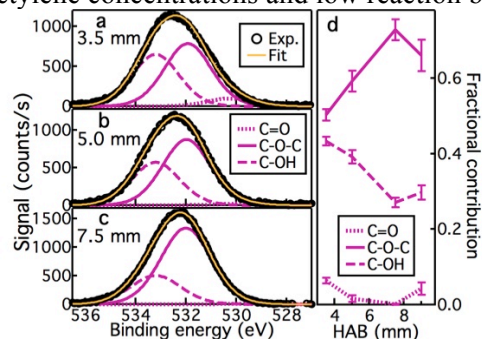


Figure 5. XPS O 1s spectra of soot sampled from a premixed flame. Spectra are shown for particles extracted from HABs of (a) 3.5 mm, (b) 5.0 mm, and (c) 7.5 mm. (d) Fractional contributions of oxygenated functional groups were inferred from fits to XPS O 1s spectra. Error bars are  $\pm$  one standard deviation of the uncertainties associated with the peak fits. From Ref. 5.

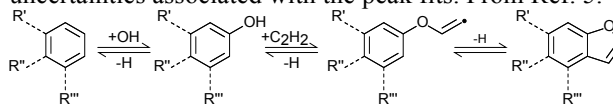


Figure 6. Probable reaction sequence for formation of a furan group. Left-to-Right: H-abstraction, then OH addition to the radical free-edge site on an aromatic ring; H-abstraction from the OH group, then acetylene addition, forming an ether group; H-elimination during ring closure to form a furan group. From Ref. 5.

particle mass analysis (CPMA), Raman spectroscopy, near-edge X-ray absorption fine-structure spectroscopy (NEXAFS), and XPS, making an effort to deploy all of these diagnostics on selected combustion systems. We plan to eventually apply these diagnostics to combustion systems at higher pressure to study the influence of pressure on nucleation and oxidation processes.

#### IV. References

1. Johansson, K. O.; El Gabaly, F.; Schrader, P. E.; Campbell, M. F.; Michelsen, H. A., Evolution of particle surface and bulk maturity level during soot growth and oxidation in a flame. *Aerosol Sci. Technol.* **2017**, submitted.
2. Michelsen, H. A., Probing soot formation, chemical and physical evolution, and oxidation: A review of *in situ* diagnostic techniques and needs. *Proc. Combust. Inst.* **2017**, *36*, 717-735.
3. López-Yglesias, X.; Schrader, P. E.; Michelsen, H. A., Soot maturity and absorption cross sections. *J. Aerosol Sci.* **2014**, *75*, 43-64.
4. (a) Frenklach, M.; Wang, H., Detailed modeling of soot particle nucleation and growth. *Twenty-Third Symp. (Internat.) Combust.* **1991**, *23*, 1559-1566; (b) Richter, H.; Howard, J. B., Formation and consumption of single-ring aromatic hydrocarbons and their precursors in premixed acetylene, ethylene and benzene flames. *Phys. Chem. Chem. Phys.* **2002**, *4*, 2038-2055.
5. Johansson, K. O.; Dillstrom, T.; Monti, M.; El Gabaly, F.; Campbell, M. F.; Schrader, P. E.; Popolan-Vaida, D. M.; Richards-Henderson, N. K.; Wilson, K. R.; Violi, A.; Michelsen, H. A., Formation and emission of large furans and oxygenated hydrocarbons from flames. *Proc. Natl. Acad. Sci. USA* **2016**, *113* (30), 8374-8379.

#### V. Publications and submitted journal articles supported by this project 2015-2017

1. K. O. Johansson, F. El Gabaly, P. E. Schrader, M. F. Campbell, and H. A. Michelsen, "Evolution of particle surface and bulk maturity level during soot growth and oxidation in a flame", *Aerosol Sci. Technol.* **XX**, submitted (2017).
2. K. O. Johansson, M. F. Campbell, P. Elvati, P. E. Schrader, J. Zádor, N. K. Richards-Henderson, K. R. Wilson, A. Violi, and H. A. Michelsen, "Photoionization efficiencies of five polycyclic aromatic hydrocarbons", *J. Phys. Chem. A* **XX**, submitted (2017).
3. K. O. Johansson, J. Zádor, P. Elvati, M. F. Campbell, P. E. Schrader, N. K. Richards-Henderson, K. R. Wilson, A. Violi, and H. A. Michelsen, "Critical assessment of photoionization efficiency measurements for characterization of soot-precursor species", *J. Phys. Chem. A* **XX**, submitted (2017).
4. H. A. Michelsen, "Probing soot formation, chemical and physical evolution, and oxidation: A review of *in situ* diagnostic techniques and needs", *Proc. Combust. Inst.* **36**, 717-735 (2017).
5. K. O. Johansson, T. Dillstrom, P. Elvati, M. F. Campbell, P. E. Schrader, D. M. Popolan-Vaida, N. K. Richards-Henderson, K. R. Wilson, A. Violi, and H. A. Michelsen, "Radical-radical reactions, pyrene nucleation, and incipient soot formation in combustion", *Proc. Combust. Inst.* **36**, 799-806 (2017).
6. M. F. Campbell, A. Bohlin, P. E. Schrader, R. P. Bambha, C. J. Kliewer, K. O. Johansson, and H. A. Michelsen, "Design and characterization of a linear Hencken-type burner", *Rev. Sci. Instrum.* **87**, 115114 (2016).
7. K. O. Johansson, T. Dillstrom, M. F. Campbell, M. Monti, F. El Gabaly, P. E. Schrader, D. M. Popolan-Vaida, N. K. Richards-Henderson, K. R. Wilson, A. Violi, and H. A. Michelsen, "Toxins, carcinogens, fire, and soot: Explaining large furan and oxygenated hydrocarbon formation and emission from flames", *Proc. Natl. Acad. Sci. USA* **113**, 8374-8379 (2016).
8. R. P. Bambha and H. A. Michelsen, "Effects of aggregate morphology and size on laser-induced incandescence and scattering from black carbon (mature soot)", *J. Aerosol Sci.* **88**, 159-181 (2015).
9. H. A. Michelsen, C. Schulz, G. J. Smallwood, and S. Will, "Laser-induced incandescence: Particulate diagnostics for combustion, atmospheric, and industrial applications", *Progress Energy Combust. Sci.* **51**, 2-48 (2015).
10. K. O. Johansson, J. Y. W. Lai, S. A. Skeen, K. R. Wilson, N. Hansen, A. Violi, and H. A. Michelsen, "Soot precursor formation and limitations of the stabilomer grid", *Proc. Combust. Inst.* **35**, 1819-1826 (2015).

# Reaction Dynamics in Polyatomic Molecular Systems

William H. Miller

Department of Chemistry, University of California, and  
Chemical Sciences Division, Lawrence Berkeley National Laboratory  
Berkeley, California 94720-1460  
millerwh@berkeley.edu

## I. Program Scope

The goal of this program is the development of theoretical methods and models for describing the dynamics of chemical reactions, with specific interest for application to polyatomic molecular systems of special interest and relevance. There is interest in developing the most rigorous possible theoretical approaches and also in more approximate treatments that are more readily applicable to complex systems.

## II. Recent Progress

Effort in earlier years focused on developing *semiclassical* (SC) theory<sup>1-3</sup> into a practical way for adding quantum mechanical effects to classical molecular dynamics (MD) simulations, which are so ubiquitously applied to all types of dynamical processes in complex molecular systems, e.g., chemical reactions in clusters, nano-structures, molecules on or in solids, bio-molecular systems, etc. More recently, however, we have been exploring how successful even simpler, *purely classical* MD approaches can be (with some judicious SC ideas incorporated), especially for the important case of *electronically non-adiabatic processes*, i.e., those which involve transitions between different electronic states. The two essential ingredients to the approach, (a) how are the electronic degrees of freedom described within a classical mechanics framework, and (b) how one identifies specific electronic states (initially and finally) within a classical picture.

The Meyer-Miller (MM) classical vibronic Hamiltonian<sup>4</sup> maps the electronic degrees of freedom (DOF) of a coupled electronic-nuclear system onto a set of classical harmonic oscillators, each oscillator representing the occupation of the various electronic states. Since the electronic as well as the nuclear DOF are thus described classically, a standard classical MD simulation treats these DOF and their interaction dynamically consistently (albeit at the level of classical mechanics). (If all these DOF were treated quantum mechanically, the MM Hamiltonian becomes a representation of the exact QM *operator* and would thus provide the exact QM vibronic dynamics.) In a recent series of papers, a symmetrical quasi-classical (SQC) windowing methodology<sup>5</sup> has been described and applied to the MM Hamiltonian in order to “quantize” these electronic DOF both initially and finally<sup>6</sup>. It was found that this approach provides a very reasonable description of non-adiabatic dynamics exhibited in a suite of standard benchmark model problems for which exact quantum mechanical (QM) results are available for comparison. Among the examples were systems exhibiting strong quantum coherence effects and systems representative of condensed-phase non-adiabatic dynamics, including some which other simple approaches have difficulty in describing



correctly (e.g., the asymmetric spin-boson problem<sup>6</sup> and the inverted regime in electron transfer processes<sup>7</sup>).

It was also discussed in these recent papers how various aspects of the SQC/MM model are appealing from a theoretical perspective<sup>8</sup>: e.g., it has a straightforward theoretical justification, and by providing an equivalent treatment of the electronic and the nuclear DOF (i.e., via classical mechanics) it is able to describe “quantum” coherence and de-coherence without resorting to any “add ons” to the theory. The (classical) time evolution of the nuclear and electronic DOF is continuous at all times (as it is QM'ly), and it gives equivalent results whether implemented in adiabatic or diabatic representations. It was also emphasized that though the equations of motion that result from the MM Hamiltonian are “Ehrenfest” — in that the force on the nuclei at any time is the coherent average of that over all electronic states — the fact that zero point energy is included in the electronic oscillators means that there is an ensemble of trajectories for each initial state (rather than only one trajectory as in the “Ehrenfest method” itself), and the population of each final electronic state is determined by the fraction of that ensemble that end up in that state. I.e., each trajectory in this ensemble contributes to only one final electronic state. The approach thus does not suffer from the well-known “Ehrenfest disease” of having all final electronic states determined by one (average) nuclear trajectory. As a result, the SQC method of quantizing the electronic DOF initially and finally leads to detailed balance being described correctly<sup>9</sup>. From a practical perspective, the SQC/MM is attractive since it is trajectory-based and can be straightforwardly incorporated within the framework of a standard classical MD simulation. One has only to add one vibrational-like DOF for each electronic state, which are propagated along with the (perhaps very many) nuclear DOF via Hamilton's equations that result from the MM Hamiltonian.

Recent developments and extensions of the SQC/MM approach have been (1) to show that it can treat very weak electronic coupling as well as it does strong coupling (which most examples treated by us and others have been), and (2) how off-diagonal elements of the electronic density matrix can be obtained within the same ensemble of trajectories that gives the diagonal elements (i.e., the populations):

(1) Very weak electronic coupling is accurately treated by using a modification of the ‘window functions’ of the SQC model for ‘quantizing’ the electronic degrees of freedom initially and finally.<sup>10</sup> Since these window functions are essentially pre-limit delta functions (about the Bohr-Sommerfeld integer values for the electronic action variables that define the electronic states), there is considerable room for choosing them; this is the modelistic aspect of the approach. Thus it was found that triangle window functions centered about the quantum integer values (but which touch at a corner) describe the weak coupling regime extremely well, as well as also the strong coupling regime at least as well (or better) than the square histogram window functions that had been to date been the ‘standard’ choice. Ref 10 gives the specifics of this modification, and Figure 1 shows as example (for a 1d scattering problem) of the electronic transition probability versus electronic coupling strength. Both the square and the triangle window functions work quite well for transition probabilities  $>/\sim 0.1$ , but one sees that the square histogram windows fail precipitously for smaller transition

probabilities, while the triangle window functions give excellent results over the whole region of large and small transition probabilities.

(2) Reference 11 shows how (square or triangle) window functions can be defined for off-diagonal elements of the electronic density matrix that are completely consistent with the Bohr-Sommerfeld window functions for the diagonal elements (i.e., populations). Figure 2 shows an example of the full density matrix for the 2-state site exciton model treated by Ishizaki and Fleming<sup>12</sup> using the HEOM method (which should give the exact quantum results for this spin-boson type system).

A review of the body of SQC/MM work to date is given in the Introductory Lecture for a recent Faraday Discussion on Reaction Rate Theory.<sup>13</sup>

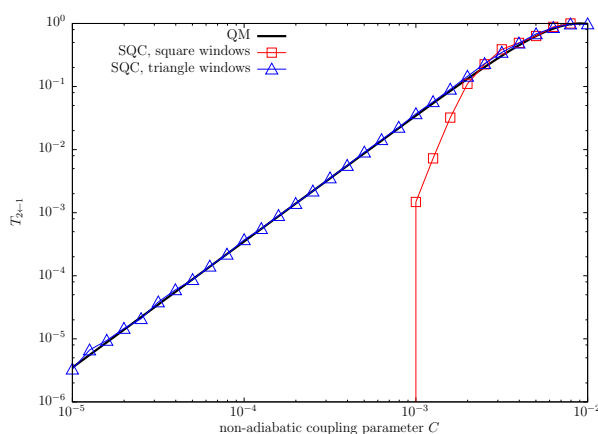


Figure 1. SQC/MM results calculated using square Histogram and triangle window functions *versus* energy-domain QM scattering calculations ( $P = 15\text{AU}$ ).

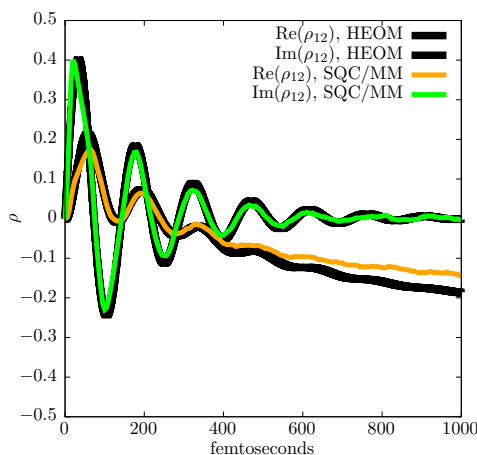
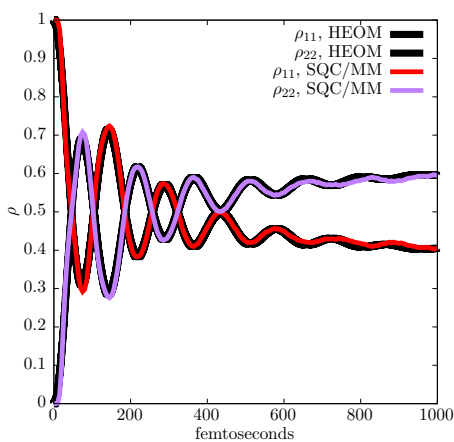


Figure 2. SQC/MM computed density matrix  $\{\rho_{ij}(t)\}$  *versus* HEOM results for 2-state site-exciton model (difference in site energies  $\varepsilon_1 - \varepsilon_2 = 100\text{cm}^{-1}$ , non-adiabatic coupling  $\Delta = 100^{-1}$ , bath characteristics frequency  $\omega_c = 53.08\text{cm}^{-1}$ , reorganization energy  $\lambda = 20\text{cm}^{-1}$ , and  $T = 300\text{K}$ ; see Fig. ? of Ref. ?).

### III. Future Plans

Since this quasi-classical model has proved quite reliable for describing electronically non-adiabatic dynamics in these simple model problems, work is in progress to extend its application to more general and complex non-adiabatic processes.

## References

1. For reviews, see W. H. Miller, *Adv. Chem. Phys.* **25**, 69-177 (1974); **30**, 77-136 (1975).
2. W. H. Miller, *J. Chem. Phys.* **53**, 1949-1959 (1970).
3. For reviews, see W. H. Miller, (a) *J. Phys. Chem. A* **105**, 2942-2955 (2001); (b) *Proc. Natl. Acad. Sci. USA* **102**, 6660-6664 (2005); (c) *J. Chem. Phys.* **125**, 132305.1-8 (2006).
4. H. D. Meyer and W. H. Miller, *J. Chem. Phys.* **71**, 2156-2169 (1979).
5. S. J. Cotton and W. H. Miller, *J. Phys. Chem. A* **117**, 7190-7194 (2013).
6. S. J. Cotton and W. H. Miller, *J. Chem. Phys.* **139**, 234112.1-9 (2013).
7. S. J. Cotton, K. Igumenshchev and W. H. Miller, *J. Chem. Phys.* **141**, 084104.1-14 (2014).
8. S. J. Cotton and W. H. Miller, *J. Phys. Chem. A* **119**, 12138-12145 (2015).
9. W. H. Miller and S. J. Cotton, *J. Chem. Phys.* **142**, 131103.1-3 (2015).
10. S. J. Cotton and W. H. Miller, *J. Chem. Phys.* **145**, 144108.1-16 (2016).
11. W. H. Miller and S. J. Cotton, *J. Chem. Phys.* **145**, 081101.1-4 (2016).
12. A. Ishizaki and G. R. Fleming, *J. Chem. Phys.* **130**, 23411 (2009).
13. W. H. Miller and S. J. Cotton, *Faraday Discuss.* **195**, 9-30 (2016).

## IV. 2014 - 2016 DOE Publications

1. W. H. Miller, A Journey Through Chemical Dynamics, *Annu. Rev. Phys. Chem.* **65**, 1-19 (2014).
2. B. Li, E. Y. Wilner, M. Thoss, E. Rabani and W. H. Miller, A Quasi-Classical Mapping Approach to Vibrationally Coupled Electron Transport in Molecular Junctions, *J. Chem. Phys.* **140**, 104110.1-7 (2014)
3. B. Li, W. H. Miller, T. J. Levy and E. Rabani, Classical Mapping for Hubbard Operators: Application to the Double-Anderson Model, *J. Chem. Phys.* **140**, 204106.1-7 (2014).
4. S. J. Cotton, K. Igumenshchev and W. H. Miller, Symmetrical Windowing for Quantum States in Quasi-Classical Trajectory Simulations: Application to Electron Transfer, *J. Chem. Phys.* **141**, 084104.1-14 (2014).
5. W. H. Miller and S. J. Cotton, Communication: Note on Detailed Balance in Symmetrical Quasi-Classical Models for Electronically Non-Adiabatic Dynamics, *J. Chem. Phys.* **142**, 131103.1-3 (2015).
6. S. J. Cotton and W. H. Miller, A Symmetrical Quasi-Classical Spin-Mapping Model for the Electronic Degrees of Freedom in Non-Adiabatic Processes, *J. Phys. Chem. A* **119**, 12138-12145 (2015).
7. S. J. Cotton and W. H. Miller, The Symmetrical Quasi-Classical Model for Electronically Non-Adiabatic Processes Applied to Energy Transfer Dynamics in Site-Exciton Models of Light-Harvesting Complexes, *J. Chem. Theory Comput.* **12**, 983-991 (2016).
8. W. H. Miller and S. J. Cotton, Communication: Wigner Functions in Action-Angle Variables, Bohr-Sommerfeld Quantization, the Heisenberg Correspondence Principle, and a Symmetrical Quasi-Classical Approach to the Full Electronic Density Matrix, *J. Chem. Phys.* **145**, 081101.1-4 (2016).
9. S. J. Cotton and W. H. Miller, A New Symmetrical Quasi-Classical Model for Electronically Non-Adiabatic Processes: Application to the Case of Weak Non-Adiabatic Coupling, *J. Chem. Phys.* **145**, 144108.1-16 (2016).
10. W. H. Miller and S. J. Cotton, Classical Molecular Dynamics Simulation of Electronically Non-Adiabatic Processes, *Faraday Discuss.* **195**, 9-30 (2016).

# Reacting Flow Modeling with Detailed Chemical Kinetics

Habib N. Najm

Sandia National Laboratories  
P.O. Box 969, MS 9051, Livermore, CA 94551  
hnnajm@sandia.gov

## I. Program Scope

The goal of this research program is to improve fundamental understanding of reacting flow, thereby advancing the state of the art in predictive modeling of combustion. The work involves: (1) Developing numerical methods for the efficient solution of reacting flow systems of equations with detailed kinetics and transport, massively parallel codes for computing large scale reacting flow with detailed kinetics, and techniques for analysis of multidimensional reacting flow; (2) Using computations to investigate the structure and dynamics of flames using detailed chemical kinetics; (3) Developing numerical methods for uncertainty quantification (UQ) in reacting flow computations; (4) Estimation of chemical model parameters, and calibration/validation of reacting flow models, based on experimental data and computational predictions; and (5) UQ studies in computations of chemical systems and reacting flow. In the following, recent progress and future plans in this overall area are discussed.

## II. Recent Progress

### A. Statistical Inference of Reaction Rate Coefficients

We have continued to work on statistical estimation of chemical rate coefficients from summary statistics, as opposed to actual measurements, using a combination of Maximum Entropy and approximate Bayesian computation methods. This situation, where inference is necessary in the absence of data, is in fact quite common in the combustion field, where actual raw data on chemical rate measurements is not published. Rather, available publications report summary statistics on chemical rate constants, such as the nominal value and error bars of  $k(T)$  at different temperatures, or nominal values and error bars on the pre-exponential and/or activation energy. Our goal in this context is to take this published information and arrive at a joint density, including correlations, on uncertain model parameters. Our earlier developments of our “data free inference” (DFI) procedure in this context included both synthetic data problems, as well as the estimation of the rate of the  $\text{H} + \text{O}_2 \longrightarrow \text{O} + \text{OH}$  reaction based on reported summary statistics from shock tube measurements [B3, B5]. More recently, we have been working on the application of the algorithm to other reactions in the  $\text{H}_2\text{-O}_2$  system, focusing on the investigation of the thermal decomposition reaction,  $\text{H}_2\text{O}_2 + \text{M} \longrightarrow 2\text{OH} + \text{M}$ , a critical pathway in both high-pressure and intermediate temperature  $\text{H}_2\text{-O}_2$  kinetics. The data inference is conducted subject to constraints imposed in the form of error bounds on Arrhenius parameters consistent with the uncertain Arrhenius fit expression reported in the target experiment. Model data in the form of species decay profiles are generated using a polynomial chaos expansion (PCE) surrogate using Legendre polynomials of a uniform random variable. We employed algorithmic refinements through the imposition of a determinism requirement on the approximate data likelihood function, improving the convergence of the data inference.

The utility of the correlated parameter probability density function obtained by performing Bayesian inference of the DFI generated data was investigated by constructing forward model predictions of the characteristic Z-curve describing the explosion limits of  $\text{H}_2\text{-O}_2$  mixtures, which is known to be highly sensitive to this particular reaction at high pressures. Forward sampling from the correlated DFI-sourced Arrhenius parameter PDF showed drastic reduction in Z-curve location uncertainty compared with using samples drawn from an incorrect uniform PDF defined by the reported parameter error bounds.

### B. Laminar premixed flame–wall interaction

We have begun testing potential configurations for numerically investigating side-wall quenching of laminar flames using our 2D low Mach number *dflame* solver. Current efforts are focused on developing an idealized steady flame configuration for comparison with recent published side-wall quenching studies while avoiding the necessity to

resolve the complicated details of the experimental setup in the simulations, *e.g.* flame anchoring and quenching region stabilization. The objective of this study is ultimately to probe the behavior of flame chemistry and structure in the presence of strong heat losses and boundary layer transport effects.

### C. Laser-perturbed Flame Modeling

In joint work with J. Frank, we have begun a computational study of transient laminar flame behavior under a modeled perturbation designed to simulate the effect of laser energy deposition and species photo-dissociation. Specifically, 1D simulations have been used to investigate the increase in CH<sub>4</sub>-air flame reactivity arising from pulsed energy deposition in the flame zone, modeled using a “dynamic” chemical sub-mechanism where two CH<sub>2</sub>O decomposition pathways are defined with time-dependent rates proportional to a defined pulse signal. We have examined simulations using the dynamic sub-mechanism with a prescribed branching ratio between the two decomposition pathways sourced from experimental data. For a range of Gaussian shaped temporal pulses of nominal strength and varying width, the laminar flame shows an approximately 15% limited increase in the instantaneous flame consumption speed, resulting from the increased reactivity arising from the larger radical pool created by CH<sub>2</sub>O fracturing until all CH<sub>2</sub>O has been consumed. These preliminary results provide useful information toward experimental design of a laser-forced flame experiment, and will be used going forward for detailed comparisons to resulting measurements.

### D. Chemical Model Reduction under Uncertainty

We have continued to work on the development of computational singular perturbation (CSP) methods [1] for analysis and reduction of chemical models under uncertainty. We finalized our study on the analysis and reduction of an n-butane mechanism with 1111 uncertain rate constants [B6]. In this first instance, we focused on the examination of the utility of the method for identifying robust simplified mechanisms. We used marginal statistics exclusively, including reactions whose marginal probability of being in the mechanism exceeds a specified threshold  $\theta$ . This threshold, along with the conventional dynamical threshold  $\tau$  on CSP importance indices, provide the requisite control knobs that specify the degree of reduction. Controlling  $(\tau, \theta)$  enables generation of a spectrum of simplified mechanisms having a wide range of accuracy and size, each of which is both dynamically and probabilistically self-consistent. In particular, we were able to show the utility of the probabilistic reduction strategy in terms of achieving robust reduction. Given uncertainty in the detailed model parameters, we showed that a reduction strategy that ignores uncertainty results in simplified mechanisms that can violate prescribed *a-posteriori* error thresholds with high probability. On the other hand, the simplified mechanisms developed with this new approach do not exhibit this behavior. Rather, they satisfy specified error thresholds with high probability.

### E. Analysis and Reduction of Stochastic Chemical Systems

When the number of molecules of a chemical species within a volume of interest is small,  $O(100)$ , the accurate description of chemical processes requires the inclusion of stochastic effects. In this regime, chemical system dynamics are well represented using the chemical Langevin equation (CLE), a stochastic differential equation (SDE). In many systems of practical interest, the resulting CLE system is large and stiff, involving reaction rates spanning a wide range of time scales. While there are well-founded methods for dynamical analysis and reduction of ordinary differential equation systems, using computational singular perturbation (CSP) theory [1, 2], which have been used extensively for simplification of macroscale chemical system models, there is relatively little work done on analysis/reduction of SDEs by comparison. In recent work, we developed and demonstrated a stochastic CSP (SCSP) method to address this challenge [B9]. The method involves an operator-split construction following similar CSP-based time integration for ODEs [3]. The method models the effect of fast time scales by projecting any initial condition toward the deterministic slow-manifold underlying the SDE, and forming the backbone of the basin of attraction for the stochastic motions. This is followed by explicit large time-step integration of the residual slow dynamics within the basin of attraction. This process is repeated for each time step. The net result is fast and stable explicit time integration of stiff SDEs. The method was outlined and demonstrated in [B9], using a model stiff SDE system, revealing significant computational savings. We observed second-order accuracy in capturing the time-dependent mean and standard deviation of species controlled by slow processes, and the mean of species controlled by fast processes. The fast statistics of the latter are, by construction, not computed in detail, hence the loss of accuracy in their standard deviation. Next will come the application of the scheme to a model CLE. The

underlying dynamical structure will also be useful as a basis for analysis of stochastic chemical system dynamics and identification of associated simplified systems.

### **III. Future Plans**

#### **A. Estimation of Model Error in Chemical Systems**

We are continuing our earlier work on modeling and estimation of model error in chemical systems [B8, B2]. Going forward, we will be applying the method in the context of Bayesian calibration of one (simple) chemical model against another, more complex, model. Earlier work had targeted simple quantities of interest (QoIs), such as ignition time, spanned limited variation of operating conditions, and pursued estimation of a subset of available parameters. We will relax these constraints going forward, providing estimation of model error for prediction of more complex QoIs, such as the structural features of ignition profiles. We will do this over ranges of initial equivalence ratio, temperature, and pressure; and will explore fitting of a larger set of model parameters. Initial studies will focus on model error in single-step global methane models, versus detailed kinetic methane mechanisms, to be followed later with an exploration of model error in skeletal methane mechanisms.

#### **B. Statistical Inference of Reaction Rate Constants**

We plan to continue the application of the DFI procedure to other reactions in the H<sub>2</sub>-O<sub>2</sub> system to determine the joint probability density function on all relevant uncertain rate parameters in this system. We will also apply DFI to experiments investigating the same reaction at different temperature ranges such that these distinct data sets can be effectively pooled, with a resulting pooled data inference delivering a consensus Arrhenius expression and parameter uncertainty structure across these temperature ranges. We plan to include additional nuisance parameters in the DFI procedure in the form of uncertainty in the experimental conditions, e.g. temperature, to further generalize the uncertainty framework. We will also explore different avenues for utilizing the DFI data itself beyond informing forward UQ studies, e.g. using the parameter posterior density constructed using the DFI data to inform parameter priors for optimal experimental design (OED) studies.

#### **C. Laminar premixed flame-wall interaction**

We plan to investigate side-wall quenching behavior for a range of wall temperatures to investigate the activation and de-activation of important chemical pathways and their effect on flame behavior. Ultimately this study will help to inform strategies for performing chemical model reduction with appropriate attention to processes that dictate flame behavior in the extinction limit due to heat loss. We are currently experimenting with alternate means of anchoring the computational flame in the vicinity of a solid wall.

#### **D. Laser-perturbed Flame Modeling**

We will continue studying modeled laser pulsing and its effects on CH<sub>2</sub>O chemistry by exploring varying pulsing strategies. We will then extend the simulation framework to enable modeling of 2D opposed flow flames, thereby mimicking the experimental geometry. This will allow us to investigate the interaction of the photo-dissociation chemistry with extinction and re-ignition events in the flame, with detailed comparisons to experimental data.

#### **E. Chemical Model Reduction under Uncertainty**

We have started to examine joint statistics among sets of reactions, moving beyond analysis and reduction based on marginal probabilities. In principle, this approach, if sufficient samples are available, allows the examination of joint statistics for full sub-mechanisms, facilitating the identification of the simplified mechanism with highest probability, for a given CSP importance index threshold. Of course, there is no guarantee that any given mechanism will have overwhelmingly large probability, as compared with others. In this case, one may resort to inclusion of the union of some set of mechanisms that capture the bulk of the probability. Further, the approach enables examination of pair-wise or path-wise statistics, providing much insight on mechanism network structure and associated constraints. It is interesting, e.g., to identify pairs of reactions that are always included together or not, but never one without the other. Similarly for pathways.

## F. Coupling with Experiments

Going forward, and in joint work with J. Frank and J. Oefelein, we will explore avenues for effective utilization of statistical data analysis and probabilistic modeling in the analysis of experimental and computational turbulent reacting flow data. This includes estimation of uncertainty in tomographic PIV measurements of flow velocity fields, and the study of turbulent flow structures, combining information from both computations and experiments.

## G. Analysis and Reduction of Stochastic Chemical Systems

Our future targets in the context of stochastic chemical systems include a range of planned developments. To begin with, we will extend the current SCSP time integration method to the full CLE, focusing to begin with on stochastic Michaelis-Menten kinetics. This pursuit will result in significant additional complexity given the CLE structure, and the multiplicity of Brownian motion source terms when dealing with multiple reactions. The resulting challenge will require requisite algorithmic and code developments. At the same time, we will be looking at the utilization of the method for analysis purposes given computational databases of CLE solutions. This will require formulation of appropriate projections of reaction processes onto both the slow and fast subspaces, and estimation of important processes in each subspace. Doing this in a stochastic setting will require some care, and significant effort.

## References

- [1] S.H. Lam and D.A. Goussis. The CSP Method for Simplifying Kinetics. *International Journal of Chemical Kinetics*, 26:461–486, 1994.
- [2] M. Valorani, F. Creta, F. Donato, H.N. Najm, and D.A. Goussis. Skeletal Mechanism Generation and Analysis for *n*-heptane with CSP. *Proc. Comb. Inst.*, 31:483–490, 2007.
- [3] M. Valorani and D.A. Goussis. Explicit Time-Scale Splitting Algorithm For Stiff Problems: Auto-Ignition Of Gaseous-Mixtures Behind A Steady Shock. *J. Comput. Phys.*, 169:44–79, 2001.

## BES-Supported Published/In-Press/Submitted Publications [2015-2017]

- [B1] L. Hakim, G. Lacaze, M. Khalil, H. Najm, and J. Oefelein. Modeling auto-ignition transients in reacting Diesel jets. *ASME J. Eng. Gas Turb. Power*, 138(11):112806–112806–8, 2016. Paper #: GTP-16-1054.
- [B2] L. Hakim, G. Lacaze, M. Khalil, K. Sargsyan, H. Najm, and J. Oefelein. Probabilistic parameter estimation in a 2-step chemical kinetics model for *n*-dodecane jet autoignition. *Combustion Theory & Modelling*. submitted.
- [B3] M. Khalil, K. Chowdhary, C. Safta, K. Sargsyan, and H.N. Najm. Inference of reaction rate parameters based on summary statistics from experiments. *Proc. Comb. Inst.*, 36(1):699–708, 2017.
- [B4] M. Khalil, G. Lacaze, J.C. Oefelein, and H.N. Najm. Uncertainty quantification in LES of a turbulent bluff-body stabilized flame. *Proceedings of the Combustion Institute*, 35:1147–1156, June 2015.
- [B5] M. Khalil and H.N. Najm. Probabilistic Inference of Reaction Rate Parameters from Summary Statistics. *Combustion Theory and Modeling*. submitted.
- [B6] R. Malpica-Galassi, M. Valorani, H.N. Najm, C. Safta, M. Khalil, and P.P. Ciottoli. Chemical Model Reduction under Uncertainty. *Combustion and Flame*, 179:242–252, 2017.
- [B7] C. Safta, M. Blaylock, J. Templeton, S. Domino, K. Sargsyan, and H. Najm. Uncertainty quantification in les of channel flow. *International Journal for Numerical Methods in Fluids*, 83:376–401, 2017.
- [B8] K. Sargsyan, H. N. Najm, and R. Ghanem. On the Statistical Calibration of Physical Models. *International Journal for Chemical Kinetics*, 47(4):246–276, 2015.
- [B9] L. Wang, X. Han, Y. Cao, and H.N. Najm. Computational Singular Perturbation Analysis of Stochastic Chemical Systems with Stiffness. *J. Comput. Phys.*, 335:404–425, 2017.

## Spectroscopy, Kinetics and Dynamics of Combustion Radicals

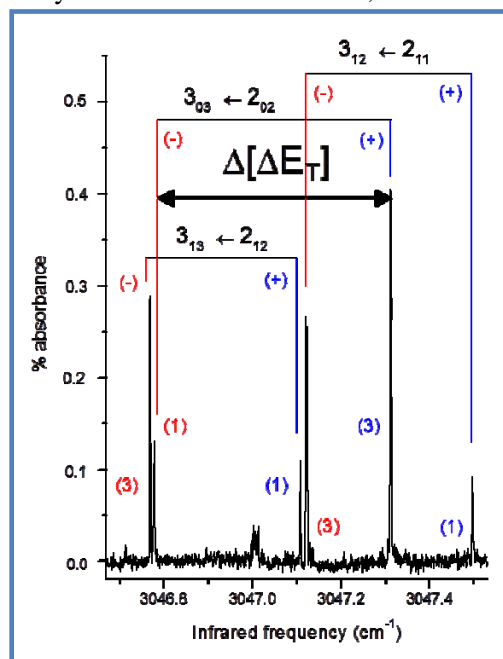
David. J. Nesbitt

Our research program involves combined experimental and theoretical study of transient chemical species relevant to fundamental combustion processes. The work specifically focuses on spectroscopy and unimolecular/bimolecular dynamics of highly reactive radical intermediates, combining i) high-resolution direct IR laser absorption methods at the quantum shot noise sensitivity limit, ii) high densities ( $10^{12}$ - $10^{14}$  #/cm<sup>3</sup>) of jet-cooled hydrocarbon radicals in slit supersonic discharge expansions, and iii) high-level *ab initio* potential surface and multidimensional quantum mechanics calculations. Key advantages of the slit discharge expansion are i) generation of high concentrations of transient species under typical combustion conditions, yet ii) rapid subsequent cooling of these reactive intermediates to  $T_{\text{rot}} \approx 15$  K in a multipass geometry ideal for sub-Doppler laser absorption spectroscopy and quantum shot-noise limited detection sensitivity. The unifying themes of this program have continued to be i) spectroscopic characterization of critical combustion intermediates, ii) elucidation of large-amplitude conformational dynamics, and iii) fundamental tests of *ab initio* combustion modeling efforts. Over the past year, our group has explored multiple jet-cooled transients via high-resolution IR laser spectroscopy, highlights of which will be discussed below.

### A. Hydroxymethyl Radical: Large Amplitude Quantum Tunneling Dynamics in CH<sub>2</sub>OH

Hydroxymethyl radical (CH<sub>2</sub>OH) is a highly reactive intermediate<sup>1</sup> that plays an important role in many fields, ranging from methanol combustion to atmospheric chemistry.<sup>2</sup> Hydroxymethyl is also thought to be important in the tropospheric removal of oxygenated biogenic volatile organic compounds and in turn is removed via reaction with O<sub>2</sub> to form formaldehyde and hydroperoxy radical.<sup>3</sup> The search for hydroxymethyl radicals in interstellar space is also of interest, since these species are key precursors to the formation of astrobiological molecules.<sup>4</sup> Interestingly, recent surveys have determined that interstellar grains coated primarily with water and methanol, demonstrate production of complex organic molecules with hydroxymethyl as a key radical intermediate.<sup>5</sup> Confirmation of such pathways will require observation of CH<sub>2</sub>OH mm-wave spectra, which have been challenging to obtain due to the complex spectral background from methanol under typical conditions. Indeed, stimulated by our high-resolution IR efforts, a mm-wave spectrum has been recently obtained,<sup>6</sup> which now provide precise COH torsional tunneling splittings and incentive for further high-resolution IR studies.

Over the past granting period, the sub-Doppler CH symmetric stretch ( $\nu_3$ ) infrared absorption spectrum of hydroxymethyl (CH<sub>2</sub>OH) radical has been observed and analyzed (Fig. 1), with the radical formed in a slit-jet supersonic discharge expansion ( $T_{\text{rot}} \approx 18$  K) via Cl abstraction of an H atom from methanol.<sup>7,8</sup> The high-sensitivity of the spectrometer and reduced spectral congestion in a jet-cooled expansion permits spectroscopic observation of transitions from levels split by large-amplitude COH torsional tunneling as well as spin-rotation. Nuclear spin statistics due to exchange of the two methyl H atoms aid in unambiguous rovibrational assignment of  $K_a = 0 \leftarrow 0$  and  $K_a = 1 \leftarrow 1$  a-type bands from each of the two tunneling states. The assigned transitions are least-squares fit to a Watson A-reduced asymmetric top Hamiltonian, yielding A, B and C constants for the  $\nu_3 = 0, 1$  states of both tunneling levels. Spin-





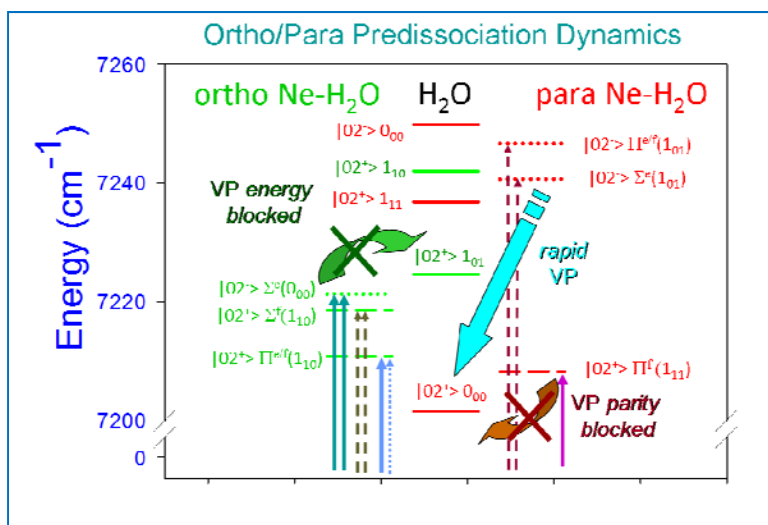
rotation fine structure splittings also permit analysis of spin-rotation coupling constants and changes upon vibrational excitation. In conjunction with recent mm-wave data,<sup>6</sup> the current IR results permit unambiguous assignment of *ortho/para* transitions *across* the tunneling gap, which therefore constitute first precision measurements for in situ detection outside the laboratory setting and for tunneling dynamics in the vibrationally excited  $\nu_3 = 1$  manifold.

## B. Spectroscopy and *Ab Initio* Rovibrational Dynamics of H<sub>2</sub>O Containing Clusters

Noncovalent interactions between molecules play a critical role in an extraordinary variety of physical and chemical phenomena. Though such binding energies are small with respect to room temperature  $kT$ , they nevertheless can be of major significance. Indeed, non-covalent interactions in species such as N<sub>2</sub>-H<sub>2</sub>O are thought to be responsible for transient dimer formation in colder regions of the upper Earth atmosphere, as well as directly influencing metastable structures in a variety of low-temperature noble-gas matrices, doped helium nanodroplets, and supersonic jets. Weak attractive forces also play a critical role in stabilizing pre-reactive complexes in early stages of a chemical reaction.<sup>9</sup> Such interactions have been speculated to control the solvation of non-polar hydrophobic molecules in water and thus the propensity to produce clathrates under high pressure conditions.<sup>10</sup> Insights into the potential energy surfaces associated with these interactions can be obtained via high-resolution spectroscopy of strong infrared chromophores such as H<sub>2</sub>O complexed with rare gas atoms, for which the "supermolecules" are bound non-covalently by combination of i) van der Waals attraction between two polarizable species and ii) dipole-induced dipole interaction between a permanent dipole and the polarizable species.

In particular, we have undertaken a triple-resonance IR-UV-UV study of Ne-H<sub>2</sub>O, a very weakly bound van der Waals structure in which the presence of shallow minima and low barriers in the potential energy surface allow for extreme large-amplitude motion effects.<sup>11</sup> Vibrationally state-selective spectroscopy and dynamics of weakly-bound Ne-H<sub>2</sub>O complexes ( $D_0 = 31.67 \text{ cm}^{-1}$  (*para*) and  $34.66 \text{ cm}^{-1}$  (*ortho*)) are reported, based on near

infrared excitation of van der Waals cluster bands correlating with  $\nu_{\text{OH}} = 2 \leftarrow 0$  overtone transitions ( $|02^{\pm}\rangle$  and  $|02^{+\pm}\rangle$ ) out of both the *ortho* ( $1_{01}$ ) and *para* ( $0_{00}$ ) internal-rotor states of the H<sub>2</sub>O moiety. Fully converged quantum theoretical calculations for nuclear motion on a high-level potential energy surface (CCSD(T)/VnZf12 ( $n=3,4$ ), corrected for BSSE and extrapolated to the CBS limit) have been employed to assign  $\Pi$ - $\Sigma$ ,  $\Sigma$ - $\Sigma$ , and  $\Sigma$ - $\Pi$  infrared bands in the spectra, where  $\Sigma$  or  $\Pi$  represent approximate projections of the body-fixed H<sub>2</sub>O angular momentum along the Ne-H<sub>2</sub>O internuclear axis. End-over-end tumbling of the Ne-H<sub>2</sub>O cluster is evident via rotational band contours observed for the *ortho* species, with band origins and rotational progressions in remarkable agreement with *ab initio* predictions. In addition, IR-UV pump-probe experimental capabilities have permitted real-time measurements of vibrational predissociation dynamics, which indicate facile intramolecular energy transfer from the H<sub>2</sub>O  $\nu_{\text{OH}} = 2$  overtone vibrations into the VdW dissociation coordinate on the  $\tau_{\text{prediss}} \approx 15\text{-}25 \text{ ns}$  timescale. Surprisingly, VMP spectra for the corresponding *para* Ne-H<sub>2</sub>O complexes are conspicuously absent, despite *ab initio* predictions of intensities with  $S/N > 20\text{-}40$ . Such behavior signals the presence of highly *ortho-para* selective predissociation dynamics in the upper state, for which we offer a simple mechanism based on *cluster mediated* intramolecular vibrational energy

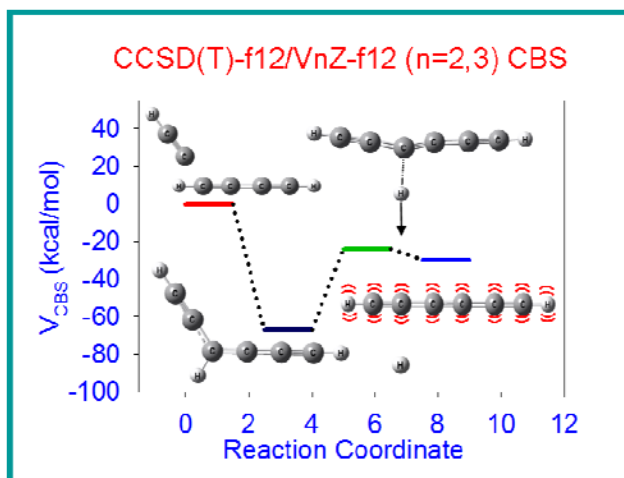


relaxation in the H<sub>2</sub>O subunit (i.e.,  $|02^{+/-}\rangle \rightarrow \{|01^{+/-}\rangle; \nu_2 = 2\}$ ), confirmed by *ab initio* predictions and nascent OH rotational (N), spin-orbit ( $\Pi_{1/2, 3/2}$ ) and lambda-doublet product distributions. Of particular dynamical interest, our spectral analysis reveals the presence of long-lived *para*  $\Pi^f(1_{11})$  states at energies *in excess* of the Ne + H<sub>2</sub>O (0<sub>00</sub>) dissociation limit, elucidating a novel mechanism for *eff parity-dependent* predissociation and metastability in Ne-H<sub>2</sub>O clusters. Finally, Boltzmann analysis of the rotational spectra reveal anomalously low jet temperatures ( $T_{rot} \approx 4(1)$  K), which we attribute to evaporative cooling of the weakly bound Ne-H<sub>2</sub>O clusters and which provides support for similar cooling dynamics playing a role in rare-gas-tagging studies.<sup>12</sup>

### C. Chemistry in Supersonic Jets: Polymer Growth via Ethynyl Radical Accretion

Diacetylene (H-C≡C-C≡CH) is the smallest member of the polyynyl family and represents an ubiquitous species in the combustion chemistry of unsaturated hydrocarbons and fuel-rich flames. What makes these linear polyynes so chemically interesting is that they form readily via addition with CCH ethynyl radical, e.g.,  $\text{HC}\equiv\text{CH} + \text{C}\equiv\text{C}\cdot\text{H} \rightarrow [\text{H}\cdot\text{C}\equiv\text{C}(\text{H})\text{-C}\equiv\text{C}\cdot\text{H}] \rightarrow \text{H}\cdot\text{C}\equiv\text{C}\text{-C}\equiv\text{C}\cdot\text{H} + \text{H}$ , where the subsequent regeneration of CCH to complete the chain-reaction can occur via H-atom abstraction, e.g.,  $\text{H} + \text{H}\cdot\text{C}\equiv\text{C}\text{-H} \rightarrow \text{H}_2 + \text{C}\equiv\text{C}\cdot\text{H}$  at sufficiently elevated combustion temperatures. It is worth noting that the intermediate H-C≡C(H)-C≡C-H species is not a high-energy transition state but rather a stable radical adduct,  $\approx 63$  kcal/mol *lower* in energy than HCCH + CCH reactants, with little or no barrier to insertion and therefore resulting in reaction rate constants near the gas-kinetic limit.<sup>13,14</sup> Furthermore, this process can continue by subsequent exothermic attack of CCH into one of the diacetylenic C≡C bonds, which then can in principle form even higher order polyynes such as triacetylene, tetraacetylene, etc. Indeed, such chain-reaction kinetics are extremely rapid under non-oxidizing flame conditions at normal pressures and temperatures, which makes diacetylene (as well as each of the successive polyynes) a key crucial intermediate in the formation chemistry of soot.<sup>15,16</sup> Furthermore, since exposure of these polyynes to solar VUV radiation yields highly reactive radical CCH fragments, this provides a photolysis mechanism for radical chain production of high molecular weight species, which indeed are proposed as key intermediates in formation of organic aerosols (tholines)<sup>17</sup> and polycyclic aromatic hydrocarbons (PAH).<sup>18</sup>

During the previous granting period, fundamental, bending ( $\nu_6, \nu_7, \nu_8, \nu_9$ ), and CC-stretch ( $\nu_2, \nu_3$ ) hot-band spectra in the antisymmetric CH stretch ( $\nu_4$ ) region near  $3330\text{ cm}^{-1}$  have been observed and analyzed for jet-cooled diacetylene (HC≡C-C≡CH) under sub-Doppler conditions, with parallel studies also performed for subsequent formation of triacetylene (HC≡C-C≡C-C≡CH).<sup>19,20</sup> The polyynyl is generated *in situ* in the throat of a pulsed supersonic slit expansion by discharge dissociation of acetylene to form ethynyl (C≡CH) + H, followed by radical attack (C≡CH + C≡C-H) to form HC≡C-C≡CH + H. The combination of i) sub-Doppler line widths and ii) absence of spectral congestion permit rotational structure and Coriolis interactions in the  $\nu_4$  CH stretch fundamental to be observed and analyzed with high precision. Of particular dynamical interest, the spectra reveal diacetylene formation in highly excited internal vibrational states. Specifically, multiple  $\Pi \leftarrow \Pi$  and  $\Delta \leftarrow \Delta$  hot bands built on the  $\nu_4$  CH stretch fundamental are observed, due to doubly degenerate bending vibrations [cis C≡C-H bend ( $\nu_6$ ), trans C-C≡C bend ( $\nu_7$ ), trans C≡C-H bend ( $\nu_8$ ) and cis C-C≡C bend ( $\nu_9$ )], as well as a  $\Sigma \leftarrow \Sigma$  band assigned to excitation of  $\nu_2$  or  $2\nu_3$  CC stretch. Boltzmann analysis yields populations consistent with universally cold rotations ( $T_{rot} \approx 15 \pm 5$  K) and *superthermal* vibrations ( $T_{vib} \approx 85\text{-}430$  K), the latter of which



is quite anomalous for collision densities in a slit jet expansion. To elucidate the physical mechanism for this excess vibrational excitation, high-level *ab initio* MOLPRO/CCSD(T) calculations have been pursued with explicitly correlated basis sets (VnZ-f12; n=2,3) and extrapolated to the complete basis set (CBS) limit.<sup>21</sup> The results suggest that the extensive hot-band structure observed arises from i) exothermic CCH + HCCH addition to yield a strongly bent HCCHCCH radical intermediate ( $\Delta H = -62.6$  kcal/mol), followed by ii) rapid fragmentation over a submerged transition state barrier ( $\Delta H = -18.9$  kcal/mol) to form vibrationally hot diacetylene + H products ( $\Delta H = -25.6$  kcal/mol), consistent with crossed molecular beam studies by Kaiser *et al.*<sup>14</sup> Finally, RRKM fragmentation rates for this complex are calculated, which exceed collision frequencies in the slit jet expansion and suggest near-unity quantum efficiency for diacetylene as well as triacetylene formation.<sup>19,20</sup>

- 1 B. Ruscic, J. E. Boggs, A. Burcat, A. G. Csaszar, J. Demaison, R. Janoschek, J. M. L. Martin, M. L. Morton, M. J. Rossi, J. F. Stanton, P. G. Szalay, P. R. Westmoreland, F. Zabel, and T. Berces, *J. Phys. Chem. Ref. Data* **34** (2), 573 (2005).
- 2 R. Atkinson and J. Arey, *Atmos. Environ.* **37**, S197 (2003).
- 3 S. Olivella, J. M. Bofill, and A. Sole, *Chem.-Eur. J.* **7** (15), 3377 (2001).
- 4 S. Maity, R. I. Kaiser, and B. M. Jones, *Phys. Chem. Chem. Phys.* **17** (5), 3081 (2015).
- 5 R. J. Shannon, M. A. Blitz, A. Goddard, and D. E. Heard, *Nature Chem.* **5** (9), 745 (2013).
- 6 C. Bermudez, S. Bailleux, and J. Cernicharo, *Astron. Astrophys.* (in press).
- 7 M. A. Roberts, E. N. Sharp-Williams, and D. J. Nesbitt, *J. Phys. Chem. A* **117** (32), 7042 (2013).
- 8 M. D. Schuder, F. Wang, C.-H. Chang, and D. J. Nesbitt, *J. Chem. Phys.* (in press).
- 9 V. Vaida, *J. Chem. Phys.* **135** (2) (2011).
- 10 Y. A. Dyadin, E. G. Larionov, A. Y. Manakov, F. V. Zhurko, E. Y. Aladko, T. V. Mikina, and V. Y. Komarov, *Mendeleev Comm.* (5), 209 (1999).
- 11 M. P. Ziemkiewicz, C. Pluetzer, M. Wojcik, J. Loreau, A. v. d. Avoird, and D. J. Nesbitt, *J. Chem. Phys.* (in press).
- 12 C. J. Johnson, A. B. Wolk, J. A. Fournier, E. N. Sullivan, G. H. Weddle, and M. A. Johnson, *J. Chem. Phys.* **140** (22), 221101 (2014).
- 13 D. L. Baulch, C. J. Cobos, R. A. Cox, C. Esser, P. Frank, T. Just, J. A. Kerr, M. J. Pilling, J. Troe, R. W. Walker, and J. Warnatz, *J. Phys. Chem. Ref. Data* **21** (3), 411 (1992).
- 14 R. I. Kaiser, F. Stahl, P. V. Schleyer, and H. F. Schaefer, *Phys. Chem. Chem. Phys.* **4** (13), 2950 (2002).
- 15 M. Frenklach, *Phys. Chem. Chem. Phys.* **4** (11), 2028 (2002).
- 16 A. Jamal and A. M. Mebel, *J. Phys. Chem. A* **115** (11), 2196 (2011).
- 17 J. H. Waite, D. T. Young, T. E. Cravens, A. J. Coates, F. J. Crary, B. Magee, and J. Westlake, *Science* **316** (5826), 870 (2007).
- 18 F. Shindo, Y. Bénilan, P. Chaquin, J. C. Guillemin, A. Jolly, and F. Raulin, *J. Mol. Spec.* **210** (2), 191 (2001).
- 19 C.-H. Chang and D. J. Nesbitt, *J. Phys. Chem. A* **119** (28), 7940 (2015).
- 20 C. H. Chang, J. Agarwal, W. D. Allen, and D. J. Nesbitt, *J. Chem. Phys.* **144** (7) (2016).
- 21 K. A. Peterson, R. A. Kendall, and T. H. Dunning, *J. Chem. Phys.* **99** (3), 1930 (1993).

# Large Eddy Simulation of Reacting Flow Physics

Joseph C. Oefelein

Combustion Research Facility, Sandia National Laboratories

Livermore, CA 94551-0969

oefelei@sandia.gov

## Program Scope

Application of the Large Eddy Simulation (LES) technique within the Chemical Sciences program is aimed at establishing a series high-fidelity computational benchmarks that identically match the geometry and operating conditions of selected experimental target flames. The goal is to provide a one-to-one correspondence between simulations and experiments at conditions unattainable using Direct Numerical Simulation (DNS) by performing a series of high-resolution calculations using first-principles sub-models that progressively incorporate the fully-coupled dynamic behavior of reacting flows with detailed thermodynamics, transport, chemistry, and realistic spectra of turbulence. Results provide a strong scientific link between theory, experiments, and relevant scientific questions by providing fundamental information that cannot be measured. The insights gained provide a basic science foundation for the development of predictive models required to understand and design advanced propulsion, and power systems.

## Recent Progress

A major goal in the development of closure strategies for turbulent combustion is to use first principles models designed specifically for LES (i.e., using all the information available from the LES formalism in contrast to conventional RANS-based combustion closures that make use of relatively limited information). Recently, for example, a class of reconstruction models has been proposed [1, 2] that combines the purely mathematical approximate deconvolution procedure [3, 4] with physical information from an assumed scalar spectrum to match specific scalar moments. Using this method, a surrogate to the exact scalar field can be estimated such that filtered moments match to a specified order. In principle, the surrogate field can be used to calculate the subfilter contribution of any related nonlinear function. In practice, however, the extent of the nonlinearity limits the accuracy and it has been shown that the method cannot be used reliably to close the filtered chemical source terms directly. It can be used, on the other hand, to obtain highly accurate representations of polynomial nonlinearities such as the subfilter variances and covariances if appropriate levels of resolution are applied. These are precisely the input required to generate subfilter fluctuations stochastically. Given these findings, an extension to the reconstruction approach has been derived by coupling it to a stochastic technique. The matrix of subfilter variances and covariances are obtained via reconstruction, then used as input to a Cholesky decomposition to obtain a correlated approximation of the subfilter velocity and scalar fluctuations in time. The modeled instantaneous fields (i.e.,  $\phi_i = \tilde{\phi}_i + \phi_i''$ , where  $\tilde{\phi}_i$  is the Favre averaged resolved-scale contribution of an arbitrary scalar and  $\phi_i''$  the correlated subfilter fluctuation) are used to evaluate the filtered chemical source terms directly. The filtered source terms are closed by selecting an appropriate chemical kinetics mechanism (e.g., detailed or skeletal), and the model coefficients are evaluated locally in a manner consistent with the dynamic modeling procedure. The only adjustable parameters are the filter-size, time-step, and boundary conditions. In the limit as the filter-size and time-step approach the smallest relevant scales, subfilter contributions approach zero and the solution converges to a DNS. A novel feature of this approach is that it naturally accounts for multiscale mixing.

A representative result using this model is given in Fig. 1, which shows a photograph of the Sandia high-pressure combustion vessel (top left) with representative shadowgraphs highlighting the flow structure as autoignition occurs (bottom left). The calculations were performed using the RAPTOR code framework. Unlike conventional LES codes, RAPTOR is a DNS solver that has been optimized to meet the strict algorithmic requirements imposed by the LES formalism. The theoretical framework solves the fully-coupled conservation equations of mass, momentum, total-energy, and species for a chemically reacting flow. It is designed to handle high Reynolds number, high-pressure, real-gas and/or liquid conditions over a wide Mach operating range using non-dissipative, discretely conservative,

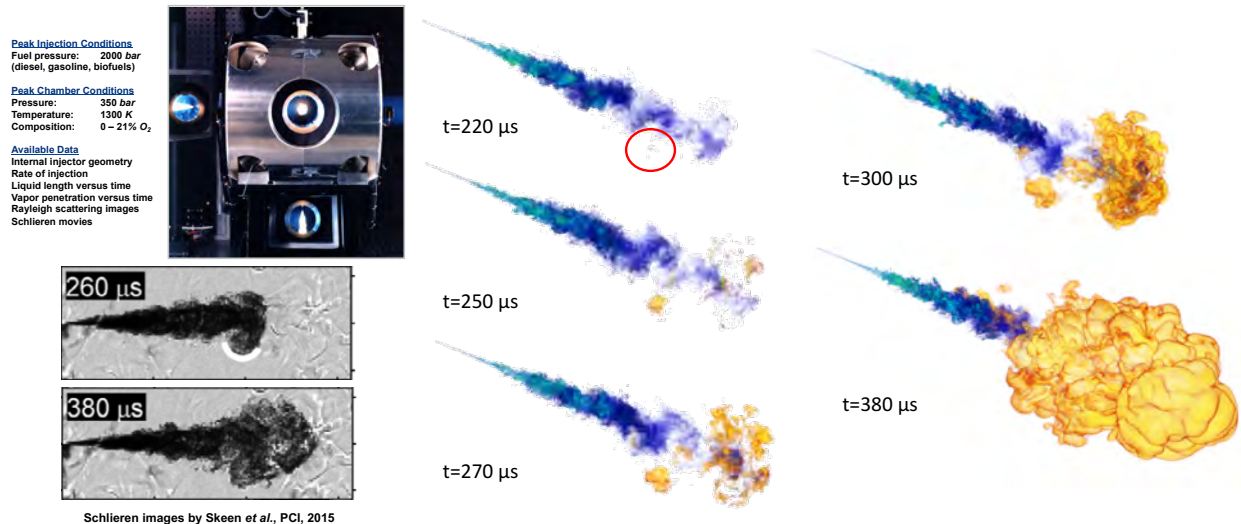


**Figure 1.** Photograph of the Sandia high-pressure combustion vessel (top left) with representative shadowgraphs highlighting the flow structure as autoignition occurs (bottom left). On the right is a representative result from LES showing the corresponding transient ignition sequence at conditions identical to the experiment. The jet Reynolds number for this case is 120,000.

staggered, finite-volume differencing. This eliminates numerical contamination of the subfilter models due to artificial dissipation and provides discrete conservation of mass, momentum, energy, and species, which is required for high quality LES. Details related to the baseline formulation and subfilter models are given by Oefelein [5]. Representative results and case studies are given by Oefelein *et al.* [6–14].

On the right of Fig. 1 is a result from LES showing the corresponding transient ignition sequence at conditions identical to the experiment. Note that the jet Reynolds number for this case is 120,000. A three-dimensional rendering of a liquid n-dodecane fuel jet is shown, which is injected at a temperature of 363 K into the high-pressure chamber at 60 bar, 900 K, with 15-percent oxygen. Scalar mixing is represented by a blue volume rendering based on the fuel mixture fraction. The development of ignition kernels and resultant flame structure are tracked by a yellow volume rendering based on temperature. The locations of the first flame kernels are in good agreement with the experimental shadowgraphs. The first kernels appear initially in the downstream region of the jet where large vortical structures carry fuel away from the high-speed jet. In those regions, turbulence and hot ambient conditions enhance the mixing of the fuel with the ambient. Subsequently, other locations reach a burning state by either autoignition or propagation mechanisms. This case exemplifies the complementary synergy our LES approach provides between programs within the DOE. Development of the combustion closure described above and real fluid thermodynamics and transport for complex hydrocarbon mixtures in high-pressure systems were enabled through our research under BES. Application of these constitutive models for advanced engine combustion research was performed under the DOE Vehicle Technologies program. The net result are one-of-a-kind simulations that capture complex dynamics that cannot be characterized experimentally or with DNS. The spatial and temporal fidelity provides access to the full broadband three-dimensional characteristics of injection, ignition, and combustion at conditions that 1) identically match the experiment, and 2) are directly relevant to practical systems. Details can be found in Refs. [10, 12, 15].

## Future Plans

We will continue to apply the approach and framework described above with emphasis on three interrelated areas of research: 1) Maintain close coordination between LES and experimental reacting flow research with emphasis on the collaborative activities of the TNF Workshop. 2) Maintain a significant effort in the development of quality assessment and uncertainty quantification (UQ) techniques for LES aimed at understanding and controlling the myriad of errors that complicate the development of predictive models. 3) Continue to develop advanced models and simulation techniques aimed at accurate prediction of flame behavior (and related flow physics) across a broad range of combustion regimes and fuels. Tasks related to research area 1 will be pursued through close collaborations with Barlow and Frank *et al.* following the proposed series of experiments outlined in their respective abstracts. Tasks related to research area 2 will be pursued through close collaborations with Najm *et al.* (e.g., see Najm’s abstract). Tasks will continue to focus on advanced model development in a manner that effectively bridges the gap between the idealized jet flame processes studied under this program and application relevant processes exhibited at the device scale.

## Literature Cited

- [1] C. Pantano and S. Sarkar. A subgrid model for nonlinear functions of a scalar. *Physics of Fluids*, 13(12): 3803–3819, 2001.
- [2] J. P. Mellado, S. Sarkar, and C. Pantano. Reconstruction subgrid models for non-premixed combustion. *Physics of Fluids*, 15(11):3280–3307, 2003.
- [3] B. J. Geurts. Inverse modeling for large eddy simulation. *Physics of Fluids*, 9(12):3585–3587, 1997.
- [4] S. Stolz and N. A. Adams. An approximate deconvolution procedure for large eddy simulation. *Physics of Fluids*, 11(7):1699–1701, 1999.
- [5] J. C. Oefelein. Large eddy simulation of turbulent combustion processes in propulsion and power systems. *Progress in Aerospace Sciences*, 42(1):2–37, 2006.
- [6] J. H. Frank, S. A. Kaiser, and J. C. Oefelein. Analysis of scalar mixing dynamics in LES using high-resolution imaging of laser Rayleigh scattering in turbulent non-reacting jets and non-premixed jet flames. *Proceedings of the Combustion Institute*, 33:1373–1381, 2011.
- [7] A. M. Kempf, B. J. Geurts, and J. C. Oefelein. Error analysis of large eddy simulation of the turbulent non-premixed Sydney bluff-body flame. *Combustion and Flame*, 158:2408–2419, 2011.
- [8] G. Lacaze and J. C. Oefelein. A non-premixed combustion model based on flame structure analysis at supercritical pressures. *Combustion and Flame*, 159:2087–2103, 2012.
- [9] J. C. Oefelein, R. N. Dahms, and G. Lacaze. Detailed modeling and simulation of high-pressure fuel injection processes in diesel engines. *SAE International Journal of Engines*, 5(3):1–10, 2012.
- [10] J. Oefelein, G. Lacaze, R. Dahms, A. Ruiz, and A. Misdariis. Effects of real-fluid thermodynamics on high-pressure fuel injection processes. *SAE International Journal of Engines*, 7(3):1–12, 2014.
- [11] M. Khalil, G. Lacaze, J. C. Oefelein, and H. N. Najm. Uncertainty quantification in LES of a turbulent bluff-body stabilized flame. *Proceedings of the Combustion Institute*, 35:1147–1156, 2015.
- [12] G. Lacaze, A. Misdariis, A. Ruiz, and J. C. Oefelein. Analysis of high-pressure diesel fuel injection processes using LES with real-fluid thermodynamics and transport. *Proceedings of the Combustion Institute*, 35: 1603–1611, 2015.
- [13] A. M. Ruiz, G. Lacaze, and J. C. Oefelein. Flow topologies and turbulence scales in a jet-in-cross-flow. *Physics of Fluids*, 27(045101):1–35, 2015.
- [14] A. M. Ruiz, G. Lacaze, J. C. Oefelein, R. Mari, B. Cuenot, L. Selle, and T. Poinsot. A numerical benchmark for high-reynolds number supercritical flows with large density gradients. *AIAA Journal*, 54(5):1445–1460, 2016.
- [15] L. Hakim, G. Lacaze, and J. C. Oefelein. Large eddy simulation of autoignition transients in a model diesel injector configuration. *SAE International Journal of Fuels and Lubricants*, 9(1):165–176, 2016.
- [16] X. Huan, C. Safta, K. Sargsyan, M. S. Eldred, Z. P. Vane, G. Lacaze, J. C. Oefelein, and H. N. Najm. Global sensitivity analysis and quantification of model error in scramjet computations. *AIAA Journal*, 2017. Submitted.
- [17] A. M. Ruiz, G. Lacaze, B. Corriton, J. H. Frank, and J. C. Oefelein. Nozzle flow dynamics and boundary conditions in the Yale-Sandia turbulent opposed jet flame configuration. *Combustion and Flame*, 2017. Submitted.
- [18] L. Hakim, G. Lacaze, M. Khalil, K. Sargsyan, H. Najm, and J. Oefelein. Probabilistic parameter estimation of a 2-step chemical kinetics model for n-dodecane jet autoignition. *Combustion Theory and Modelling*, 2017. Submitted.
- [19] F. Doisneau, M. Arienti, and J. C. Oefelein. A semi-Lagrangian transport method for kinetic problems with application from dense to dilute polydisperse reacting spray flows. *Journal of Computational Physics*, 2017. In press.
- [20] F. Doisneau, M. Arienti, and J. C. Oefelein. On multi-fluid models for spray-resolved LES of reacting jets. *Proceedings of the Combustion Institute*, 36:2441–2450, 2017.
- [21] J. Ling, A. Ruiz, G. Lacaze, and J. C. Oefelein. Uncertainty analysis and data-driven model advances for a jet-in-crossflow. *Journal of Turbomachinery*, 139(021008):1–9, 2017.
- [22] J. C. Oefelein. Dynamics of gas-liquid interfaces in high-pressure systems. *24th International Congress of Theoretical and Applied Mechanics, Invited Topical Lecture and Paper*, August 21-26 2016. Montreal, Canada.
- [23] R. N. Dahms and J. C. Oefelein. The significance of drop non-sphericity in sprays. *International Journal of Multiphase Flow*, 86:67–85, 2016.
- [24] L. Hakim, G. Lacaze, M. Khalil, H. N. Najm, and J. C. Oefelein. Modeling auto-ignition transients in reacting diesel jets. *Journal of Engineering for Gas Turbines and Power*, 138:112806 1–8, 2016.

- [25] R. N. Dahms and J. C. Oefelein. Atomization and dense-fluid breakup regimes in liquid rocket engines. *Journal of Propulsion and Power*, 31(5):1221–1231, 2015.
- [26] R. N. Dahms and J. C. Oefelein. Liquid jet breakup regimes at supercritical pressures. *Combustion and Flame*, 162:3648–3657, 2015.
- [27] R. N. Dahms and J. C. Oefelein. Non-equilibrium gas-liquid interface dynamics in high-pressure liquid injection systems. *Proceedings of the Combustion Institute*, 35:1587–1594, 2015.

### **BES Sponsored Publications (2015–Present)**

- X. Huan, C. Safta, K. Sargsyan, M. S. Eldred, Z. P. Vane, G. Lacaze, J. C. Oefelein, and H. N. Najm. Global sensitivity analysis and quantification of model error in scramjet computations. *AIAA Journal*, 2017. Submitted.
- A. M. Ruiz, G. Lacaze, B. Corriton, J. H. Frank, and J. C. Oefelein. Nozzle flow dynamics and boundary conditions in the Yale-Sandia turbulent opposed jet flame configuration. *Combustion and Flame*, 2017. Submitted.
- L. Hakim, G. Lacaze, M. Khalil, K. Sargsyan, H. Najm, and J. Oefelein. Probabilistic parameter estimation of a 2-step chemical kinetics model for n-dodecane jet autoignition. *Combustion Theory and Modelling*, 2017. Submitted.
- F. Doisneau, M. Arienti, and J. C. Oefelein. A semi-Lagrangian transport method for kinetic problems with application from dense to dilute polydisperse reacting spray flows. *Journal of Computational Physics*, 2017. In press.
- F. Doisneau, M. Arienti, and J. C. Oefelein. On multi-fluid models for spray-resolved LES of reacting jets. *Proceedings of the Combustion Institute*, 36:2441–2450, 2017.
- J. Ling, A. Ruiz, G. Lacaze, and J. C. Oefelein. Uncertainty analysis and data-driven model advances for a jet-in-crossflow. *Journal of Turbomachinery*, 139(021008):1–9, 2017.
- J. C. Oefelein. Dynamics of gas-liquid interfaces in high-pressure systems. *24th International Congress of Theoretical and Applied Mechanics, Invited Topical Lecture and Paper*, August 21-26 2016. Montreal, Canada.
- R. N. Dahms and J. C. Oefelein. The significance of drop non-sphericity in sprays. *International Journal of Multiphase Flow*, 86:67–85, 2016.
- L. Hakim, G. Lacaze, M. Khalil, H. N. Najm, and J. C. Oefelein. Modeling auto-ignition transients in reacting diesel jets. *Journal of Engineering for Gas Turbines and Power*, 138:112806 1–8, 2016.
- A. M. Ruiz, G. Lacaze, J. C. Oefelein, R. Mari, B. Cuenot, L. Selle, and T. Poinot. A numerical benchmark for high-reynolds number supercritical flows with large density gradients. *AIAA Journal*, 54(5):1445–1460, 2016.
- L. Hakim, G. Lacaze, and J. C. Oefelein. Large eddy simulation of autoignition transients in a model diesel injector configuration. *SAE International Journal of Fuels and Lubricants*, 9(1):165–176, 2016.
- R. N. Dahms and J. C. Oefelein. Atomization and dense-fluid breakup regimes in liquid rocket engines. *Journal of Propulsion and Power*, 31(5):1221–1231, 2015.
- R. N. Dahms and J. C. Oefelein. Liquid jet breakup regimes at supercritical pressures. *Combustion and Flame*, 162:3648–3657, 2015.
- A. M. Ruiz, G. Lacaze, and J. C. Oefelein. Flow topologies and turbulence scales in a jet-in-cross-flow. *Physics of Fluids*, 27(045101):1–35, 2015.
- G. Lacaze, A. Misdariis, A. Ruiz, and J. C. Oefelein. Analysis of high-pressure diesel fuel injection processes using LES with real-fluid thermodynamics and transport. *Proceedings of the Combustion Institute*, 35:1603–1611, 2015.
- M. Khalil, G. Lacaze, J. C. Oefelein, and H. N. Najm. Uncertainty quantification in LES of a turbulent bluff-body stabilized flame. *Proceedings of the Combustion Institute*, 35:1147–1156, 2015.
- R. N. Dahms and J. C. Oefelein. Non-equilibrium gas-liquid interface dynamics in high-pressure liquid injection systems. *Proceedings of the Combustion Institute*, 35:1587–1594, 2015.

## KINETICS, DYNAMICS, AND SPECTROSCOPY OF GAS PHASE CHEMISTRY

David L. Osborn

*Combustion Research Facility, Mail Stop 9055, Sandia National Laboratories*

*Livermore, CA 94551-0969*

[dlosbor@sandia.gov](mailto:dlosbor@sandia.gov)

### PROGRAM SCOPE

The goal of this program is to elucidate mechanisms of elementary chemical reactions through the use of multiplexed spectroscopy and mass spectrometry. We developed a technique known as time-resolved multiplexed photoionization mass spectrometry (MPIMS), which is used to sensitively and selectively probe chemical reactions and reaction intermediates. This work is in collaboration with Sandia chemists Craig Taatjes, Leonid Sheps, and Judit Zádor, and a large group of scientists from other institutions in the US and abroad. The Sandia-designed MPIMS instrument utilizes tunable vacuum ultraviolet light from the Advanced Light Source (ALS) synchrotron at Lawrence Berkeley National Laboratory (LBNL) for sensitive, isomer-specific ionization of reactant and product molecules sampled from chemical reactions.

As a complementary approach, we also use Fourier transform spectroscopy (FTS), in both its continuous scanning and step-scan variants, to probe multiple species in chemical reactions. We have begun a new push to move photoelectron photoion coincidence spectroscopy past its roots in thermochemistry and ultrafast dynamics. Our innovations promise to make PEPICO a powerful tool for time-resolved probing of gas phase chemical reactions with superior performance in many areas compared to MPIMS.

### RECENT PROGRESS

#### Isomer-resolved mass spectrometry

The multiplexed chemical kinetics photoionization mass spectrometer operates both at Sandia National Laboratories (using various discharge lamps to create vacuum ultraviolet radiation), and at the Chemical Dynamics Beamline of the ALS synchrotron of LBNL. The chemical reactor is based on the Gutman design, which allows the study of photodissociation and bimolecular reactions at pressures of 1 – 40 Torr and temperatures of 250 – 1000 K.

During the past 3-year period, we have applied this apparatus to a broad array of chemical problems, including the influence of hetero atoms on low temperature combustion chemistry, astrophysically relevant reactions of C(<sup>3</sup>P) atoms with hydrocarbons, effects of resonance stabilization on reactivity, molecular weight growth chemistry, new reactions of Criegee Intermediates impacting Earth's troposphere, and reactions on multiple potential energy surfaces.

#### Photo-tautomerization of acetaldehyde to vinyl alcohol

The photochemistry of aldehydes and ketones has been extensively studied over the past 100 years. Simultaneously, the less stable enol tautomers of carbonyl compounds are well known in organic chemistry for their role as reactive intermediates. It is therefore somewhat surprising that there has been no consideration of whether electronic excitation of carbonyl molecules could cause photo-tautomerization that creates enols. We showed in 2013 that  $S_1 \leftarrow S_0$  excitation of neat acetaldehyde ( $\text{CH}_3\text{CHO}$ ) at low pressure generates vinyl alcohol (VA,  $\text{H}_2\text{C}=\text{CHOH}$ ). We proposed a model for pressure dependence of VA yield that predicts zero yield at both infinite and zero pressure, with finite yields at intermediate pressures. In this review period we have measured the photo-tautomerization yield in a bath gas of  $\text{N}_2$  at up to 1



atm pressure, from  $\lambda = 300 - 330$  nm. The observed pressure and wavelength dependence of VA yield is a sensitive probe of both coupling between singlet and triplet electronic states, and collisional energy transfer dynamics. In addition to the fundamental photochemical knowledge gained, the observation that photo-tautomerization is relevant at atmospheric pressure provides evidence that it contributes organic acid sources to Earth's atmosphere. In the case of acetaldehyde, there is evidence that the OH + VA reaction creates formic acid, a critical molecule whose globally averaged concentration is 2 -3 times higher than predicted by atmospheric models. This work is submitted for publication.

### **Spectroscopy of larger enols**

Of all the enols, the only known gas phase infrared spectrum in the literature is of the simplest enol, vinyl alcohol (VA). We recently completed a project to measure gas phase spectra of the 3-carbon enols, 1-propenol and 2-propenol. In doing so, we learned that a portion of the VA spectrum had been mis-assigned. VA has both *syn*- and *anti*- conformers, with the OH group pointing towards or away from the C=C bond, respectively. The literature infrared spectrum had been assigned to the *syn*- form. By comparison with anharmonic calculations of the spectrum, we have reassigned the vibrational band at  $1,260\text{ cm}^{-1}$  to the  $\nu_8$  mode of *anti*-VA. In this project, we create enols by the Norrish Type II dissociation pathway of aldehydes and ketones. In the larger 1-propenol molecule, *cis*- and *trans*- forms exist in addition to the *syn*- and *anti*- conformers. We have identified bands from all four resulting isomers, and extract a non-equilibrium experimental *cis:trans* ratio of 1:9, implying that the ratio is determined by the dissociation dynamics of the NTII process rather than by thermochemistry. In addition to these fundamental discoveries in the mechanism of NTII photodissociation, and the molecular structure of larger enols, this work provides benchmark infrared spectra with absolute cross sections for the future identification of 3-carbon enols in the laboratory and atmosphere. This work is submitted for publication.

### **Following multi-well chemical reactions with PEPICO (Photoelectron Photoion Coincidence Spectroscopy)**

We and others have made great use of photoionization spectroscopy as a tool for quantitative chemical analysis in complex chemical environments such as flames and time-evolving chemical reactions. The technique provides an efficient method to sort a chemical mixture first by mass-to-charge ( $m/z$ ) ratio, and further by ionization energy and spectral shape at each  $m/z$  ratio for isomer identification. Photoelectron spectroscopy would provide an improved spectral fingerprint, but for analysis of a time-varying mixture of neutral molecules, we must use photoelectron photoion coincidence, pioneered by Tom Baer in this program, to collect such spectra. We recently published both the concept and demonstrated the practice of a new technique to eliminate almost all false coincidences from PEPICO experiments (see pub. 11). This breakthrough increases the dynamic range of PEPICO from  $\sim 10^3$  to  $10^5$  or better, a crucial goal in enabling its use for the study of multi-channel chemical reactions in the gas phase.

In collaboration with Drs. Andras Bodi and Patrick Hemberger of the Swiss Light Source, and Prof. Bálint Sztáray of the University of the Pacific, we have built and tested a new prototype time-resolved PEPICO spectrometer that features a unique ion/electron optics design. This design provides Wiley-McLaren space focusing of cations, which provides good mass resolution, while simultaneously enabling independent velocity map imaging of both electrons and cations. The key to this gridless design is a larger number of closely spaced plates, creating a linear, low electric field surrounding the ionization point, with steeper, curved fields on both

the electron and cation side that can be independently adjusted for optimal velocity map focusing. We have tested this apparatus with neutral samples from either supersonic molecular beam expansion, or from a low-pressure quartz reactor tube similar to what we use in the MPIMS apparatus. The prototype spectrometer enables one to obtain threshold photoelectron spectra, slow photoelectron spectra, and photoionization spectra simultaneously. In addition, a scanning source of vacuum ultraviolet photons is not required, because photoelectron spectra can be obtained from reconstruction of the electron velocity map image. This research is submitted for publication.

### Future Plans

Building on the advances we designed and tested in the prototype PEPICO spectrometer described above, in the next review period we will design and build the new CRF-PEPICO spectrometer for operation at Sandia and the Advanced Light Source. It will enable better molecular fingerprints to help resolve chemical reaction mechanisms that are beyond our capabilities at present. Among chemistry goals, we will pursue the investigation of how non-thermal reactant internal energy distributions affect chemical reaction mechanisms and outcomes. We will also attempt to synthesize precursors for several additional hydroperoxyalkyl isomers (QOOH), whose fundamental reactivity is still not sufficiently understood both in a fundamental and practical sense.

### BES-sponsored publications, 2015 – present

- 1) CRF-PEPICO: double velocity map imaging photoelectron photoion coincidence spectroscopy for reaction kinetics studies, B. Sztaray, K. Voronova, K. Torma, K. Covert, A. Bodi, P. Hemberger, T. Gerber, and D. L. Osborn, *J. Chem. Phys.*, submitted (2017).
- 2) Infra-red spectra of gas-phase 1- and 2-propenol isomers, M. F. Shaw, D. L. Osborn, M. J. T. Jordan, and S. H. Kable, *J. Phys. Chem. A*, submitted (2017).
- 3) Photo-tautomerization of acetaldehyde is a significant photochemical source of organic acids in the troposphere, M. Shaw, B. Sztaray, L. K. Whalley, D. Heard, M. J. T. Jordan, D. L. Osborn, and S. H. Kable, *Nat. Chem.*, submitted (2017).
- 4) Influence of oxygenation in cyclic hydrocarbons on chain-termination reactions from  $R + O_2$ : tetrahydropyran and cyclohexane, B. Rotavera, J. D. Savee, I. O. Antonov, R. L. Caravan, L. Sheps, D. L. Osborn, J. Zador, and C. A. Taatjes, *Proc. Combust. Inst.* **36**, 597 (2017).
- 5) Reactions of atomic carbon with butene isomers: implications for molecular growth in carbon-rich environments, J. Bourgalais, M. Spencer, D. L. Osborn, F. Goulay, S. D. Le Picard, *J. Phys. Chem. A* **120**, 9138 (2016).
- 6) Direct measurements of unimolecular and bimolecular reaction kinetics of the Criegee intermediate  $(CH_3)_2COO$ , R. Chhantyal-Pun, O. Welz, J. D. Savee, A. J. Eskola, E. P. F. Lee, L. Blacker, H. Hill, M. Ashcroft, M. A. Khan, G. Lloyd-Jones, L. Evans, B. Rotavera, H. Huang, D. L. Osborn, D. Mok, J. M. Dyke, D. E. Shallcross, C. Percival, A. J. Orr-Ewing, and C. A. Taatjes, *J. Phys. Chem. A* **121**, 4 (2016).
- 7) Hydroxyacetone production from  $C_3$  Criegee intermediates, C. A. Taatjes, F. Liu, B. Rotavera, M. Kumar, R. L. Caravan, D. L. Osborn, W. H. Thompson, M. I. Lester, *J. Phys. Chem. A* **121**, 16 (2016).
- 8) Resonance stabilization effects on ketone autoxidation: isomer-specific cyclic ether and ketohydroperoxide formation in the low-temperature (400 – 625 K) oxidation of diethyl ketone, A. M. Scheer, A. J. Eskola, D. L. Osborn, L. Sheps, C. A. Taatjes, *J. Phys. Chem. A* **120**, 8625 (2016).
- 9) Laser-driven hydrothermal process studied with excimer laser pulses, R. Mariella Jr., A. Rubenchik, E. Fong, M. Norton, W. Hollingsworth, J. Clarkson, H. Johnsen, and D. L. Osborn, *J. Appl. Phys.* (2016), *submitted*.
- 10) Reaction mechanisms on multi-well potential energy surfaces in combustion (and atmospheric) chemistry, D. L. Osborn, *Ann. Rev. Phys. Chem.* **68**, DOI: 10.1146/annurev-physchem-040215-112151 (2016).
- 11) Breaking through the false coincidence barrier in electron-ion coincidence experiments, D. L. Osborn, C. C. Hayden, P. Hemberger, A. Bodi, K. Voronova, and B. Sztaray, *J. Chem. Phys.* **145**, 164202 (2016).

- 12) Pressure-dependent competition among reaction pathways from first- and second-O<sub>2</sub> additions in the low-temperature oxidation of tetrahydrofuran, I. O. Antonov, J. Zador, B. Rotavera, E. Papajak, D. L. Osborn, C. A. Taatjes, and L. Sheps, *J. Phys. Chem. A* **120**, 6582 (2016).
- 13) Formation and stability of gas-phase o-benzoquinone from oxidation of orth-hydroxyphenyl: a combined neutral and distonic radical study, M. B. Prendergast, B. B. Kirk, J. D. Savee, D. L. Osborn, C. A. Taatjes, K. S. Masters, S. J. Blanksby, G. da Silva, A. J. Tretiff, *Phys. Chem. Chem. Phys.* **18**, 4320 (2016).
- 14) Low temperature chlorine-initiated oxidation of small-chain methyl esters: quantification of chain-terminating HO<sub>2</sub>-elimination channels, G. Muller, A. Scheer, D. L. Osborn, C. A. Taatjes, and G. Meloni, *J. Phys. Chem. A* DOI: 10.1021/acs.jpca.6b00148 (2016)
- 15) Photoelectron wave function in photoionization: plane wave or coulomb wave?, S. Gozem, A. O. Gunina, T. Ichino, D. L. Osborn, J. F. Stanton, and A. I. Krylov, *J. Phys. Chem. Lett.* **6**, 4532 (2015)
- 16) The C(<sup>3</sup>P) + NH<sub>3</sub> reaction in interstellar chemistry. I. Investigation of the product formation channels, J. Bourgalais, M. Capron, R.K.A. Kailasanathan, D. L. Osborn, K. M. Hickson, J. C. Loison, V. Wakelam, F. Goulay, and S. D. Le Picard, *Astrophys. J.*, **812**, 106 (2015).
- 17) Flow tube studies of the C(<sup>3</sup>P) reactions with ethylene and propylene, M. Capron, J. Bourgalais, R.K.A. Kailasanathan, D. L. Osborn, S. D. Le Picard, and F. Goulay, *Phys. Chem. Chem. Phys.* **17**, 23833 (2015).
- 18) Molecular weight growth in Titan's atmosphere: branching pathways for the reaction of 1-propynyl radical (H<sub>3</sub>CC≡C•) with small alkenes and alkynes, B. B. Kirk, J. D. Savee, A. J. Trevitt, D. L. Osborn, and K. R. Wilson, *Phys. Chem. Chem. Phys.* **17**, 20754 (2015).
- 19) Time- and Isomer-Resolved Measurements of Sequential Addition of Acetylene to the Propargyl Radical, J. D. Savee, T. M. Selby, O. Welz, C. A. Taatjes, and D. L. Osborn, *J. Phys. Chem. Lett.* **6**, 4153 (2015).
- 20) Multiscale Informatics for Low-Temperature Propane Oxidation: Further Complexities in Studies of Complex Reactions, M. P. Burke, C. F. Goldsmith, S. J. Klippenstein, O. Welz, H. Huang, I. O. Antonov, J. D. Savee, D. L. Osborn, J. Zador, C. A. Taatjes, and L. Sheps, *J. Phys. Chem. A* **119**, 7095 (2015).
- 21) New insights into low-temperature oxidation of propane from synchrotron photoionization mass spectrometry and multiscale informatics modeling, O. Welz, M. P. Burke, I. O. Antonov, C. F. Goldsmith, J. D. Savee, D. L. Osborn, C. A. Taatjes, S. J. Klippenstein, and L. Sheps, *J. Phys. Chem. A* **119**, 7116 (2015).
- 22) The physical chemistry of Criegee intermediates in the gas phase, D. L. Osborn and C. A. Taatjes, *Int. Rev. Phys. Chem.* **34**, 309 (2015).
- 23) Multiplexed photoionization mass spectrometry investigation of the O(<sup>3</sup>P) + propyne reaction, J. D. Savee, S. Borkar, O. Welz, B. Sztáray, C. A. Taatjes, and D. L. Osborn, *J. Phys. Chem. A* **119**, 7388 (2015).
- 24) Low temperature (550-700 K) oxidation pathways of cyclic ketones: dominance of HO<sub>2</sub>-elimination channels yielding conjugated cyclic coproducts, A. M. Scheer, O. Welz, S. S. Vasu, D. L. Osborn, C. A. Taatjes, *Phys. Chem. Chem. Phys.* **17**, 12124 (2015).
- 25) Synchrotron-based double imaging photoelectron/photoion coincidence spectroscopy of radicals produced in a flow tube: OH and OD, G. A. Garcia, X. F. Tang, J. F. Gil, L. Nahon, M. Ward, S. Batut, C. Fittschen, C. A. Taatjes, D. L. Osborn, and J. C. Loison, *J. Chem. Phys.* **142**, 164201 (2015).
- 26) VUV photoionization cross sections of HO<sub>2</sub>, H<sub>2</sub>O<sub>2</sub>, and H<sub>2</sub>CO, L. G. Dodson, L. H. Shen, J. D. Savee, N. C. Eddingsaas, O. Welz, C. A. Taatjes, D. L. Osborn, S. P. Sander, and M. Okumura, *J. Phys. Chem. A* **119**, 1279 (2015).
- 27) Formation of fulvene in the reaction of C<sub>2</sub>H with 1,3-butadiene, J. F. Lockyear, M. Fournier, I. R. Sims, J. C. Guilemin, C. A. Taatjes, D. L. Osborn, and S. R. Leone, *Int. J. Mass Spec.* **378**, 232 (2015).
- 28) Threshold photoelectron spectrum of the benzyl radical, J. D. Savee, J. Zádor, P. Hemberger, B. Sztáray, A. Bodi, and D. L. Osborn, *Mol. Phys.* **113**, 2217 (2015).
- 29) Chlorine atom-initiated low-temperature oxidation of prenyl and isoprenol: The effect of C=C double bonds on the peroxy radical chemistry in alcohol oxidation, O. Welz, J. D. Savee, D. L. Osborn, and C. A. Taatjes, *Proc. Combust. Inst.* **35**, 401 (2015).
- 30) Direct observation and kinetics of a hydroperoxyalkyl radical (QOOH), J. D. Savee, E. Papajak, B. Rotavera, H. Huang, A. J. Eskola, O. Welz, L. Sheps, C. A. Taatjes, J. Zador, and D. L. Osborn, *Science* **347**, 643 (2015).
- 31) Probing the low-temperature chain-branching mechanism of *n*-butane autoignition chemistry via time-resolved measurements of ketohydroperoxide formation in photolytically initiated *n*-C<sub>4</sub>H<sub>10</sub> oxidation, A. J. Eskola, O. Welz, J. Zador, I. O. Antonov, L. Sheps, J. D. Savee, D. L. Osborn, C. A. Taatjes, *Proc. Combust. Inst.* **35**, 291 (2015).
- 32) Influence of temperature and resonance-stabilization on the ortho- effect in cymene oxidation, B. Rotavera, A. M. Scheer, H. Huang, D. L. Osborn, and C. A. Taatjes, *Proc. Combust. Inst.* **35**, 543 (2015).

# Chemical Kinetic Modeling of Combustion Chemistry

William J. Pitz, Charles K. Westbrook  
Lawrence Livermore National Laboratory, Livermore, CA 94550  
pitz1@llnl.gov

## 1. Program Scope

We develop chemical kinetic reaction mechanisms to describe the combustion of hydrocarbons and other related fuels, including bio-derived fuels. These mechanisms are validated through comparisons between computations and experimental results in carefully controlled laboratory-scale facilities including shock tubes, laminar flames, stirred reactors, and rapid compression machines. After validation, these mechanisms are then used to understand more complex combustion phenomena in practical engines and other combustion systems. We identify particularly sensitive parts of these mechanisms and provide that information to other DOE/BES researchers who can use theory and new experiments to refine the kinetic models. We try to anticipate kinetic modeling needs of the DOE combustion community, so other researchers can have accurate models to assist in their own research projects. Our kinetic mechanisms are freely available at <https://combustion.llnl.gov/> and provide a valuable service to the combustion community.

## 2. Recent Progress

Our work has been focused towards improving the chemical kinetic models of transportation fuels, including fuels to represent gasoline and diesel fuels. Recently we have been improving and developing chemical kinetic models for representative components for gasoline and diesel fuels, and for bio-derived fuels that are low-carbon replacements for fossil fuels.

### A. Improvements to gasoline-component kinetic mechanisms

One gasoline fuel component that we have been improving is cyclopentane that is a fuel component with a high research octane number (RON) and high octane sensitivity (OS). Both of these engine properties make cyclopentane attractive for advanced spark ignition (SI) engines for automotive applications. We collaborated with Prof. Sarathy's group at KAUST and with Dr. Zador at Sandia to develop a chemical model for cyclopentane. Dr. Al Rashidi visited LLNL and worked with Dr. Zador to compute temperature and pressure dependent rate constants for the low temperature chemistry of cyclopentane, which were not previously available. The work showed that cyclopentane is particularly resistant to autoignition in the high temperature, high pressure, unreacted gases in a SI engine because its five-membered ring greatly reduces the rate of RO2 isomerization reactions leading to low-temperature chain branching compared analogous rates in acyclic alkanes [1]. One of the issues found in the development of cyclopentane mechanism was the lack of availability of robust methods in kinetic modeling software of incorporating rate constants that are pressure and temperature dependent.

For other improvements to gasoline component mechanisms, we have focused on improving the mechanisms for toluene and isooctane. For toluene, we have collaborated with the Prof. Curran's group at National University of Ireland, Galway (NUIG) to improve some of the chemical kinetic pathways so that the behavior of toluene over wide pressure and temperature ranges can be better predicted. The notable improvements to the mechanism involved the combination of benzyl radicals to form bi-benzyl and subsequent reactions. This is a termination pathway that reduces the oxidation rate of toluene in fuel mixtures as the toluene concentration is increased. In this work, toluene was mixed with dimethyl ether (DME) so that the interaction between a relatively unreactive fuel (toluene) and reactive fuel (DME) could be investigated [2]. This is a typical situation in practical fuels like gasoline where highly reactive and less reactive components are blended together.

The second gasoline component whose mechanism was recently improved was isooctane [3]. This work was done in collaboration with Prof. Sarathy's group at KAUST and Prof. Curran's group at NUIG. This work focused on improving the accuracy of its low temperature mechanism by incorporating reaction rates computed by fundamental methods from various groups over the last 7 years. Since rate constants for large species were needed for treating the low temperature chemistry of isooctane, computed rate constants were considered from groups that have focused on such large species such as Prof. Green's group at MIT, Prof. Dean's group at CSM, and Prof. Miyoshi at University Tokyo. The various reaction classes for the low temperature chemistry in the mechanism were updated based on fundamental work from these groups. These classes included R + O<sub>2</sub> addition rates, RO<sub>2</sub> isomerization rates, HO<sub>2</sub> elimination reactions to form alkenes, reactions forming cyclic ethers, and analogous reactions occurring with the second addition of O<sub>2</sub>. Alternative RO<sub>2</sub> isomerization reactions were also included. Rate constants specific to isooctane low-temperature chemistry were included based on Prof. Bozzelli's group at NJIT. After testing the mechanism by comparing predictions with many experimental data sets, a set of reaction rate rules for each of the low-temperature reaction classes was found that allowed accurate simulation of the experimental data. In this work, we found that the results were sensitive to the thermodynamic properties of some isooctane species and more work is needed to reduce the uncertainty in the thermodynamic properties so that greater accuracy can be achieved. Since the availability of studies on species larger than C<sub>6</sub> is limited, fundamental rate constant calculations are needed that address large molecules such as isooctane so that the specific molecular structures can be fully accounted for and chemical kinetic models can achieve greater accuracy.

#### A. The development of chemical kinetic models for bio-derived fuels

We have also focused on developing chemical kinetic models for bio-derived fuels. One such fuel was cyclopentanone which is a bio-derived fuel with a high RON and high OS. Collaborating with the group at NUIG, we computed H-abstraction rate constants for the reaction of H, OH, and OH, with cyclopentanone as a step towards developing a chemical model for cyclopentanone [4]. Additionally, we are working on developing chemical models for other bio-derived fuel molecules that have similar engine properties of high RON and OS.

### 3. Future Plans

In the future, we plan to continue our development of chemical kinetic models for bio-derived fuels that can displace fossil fuel components in gasoline and diesel fuels. We will be focusing on components that are attractive for advanced spark ignition engines and advanced compression ignition engines. Our work will be focused on understanding how the chemical kinetics of some fuel components help enable attractive engine performance properties. We also continue to improve the chemical kinetic models for fuel components representative of practical fuels and their mixtures so that the predictability of these models can be improved.

### Acknowledgements

This work was performed under the auspices of the U.S. Department of Energy by Lawrence Livermore National Laboratory under Contract DE-AC52-07NA27344.

### References

1. Paper 5 below.
2. Paper 3 below.
3. Paper 6 below.
4. Paper 7 below.

### Published papers in 2015 to 2017

1. Westbrook, C. K., Mehl, M., Pitz, W. J. and Sjöberg, M., "Chemical Kinetics of Octane Sensitivity in a Spark-Ignition Engine," *Combustion and Flame* 175 (2017) 2-15.
2. Fridlyand, A., Johnson, M. S., Goldsborough, S. S., West, R. H., McNenly, M. J., Mehl, M. and Pitz, W. J., "The Role of Correlations in Uncertainty Quantification of Transportation Relevant Fuel Models," *Combustion and Flame* (2017).
3. Zhang, Y., Somers, K. P., Mehl, M., Pitz, W. J., Cracknell, R. F. and Curran, H. J., "Probing the Antagonistic Effect of Toluene as a Component in Surrogate Fuel Models at Low Temperatures and High Pressures. A Case Study of Toluene/Dimethyl Ether Mixtures," *Proceedings of the Combustion Institute* 36 (1) (2017) 413–421.
4. Sun, W., Wang, G., Li, S., Zhang, R., Yang, B., Yang, J., Li, Y., Westbrook, C. K. and Law, C. K., "Speciation and the Laminar Burning Velocities of Poly(Oxymethylene) Dimethyl Ether 3 (Pomdme3) Flames: An Experimental and Modeling Study," *Proceedings of the Combustion Institute* 36 (1) (2017) 1269-1278.
5. Al Rashidi, M. J. A., Thion, S., Togbé, C., Dayma, G., Mehl, M., Dagaut, P., Pitz, W. J., Zádor, J. and Sarathy, S. M., "Elucidating Reactivity Regimes in Cyclopentane Oxidation: Jet Stirred Reactor Experiments, Computational Chemistry, and Kinetic Modeling," *Proceedings of The Combustion Institute* Volume 36, Issue 1, 2017, Pages 469–477.
6. Atef, N., Kukkadapu, G., Mohamed, S. Y., Rashidi, M. A., Banyon, C., Mehl, M., Heufer, K. A., Nasir, E. F., Alfazazi, A., Das, A. K., Westbrook, C. K., Pitz, W. J., Lu, T., Farooq, A., Sung, C.-J., Curran, H. J. and Sarathy, S. M., "A Comprehensive Iso-Octane Combustion Model with Improved Thermochemistry and Chemical Kinetics," *Combustion and Flame* 178 (2017) 111-134.

7. Zhou, C.-W., Simmie, J. M., Pitz, W. J. and Curran, H. J., "Towards the Development of a Fundamentally-Based Chemical Model for Cyclopentanone: High Pressure Limit Rate Constants for H-Atom Abstraction and Fuel Radical Decomposition," *Journal of Physical Chemistry A* 120 (36) (2016) 7037-7044.
8. Sun, W., Yang, B., Hansen, N., Westbrook, C. K., Zhang, F., Wang, G., Moshhammer, K. and Law, C. K., "An Experimental and Kinetic Modeling Study on Dimethyl Carbonate (DMC) Pyrolysis and Combustion," *Combustion and Flame* 164 (2016) 224–238.
9. Sarathy, S. M., Kukkadapu, G., Mehl, M., Javed, T., Ahmed, A., Naser, N., Tekawade, A., Kosiba, G., Abbad, M. A., Singh, E., Park, S., Rashidi, M. A., Chung, S. H., Roberts, W. L., Oehlschlaeger, M. A., Sung, C.-J. and Farooq, A., "Compositional Effects on the Ignition of Face Gasoline Fuels," *Combustion and Flame* 169 (2016) 171-193.
10. Westbrook, C. K., Pitz, W. J., Mehl, M., Glaude, P. A., Herbinet, O., Bax, S., Battin-Leclerc, F., Mathieu, O., Petersen, E. L., Bugler, J. and Curran, H. J., "Experimental and Kinetic Modeling Study of 2-Methyl-2-Butene: Allylic Hydrocarbon Kinetics," *Journal of Physical Chemistry A* 119 (28) (2015) 7462-7480.
11. Mehl, M., Herbinet, O., Dirrenberger, P., Bounaceur, R., Glaude, P.-A., Battin-Leclerc, F. and Pitz, W. J., "Experimental and Modeling Study of Burning Velocities for Alkyl Aromatic Components Relevant to Diesel Fuels," *Proc. Combust. Inst.* 35 (2015) 341-348.
12. Goldsborough, S. S., Johnson, M. V., Banyon, C., Pitz, W. J. and McNewly, M. J., "Experimental and Modeling Study of Fuel Interactions with an Alkyl Nitrate Cetane Enhancer, 2-Ethyl-Hexyl Nitrate," *Proc. Combust. Inst.* 35 (1) (2015) 571–579.
13. Nakamura, H., Curran, H., Córdoba, A. D. P., Pitz, W. J., Dagaut, P., Togbé, C., Sarathy, S. M., Mehl, M., Agudelo, J. and Bustamante, F., "An Experimental and Modeling Study of Diethyl Carbonate Oxidation," *Combust. Flame* 162 (4) (2015) 1395–1405.
14. Kukkadapu, G., Kumar, K., Sung, C.-J., Mehl, M. and Pitz, W. J., "Autoignition of Gasoline Surrogates at Low Temperature Combustion Conditions," *Combustion and Flame* 162 (5) (2015) 2272-2285.
15. Korobeinichev, O.P., Gerasimov, I.E., Knyazkov, D.A., Shmakov, A.G., Bolshova, T.A., Hansen, N., Westbrook, C.K., Dayma, G., and Yang, B., "An Experimental and Kinetic Modeling Study of Premixed Laminar Flames of Methyl Pentanoate and Methyl Hexanoate", *Z. Phys. Chem.* 229 (5) (2015) 759-780.
16. Kumar, K., Zhang, Y., Sung, C.-J. and Pitz, W. J., "Autoignition Response of N-Butanol and Its Blends with Primary Reference Fuel Constituents of Gasoline," *Combustion and Flame* 162 (6) (2015) 2466-2479.
17. Burke, U., Pitz, W. J. and Curran, H. J., "Experimental and Kinetic Modeling Study of the Shock Tube Ignition of a Large Oxygenated Fuel: Tri-Propylene Glycol Mono-Methyl Ether," *Combustion and Flame* Propylene Glycol Mono-Methyl Ether," *Combustion and Flame* 162 (7) (2015) 2916–2927.

# INVESTIGATION OF NON-PREMIXED TURBULENT COMBUSTION

Grant: DE-FG02-90ER14128

Stephen B. Pope & Perrine Pepiot  
Sibley School of Mechanical & Aerospace Engineering  
Cornell University, Ithaca, NY 14853  
s.b.pope@cornell.edu, pp427@cornell.edu

## 1 Scope of the Research Program

The underlying theme of this work is the development of computational approaches which allow our detailed knowledge of the chemical kinetics of combustion to be applied to the modeling and simulation of combustion devices. The principal modeling approaches used are large-eddy simulation (LES) to describe the flow and turbulence, and particle-based probability density function (PDF) methods to treat the turbulence-chemistry interactions. Research is currently focused on the validation and optimization of a pre-partitioned adaptive chemistry (PPAC) approach for use in LES-PDF simulations, in which individual particles evolve according to an adaptively chosen reduced set of kinetic equations tailored for their specific compositions. The main objective is to significantly reduce both the time and memory required for a computation with a given kinetic mechanism, and enable affordable computations with significantly more detailed chemistry descriptions.

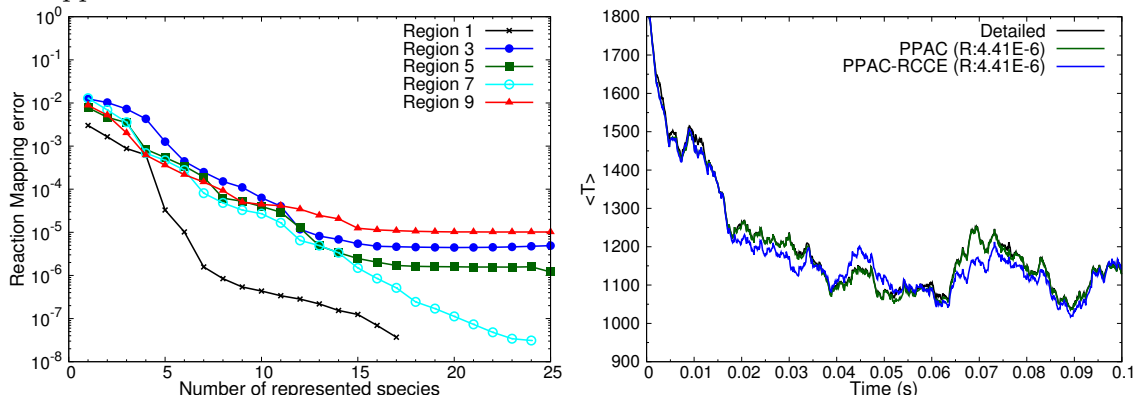
## 2 Recent Progress - An Adaptive Methodology to Implement Detailed Chemistry in LES/PDF

The project has been focused on the improvement and validation of a pre-partitioned adaptive chemistry (PPAC) methodology tailored to LES/PDF simulations, in which each particle is assigned a specialized reduced representation and chemical model tailored to their individual composition. Instead of performing chemical reduction at runtime to determine the optimal set of equations to use for a given particle, an analysis of the composition space region likely accessed during the turbulent flow simulation is conducted first, in order to *a priori* partition the composition space into a user-specified number of regions. Suitable reduced chemical representations and chemical models are then identified for each region. This is done automatically using the Directed Relation Graph with Error Propagation (DRGEP) method, extended to simultaneously eliminate non-important species and reactions. In the LES/PDF simulation, a computational particle evolves according to, and carries only the variables present in the reduced representation corresponding to the composition space region it belongs to, thereby simultaneously reducing both the CPU time and memory cost of the simulation. This region is identified using a low-dimensional binary tree search algorithm, thereby keeping the run-time overhead associated with the adaptive approach to a minimum. Two main directions for improvement are being explored, on the efficiency side first, by enabling more compact reduced representations of the chemical compositions, and on the accuracy side, by exploring how to best capture the relevant kinetics observed in turbulent flames in the *a priori* determination of reduced models and representations. An overview is provided below, the methodology and results will be reported in journal articles currently in preparation.



We have combined the PPAC approach with the rate constrained chemical equilibrium (RCCE) method. This further reduces the number of variables for individual particles to the specific moles of the represented species and elements. A key element in the success of RCCE is using appropriate represented species. This is done here by using a parallel implementation of the greedy algorithm with local improvement (GALI) of Hiremath et al. [1]. GALI is used to identify represented species for individual reduced models identified by DRGEP, which correspond to a single reduction error threshold. GALI is run on a collection of reduced models as opposed to the detailed model to significantly speed-up the selection process and avoid situations where GALI identifies represented species which have been removed during reduction. At runtime, individual particles only carry the specific moles of reduced represented variables, elements and mass fractions of locally significant species. During the reaction fractional step, the relevant reduced model compositions are reconstructed from the reduced represented species and atoms. These are integrated using the reduced model and finally the integrated composition is converted back to the reduced represented variables and atoms.

A preliminary assessment of the coupled PPAC-RCCE approach has been performed using a Sandia flame D-like non-premixed partially stirred reactor (PaSR) configuration. A partitioned subset of compositions from a PaSR run using the detailed mechanism are used by GALI to determine the near optimal represented species for individual reduced models. The results from GALI are shown in figure 1(a) for a subset of reduced models corresponding to a reduction error threshold of  $4.41 \times 10^{-6}$ . The first 12 represented species identified by GALI for individual reduced models are used to run a coupled PPAC-RCCE simulation. Figure 1(b) compares the mean temperature obtained from simulations using the detailed mechanism, PPAC approach, and a coupled PPAC-RCCE approach. The coupled PPAC-RCCE approach provides mean temperature predictions with  $\approx 5\%$  of the detailed mechanism and PPAC approach using only approximately half the variables required in the PPAC approach. Ongoing work is focused on combining PPAC-RCCE with in situ adaptive tabulation (ISAT), which will significantly enhance the efficiency of the coupled PPAC-RCCE approach.

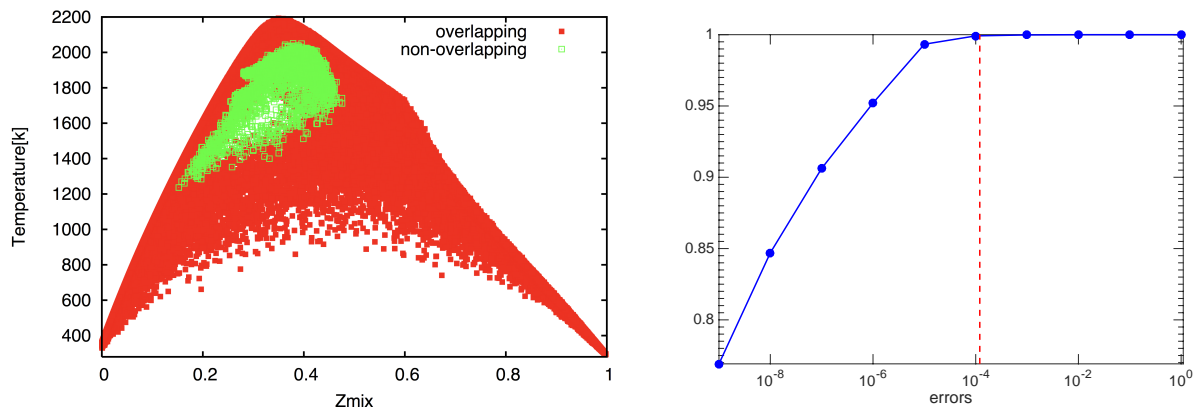


(a) Reaction mapping error as a function of number of represented species determined by GALI for a subset of reduced models (b) Comparison of temporal evolution of mean temperature in flame D like PaSR configuration obtained using a detailed mechanism, PPAC and a combined PPAC-RCCE approach

Figure 1: Preliminary results from a PPAC-RCCE coupling.

Our second focused effort aims at guaranteeing the relevance of the *a priori* generated reduced representations and kinetic models used in PPAC. One key assumption in the PPAC methodology is

that the composition database used in pre-partitioning to derive those reduced representations and models is representative of compositions found in the turbulent flame simulations. In this project, partially stirred reactors (PaSR) have been most commonly used as a convenient and inexpensive way to build such databases. We have made progress in 1) characterizing how representative a PaSR-derived database is of the chemistry occurring in a non-premixed turbulent flame, and 2) developing practical algorithms to address the identified short-comings of such databases. This is done by comparing accessed regions of the composition space in both LES/PDF and in PaSR using the ellipsoid framework at the core of the ISAT algorithm. For example, Fig. 2(a) shows, projected in a simple two-dimensional temperature *vs.* mixture fraction plot, the LES/PDF compositions that are adequately represented in a PaSR-derived database (red), and those that may not be (green). Yet, initial tests show that those LES/PDF-observed compositions that are *not* included in the PPAC database are accurately handled by the PPAC strategy, with less than 0.1% of them leading to integration errors above the error tolerance set in PPAC (Fig. 2(b)). A dynamic approach to identify and more robustly handle those compositions is being developed.



(a) Visualization of overlapping and non-overlapping portions of LES/PDF accessed composition database and PaSR database. Overlapping portion (99.6%) is in red, and non-overlapping portion (0.4%) is in green.

(b) Cumulative distribution function of integration errors evaluated over one time step of a PPAC/LES/PDF simulation of a methane/air flame. Less than 0.1% of all compositions result in an integration error larger than the preset PPAC error tolerance of  $10^{-4}$  (dashed red line).

Figure 2: Initial analysis of the adequacy of PaSR simulations as surrogates for turbulent flames for the pre-processing stage of PPAC.

### 3 Future Plans

The work in the near future will focus on further algorithmic and methodology improvements of PPAC for practical simulations, in particular on ISAT integration and optimal data structures and parallelization strategies.

### 4 Publications from DOE Research 2014-2017

1. Jaravel, T., Riber, E., Cuenot, B., Pepiot, P. (2017) “Large Eddy Simulation of the Sandia flame D using reduced mechanism for accurate pollutant prediction”, Combust. Flame, under review.

2. R.R. Tirunagari, S.B. Pope (2016) “Characterization of extinction/re-ignition events in turbulent premixed counterflow flames using strain-rate analysis”, Proc. Combust. Inst., accepted.
3. R.R. Tirunagari, S.B. Pope (2016) “An Investigation of Turbulent Premixed Counterflow Flames using Large-Eddy Simulations and Probability Density Function Methods”, Combust. Flame 166, 229–242.
4. R.R. Tirunagari, M.W.A. Pettit, A.M. Kempf, S.B. Pope (2015) “A Simple Approach for Specifying Velocity Inflow Boundary Conditions in Simulations of Turbulent Opposed-Jet Flows”, Flow, Turb. Combust., submitted for publication.
5. R.R. Tirunagari, S.B. Pope (2015) “LES/PDF for Premixed Combustion in the DNS Limit”, Combust. Th. Model., submitted for publication.
6. Y. Liang, S. B. Pope, and P. Pepiot (2015) “An adaptive methodology for the efficient implementation of combustion chemistry in particle PDF methods”, Combust. Flame 162, 3236–3253.
7. M. Mehta, R. O. Fox, and P. Pepiot. (2015) “Reduced chemical kinetics for the modeling of TiO<sub>2</sub> nanoparticle synthesis in flame reactors”, Ind. Eng. Chem. Res. 54, 5407–5415.
8. K. Narayanaswamy, P. Pitsch, and P. Pepiot (2015) “A chemical mechanism for low to high temperature oxidation of methylcyclohexane as a component of transportation fuel surrogates”, Combust. Flame, 162, 1193–1213.
9. Pope, S. B. (2014) “The determination of turbulence-model statistics from the velocity-acceleration correlation”, J. Fluid Mech. 757, R1, DOI:10.1017/jfm.2014.563.
10. Pope, S. B. and R. Tirunagari (2014) “Advances in probability density function methods for turbulent reactive flows”, In Proceedings of the Nineteenth Australasian Fluid Mechanics Conference. RMIT University, Melbourne.
11. Popov, P. and S. B. Pope (2014) “Large eddy simulation/probability density function simulations of bluff body stabilized flames”, Combust. Flame 161, 3100–3133.
12. K. Narayanaswamy, P. Pepiot, and P. Pitsch (2014) “A chemical mechanism for low to high temperature oxidation of *n*-dodecane as a component of transportation fuel surrogates”, Combust. Flame, 161, 866–884.

## References

- [1] V. Hiremath, Z. Ren and S.B. Pope. *Combust. Flame*, 158 (2011) 2113-2127.

## OPTICAL PROBES OF ATOMIC AND MOLECULAR DECAY PROCESSES

S.T. Pratt  
Building 200, B-125  
Argonne National Laboratory  
9700 South Cass Avenue  
Argonne, Illinois 60439  
E-mail: spratt@anl.gov

### PROGRAM SCOPE

The study of molecular photoabsorption, photoionization, and photodissociation dynamics can provide considerable insight into how energy and angular momentum flow among the electronic, vibrational, and rotational degrees of freedom in isolated, highly energized molecules. This project involves the study of these dynamics in small molecules, with an emphasis on understanding the mechanisms of intramolecular energy flow and determining how these mechanisms influence decay rates and product branching ratios. Such studies also shed light on related collision processes such as dissociative recombination, providing a connection between spectroscopy and dynamics. One recent focus of the project has been understanding the factors that determine and influence photoabsorption and photoionization cross sections. The experimental approach combines a variety of laser-based techniques, including nonlinear methods to generate tunable vacuum ultraviolet light, and double-resonance methods to prepare selected excited states of the species of interest. Synchrotron-based techniques are also being used. The detection methods include mass spectrometry, photoion- and photoelectron-imaging, and high-resolution photoelectron spectroscopy, which are used to characterize the decay processes of the selected excited states. Currently, photoelectron imaging is also allowing the study of circular dichroism in photoelectron angular distributions as a means to characterize chiral molecules. Finally, experiments enabled by new vuv and x-ray free electron laser sources are being explored.

### RECENT PROGRESS

Over the past year, new experiments have been performed both in the laboratory at Argonne and at the Linac Coherent Light Source. I have also spent time analyzing results from previous experiments and preparing them for publication. I have been allocated beamtime at SOLEIL in June to record high-resolution photoionization data on a series of butynyl radicals generated by using a fluorine abstraction technique developed by J. C. Loison (ISM, Bordeaux). The goal of this work is to see if the shape resonances observed in closed shell alkyne molecules with internal triple bonds are also observed in radical systems, and if these resonances are absent in closed shell molecules with terminal triple bonds. Because the HOMO in the radical systems only contains a single electron, the intensity of this shape resonance is expected to be approximately half that of the closed shell molecule, but that also remains to be seen. The high-resolution monochromator available at SOLEIL should allow the resolution of autoionizing structure that may also prove informative. This would be the first demonstration of a shape resonance in such a system, and its characterization will be useful in developing qualitative and quantitative methods for estimating radical photoionization cross sections.

#### *Circular Dichroism in Imaging Experiments*

The new work on butynyl radicals will be complemented by laboratory work in which butynyl bromides and iodides are photodissociated with the goal of studying the photoionization dynamics of the butynyl radicals and characterizing the radical photoionization cross section. This work will also be extended to some unsaturated butyl halides to explore a new direction of our work: using photoelectron angular distributions to characterize the photoionization dynamics of chiral molecules. When chiral molecules are photoionized with circular polarized light, the photoelectron angular distributions can display forward backward asymmetry that depends on the direction of circular polarization and the particular enantiomer. Switching the polarization or the enantiomer will flip the photoelectron asymmetry. In the last decade, this photoelectron circular dichroism (PECD) has become an active area of research, and the possibility of extending such studies to reactive species is being investigated. For example, pure enantiomers of the chiral molecule 2-methyl-1-bromobutane are available, and these should give rise to a PECD signal. If a

single enantiomer of this molecule is photodissociated in the near ultraviolet, the resulting 2-methyl-but-1-yl radical should also be chiral, and produce its own PECD signal. Isomerization of this radical to the other enantiomer should be reasonably slow, and may be captured by monitoring the time dependence of the PECD signal.

In the course of testing the PECD set up, preliminary experiments were performed on a non-chiral molecule, nitric oxide. In these experiments, circular dichroism is induced by excitation to the  $A^2\Sigma^+$  state with a circular polarized pump, and probed by ionization with a circular polarized probe beam. Rotationally resolved photoelectron images show significant circular dichroism for some rotational transitions, and can be used to provide insight into the details of the photoionization dynamics. This imaging approach greatly simplifies previous circular dichroism studies on NO, and the experimental results compare favorably with the earlier work. [See, for example, Appling et al. *J. Chem. Phys.* **87**, 6927 (1987) and Leahy et al. *J. Chem. Phys.* **97**, 4948 (1992).]

#### *Photoionization of Molecular Nitrogen*

The near-threshold single-photon ionization spectrum of  $N_2$  shows significant resonant structure corresponding to autoionizing Rydberg states converging to vibrational levels of the  $X^2\Sigma_g^+$ ,  $A^2\Pi_u$ , and  $B^2\Sigma_u^+$  states of the ion, as well as to high vibrational levels of the  $b'^1\Sigma_u^+$  valence state. In particular, two intense complex resonances are observed between  $126100\text{ cm}^{-1}$  and  $126500\text{ cm}^{-1}$  that have the appearance of the two towers of a cathedral. Although the assignment of one of the towers is well accepted, it is surprising for a molecule as fundamental as  $N_2$  that the assignment of the second remains contested. Several years ago, we recorded high-resolution spectra of this region using the SOLEIL synchrotron, including photoelectron angular distributions of rotationally resolved autoionizing resonances. The goal was to use these distributions to help assign the resonances, but this has proved difficult. We have, however, developed a simple approach to calculate the angular distribution parameters for rotational levels of the  $9p\sigma$ ,  $v=1$  state, and we are working to extend this model to other resonances.

Because of the difficulty of extracting detailed information from the photoelectron angular distributions of  $N_2$ , new double resonance experiments have been performed at Argonne on the photoionization spectrum of  $N_2$  just above the ionization threshold. In these experiments, the  $a''^1\Sigma_g^+$ ,  $v'=0$  state is pumped via a two-photon transition, and a second tunable laser drives the transition from there into the region of interest. Because the overall process involves three photons, the same parity levels are accessed as in a single-photon transition from the ground state of  $N_2$ . The  $a''^1\Sigma_g^+$  state corresponds to the  $(X^2\Sigma_g^+)3s\sigma_g$  Rydberg state, and the probe transition accesses the same region as in the SOLEIL experiments. Several types of probe transitions are possible. First, the probe photon can further excite the  $3s\sigma_g$  electron. Because the  $a''^1\Sigma_g^+$  state has a potential curve similar to that of the  $X^2\Sigma_g^+$  state of the ion, the Franck-Condon factor between the  $v^+ = v' = 0$  levels is nearly unity. In the region of interest, such transitions lead to direct photoionization of the intermediate state. The corresponding transitions to levels with  $v^+ \neq v'$  will have much smaller Franck-Condon factors, and will populate vibrationally autoionizing levels converging to the  $N_2^+ X^2\Sigma_g^+$  levels with  $v^+ \geq 1$ . The second type of transition can involve excitation of the  $N_2^+ X^2\Sigma_g^+$  core of the  $a''^1\Sigma_g^+$  Rydberg state, with the  $3s\sigma_g$  electron acting as a spectator (or nearly as a spectator). In the region of interest, the two possible transitions of the ion core correspond to the  $X^2\Sigma_g^+ \rightarrow A^2\Pi_u$  and  $X^2\Sigma_g^+ \rightarrow B^2\Sigma_u^+$  transitions, which have been very well characterized. In principle, such a core transition would produce an electronically autoionizing level with an  $A^2\Pi_u$  or  $B^2\Sigma_u^+$  core and a  $3s\sigma_g$  electron. However, such a transition of the core creates an impulsive change in the character of the ion core that can "shake up" the Rydberg electron into a different Rydberg state. Of course, the electronic parity must remain ungerade, and since the A or B state cores are also ungerade, the Rydberg electron must have gerade symmetry. The third type of transition is to the high vibrational levels of the  $b'^1\Sigma_u^+$  mentioned above. In principle, the simplification of rotational structure in the spectra resulting from the double resonance approach should provide significant help in assigning the resulting spectrum.

Although most of the previous efforts aimed at unraveling the assignments of this region of the  $N_2$  photoionization spectrum have involved single-photon excitation from the  $X^1\Sigma_g^+$  ground state, one previous double-resonance experiment has been performed via the  $a^1\Pi_g$  valence state. In that experiment,

no transitions were observed corresponding to the higher energy tower of the cathedral bands. In the present experiments, strong features are observed for both towers. The analysis of these data is currently underway, and the effort should be completed by the summer.

## **FUTURE PLANS**

In the coming year, I will complete my analysis of the two datasets on the near-threshold photoionization of  $N_2$ , and write up the papers for submission. My hope is that the new data will provide a definitive assignment of the complex resonances and autoionizing structure that appears in this region, and answer some long-standing questions. These results should also help in the analysis of planned experiments on  $N_2$  using FELs, as well as for the interpretation of recent attosecond time-resolved studies of the  $N_2$  absorption spectrum, where the nature of the wavepacket (i.e., the nature of the resonances contributing to it) is expected to have a significant effect on the observed time evolution [Warrick et al. J. Phys. Chem. A 120, 3165 (2016)].

I will continue experiments on the photodissociation of more complex alkyl-halide molecules, and on the photoionization of the resulting alkyl radicals. Particular attention will be paid to chiral molecules and radicals, and to using PECD techniques to characterize their photoionization dynamics. While additional small chiral molecules are also of interest, the simplicity of the dissociation dynamics of the alkyl halides makes them particularly interesting targets.

As mentioned above, I have beamtime at SOLEIL in June for the study of the photoionization cross sections of the butynyl radicals. I will also have a second beamtime at SOLEIL (to be scheduled) to study the inner-valence and core-shell ionization of  $CH_3I$  with David Holland, Ruaridh Forbes (Ottawa), and Jonathan Underwood (University College London). I am already working with these collaborators to analyze and interpret some of their earlier results, and the new experiments will build on this analysis.  $CH_3I$  has become a popular target for pump-probe experiments using x-ray FELs, and our results should be helpful for interpreting the new results from those experiments.

I will also continue to collaborate with researchers at x-ray FELs. This past year, I co-authored two papers that were published about the experiments performed at the LCLS in 2014. These papers explored the time-dependent decay processes of  $XeF_2$  and  $N_2$  following core-hole formation by looking at the fragment time of flight distributions. These were some of the first x-ray pump/x-ray probe experiments to be performed at the LCLS. This past year I also participated in new beamtime at the LCLS with the AMO Physics Group, coupling an x-ray/x-ray pump-probe technique and photoelectron spectroscopy to study the electron and nuclear dynamics following core excitation in CO. The data from that experiment are currently being analyzed. I also worked on a proposal with David Holland and Katharine Reid for beamtime at the FERMI FEL, which has narrow bandwidth in the vacuum ultraviolet region. This proposal focuses on photoelectron angular distributions from electronically autoionizing states in fixed-in-space  $N_2$ , and will be submitted following the next call for beamtime proposals.

I will continue to collaborate with Christian Jungen on using results from *ab initio* photoionization calculations to try to characterize the importance and interactions among the bound Rydberg states of the alkynes and related molecules. At the moment we are waiting for new theoretical calculations by Robert Lucchese to try to assess the energy dependence of the transition moments and quantum defects. As stated previously, if the approach is successful, it would provide a new way to connect the continuum and bound-state portions of photoabsorption and photoionization spectra, and provide insight into the assignment of the absorption spectra of large molecules.

## **ACKNOWLEDGEMENTS**

This work was performed in collaboration with Ananya Sen. Work on oriented NO was performed in collaboration with K. L. Reid (Nottingham). Work at Soleil was performed in collaboration with S. Boyé-Péronne and B. Gans (Institut des Sciences Moléculaires d'Orsay), D. M. P. Holland (STFC, Daresbury), U. Jacovella (ETH-Zürich), R. R. Lucchese (Texas A&M), E. F. McCormack (Bryn Mawr College), and N. de Oliveira (Soleil). Work on dissociative recombination was performed in collaboration with Ch.

Jungen (Laboratoire Aime Cotton). This work was supported by the U.S. Department of Energy, Office of Science, Office of Basic Energy Sciences, Division of Chemical Sciences, Geosciences, and Biological Sciences under contract No. DE-AC02-06CH11357.

### DOE-SPONSORED PUBLICATIONS SINCE 2015

1. S. T. Pratt and Ch. Jungen  
GENERAL FEATURES OF THE DISSOCIATIVE RECOMBINATION OF POLYATOMIC MOLECULES  
EPJ Web of Conf. **84**, 04001 (5 pages) (2015).
2. Hong Xu and S. T. Pratt  
PHOTODISSOCIATION OF METHYL IODIDE VIA SELECTED VIBRATIONAL LEVELS OF THE  $\tilde{B}$  ( $^2E_{3/2}$ )6s RYDBERG STATE  
J. Phys. Chem. A, **119**, 7548-7558 (2015).
3. U. Jacovella, D. M. P. Holland, S. Boyé-Péronne, B. Gans, N. de Oliveira, D. Joyeux, L. E. Archer, R. R. Lucchese, Hong Xu, and S. T. Pratt  
HIGH-RESOLUTION VACUUM-ULTRAVIOLET PHOTOABSORPTION SPECTRA OF 1-BUTYNE AND 2-BUTYNE  
J. Chem. Phys. **143**, 034304 (14 pages) (2015).
4. S. J. Klippenstein and S. T. Pratt  
A TRIBUTE TO LAWRENCE B. HARDING, JOE V. MICHAEL, AND ALBERT F. WAGNER FOR THEIR 100 YEARS OF COMBUSTION KINETICS STUDIES AT ARGONNE  
J. Phys. Chem. A. **119**, 7075-7077 (2015).
5. U. Jacovella, D. M. P. Holland, S. Boyé-Péronne, B. Gans, N. de Oliveira, K. Ito, D. Joyeux, L. E. Archer, R. R. Lucchese, Hong Xu, and S. T. Pratt  
A NEAR-THRESHOLD SHAPE RESONANCE IN THE VALENCE SHELL PHOTOABSORPTION OF LINEAR ALKYNES  
J. Phys. Chem. A. **119**, 12339-12348 (2015).
6. N. Saquet, D.M.P. Holland, S.T. Pratt, D. Cubaynes, X. Tang, G. A. Garcia, L. Nahon, and K.L. Reid  
EFFECT OF ELECTRONIC ANGULAR MOMENTUM EXCHANGE ON PHOTOELECTRON ANISOTROPY FOLLOWING THE TWO-COLOUR IONIZATION OF KRYPTON ATOMS  
Phys. Rev. A **93**, 033419 (11 pages) (2016).
7. A. Piçon, C. S. Lehmann, C. Bostedt, A. Rudenko, A. Marinelli, T. Osipov, D. Rolles, N. Berrah, C. Bomme, M. Bucher, G. Doumy, B. Erk, K. R. Ferguson, T. Gorkhover, P. J. Ho, E. P. Kanter, B. Krässig, J. Krzywinski, A. A. Lutman, A. M. March, D. Moonshiram, D. Ray, L. Young, S. T. Pratt, and S. H. Southworth  
HETERO-SITE-SPECIFIC ULTRAFAST INTRAMOLECULAR DYNAMICS  
Nat. Commun. **7**, 11652 (6 pages) (2016).
8. C. S. Lehmann, A. Piçon, C. Bostedt, A. Rudenko, A. Marinelli, D. Moonshiram, T. Osipov, D. Rolles, N. Berrah, C. Bomme, M. Bucher, G. Doumy, B. Erk, K. R. Ferguson, T. Gorkhover, P. J. Ho, E. P. Kanter, B. Krässig, J. Krzywinski, A. A. Lutman, A. M. March, D. Ray, L. Young, S. T. Pratt, and S. H. Southworth  
ULTRAFAST X-RAY-INDUCED NUCLEAR DYNAMICS IN DIATOMIC MOLECULES USING FEMTOSECOND X-RAY-PUMP - X-RAY-PROBE SPECTROSCOPY  
Phys. Rev. A **94**, 013426 (7 pages) (2016).
9. A. Sen, S. T. Pratt, and K. L. Reid  
CIRCULAR DICHROISM IN PHOTOELECTRON IMAGES FROM ALIGNED NITRIC OXIDE MOLECULES  
Submitted to J. Chem. Phys. (2017).

# Chirped-Pulse Fourier Transform Millimeter-Wave Spectroscopy for Dynamics and Kinetics Studies of Combustion-Related Reactions

Kirill Prozument  
Chemical Sciences and Engineering Division  
Argonne National Laboratory  
Argonne, IL 60439  
[prozument@anl.gov](mailto:prozument@anl.gov)

## 1. Scope of the Program

I am developing a new program to use millimeter-wave rotational spectroscopy to probe stable and reactive species relevant to combustion chemistry, and to use this capability to study reaction dynamics and kinetics. Rotational spectroscopy is known for its unsurpassed resolution and precision in determining molecular structure. The program is based on chirped-pulse Fourier transform millimeter-wave (CP-FTmmW) spectroscopy, which has revolutionized the field of molecular spectroscopy.[1-3] The CP-FTmmW spectroscopy is capable acquiring ~10 GHz-wide rotational spectra with sub-MHz resolution in several microseconds with meaningful relative intensities of the transitions of multiple reaction products. The technique is nearly universal (applicable to all polar species) chemical tool that is conformer- and state-specific, quantitative and non-destructive, and suitable for studies of stable and transient species. The versatility of the CP-FTmmW technique is sufficient for its application to a wide range of experiments in reaction dynamics and kinetics in the gas phase. The program is currently focused of three directions: i) investigation of pyrolysis chemistry in the Chen tubular reactor at 1000–1800 K, ii) *in situ* time-resolved chirped-pulse spectroscopy of photoproducts at room temperature and iii) automating rotational spectral pattern recognition using deep machine learning.

## 2. Recent Progress

In the year since our last meeting my group has implemented the chirped-pulse rotational spectroscopy to investigate chemical dynamics processes at room temperature and in two regimes: the *fine time-resolution mode* (~10  $\mu$ s) and *medium time-resolution mode* (~1 ms) for studying evolution of reaction products' concentrations and their quantum state distributions. Combined with previously reported chirped-pulse spectrometer by BrightSpec Company, suited for continuous (CW) acquisition of rotational spectra, these tools equip us to study vast range of chemical and physical phenomena.

### a. Dynamic Time-Resolved Chirped-Pulse Rotational Spectroscopy in a Room Temperature Flow Reactor

The branching ratios that are experimentally detectable in a chirped-pulse experiment can be compared to accurate kinetic calculations to understand the reaction mechanisms. It is imperative then to have a reactor with well-defined thermodynamic conditions that would be amenable to modeling. Recently, the Suits group has implemented such a reactor based on the Laval flow for low-temperature studies. In our program we have developed a room flow-tube reactor operating at



room temperature coupled with chirped-pulse spectrometer, which is shown in Fig. 1. The present approach allows to i) study chemical dynamics at room temperature and, potentially, at elevated temperature in a heated version of the flow tube, ii) ability to accurately control and vary pressure in the 1–100 mTorr range, iii) up to  $\sim 10$  ms flight times through the reactor, iv) generally richer rotational spectra that would allow for experimental determination of the rotational temperature of reaction products. The latter consideration also carries potential challenges in detecting rotational transitions due to spread of population among rotational levels.

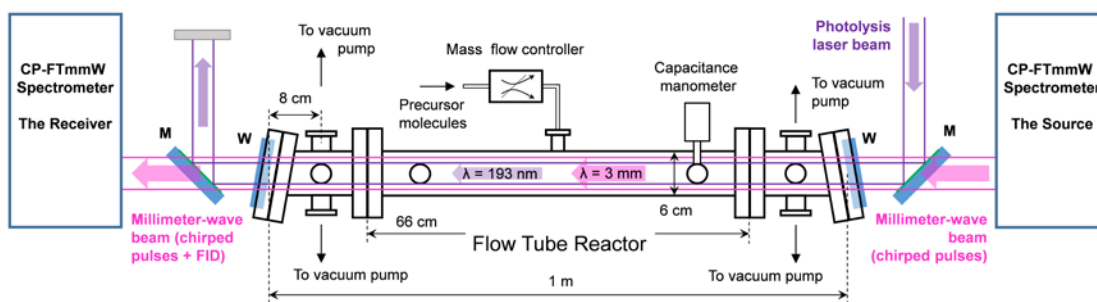


Fig 1. The schematic of the DTR CP-FTmmW experimental setup. The laser beam is coupled into the flow tube reactor with a pair of mirrors M that are transparent to the mm-wave beam of the spectrometer. The precursor vinyl cyanide molecules are introduced at the middle of the reactor and evacuated by a vacuum pump (not shown) through the four ports near the ends of the tube. Tilted laser windows W help quench reflections and standing waves. The reactor is designed to maximize the overlap between the gas sample, photolysis laser beam, and millimeter-wave beam of a CP-FTmmW spectrometer for better signal. The relative timing of the laser pulse and the mm-wave chirped pulses is set to investigate the dynamics of the post-photolysis chemistry. The repetition rate of the laser and train of chirped mm-wave pulses is set to ensure effective evacuation of photoproducts between the cycles.

The time evolution of the HCN, HNC and HCCCN products of 193 nm photolysis of vinyl cyanide,  $\text{CH}_2\text{CHCN}$ , detected in the flow tube reactor is shown in Fig. 2. The initial growth of all products is associated with rotational equilibration of the hot nascent photoproducts at  $t < 1$  ms. Slower growth of the HCCCN signal compared to that of HCN indicates that more excitation is deposited into HCCCN upon passing through its transition state than is the case with HCN. The HNC signal is rapidly decaying starting at 200  $\mu\text{s}$ , most likely upon  $\text{HNC} \rightarrow \text{HCN}$  isomerization. The W-band (75–110 GHz) DTR CP-FTmmW spectrometer used here is a variation of the Argonne E-band CP-FTmmW spectrometer in combination with the BrightSpec W-band spectrometer.

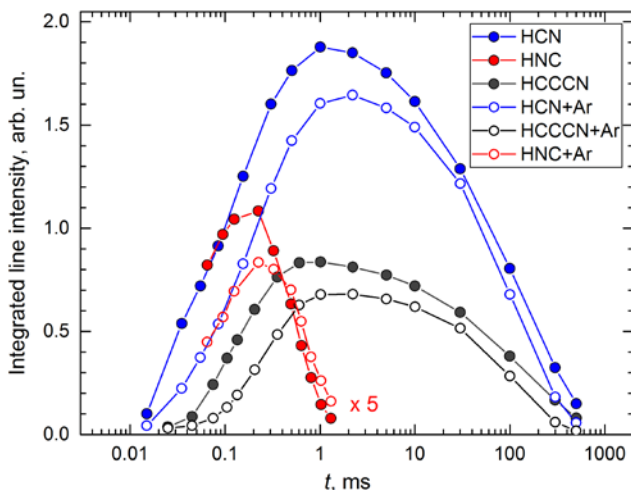


Fig. 2. The time evolution of the CP-FTmmW signals of HCN, HNC, and HCCCN following photodissociation of  $\text{CH}_2\text{CHCN}$  at  $t = 0$  obtained in *fine time-resolution mode* of the spectrometer. Chirped pulses are fired at times  $t$  and with their frequencies centered around the HCN, HNC, and HCCCN, transitions. The intensities of the molecular responses plotted as a function of the initiation time  $t$  of the excitation pulses. The filled circles are the results with neat  $\text{CH}_2\text{CHCN}$  precursor at 1  $\mu\text{bar}$  (0.76 mTorr) pressure. The empty circles are from the tests in which  $\text{CH}_2\text{CHCN}$  was diluted in argon. The partial pressure of  $\text{CH}_2\text{CHCN}$  was  $\mu\text{bar}$  while the total pressure was 10  $\mu\text{bar}$ . The decline in signals after 5–10 ms is associated with evacuation of the photoproducts by the pump.

As evident from Fig. 2, the CP-FTmmW signals of the photoproducts are only slowly evolving between the 1 ms and 5 ms time-points. Neglecting these dynamics, we take advantage of the 80% duty cycle of the segmented chirp BrightSpec spectrometer and set it to acquire a broadband CP-FTmmW spectrum, but only at  $1 \text{ ms} \leq t \leq 5 \text{ ms}$ . This is implemented in the synchronized High Dynamic Range (sync-HDR) mode of the spectrometer developed by BrightSpec at our request. In this *medium time-resolution* mode we are trading the time resolution of the *fine time-resolution* mode for the ability to acquire a spectrum over the entire W-band with similar S/N. The broadband sync-HDR spectrum shows several rotational transitions of vibrationally excited HCCCN that are Boltzmann-distributed with the vibrational temperature near 300 K. Similar results is obtained for the  $0 \leq t \leq 400 \mu\text{s}$  time-window, indicating that vibrational relaxation, if any, is faster than rotational relaxation. A possibility of bimolecular chemistry contribution is excluded by an experiment with isotopically labeled precursors. Assuming complete thermalization of HCN and HNC to the ambient temperature of 295 K, the  $[\text{HCN}]/[\text{HCCCN}] = 1.64 \pm 0.25$  branching ratio is determined.

### b. Rotational Spectral Pattern Recognition using Artificial Neural Networks

A typical broadband rotational spectrum may contain several thousand observable transitions, spanning many species. Identifying the individual spectra, particularly when the dynamic range reaches 1,000:1 or even 10,000:1, can be challenging. One approach is to apply automated fitting routines. In this approach, combinations of 3 transitions can be created to form a “triple”, which allows fitting of the A, B, and C rotational constants in a Watson-type Hamiltonian. On a standard desktop computer, with a target molecule of interest (to a first approximation only one species can be searched for at a time), a typical AUTOFIT routine[4] takes 4–12 hours depending on the spectral density. A new approach is to utilize machine learning to train a computer to recognize the patterns (frequency spacing and relative intensities) inherent in rotational spectra and to identify the individual spectra in a raw broadband rotational spectrum.

The first approach employed in my group is to train a recurrent neural network to identify different types of rotational spectra and classify them accordingly. For this type of artificial neural network (ANN), the computer learns the spectral patterns associated with several different types of molecules (linear, symmetric, and asymmetric tops). Spectral parameters are randomly generated (with some filters to assure they remain physically meaningful) and several thousand spectra are generated using an appropriate Hamiltonian, along with a label denoting the type of spectrum. The neural network then trains on these spectra, learning the frequency spacings and intensity patterns. Training the network takes only a few seconds. The typical accuracy of the network after training ranges between 96–98%. This is a desirable range, as 100% would indicate the neural network is just memorizing the training set instead of generalizing. The problem with this type of neural network, however, is that it is not particularly useful. First, the input to the network must be a set of frequencies and intensities equal in length to the training set. This means, in a practical sense, that the experimental spectrum must first be processed (e.g. peakpicked). If the network was trained on 60 transitions, as was the case here, then 60 random transitions would have to be pulled from the original experimental spectrum. It is unlikely they would match. Of course, every possible combination could be created, but that is no better than the automated fitting option described earlier. It is not clear that this type of ANN could separate a spectrum from the noise, whether it is actual noise or the noise of other spectra. However, it does demonstrate that a neural network can be trained to identify the different types of rotational spectra.

A second type of ANN, the convolutional neural network (CNN), has also been developed. CNN’s are most notably used for object recognition, like facial recognition in a photo or voice recognition in a waveform. The idea is then, can a CNN identify rotational spectra in an experimental spectrum? To continue the analogy, the experimental spectrum is the photo and the

rotational spectrum the face. Early results in applying CNN's for spectral object recognition in broadband rotational spectra appear promising.

### 3. Future Plans

We plan to apply the newly developed DTR chirped-pulse spectroscopy to bimolecular reactions studies. Initial chemistry can be initiated by photolysis of cyanogen, NCCN. The resulting CN radicals will readily abstract H-atoms from hydrocarbons, ketones or aldehydes thus creating a pool of radicals. We plan on advancing our spectrometer to the 260–290 GHz spectral region to improve the sensitivity of room temperature measurements by a factor of 5–10. Initial studies may involve CH<sub>3</sub>OH or CH<sub>2</sub>O molecules. In particular, we are interested in vibrational and rotational energy distribution in the reaction products.[5] We aim at observing how that internal energy affects the chemical pathways of reactive intermediates.

The pyrolysis experiments that are underway in my group and that have been described in the last year's report are an important part of this program. We plan collaboration with Robert Kee of Colorado School of Mines to conduct detailed computer fluid dynamics (CFD) characterization of the gas flow inside the Chen reactor and merge those with chemical kinetic modeling by my colleague Raghu Sivaramakrishnan. An important part of this collaboration will be the x-ray fluorescence measurements by my colleague Robert Tranter. Recently, he used that method to map the gas density inside the reactor, which can serve as an experimental benchmark for CFD calculations. The combination of these approaches with CP-FTmmW measurements will lead to detailed models of very complex pyrolysis and combustion reactions.

We plan further developing the spectral pattern recognition project using the convolutional artificial neural networks. The ANN's will be redeveloped in Java and we expect noticeable performance improvements in manipulating large amounts of data. In the future we plan employing Argonne super-computer for this project.

[1] G.G. Brown, B.C. Dian, K.O. Douglass, S.M. Geyer, S.T. Shipman, B.H. Pate, A broadband Fourier transform microwave spectrometer based on chirped pulse excitation, *Rev Sci Instrum* 79(5) (2008) 053103.

[2] B.C. Dian, G.G. Brown, K.O. Douglass, B.H. Pate, Measuring Picosecond Isomerization Kinetics via Broadband Microwave Spectroscopy, *Science* 320(5878) (2008) 924-928.

[3] G.B. Park, A.H. Steeves, K. Kuyanov-Prozument, J.L. Neill, R.W. Field, Design and Evaluation of a Pulsed-Jet Chirped-Pulse millimeter-Wave Spectrometer for the 70-102 GHz Region, *J. Chem. Phys.* 135(2) (2011) 024202.

[4] N.A. Seifert, I.A. Finneran, C. Perez, D.P. Zaleski, J.L. Neill, A.L. Steber, R.D. Suenram, A. Lesarri, S.T. Shipman, B.H. Pate, AUTOFIT, an automated fitting tool for broadband rotational spectra, and applications to 1-hexanal, *J Mol Spectrosc* 312 (2015) 13-21.

[5] N.J. Labbe, R. Sivaramakrishnan, C.F. Goldsmith, Y. Georgievskii, J.A. Miller, S.J. Klippenstein, Weakly Bound Free Radicals in Combustion: "Prompt" Dissociation of Formyl Radicals and Its Effect on Laminar Flame Speeds, Submitted (2015).

#### DOE-Sponsored Publications Since 2016

1. D.P. Zaleski, C. Duan, M. Carvajal, I. Kleiner, K. Prozument, The Broadband Rotational Spectrum of Fully Deuterated Acetaldehyde (CD<sub>3</sub>CDO) in a CW Supersonic Expansion, *J. Mol. Spectrosc.* (2017) <http://dx.doi.org/10.1016/j.jms.2017.01.010>.
2. D.P. Zaleski, K. Prozument, Design of an E-Band CP-FTmmW Spectrometer and Identification of Pseudo-Equilibrium structure of HNO. Submitted (2017).

# Spectroscopic probes of dynamics on multiple potential energy surfaces

Krupa Ramasesha  
Combustion Research Facility, Mail Stop 9055  
Sandia National Laboratories  
Livermore, CA 94551  
[kramase@sandia.gov](mailto:kramase@sandia.gov)

## I. Program Scope

This program is a new thrust within Sandia National Laboratories' Combustion Research Facility, and aims to apply ultrafast spectroscopy to time-resolve fundamental gas-phase molecular dynamics. The proposed work will develop molecular structure-specific probes to follow coupled electronic and nuclear motion on femtosecond to picosecond timescales in gas-phase small molecules. The coupling of electronic and nuclear degrees of freedom, representing a breakdown of the Born-Oppenheimer approximation, gives rise to complex pathways of non-radiative energy dissipation in electronically excited molecules, which often involve participation of several electronic states. Identifying the motions that couple electronic states, the timescales and dynamics of excited state population relaxation, and the role of the coupled vibrational modes of a molecule in guiding energy flow are crucial to our understanding of non-equilibrium dynamics, and will form the mainstay of this proposed program.

## II. Recent Progress

During the last review period, I started a collaboration with David Osborn and Judit Zádor to investigate the reaction of  $O(^3P)$  + cyclopentene. Fitting with the program scope just discussed, all reactions of  $O(^3P)$  atoms with closed shell molecules are of fundamental importance because they may occur on multiple electronic surfaces. Practically, reaction of ground state atomic oxygen,  $O(^3P)$ , with alkenes is a crucial process in combustion chemistry. This general class of reactions is known to proceed with the addition of the O atom to the alkene double bond to form a triplet biradical adduct<sup>1</sup>, which can isomerize or dissociate into bimolecular products either on the triplet potential energy surface (PES) or on the singlet PES following inter-system crossing. Studies of  $O(^3P)$  reaction with acyclic unsaturated hydrocarbons<sup>2-4</sup> show bimolecular pathways where products are formed both on the singlet and the triplet PES. This prior work provides a benchmark for comparison to reactions of  $O(^3P)$  with cyclic alkenes, where the more rigid structure of a ring may constrain viable reaction pathways.

We are studying the reaction of  $O(^3P)$  with cyclopentene at 4 Torr, 298 K using time-resolved multiplexed photoionization mass spectrometry<sup>5</sup>, where  $O(^3P)$  radicals are generated by 351 nm photolysis of  $NO_2$  and are allowed to react with excess cyclopentene in He under pseudo-first order conditions. The resulting products are sampled and characterized by tunable ionizing vacuum ultraviolet radiation produced by the Advanced Light Source of Lawrence Berkeley National Laboratory and an orthogonal acceleration time-of-flight mass spectrometer. This technique enables measurement of both mass spectra and photoionization spectra at various times following the initiation of the reaction. The majority of detected primary product branching is to channels that have not been observed before. We observe propylketene (40%), acrolein + ethene (37%), 1-butene + CO (20%) and cyclopentene oxide (3%), of which the propylketene and 1-butene + CO pathways were previously unidentified experimentally<sup>6,7</sup> and theoretically<sup>8</sup>. Quantum chemical calculations point to an essentially barrier-less formation of cyclopenteneoxide on the singlet PES, pathways for propylketene formation on the triplet and singlet PES, and pathways to bimolecular products on the singlet PES. Unlike reactions of  $O(^3P)$  with acyclic unsaturated molecules, we do not observe any doublet + doublet (i.e., radical) products. This observation, and comparison of experimental ionization energies with those calculated using CBS-QB3, suggest that all products are detected on the singlet PES, providing evidence for a much more efficient competition of intersystem crossing with decay pathways on the triplet surface when compared to previously studied acyclic systems. Current work is aimed at locating minimum energy crossings between the triplet and

singlet PES, calculating the flux through these crossings, and performing master equation calculations to explain the experimentally measured product yields.

### III. Future Work

A laboratory is being designed and renovated to support new work on ultrafast chemical dynamics. Ultrafast spectroscopy of non-adiabatic dynamics will initially involve the use of two techniques to study molecular structure evolution, allowing investigation of systems that vastly differ in size and complexity. First, UV pump—supercontinuum infrared probe spectroscopy will be used as a means of probing nuclear motions that bring about electronic degeneracies, by using high frequency molecular vibrations as reporters of large-scale structural deformations in polyatomic molecules. Specifically, we will study non-adiabatic dynamics in acetyl acetone (AcAc) using vibrational spectroscopy, since the presence of a strong intramolecular hydrogen bonding interaction between O-H and C=O moieties allows the O-H and C=O stretch frequencies to be used as sensitive reporters of backbone deformations of the molecule that modify the strength of this interaction. It has been shown theoretically that relaxation of electronically excited AcAc from  $S_2$  ( $\pi\pi^*$ ) involves significant changes to the backbone structure as it traverses through conical intersections<sup>9,10</sup>, and probing the evolution of high frequency vibrations in the molecule can effectively constrain possible structures as a function of time. Second, UV pump—soft X-ray probe spectroscopy will be employed to report on electronic and structural dynamics via changes to the energies and oscillator strengths of sulfur  $L_{2,3}$ -edge and carbon  $K$ -edge transitions in small molecules with single carbon and sulfur atoms and with minimal internal degrees of freedom. The first candidate for these studies will be carbonyl sulfide (OCS), where it has been shown that 220 nm excitation breaks the C-S bond<sup>11</sup>, and that both electronic excitation and dissociation of the molecule involve bending deformations that have been predicted to evolve on sub-picosecond timescales<sup>12</sup>. Bending of OCS has been theoretically shown to result in significant changes to the valence molecular orbital energies<sup>2</sup>, suggesting the use of near-edge core level transitions (i.e., transition of a 1s electron to an unoccupied valence orbital) as a powerful probe of evolving structural dynamics.

### IV. References:

1. Cvetanović, R. J. Evaluated Chemical Kinetic Data for the Reactions of Atomic Oxygen O ( 3P ) with Unsaturated Hydrocarbons Evaluated chemical kinetic data for the reactions of atomic oxygen O ( 3P ) with unsaturated hydrocarbons. *J. Phys. Chem. Ref. Data* **16**, 261 (1987).
2. Savee, J. D. *et al.* Multiplexed Photoionization Mass Spectrometry Investigation of the O( 3 P ) + Propyne Reaction. *J. Phys. Chem. A* **119**, 7388–7403 (2015).
3. Savee, J. D., Welz, O., Taatjes, C. A. & Osborn, D. L. New mechanistic insights to the O(3P) + propene reaction from multiplexed photoionization mass spectrometry. *Phys. Chem. Chem. Phys.* **14**, 10410 (2012).
4. Baulch, D. L. Evaluated Kinetic Data for Combustion Modeling: Supplement II. *J. Phys. Chem. Ref. Data* **34**, 757 (2005).
5. Osborn, D. L. *et al.* The multiplexed chemical kinetic photoionization mass spectrometer: A new approach to isomer-resolved chemical kinetics. *Rev. Sci. Instrum.* **79**, 104103 (2008).
6. Cvetanović, R. J., Ring, D. F. & Doyle, L. C. Reaction of oxygen atoms with cyclopentene. *J. Phys. Chem.* **75**, 3056 (1971).
7. Hoyermann, K., Nothdurft, J., Olzmann, M., Wehmeyer, J. & Zeuch, T. Formation and decomposition of chemically activated cyclopentoxy radicals from the *c*-C<sub>5</sub>H<sub>9</sub> + O reaction. *J. Phys. Chem. A* **110**, 3165–3173 (2006).
8. Zhao, H., Liu, K., Song, D. & Su, H. Nonadiabatic reaction mechanisms of the O((3)P) with cyclopentene. *J. Mol. Graph. Model.* **51**, 184–192 (2014).
9. Coe, J. D. & Martínez, T. J. Ab initio molecular dynamics of excited-state intramolecular proton transfer around a three-state conical intersection in malonaldehyde. *J. Phys. Chem. A* **110**, 618–630 (2006).
10. Upadhyaya, H. P., Kumar, A. & Naik, P. D. Photodissociation dynamics of enolic acetylacetone at

- 266, 248, and 193 nm: Mechanism and nascent state product distribution of OH. *J. Chem. Phys.* **118**, 2590 (2003).
11. Katayanagi, H., Mo, Y. & Suzuki, T. 223 nm photodissociation of OCS. Two components in S(1D2) and S(3P2) channels. *Chem. Phys. Lett.* **247**, 571–576 (1995).
  12. Suzuki, T., Katayanagi, H., Nanbu, S. & Aoyagi, M. Nonadiabatic bending dissociation in 16 valence electron system OCS. *J. Chem. Phys.* **109**, 5778–5794 (1998).



## Photoinitiated Reactions of Radicals and Diradicals in Molecular Beams

Hanna Reisler

Department of Chemistry, University of Southern California

Los Angeles, CA 90089-0482

reisler@usc.edu

### Program Scope

Open shell species such as radicals, diradicals and excited electronic states are central to reactive processes in combustion and environmental chemistry. Our program is concerned with photoinitiated reactions of radicals, carbenes, and other open shell species. The goal is to investigate the detailed dynamics of dissociation of species in which multiple pathways participate, including molecular rearrangements, and compare them with high-level calculations. Studies include unimolecular reactions on the ground state as well as photodissociation dynamics on excited Rydberg and valence states that involve multiple potential energy surfaces.

### Recent Progress

#### Photodissociation of Highly Vibrationally Excited CO<sub>2</sub>

Last year we described preliminary results on the 205-230 nm photodissociation of vibrationally excited CO<sub>2</sub> at temperatures up to 1800 K. CO<sub>2</sub> molecules seeded in He were heated in a SiC tube attached to a pulsed valve and supersonically expanded to create a molecular beam of rotationally cooled but vibrationally hot CO<sub>2</sub>. Photodissociation was observed from vibrationally excited CO<sub>2</sub> with internal energies up to about 20,000 cm<sup>-1</sup>, and CO(*X*<sup>1</sup>Σ<sup>+</sup>), O(<sup>3</sup>P) and O(<sup>1</sup>D) products were detected by 2+1 REMPI. The large enhancement in the absorption cross-section with increasing CO<sub>2</sub> vibrational excitation made this investigation feasible. The internal energies of heated CO<sub>2</sub> molecules that absorbed 230 nm radiation were estimated from the kinetic energy release (KER) distributions of CO(*X*<sup>1</sup>Σ<sup>+</sup>) products in *v*" = 0. We found that at 230 nm, CO<sub>2</sub> needs to have at least 4,000 cm<sup>-1</sup> of rovibrational energy to absorb the UV radiation and produce CO(*X*<sup>1</sup>Σ<sup>+</sup>) + O(<sup>3</sup>P). CO<sub>2</sub> internal energies in excess of 16,000 cm<sup>-1</sup> were confirmed by observing O(<sup>1</sup>D) products. The CO product internal energy distributions changed with increasing CO<sub>2</sub> temperature, suggesting the participation of more than one dynamical pathway when the internal energy of the parent CO<sub>2</sub> (and the corresponding available energy) increases. The KER distributions of O(<sup>1</sup>D) and O(<sup>3</sup>P) showed broad internal energy distributions in the CO(*X*<sup>1</sup>Σ<sup>+</sup>) cofragment, extending up to the maximum allowed by energy but peaking at low KER values.

We have now completed the study, and below we discuss the implications of our observations to the dissociation mechanism of CO<sub>2</sub>. In addition, we describe aspects of the 2+1 REMPI spectroscopy of CO at ~230 nm, which are still poorly understood.

The CO product energy distributions determined by velocity map imaging (VMI) of O(<sup>3</sup>P) fragments demonstrate the increased complexity of the dissociation dynamics at higher temperatures, and suggest that bending and stretch excitation of ground state CO<sub>2</sub> influence the dissociation efficiency and dynamics. With low CO<sub>2</sub> heating, the KER distributions obtained by monitoring O(<sup>3</sup>P) are broad and unstructured, corresponding to highly rovibrationally excited CO cofragments. At higher temperatures, a second unstructured component centered at high KER values appears, indicating the opening of another, more direct, dissociation pathway. Following 205 nm photodissociation, the KER distributions obtained by monitoring the O(<sup>1</sup>D) fragment, which have 16,000 cm<sup>-1</sup> internal energy, peak at lower KER values but



extend up to about  $6000\text{ cm}^{-1}$ . These distributions show that CO fragments associated with the  $\text{O}(^1\text{D}) + \text{CO}$  channel are also born with a broad distribution of rovibrational levels.

Several theoretical studies have focused on the excited electronic states of  $\text{CO}_2$  at 4-9 eV, and on the interactions among states involved in the dissociation (see Fig. 1).<sup>1</sup> It was concluded in theoretical and experimental studies that whereas absorption is mainly to the  $A^1B_2$  state at the vertical maximum, at longer wavelengths the  $B^1A_2$  state can be excited as well, and the long wavelength absorption spectrum reflects also mixing between the  $A^1B_2$  and the ground state.<sup>1,2</sup> The energy differences between the ground and excited states decrease with decreasing OCO bond angle, e.g. with increased bending excitation in the

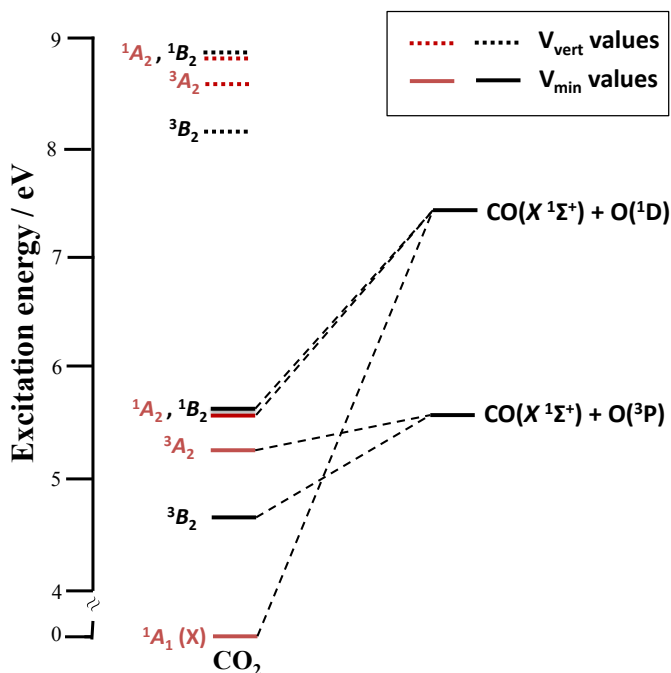


Fig. 1. Energy diagram showing adiabatic ( $V_{\min}$ , solid line) and vertical ( $V_{\text{vert}}$ , dotted line) energies of the excited electronic states of  $\text{CO}_2$  listed in Ref. 1. *A* and *B* states are shown in red and black, respectively.

In our experiments, a likely reason for the reduced anisotropy is also the concurrent excitation of the  $A^1B_2$  and  $B^1A_2$  states. Schmidt et al. showed that at long wavelengths there are reasonable transition dipole moments (TDMs) to both these states, and bending and asymmetric stretch excitations increase the TDM to  $^1A_2$ .<sup>1</sup> Spielfiedel *et al.* assigned a long bending progression of perpendicular vibronic bands to transitions to the  $B^1A_2$  state at the long wavelength absorption tail, in addition to the main bands to the  $A^1B_2$  excited state.<sup>2</sup> The nearly isotropic KER distributions of the products measured in our experiments suggest that these two excited states participate in the initial electronic excitation, and this may be a major cause for the reduction in anisotropy.

The main photodissociation products observed in our studies derive from the spin-forbidden channel, and therefore the reverse spin-forbidden recombination reaction,  $\text{O}(^3\text{P}) + \text{CO}$ , is also relevant. The recent theoretical papers that examined the recombination reaction, identified spin-orbit couplings and conical intersections, and suggested that more than one reaction mechanism is involved.<sup>3,4</sup> These papers describe

the ground electronic state. Due to more favorable FC factors, vibrationally excited  $\text{CO}_2$  molecules absorb 205-230 nm radiation more efficiently, allowing studies of  $\text{CO}_2$  photodissociation closer to the origins ( $V_{\min}$ ) of the lowest excited states and to the dissociation threshold, where the  $\text{O}(^3\text{P}) + \text{CO}$  channel dominates.

Notably, the images recorded in our experiments are nearly isotropic ( $\beta \sim 0$ ), even though dissociation is fairly fast. A common reason for an isotropic product angular distribution is a dissociation lifetime that is longer than the rotational period of the molecule. In our case, the dissociation lifetime is unknown, and the average classical rotational period of  $\text{CO}_2$  molecules at 100 K is roughly 0.9 ps. This may cause some decrease from the maximum recoil anisotropy value of 2.0 for a parallel transition. Another plausible argument is that dissociation occurs from bent vibrational configurations or high rotational levels that reduce the anisotropy by changing the fragments' recoil direction.

the participation of a direct (or non-statistical) mechanism, which is too fast to allow for randomization of energy, and an indirect (or statistical-like) route, in which at least some energy randomization takes place. The exact nature of the dynamics via these two pathways is not settled yet, but both the  $a^3B_2$  and  $b^3A_2$  triplet states are shown to be involved in the spin-forbidden reaction  $O(^1D) + CO \rightarrow CO + O(^3P)$ .<sup>3,4</sup> The existence of multiple dynamical channels is amply evidenced in the observed KER distributions of the CO and O products, and also in the CO REMPI spectra obtained as a function of CO<sub>2</sub> heating. In photodissociation events that start closer to the reaction threshold, as is the case in our work, it is not hard to imagine that following initial excitation to either the  $A^1B_2$  or  $B^1A_2$  state or both, the  $a^3B_2$  and  $b^3A_2$  triplet states and even the ground electronic state are involved, giving rise to multiple crossings and dissociation pathways that depend sensitively on initial vibrational excitation of parent CO<sub>2</sub>.

The 2+1 REMPI spectra of the CO products show that  $v''=0$  and 1 are generated each with a broad distribution of rotational states, and that the rotational distribution in  $v''=0$  is bimodal and can be fit with a  $\sim 1700$  K Boltzmann component at low to medium  $J''$  levels, and a narrow Gaussian-shaped component centered at  $J'' > 40$ . The 2+1 REMPI identification of higher vibrational levels is hampered by uncertainties in the spectroscopic constants of CO as described below.

### Uncertainties in the 2+1 REMPI spectroscopy of the CO products at $\sim 230$ nm

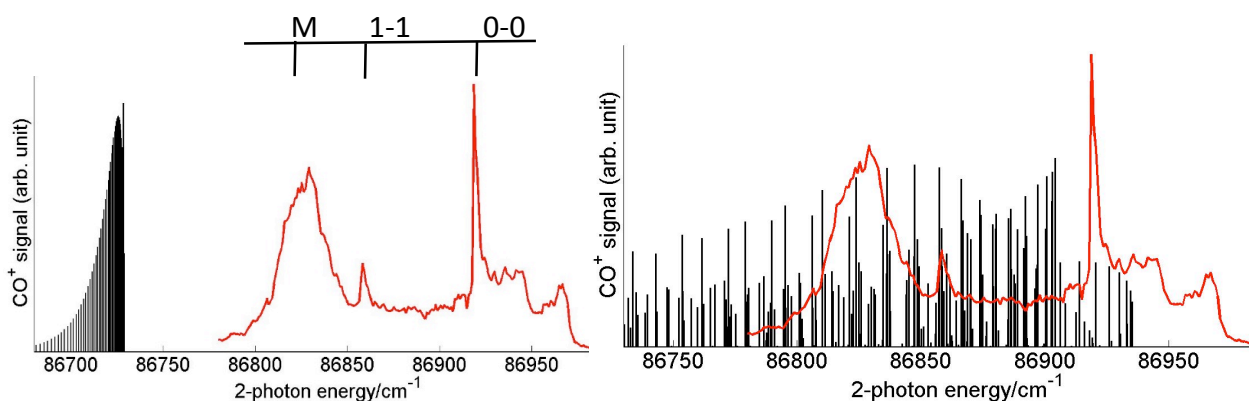


Fig. 2. The red spectrum shows the measured 2+1 REMPI spectrum of the CO product recorded with high heating of the CO<sub>2</sub> parent. The  $B^1\Sigma^+ \leftarrow X^1\Sigma^+$  0-0 and 1-1 vibronic transitions are indicated on the left panel. The assignment of the M band is uncertain. On the left, a simulated spectrum of the  $B^1\Sigma^+ \leftarrow X^1\Sigma^+$  2-2 band is shown at 1700 K, and on the right, the  $k^3\Pi \leftarrow X^1\Sigma^+$  1-2 vibronic band is simulated at 500 K.

In Fig. 2 the CO 2+1 REMPI spectrum obtained with high heating of CO<sub>2</sub> is shown in red. Whereas the spectra associated with  $v'' = 0$  and 1 are clear and easily simulated by using the known spectroscopic constants of the  $B^1\Sigma^+ \leftarrow X^1\Sigma^+$  0-0 and 1-1 vibronic transitions, the origin of the broad spectral feature with a maximum at  $\sim 86,830$  cm<sup>-1</sup> (denoted henceforth by M) remains puzzling. This feature appears only at mass 28 in the time-of-flight mass spectrum, and only in the photolysis of hot CO<sub>2</sub>. It has been observed before in the 193 nm photodissociation of HNCO and assigned tentatively as the 2-2 vibronic band of the  $B \leftarrow X$  transition. However, we could not reproduce this feature using the known spectroscopic constants of the  $B \leftarrow X$  transition (see Fig. 2 left panel). The  $B$  state is severely predissociated at  $v' > 1$ , and as a result, the assignments of the band origins of the  $B \leftarrow X$  vibronic transitions involving  $v' > 1$  are quite uncertain. Using the known spectroscopic constants of the ground state, and the experimental values for the  $v'$  levels in the  $B$  state, we have estimated the band origin frequencies of diagonal transitions from 2-2 to 9-9 and none fits the M feature. The 2-2 band spectral simulation is shown in Fig. 2. It is possible that the M band originates in a different electronic transition than  $B \leftarrow X$ . The three electronic states closest to this

energy region are  $k^3\Pi$ ,  $C^1\Sigma_g^+$  and  $E^1\Pi$ . The different vibronic transitions were estimated from the known spectroscopic constants of these states. The only transition close to the M band is  $k(v'=1) \leftarrow X(v''=2)$ . The 500 K thermal rotational distribution of this vibronic transition is simulated (using PGOPHER) and shown in the right panel of Fig. 2. The simulated REMPI spectrum spans frequencies extending from near the bandhead of the 0-0 peak of the  $B \leftarrow X$  transition to the low frequency end of the observed M band. The peak of the M band corresponds to  $J'' = 5-10$  of  $v''=2$  of the ground state. This transition may contribute to the REMPI signal originating in  $v''=2$  of CO, but other (yet unknown) transitions may contribute as well.

The KER distribution obtained by monitoring the peak of the M band exhibits only a fairly sharp feature centered at  $5000\text{ cm}^{-1}$ , with a  $1000\text{ cm}^{-1}$  width. Similar KER features centered at  $5000\text{ cm}^{-1}$  appear in images obtained by monitoring the bandheads of the 1-1 and 0-0 transitions with high CO<sub>2</sub> heating, but not in those obtained by monitoring higher rotational levels of the 0-0 band (higher energies in Fig. 2). We conclude that the M band extends to frequencies that overlap the 0-0 and 1-1 bands, and that a different dissociation mechanism, presently unknown, gives rise to the feature centered at  $\sim 5000\text{ cm}^{-1}$ .

### Future Work

We plan to elucidate the effect of vibrational excitation on CO<sub>2</sub> photodissociation dynamics by using vibrationally-mediated photodissociation. Several singlet and triplet states of CO<sub>2</sub> are located near the bright singlet state, and these states interact by conical intersections and spin-orbit couplings with other singlet and triplet states, including the ground state. Theoretical calculations identify multiple surface crossings.<sup>1-4</sup> Conical intersections are predicted to be strongest for CO<sub>2</sub> with bent and asymmetric stretch excitations, and hence state specific effects are expected. We have also initiated work on the state-specific dissociation and isomerization of HCOH on the ground and electronic excited states. We plan to characterize CO<sub>2</sub> and HCOH as products of the UV photolysis of glyoxylic and pyruvic acids.

### References

1. Schmidt, J. A.; Johnson, M. S.; Schinke, R., *Proc. Natl. Acad. Sci. USA* **2013**, *110* (44), 17691-17696.
2. Spielfiedel, A.; Feautrier, N.; Cossart-Magos, C.; Chambaud, G.; Rosmus, P.; Werner, H. J.; Botschwina, P., *J. Chem. Phys.* **1992**, *97* (11), 8382-8388.
3. Jasper, A. W., Dawes, R., *J. Chem. Phys.* **2013**, *139*, 154313.
4. Hwang, D.-Y.; A. M. Mebel, A. M., *Chem. Phys.* **2000**, *256*, 169.

### Publications, 2014-2017

1. C.P. Rodrigo, S. Sutradhar, and H. Reisler, "Imaging studies of excited and dissociative states of hydroxymethylene produced in the photodissociation of the hydroxymethyl radical", *J. Phys. Chem. A* (Yarkonly Festschrift), *118*(51), 11916-11925 (2014).
2. S. Sutradhar, B.R. Samanta, A.K. Samanta, and H. Reisler, "Temperature dependence of the photodissociation of CO<sub>2</sub> from high vibrational levels: 205-230 nm imaging studies of CO( $X^1\Sigma^+$ ) and O( $^3P$ ,  $^1D$ ) products", *J. Chem. Phys.* (in press).

## Active Thermochemical Tables

Branko Ruscic  
Chemical Sciences and Engineering Division, Argonne National Laboratory,  
9700 South Cass Avenue, Argonne, IL 60439  
ruscic@anl.gov

### Program Scope

The *spiritus movens* of this program is the need to provide the scientific community with accurate and reliable thermochemical information on chemical species that are relevant in combustion or play prominent roles in related post-combustion environmental chemistry. Detailed knowledge of thermodynamic parameters for a broad array of stable and ephemeral chemical species is pivotal to chemistry and essential in many industries. In particular, the availability of accurate, reliable, and internally consistent thermochemical values is a *conditio sine qua non* in kinetics, reaction dynamics, formulation of plausible reaction mechanisms, and construction of predictive models of complex chemical environments. In addition, the availability of accurate thermochemical values has historically been the prime driver for steady advancement of increasingly sophisticated electronic structure theories.

The focus of this program is on bringing substantial innovations to the field of thermochemistry through development of new methodologies, and utilizing them to systematically improve both the quality and quantity of available thermochemical data relevant to energy-producing processes. In order to achieve the stated goals, this program has developed a novel approach that is centered on analyzing and optimally utilizing the information content of *all available* thermochemically relevant determinations. The aim is not only to dynamically produce the best currently possible thermochemical parameters for the targeted chemical species, but also to allow efficient updates with new knowledge, properly propagating its consequences through all affected chemical species, as well as to provide critical tests of new experimental or theoretical data, and, when possible, to develop pointers to additional determinations that are most likely to efficiently improve the overall thermochemical knowledge base. In order to provide a broad perspective of this area of science, the effort of this program is synergistically coordinated with related experimental and theoretical efforts within the Gas-Phase Chemical Dynamics Group at Argonne.

### Recent Progress

Over the past year we have continued the development of various aspects of Active Thermochemical Tables (ATcT). ATcT are a new paradigm for developing accurate and reliable thermochemical values for stable and reactive chemical species. With very few exceptions, enthalpies of formation are not directly measured quantities. Rather, they are intrinsically defined via intricate manifolds of intertwined dependencies. Thermochemical determinations (such as reaction enthalpies, equilibrium constants, bond dissociation energies, etc.) involve simultaneously several chemical species, and thus define the enthalpy of formation of the target chemical species only *relative* to other species. Historically, extracting the enthalpies of formation from intertwined (and frequently inconsistent) dependencies was viewed as an intractable proposition, resulting in the adoption of a simplified *sequential* approach of inferring the enthalpies of formation one at the time (A begets B, B begets C, etc.), which is bound to produce static sets of enthalpies of formation that contain hidden progenitor-progeny relationships and are thus impossible to update with new knowledge without introducing new inconsistencies. The success of ATcT is rooted in treating the intertwined determinations as a network of simultaneous dependences that is amenable to mathematical and statistical manipulation, effectively converting the originally intractable problem into an information-rich environment that drives the quantum leap in the quality and reliability of the resulting thermochemistry. The Thermochemical Network (TN) represents a system of qualified constraints that have to be simultaneously satisfied to produce a set of enthalpies of formation that correctly reflects the entire knowledge content of the TN, providing that the individual uncertainties associated with the determinations present in the TN are realistic. Because of the unavoidable presence of determinations with 'optimistic' uncertainties (i.e. erroneous determinations), ATcT first performs an iterative analysis, which isolates them and brings the TN to self-consistency. Once self-consistency is

achieved, ATcT proceeds to solve the TN simultaneously for all included species.

We are currently working on ver. 1.122i of the ATcT TN. Version 1.122 of the TN (containing 1183 species) originally started as the source of the best currently available 0 K and 298 K thermochemistry for a group of essential combustion-related species that can be obtained if one starts with three prototypical fuels: methane, ethane, or methanol, and considers all possible sequences of bond dissociations, producing  $\text{CH}_n$ ,  $n = 4 - 0$  (methane, methyl, methylene, methylidyne, and carbon atom),  $\text{C}_2\text{H}_n$ ,  $n = 6 - 0$  (ethane, ethyl, ethylene, ethylidene, vinyl, ethylidyne, acetylene, vinylidene, ethynyl, and ethynylene),  $\text{COH}_n$ ,  $n = 4 - 0$  (methanol, hydroxymethyl, methoxy, formaldehyde, hydroxymethylene, formyl, isoformyl, and carbon monoxide), as well as  $\text{OH}_n$ ,  $n = 2 - 0$  (water, hydroxyl, oxygen atom), and carbon dioxide. This version of the TN was subsequently expanded (ver. 1.122a and 1.122b) to produce the best currently available energy of the prototypical  $\text{HCN} \leftrightarrow \text{HNC}$  isomerization (both species are playing important roles not only in  $\text{NO}_x$ -related combustion processes, but also in many other areas of chemistry, including astrochemistry). Version 1.122b was further expanded in various additional projects over the last year (some of which are mentioned below), leading to the current ver. 1.122i, which at last count includes no less than 1625 species (corresponding to a rather spectacular growth by 37%), interlinked by >21,000 active determinations (as well as several thousand additional determinations that have been rendered inactive).

One important background activity during this project, which is necessary in order to allow ATcT to produce as accurate values as possible even at elevated temperatures, consisted of improving the ubiquitous RRHO partition functions for the target species to non-rigid-rotator anharmonic-oscillator (NRRAO) partition functions. In ATcT, these are obtained by incorporating first- (NRRAO1) or second-order (NRRAO2) anharmonic corrections to the initial RRHO partition function (which itself is based on fundamental frequencies and ground-state rotational constants), and including further corrections for effects of rotation-vibration interaction, centrifugal distortion, Darling-Dennison and Fermi resonances, as well as the Strip-Kirkwood correction. At the lowest temperatures the NRRAO partition function is combined with direct counts. For internal rotors and inversions the corrections are typically obtained by replacing the corresponding contribution of the mode with a direct count of the corresponding levels. If the mode is approximately separable, this involves computing the potential energy along that mode and solving it, and then computing the relevant contribution to the partition function (and its first and second derivative) by a level count. However, there is a considerable number of species where the targeted mode is strongly coupled to some other mode. Textbook examples are the hydroxymethyl and ethyl radical, where the internal rotor motion strongly couples to the  $\text{CH}_2$  wag, and the molecule undergoes a complex periodic motion that involves a partial internal rotation in synchrony with a wag. We are currently making progress in the development of the practical details of a generally applicable approach that involves computing to sufficiently high energies the appropriate a 2D (or higher) potential energy surface (in collaboration with L. Harding), extracting from it the proper DVR grid, and solving it.

In general, the effects of anharmonicity can be rather pronounced, particularly at higher temperatures relevant in combustion. Anharmonicity normally increases the density of states at excitation energies relevant to combustion temperatures, leading to heat capacities and enthalpy increments that exceed those predicted by RRHO, such as, for example, in methylene. However, in some cases the opposite is true, as in methyl, where the inversion mode leads to a decrease in the relevant density of states, producing heat capacities lower than the RRHO prediction. The consequences of the ATcT thermochemistry (which includes NRRAO partition functions) for several fundamental combustion species - including these two - are currently being probed in interpretations of kinetic measurements in collaboration with R. Tranter, and in several combustion models in collaboration with R. Sivaramakrishnan, N. Labbe, S. Klippenstein, and A. Jasper. So far, the tests indicate that the new ATcT thermochemistry has a rather significant effect on combustion modeling, changing, for example, the flame speed in existing  $\text{CH}_4$ /air combustion models by as much as 30%, but also strongly suggesting that the important rate of recombination of  $\text{CH}_3 + \text{H}$ , which is normally derived from the forward (dissociation) rate of  $\text{CH}_4$  and the equilibrium constant, needs to be seriously reevaluated. The new ATcT thermochemistry changes the high-temperature equilibrium concentration of  $\text{CH}_3$ , which cascades further down the relevant chemical mechanisms, impacting the

concentration and chemistry of methylene and other small carbon-containing species.

On the front of disseminating the ATcT values, including interim results for species that have not been yet completely ‘finalized’, we have continued to maintain and expand our website, ATcT.anl.gov, which lately receives about 100 unique visitors per day. As requested by popular demand, the website has now a search function (based on the full ATcT Species Dictionary). Another important recent expansion of the web-available content is the addition of the provenance of the listed ATcT enthalpy of formation for each chemical species, implemented by extending the current website information for TN ver. 1.118. In sequential thermochemistry, the provenances are usually rather succinct and straightforward. In contrast to this, the provenances of ATcT values are typically highly distributed, sometimes over a hundred or more relevant determinations. The distributed provenance is one of the important factors contributing to the robustness of ATcT values, since this insures that the value does not critically depend on any single determination (unlike values obtained by sequential thermochemistry). We are currently preparing the ATcT results from TN ver. 1.122 and 1.122b for web release. These versions will continue to have the search capabilities, as well as the per-species provenance information. However, we are working on adding other helpful information for each species, such as the list of the most strongly correlated species, a list of high-leverage determinations involving the relevant species (based on analyzing the hat-matrix, with some guidance from M. Davis), as well as a visual display of the species geometry.

We also have a number of ongoing national and international collaborations. One such collaboration, with P. Glarborg at DTU and with the Italian team at the Politecnico di Milano, aims to improve  $C_0$ ,  $C_1$ , and higher mechanisms using ATcT thermochemistry. Another collaboration with P. Glarborg relates to the thermochemistry of  $NO_x$  species in combustion. With G. Bacskay and K. Peterson we are working on developing high-accuracy computational results for I and Br-containing species. Finally, we have developed a very active ATcT Task Group involving J. Stanton, T. L. Nguyen, G. B. Ellison, J. Baraban, B. Changala, and their students, and are in the process of establishing two more ATcT Workgroups involving PIs and their students, one with K. Peterson, and another with R. Dawes.

### Future Plans

Future plans of this program pivot around further development and expansion of the Active Thermochemical Tables approach, continuing to provide accurate thermochemistry, and driving targeted thermochemically-relevant theoretical and experimental investigations of radicals and transient species that are intimately related to combustion and post-combustion atmospheric processes. A significant part of the effort during the forthcoming period will be focused on continued ‘finalization’ and dissemination of the resulting ATcT thermochemistry. A crucial component of the process of ‘finalization’ of results (usually done on a group of related chemical species) consists of testing and analyzing their TN dependencies (in part by using the variance/covariance decomposition approach and exploring the influences of related determinations via a hat-matrix analysis) as well as enhancing the accuracy of their partition functions (by gradually replacing them with fully corrected NRRAO partition functions), and, when suggested by ATcT analyses, adding new high-quality results (either virtual, i.e. computational, or actual, i.e. experimental) to coerce the resulting thermochemistry toward stable, ‘release quality’ values. This iterative process unavoidably results in an expansion of the TN with new related chemical species, which is an added benefit. Another important component in the future plans is the continuation of the current effort of designing and producing a computer-generated web site that will display the current ATcT thermochemistry, as well as the pertinent metadata, with a rigorous archival capability. One set of pertinent metadata that we will continue generating relates to documenting the provenance for each thermochemical value, which entails a variance decomposition analysis for each of the chemical species. Finally, a significant long-term component of future progress consists in developing the next generation of ATcT software. This will be based on further overhaul of the ATcT kernel, with the aim of making the software even more efficient and streamlined, but also allowing sufficient flexibility that will enable the adoption and utilization of emerging computing technologies as they become available.

*This work is supported by the U.S. Department of Energy, Office of Basic Energy Sciences, Division of Chemical Sciences, Geosciences, and Biosciences, under Contract No. DE-AC02-06CH11357.*

## Publications resulting from DOE sponsored research (2014 – present)

- *Extended Third Millennium Ideal Gas and Condensed Phase Thermochemical Database for Combustion with updates from Active Thermochemical Tables*, E. Goos, A. Burcat, and B. Ruscic (2014); (includes complete ATcT values from TN ver. 1.112); progressive updates are currently available at <http://burcat.technion.ac.il/dir/> and mirrored at <http://garfield.chem.elte.hu/Burcat/burcat.html>
- *Improved Accuracy Benchmarks of Small Molecules Using Correlation Consistent Basis Sets*, D. Feller, K. A. Peterson, and B. Ruscic, *Theor. Chem. Acc.* **133**, 1407/1-16 (2014), DOI: 10.1007/s00214-013-1407-z
- *Active Thermochemical Tables: Dissociation Energies of Several Homonuclear First-Row Diatomics and Related Thermochemical Values*, B. Ruscic, D. Feller, and K. A. Peterson, *Theor. Chem. Acc.* **133**, 1415/1-12 (2014), DOI: 10.1007/s00214-013-1415-z
- *Uncertainty Quantification in Thermochemistry, Benchmarking Electronic Structure Computations, and Active Thermochemical Tables*, B. Ruscic, *Int. J. Quantum Chem.* **114**, 1097-1101 (2014), DOI: 10.1002/qua.24605
- *Electronic States of the Quasilinear Molecule Propargylene (HCCCH) from Negative Ion Photoelectron Spectroscopy*, D. L. Osborn, K. M. Vogelhuber, S. W. Wren, E. M. Miller, Y.-J. Lu, A. S. Case, L. Sheps, R. J. McMahon, J. F. Stanton, L. B. Harding, B. Ruscic, and W. C. Lineberger, *J. Am. Chem. Soc.* **136**, 10361-10372 (2014), DOI: 10.1021/ja5039984
- *Active Thermochemical Tables enthalpies of formation based on ver. 1.112 of the Thermochemical Network*, B. Ruscic, <http://atct.anl.gov/Thermochemical%20Data/version%201.112/> (2014)
- *High-Temperature Chemistry of HCl and Cl<sub>2</sub>*, M. Pelucchi, A. Frassoldati, T. Faravelli, B. Ruscic, and P. Glarborg, *Combust. Flame* **162**, 2693-2704 (2015), DOI: 10.1016/j.combustflame.2015.04.002
- *IUPAC Technical Report: Standard Electrode Potentials Involving Radicals in Aqueous Solution: Inorganic Radicals*, D. A. Armstrong, R. E. Huie, W. H. Koppenol, S. V. Lyman, G. Merényi, P. Neta, B. Ruscic, D. M. Stanbury, S. Steenken, and P. Wardman, *Pure Appl. Chem.* **87**, 1139-1150 (2015), DOI: 10.1515/pac-2014-0502
- *Active Thermochemical Tables: Sequential Bond Dissociation Enthalpies of Methane, Ethane, and Methanol and the Related Thermochemistry*, B. Ruscic, *J. Phys. Chem. A* **119**, 7810-7837 (2015), DOI: 10.1021/acs.jpca.5b01346
- *Thermal Dissociation and Roaming Isomerization of Nitromethane: Experiment and Theory*, C. J. Annesley, J. B. Randazzo, S. J. Klippenstein, L. B. Harding, A. W. Jasper, Y. Georgievski, B. Ruscic, and R. S. Tranter, *J. Phys. Chem. A* **119**, 7872-7893 (2015), DOI: 10.1021/acs.jpca.5b01563
- *On the HCN – HNC Energy Difference*, T. L. Nguyen, J. H. Baraban, B. Ruscic, and J. F. Stanton, *J. Phys. Chem. A* **119**, 10929–10934 (2015), DOI: 10.1021/acs.jpca.5b08406
- *Active Thermochemical Tables (ATcT) Enthalpies of Formation Based on version 1.118 of the Thermochemical Network (with a New Search Functionality Based on the ATcT Species Dictionary)*, B. Ruscic and D. H. Bross, <http://atct.anl.gov/Thermochemical%20Data/version%201.118/> (2016)
- *Extension of Active Thermochemical Tables (ATcT) Values ver. 1.118 with Provenances of the Enthalpies of Formation Based on Variance Decomposition Analysis and References*, B. Ruscic and D. H. Bross, <http://atct.anl.gov/Thermochemical%20Data/version%201.118/index.php> (2016)
- *Active Thermochemical Tables Kernel Software ver.1.50*, B. Ruscic and D. H. Bross, Argonne National Laboratory, Argonne, Ill. (2016) (64-bit, platform independent, parallelized overhaul of the original 32-bit Windows sequential ATcT Kernel Software)
- *Bond Dissociation Energies for Diatomic Molecules Containing 3d Transition Metals: Benchmark Scalar-Relativistic Coupled-Cluster Calculations for Twenty Molecules*, L. Cheng, J. Gauss, B. Ruscic, P. Armentrout, and J. Stanton, *J.Chem. Theory Computat.* **13**, 1044-1056 (2017), DOI: 10.1021/acs.jctc.6b00970
- *A Vacuum Ultraviolet laser Pulsed Field Ionization-Photoion Study of Methane (CH<sub>4</sub>): Determination of the Appearance Energy of Methylum From Methane with Unprecedented Precision and the Resulting Impact on the Bond Dissociation Energies of CH<sub>4</sub> and CH<sub>4</sub><sup>+</sup>*, Y.-C. Chang, B. Xiong, D. H. Bross, B. Ruscic, and C. Y. Ng, *Phys. Chem. Chem. Phys.* **19**, 9592-9605 (2017), DOI: 10.1039/c6cp08200a
- *An Experimental and Theoretical Study of the Thermal Decomposition of C<sub>4</sub>H<sub>6</sub> Isomers*, J. P. A. Lockhart, C. F. Goldsmith, J. B. Randazzo, B. Ruscic, and R. S. Tranter, *J. Phys. Chem. A* (in press) (2017)
- *Thermal Decomposition of Potential Ester Biofuels, Part I: Methyl Acetate and Methyl Butanoate*, J. P. Porterfield, D. H. Bross, B. Ruscic, J. H. Thorpe, T. L. Nguyen, J. H. Baraban, J. F. Stanton, J. W. Daily, and G. B. Ellison, *J. Chem. Phys. A* (submitted) (2017)

# GAS-PHASE MOLECULAR DYNAMICS: HIGH RESOLUTION SPECTROSCOPY AND COLLISION DYNAMICS OF TRANSIENT SPECIES

Trevor J. Sears  
Chemistry Division, Brookhaven National Laboratory  
Upton, NY 11973-5000  
[sears@bnl.gov](mailto:sears@bnl.gov)

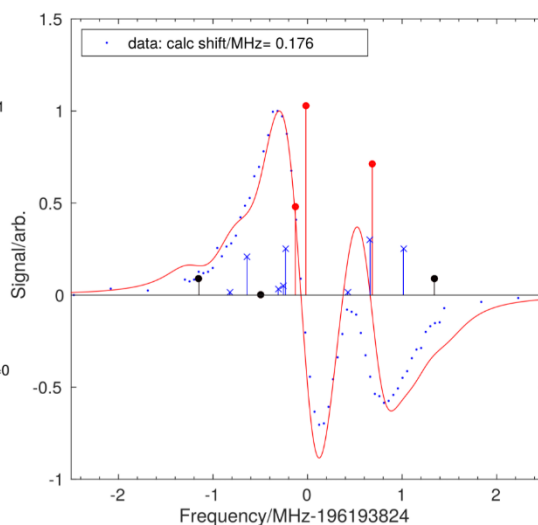
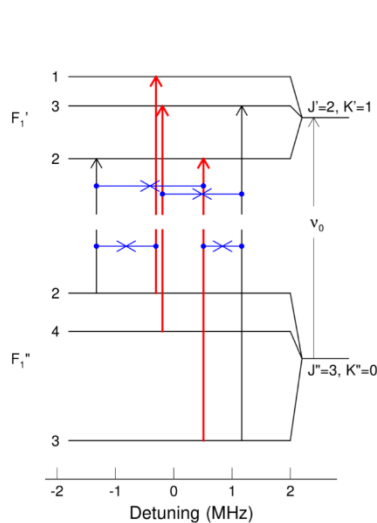
## Program Scope

This research is carried out as part of the Gas-Phase Molecular Dynamics program in the Chemistry Division at Brookhaven National Laboratory. High-resolution spectroscopic methods, augmented by theoretical and computational work, are used to investigate the structure, collision dynamics and chemical behavior of intermediates in the elementary gas-phase reactions involved in combustion chemistry. There is an emphasis on new technique development with the aim of improving both the sensitivity and resolution of spectroscopic measurements.

## I. Recent Progress

### A. $^{14}\text{N}$ quadrupole splittings in the near-IR spectrum of $\text{NH}_3$

Sub-Doppler, saturation dip, spectra of lines in the  $\nu_1 + \nu_3$ ,  $\nu_1 + 2\nu_4$  and  $\nu_3 + 2\nu_4$  bands of  $^{14}\text{NH}_3$  have been measured by frequency comb-referenced diode laser absorption spectroscopy. The observed spectral line widths are due to a combination of transit time broadening and residual lifetime broadening due to large cross-section velocity changing collisions. They show resolved or partially-resolved hyperfine splittings that are primarily determined by the  $^{14}\text{N}$  quadrupole coupling. Modeling of the observed line shapes based on the known hyperfine level structure of the ground state of the molecule shows that, in nearly all cases, the excited state level has hyperfine splittings similar to the same rotational level in the ground state. The data provide accurate frequencies for the line positions and easily separate lines overlapped in the most precise Doppler-limited spectra. The observed hyperfine splittings are diagnostic to the rotational quantum number change in the transition and can be used to confirm or refute rotational assignments. Ground state combination differences obtained from the measured frequencies are comparable in accuracy to those obtained from conventional microwave spectroscopy. Several of the measured transitions do not show the quadrupole hyperfine splittings expected based on their existing rotational assignments. Either the assignments are incorrect or (less likely) the upper levels involved are perturbed in a way that affects the



nuclear hyperfine structure.

The figure shows the quadrupole hyperfine structure for the  $P(3,0)$  transition in the  $\nu_1 + \nu_3$  band at 196 193 824. 176(30) GHz and how transitions between the different components build up to give the observed saturation dip spectrum (blue dots) in the right hand panel. Crossover resonances which share a common upper or lower hyperfine



component, shown in blue in the simulation, contribute significantly to the observed line shape in which the  $\Delta J = \Delta F_1$  transitions are the strongest and shown in red. Here,  $F_1$  is the resultant of the rotational angular momentum,  $J$ , and the nuclear spin,  $I_N$ , of the nitrogen nucleus. The calculated profile is not exactly as the observed spectrum, probably due to subtle changes in the quadrupole coupling compared to the ground state, in the excited vibrational level.

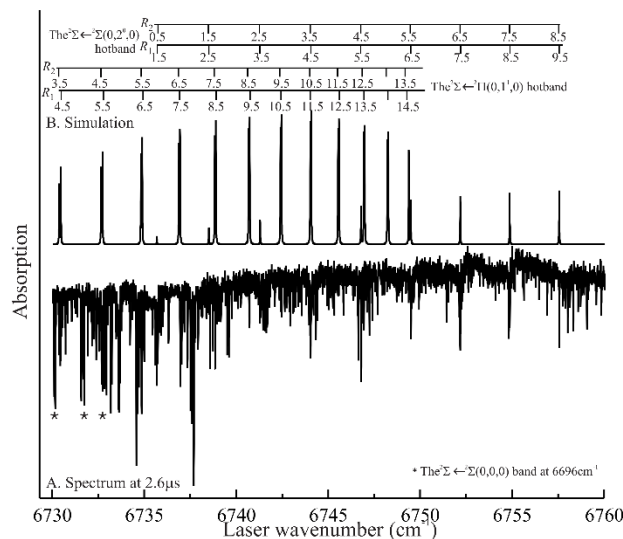
## B. The near-IR spectrum of C<sub>2</sub>H

Transient diode laser absorption spectroscopy has been used to measure three strong vibronic bands in the near infrared spectrum of the C<sub>2</sub>H, ethynyl, radical not previously observed in the gas phase. The radical was produced by ultraviolet excimer laser photolysis of either acetylene or (1,1,1)-trifluoropropyne in a slowly flowing sample of the precursor diluted in inert gas, and the spectral resolution was Doppler-limited. The character of the upper states was determined from the rotational and fine structure in the observed spectra and assigned by measurement of ground state rotational combination differences. The upper states include a  $^2\Sigma^+$  state at 6696 cm<sup>-1</sup>, a second  $^2\Sigma^+$  state at 7088 cm<sup>-1</sup>, and a  $^2\Pi$  state at 7110 cm<sup>-1</sup>. By comparison with published calculations (R. Tarroni and S. Carter, *J. Chem. Phys* **119**, 12878 (2003) and *Mol. Phys.* **102**, 2167 (2004)), the vibronic character of these levels was also assigned. The observed states contain both X  $^2\Sigma^+$  and A $^2\Pi$  electronic character. Several local rotational level perturbations were observed in the excited states. Kinetic measurements of the time-evolution of the ground state populations following collisional relaxation and reactive loss of the radicals formed in a hot, non-thermal, population distribution were made using some of the strong rotational lines observed. The case of C<sub>2</sub>H may be a good place to investigate the behavior at intermediate pressures of inert colliders, where the competition between relaxation and reaction can be tuned and observed to compare with master equation models, rather than deliberately suppressed to measure thermal rate constants.

## II. Current and Future Work

### A. Hot bands and kinetics in the near-IR Spectrum of C<sub>2</sub>H

Some preliminary measurements of the kinetics of the mixed collisional deactivation and chemical loss of this radical were made previously in the work described immediately above and in G. Hall's abstract elsewhere in this publication. In particular, the chemical reactivity of the radical with H<sub>2</sub> and acetylene is of interest, and there are some indications that these reactions, and others of C<sub>2</sub>H, do not proceed at rates that can be described by standard thermal rate constant approaches. This is because the ground state and



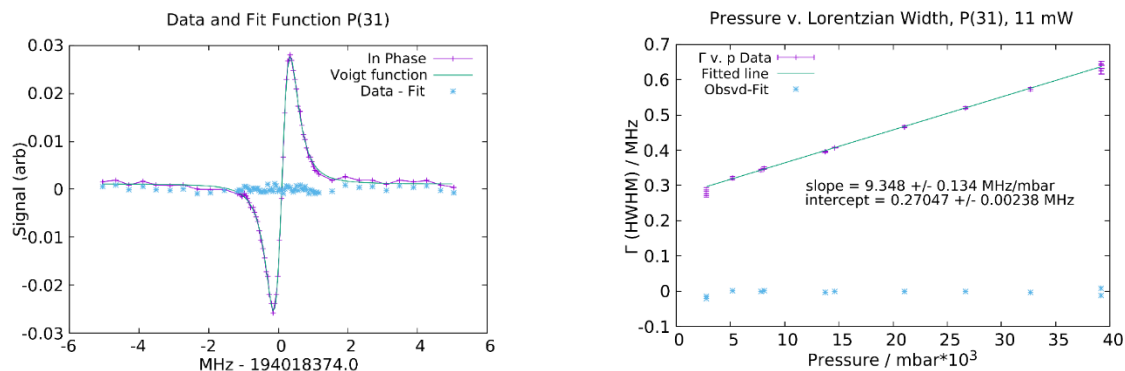
low-lying A $^2\Pi$  states have markedly different chemical reactivity, and the vibrational levels of the ground state possess varying amounts of electronic character of the two states. Convenient spectroscopic probes of the various low-lying vibrational levels are therefore desirable. We are presently working to assign absorptions from vibrationally hot levels in the spectrum and the figure shows some assignments of transitions from the X $^2\Pi$  (0,1<sup>1</sup>,0) level. This and transitions from one component of the doubly excited bending vibration X $^2\Sigma^+$ (0,2<sup>0</sup>,0) have now been assigned. Further work on the spectrum can be expected to lead to more assignments, and kinetics studies are also planned in the near future.

## B. Other radical spectroscopy

Guided by calculations by H.-G. Yu in our group, we are planning to search for transitions in vinyl radical,  $C_2H_3$ , also in the near-IR region. The radical is of fundamental interest because of the low-frequency inversion motion associated with CCH bending at the radical center, which leads to spectroscopically observable tunneling splittings of the lowest rotational levels and the two equivalent protons on the  $\beta$ -carbon leading to 3:1 nuclear spin-statistics. Published work by others suggests that in vibrationally excited levels this symmetry is not preserved, possibly due to a large geometrical distortion or some large-amplitude motion that leads to a symmetry breakdown. The radical is also the equilibrium structure of the intermediate in the  $C_2H+H_2$  reaction and therefore provides another view of the potential energy surface for the reaction discussed above and in G. Hall's abstract.

## C. Different views of the effects of velocity-changing collisions

Several of the current projects in the group are concerned with the fine details of collisional energy transfer in gas mixtures. The kinetics of thermalization of a sub-Doppler hole in the speed distribution of single rotational levels of CN radical, discussed in G. Hall's abstract, provides one direct view of the relative probabilities of elastic, velocity-changing, versus hard, non-elastic, state- or phase-changing collisions in molecules. Another view of the processes involved can come from the observation of lifetime broadening of sub-Doppler resonances in molecular spectra. The figure below shows an example of a lifetime-broadened sub-Doppler saturation dip of the P(31) line in the  $v_1+v_3$  band of  $C_2H_2$  and the results of a fit to a convolution of a transit-time broadened Gaussian and a lifetime broadened Lorentzian profile. Measurement of the lifetime broadening as a function of pressure, results in the plot in the right hand panel.



The slope of the plot is the definition of the pressure broadening coefficient,  $\gamma$ , and the value obtained is several times that measured in a conventional Doppler-broadened line for the same transition. At all the pressures involved in the sub-Doppler measurements here, the hard collision rate, from gas-kinetic theory is much slower than the transit time of the molecules through the laser beam, so the broadening observed is solely due to large cross-section velocity changing collisions (VCCs) that result in angular deflection of the molecule, removing it from the sub-Doppler saturated sample. The rate of these collisions is significantly higher than the hard collisions, resulting in a faster broadening with pressure than seen in conventional measurements. In linear absorption spectra, the broadening effects of the hard collisions dominate, because the effects of VCCs are confined to the Gaussian, Doppler, contribution to the line profile and do not change the area of the absorption peak. However, VCCs are responsible for the Dicke-narrowing phenomenon seen in all precision line shape measurements and our experiments provide direct information on the relative magnitudes of the contributions from the soft and hard collisions. Work to further understand and quantify these measurements is ongoing in the group.

## III. Publications supported by this project since 2015

Doppler-Resolved Kinetics of Saturation Recovery, D. Forthomme, M. L. Hause, H.-G. Yu, P. J. Dagdigian, T. J. Sears, and G. E. Hall, *J. Phys. Chem. A* 119, 7439-7450 (2015).

- Application of the Hartmann–Tran profile to precise experimental data sets of  $^{12}\text{C}_2\text{H}_2$ , D. Forthomme, M.J. Cich, S. Twagirayezu, G.E. Hall, T.J. Sears, *Journal of Quantitative Spectroscopy & Radiative Transfer* **165** (2015) 28–37.
- Frequency-comb referenced spectroscopy of  $\nu_4$  and  $\nu_5$  hot bands in the  $\nu_1 + \nu_3$  combination band of  $\text{C}_2\text{H}_2$ , S. Twagirayezu, M. J. Cich, T. J. Sears, C. P. McRaven, and G. E. Hall, *J. Molec. Spectrosc.* **316** 64-71 (2015).
- Photo-assisted intersystem crossing: The predominant triplet formation mechanism in some isolated polycyclic aromatic molecules excited with pulsed lasers, P. M. Johnson, and T. J. Sears, *J. Chem Phys.*, **143**, 045305 (2015).
- Further investigation of g-factors for the lead monofluoride ground state, L. V. Skripnikov, A. N. Petrov, A. V. Titov, R. J. Mawhorter, A. L. Baum, T. J. Sears, and J.-U. Grabow, *Phys. Rev. A* **92**, 032508 (2015).
- Detection and characterization of singly deuterated silylene, SiHD, via optical spectroscopy, D. Kokkin, T. Ma, T. Steimle and T. J. Sears, *J. Chem. Phys.* **144**, 244304(13) (2016).
- The near infrared spectrum of ethynyl radical, A. T. Le, G. E. Hall and T. J. Sears, *J. Chem. Phys.* **145**, 074306(11) 2016).
- Quadrupole splittings in the near-infrared spectrum of  $^{14}\text{NH}_3$ , S. Twagirayezu, G. E. Hall and T. J. Sears, *J. Chem. Phys.* **145**, 144302(8) (2016).

# Theoretical Studies of Potential Energy Surfaces and Computational Methods

Ron Shepard

Chemical Sciences and Engineering Division,  
Argonne National Laboratory, Argonne, IL 60439  
[email: shepard@tcg.anl.gov]

**Program Scope:** This project involves the development, implementation, and application of theoretical methods for the calculation and characterization of potential energy surfaces (PES) involving molecular species that occur in hydrocarbon combustion. These potential energy surfaces require an accurate and balanced treatment of reactants, intermediates, and products. This difficult challenge is met with general multiconfiguration self-consistent field (MCSCF) and multireference single- and double-excitation configuration interaction (MR-SDCI) methods. In contrast to the more common single-reference electronic structure methods, this approach is capable of describing accurately molecular systems that are highly distorted away from their equilibrium geometries, including reactant, fragment, and transition-state geometries, and of describing regions of the potential surface that are associated with electronic wave functions of widely varying nature. The MCSCF reference wave functions are designed to be sufficiently flexible to describe qualitatively the changes in the electronic structure over the broad range of molecular geometries of interest. The necessary mixing of ionic, covalent, and Rydberg contributions, along with the appropriate treatment of the different electron-spin components (e.g. closed shell, high-spin open-shell, low-spin open-shell, radical, diradical, etc.) of the wave functions are treated correctly at this level. Further treatment of electron correlation effects is included using large-scale multireference CI wave functions, particularly including the single and double excitations relative to the MCSCF reference space. The recent focus has included the development and application of the Graphically Contracted Function (GCF) method.

**Recent Progress:** ELECTRONIC STRUCTURE CODE MAINTENANCE, DEVELOPMENT, AND APPLICATIONS: A major component of this project is the development and maintenance of the COLUMBUS Program System. The COLUMBUS Program System computes MCSCF and MR-SDCI wave functions, MR-ACPF (averaged coupled-pair functional) energies, MR-AQCC (averaged quadratic coupled cluster) energies, spin-orbit CI energies, analytic energy gradients, and nonadiabatic coupling. Geometry optimizations to equilibrium and saddle-point structures can be done automatically for both ground and excited electronic states. The COLUMBUS Program System is maintained and developed collaboratively with several researchers including Russell M. Pitzer (Ohio State University), Thomas Mueller (Jülich Supercomputer Center, Germany), and Hans Lischka (Tianjin University, China, University of Vienna, Austria, and Texas Tech University). The nonadiabatic coupling and geometry optimization for conical intersections is done in collaboration with David R. Yarkony (Johns Hopkins University). The distributed development effort and software coordination uses an svn repository of source code. The parallel sections of the code are based on the single-program multiple-data (SPMD) programming model with explicit

This work was performed under the auspices of the Office of Basic Energy Sciences, Division of Chemical Sciences, Geosciences, and Biosciences, U.S. Department of Energy, under contract number DE-AC02-06CH11357.

message passing using the portable MPI library, and the portable Global Array Library (distributed from PNNL) is used for data distribution. The COLUMBUS codes incorporate several of the newer language features of F90 and later in order to facilitate future development and maintenance efforts. Development versions of the single-facet and multifacet GCF methods are included within the COLUMBUS repository.

**GRAPHICALLY CONTRACTED FUNCTION METHOD:** We have developed a novel expansion basis for electronic wave functions [see *J. Chem. Phys.* **141**, 064105 (2014) and references therein]. In this approach, the wave function is written as a linear combination of *graphically contracted functions* (GCF), and each GCF in turn is formally equivalent to a linear combination of configuration state functions (CSFs) that comprise an underlying full-CI linear expansion space of dimension  $N_{\text{CSF}}$ . The CSF coefficients that define the GCFs are nonlinear functions of a smaller number of essential variables  $N_{\phi} \ll N_{\text{CSF}}$ . The initial implementation of the GCF method relied on the nonlinear basis dimension  $N_{\text{GCF}}$  to extend the wave function flexibility and to converge molecular properties toward the full-CI limit. We have now implemented an alternative, and potentially more efficient, approach to enhance the wave function flexibility that consists of allowing multiple partially contracted wave functions to be associated with each Shavitt graph node within each GCF. The initial approach is now called the single-facet GCF (SFGCF) method, and this new approach is called the multifacet GCF (MFGCF) method. All of the properties and algorithms previously developed for the SFGCF method are being implemented within the MFGCF code: state-averaging, Hamiltonian matrix construction, one- and two-particle reduced density matrix (RDM) construction, Slater determinant overlaps, graph density computation and display, and spin-density matrix computation. MFGCF expansions with facet counts in the range  $f_{\text{MAX}} \approx 4$  to 10 have been shown to approach the full-CI PES to within chemical accuracy (1 kcal/mole or better). The GCF method is formulated in terms of spin eigenfunctions using the Graphical Unitary Group Approach (GUGA) of Shavitt, and consequently it does not suffer from spin contamination or spin instability. This is an important feature for the study of radicals and excited states that occur in hydrocarbon combustion. The GCF method scales much better with orbital basis function dimension and with the number of electrons than traditional high-level electronic structure methods. No intrinsic restrictions are imposed on the orbital occupations, and in particular there are no artificial excitation-level or occupation restrictions with respect to a reference function or reference space; in this sense, the method is more correctly characterized as a multiconfigurational method rather than a multireference method. Because the wave function is a linear combination of GCF basis functions rather than a single expansion term, this allows the method to be used for both ground and excited electronic states, the increased wave function flexibility leads to higher accuracy, and this expansion form facilitates the computation of transition moments, nonadiabatic coupling, and other properties that at present can only be computed reliably with multireference and multiconfigurational approaches.

The optimization of the nonlinear arc factor parameters has proven to be a difficult computational task for traditional optimization methods such as quasi-Newton and conjugate gradient methods. Such methods typically display superlinear convergence in some neighborhood near the converged solution, but, when applied to the GCF optimization, these methods typically display slower sublinear power-law convergence. For tight convergence, appropriate for computing molecular properties, analytic gradients

for geometry optimization, etc., this might require  $10^4$  to  $10^6$  iterations. We have begun to explore the nature of these convergence difficulties, and a first step includes the implementation of a Direct Inversion in the Iterative Subspace (DIIS) interpolation within an L-BFGS quasi-Newton optimization. This results in an interesting and potentially useful general optimization algorithm for other optimization problems. In the L-BFGS algorithm [J. Nocedal, *Math. Comput.* **35**, 773(1980)], the quasi-Newton step direction each iteration is determined as  $\mathbf{d} = -\mathbf{B}\mathbf{g}_k$  where  $\mathbf{g}_k = \partial f(\mathbf{x})/\partial \mathbf{x}$  is the gradient and  $\mathbf{B}$  is an approximation to the inverse hessian matrix at the point  $\mathbf{x}_k$ . The actual step taken is determined from a line search of  $f(\mathbf{x}+\alpha\mathbf{d})$  to determine an  $\alpha_{\text{opt}}$  step size for the next trial vector. Starting from an initial  $\mathbf{x}_0$  and  $\mathbf{B}_0$ , the matrix  $\mathbf{B}$  is updated recursively as

$$\mathbf{B}_j = \mathbf{T}_j^T \mathbf{B}_{j-1} \mathbf{T}_j + \rho_j \mathbf{s}_j \mathbf{s}_j^T$$

with  $\mathbf{T}_j = \mathbf{1} - \rho_j \mathbf{y}_j \mathbf{s}_j^T$ ,  $\mathbf{s}_j = \mathbf{x}_j - \mathbf{x}_{j-1}$ ,  $\mathbf{y}_j = \mathbf{g}_j - \mathbf{g}_{j-1}$ , and  $\rho_j = 1/\mathbf{s}_j^T \mathbf{y}_j$ . The *secant condition*  $\mathbf{B}_j \mathbf{y}_j = \mathbf{s}_j$  is satisfied for this approximation as it would be for the exact inverse hessian matrix for an infinitesimal step. In the L-BFGS algorithm, the approximations  $\mathbf{B}_j$  are not computed and stored explicitly. Instead, the history vectors  $\mathbf{s}_j$  and  $\mathbf{y}_j$  are stored, and the matrix-vector products  $\mathbf{B}_j \mathbf{g}_k$  are computed from these history vectors using a recursive algorithm based on the above expression for  $\mathbf{B}_j$ . The L-BFGS optimization procedure then consists of adding new history vectors and computing new trial vectors iteratively until convergence is achieved. Typically a limited number of history vectors are kept. This has the effect of limiting the storage requirements (which is important for optimizations involving large numbers of variables), of reducing the computational effort each iteration (since only a few vector operations are required for each history vector), and also of discarding unreliable information from the distant past that no longer reflects accurately the local approximate hessian information.

DIIS interpolation [P. Pulay, *Chem. Phys. Lett.* **73**, 393(1980); R. Shepard and M. Minkoff, *Mol. Phys.* **105**, 2839(2007) (SM)] may be imposed on the optimization procedure by periodically computing the step  $\mathbf{d}$  using an interpolation procedure rather than from the quasi-Newton procedure. In the DIIS procedure, a new trial vector is obtained by first computing the constrained least-squares (CLS) solution

$$\min_{\mathbf{c}} \|\mathbf{E}\mathbf{c}\| \quad \text{with } \mathbf{u} \cdot \mathbf{c} = 1.$$

The columns of the matrix  $\mathbf{E}$  are error vectors associated with the most recent trial vectors. These may be the gradient vectors  $\mathbf{g}_k$ , preconditioned gradient vectors, or some other measure of the error associated with each trial vector. The *uno vector* is defined as  $\mathbf{u}=[1,1\dots 1]$ . The above CLS equation may be interpreted as a minimum-error interpolation constrained to the hyperplane that is perpendicular to the vector  $\mathbf{u}$ . The solution  $\mathbf{c}$  is usually found from the augmented equation

$$\begin{pmatrix} \mathbf{M} & -\mathbf{u}^T \\ -\mathbf{u} & 0 \end{pmatrix} \begin{pmatrix} \mathbf{c} \\ \lambda \end{pmatrix} = \begin{pmatrix} \mathbf{0} \\ -1 \end{pmatrix}$$

where  $\mathbf{M}=\mathbf{E}^T\mathbf{E}$ . This is the normal equation form of the CLS problem. Because  $\kappa(\mathbf{M})=\kappa(\mathbf{E})^2$ , this solution displays numerical problems when the condition number  $\kappa$  is large, which in turn can occur when the columns of  $\mathbf{E}$  are nearly linearly dependent. A

more complete discussion of this feature is given in the above SM reference. After the solution vector  $\mathbf{c}$  has been determined, then the interpolated vector is given by  $\mathbf{x}_{\text{DIIS}} = \mathbf{X}\mathbf{c}$ , where the columns of  $\mathbf{X}$  are the most recent trial vectors, and the corresponding step direction is given as  $\mathbf{d} = \mathbf{x}_{\text{DIIS}} - \mathbf{x}_{\text{last}}$ .

Because  $\mathbf{X}$  and  $\mathbf{E}$  are not stored during the L-BFGS procedure, there are two approaches that may be taken to perform the DIIS interpolation. One is to extract  $\mathbf{X}$  and  $\mathbf{E}$  from the history vectors, and then proceed according to the above CLS procedure. A second option, which we now describe, is to transform the DIIS equations to use the L-BFGS history vectors. The LS equation is rewritten as  $\|\mathbf{E}\mathbf{c}\| = \|\mathbf{E}\mathbf{D}\mathbf{D}^{-1}\mathbf{c}\| = \|(\mathbf{Y}, \mathbf{g}_{\text{last}})\tilde{\mathbf{c}}\|$  where  $\tilde{\mathbf{c}} = \mathbf{D}^{-1}\mathbf{c}$  and where

$$\mathbf{E}\mathbf{D} = (\mathbf{g}_0 \mathbf{g}_1 \mathbf{g}_2 \dots \mathbf{g}_{\text{last}}) \begin{pmatrix} -1 & 0 & \dots & 0 \\ +1 & -1 & \dots & 0 \\ 0 & +1 & \dots & 0 \\ 0 & 0 & \dots & +1 \end{pmatrix} = (\mathbf{Y}, \mathbf{g}_{\text{last}})$$

The constraint transforms as  $\mathbf{u} \cdot \mathbf{c} = \mathbf{u}\mathbf{D}\mathbf{D}^{-1}\mathbf{c} = [0, 0, \dots, 1] \cdot \tilde{\mathbf{c}} = \tilde{c}_{\text{last}} = 1$ . Since the last element is fully determined from the constraint, the CLS equation may be written in the standard unconstrained LS form as  $\|\mathbf{Y}\tilde{\mathbf{c}}' + \mathbf{g}_{\text{last}}\|$ . The  $\mathbf{x}_{\text{DIIS}}$  vector can be similarly transformed, and the resulting step is given simply by  $\mathbf{d} = \mathbf{S}\tilde{\mathbf{c}}'$  where the columns of  $\mathbf{S}$  are the LBFGS history vectors. The transformation  $\mathbf{D}$  has condition number  $\kappa(\mathbf{D})=1$ , so it introduces no additional numerical errors, and the LS solution can be obtained with a Singular Value Decomposition (SVD) algorithm that is robust for large  $\kappa(\mathbf{Y})$ . In this form, the DIIS interpolation meshes very well with the underlying L-BFGS procedure, and it enjoys some additional numerical stability relative to the normal equation form.

### Publications:

- “Comparison of Multireference Configuration Interaction Potential Energy Surfaces for  $\text{H} + \text{O}_2 \rightarrow \text{HO}_2$ : The Effect Of Internal Contraction,” L. B. Harding, S. J. Klippenstein, H. Lischka, and R. Shepard, *Theor. Chem. Acc.* **133**, 1429 (2014).
- “Wave Function Analysis with Shavitt Graph Density in the Graphically Contracted Function Method,” G. Gidofalvi, S. R. Brozell, and R. Shepard. *Theor. Chem. Acc.* **133**, 1512 (2014).
- “Wave function analysis with Shavitt graph density in the graphically contracted function method,” G. Gidofalvi, S. Brozell, R. Shepard, *Abstracts of Papers of the American Chemical Society* **248**, 450-COMP (2014).
- “The Multifacet Graphically Contracted Function Method. I. Formulation and Implementation,” R. Shepard, G. Gidofalvi, and S. R. Brozell. *J. Chem. Phys.* **141**, 064105 (2014).
- “The Multifacet Graphically Contracted Function Method. II. A General Procedure for the Parameterization of Orthogonal Matrices and its Application to Arc Factors,” R. Shepard, G. Gidofalvi, and S. R. Brozell. *J. Chem. Phys.* **141**, 064106 (2014).
- “The Representation and Parametrization of Orthogonal Matrices,” R. Shepard, S. R. Brozell, and G. Gidofalvi. *J. Phys. Chem. A* **119**, 7924-7939 (2015).
- “Shavitt Memorial Festschrift Collection,” *Theor. Chem. Acc.* (2016). ISSN: 2194-8666, ISSN 2194-8674 (electronic). Edited by R. Shepard, T. H. Dunning, Jr., and R. M. Pitzer.

# Mechanisms and Models for Combustion Simulations

Raghu Sivaramakrishnan

Chemical Dynamics Group, Chemical Sciences & Engineering Division

Argonne National Laboratory, Argonne, IL 60439

[raghu@anl.gov](mailto:raghu@anl.gov)

## I. Program Scope

Mechanisms describing the combustion chemistry of even simple fuels can be complex involving a myriad of unimolecular and bimolecular elementary steps. The primary scope of this program is to develop and validate detailed chemical kinetics mechanisms and models for use in combustion simulations.

The kinetics models will be developed on the basis of a consistent framework incorporating theoretical predictions, experimental measurements, and evaluations of elementary reaction rate coefficients including feedback loops between them. The detailed models will subsequently be used for simulations of data from reactors, shock-tubes, rapid compression machines, and flames, the aim being the validation of the mechanistic and kinetic aspects of these models over practical combustion regimes.

## II. Recent Progress

### A. Probing Variational Effects in the Thermal Decompositions of Hydroxyalkyl Radicals

Hydroxyalkyl radicals are often the dominant intermediates formed by H-atom abstractions from alcohols. These radicals are stable and have bond energies large enough that they persist even in high temperature flame-environments.<sup>1</sup> Recent studies on the thermal decomposition of the simplest hydroxyalkyl radical, CH<sub>2</sub>OH, reveals that variational effects impact the predicted kinetics for the C-H β-bond scission reaction. These variational effects predominantly stem from the substantial changes (> factor of 3) in the O-H torsional frequency (with changes in the O-H bond length) in the transition state for the CH<sub>2</sub>OH → H + CH<sub>2</sub>O (β-bond scission) reaction. As a result of including this effect, the dominant decomposition pathway at high temperatures (>1000K) is predicted to be a well-skipping process (CH<sub>2</sub>OH → CH<sub>3</sub>O → H + CH<sub>2</sub>O), in agreement with shock tube experiments<sup>2</sup> on the deuterated analogs of CH<sub>2</sub>OH (CH<sub>2</sub>OD and CD<sub>2</sub>OH). These theoretical predictions and experimental data confound recent theoretical analyses that conclude that β-bond scission is the dominant mechanism for the decomposition of CH<sub>2</sub>OH to eventual end products, H + CH<sub>2</sub>O.

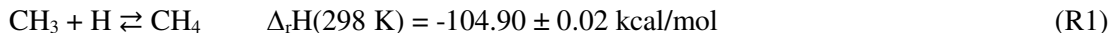
Larger hydroxyalkyl radicals such as CH<sub>3</sub>CHOH and CH<sub>3</sub>C(OH)CH<sub>3</sub> are the dominant radicals produced from hydrogen abstractions in ethanol and iso-propanol. Prior theoretical studies,<sup>3,4</sup> without consideration of variational effects have concluded that the lowest energy pathways for the decomposition of these two radicals through O-H bond β-scission, (CH<sub>3</sub>CHOH → H + CH<sub>3</sub>CHO and CH<sub>3</sub>C(OH)CH<sub>3</sub> → H + CH<sub>3</sub>COCH<sub>3</sub>) were kinetically dominant even under combustion (>1000 K) conditions. In light of our recent observations<sup>2</sup> for CH<sub>2</sub>OH decomposition, the impact of including variational effects are assessed for the decompositions of these two larger hydroxyalkyl radicals. A preliminary analysis reveals similar changes (as in CH<sub>2</sub>OH) in OH torsional frequencies in the transition states for the O-H bond β-scissions in CH<sub>3</sub>CHOH and CH<sub>3</sub>C(OH)CH<sub>3</sub>. The kinetics implications of these variational analyses on the dissociations these hydroxyalkyl radicals will be assessed through master-equation calculations in collaboration with S. J. Klippenstein.

### B. High Accuracy Thermochemical Kinetics for H + CH<sub>3</sub> (+M) ⇌ CH<sub>4</sub> (+M)

CH<sub>3</sub>, the simplest alkyl radical, is an extremely stable intermediate with a C-H bond dissociation enthalpy of 110.69 ± 0.03 kcal/mol at 298 K.<sup>5,6</sup> As a consequence, it persists in large concentrations even in high-temperature chemically reacting systems such as flames. The relatively strong C-H bonds preclude unimolecular dissociation of CH<sub>3</sub> at T < 2000 K,<sup>7</sup> and the predominant mechanism by which CH<sub>3</sub> radicals are consumed in most chemical processes is through bimolecular reactions.<sup>8</sup> In particular,



the facile barrierless reaction of CH<sub>3</sub> radicals with H-atoms (R1) is a major process for its removal in high temperature combustion.<sup>8,9</sup>



Due to its paramount role as a chain-terminating process, the chemical kinetics of reaction (R1) has received substantial attention<sup>10</sup> from the atmospheric and combustion chemistry communities. With the exception of the inferred high-pressure limiting rate constants,  $k_{1\infty}$ , from a shock tube study<sup>11</sup> of D + CH<sub>3</sub>, direct measurements of reaction (R1) in the recombination direction are limited to low temperatures<sup>12</sup> (<600 K). On the other hand, direct shock tube measurements<sup>13-15</sup> of the rate constants in the dissociation direction,  $k_1$ , span a higher temperature range 1500 - 4500 K, primarily due to the strong C-H bond in CH<sub>4</sub>. Reconciling the thermally disparate experimental database on  $k_1$  and  $k_{-1}$  requires accurate equilibrium constants for reaction (R1) that span an extended range of temperatures (300-4500 K).

In a CH<sub>4</sub> dissociation study, Sutherland et al.<sup>15</sup> have utilized equilibrium constants ( $K_{\text{eq}}$ ) calculated earlier by Ruscic<sup>16-18</sup> to obtain Troe fits to the relevant experimental data<sup>12-15</sup> on  $k_1$  and  $k_{-1}$ . These  $K_{\text{eq}}$  values (300-4500 K) relied on thermochemical parameters for the CH<sub>3</sub> radical that were calculated using the usual rigid-rotor harmonic-oscillator (RRHO) approximation. Similarly, the IUPAC evaluation<sup>19</sup> for the thermochemistry of CH<sub>3</sub>, which provides NASA polynomials that are widely used in combustion for simulations over extended T-ranges, also uses the same RRHO approximation.

However, a theoretical study<sup>20</sup> of the CH<sub>3</sub> radical concluded that for this species the RRHO approximation is inadequate at high temperatures relevant to flame chemistry. Theoretical kinetics<sup>21</sup> has now advanced to the point that *a priori* predictions for pressure-dependent reactions such as (R1) are becoming as accurate, if not better, than experimental determinations. Incorporating these accurate predictions for  $k_{-1}$  in simulation tools like CHEMKIN<sup>22</sup> also requires accurate thermochemistry for all the species in order to maintain the integrity of  $k_1$ .

In collaboration with Ruscic, accurate equilibrium constants were determined for the title reaction using the ATcT approach.<sup>23-26</sup> These accurate equilibrium constants were used along with results from a two-dimensional master equation approach<sup>21</sup> (in collaboration with Jasper and Klippenstein) and literature experiments on  $k_1$  and  $k_{-1}$  to obtain an accurate representation for the kinetics of reaction R1 (see Figure 1 below). The impact of using this updated fit for reaction R1 is assessed through simulations of laminar flame speeds. Simulations of 1-10 atm CH<sub>4</sub>-air flames ( $T_u = 298 \text{ K}$ ) were performed using two popular combustion models, USC-Mech<sup>27</sup> and Aramco Mech.<sup>28</sup> Replacing  $k_1(T,P)$  and CH<sub>3</sub> thermo with the present recommendations (fit depicted in Fig. 1) in either of these models<sup>27,28</sup> leads to a noticeable 30% increase in flame speed predictions (relative to simulations with the raw models).

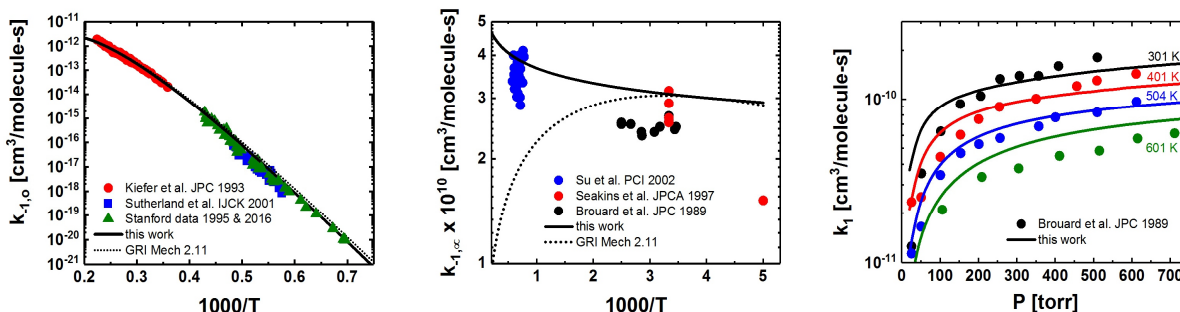


Figure 1: Comparison of the present fit for reaction (R1) to literature experimental data.

### C. Thermal Decompositions of Xylyl Radicals

In collaboration with J.V. Michael, S.J. Klippenstein, and C. Cavallotti (Politecnico Milano), we have initiated a joint experiment-theory study of o-xylylbromide dissociation as a source for o-xylyl

radicals and the subsequent dissociation kinetics of *o*-xylyl. The high sensitivity H-atom ARAS detection technique was used to obtain quantitative measurements of the H-atom yields and rate constants for *o*-xylyl decomposition ( $1267\text{ K} \leq T \leq 1597\text{ K}$ ;  $P \sim 0.3\text{-}1.0\text{ atm}$ ). The results from these studies and comparisons to earlier studies are discussed in terms of two processes; *o*-xylyl  $\rightarrow$  H + *o*-xylylene and *o*-xylyl  $\rightarrow$  non-H-atom channel. The experimental data have been subsequently compared with the results of a computational investigation performed in collaboration. The full PES is composed of 20 wells connected by 37 transition states. Master equation simulations were performed to determine channel specific rate constants for the decomposition of *o*-, *m*-, and *p*-xylyl for a wide range of temperatures and pressures. The simulations predict that the main products of decomposition are *o*-xylylene + H, *p*-xylylene + H, styrene + H, phenyl + C<sub>2</sub>H<sub>4</sub> and fulvenallene + CH<sub>3</sub>, with H channels accounting for about 80% of the decomposition products. It was also found that *ortho-meta-para* isomerization is a fast process, with a rate that is competitive with that of decomposition. The theoretical analysis also helped clarify the decomposition kinetics of the *o*-xylylbromide precursor. A publication describing these joint experiment/theory studies is nearing submission.

#### ***D. A detailed analysis of methanol combustion kinetics***

In collaboration with N.J. Labbe, S.J. Klippenstein, and the group of Y. Ju (Princeton University), an updated model for methanol combustion was developed. Initial simulations indicated that methanol (as the dominant intermediate from methylformate) and its sub-set mechanisms required a substantial update. In particular, the methanol model includes new theoretical kinetics predictions for OH + CH<sub>3</sub>OH and decompositions of CH<sub>2</sub>OH and CH<sub>3</sub>O, with a re-analysis of the H-atom abstractions from methanol by H, CH<sub>3</sub>, HO<sub>2</sub>, and O<sub>2</sub>. Simulations with the model indicate good agreement with literature data from shock-tubes, reactors, and flames. Recommendations for methanol combustion studies are also presented.

### **III. Future work**

In collaboration with Klippenstein and Jasper we have initiated the development of a theory informed kinetics database for combustion relevant reactions on the H<sub>n(=1-5)</sub>CO potential energy surfaces. There are high-level theoretical studies on the thermal dissociations of the smaller C<sub>2</sub> and C<sub>3</sub> radicals. However, such studies are lacking for the larger C<sub>4</sub> and C<sub>5</sub> radicals. In collaboration with Klippenstein, we propose to theoretically characterize the thermal dissociations of the four C<sub>4</sub>H<sub>9</sub> radical isomers, and additionally calculate prompt dissociation fractions for inclusion in combustion modeling. In collaboration with Klippenstein and Nils Hansen (CRF-Sandia), we propose to simulate the formation of intermediates in fuel-rich flames of small alkenes/alkynes. A particular focus is on the formation and destruction of larger aromatics, and PAH's to further our understanding of soot precursor chemistry.

### **IV. Acknowledgements**

This work was supported by the U.S. Department of Energy, Office of Science, Office of Basic Energy Sciences, Division of Chemical Sciences, Geosciences, and Biosciences under Contract No. DE-AC02-06CH11357.

### **V. References**

1. N.J. Labbe, R. Sivaramakrishnan, S.J. Klippenstein, Proc. Combust. Inst. 35 (2015) 447-455.
2. N.J. Labbe, S.L. Peukert, L. Ye, R. Sivaramakrishnan, S.J. Klippenstein, J.V. Michael, "OH + CH<sub>3</sub>OH Experiments and Theory Probe Mechanistic Aspects of CH<sub>2</sub>OH Decomposition: Well-skipping or  $\beta$ -scission?", In Preparation, J. Phys. Chem. A, (2017).
3. J.P. Senosiain, S.J. Klippenstein, J.A. Miller, J. Phys. Chem. A 110 (2006) 6960-6970.
4. J. Zador, A.W. Jasper, J.A. Miller, Phys. Chem. Chem. Phys. 11 (2009) 11040-11053.
5. B. Ruscic, J. Phys. Chem. A 119 (2015) 7810-7837.
6. B. Ruscic, Active Thermochemical Tables (ATcT) Values Based on Ver. 1.118 of the Thermochemical Network (2015); available at <https://ATcT.anl.gov>
7. K.P. Lim, J. V. Michael, Proc. Combust. Inst. 25 (1994) 713-719.

8. W. C. Gardiner, Jr. *Combustion Chemistry*; Springer Verlag: New York, 1984.
9. J. Warnatz, *Proc. Combust. Inst.* 18 (1981), 369-384.
10. D.L. Baulch, C.T. Bowman, C.J. Cobos, R.A. Cox, Th. Just, J.A. Kerr, M.J. Pilling, D. Stocker, J. Troe, W. Tsang, R.W. Walker, J. Warnatz, *J. Phys. Chem. Ref. Data* 34 (2005) 757-1397.
11. M.-C. Su, J.V. Michael, *Proc. Combust. Inst.* 29 (2002) 1219-1227
12. M. Brouard, M.T. Macpherson, M.J. Pilling, *J. Phys. Chem.* 93 (1989) 4047.
13. J.H. Kiefer, S.S. Kumaran, *J. Phys. Chem.* 97 (1993) 414-420.
14. (a) D.F. Davidson, M.D. Di Rosa, A.Y. Chang, R.K. Hanson, C.T. Bowman, *Symp. Int. on Combust.* 24 (1992) 589-596. (b) D.F. Davidson, R.K. Hanson, C.T. Bowman, *Int. J. Chem. Kin.* 27 (1995) 305-308. (c) S.K. Wang, D.F. Davidson, R.K. Hanson, *J. Phys. Chem. A* 120 (2016) 5427-5434.
15. J.W. Sutherland, M.-C. Su, J.V. Michael, *Int. J. Chem. Kin.* 33 (2001) 669-684.
16. B. Ruscic Private communication (Sept. 2000) to the authors of Ref. 15 **Error! Bookmark not defined.**
17. (a) B. Ruscic, M. Litorja, R.L. Asher, *J. Phys. Chem. A* 103 (1999) 8625 - 8633 (b) G. Herzberg, *J. Mol. Spectrosc.* 33 (1970) 147-168.
18. M.W. Chase, Jr., C.A. Davies, J.R. Downey, Jr., D.J. Frurip, R.A. McDonald, A.N. Syverud, *J. Phys. Chem. Ref. Data* 14 (1985) (Suppl. 1) 1-926.
19. B. Ruscic, J.E. Boggs, A. Burcat, A.G. Csaszar, J. Demaison, R. Janoschek, J.M.L. Martin, M.L. Morton, M.J. Rossi, J.F. Stanton, P.G. Szalay, P.R. Westmoreland, F. Zabel, T. Berces, *J. Phys. Chem. Ref. Data* 34 (2005) 573.
20. D.M. Medvedev, L.B. Harding, S.K. Gray, *Mol. Phys.* 104 (2006) 104, 73.
21. A.W. Jasper, K.M. Pelzer, J.A. Miller, E. Kamarchik, L.B. Harding, S.J. Klippenstein, *Science* 346 (2014) 1212.
22. ANSYS CHEMKIN 18.0 (Release Date 27-Jan-2017), ANSYS Inc., 2016.
23. B. Ruscic, R.E. Pinzon, M.L. Morton, G. von Laszewski, S. Bittner, S.G. Nijssure, K.A. Amin, M. Minkoff, A.F. Wagner, *J. Phys. Chem. A* 108 (2004) 9979-9997.
24. B. Ruscic, R.E. Pinzon, G. von Laszewski, D. Kodeboyina, A. Burcat, D. Leahy, D. Montoya, A.F. Wagner, *J. Phys. Conf. Ser.* 16 (2005) 561-570.
25. B. Ruscic, R.E. Pinzon, M.L. Morton, N.K. Srinivasan, M.-C. Su, J.W. Sutherland, J.V. Michael, *J. Phys. Chem. A* 110 (2006) 110, 6592-6600.
26. B. Ruscic, D. Feller, K.A. Peterson, *Theor. Chem. Acc.* 133 (2014) 1415.
27. H. Wang, X. You, A.V. Joshi, S.G. Davis, A. Laskin, F. Egolfopoulos, C.K. Law, USC Mech Version II. High-Temperature Combustion Reaction Model of H<sub>2</sub>/CO/Cl-C<sub>4</sub> Compounds. [http://ignis.usc.edu/USC\\_Mech\\_11.htm](http://ignis.usc.edu/USC_Mech_11.htm)
28. W.K. Metcalfe, S.M. Burke, S.S. Ahmed, H.J. Curran, *Int. J. Chem. Kin.* 45 (2013) 638-675.

## VI. Journal articles supported by this project 2015-2017

1. N. J. Labbe, R. Sivaramakrishnan, S. J. Klippenstein, "The Role of Radical + Fuel-Radical Well-Skipping Reactions in Ethanol and Methylformate Low-pressure Flames", *Proc. Combust. Inst.* **35** (2015) 447-455.
2. R. Sivaramakrishnan, J. V. Michael, L. B. Harding and S. J. Klippenstein, "Resolving some paradoxes in the thermal decomposition mechanism of CH<sub>3</sub>CHO", *J. Phys. Chem. A* **119** (2015) 7724-7733.
3. M. J. Davis, W. Liu, R. Sivaramakrishnan, "Global Sensitivity Analysis with Small Sample Sizes: Ordinary Least Squares Approach", *J. Phys. Chem. A* **121** (2017) 553-570.
4. N. J. Labbe, A. W. Jasper, S. J. Klippenstein, J. A. Miller, R. Sivaramakrishnan, B. Ruscic, "From Anharmonic Partition Functions to Flame Chemistry: High Accuracy Thermochemical Kinetics for H + CH<sub>3</sub> (+M) ⇌ CH<sub>4</sub> (+M)", In Preparation, *J. Phys. Chem. A* (2017).
5. N. J. Labbe, P. Dievart, X. L. Yang, R. Sivaramakrishnan, S. J. Klippenstein, Y. Ju, "A detail analysis of the kinetics of methanol combustion", In Preparation, *Comb. And Flame* (2017).
6. D. Polino, R. Sivaramakrishnan, S. J. Klippenstein, J. V. Michael, C. Cavallotti "Experimental and theoretical studies on the thermal decomposition of xylyl radicals", In Preparation, *J. Phys. Chem. A* (2017).
7. S. L. Peukert, R. Sivaramakrishnan, S. J. Klippenstein, J. V. Michael, "Shock tube and theoretical kinetics studies on the thermal decomposition of iso-propanol and it's reaction with D-atoms", In Preparation, *J. Phys. Chem. A* (2017).

# Quantum Chemistry of Radicals and Reactive Intermediates

John F. Stanton  
Quantum Theory Project  
Departments of Chemistry and Physics  
University of Florida  
Gainesville, FL 32611  
johnstanton@ufl.edu

## Scope of Research

My research group works in the area of theoretical chemical physics, especially on the properties and chemistry of organic radicals and other reactive intermediates. This research follows a number of paths, including first-principles calculation of bond energies and other thermochemical information (as well as development of methodology needed for such calculations), methods for the simulation and analysis of molecular spectra (especially those relevant to experiments that can be used to glean thermochemical information), the development of *ab initio* quantum chemical methods needed for the accurate treatment of fundamental aspects of electronic structure and potential energy surfaces, and computational kinetics including semiclassical transition state theory and master equation modeling of chemical reactions.

## Summary of Selected Recent Accomplishments

- For some time, my group has worked on extension of the perturbation theory based on the Watson molecular Hamiltonian (which is generally known as vibrational perturbation theory, or VPT), specifically in extending the familiar and quite successful second-order variant (VPT2) to the next non-vanishing order (VPT4). While most perturbation theories are easily extended in a similar fashion, the mathematics associated with going from VPT2 to VPT4 is starkly tedious and only numerical implementations had been carried out previously. Our motivation to work out VPT4 - algebraically - was largely driven by potential application of this approach to the corresponding semiclassical transition state theory (SCTST)<sup>1</sup>, as SCTST is based on an algebraic relation between the good action-angle variables (the vibrational quantum numbers plus one-half) and the energy. VPT2-based SCTST has proven to be a valuable addition to the toolkit of computational chemical kinetics, although it is not without its shortcomings<sup>2</sup>; it is consequently of interest to explore its performance in the context of the more elaborate VPT4 framework. An illustrative calculation of the tunneling probability involving the symmetric Eckart potential revealed that VPT4 gives very accurate results quite deep into the tunneling regime, at energies well below those where VPT2-based SCTST begins to have problems. In fact, VPT4-SCTST is within 1% of the exact result down to energies where  $P(\textit{transmission})$  falls to *ca.*  $10^{-10}$ . Analysis of the VPT4-SCTST and exact SCTST results<sup>3</sup> suggests a simple empirical correction to VPT2-SCTST to account for higher order effects without having to do the much more elaborate potential energy surface calculations necessitated by VPT4. An initial as-yet unpublished study on the  $\text{NH}_3 + \text{OH}$  reaction indicates

<sup>1</sup>W.H. Miller *Trans. Farad. Soc.* 62, 40 (1977).

<sup>2</sup>A.H. Wagner *J. Phys. Chem. A* 117, 13089 (2013).

<sup>3</sup>V. Ryaboy and N. Moiseyev *J. Chem. Phys.* 98, 9618 (1993).

that this correction has promise. In addition, an ongoing collaboration with the Schaefer/Allen group at Georgia involves, amongst other things, application of the conventional bound-state VPT4 treatment to the vibrational levels of the formaldehyde molecule.

- My group has identified a new algorithm for carrying out Franck-Condon FC simulations of electronic spectra. Although most of our work on electronic spectra (see below, for example) involves cases in which more than one, and coupled, electronic state(s) are involved, the FC method is enormously useful in cases which are adequately treated by the Born-Oppenheimer approximation. For polyatomic molecules, FC calculations are usually based on approaches developed long ago that are based on recurrence relations. Our new algorithm is similar in spirit, but uses a new way to organize the information and data needed for these recursions and is significantly faster than conventional algorithms for medium-sized and large polyatomic molecules. Factors of roughly 30-50 are typically found. The initial report of the algorithm also reported its application to the photoelectron spectrum of cyclopentadienone, a ubiquitous combustion intermediate that was involved in a number of previous collaborative studies by our group.

- In collaboration with the Continetti group, we have studied the photoelectron spectrum of the propioly anion ( $\text{HCCCO}_2^-$ ), a species that is conceptually similar to the formyl anion ( $\text{HCO}_2^-$ ). Like formyloxyl, the neutral species is characterized by profound vibronic coupling between  $^2A_1$  and  $^2B_2$  electronic states, which significantly complicates the appearance of the spectrum in addition to the description of the  $\text{CO}_2$  loss process which nominally occurs only via the  $^2A_1$  state. Unlike formyloxyl, however, the system is sufficiently large to make the vibronic simulation calculations much more challenging (twelve vibrational modes *v.* six) as well as the quantum chemical calculations needed to construct the vibronic Hamiltonian (35 electrons *v.* 25). However, through use of a massively parallel code for the former and the recently-developed *ncc* coupled-cluster code, both developed as part of our GPCP-sponsored research, a faithful simulation of the spectrum could be obtained. Significantly, it was very important to establish the vertical electron detachment energies accurately for this study, and the full EOMIP-CCSDTQ was used for this purpose. Application of such a method to a system of this size for chemical applications is unprecedented, and the high-quality result obtained attests to the predictive power of CC calculations including quadruple excitation (correlation) effects. The calculations made possible the definitive assignment of  $\text{HCCCO}_2$  as the carrier of the spectrum; lower-level theory and simpler (FC) simulations were also largely consistent with the two (*cis*- and *trans*-) isomers of  $\text{CCCO}_2\text{H}$ . The assignment also aided the explanation of the distinctly different nature of the detachment process in  $\text{HCCCO}_2^-$  (relative to  $\text{HCO}_2^-$ ), as  $\text{CO}_2$  loss occurs only far above the detachment threshold in the former while it is conspicuous at all energies above the electron affinity of the latter.

- Recent work by the Field group at MIT has established an approach which can be used to determine classical barrier heights for isomerization reactions from experimental vibrational level structure below and in the relative vicinity of the barrier<sup>4</sup>. One of the first applications of this method was to the barrier height for the prototypical *cis-trans* isomerization of the  $S_1$  excited state of acetylene, which takes place on a single (adiabatic and diabatic) potential energy surface. This favorable example provides a benchmark for theoretical calculation of barrier heights, and our group – again employing the *ncc* module, which is considerably faster than any other extant program for doing coupled-cluster calculations involving quadruple excitations – has carried out such a benchmark study. Results for the barrier height obtained with a variant of the HEAT thermochemical protocol (as applied to a transition state) are in excellent agreement with the experimentally inferred barrier height. This is an important result for calibration purposes, as HEAT-based barrier calculations have been a major part of our chemical kinetics applications in

---

<sup>4</sup>J.H. Baraban, P.B. Changala, G.C. Mellau, J.F. Stanton, A.J. Merer and R.W. Field *Science* 350, 1338 (2015).

recent years.

• My associate L.T. Nguyen has continued his excellent work in chemical kinetics. He has developed a user-friendly program for doing kinetic simulations based on his approximate (steady-state) two-dimensional (E and J) master equation approach, which has recently become a part of the MULTIWELL program package that has historically been maintained by J.R. Barker at the University of Michigan. Our group is one of two others that are now part of the MULTIWELL development team, and our previous work on SCTST (VPT2-SCTST) is a part of the distributed version along with that based on the above-mentioned VPT4-motivated correction. Application studies in the last year included kinetic analyses of two interesting reactions that were observed by M.C. McCarthy (Harvard). The first of these is the remarkably selective production of the simplest Criegee intermediate ( $\text{CH}_2\text{COO}$ ) when methane is discharged with molecular oxygen and hydrogen; the second is the similarly selective production of the biologically important HSNO molecule when  $\text{H}_2\text{S}$  is mixed with  $\text{N}_2\text{O}_3$ . In the former case, kinetic analysis was able to rationalize the laboratory observations, but a master-equation study suggests that the latter observation is not a result of a homogenous gas-phase reaction. In more recent work that has just been published, we have collaborated with R.I. Kaiser (Hawaii) to help analyze the interesting kinetically-driven production of the (vinylidene-like)  $\text{H}_2\text{SiSi}$  isomer in the gas-phase reaction of silane with silicon atoms.

#### **Students and Postdoctoral Supported:**

T.L. Nguyen (postdoc)

C.A. Lopez (student)

S.A. Rabidoux (student)

## **References from 2016 acknowledging DE-FG02-07ER15884**

S.M. Rabidoux and J.F. Stanton “A Highly-Efficient Implementation of the Doktorov Recurrence Relations for Franck-Condon Calculations *J. Comp. Theo. Chem.* 12, 728 (2016).

M. Nava, M.A. Martin-Drumel, C.A. Lopez, K.N. Crabtree, C.C. Womack, T.L. Nguyen, S. Thorwirth, J.F. Stanton and M.C. McCarthy “Spontaneous and Selective Formation of HSNO, a Crucial Intermediate Linking  $\text{H}_2\text{S}$  and NO Chemistries *J. Amer. Chem. Soc.* (communication) 138, 11441 (2016).

T.L. Nguyen, M.C. McCarthy and J.F. Stanton “Relatively Selective Production of the Simplest Criegee Intermediate in a  $\text{CH}_4/\text{O}_2$  Electric Discharge: Kinetic Analysis of a Plausible Mechanism *J. Phys. Chem. A* 119, 7197 (2015).

J.P. Porterfield, J.H. Baraban, T.P. Troy, M. Ahmed, M.C. McCarthy, K.M. Morgan, J.W. Daily, T.L. Nguyen, J.F. Stanton and G.B. Ellison “Pyrolysis of the Simplest Carbohydrate, Glycoaldehyde ( $\text{CHO-CH}_2\text{OH}$ ), and Glyoxal in a Heated Micro-Reactor *J. Phys. Chem. A* 120, 2161 (2016).

M.C. McCarthy, O. Martinez, B.A. McGuire, K.N. Crabtree, M.-A. Martin-Drumel and J.F. Stanton, “Isotopic Studies of trans- and cis-HOCO Using Rotational Spectroscopy: Formation, Chemical Bonding, and Molecular Structures” *J. Chem. Phys.* 144, 124304 (2016).

J.H. Baraban, D.A. Matthews and J.F. Stanton “An Accurate Calculation of the  $\text{S}_1$   $\text{C}_2\text{H}_2$  cis-trans Barrier Height *J. Chem. Phys.* (communication) 144, 111102 (2016).



# Universal and State-Resolved Imaging Studies of Chemical Dynamics

Arthur G. Suits

Department of Chemistry, University of Missouri, Columbia MO 65211  
suitsa@missouri.edu

## I. Program Scope

The focus of this program is on combining universal ion imaging probes providing global insight, with high-resolution state-resolved probes providing quantum mechanical detail, to develop a molecular-level understanding of chemical phenomena. Particular emphasis is placed upon elementary reactions important in understanding and predicting combustion chemistry. This research is conducted using state-of-the-art molecular beam machines, photodissociation, reactive scattering, and vacuum ultraviolet lasers in conjunction with ion imaging techniques. A major focus of our effort remains crossed-beam reactive scattering, with new directions introduced below. We have moved our effort from Wayne State University to the University of Missouri a year ago, and the new grant at Missouri has just begun in January of this year.

## II. Recent Progress

Our current DOE research is directed to investigations of polyatomic reaction dynamics using crossed-beams with DC slice imaging. Our recent efforts have turned to focusing on fluorine atom reactions with larger hydrocarbons, contrasting them with the Cl atom reaction extensively studied in our laboratory, and recently reactions of ground state oxygen atoms.

### F atom reactions with alkenes

In recent years we have pursued a wide range of crossed-beam imaging studies of bimolecular reactions using the F<sub>2</sub> excimer at 157nm as a “universal” probe for C<sub>3</sub> and larger hydrocarbons and related systems for which the radical products have ionization energies below 7.9 eV. As mentioned last year, we have begun investigation of F atom reactions with a range of target molecular systems. F atoms offer a very revealing contrast to the Cl atom reactions that we and others have extensively studied in recent years. Recently we have extended these studies to F atom reaction with alcohols and alkenes. The experimental results, summarized in Fig. 1, show some

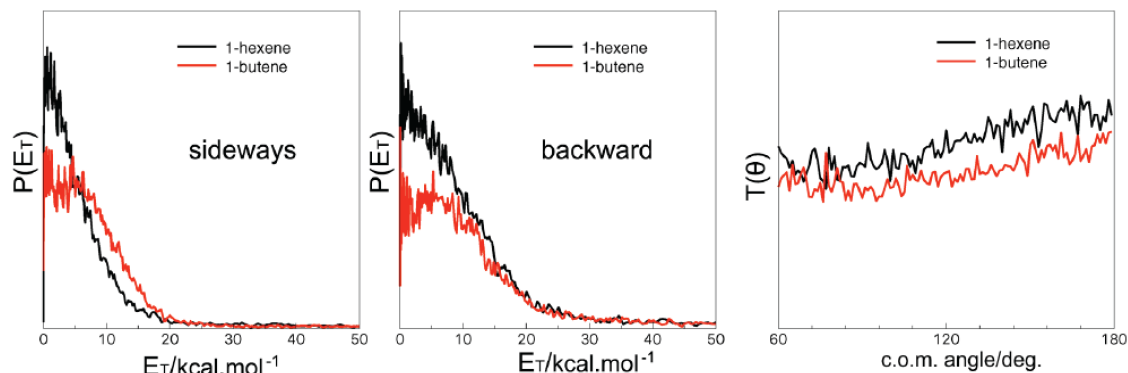


Figure 1. Sideways and backward translational energy distributions of allylic radical products of F + 1-butene and F + 1-hexene reaction (left); right is the center-of-mass angular distributions for each.



evidence of addition/elimination even for the F atom case, although our probe is only sensitive to the allylic radical product, while the vinylic channel may be dominant. This may be seen in the theoretical calculations shown in Fig. 2.

In the Cl atom reactions with alkenes, we showed that the addition/elimination proceeds via a “roaming” mechanism in which the Cl atom can undergo electrophilic addition to the C1 site (“anti-Markovnikov”) or less favorably to the C2 site, then re-dissociate to find a roaming-type transition state at very long-range C-Cl and Cl-H distances leading to HCl elimination. The analogous situation for F atom reaction is very different, as seen in Fig. 1 at various levels of theory. In this case adduct formation is more favorable at the C2 carbon (“Markovnikov addition”). Moreover, despite >20 kcal/mol deficit in exoergicity, 2,2 HCl elimination involving the vinylic H atom is favored over the 2,3 HCl elimination owing to the lower barrier.

As seen in Fig. 2, the transition state energies are strongly dependent on the level of theory applied, but in all cases, the 2,2 elimination threshold is significantly lower than 2,3. It is also interesting to compare the transition state structures here with those of the corresponding Cl atom reactions. In the Cl case, the C-Cl distance at the roaming TS is 3.5 Å, compared to 2.3 for the F atom case, and the Cl-H distance is 2.4 Å compared to 1.5 Å for the F atom case. It is also interesting that, at the highest level of theory applied, both F-butene and Cl-butene HX elimination TSs are within 2 kcal/mol of the separated reactants.

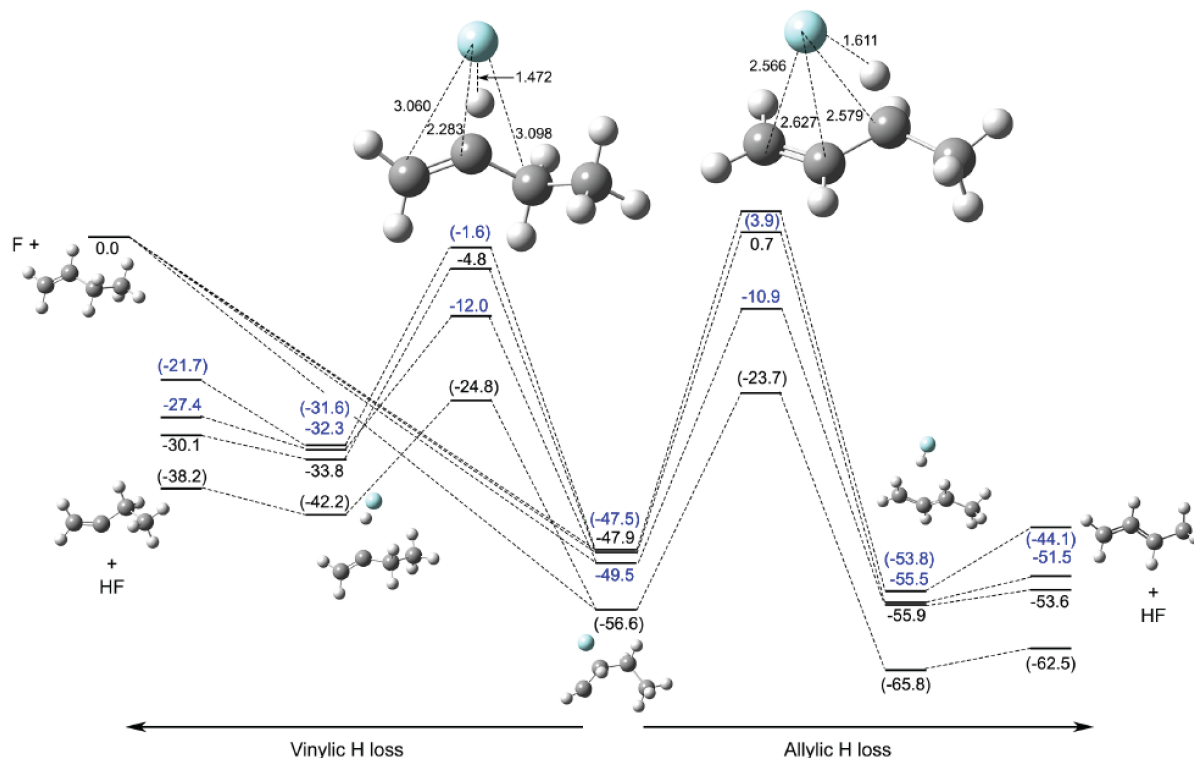


**Figure 2.** Key stationary points on the potential energy surface of the fluorine + 1-butene reaction. Numbers are relative energies with zero point correction for various model chemistries. CBS-QB3 results are in black, B3LYP/6-31+G(d,p) in black with parentheses, WB97XD/6-31+G(d,p) in blue, and G3MP2 using the WB97XD/6-31+G(d,p) geometries in blue with parentheses. Structures shown are from CBS-QB3.

### Crossed-beam $O(^3P)$ reactions

We are now turning our attention to oxygen atom reactions in crossed-beams using a photolytic O atom source and our “universal” VUV probe. Our initial studies are focused on oxygen atom reactions with alkylamines. Fig. 3 shows the preliminary imaging result for  $O(^3P)$  reaction with

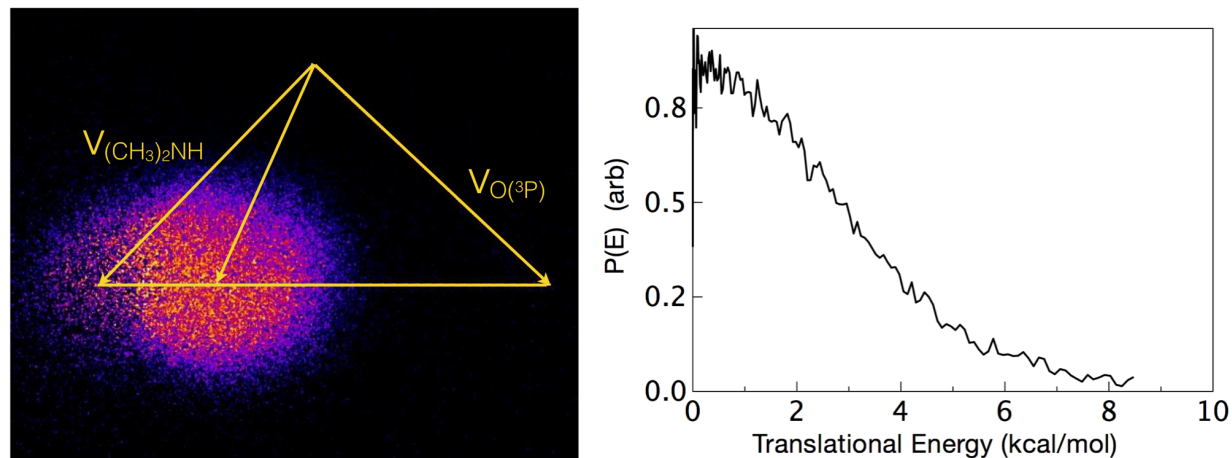


**Figure 3.** DC sliced image of the OH elimination product of the  $O(^3P)$  + dimethylamine reaction at 5.8 kcal/mol collision energy with Newton diagram superimposed (left). Total translational energy distribution (right).

dimethylamine (DMA) at 5.8 kcal/mol collision energy. We see very strong signal for the OH elimination channel likely producing dimethyl amidogen. In addition, we also see, weakly, the  $CH_3CH_2N$  product corresponding to water elimination. Stationary points on the O + DMA surface are shown in Fig. 4. Oxygen atom can add to the nitrogen to form a strongly bound complex,

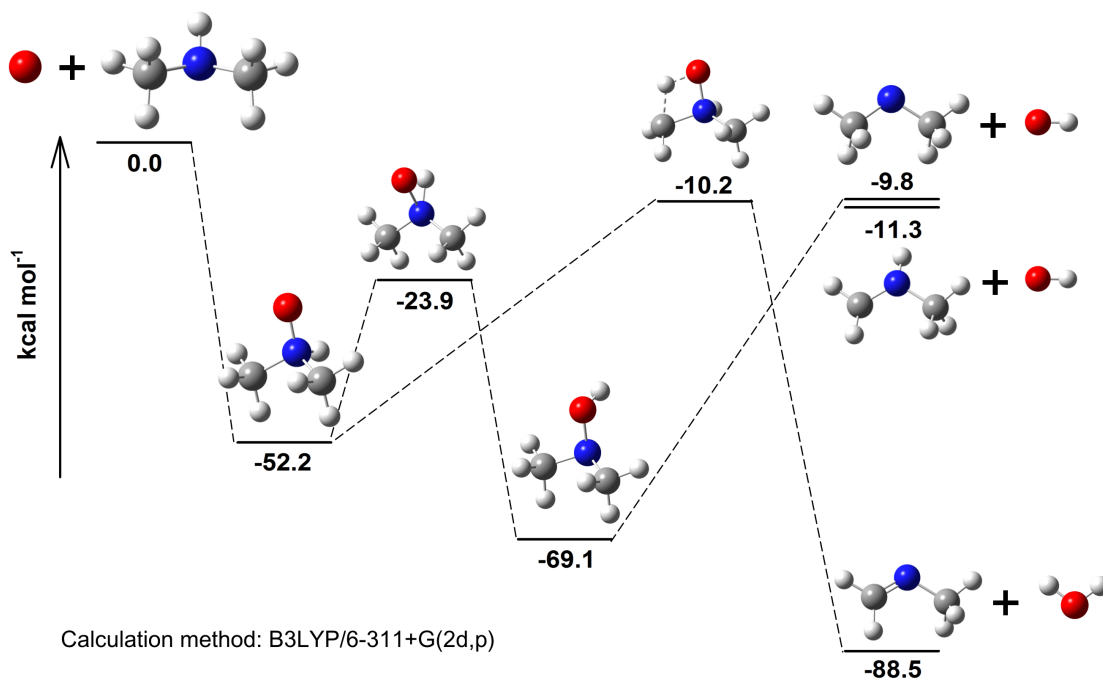


**Figure 4.** Stationary points on the  $O(^3P)$ +DMA potential energy surface.

followed by rearrangement over a modest barrier to the hydroxylamine. We also find a 4-center TS from the adduct to H<sub>2</sub>O elimination. We are currently optimizing our O atom source for ongoing systematic studies, and for the high-resolution O + HCl reaction described in the next section.

### III. Future Directions

We plan to continue our crossed-beam imaging studies with VUV probe of O atom reactions with a variety of alkylamines to characterize more fully the reaction products and pathways. We will then turn to O atom reaction with alcohols. Our more ambitious goals for the oxygen atom studies is to study the O(<sup>3</sup>P)+HCl reaction probing the Cl atom product. Bowman and coworkers have shown theoretical evidence for very strong reactive resonances below the barrier of ~0.5 eV owing to van der Waals wells, but these have not been experimentally detected. The first very sharp resonance for J=0 is predicted at 5.4 kcal/mol, and a number of other strong features appear at increasing energy. This will require intense beams and tight control over the collision energy, but we believe this will be feasible.

### IV. DOE Publications 2013-present

B. Joalland, Van Camp, R. D., Shi, Y., Patel, N., & Suits, A. G., "Crossed-Beam Slice Imaging of Cl Reaction Dynamics with Butene Isomers." *J. Phys. Chem. A*. (2013) DOI: 10.1021/jp403030s.

L. Yan, F. Cudry, W. Li, and A. G. Suits, "Isomer-Specific Mass Spectrometric Detection Via Semi-Soft Strong-Field Ionization," *J. Phys. Chem. A* (2013) DOI: 10.1021/jp403118c.

B. Joalland, Shi, Y., Patel, N., Van Camp, R., & Suits, A., "Dynamics of Cl+ Propane, Butanes Revisited: A Crossed Beam Slice Imaging Study." *Phys. Chem. Chem. Phys.* (2014) DOI: 10.1039/C3CP51785C.

B. Joalland, Y. Shi, A. G. Suits and A. M. Mebel, "Roaming dynamics in radical addition/elimination reactions," *Nature Comm.* (2014) DOI: 10.1038/ncomms5064

B. Joalland, Y. Shi, A. D. Estillore, A. Kamasah, A. M. Mebel, A. G. Suits, "Dynamics of chlorine atom reactions with hydrocarbons: Insights from imaging the radical product in crossed beams," *J. Phys. Chem. A* (2014) doi:10.1021/jp504804n (Feature Article).

F. Cudry, J. M. Oldham, S. Lingenfelter, and A. G. Suits. "Strong-Field Ionization of Flash Pyrolysis Reaction Products." *J. Phys. Chem. A* (2015) **119**, 460-467. DOI: 10.1021/jp510552a.

Y. Shi, A. Kamasah, B. Joalland, and A. G. Suits. "Crossed-Beam DC Slice Imaging of Fluorine Atom Reactions with Linear Alkanes." *J. Chem. Phys.* (2015) **142**, 184309.

Shi, Y. Kamasah, A., Suits, A. G., "'H Abstraction Channels in the Crossed-Beam Reaction of F + 1-Propanol, 1-Butene and 1-Hexene by DC Slice Imaging" *J. Phys. Chem. A*, 120.45 (2016): 8933-8940. DOI: 10.1021/acs.jpca.6b08408.

# An Update on a Novel Multiscale Simulation Strategy for Reacting Flows

PI: James C. Sutherland  
Department of Chemical Engineering, The University of Utah  
Salt Lake City, UT 84112-9203  
James.Sutherland@utah.edu  
Project start date: October, 2012

## I. LBMS Progress Update

We have previously proposed a new methodology to bridge the gap between Large Eddy Simulation (LES) and DNS. This methodology, termed Lattice-Based Multiscale Simulation (LBMS), creates a system of ODT models that overcomes the shortcomings of ODT at a cost significantly cheaper than DNS. Furthermore, by fully solving all governing equations at the smallest scales, all phenomena associated with turbulent combustion can be accurately captured.

### A. Timings

For Lattice-Based Multiscale Simulation (LBMS) to compete with Direct Numerical Simulation (DNS) and Large Eddy Simulation (LES), reasonable speed up must be obtained as the number of grid points is decreased through coarsening. The fine grid spacing,  $\delta_{LBMS}$ , however, is constrained by the turbulent length scales in order for the One-Dimensional Turbulence (ODT) model to appropriately resolve eddies down to the smallest length scales. However, the perpendicular flux reconstruction treatment, which utilizes fully resolved coarse fluxes from other bundles as well as high wave number fluxes from the native bundle, will not necessarily decrease in cost with a decrease in the number of coarse grid cells.

We investigated computational speed ups by maintaining 256 fine grid points while varying the fine to coarse ratio,  $\delta_{LBMS}/\Delta_{LBMS}$ , between  $1/2$ ,  $1/4$ ,  $1/8$ ,  $1/16$ ,  $1/32$ , and  $1/64$ . This case was a cold flow, compressible simulation with periodic boundary conditions. The results were obtained by running the case on three processors. This ensures that communication between processors must occur, as each bundle,  $(x,y,z)$  is decomposed onto its own core. Figure 1 shows that, as LBMS coarsens, flux reconstruction does indeed begin to dominate the computational costs. However, even when coarsening from  $1/32$  to  $1/64$ , there is still a 49% speed up. The bottom axis shows the total number of points on each bundle while the top axis shows the ratio. For example the fastest case has 256 by 4 by 4 control volumes for a total of 4096 cells on its  $x$ -bundle. For this same case, the ratio is  $1/64$ . This speedup shows that, while an asymptotic limit may exist, dramatic coarsening still provides a significant reduction in computational costs. As such, LBMS has the potential to be a viable method for reducing the high computational costs often associated with turbulent flow simulations.

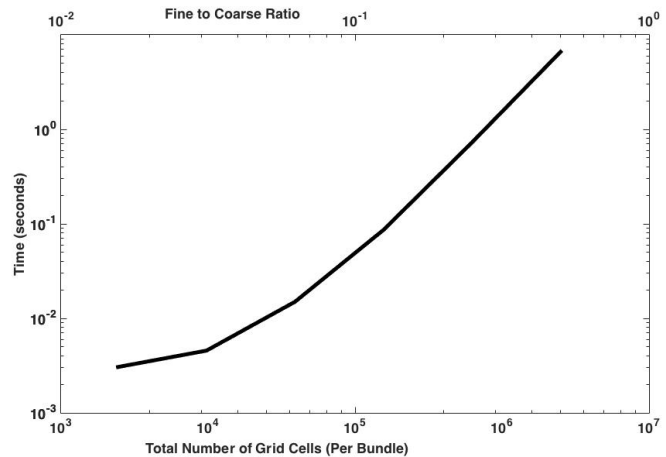


Figure 1: Average time to execute a single time step while varying the coarse grid spacing (*i.e.* the number of ODT lines on each bundle).

### B. Dynamic Eddy Rate Constant

The eddy rate parameter,  $C$ , is fundamental to controlling the “eddy events” associated with ODT modeling. For Reynolds numbers above  $Re > 9000$ , where turbulence is fully developed, an eddy rate constant of  $C = 10$  allows stand alone ODT models to accurately capture the effects of turbulence. However, at Reynolds numbers between  $2250 > Re > 9000$ , in the transitional regime, the eddy rate constant must be increased in order to ensure that enough triplet mapping events are produced. While current literature in this area is lacking, preliminary research suggests an empirical formulation,

$$C = \begin{cases} 10 & Re > 9000 \\ bRe^a & 2250 \leq Re \leq 9000 \end{cases}$$

where  $a = -1.49$  and  $b = e^{15.1}$ , represents this transitional regime appropriately [1]. When attempting to reproduce the kinetic energy decay from the Comte-Bellot and Corrsin grid generated isotropic turbulence experimental data, the decreasing Reynolds number has given LBMS issues, as shown in Figure 2. This corroborates other research that suggests that the eddy rate constant must increase as the Reynolds number decreases [2, 3]. As such, a dynamic eddy rate constant will need to be implemented. This area is ripe for investigation, not just for LBMS but for traditional ODT as well. However, as LBMS is a three-dimensional model that consists of many ODT lines, it may be particularly important to have eddy rate constants local to each individual ODT line within a bundle.

### C. Investigating Coarse to Fine Ratios

Maintaining a constant eddy rate and increasing the coarse grid spacing also affects decay as well, as shown in Figure 3. These results have important implications for tuning the turbulent decay. As we refine our coarse ratio (i.e. add more ODT lines in each bundle), the total kinetic energy decay is increased dramatically. This implies that decreasing the eddy rate constant with respect to the number of ODT lines on each bundle will be necessary to accurately capture the decay rate. A parametric study is being completed at  $Re > 9000$ , to determine an appropriate scaling without introducing effects due to a transitional regime. The result will then be tested against a range of Reynolds numbers to ensure that the scaling is appropriate. Unlike a dynamic eddy rate constant, however, scaling based on the coarse to fine ratio will be static, though, allowing for a practically computationally free implementation.

### D. Ignition, Flame Stand-off and Future Work

The ultimate goal of this project is to create a novel methodology that can accurately capture lifted flame fronts within a computationally cost effective framework. We have now demonstrated ignition of a cold fuel jet in a hot oxidizer environment. Figure 4 shows a streamwise line of sight down a two-dimensional delayed ignition case where a cold fuel is injected into a hot oxidizer. While this case is laminar, we finally have every tool implemented that is necessary to reach our goals. Focus will now be shifted from implementation to performing and publishing studies on everything from ODT parameter tuning to investigating mixing rates in a turbulent cold flow planar jets to simulating turbulent jet flames.

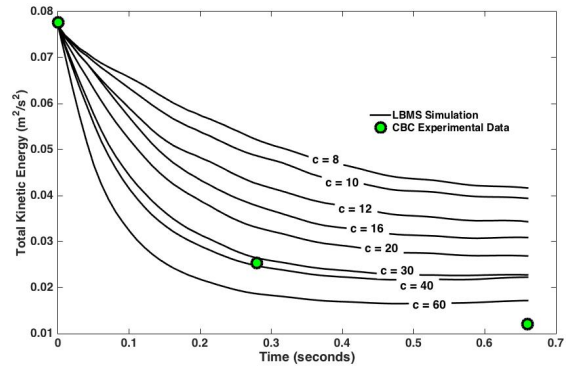


Figure 2: Isotropic Turbulence Decay with  $[4, 4, 4]$  coarse points and  $[512, 512, 512]$  fine grid points. The Eddy Rate Constant,  $C$ , is increased from 8 to 60. Experimental data points at  $t = 0, 0.28$  and  $0.66$  s.

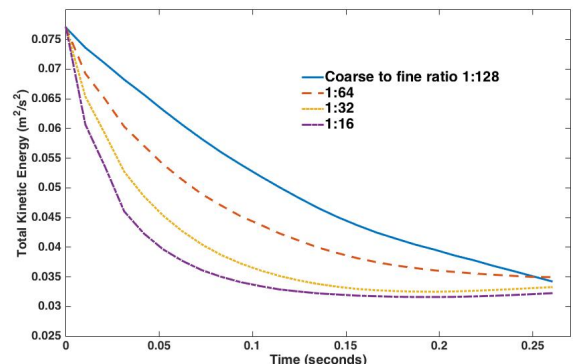


Figure 3: Isotropic Turbulence Decay with an eddy rate constant of  $C = 20$  and  $[512, 512, 512]$  fine grid points.

## II. Tools for Analysis of Chemical Dynamics

### A. Web-Application for Zero-Dimensional Reactor Simulation

In connection with a senior design project for computer science students, we have developed a robust, efficient, web-based tool for parametric simulation of zero dimensional reactors with finite residence time. This leverages recent advances in robust time integration for combustion chemistry [4, 5] to provide a convenient way of analyzing chemical mechanisms and obtaining physical insight into the behavior of large mechanisms such as those for biofuels.

This web interface allows the user to specify different chemical mechanisms, residence times, as well as initial temperature, pressure and species mole fractions as parametric inputs and can provide either transient or steady-state solutions. This work was recently presented at the SIAM International Numerical Combustion Meeting in April 2017 in Orlando, Florida [6].

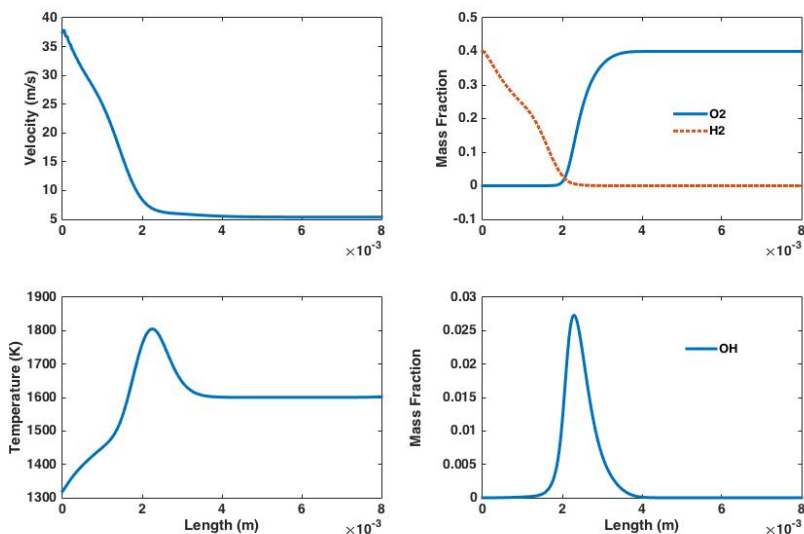


Figure 4: Centerline profiles of a reacting jet case with an inlet velocity of  $40\text{ m/s}$ , a cold hydrogen fuel jet at  $800\text{ K}$  into a heated oxidizer at  $1600\text{ K}$ .

### B. Stiffness Reduction via Principal Component Analysis

Finally, we have provided formal analysis of principal component analysis (PCA) based modeling frameworks recently proposed [7, 8]. The motivation for this work came from the empirical observations from previous work that suggest when PCA is used to reduce the dimensionality of a system, it also reduces the stiffness.

We have studied stiffness of the original system as well as a reduced PC-space systems by comparing eigenvalues of the Jacobian matrices of the conserved chemical source terms and of the principal components once the PC space has been truncated. Two methods are evaluated for obtaining the Jacobian in PC space: performing a similarity transformation on the Jacobian in state space using the PCA transformation matrix and using a finite-differenced Jacobian from the regression of the source terms in PC space on the PCs. Autoignition training data for adiabatic, constant volume batch reactors was first generated. Variables that did not deviated from zero were removed, and the remaining variables were centered and scaled before applying PCA. Timescales (inverse eigenvalues) were then compared for the two methods of obtaining the Jacobian in PC space with the Jacobian in state space.

Results for a 57-species ethanol mechanism are shown in Figure 5 for the similarity transform method with different PCA scalings, which shows that PCA eliminates the fastest timescales, thereby reducing stiffness in the resulting system. We also found that the timescales in PC space, regardless of the method used to calculate them, show sharp peaks at various times during the autoignition events. This suggests that, when using an implicit time integrator, it may be difficult to reach a physically realizable solution in PC space for autoignition. Future work will explore the performance of these cases in solving the governing equations in PC space compared to those in state space. Including more training data as well as possibly training with steady flamelets or one-dimensional premixed systems could result in better manifolds in PC space, reducing the nonlinearities in the timescales. This work will be presented at the US National Combustion meeting in April, 2017 [9].

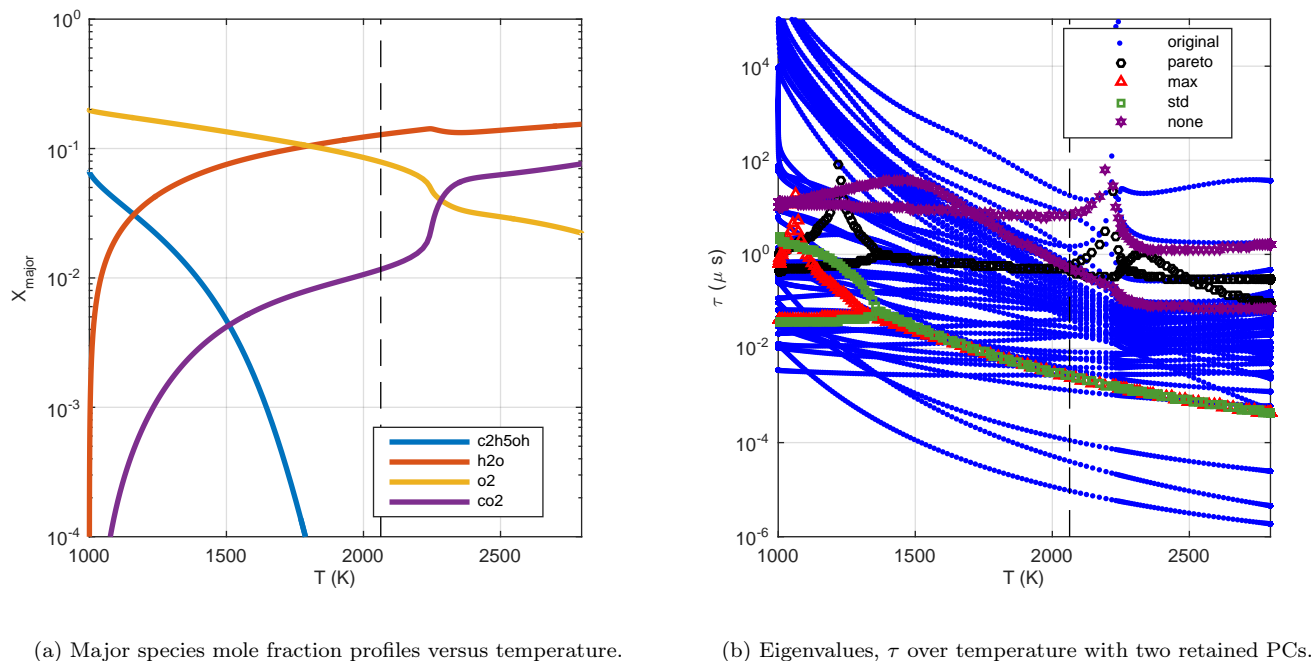


Figure 5: Ethanol autoignition event in air at 1000 K, one atm. The dashed black line shows the temperature at the ignition delay.

## References

- [1] Naveen Punati. *An Eulerian One-Dimensional Turbulence Model : Application to Turbulent and Multi-phase Reacting Flows*. PhD thesis, University of Utah, 2012.
- [2] Esteban D. Gonzalez-Juez, Rodney C. Schmidt, and Alan R. Kerstein. ODTLES simulations of wall-bounded flows. *Physics of Fluids*, 23(12):125102, 2011.
- [3] R. Schmidt, A. Kerstein, and R. McDermott. ODTLES: A multi-scale model for 3D turbulent flow based on one-dimensional turbulence modeling. *Comp. Methods in Appl. Mech. and Eng.*, 199:865–880, 2010.
- [4] M A Hansen and J C Sutherland. Pseudotransient Continuation for Combustion Simulation with Detailed Reaction Mechanisms. *SIAM Journal on Scientific Computing*, 38(2):B272–B296, jan 2016.
- [5] Michael Alan Hansen and James Clayton Sutherland. Dual timestepping methods for detailed combustion chemistry. *Combustion Theory and Modelling*, pages 1–17, oct 2016.
- [6] E. Armstrong, M. A. Hansen, and J. C. Sutherland. A Web-Based Tool for Simulation and Numerical Analysis of Zero-Dimensional Combustion Problems. In *16<sup>th</sup> Intl. Conference on Numerical Combustion*, Orlando, FL, April 2017.
- [7] J. Sutherland and A. Parente. Combustion modeling using principal component analysis. *Proc. Combust. Inst.*, 32(1):1563–1570, 2009.
- [8] Amir Biglari and James C Sutherland. An a-posteriori evaluation of principal component analysis-based models for turbulent combustion simulations. *Combustion and Flame*, 162(10):4025–4035, oct 2015.
- [9] E Armstrong, M A Hansen, and J C Sutherland. Assessment of Stiffness Reduction in Chemical Reacting Systems Using Principal Component Analysis. In *10<sup>th</sup> US National Combustion Meeting*, College Park, MD, April 2017.

# Elementary Reaction Kinetics of Combustion Species

Craig A. Taatjes

*Combustion Research Facility, Mail Stop 9055, Sandia National Laboratories,  
Livermore, CA 94551-0969  
cataatj@sandia.gov*

## SCOPE OF THE PROGRAM

This program aims to develop new methods for studying chemical kinetics and to apply these methods to the investigation of fundamental chemistry relevant to hydrocarbon oxidation and combustion science. One central goal is to perform accurate measurements of the rates at which important free radicals react with each other and with stable molecules. Another goal is to characterize complex reactions that occur via multiple potential wells by investigating the formation of products. These investigations employ simultaneous time-resolved detection of multiple species in well-characterized photolytically-initiated reaction systems where multiple consecutive and competing reactions may occur. Detailed characterization of these reactions under accessible experimental conditions increases the confidence with which these and similar reactions can be predicted for energy mission applications. This research often requires the development and use of new detection methods for precise and accurate kinetics measurements. Absorption-based techniques and mass-spectrometric methods have been emphasized, because many key intermediates are not amenable to fluorescence detection.

An important part of our strategy, especially for complex reaction systems, is using experimental data to test and refine detailed calculations (working in close cooperation with Stephen Klippenstein and Ahren Jasper at Argonne and Judit Zádor at Sandia), where the theory enables rigorous interpretation of experimental results and guides new measurements that will probe key aspects of potential energy surfaces. Moreover, we have increasingly aimed at producing elusive and scientifically important species that are intermediates in oxidation systems (e.g., Criegee intermediates, hydroperoxyalkyl radicals) and characterizing their reactivity through direct probing of their kinetics.

## RECENT PROGRESS

We continue to apply frequency-modulation and direct absorption spectroscopy to measurements of OH and HO<sub>2</sub> product formation in reactions of hydrocarbon and oxygenated hydrocarbon radicals with O<sub>2</sub>. These experiments are often coordinated with measurements of other products using the multiplexed photoionization mass spectrometric reactor at the Advanced Light Source (ALS), an experimental effort led by David Osborn (see his abstract). We have also continued to expanding our understanding of the chemistry of carbonyl oxides (Criegee intermediates), closed-shell singlet species that are nevertheless reactive with stable molecules. Their unusual electronic structure may make their reactivity a probe of multiple-state interactions.<sup>1</sup>

**Ketohydroperoxide formation in neopentane oxidation.** Product formation in time-resolved, Cl-atom initiated neopentane oxidation experiments in the temperature range 550 K – 675 K using synchrotron photoionization time-of-flight mass spectrometry. Experiments were performed both at 1 – 2 atm pressure using a high-



pressure reactor and also at ~ 9 Torr pressure employing a low-pressure reactor for comparison. Because of the highly symmetric structure of neopentane, ketohydroperoxide signal is can be attributed to a 3-hydroperoxy-2,2-dimethylpropanal isomer, i.e. from a  $\gamma$ -ketohydroperoxide ( $\gamma$ -KHP). The photoionization spectra of the  $\gamma$ -KHP measured at low- and high pressures and varying oxygen concentrations agree well with each other, further supporting they originate from the single isomer. Measurements of the products of the oxidation suggest that the “Korcek” mechanism may play an important role in the decomposition of 3-hydroperoxy-2,2-dimethylpropanal, especially at lower temperatures. However, at higher temperatures where  $\gamma$ -KHP decomposition to hydroxyl radical and oxy-radical dominates, oxidation of the oxy-radical yields a new important channel leading to acetone, carbon monoxide, and OH radical. A strongly temperature-dependent reaction product is observed at  $m/z = 100$ , likely attributable to 2,2-dimethylpropanedial.

**Reactions of Carbonyl Oxides.** The investigation of the reactions of carbonyl oxides, or Criegee intermediates, has also continued in the past year, in collaboration with Carl Percival (Manchester) and Dudley Shallcross and Andrew Orr-Ewing (Bristol). Partly through a new collaboration with Marsha Lester (Penn), we have interest in isomerization reactions of Criegee intermediates, particularly isomerization that is assisted via bimolecular interactions. Criegee intermediate reactions often form bound intermediates whose subsequent decomposition can follow several possible channels.

We measured the reactions of acetone oxide,  $(\text{CH}_3)_2\text{COO}$  and  $(\text{CD}_3)_2\text{COO}$  with  $\text{SO}_2$  and  $\text{NO}_2$  by synchrotron photoionization mass spectrometry. The rate coefficient of the reaction of the Criegee intermediate with  $\text{SO}_2$  was measured using photoionization mass spectrometry and pseudo-first order methods to be  $(7.3 \pm 0.5) \times 10^{-11} \text{ cm}^3 \text{ s}^{-1}$  at 298 K and 4 Torr and  $(1.5 \pm 0.5) \times 10^{-10} \text{ cm}^3 \text{ s}^{-1}$  at 298 K and 10 Torr (He buffer). Measurements with deuterated acetone oxide at 4 Torr show an inverse deuterium kinetic isotope effect,  $k_{\text{H}}/k_{\text{D}} = (0.53 \pm 0.06)$ , for reactions with  $\text{SO}_2$ . Both observations may be consistent with recent suggestions that the formation of an association complex affects the rate coefficient. Product measurements of the reactions of  $(\text{CH}_3)_2\text{COO}$  with  $\text{NO}_2$  and with  $\text{SO}_2$  suggest that these reactions may facilitate isomerization to 2-hydroperoxypropene, possibly by subsequent reactions of association products.

In collaboration with Marsha Lester (Penn) and Ward Thompson (Kansas), hydroxyacetone ( $\text{CH}_3\text{C}(\text{O})\text{CH}_2\text{OH}$ ) was observed as a stable end product from the  $(\text{CH}_3)_2\text{COO}$  Criegee intermediate in a flow tube coupled with multiplexed photoionization mass spectrometer detection. Complementary electronic structure calculations reveal multiple reaction pathways for hydroxyacetone formation, including unimolecular isomerization via hydrogen atom transfer and  $-\text{OH}$  group migration as well as self-reaction of Criegee intermediates. The hydroxyacetone end product provides an effective, stable marker for the production of Criegee intermediates in future studies of alkene ozonolysis.

The reactions of Criegee intermediates with  $\text{NO}_2$  have been proposed to form  $\text{NO}_3$ , which is an important nighttime oxidant in Earth’s troposphere. However, previous efforts to characterize the yield of  $\text{NO}_3$  from these reactions have been inconclusive, with many studies failing to detect  $\text{NO}_3$ . We studied the reactions of formaldehyde oxide

(CH<sub>2</sub>OO) and acetaldehyde oxide (CH<sub>3</sub>CHOO) with NO<sub>2</sub> to further explore the product formation over a pressure range of 4-40 Torr. We were unable to observe NO<sub>3</sub> under any of these conditions, and through quantification of the carbonyl species that would be the co-product of NO<sub>3</sub> formation derived an upper limit for NO<sub>3</sub> of 30%. However, temporally resolved and [NO<sub>2</sub>]-dependent signal is observed at the mass of the Criegee-NO<sub>2</sub> adduct for both formaldehyde- and acetaldehyde- oxide systems. The photoionization spectrum of the adduct has been measured.

## FUTURE DIRECTIONS

We will continue our collaboration with David Osborn and Lenny Sheps, using their photoionization mass spectrometry machines at the Advanced Light Source, and explore effects of unsaturation and oxygenation on low-temperature oxidation chemistry in coordination with Judit Zádor, Ahren Jasper, and Stephen Klippenstein. Measurements of elementary oxidation reactions of representative hydrocarbon and substituted hydrocarbon molecules will continue, with a goal of reaching an understanding of the complex interactions that govern the product formation in these reactions.

## References

1. Miliordos, E.; Xantheas, S. S., The Origin of the Reactivity of the Criegee Intermediate: Implications for Atmospheric Particle Growth. *Angew. Chem. Int. Ed.* **2016**, *55*, 1015 –1019.

## Publications acknowledging BES support for CAT, 2015 –

- a. Arkke J. Eskola, Ivan O. Antonov, Leonid Sheps, John D. Savee, David L. Osborn, and Craig A. Taatjes, “Time-resolved measurements of product formation in the low-temperature (550 – 675 K) oxidation of neopentane: a probe to investigate chain-branching mechanism,” accepted to *Phys. Chem. Chem. Phys.*
- b. Craig A. Taatjes, “Criegee Intermediates: What Direct Production and Detection Can Teach Us about Reactions of Carbonyl Oxides,” *Annu. Rev. Phys. Chem.* in press, doi:10.1146/annurev-physchem-052516-050739.
- c. Rebecca L. Caravan, M. Anwar H. Khan, Brandon Rotavera, Ewa Papajak, Ivan O. Antonov, Ming-Wei Chen, Kendrew Au, Wen Chao, David L. Osborn, Jim Jr-Min Lin, Carl J. Percival, Dudley E. Shallcross, Craig A. Taatjes, “Products of Criegee Intermediate Reactions with NO<sub>2</sub>: Experimental Measurements and Tropospheric Implications,” *Faraday Discuss.* in press (2017).
- d. Craig A. Taatjes, Fang Liu, Brandon Rotavera, Manoj Kumar, Rebecca Caravan, David L. Osborn, Ward H. Thompson, and Marsha I. Lester, “Hydroxyacetone Production from C<sub>3</sub> Criegee Intermediates,” *J. Phys. Chem. A* **121**, 16–23, (2017).
- e. Rabi Chhantyal-Pun, Oliver Welz, John D. Savee, Arkke J. Eskola, Edmond P. F. Lee, Lucy Blacker, Henry R. Hill, Matilda Ashcroft, M. Anwar H. Khan, Guy C. Lloyd-Jones, Louise Evans, Brandon Rotavera, Haifeng Huang, David L. Osborn, Daniel K. W. Mok, John M. Dyke, Dudley E. Shallcross, Carl J. Percival, Andrew J. Orr-Ewing, and Craig A. Taatjes “Direct measurements of unimolecular and bimolecular reaction kinetics of the Criegee intermediate (CH<sub>3</sub>)<sub>2</sub>COO,” *J. Phys. Chem. A* **121**, 4–15 (2017)
- f. Adam M. Scheer, Arkke J. Eskola, David L. Osborn, Leonid Sheps, Craig A. Taatjes, “Resonance Stabilization Effects on Ketone Autoxidation: Isomer-Specific Cyclic Ether and Ketohydroperoxide Formation in the Low-Temperature (400 – 625 K) Oxidation of Diethyl Ketone,” *J. Phys. Chem. A* **120**, 8625–8636 (2016).
- g. Kai Moshhammer, Ahren W. Jasper, Denisia M. Popolan-Vaida, Zhandong Wang, Vijai Shankar Bhavani Shankar, Lena Ruwe, Craig A. Taatjes, Philippe Dagaut, and Nils Hansen, “Quantification of the Keto-hydroperoxide (HOCH<sub>2</sub>OCHO) and Other Elusive Intermediates during Low-Temperature Oxidation of Dimethyl Ether,” *J. Phys. Chem. A* **120**, 7890–7901 (2016).
- h. Ivan O. Antonov, Judit Zádor, Brandon Rotavera, Ewa Papajak, David L. Osborn, Craig A. Taatjes, and Leonid Sheps, “Pressure-Dependent Competition among Reaction Pathways from First- and Second-O<sub>2</sub> Additions in the Low-Temperature Oxidation of Tetrahydrofuran,” *J. Phys. Chem. A*, **120**, 6582–6595 (2016).
- i. Zhandong Wang, Lidong Zhang, Kai Moshhammer, Denisia M. Popolan-Vaida, Vijai Shankar Bhavani Shankar, Arnas Lucassen, Christian Hemken, Craig A. Taatjes, Stephen R. Leone, Katharina Kohse-Hoeinghaus, Nils

- Hansen, Philippe Dagaut, and S. Mani Sarathy, "Additional chain-branching pathways in the low-temperature oxidation of branched alkanes," *Combust. Flame* **164**, 386-396 (2016).
- j. Matthew B. Prendergast, Benjamin B. Kirk, John D. Savee, David L. Osborn, Craig A. Taatjes, Kye-Simeon Masters, Stephen J. Blanksby, Gabriel da Silva, and Adam J. Trevitt, "Formation and stability of gas-phase o-benzoquinone from oxidation of ortho-hydroxyphenyl: a combined neutral and distonic radical study," *Phys. Chem. Chem. Phys.* **18**, 4320-4332 (2016).
- k. Giel Muller, Adam Scheer, David L. Osborn, Craig A. Taatjes, and Giovanni Meloni, "Low Temperature Chlorine-Initiated Oxidation of Small-Chain Methyl Esters: Quantification of Chain-Terminating HO<sub>2</sub>-Elimination Channels," *J. Phys. Chem. A* **120**, 1677-1690 (2016).
- l. Oliver Welz, John D. Savee, David L. Osborn, and Craig A. Taatjes, "Chlorine atom-initiated low-temperature oxidation of prenil and isoprenol: The effect of C=C double bonds on the peroxy radical chemistry in alcohol oxidation," *Proc. Combust. Inst.* **35**, 401-408 (2015).
- m. Adam M. Scheer, Oliver Welz, Subith S. Vasu, David L. Osborn, and Craig A. Taatjes, "Low temperature (550-700 K) oxidation pathways of cyclic ketones: dominance of HO<sub>2</sub>-elimination channels yielding conjugated cyclic coproducts," *Phys. Chem. Chem. Phys.* **17**, 12124-12134 (2015).
- n. John D. Savee, Talitha M. Selby, Oliver Welz, Craig A. Taatjes, and David L. Osborn, "Time- and Isomer-Resolved Measurements of Sequential Addition of Acetylene to the Propargyl Radical," *J. Phys. Chem. Lett.* **6**, 4153-4158 (2015).
- o. John D. Savee, Ewa Papajak, Brandon Rotavera, Haifeng Huang, Arkke J. Eskola, Oliver Welz, Leonid Sheps, Craig A. Taatjes, Judit Zador, and David L. Osborn, "Direct observation and kinetics of a hydroperoxyalkyl radical (QOOH)," *Science* **347**, 643-646 (2015).
- p. John D. Savee, Sampada Borkar, Oliver Welz, Balint Sztaray, Craig A. Taatjes, and David L. Osborn, "Multiplexed Photoionization Mass Spectrometry Investigation of the O(<sup>3</sup>P) + Propyne Reaction," *J. Phys. Chem. A* **119**, 7388-7403 (2015).
- q. Kai Moshhammer, Ahren W. Jasper, Denisia M. Popolan-Vaida, Arnas Lucassen, Pascal Dievarti, Hatem Selim, Arkke J. Eskola, Craig A. Taatjes, Stephen R. Leone, S. Mani Sarathy, Yiguang Ju, Philippe Dagaut, Katharina Kohse-Hoeinghaus, and Nils Hansen, "Detection and Identification of the Keto-Hydroperoxide (HOOCH<sub>2</sub>OCHO) and Other Intermediates during Low-Temperature Oxidation of Dimethyl Ether," *J. Phys. Chem. A* **119**, 7361-7374 (2015).
- r. Jessica F. Lockyear, Martin Fournier, Ian R. Sims, Jean-Claude Guillemin, Craig A. Taatjes, David L. Osborn, and Stephen R. Leone, "Formation of fulvene in the reaction of C<sub>2</sub>H with 1,3-butadiene," *Int. J. Mass Spectrom.* **378**, 232-245 (2015).
- s. Gustavo A. Garcia, Xiaofeng Tang, Jean-Francois Gil, Laurent Nahon, Michael Ward, Sebastien Batut, Christa Fittschen, Craig A. Taatjes, David L. Osborn, and Jean-Christophe Loison, "Synchrotron-based double imaging photoelectron/photoion coincidence spectroscopy of radicals produced in a flow tube: OH and OD," *J. Chem. Phys.* **142**, 164201 (2015).
- t. A. J. Eskola, O. Welz, J. Zador, I. O. Antonov, L. Sheps, J. D. Savee, D. L. Osborn, and C. A. Taatjes, "Probing the low-temperature chain-branching mechanism of *n*-butane autoignition chemistry via time-resolved measurements of ketohydroperoxide formation in photolytically initiated *n*-C<sub>4</sub>H<sub>10</sub> oxidation," *Proc. Combust. Inst.* **35**, 291-298 (2015).
- u. Oliver Welz, Michael P. Burke, Ivan O. Antonov, C. Franklin Goldsmith, John D. Savee, David L. Osborn, Craig A. Taatjes, Stephen J. Klippenstein, and Leonid Sheps, "New Insights into Low-Temperature Oxidation of Propane from Synchrotron Photoionization Mass Spectrometry and Multiscale Informatics Modeling," *J. Phys. Chem. A* **119**, 7116-7129 (2015).
- v. Michael P. Burke, C. Franklin Goldsmith, Stephen J. Klippenstein, Oliver Welz, Haifeng Huang, Ivan O. Antonov, John D. Savee, David L. Osborn, Judit Zador, Craig A. Taatjes, and Leonid Sheps, "Multiscale Informatics for Low-Temperature Propane Oxidation: Further Complexities in Studies of Complex Reactions," *J. Phys. Chem. A* **119**, 7095-7115 (2015).
- w. Leah G. Dodson, Linhan Shen, John D. Savee, Nathan C. Eddingsaas, Oliver Welz, Craig A. Taatjes, David L. Osborn, Stanley P. Sander, and Mitchio Okumura, "VUV Photoionization Cross Sections of HO<sub>2</sub>, H<sub>2</sub>O<sub>2</sub>, and H<sub>2</sub>CO," *J. Phys. Chem. A* **119**, 1279-1291 (2015).
- x. David L. Osborn and Craig A. Taatjes, "The physical chemistry of Criegee intermediates in the gas phase," *Int. Rev. Phys. Chem.* **34**, 309-360 (2015).

# Elementary Reactions of PAH Formation

Robert S. Tranter

Chemical Sciences and Engineering Division, Argonne National Laboratory

Argonne, IL-60439

tranter@anl.gov

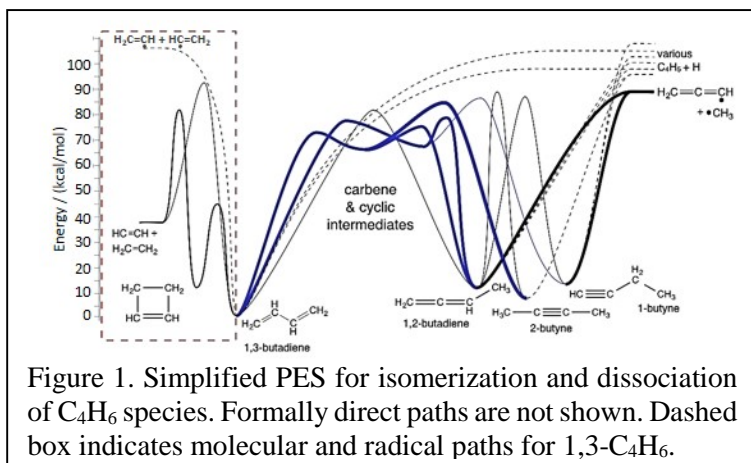
## I. Program Scope

This program is focused on the experimental determination of kinetic and mechanistic parameters of elementary reactions, in particular those involved in the formation and destruction of the building blocks for aromatic species. The program also encompasses dissociation of novel fuels such as ethers and cyclic species and their dissociation products that are representative of oxygenated intermediates in combustion mechanisms. Thermal sources of radicals are investigated and characterized for use in more complex reaction systems where secondary chemistry can be significant. Recently, the scope has been increased to include thermally initiated roaming reactions. The approach involves a diaphragmless shock tube (DFST) equipped with laser schlieren (LS) and a time-of-flight mass spectrometer (TOF-MS). The combination of these techniques accesses a wide range of reaction temperatures and pressures. Finally, X-ray diagnostics have recently been used to study flows in hostile environments to obtain a better understanding of how to accurately interpret information from some common experimental devices.

## II. Recent Progress

### A. Pyrolysis of $C_4H_6$ isomers and the importance of formally direct reactions

The chemistry of small unsaturated hydrocarbons, such as 1,3-butadiene (1,3- $C_4H_6$ ), 1,2-butadiene (1,2- $C_4H_6$ ), 2-butyne (2- $C_4H_6$ ) and 1-butyne (1- $C_4H_6$ ), is of central importance to the modeling of combustion systems. These species are important intermediates, yet their high-temperature chemistry remains poorly understood. For instance, several groups have studied the dissociation of 1,3- $C_4H_6$  and proposed dissociation pathways leading to radical products<sup>1</sup> or molecular products<sup>2</sup> (dashed box, Fig. 1) or isomerization.<sup>3</sup>



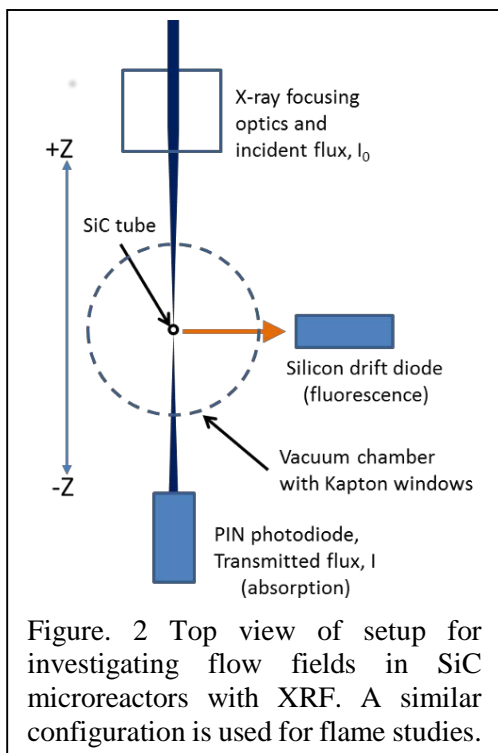
The simplified PES shown in Fig. 1 shows the intimate linkage between the isomers. Thus understanding the chemistry of one  $C_4H_6$  isomer necessitates developing a model that treats all the isomers simultaneously. Consequently, we have investigated the thermal decompositions of 1,3- $C_4H_6$ , 1,2- $C_4H_6$ , 2- $C_4H_6$  and 1- $C_4H_6$  behind incident shock waves (total of 382 experiments), at incident shock pressures,  $P_2$ , of 26–261 Torr and temperatures,  $T_2$ , of 1428–2354 K, using laser schlieren densitometry. The

experimental work was complemented by an ab initio/master equation study in collaboration with Goldsmith (Brown). The theoretical work provided constraints for modeling the experiments; initial estimates of branching ratios for competing paths; and most importantly, identified two formally direct dissociation paths. These paths have not been previously reported but are critical to simulate the current work and the literature accurately. The formally direct paths connect 1,3-butadiene and 2-butyne to the major products  $CH_3$  and  $C_3H_3$  avoiding the need for the isomerization steps that by Hidaka et al.<sup>3,4</sup> considered important. A chemical kinetic model has been constructed including isomerization and dissociation channels or the four isomers and the formally direct paths for 1,3- $C_4H_6$  and 1- $C_4H_6$ . The thermochemical data include the latest ATcT evaluation from Ruscic for  $CH_3$ ,  $^3CH_2$  and  $C_2H_6$  that include

anharmonic corrections. From simulation of the LS profiles it was determined that the isomerization paths are actually quite minor, contrary to the literature, and that the formally direct and direct dissociation paths to  $\text{CH}_3 + \text{C}_3\text{H}_3$  dominate. The product distributions that led Hidaka et al. to propose a dominant role for isomerization of  $\text{C}_4\text{H}_6$  can be explained by recombination of  $\text{CH}_3 + \text{C}_3\text{H}_3$  and a minor role of isomerization. The final model provides very good simulations of all the LS experiments and reproduces Hidaka's single pulse shock tube results for all four isomers very well, and Kern and Kiefer's ST/TOFMS results for 1,2-butadiene. Rate coefficients for the major dissociation paths have been obtained for each isomer and all display strong pressure dependencies. For 1,2- $\text{C}_4\text{H}_6$ , 1- $\text{C}_4\text{H}_6$  and 2- $\text{C}_4\text{H}_6$  these are in very good agreement with the values predicted by Goldsmith. However, there are differences of up to a factor of 4 for 1,3- $\text{C}_4\text{H}_6$ . The phase space theory used by Goldsmith has uncertainties of up to a factor of 5 and refining the theoretical model will be the focus of future work.

## B. Dissociation of cyclic species-Cyclopentane

Cyclic species form a significant fraction of fuels but the pyrolytic chemistry of many of these is poorly described. The dissociation of cyclopentane and cycloheptane have been studied by DFST/LS to complement prior investigations by Kiefer et al.<sup>5</sup> on cyclohexane. The work on cycloheptane is ongoing whereas that of cyclopentane is complete. The pyrolysis of cyclopentane was studied at  $P_2$  of 35-300 Torr and  $T_2$  of 1472-2074 K. As usual, rate coefficients for key steps were obtained by simulating the LS profiles. The primary reaction removing cyclopentane is C-C scission to form a biradical which rapidly isomerizes to 1-pentene, similar to cyclohexene dissociation. Over most of the experimental range 1-pentene readily dissociates to  $\text{C}_2\text{H}_5 + \text{C}_3\text{H}_5$  and  $\text{C}_2\text{H}_5$  immediately yields  $\text{H} + \text{C}_2\text{H}_4$ . Thus unlike the cyclohexane system which generates two stable allyl radicals the secondary chemistry of cyclopentane is dominated by H-atom reactions and H + cyclopentane has to be accounted for. The rate coefficients for formation of 1-pentene from cyclopentane show a modest pressure dependence that is well replicated by RRKM calculations with  $E_0 = 80.0 \text{ kcal mol}^{-1}$  and  $\langle \Delta E_{\text{down}} \rangle = 300 \text{ cm}^{-1}$ . The calculated rate coefficients are given by:  $k_{1(35\text{Torr})} = (7.93 \pm 3.96) \times 10^{84} \text{ T}^{-19.815} \exp(-64366/\text{T}) \text{ s}^{-1}$ ,  $k_{1(70\text{Torr})} = (4.79 \pm 2.39) \times 10^{77} \text{ T}^{-17.705} \exp(-62316/\text{T}) \text{ s}^{-1}$ ,  $k_{1(150\text{Torr})} = (2.42 \pm 1.21) \times 10^{69} \text{ T}^{-15.295} \exp(-59862/\text{T}) \text{ s}^{-1}$ ,  $k_{1(300\text{Torr})} = (4.66 \pm 2.33) \times 10^{61} \text{ T}^{-13.065} \exp(-57493/\text{T}) \text{ s}^{-1}$ , and  $k_{1\infty} = (1.69 \pm 0.85) \times 10^{16} \text{ T}^{-0.005} \exp(-42983/\text{T})$ . The high-pressure limit rates for cyclopentane dissociation are also compared with previous results in the literature and show good agreement with a study by Tsang.<sup>6</sup> In a separate study, dissociation of 1-pentene ( $P_2=30\text{-}300 \text{ Torr}$ ,  $T_2=1250\text{-}1900 \text{ K}$ ) has been investigated. While this work is ongoing to unravel the complicated secondary chemistry which is driven by H-atoms it has yielded solid rate coefficients for dissociation of 1-pentene that form a key part of the cyclopentane model.



## C. X-ray fluorescence investigations of high temperature flow fields

Obtaining 2D images of flow fields in hostile environments is challenging and this can be exacerbated by optical access to the chamber and, the opacity of the fluid and environment. Recently, in collaboration with Alan Kastengren (APS, 7BM), X-ray fluorescence (XRF) of rare gases has been exploited to obtain 2D raster scan images of gas densities and hence temperatures in flowing fluids. These images reveal unprecedentedly detailed information of the flow fields under study. Two examples are given below. The first study imaged flow fields inside a heated, SiC microreactor which is opaque to normal light sources. These data are intended for testing CFD simulations of flows in microreactors and developing

methods of extracting kinetic data from reactions in the reactors. The second study is an ongoing project with Hansen (Sandia) to probe, in low pressure flame/mass spectrometry experiments, the perturbation of the flame by the sampling cone.

**SiC:** Density profiles of flowing gases within an opaque, heated, silicon carbide (SiC) miniature flow tube (1mm i.d with 0.5mm walls) were measured, for the first time, by XRF using krypton dilute in He as the fluorescent species. These measurements are particularly challenging because SiC is opaque and absorbs X-rays quite strongly. However, sufficient  $\alpha$  fluorescence (12.65 keV) from Kr escapes the tube and gas densities can be obtained from the intensity of the fluorescence signal. The experiments were performed with the flow tube at various fixed exterior wall temperatures between 300 K and 1100 K and a highly focused X-ray beam ( $5 \mu\text{m} \times 7 \mu\text{m}$ ; 15 keV). Spatially resolved raster scan maps of gas densities in the miniature reactor and the nearly supersonic jet eluting from the reactor were obtained. The intensity of the fluorescence signal was attenuated by the microreactor walls, and a signal trapping model based on the tube morphology is required to convert the raw fluorescence signal into gas densities. This model was obtained, in part, from simultaneous measurements of the absorption of the incident X-rays by the SiC. Additional radiographic experiments with an unfocused beam were performed to image the SiC tube and complement the raster scans. Excellent correlation was found between the flow pattern revealed by the fluorescence measurements and the wall structure observed from the absorption measurements. In future experiments a more sophisticated calibration method will be used to obtain accurate correlations between signal intensity and density.

**Low pressure flames:** Mass spectrometric studies of the radicals and products produced in low pressure flames has produced much of our understanding of the elementary reactions involved in the combustion of fuels. However, extracting kinetic data from these measurements as well as mechanistic information is problematic due to the influence of the sampling cone on the flame structure. Undoubtedly, the flame is perturbed from the ideal 1D approximation. Measuring 2D spatially resolved, temperature profiles in these flames is challenging but necessary to allow models to be constructed that accurately represent the distortions created by the probe and hence accurate interpretation of the temperature history experienced by species in the flame.

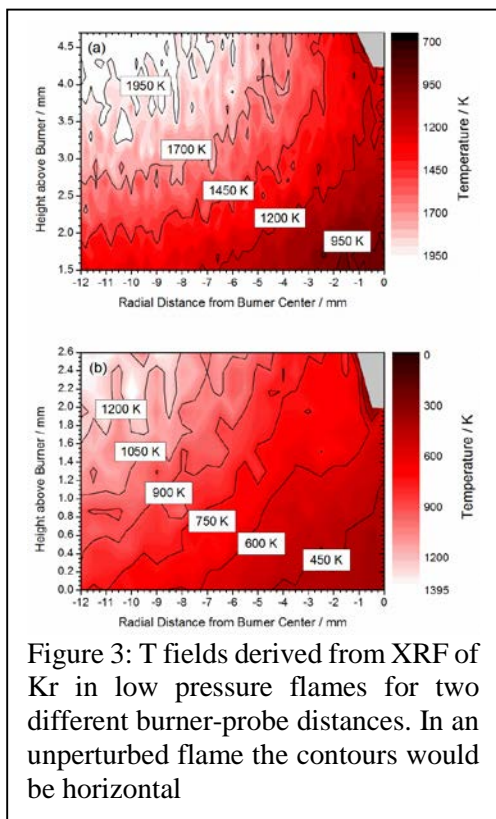


Figure 3: T fields derived from XRF of Kr in low pressure flames for two different burner-probe distances. In an unperturbed flame the contours would be horizontal

information is problematic due to the influence of the sampling cone on the flame structure. Undoubtedly, the flame is perturbed from the ideal 1D approximation. Measuring 2D spatially resolved, temperature profiles in these flames is challenging but necessary to allow models to be constructed that accurately represent the distortions created by the probe and hence accurate interpretation of the temperature history experienced by species in the flame. In collaboration with Hansen, a series of experiments have been started to obtain highly spatially resolved measurements of gas densities and therefore temperature in a standard ethylene/oxygen/argon flame doped with krypton. Similar to the SiC experiments the Kr acts as a fluorescent species however much lower concentrations can be used as the photons are no longer absorbed by SiC. In an improvement on the SiC work a polycapillary optic was placed between the detector and flame allowing efficient collection of photons by confocal microscopy. The imaged spot was approximately  $5 \times 7 \times 300 \mu\text{m}$ . One and two dimensional scans, Fig. 3, of the temperature field were obtained by translating the entire flame chamber through a pre-programmed sequence of positions on high precision translation stages and measuring the X-ray fluorescence at each location. Multiple measurements were performed at various separations between the burner surface and probe tip, representing sampling positions from the preheat, reaction, and postflame zones of the low-pressure flame. Distortions of up to

1000 K of the burner-probe centerline flame temperature were found with the tip of the probe in the preheat zone and distortions of up to 500 K were observed with it in the reaction and postflame zones. Furthermore,

perturbations of the temperature field have been revealed that reach radially as far as 20 mm from the burner-probe centerline and about 3 mm in front of the probe tip. These results clearly reveal the limitations of one-dimensional models for predicting flame-sampling experiments.

#### D. Future work

The DFST/TOF-MS/LS studies of aromatics and resonantly stabilized radicals are being expanded to include reactions between radicals and oxygen molecules. These represent a new application of the LS technique and initial efforts are focusing on phenyl + O<sub>2</sub>. An ongoing study of chlorobenzene pyrolysis and the dissociation/recombination reaction of phenyl and o-benzyne radicals is coming to completion. This is being complemented by theoretical work from Mebel and Klippenstein. The XRF studies with Hansen are ongoing and future studies will involve different nozzle geometries with the aim of providing guidance on the optimal design of sampling nozzles to minimize flame perturbations and a long term goal methods of accurately simulating the flame structures to permit more accurate interpretation of the flame/MS studies.

### III. References

- 1) Kiefer, J. H., Wei, H. C., Kern, R. D., Wu, C. H., Int. J. Chem. Kinet. **1985**, 17, 225–253.
- 2) Rao, V. S., Takeda, K., Skinner, G. B., Int. J. Chem. Kinet. **1988**, 20, 153.
- 3) Hidaka, Y., Higashihara, T., Ninomiya, N., Masaoka, H., Nakamura, T., Kawano, H., Int. J. Chem. Kinet. **1996**, 28, 137–151.
- 4) Hidaka, Y., Higashihara, T., Ninomiya, N., Oshita, H., J. Phys. Chem. 1993, 97, 10977–10983.
- 5) Kiefer J.H., Gupte K.S., Harding L.B., Klippenstein S.J., J. Phys. Chem. A 2009, 113, 13570–13583.
- 6) Tsang W., Int. J. Chem. Kinet., **1978**, 10, 1119–1138.

### IV. Publications and submitted journal articles supported by this project 2015-2017

- 1) Lockhart J. P. A., Goldsmith C. F., Randazzo J. B., Ruscic B. and Tranter R. S. ‘An Experimental and Theoretical Study of the Thermal Decomposition of C<sub>4</sub>H<sub>6</sub> Isomers’ J. Phys. Chem. A, Submitted (2017).
- 2) Hansen N., Tranter R.S., Moshhammer K., Randazzo J.B., Lockhart J.P.A., Fugazzi P. G., Tao T., and Kastengren A.L. ‘2D-Imaging Of Sampling-Probe Perturbations in Laminar Premixed Flames Using Kr X-Ray Fluorescence’ Combust. Flame, In-press (2017)
- 3) Tranter R. S., Jasper A. W., Randazzo J. B., Lockhart J. P. A., and Porterfield J. P. ‘Recombination and Dissociation of 2-Methyl Allyl Radicals: Experiment and Theory’ Proc. Combust. Inst. **2017**, 36, 211-218.
- 4) Randazzo J. B., Annesley C. J., Bell K., and Tranter R. S. ‘A Shock Tube Laser Schlieren Study of Cyclopentane Pyrolysis’ Proc. Combust. Inst. **2017**, 36, 273-280.
- 5) Tranter R. S., Kastengren A. L., Porterfield J. P., Randazzo J. B., Lockhart J. P. A., Baraban J. H., and Ellison G. B. ‘Measuring Flow Profiles in Heated Miniature Reactors With X-ray Fluorescence Spectroscopy’ Proc. Combust. Inst. **2017**, 36, 4603-4610.
- 6) Ossler F., Canton S. E., Seifert S., Hessler J. P., and Tranter R. S. ‘Measurements of Structures and Concentrations of Carbon Particle Species in Premixed Flames by the use of *In-Situ* Wide Angle X-ray Scattering’ Carbon **2016**, 96, 782-798.
- 7) Annesley C. J., Randazzo J. B., Klippenstein S. J., Harding L. B., Jasper A. W., Georgievskii Y., Ruscic B., and Tranter R. S. ‘Thermal Dissociation and Roaming Isomerization of Nitromethane: Experiment and Theory’ J. Phys. Chem. A **2015**, 119, 7872-7893.
- 8) Randazzo J. B., Annesley C. J. and Tranter R. S., ‘Note: an improved driver section for a diaphragmless shock tube’ Rev. Sci. Instrum. **2015**, 86, 016117
- 9) Lynch P. T., Annesley C. J. and Tranter R. S. ‘Dissociation of *ortho*-Benzyne Radicals in the High Temperature Fall-off Regime’ Proc. Combust. Inst. **2015**, 35, 145-152.

# HIGH PRESSURE DEPENDENCE OF COMBUSTION REACTIONS AND SEMICLASSICAL BIMOLECULAR TUNNELING APPROACHES

Albert Wagner  
Chemical Sciences and Engineering Division  
Argonne National Laboratory  
9700 South Cass Avenue  
Argonne, IL 60439  
Email: [wagner@anl.gov](mailto:wagner@anl.gov)

## PROJECT SCOPE

This program is aimed both at improved semiclassical tunneling processes in bimolecular reactions and at understanding pressure effects on relaxation and reaction processes in higher pressure regimes where collisions between two species may be frequently interrupted by other species.

## RECENT PROGRES

*High Pressure Relaxation:* The pressure dependence of reaction kinetics is typically modeled by Master Equation (ME) methods that incorporate the isolated binary collision (IBC) approximation that inelastic collisions are binary events uninterrupted by collisions with other species. Since higher maximum pressures are becoming the norm in internal combustion engine design, we have developed a program to study IBC breakdown starting with an initial focus on energy relaxation. We use molecular dynamics simulations to study the transition from low-pressure behavior where bath-gas/molecule collisions are binary to high-pressure behavior where many collisions may involve multiple bath gas atoms. In collaboration with the Sewell group (U. Missouri) and Rivera-Rivera group (Ferris State University), we are currently examining the vibrational and rotational relaxation of initially excited  $\text{CH}_3\text{NO}_2$  or OH molecules in a periodic box filled with 1000 thermal Ar atoms at 300K and at pressures that range from 10 atm to 400 atm. For these two systems, the *intramolecular* potentials and pairwise additive Exp-6 or Lennard-Jones *intermolecular* potentials are already available in the literature.<sup>1,2</sup>

In our OH simulations,<sup>2</sup> OH starts with zero rotational energy and a classical vibrational excitation equal to the  $\nu = 4$  vibrational level. In Fig. 1a, the vibrational decay is plotted for five different pressures from 50 atm to 400 atm. In the figure  $\text{En}_{\text{rm-vib}}$  is the ensemble average of *excess* vibrational energy over the thermal vibrational energy all normalized to unity at zero time. The color-code lines are the trajectory results and the dotted black lines are an optimized Lendvay-Schatz (LS) fit of the form of  $\text{En}_{\text{rm-vib}}(t) = [1 - (1-m)k_i t]^{1/(1-m)}$  where  $m$  and  $k_i$  are two adjustable constants at each pressure. From the form, the rate of decay at  $t = 0$  is  $k_i$ . Unlike our past results  $\text{CH}_3\text{NO}_2$ <sup>1</sup>

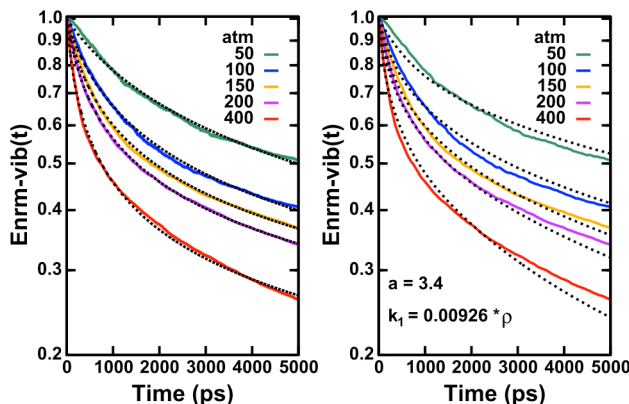


Fig. 1. OH vibrational energy decay with two fits (a) Lendvay-Schatz, (b) Exponential gap (see text).



and  $\text{HO}_2$ ,<sup>3</sup>  $k_i$  is proportional to Ar density (i.e., equivalent to the binary collision frequency) over the entire pressure range, suggesting that if the IBC approximation breaks it leaves no discernable mark on vibrational decay. The other parameter  $m$  measures the global curvature of the decay from a straight line, single exponential decay on a semi-log plot. A low pressure experimental study<sup>4</sup> of OH/He measured  $k_v$ , the de-excitation rate from the  $v^{\text{th}}$  vibrational level, and found a  $v$  dependence of  $k_v = a^{(v-1)}k_l$ , a form based on an exponentially sensitivity of the rate to the anharmonic narrowing of the energy gap between adjacent states. Fig. 1b shows this model reasonably well represents the trajectory data with listed value of  $a$  and  $k_l$  (directly proportional to Ar density  $\rho$ ). This means vibrational relaxation slows with time because anharmonicity decreases with vibrational energy, thereby stiffening the OH bond. Additional simulations with an OH harmonic oscillator potential show dramatically reduced curvature.

OH has no initial rotational energy. In Fig. 2a the rotational decay is plotted versus  $\rho \cdot \text{Time}$  (a product directly proportional to the number of binary collisions). The figure shows the rotational energy overshoots the asymptotic energy ( $kT$ ) in pressure dependent ways that go beyond the collision frequency. Collision-induced conversion of vibrational into rotational energy causes the overshoot. We have developed a model in which at each pressure a fraction  $F$  of the vibrational energy lost in Fig. 1 is converted to rotational energy. If we assume  $F$  is a pressure-dependent function of the vibrational energy, i.e.,  $\text{En}_{\text{rm-vib}}$ , then we can produce an analytic model of the competition between vibrationally-fed rotational energy and bath-gas-depleted rotational energy (via a rate  $k_r$ ). In Fig. 2b, the optimized value of  $k_r$  is restricted to be

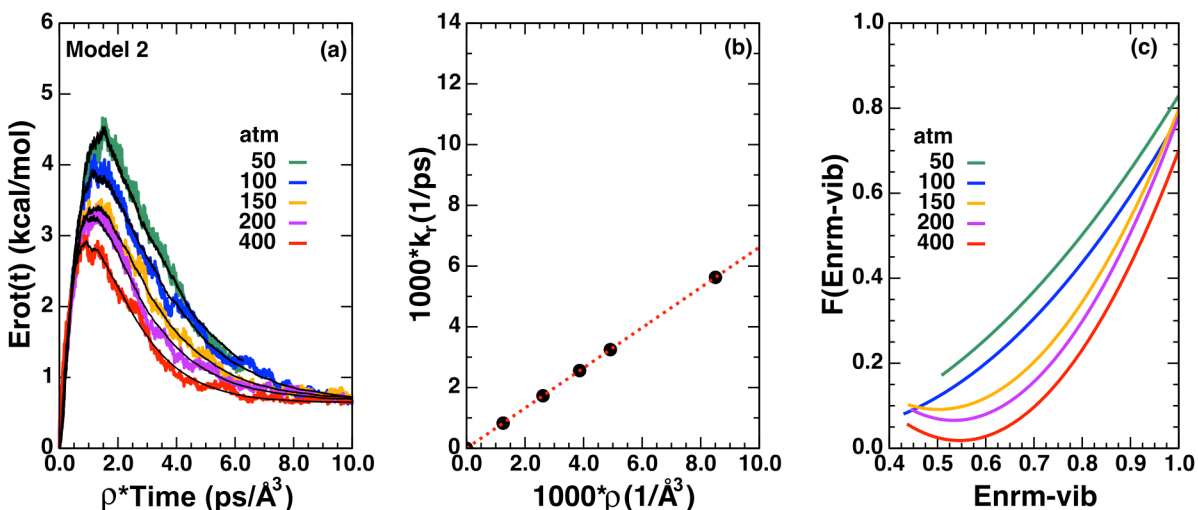


Fig. 2. (a) Rotational energy decay; (b) rotational relaxation rate constant; (c) fraction of vibrational energy converted to rotational energy (see text).

directly proportional to  $\rho$  with the associated fraction  $F$  reported in Fig. 2c. The black lines in Fig. 2a are the resulting fit that reproduces the trajectory data.  $F$  decreases rapidly as the vibrational energy content drops, consistent with decreasing opportunity to resonantly convert (low-rotation/high-vibration) conditions into (high-rotation/low-vibration) conditions. This process occurs in some degree for all molecules but is prominent in diatomic molecules with just one vibrational and two rotational degrees of freedom.

In our  $\text{CH}_3\text{NO}_2$  simulations, we are decomposing previously published<sup>1</sup> vibrational and rotational energies into contributions from the 15 vibrational and 3 rotational normal modes. With the formulation of Rhee and Kim<sup>5</sup>, we can show that vibrational energy is exclusively

decomposed into vibrational normal modes while both the rotational and vibrational-rotational (coriolis) energies are decomposed into primarily rotational and secondarily vibrational normal modes. Figure 3 gives the decomposition of the vibrational energy. In the figure, each

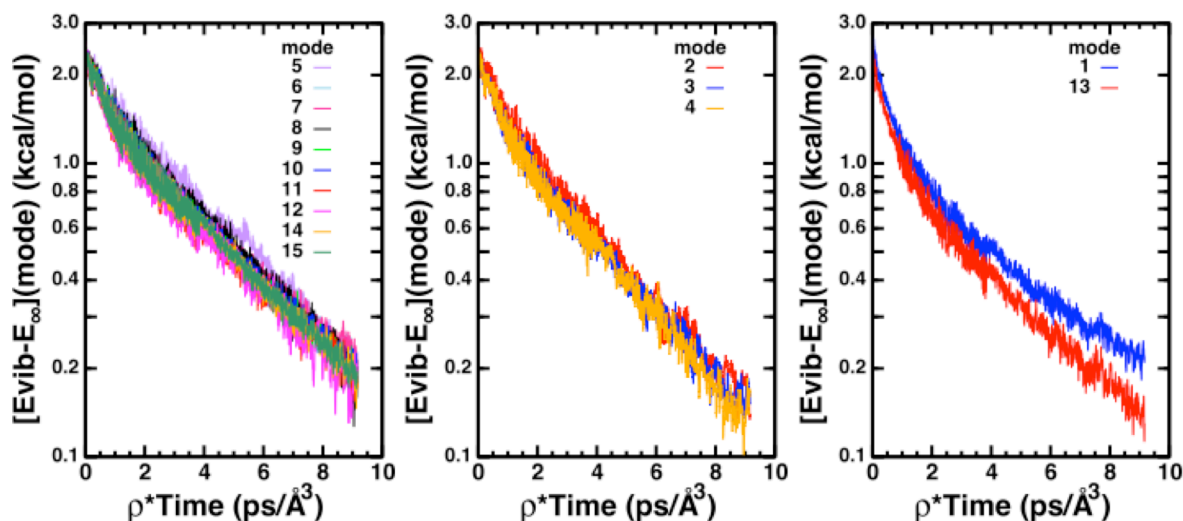


FIG. 3. Decomposition of vibrational energy into three groups of vibrational normal modes.

vibrational mode's excess vibrational energy above its asymptotic value is plotted with respect to  $\rho \cdot \text{Time}$  (proportional to the number of binary collisions). The modes are indexed from lowest to highest frequency. Each mode's trajectory data incorporates results from all pressures. This merging of data from different pressures produces some of the noise in the plots because relaxation rates for  $\text{CH}_3\text{NO}_2$  are not proportional to density over the full pressure range. Nonetheless, Fig. 3 represents the primary result that mode decomposition falls into three different groups: on the left, higher frequency modes primarily exhibiting single exponential decay; in the middle,  $\text{NO}_2$  rocks, wags, and bends primarily decaying with a higher single exponential rate; on the right, *poly*exponential decay of hindered rotation and symmetric stretch  $\text{CH}_3$  modes. These are the only two modes that retain the  $\text{CH}_3$  symmetry about the C-N axis but the physical basis of this decay is still under investigation.

In Fig. 4, the rotational mode decomposition of the rotational and vibrational-rotational excess energy is plotted in a manner similar to Fig. 3. These two energies have opposite signs and a early times a very different energy decay with the rotational energy alone having an initial rapid decay (on the order to tens of ps). All three modes have mostly comparable contributions to the rotational energy but for the vibrational-rotational energy, mode 3 (rotation about the C-N axis) dominates. Vibrational mode decomposition of both energies is similar in behavior to that of Fig. 4, but much smaller and dominated by the  $\text{CH}_3$  hindered rotational mode. Coupling of the hindered rotations and external rotations about the C-N axis is, not surprisingly, an important

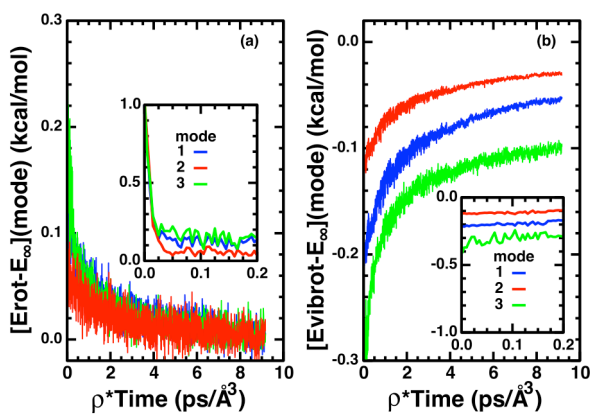


Fig. 4. Rotational and vibrational-rotational energy decomposition into rotational normal modes.

mechanism for energy flow between vibration and rotation. The implications for other modes are still being investigated.

*Tunneling in Bimolecular Reactions:* Most tunneling methods are based on reaction paths whose calculation is typically not readily parallelized. We recently developed an improved semiclassical tunneling theory<sup>6</sup> (iSCTST) that is based on readily parallelized, second order vibrational perturbation theory (VPT2) at the saddle point. Our approach required the construction of a composite 1D tunneling potential carrying VPT2 saddle point information and the calculated barrier heights in both directions. We have recently reviewed a large variety of bound 1D potentials with analytic quantum mechanical eigenvalues. The eigenvalues for all these potentials have a zero value and slope at the dissociation energy when treated as a function of the quantum number and measured from the bottom of the well. Assuming this is always true and using the usual semiclassical replacement of a quantum number by an imaginary semiclassical action, we can produce an analytic tunneling expression *without the construction of a potential*. Implementation of this approach is in progress.

## FUTURE PLANS

For pressure dependent studies we will complete the normal mode decomposition of energies for CH<sub>3</sub>NO<sub>2</sub> and subsequently extend similar analysis to HO<sub>2</sub> and OH simulations. The exponential gap model connecting curvature to anharmonicity will be extended to CH<sub>3</sub>NO<sub>2</sub> and HO<sub>2</sub>. We then intend to increase the initial energy of excitation to allow competition between energy relaxation and unimolecular dissociation in HO<sub>2</sub> and also C<sub>2</sub>H<sub>5</sub> with a new C<sub>2</sub>H<sub>5</sub> potential in collaboration with R. Dawes (MIST). For bimolecular tunneling studies, we will implement and test the new version of the iSCTST tunneling approach on several reactions (O+H<sub>2</sub>, OH+CO, OH+H<sub>2</sub>, OH+OH, Cl+CH<sub>4</sub>, and F+H<sub>2</sub>O) with published VPT2 characterizations by Nguyen/Stanton (U. Texas) and Barker (U. Michigan). In collaboration with this team, we plan comparisons of reaction-path following polyrate<sup>7</sup> and VPT2 iSCTST tunneling calculations.

---

<sup>1</sup> DOE-Sponsored publication #2 below.

<sup>2</sup> R. Chitsazi and A. F. Wagner, *Pressure Effects on the Relaxation of Vibrationally Excited OH (v, J) in an Argon Bath*, *J. Chem. Phys.* (submitted)

<sup>3</sup> DOE-Sponsored publication #1 below.

<sup>4</sup> N. Kohno, J. Yamashita, Ch. Kadochiku, H. Kohguchi, and K. Yamasaki, *J. Phys. Chem. A* **117**, 3253 (2013).

<sup>5</sup> Y.M. Rhee and M. S. Kim, *J. Chem. Phys.* **107**, 1394 (1997).

<sup>6</sup> A. F. Wagner, *J. Phys. Chem. A* **117**, 13089-13100 (2013).

<sup>7</sup> <http://comp.chem.umn.edu/polyrate/>

## DOE-SPONSORED PUBLICATIONS SINCE 2014

1. J. W. Perry and A. F. Wagner, PRESSURE EFFECTS ON THE RELAXATION OF AN EXCITED HYDROPEROXYL RADICAL IN AN ARGON BATH, *Proc. Comb. Inst.* **36**, 229 (2017).
2. L. A. Rivera-Rivera, A. F. Wagner, T. D. Sewell, and D. L. Thompson PRESSURE EFFECTS ON THE RELAXATION OF AN EXCITED NITROMETHANE MOLECULE IN AN ARGON BATH, *J. Chem. Phys.* **142**, 014303 (2015).
3. A. F. Wagner, R. Dawes, R. E. Continetti, and H. Guo, THEORETICAL/EXPERIMENTAL COMPARISON OF DEEP TUNNELING DECAY OF QUASI-BOUND H(D)OCO TO H(D)+CO<sub>2</sub>, *J. Chem. Phys.* **141**, 054304 (2014).

# GAS-PHASE MOLECULAR DYNAMICS: THEORETICAL STUDIES IN SPECTROSCOPY AND CHEMICAL DYNAMICS

Hua-Gen Yu (hgy@bnl.gov)

Chemistry Department, Brookhaven National Laboratory, Upton, NY 11973-5000

## Program Scope

The main goal of this program is the development and application of computational methods for studying chemical reaction dynamics and molecular spectroscopy in the gas phase. We are interested in developing rigorous quantum dynamics algorithms for small polyatomic systems and in implementing approximate approaches for complex ones. Our particular focus is on the dynamics and kinetics of chemical reactions and on the rovibrational spectra of species involved in combustion processes. This research also explores the potential energy surfaces of these systems of interest using state-of-the-art quantum chemistry methods, and extends them to understand some important properties of materials in condensed phases and interstellar medium as well as in combustion environments.

## Recent Progress

### Quantum dynamics calculations of molecular vibrational spectra via NNiDM

By using the recently developed neural network iterative diagonalization method (NNiDM) and multi-layer Lanczos technique, we have carried out a rigorous variational study of highly accurate vibrational energy levels for  $\text{NH}_4^+$  and its partially and completely deuterated isotopomers using an *ab initio* based full-dimensional potential energy surface.  $\text{NH}_4^+$  is of interest as an important interstellar species with similarities to isoelectronic  $\text{CH}_4$ . The infrared vibrational dipole transition spectra were simulated by using the low-order truncated *ab initio* dipole moment surfaces of  $\text{CH}_4$  of Yurchenko and co-workers. The simulated IR spectra have been used to help the level assignments. For  $\text{NH}_4^+$ , we use a very large basis set that is able to converge the energy levels up to  $9000\text{ cm}^{-1}$  to better than  $0.01\text{ cm}^{-1}$ , for a total of 284 levels. For the isotopomers, only moderate size basis sets were employed because we do not attempt to determine such highly vibrationally excited states. However, the energy levels reported

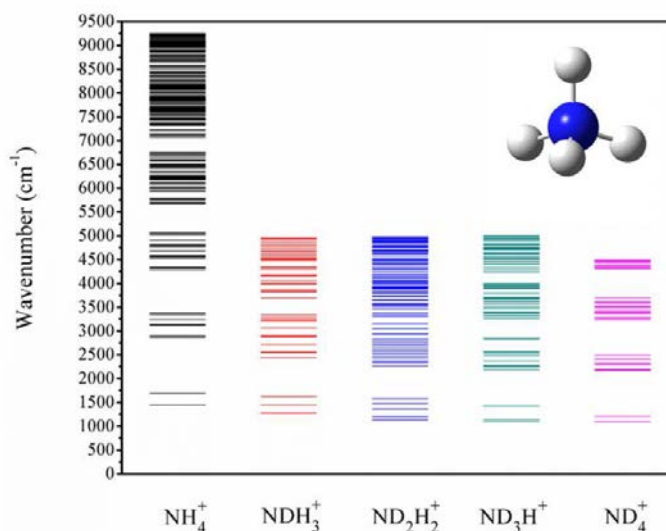


**Fig. 1:** The calculated vibrational energy levels of  $\text{NH}_4^+$  and its partially and completely deuterated isotopomers

For  $\text{NH}_4^+$ , we use a very large basis set that is able to converge the energy levels up to  $9000\text{ cm}^{-1}$  to better than  $0.01\text{ cm}^{-1}$ , for a total of 284 levels. For the isotopomers, only moderate size basis sets were employed because we do not attempt to determine such highly vibrationally excited states. However, the energy levels reported

up to about  $5000\text{ cm}^{-1}$  are still converged within  $0.05\text{ cm}^{-1}$ . Like  $\text{CH}_4$ , the vibrational levels of  $\text{NH}_4^+$  and  $\text{ND}_4^+$  exhibit a polyad structure, characterized by a collective quantum number  $P = 2(v_1 + v_3) + v_2 + v_4$  as shown in Fig. 1. The low-lying vibrational levels of all isotopomers are assigned and the agreement with available experimental data is better than one wavenumber. This work was done in collaboration with Guo at UNM.

### A universal rovibrational Hamiltonian for general many-body molecules

For semi-rigid molecules, there are a few powerful programs for calculating rovibrational spectra of molecules. Those programs usually use the Eckart-Watson Hamiltonian (mostly based on normal coordinates) so that the eigenvalue problem can be efficiently solved by using the vibrational self-consistent field (VSCF) based approach. The molecular rotations are often treated as a perturbation. However, it is difficult to calculate highly vibrationally excited states and/or to study molecules with large amplitude motion using these methods. For those systems, curvilinear coordinates are better to describe the system dynamics and the large amplitude motion is naturally taken into account. Since the choice of curvilinear coordinates, which determines the molecular Hamiltonian, is generally system-dependent, dynamics calculations require specific techniques in order to be done efficiently. The system-dependent issue is a major obstacle that prevents the development of a general code using curvilinear coordinates.

Recently, we have derived a unified rovibrational Hamiltonian for any  $N$ -body system in orthogonal polyspherical coordinates. First, we define the body-fixed (BF) frame as shown in Fig. 2 by removing the motion of the center-of-mass of the system. Therefore, only  $(N-1)$  orthogonal vectors are required to describe the rovibrational motions of the  $N$ -body system. The orthogonal vectors can be any combination of Jacobi, Radau, and orthogonal satellite vectors, chosen to most closely match the reference structure of the molecule of interest. Here, we have defined the vector  $\mathbf{r}_{N-1}$  to be coincident with the BF  $z$ -axis, and the vector  $\mathbf{r}_{N-2}$  to be in the  $xz$  plane with a positive  $x$  direction in the BF frame. That is, the spherical angle of  $\mathbf{r}_{N-1}$  and the azimuthal angle of  $\mathbf{r}_{N-2}$  are both zero by construction, which results in  $(3N-6)$  internal variables. They are defined by  $(N-1)$  radial coordinates  $\mathbf{R}=(r_1, r_2, \dots, r_{N-1})$  and  $(2N-5)$  angular variables ( $\mathbf{Q}$ ) including  $(N-2)$  polar angles  $\theta_i$  and  $(N-3)$  azimuthal angles  $\varphi_j$ . Under this convention of the BF frame, the rovibrational Hamiltonian can be written in a universal form regardless of the number ( $N>3$ ) of atoms in the system. Currently, the Hamiltonian has been numerically tested with formaldehyde, methane, and vinyl radical in full dimension. The full coupled potential energy surfaces are used. The results obtained are very promising.

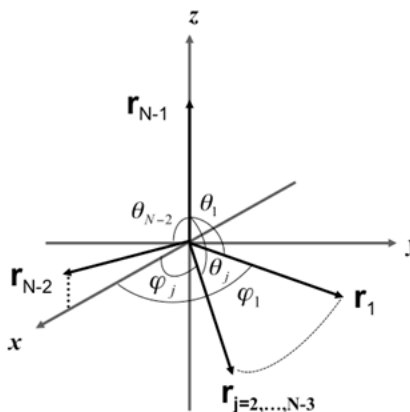


**Fig. 2:** The coordinate system of  $(N-1)$  orthogonal polyspherical vectors  $\mathbf{r}_i$  in the body-fixed (BF) frame for an  $N$ -body system.

### **Time-dependent wavepacket calculations of NO-Rg complex photodissociation**

A reduced dimension time-dependent wavepacket quantum dynamics has been carried out for molecular photodissociation in NO-rare gas complexes. The total cross sections and production rotational state distributions are calculated. The theoretical results are in good agreement with experiments by Lawrance's group at Flinders University (FU) in Australia. This work is done in collaborations with experimentalists Hall (BNL) and Lawrance (FU).

### **Future Plans**

#### **Development of a general program for calculating vibrational spectra of polyatomic systems**

In this proposal, we aim to develop computational algorithms to accurately calculate the vibrational spectra of polyatomic molecules, and to assist experimentalists in understanding their observed spectra. For polyatomic systems beyond six atoms, the challenge in rigorous quantum dynamics calculations comes from the huge basis size arising out of high-dimensional problems. The Lanczos method is an iterative eigensolver capable of solving the eigenvalue problem of a large sparse matrix with a size up to  $N \sim 10^7$ , which might be equivalent to a chemical system with six degrees of freedom. In order to overcome this difficulty, we may try to reduce the basis size by using a compact basis set. The reduction of the basis size is the crucial idea of the sequential truncation approach widely used in direct diagonalization methods. This approach however requires too much CPU time and fast memory to be tractable for polyatomic molecules beyond five-atom molecules. During the past decade, several methods to obtain a compact basis set have been developed, e.g., the pruned basis functions.

Instead, in this proposal, we will use our recently developed ZDVR method to build a compact basis set. The ZDVR is a multi-dimensional PO-DVR method so that the ZDVR basis is very compact, which can substantially reduce the basis size. Numerical tests also demonstrated that it has the Gauss convergence speed with the basis size. Importantly, the ZDVR is a grid basis representation. As a result, the matrix representation of system Hamiltonian in ZDVR is often very sparse, which guarantees the efficiency of an iterative diagonalization method as well as the low memory requirement. The new algorithm will be called ZDVRMode.

We will apply the ZDVRMode program to study the vibrational spectra of combustion-related radicals such as vinyl ( $C_2H_3$ ) and propargyl ( $C_2H_5$ ) radicals, in collaboration with Sears and Hall in the GPMD group of BNL. They will measure the overtones of both radicals using high-resolution near infrared spectroscopy. Currently, the Hamiltonian in normal mode coordinates has been numerically tested with propargyl radical in full dimension. The full coupled potential energy surface is used. The results obtained are very promising.

#### **Rovibrational spectra of polyatomic molecules with large amplitude motions**

We will continue to develop and apply the multi-layer Lanczos and neural network iterative diagonalization methods (NNiDM) to study molecular spectroscopy. Two important extensions of the current work will be implemented as an on-going project. A proposed new general program (called RoVibPLo) will no longer be restricted to  $J=0$  vibrational problems, but will accurately calculate the rovibrational spectra of polyatomic

molecules, using a method that treats the coupled vibrational angular momentum and overall rotation exactly and non-perturbatively, even for molecules undergoing large-amplitude motion. The inclusion of overall rotation in the program will be a major improvement in the assistance provided to experimentalists in the interpretation of their spectra. The other planned improvement to be implemented in the RoVibPLO program is its generality, allowing a single code to treat any polyatomic molecule with up to seven atoms, supplanting programs previously written specifically for four- or five-atom systems. An exact rovibrational Hamiltonian will be used with the specific aim of treating the overall rotation and the large amplitude vibrational motion exactly.

### **Time-dependent wavepacket calculations of the photodissociation of NO-Rg**

Following our previous work, this research will use a better quantum mechanical model to study the photodissociation of NO-Rg complexes. The new model will consider the electronic degeneracy of the system, photon polarizability, and rigorous dynamical treatment. Here, we are particularly interested in the property of differential cross sections that connect to the anisotropic dependence of angular distributions of product states as a function of photon energy.

### **Publications since 2014**

- H.-G. Yu, *Origin of anomalous electronic circular dichroism spectra of [RuPt<sub>2</sub>(tppz)<sub>2</sub>Cl<sub>2</sub>]<sup>4+</sup> in acetonitrile*, J. Phys. Chem.A **118**, 5400 (2014).
- H.-G. Yu, *A complex guided spectral transform Lanczos method for studying quantum resonance states*, J. Chem. Phys. **141**, 244114 (2014).
- H.-G. Yu, *Multi-layer Lanczos iteration approach to calculations of vibrational energies and dipole transition intensities for polyatomic molecules*, J. Chem. Phys. **142**, 044106 (2015).
- H.-G. Yu, *Neural network iterative diagonalization method to solve eigenvalue problems in quantum mechanics*, Phys. Chem. Chem. Phys. **17**, 14082 (2015).
- H.-G. Yu, S. Ndengue, J. Li, R. Dawes, and H. Guo, *Vibrational energy levels of the simplest Criegee intermediate (CH<sub>2</sub>OO) from full-dimensional Lanczos, MCTDH, and MULTIMODE calculations*, J. Chem. Phys. **143**, 084311 (2015).
- H.-G. Yu, *Accurate quantum dynamics calculations of vibrational spectrum of dideuteromethane CH<sub>2</sub>D<sub>2</sub>*, J. Chem. Phys. **142**, 194307 (2015).
- D. Forthomme, M.L. Hause, H.-G. Yu, P. J. Dagdigian, T. J. Sears, and G. E. Hall, *Doppler-resolved kinetics of saturation recovery*, J. Phys. Chem. A **119**, 7439 (2015).
- H. L. Holmes-Ross; R.J. Valenti, R. J.; H.-G. Yu, G.E. Hall, and W.D. Lawrence, *Rotational and angular distributions of NO products from NO-Rg (Rg = He, Ne, Ar) complex photodissociation*, J. Chem. Phys. **144**, 044309 (2016).
- H.-G. Yu, H. Han, and H. Guo, *Full-dimensional quantum calculations of vibrational levels of NH<sub>4</sub><sup>+</sup> and isotopomers on an accurate ab initio potential energy surface*, J. Phys. Chem. A **120**, 2185 (2016).
- H.-G. Yu, *An exact variational method to calculate rovibrational spectra of polyatomic molecules with large amplitude motion*, J. Chem. Phys. **145**, 084109 (2016).

# Chemical Kinetics of Elementary Reactions

Judit Zádor

*Combustion Research Facility, Mail Stop 9055, Sandia National Laboratories  
Livermore, CA 94551-0969  
jzador@sandia.gov*

## I. PROGRAM SCOPE

My program focuses on the theoretical determination of rate coefficients and branching fractions of reactions in the gas-phase, mostly relevant to combustion and atmospheric chemistry, such as the formation and dissociation of radicals derived from various fuel molecules and the bimolecular reactions associated with low-temperature autoignition. This program involves strong collaboration with experimentalists at the CRF (Craig A. Taatjes, David L. Osborn, Leonid Sheps), interaction with the ASC-HPCC efforts, and collaboration with the theoretical developments lead by Stephen J. Klippenstein at Argonne. An important part of the program is that I develop methods to automatically explore reactive potential energy surfaces to systematize and significantly accelerate research in elementary chemical kinetics, and study how theoretical predictions can be made more accurate. The related code, KinBot, has been used in many of the studies outlined below.

## II. RECENT PROGRESS

### A. Reactions involving the OH radical

OH radicals are the single most important chain carriers at low combustion temperatures and in the atmosphere, and alkenes are also pervasive in both environments. Between  $\sim 500$  and  $\sim 800$  K pressure-dependent adduct formation, backdissociation, isomerization, and simple H atom abstraction compete in OH + unsaturated molecule reactions.

As a continuation of my work on the reaction of OH radicals with unsaturated molecules, in collaboration with Leonid Sheps, we studied the OH + cis/trans-2-butene reactions. We used our KinBot code to explore the relevant stationary points on the PES automatically at the CCSD(T)-F12//M06-2X level, and calculated pressure-dependent rate coefficients in a master equation framework. Overall, we achieved consistency between theory and experiment, and produced rate coefficients to be used in comprehensive models. Moreover, the analysis methodology we developed is generally applicable to other OH + alkene reactions, or even more broadly, to reactions with competing timescales.

Allene and propyne, small, doubly unsaturated molecules, play an important role in the reaction sequence contributing to molecular weight growth processes. We mapped out the stationary points and the corresponding conformational space on the corresponding  $C_3H_5O$  potential energy surface relevant for the OH + allene and OH + propyne reactions systematically and automatically using our KinBot software at the UCCSD(T)-F12b//M06-2X level of theory. The double unsaturation significantly increased the number of reaction pathways. The major channel of the bimolecular reactions at high temperatures is the formation propargyl +  $H_2O$ , which makes the reactions important players in soot formation at high temperatures. However, below  $\sim 1000$  K the chemistry is more complex, involving the competition of stabilization, isomerization and dissociation processes. We found that the OH addition to the central carbon of allene has a particularly interesting and complex pressure dependence, caused by the low-lying exit channel to form ketene +  $CH_3$  bimolecular products. We compared our results to a wide range of experimental data and assessed possible uncertainties arising from certain aspects of the theoretical framework. An interesting outcome of this work was that we were able to show that automated searches can find pathways that are important but were missing in previous studies.



## B. Low-temperature autoignition chemistry

The single largest experimental obstacle when studying ephemeral species such as QOOH radicals is their generation in sufficient quantities and purity. QOOH radicals are very short-lived transients in the  $R + O_2 \rightarrow ROO \rightarrow QOOH \rightarrow \text{Products}$  sequence, and, therefore, are usually present in low concentrations when starting with an alkyl radical. We studied low-temperature oxidation using cycloheptadiene precursor in photolytically initiated oxidation experiments in collaboration with David Osborn and Craig Taatjes. One of the several possible QOOH radicals has two advantageous properties: due to double resonance stabilization it is very stable (in fact, more stable than the related ROO radical), and can be detected using photoionization mass spectrometry. Theory played a crucial role, as it enabled the systematic investigation and simplification of the fundamentally complex PES, provided strong support for the observed rate coefficients, and most importantly, enabled the interpretation of the measured quantities. The results establish that resonance stabilization dramatically changes QOOH reactivity, and, hence, oxidation of unsaturated organics can produce exceptionally long-lived QOOH intermediates, which likely contribute to secondary aerosol formation in the atmosphere as well. Also, re-examination of assumed equivalences between rate coefficients for  $R + O_2$  and  $QOOH + O_2$  reactions used in many organic oxidation models might be necessary.

In this period we investigated several other low-temperature oxidation systems, such as ketohydroperoxides in *n*-butane oxidation, tetrahydropyrene, cyclopentane, and tetrahydrofuran, with varying degree of contribution from theory. For instance, we automatically generated rate coefficients for the isomerization of radicals derived from tetrahydropyrene, which were key to interpret some of the experimental results. It turned out that ring-opening reactions compete with  $O_2$  addition and significantly alter the course of the oxidation process. For cyclopentane our model correctly predicts the lowered reactivity due to the presence of the cycle that causes the suppression of certain H-transfer reactions.

KinBot-generated PESs were key to the analysis of MPIMS experiments measuring the low-temperature oxidation products for tetrahydrofuran, a work in collaboration with Leonid Sheps. Although no rate coefficients were calculated in the work, our code allowed us to efficiently explore not just the  $R + O_2$ , but also the  $QOOH + O_2$  surfaces, and establish the lowest energy pathways. This was crucial, as we found that the second- $O_2$  addition reaction involves competing pathways, either producing OH or  $HO_2$ . Enumerating and comparing the key channels on the complicated multiwell surfaces is challenging, and was greatly enhanced by our tool.

## C. Photoionization

In collaboration with David Osborn, Balint Sztaray (University of the Pacific) and PIs from the Paul Scherrer Institut (Switzerland) we studied the photoelectron spectrum of the benzyl radical. Using the CASPT2 electronic structure method to characterize the benzyl radical's ground and excited cationic states, both triplets and singlets, from which several contribute to the measured spectrum in the 7.0–10.5 eV range. The Franck-Condon simulations are in almost perfect agreement for the lowest singlet ( $\tilde{X}^+1A_1$ ) and triplet ( $\tilde{a}^+3B_2$ ) states, and we were able to identify most of the sharp higher energy features as well associated with state  $\tilde{A}^+1B_2$  and with possible contributions from  $\tilde{b}^+3A_1$ .

## III. NEW DIRECTIONS AND ONGOING WORK

My primary research goal for the near-term is the further development of our automated kinetics code, KinBot. There are several reaction systems where it is applied either at Sandia or in collaboration with others, exploring reactions of tetrahydrofuran, pentanol, ketohydroperoxides, etc. KinBot is an expert system relying mostly on chemical rules translated into the 3-D space of molecular structures. KinBot potentially can discover pathways that were either not known or simply not thought of in the context of combustion or oxidation in general. We are planning to apply KinBot

in several key areas that can potentially benefit from it, such as the cascade O<sub>2</sub> addition reactions (reactions beyond the second O<sub>2</sub> addition), kethohydroperoxide chemistry, which is surprisingly rich and we have relatively few intuitions about it, and aromatic compound oxidation, which feature for instance ring-expansion reactions.

KinBots's approach, while very efficient and quite reliable for many problems, clearly has limitations. We are planning molecular dynamics toolsets to extend the abilities of this automated framework and also exploring the option to couple KinBot to automated reaction generators.

Methyl hydroperoxide (MHP) is the simplest organic alkylhydroperoxide, and can form the smallest QOOH radical, CH<sub>2</sub>OOH, when one of its methyl hydrogens is abstracted by an appropriate other radical, e.g., OH or Cl. However, accurate thermodynamic parameters are also absent in the literature for QOOH radicals. Establishing firm values for the heats of formation of MHP and its unimolecular dissociation products is required for strong anchor values. Moreover, future studies involving more complex organic hydroperoxides will benefit from studying the smallest homologue. The goal of this project is to establish the heat of formation values for the smallest QOOH, CH<sub>2</sub>OOH. Preliminary threshold photoelectron photoion coincidence (TPEPICO) experiments in collaboration with Balint Sztaray promise direct measurements of the ionization energy and fragmentation kinetics of the MHP cation. These observations, combined with theory, promise not only accurate thermodynamic parameters for neutral CH<sub>2</sub>OOH, but some interesting dynamical processes.

We currently investigate the unimolecular dissociation of *n*-pentanol radicals, which can be thought of as the reverse of 1-pentene + OH reaction, as a continuation of our work on OH + alkene systems. This is yet another, even larger radical system, with relevance to pyrolysis of alcohols. KinBot is used to explore the pathways, which feature mostly usual, at the same time very many isomerization and dissociation pathways, which would be very difficult and slow to study by hand. We also plan to investigate the dependence of the capture rate coefficient into the van der Waals well on the conformation of the pentene molecule as part of this project. Investigating these larger systems with rigorous methods also helps modelers assess the validity of the rules with which they estimate the rate coefficients, and as part of this project we also plan to put the calculated rate coefficients into a comprehensive pentanol pyrolysis model and compare the results to flow reactor experiments. Our initial results suggest that the rate coefficients based on the KinBot-directed AITSTME framework do matter and improve the comparison between experiment and model.

In gas-phase combustion systems the interest in acetylene stems largely from its role in molecular weight growth processes. The consensus is that above 1500 K acetylene pyrolysis starts mainly with the homolytic fission of the C–H bond creating an ethynyl radical and an H atom. However, below ~1500 K this reaction is too slow to initiate the chain reaction. It has been hypothesized that instead of dissociation, self-reaction initiates this process. Nevertheless, rigorous theoretical or direct experimental evidence is lacking, to an extent that even the molecular mechanism is debated in the literature. In our ongoing work we use rigorous ab initio transition state theory master equation methods to calculate pressure- and temperature-dependent rate coefficients for the association of two acetylene molecules and related reactions. We establish the role of vinylidene, the high-energy isomer of acetylene in this process, compare our results with available experimental data, and assess the competition between the first-order and second-order initiation steps. We also see in our calculation the effect of the rapid isomerization among the participating wells, which needs to be carefully considered in a timescale analysis when phenomenological rate coefficients are compared to certain experiments.

Experiments carried out in the Taatjes lab clearly indicate that ethylperoxy radicals (CH<sub>3</sub>CH<sub>2</sub>O<sub>2</sub>, formed in the ethyl + O<sub>2</sub> reaction) react with HO<sub>2</sub> radicals to produce a significant amount of OH radicals above 600 K. In general, low temperature and high pressure leads to high concentrations of both HO<sub>2</sub> and ROO in reacting systems, and even the slow abstraction reactions by

HO<sub>2</sub> can play a significant role under such conditions. Moreover, the reaction of alkylperoxy radicals with HO<sub>2</sub> is also important in tropospheric chemistry, where due to the even lower temperatures compared to LTC, the fate of ROO is limited to fewer channels in general, and slow reactions play an important role on these longer timescales. The literature shows that in general, ROO and HO<sub>2</sub> radicals can react both on the singlet and triplet surface, most likely producing alkyl hydroperoxides (ROOH) + O<sub>2</sub> via a barrierless entrance and a submerged barrier. The closed shell ROOH molecules act as reservoirs of highly reactive radicals, and can easily dissociate to form OH and an alkoxy radical at elevated temperatures. We plan to study this type of reaction using high-level theoretical kinetics along with the experimental studies.

#### IV. DOE SUPPORTED PUBLICATIONS, 2015-PRESENT

1. Rotavera, B., Savee, J. D., Antonov, I. O., Caravan, R. L., Sheps, L., Osborn, D. L., Zádor, J., Taatjes, C. A.: *Influence of oxygenation in cyclic hydrocarbons on chain-termination reactions from R + O<sub>2</sub>: tetrahydropyran and cyclohexane*. Proceedings of the Combustion Institute, **2017** 36 597-606.
2. Al Rashidi, M. J., Thion, S., Togbé, C., Dayma, G., Mehl, M., Dagaut, P., Pitz, W. J., Zádor, J., Sarathy, S. M.: *Elucidating reactivity regimes in cyclopentane oxidation: Jet stirred reactor experiments, computational chemistry, and kinetic modeling*. Proceedings of the Combustion Institute, **2017** 36 469-477.
3. Li, X., Jasper, A. W., Zádor, J., Miller, J. A., Klippenstein, S. J.: *Theoretical kinetics of O + C<sub>2</sub>H<sub>4</sub>*. Proceedings of the Combustion Institute, **2017** 36 219-227.
4. Antonov, I. O.; Zádor, J.; Rotavera, B.; Papajak, E.; Osborn, D. L.; Taatjes, C. A.; Sheps, L.: *Competing reaction pathways in the low-temperature oxidation of THF*. Journal of Physical Chemistry A **2016** 119 7742-7752.
5. Miller, J. A., Klippenstein, S. J., Robertson, S. H., Pilling, M. J., Shannon, R., Zádor, J., Jasper, A. W., Goldsmith, C. F., Burke, M. P.: *"Comment on "When rate constants are not enough" by John R. Barker, Michael Frenklach, and David M. Golden"*. Journal of Physical Chemistry A, **2016** 120 306-312.
6. Antonov, I. O., Kwok, J., Zádor, J., Sheps, L.: *OH + 2-butene: A combined experimental and theoretical study in the 300-800 K temperature range*. Journal of Physical Chemistry A, **2015** 119 7742-7752.
7. Burke, M. P., Goldsmith, C. F., Klippenstein, S. J., Welz, O., Huang, H., Antonov, I. O., Savee, J. D., Osborn, D. L., Zádor, J., Taatjes, C. A., Sheps, L.: *Multi-scale informatics for low-temperature propane oxidation: Further complexities in studies of complex reactions*. Journal of Physical Chemistry A, **2015** 119 7095-7115.
8. Savee, J. D., Zádor, J., Hemberger, P., Sztaray, B., Bodi, A., Osborn, D. L.: *Threshold photoelectron spectrum of the benzyl radical*. Molecular Physics, **2015** 113 2217-2227.
9. Savee, J. D., Papajak, E., Rotavera, B., Huang, H., Eskola, A. J., Welz, O., Sheps, L., Taatjes, C. A., Zádor, J., Osborn, D. L.: *Direct observation and kinetics of a critical reactive intermediate in hydrocarbon oxidation* Science, **2015** 347 643-646.
10. Zádor, J., Miller, J.A.: *Adventures on the C<sub>3</sub>H<sub>5</sub>O potential energy surface: OH + propyne, OH + allene and related reactions*. Proceedings of the Combustion Institute, **2015** 35 181-188.
11. Eskola, A.J., Welz, O., Zádor, J., Antonov, I.O., Sheps, L., Savee, J.D., Osborn, D.L., Taatjes, C.A.: *Probing the low-temperature chain-branching mechanism for n-butane autoignition chemistry via time-resolved measurements of ketohydroperoxide formation in photolytically initiated n-C<sub>4</sub>H<sub>10</sub> oxidation*. Proceedings of the Combustion Institute, **2015** 35 291-298.

# Isomer-specific spectroscopy of aromatic fuels and their radical intermediates

*Timothy S. Zwier*

Department of Chemistry, Purdue University, West Lafayette, IN 47907-2084  
zwier@purdue.edu

## Program Definition and Scope

The chemical complexity of gasoline, diesel fuels, and aviation fuels, and the fast-expanding list of potential plant-derived biofuels offer a challenge to the scientific community seeking to provide a molecular-scale understanding of their combustion, and of the incomplete combustion that leads to soot formation. Development of accurate combustion models stands on a foundation of experimental data on the kinetics and product branching ratios of individual reaction steps. Spectroscopic tools to selectively detect and characterize the widening array of fuel components and the reactive intermediates they generate upon pyrolysis and combustion. There is growing recognition that a key component of future progress in the field is the development of detection schemes that are isomer-specific and even conformation-specific. The present proposal uses an array of laser-based and broadband microwave methods to carry out conformation-specific spectroscopy on key fuel components and the reactive intermediates formed during their pyrolysis and combustion.

## Recent Progress

### A. Toward a first principles model of the alkyl CH stretch region and its application to alkylbenzenes (ref. 2, 7, 9, 14)

The alkyl CH stretch region of the infrared is a region rich in information content, but a challenge to assign, due to the ubiquitous presence of strong Fermi resonance mixing between the alkyl CH stretch and CH bend overtone levels. Conformational assignments based on a comparison of the observed alkyl CH stretch spectra with *ab initio* predictions of harmonic frequencies often fail in spectacular fashion due to these Fermi resonances, which shift and split bands to the point that comparison with harmonic calculations is fruitless. Working in collaboration with Ned Sibert (UW-Madison), we are developing a first-principles model of the alkyl CH stretch region built around a local mode Hamiltonian that explicitly takes into account anharmonic mixing via stretch-bend coupling.

Building off earlier studies that concentrated on alkyl chains containing only CH<sub>2</sub> groups (ref. 2), and extension of the model to include the more complicated Fermi coupling occurring in methyl groups (ref. 7), we have recently completed studies of the single-conformation spectroscopy of a series of alkylbenzenes, C<sub>6</sub>H<sub>5</sub>-(CH<sub>2</sub>)<sub>n</sub>-CH<sub>3</sub> with n=1-9 (ref. 9, 14). The study of ethyl-, propyl-, and butylbenzene provided a first test of the models to alkyl chains containing both CH<sub>2</sub> and CH<sub>3</sub> groups (ref. 9) in short-chain alkylbenzenes where the conformations had been assigned previously. Characteristic intra-CH<sub>n</sub> and inter-CH<sub>n</sub> coupling constants for both CH<sub>2</sub> and CH<sub>3</sub> groups were established.

Analogous studies of pentyl- through decylbenzene provided an important opportunity to extend the model to longer alkyl chains, and to establish the conformational preferences of these longer chains, with a particular interest in establishing the chain length at which the alkyl chain folds back over the ring. Laser-induced fluorescence excitation spectra, fluorescence-dip infrared spectra in the alkyl CH stretch region, and Raman spectra are combined to provide assignments for the observed conformers. Density functional theory calculations at the DFT B3LYP-D3BJ-def2TZVP level of theory provide relative energies and normal mode vibrations that serve as input

for an anharmonic local mode theory. Unique UV transitions are assigned to all-*trans* and a set of conformers containing one or more gauche defects in the chain (g1, g1g2, and g1g4'). In octylbenzene, a pair of LIF transitions shifted  $-92$  cmof the pure alkanes ( $n=18$ ), consistent with a smaller energy cost for the g1 dihedral and the increased dispersive interaction of the chain with the  $\pi$  cloud. Local site frequencies for the entire set of conformers from the local mode model show 'edge effects' that raise the site frequencies of CH<sub>2</sub>(1) and CH<sub>2</sub>(2) due to the phenyl ring and CH<sub>2</sub>( $n-1$ ) due to the methyl group. The g1g3g4 conformer also shows local sites shifted up in frequency at CH<sub>2</sub>(3) and CH<sub>2</sub>(6) due to interaction with the  $\pi$  cloud.

We have also recorded LIF and single-conformation IR spectra of a series of *para*-dialkylbenzenes, showing the explosion in conformers accompanying the presence of two independent alkyl chains on the same aromatic ring.

Finally, we have recorded high-quality IR spectra of the entire series of *n*-alkylbenzenes in the excited electronic state by detecting red-shifted fluorescence that occurs following IR excitation of the S<sub>1</sub> origin levels of the molecules.

## B. Broadband Multi-resonant Strong Field Coherence Breaking as a tool for single-component microwave spectra of mixtures (ref. 11, 13)

Using standard hardware available in chirped-pulse Fourier transform microwave (CP-FTMW) spectroscopy, we have introduced an experimental method to selectively extract from the microwave spectrum of an otherwise complicated multicomponent mixture a set of transitions due to a single component, thereby speeding spectral assignment. The method operates the broadband chirped-pulse used to excite the sample in the strong-field regime through a combination of high power and control of the sweep rate. We have developed a procedure that leads to selection of three transition frequencies that can be incorporated as a set of resonant sequential single-frequency microwave pulses that follow broadband chirped-pulse excitation, resulting in a reduction in the coherent signal from a set of transitions ascribable to the component of interest. The difference in the CP-FTMW spectrum with and without this set of multi-resonant single-frequency pulses, produces a set of transitions that can confidently be assigned to a single component of the mixture, aiding the analysis of its spectrum. In its initial applications, we have used the scheme to (i) selectively extract the spectrum of one of five singly <sup>13</sup>C-substituted isotopologues of benzonitrile in natural abundance, (ii) obtain the microwave spectra of the two structural isomers (E)- and (Z)-phenylvinyl nitrile, and (iii) record conformer-specific microwave spectra of methylbutyrate, a short-chain fatty acid methyl ester used as a biodiesel fuel surrogate. In this latter study, we have obtained and assigned the

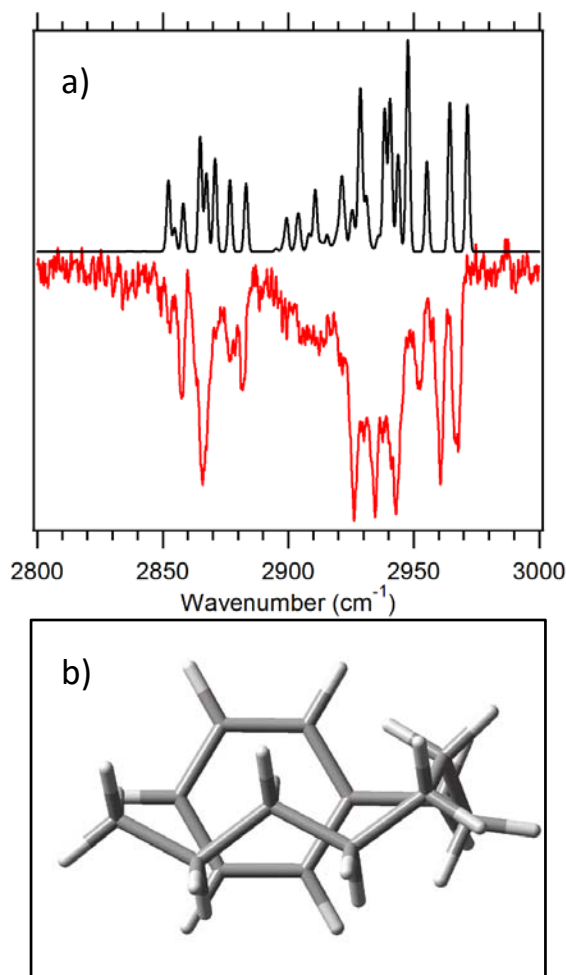
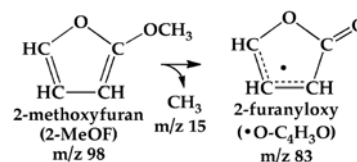


Figure 1: (a) Single-conformation IR spectrum of the g1g3g4 conformer of octylbenzene compared with the predictions of the model. (b) Optimized structure for the g1g3g4 conformer.

broadband microwave spectrum of methylbutyrate over the 8-18 GHz region. Working in collaboration with the Kleiner group, we have extended the spectrum up to 26 GHz. Two low-energy conformers, one with a fully extended, heavy-atom planar anti/anti structure (**a,a**), and the other with a gauche propyl chain (**g±,a**), were assigned in the spectrum. A/E splittings due to the internal rotation of the ester methyl group were resolved for both these lower energy conformers, and were fit to obtain an estimate of the barrier to methyl internal rotation of  $V_3 \sim 420 \text{ cm}^{-1}$ .

### C. Broadband microwave spectra of intermediates formed in flash pyrolysis

We continue to develop CP-FTMW spectroscopy as a method for characterizing the reactive intermediates formed by flash pyrolysis via a hyperthermal nozzle (or Chen nozzle). We have recently used this source to obtain the broadband microwave spectrum of the 2-furanyloxy radical, whose structure is shown to the right, formed by pyrolysis of 2-methoxyfuran.



Finally, we have built and are currently installing a VUV photoionization-TOF mass spectrometer stage to our CP-FTMW chamber that we plan to use to determine the molecular formulae of products formed by pyrolysis using 118 nm photoionization. This will help narrow our search for possible carriers of observed transitions in the microwave spectrum to species with the correct molecular formulae, adding a powerful complementary tool to this instrument.

### Future Work

- (1) We will extend our studies of long-chain alkylbenzenes to even longer-chains containing alkyl chains 10-12 in length, in order to explore a larger number of folded structures.
- (2) We will study the single-conformation spectra of a series of  $\alpha,\omega$ -diaromatic alkanes, with the goal of determining when  $\pi$  stacking begins to overcome steric constraints in the alkyl chain.
- (3) Flash pyrolysis of a series of oxygenated fuels using the combination of CP-FTMW and VUV photoionization TOF mass spectra to obtain mass-correlated broadband microwave spectra.

### Publications acknowledging DOE support, 2014-present

1. Jacob C. Dean, Patrick S. Walsh, Bidyut Biswas, P. V. Ramachandran, and Timothy S. Zwier, "Single-conformation UV and IR spectroscopy of model G-type lignin dilignols: the  $\beta$ -O-4 and  $\beta$ - $\beta$  linkages", *Chem. Sci.*, **5**, 1940 – 1955 (2014).
2. Edwin L. Sibert III, Nathanael M. Kidwell, and Timothy S. Zwier, "A First-Principles Model of Fermi Resonance in the Alkyl CH Stretch Region: Application to Hydronaphthalenes, Indanes, and Cyclohexane", *J. Phys. Chem. B* **118**, 8236-8245 (2014).
3. Nathan R. Pillsbury, Nathanael M. Kidwell, Benjamin Nebgen, Lyudmila V. Slipchenko, John R. Cable, David F. Plusquellic, and Timothy S. Zwier, "Vibronic Coupling in Asymmetric Bichromophores: I. Experimental Investigation of Diphenylmethane- $d_5$ ", *J. Chem. Phys.* **141**, 064316 (2014).
4. Nathanael M. Kidwell, Vanesa Vaquero-Vara, Thomas K. Ormond, Grant T. Buckingham, Di Zhang, Deepali N. Mehta-Hurt, Laura McCaslin, Mark R. Nimlos, John W. Daily, Brian C. Dian, John F. Stanton, G. Barney Ellison, and Timothy S. Zwier, "Chirped-Pulse Fourier Transform Microwave Spectroscopy coupled with a Flash Pyrolysis Microreactor: Structural Determination of the Reactive Intermediate Cyclopentadienone", *J. Phys. Chem. Lett.* **5**, 2201-07 (2014).

5. Jamie D. Young, Michael Staniforth, Jacob C. Dean, Gareth M. Roberts, Federico Mazzoni, Tolga N.V. Karsili, Michael N.R. Ashfold, Timothy S. Zwier, and Vasilios G. Stavros, "Towards Understanding Photodegradation Pathways in Lignins: The Role of Intramolecular Hydrogen Bonding in Excited States", *J. Phys. Chem. Lett.* **5**, 2138-43 (2014).
6. Jacob C. Dean, Ryoji Kusaka, Patrick C. Walsh, Florent Allais, and Timothy S. Zwier, "Plant Sunscreens in the UV-B: Ultraviolet Spectroscopy of Jet-Cooled Sinapoyl Malate, Sinapic Acid, and Sinapate Ester Derivatives", *J. Am. Chem. Soc.* **136**, 14780-95 (2014).
7. Edwin L. Sibert III, Daniel P. Tabor, Nathanael M. Kidwell, Jacob C. Dean, and Timothy S. Zwier, "Fermi Resonance Effects in the Vibrational Spectroscopy of Methyl and Methoxy Groups", *J. Phys. Chem. A* **118**, 11272-81 (2014).
8. Jacob C. Dean, Nicole L. Burke, John R. Hopkins, James G. Redwine, P.V. Ramachandran, Scott A. McLuckey, and Timothy S. Zwier, "UV Photofragmentation and IR Spectroscopy of Cold, G-type  $\beta$ -O-4 and  $\beta$ - $\beta$  Dilignol-Alkali Metal Complexes: Structure and Linkage-Dependent Photofragmentation", *J. Phys. Chem. A* **119**, 1917-32 (2015).
9. Daniel P. Tabor, Daniel M. Hewett, Sebastian Bocklitz, Joseph A. Korn, Anthony J. Tomaine, Arun K. Ghosh, Timothy S. Zwier, and Edwin L. Sibert III, "Anharmonic modeling of the conformation-specific IR spectra of ethyl, n-propyl, and n-butylbenzene", *J. Chem. Phys.* **144**, 224310 (2016).
10. Nathanael M. Kidwell, Deepali N. Mehta-Hurt, Joseph A. Korn, and Timothy S. Zwier, "Infrared and Electronic Spectroscopy of Jet-cooled 5-methyl-2-furanylmethyl Radical derived from the Biofuel 2,5-Dimethylfuran", *J. Phys. Chem. A* **120**, 6434-43 (2016).
11. Alicia O. Hernandez, Chamara Abeysekera, Brian M. Hays, and Timothy S. Zwier, "Broadband Multi-resonant Strong Field Coherence Breaking as a Tool for Single Isomer Microwave Spectroscopy", *J. Chem. Phys.* **145**, 114203 (2016).
12. Joseph A. Korn, Khadija Jawad, Daniel P. Tabor, Edwin L. Sibert III, and Timothy S. Zwier, "Conformation-specific Spectroscopy of Alkylbenzyl Radicals:  $\alpha$ -ethylbenzyl and  $\alpha$ -propylbenzyl radicals", *J. Chem. Phys.* **145**, 124314 (2016).
13. Alicia O. Hernandez-Castillo, Chamara Abeysekera, Brian M. Hays, Isabelle Kleiner, Ha Vinh Lam Nguyen, and Timothy S. Zwier, "Conformational Preferences and Internal Rotation of Methyl Butyrate by Microwave Spectroscopy", *J. Mol Spec.* (accepted).
14. Daniel M. Hewett, Sebastian Bocklitz, Daniel P. Tabor, Edwin L. Sibert III, Martin Suhm, and Timothy S. Zwier, "Identifying the First Folded Alkylbenzene via Ultraviolet, Infrared, and Raman Spectroscopy of Pentylbenzene through Decylbenzene", (submitted).

# *Participant List*





# 37<sup>th</sup> Annual Gas Phase Chemical Physics Research Meeting Participation List

<b>Last Name</b>	<b>First Name</b>	<b>Organization</b>	<b>Email</b>
Ahmed	Musahid	Lawrence Berkeley National Laboratory	mahmed@lbl.gov
Alexander	Millard	University of Maryland	mha@umd.edu
Barlow	Robert	Sandia National Laboratories	barlow@sandia.gov
Belkacem	Ali	Lawrence Berkeley National Laboratory	abelkacem@lbl.gov
Bellan	Josette	California Institute of Technology	Josette.Bellan@jpl.nasa.gov
Blanquart	Guillaume	Caltech	g.blanquart@caltech.edu
Chandler	David	Sandia National Laboratories	gdecast@sandia.gov
Chen	Jacqueline	Sandia National Laboratories	jhchen@sandia.gov
Continetti	Robert	UC San Diego	rcontinetti@ucsd.edu
Dagdigian	Paul	Johns Hopkins University	pjdagdigian@jhu.edu
Dahms	Rainer	Sandia National Laboratories	rndahms@sandia.gov
Davis	Michael	Argonne National Laboratory	davis@tcg.anl.gov
Davis	Harry Floyd	Cornell University	hfd1@cornell.edu
Douberly	Gary	University of Georgia	douberly@uga.edu
Field	Robert W	MIT	rwfield@mit.edu
Frank	Jonathan	Sandia National Laboratories	jhfrank@sandia.gov
Georgievski	Yuri	Argonne National Laboratory	ygeorgi@anl.gov
Green	William	MIT	whgreen@mit.edu
Hall	Gregory	Brookhaven National Lab	gehall@bnl.gov
Hansen	Nils	Sandia National Laboratories	nhansen@sandia.gov
Harding	Lawrence	Argonne National Laboratory	harding@anl.gov
Harris	Alexander	Brookhaven National Laboratory	alexh@bnl.gov
Head-Gordon	Martin	UC Berkeley	mhg@cchem.berkeley.edu

Hwang	Robert	Sandia National Laboratories	gdecast@sandia.gov
Jasper	Ahren	Argonne National Laboratory	ajasper@anl.gov
Kaiser	Ralf	University of Hawaii	ralfk@hawaii.edu
Keceli	Murat	Argonne National Laboratory	keceli@anl.gov
Kliewer	Christopher	Sandia National Laboratories	cjkliew@sandia.gov
Klippenstein	Stephen	Argonne National Laboratory	sjk@anl.gov
Krause	Jeffrey	Department of Energy	Jeff.Krause@science.doe.gov
Leone	Stephen	LBNL and University of California, Berkeley	srl@berkeley.edu
Lester	Marsha	University of Pennsylvania	milester@sas.upenn.edu
Li	Chiping	AFOSF	chiping.li@us.af.mil
Lucht	Robert	Purdue University	lucht@purdue.edu
Michelsen	Hope	Sandia National Labs	hamiche@sandia.gov
Miller	William	University of California/Lawrence Berkeley Lab	millerwh@berkeley.edu
Najm	Habib	Sandia National Laboratories	hnnajm@sandia.gov
Nesbitt	David	JILA/University of Colorado	djn@jila.colorado.edu
Neumark	Daniel	Lawrence Berkeley National Laboratory/UC Berkeley	dneumark@berkeley.edu
Neuscamman	Eric	University of California, Berkeley	eric.neuscamman@gmail.com
Oefelein	Joseph	Sandia National Laboratories	oefelei@sandia.gov
Osborn	David	Sandia National Laboratories	dlosbor@sandia.gov
Pepiot	Perrine	Cornell University	pp427@cornell.edu
Pitz	William	LLNL	pitz1@llnl.gov
Pratt	Stephen	Argonne National Laboratory	stpratt@anl.gov
Prozument	Kirill	Argonne National Laboratory	prozument@anl.gov
Reisler	Hanna	University of Southern California	reisler@usc.edu
Ruscic	Branko	Argonne National Laboratory	ruscic@anl.gov
Sears	Trevor	Brookhaven National Laboratory	sears@bnl.gov
Shaddix	Christopher	Sandia National Labs	crshadd@sandia.gov
Shepard	Ron	Argonne National Laboratory	shepard@anl.gov
Sheps	Leonid	Sandia National Laboratories	lsheps@sandia.gov
Sisk	Wade	DOE/BES	wade.sisk@science.doe.gov
Sivaramakrishnan	Raghu	Argonne National Laboratory	raghu@anl.gov
Stanton	John	University of Florida	jfstanton@gmail.com

Suits	Arthur	University of Missouri	suitsa@missouri.edu
Sutherland	James	University of Utah	James.Sutherland@utah.edu
Taatjes	Craig	Sandia National Laboratories	cataatj@sandia.gov
Tranter	Robert	Argonne National Laboratory	tranter@anl.gov
Violi	Angela	University of Michigan	avioli@umich.edu
Wagner	Albert	Argonne National Laboratory	wagner@anl.gov
Wilson	Kevin	Lawrence Berkeley National Laboratory	krwilson@lbl.gov
Yu	Hua-Gen	Brookhaven National Laboratory	hgy@bnl.gov
Zádor	Judit	Sandia National Laboratories	jzador@sandia.gov
Zwier	Timothy	Purdue University	zwier@purdue.edu

# *Critical Issues*



## Critical Issues in Gas Phase Chemical Physics that Impact Combustion

1	<b>Lean, High Pressure, Low Temperature Combustion</b>	Chandler	David	SNL/CRF
2	<b>Low-Temperature Ignition of Complex Fuels in Turbulent, Stratified Flows</b>	Chen Dahms	Jacqueline Rainer	SNL/CRF SNL/CRF
3	<b>Combustion Dynamics and Kinetics of Droplets and Nanoparticles</b>	Continetti Tranter Wagner	Robert Rob Al	UCSD ANL ANL
4	<b>Soot Formation, Growth, and Reaction</b>	Michelsen Violi	Hope Angela	SNL/CRF U Michigan
5	<b>Gas-Phase Plasma Interactions in Driven Ignition</b>	Taatjes	Craig	SNL/CRF
6	<b>Partition Functions in Thermochemistry and Kinetics under Extreme Conditions</b>	Klippenstein Ruscic	Stephen Branko	ANL ANL

# Lean, High Pressure, Low Temperature Combustion

## From Fundamentals to Accurate Models

Increase fuel efficiency (> 40%)

Difficult to ignite (plasma or stratified ignition)

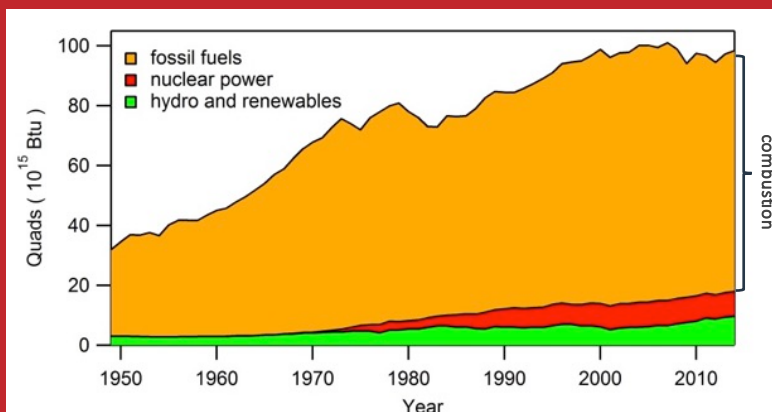
Increase pressure dependence on chemistry





DOE mission-inspired fundamental research in Gas Phase Chemical Physics impacts many energy missions of the department

U.S. Primary Energy Use



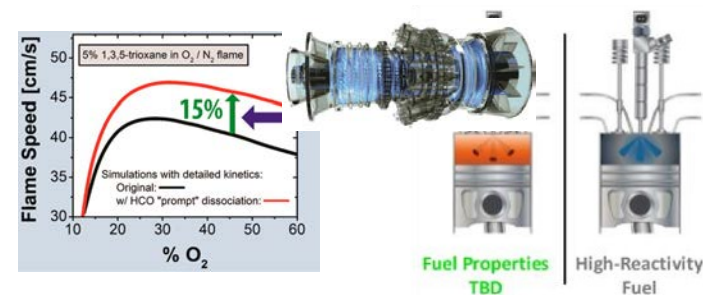
One key mission is combustion, which will remain the main process for the release of chemical energy for the foreseeable future



Theoretical chemical physics and modeling are on the frontier of constructing rigorous core kinetic mechanisms for combustion

Experiment and theory can now probe details of pressure-dependent reactions on complex potential energy surfaces

Modeling, experiment, and theory can follow consequences of nonequilibrium energy distributions in reacting systems

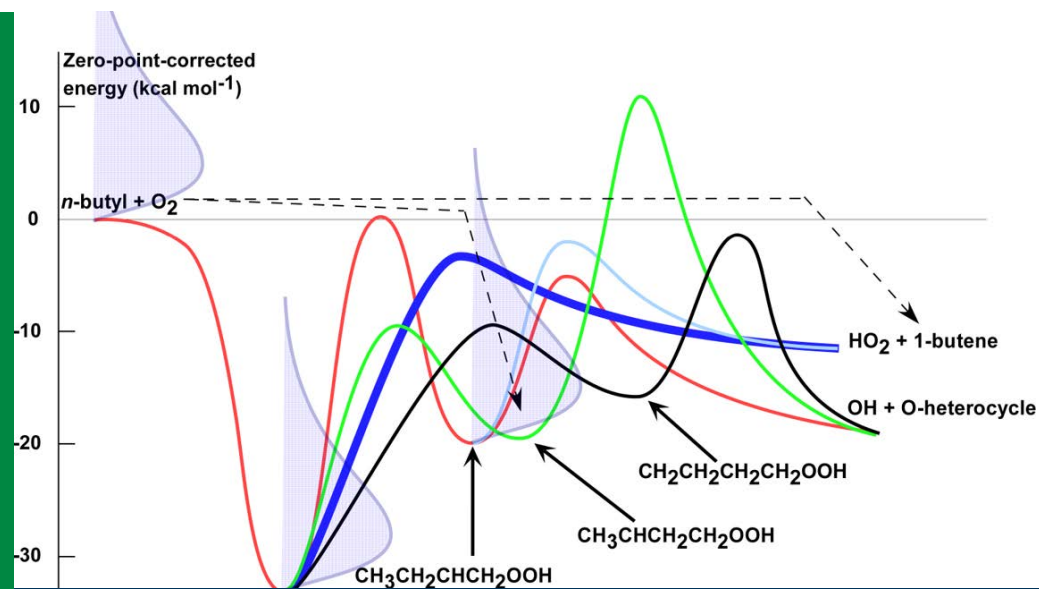


Forefront research in gas phase chemical physics on an energy mission of national importance is the goal.

## Frontiers of gas-phase chemical physics emerge in high-pressure chemistry

- Detailed rigorous description of energy transfer
- Nonequilibrium energy distributions
- Breakdown of simplifying kinetics assumptions

Combustion provides the complexity required to investigate these chemical physics frontiers



Initial energy distribution is different for direct and sequential paths

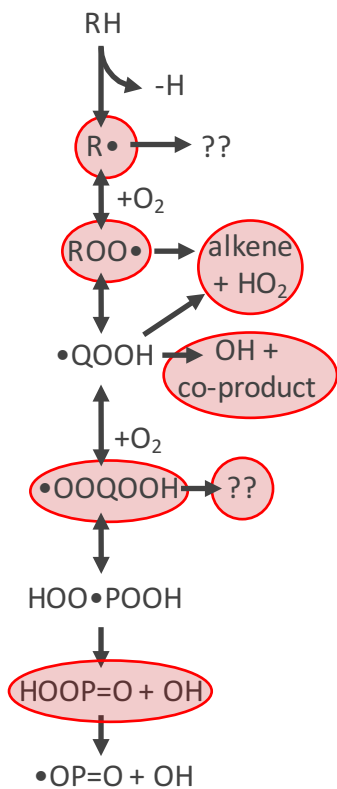
Branching fractions continue to change beyond “high pressure limit”

Product energy distributions may affect subsequent reactions

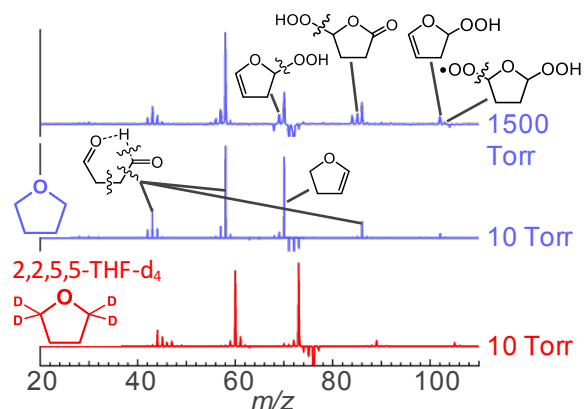
# Unexpected pathways after second O<sub>2</sub> addition in the oxidation of THF

Scientific challenge: understanding mechanisms of degenerate chain branching in autoignition

Technical challenge: extending VUV-PIMS experiments to high pressures



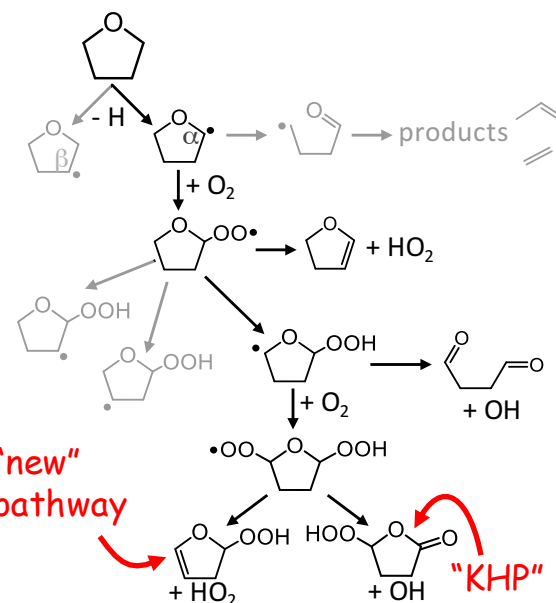
## E Experiment: tunable VUV-PIMS probing of Cl-initiated THF oxidation, P = 10 - 2000 Torr, T = 400 - 800 K



Ivan Antonov

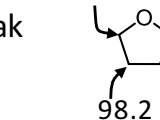


- PI spectra and THF-d<sub>4</sub> experiments → unambiguous species ID
- Simultaneous observation of OOQOOH and two of its products
- Strong P-dependence of 2<sup>nd</sup> O<sub>2</sub> addition signals



General mechanistic insight 93.7 kcal/mol

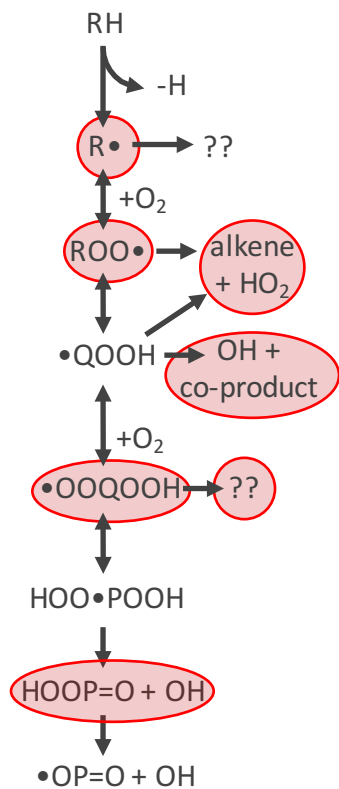
- Weak  $\alpha$ -CH bonds; weak C-O bonds in radicals
- Cyclic structure constrains reactivity



# Unexpected pathways after second O<sub>2</sub> addition in the oxidation of THF

Scientific challenge: understanding mechanisms of degenerate chain branching in autoignition

Technical challenge: extending VUV-PIMS experiments to high pressures

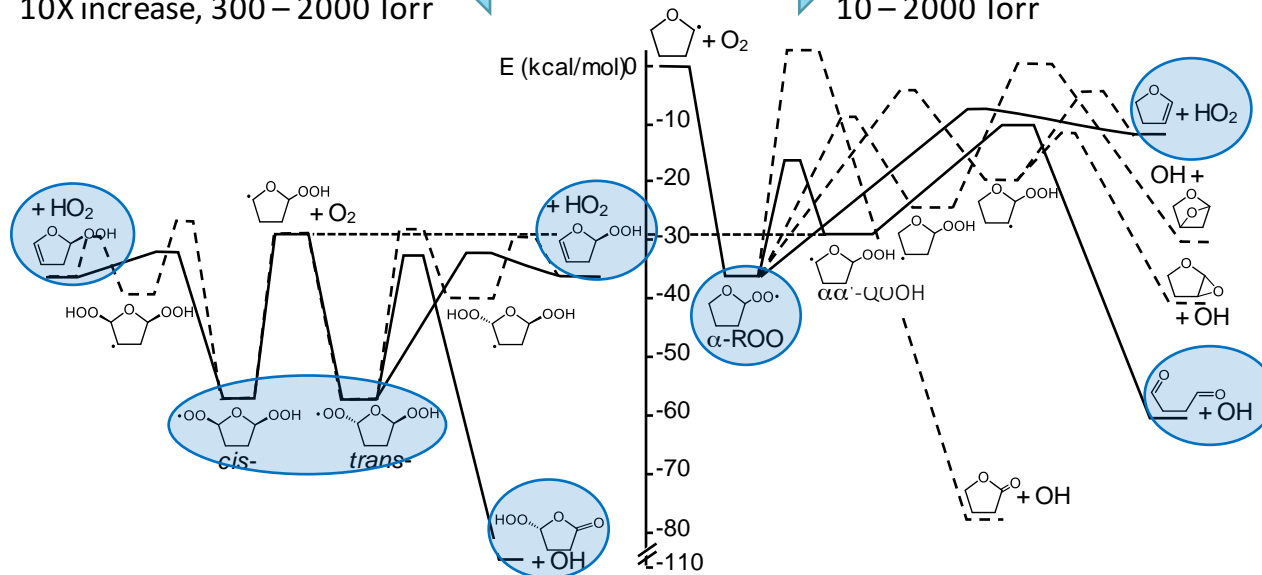


## T Theory: automated PES exploration

Strong P-dependence  
10X increase, 300 – 2000 Torr



Weak negative P-dependence  
10 – 2000 Torr



## M Modeling – part of future work

Judit Zádor



Ivan Antonov



- **Revolutionary Advances in Models, Mathematics, Algorithms, Data, and Computing**
- **Beyond Ideal Materials and Systems: Understanding the Critical Roles of Heterogeneity, Interfaces, and Disorder**
- **Mastering Hierarchical Architectures and Beyond-Equilibrium Matter**

Theoretical chemical physics and modeling are on the frontier of constructing rigorous core kinetic mechanisms for combustion

Experiment and theory can now probe details of pressure-dependent reactions on complex potential energy surfaces

Modeling, experiment, and theory can follow consequences of nonequilibrium energy distributions in reacting systems

- *Pressure-dependent system of interacting complex chemical reactions*
- *Arena to demonstrate a paradigm shift in theoretical chemical kinetics*
- *Relationships among reactions produce non-equilibrium behavior*
  
- *Target systems that capture these three themes (e.g., DME)*

Coordinating themes cross the three subtasks:

- Low-temperature oxidation
  
- Core C<sub>3</sub> mechanism
  
- Non-thermal reactions

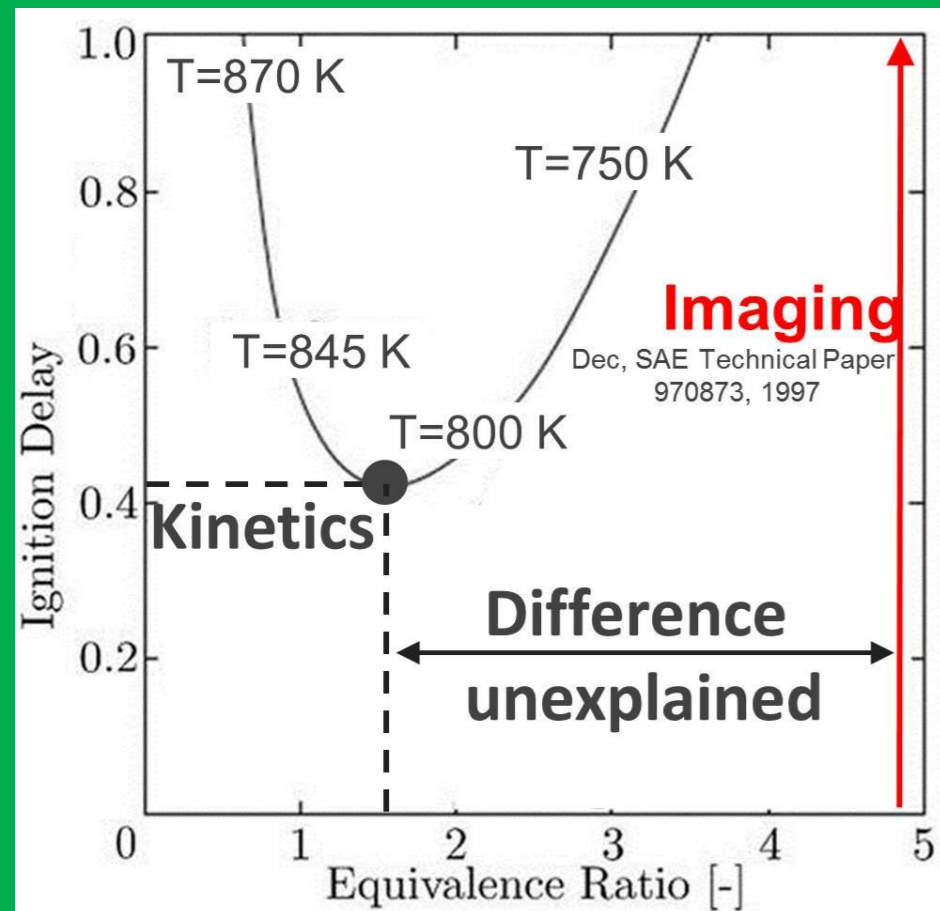


# Low-temperature ignition of complex fuels in turbulent, stratified flows

Stratified flows exhibit inhomogeneous temperature distribution  
 → Cold in fuel-rich regions  
 → Hot in fuel-lean regions (more hot air)

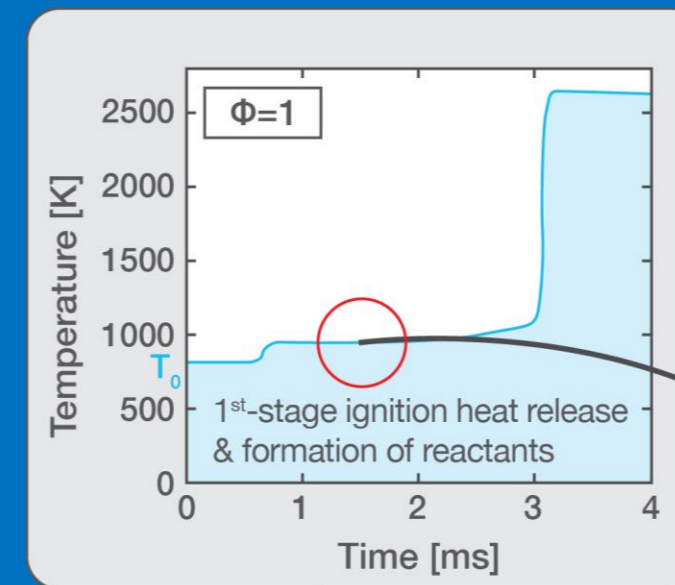
High-pressure emphasizes significance of low-temperature kinetics & two-stage ignition

Intense turbulence & molecular transport process

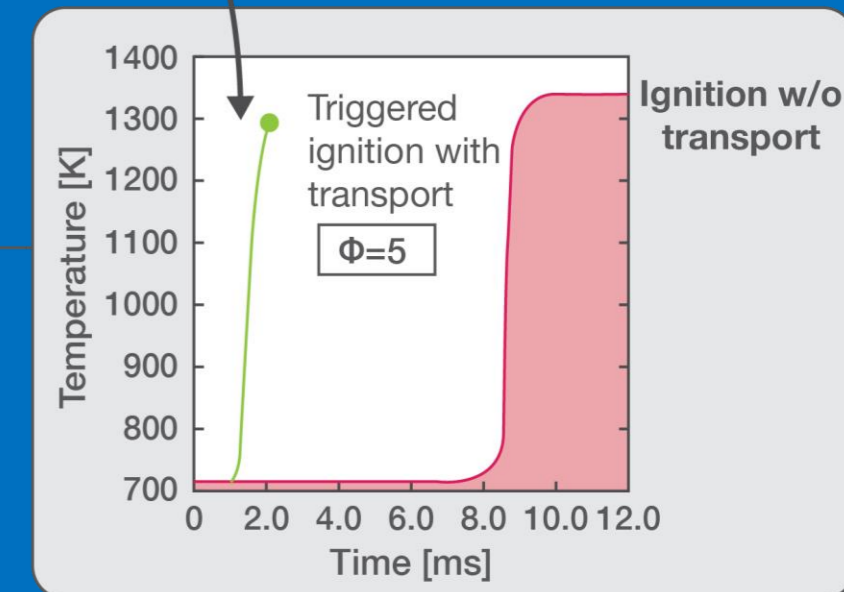
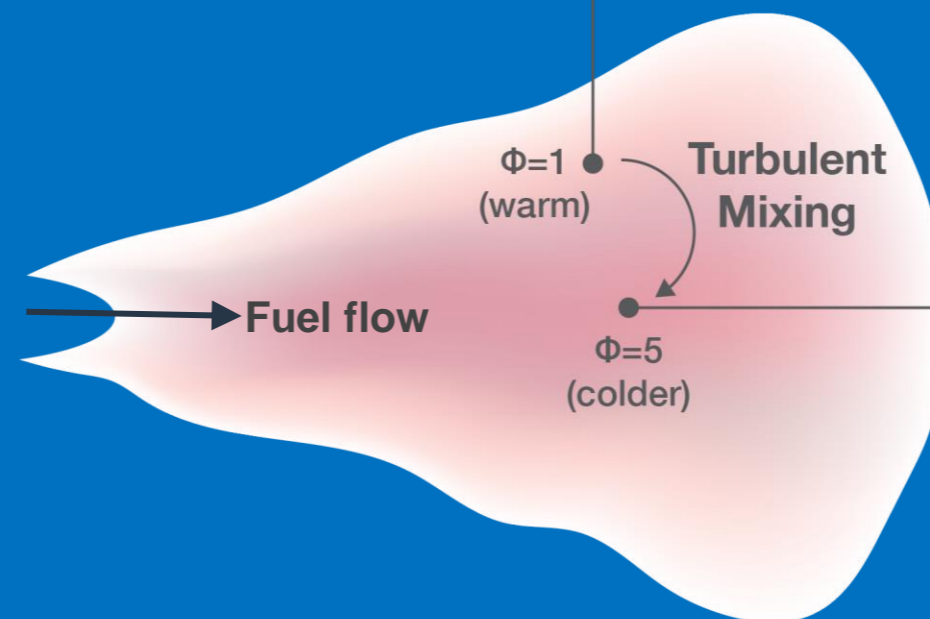


Dahms et al., *Proc. Combust. Inst.* 36:2615-2623 (2017)

Theoretical-numerical 1-D simulation shows:  
 → Low-temperature products transported into yet unburned mixtures which triggers & shortens their ignition



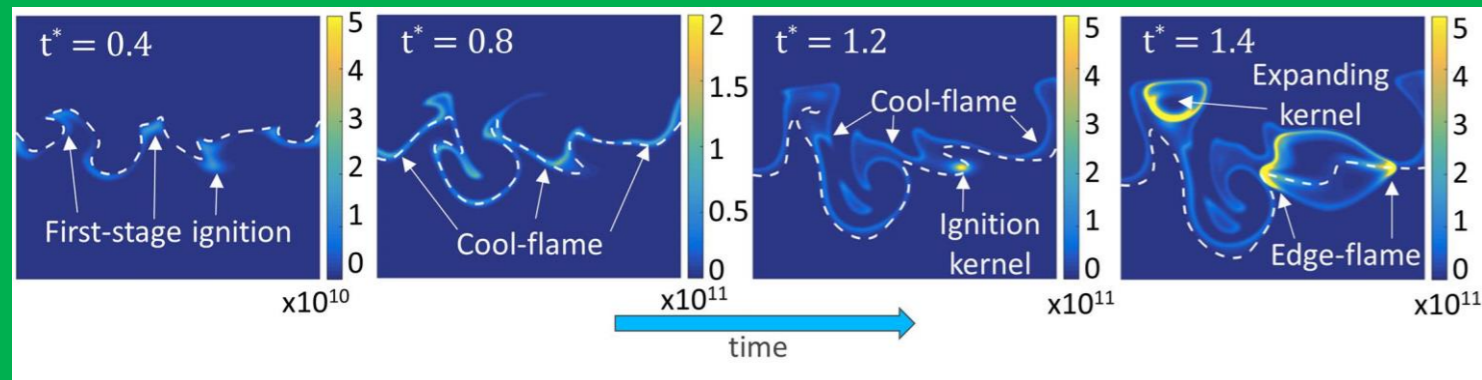
**Turbulent mixing**  
 Transports heat/reactants from reacted regions to yet unreacted mixtures to trigger their ignition



2-D direct numerical simulation of DME turbulent two-stage high-pressure ignition

→ Numerical equivalent of experiment

→ Results consistent with theoretical predictions



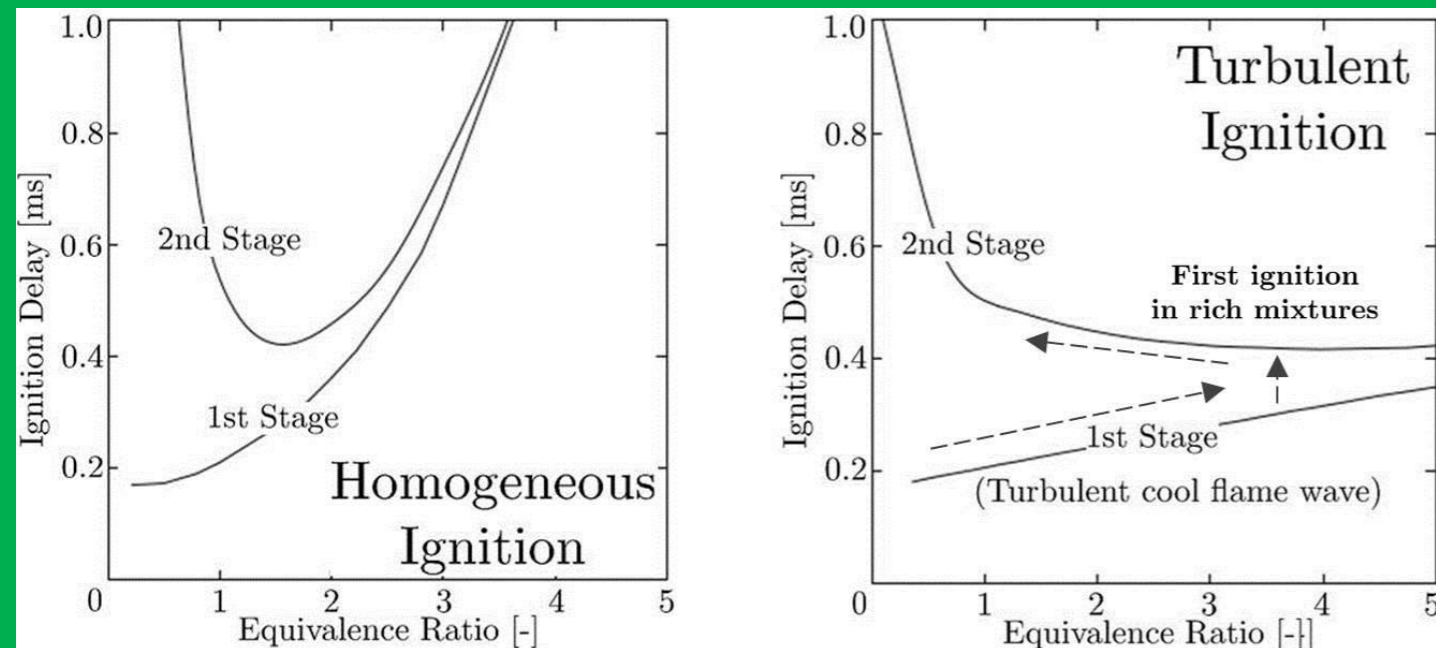
Krisman et al., *Proc. Combust. Inst.* **36**:3567-3575 (2017)

## Fundamental interactions

- Low-temperature kinetics, including possible non-equilibrium
  - Non-thermalized reactions
  - Non-equilibrium QOOH\* reactions
- Intense turbulence and molecular transport, possibly affected by (non-ideal) super-criticality and multi-component mixture properties
  - Real-fluid thermodynamics & transport
  - Non-unity Lewis number & counter-gradient diffusion

## Capabilities in the GPCP program

- Chemical kinetic models can explore & incorporate non-equilibrium chemistry
- New imaging techniques for direct measurement of transport of species
- DNS & LES modeling can enhance understanding of turbulence-chemistry interactions
- Uncertainty quantification applicable to complex problems



Dahms et al., *Proc. Combust. Inst.* **36**:2615-2623 (2017)



# Combustion Dynamics and Kinetics of Droplets and Nanoparticles

Rob Tranter (ANL), Al Wagner (ANL), and Bob Continetti (UCSD)

**Critical Issue: How do droplets/nanoparticles of fuel and fuel *blends* behave during combustion?**

- Do gas phase combustion mechanisms apply?
- Do species-specific evaporation rates and surface segregation rates influence combustion?
- Do transport properties and turbulence within the droplet influence combustion?
- How does supercriticality affect the droplet behavior of fuel blends?
- How do droplets/nanoparticles behave upon collision with surfaces? Inelastic scattering? Fragmentation?

**Implications:**

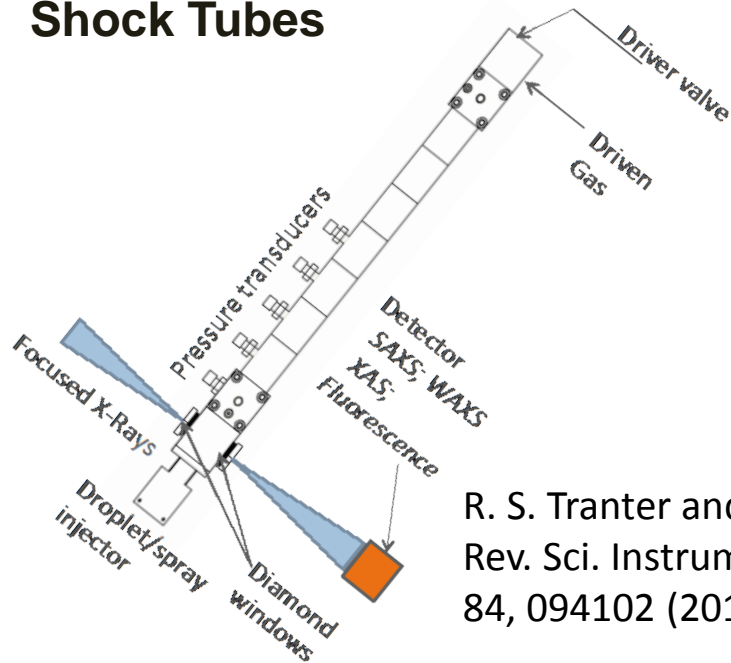
- addresses the grand challenge of matter far from equilibrium
- emphasizes chemical studies of general processes of spray breakup and condensed media oxidation/pyrolysis



# Combustion Dynamics and Kinetics of Droplets and Nanoparticles Cont'd

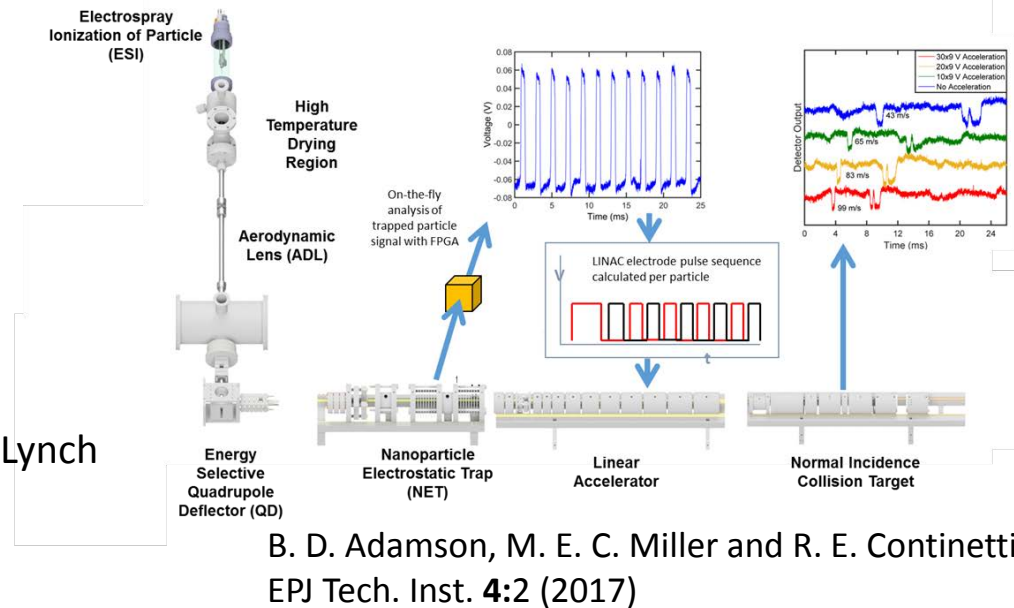
## Experimental Opportunities:

### Shock Tubes



R. S. Tranter and P. T. Lynch  
Rev. Sci. Instrum.  
84, 094102 (2013)

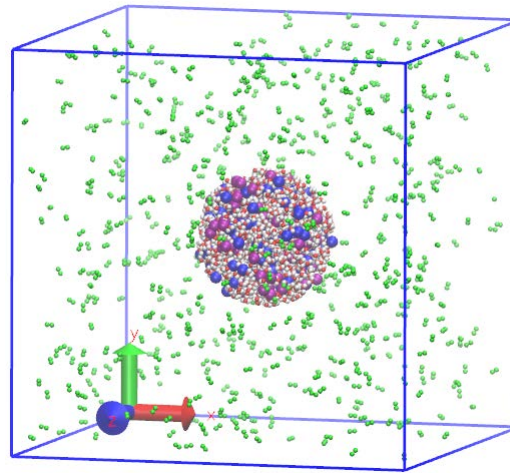
### Aerosol Impact Spectrometer



B. D. Adamson, M. E. C. Miller and R. E. Continetti  
EPJ Tech. Inst. 4:2 (2017)

## Theoretical Opportunities:

- MD simulations of 1-10 nm nanodrops/particles with high performance computing



B-B. Wang, X-D. Yang, M. Chen, and J-L. Xu,  
Entropy, 15, 1232 (2013)



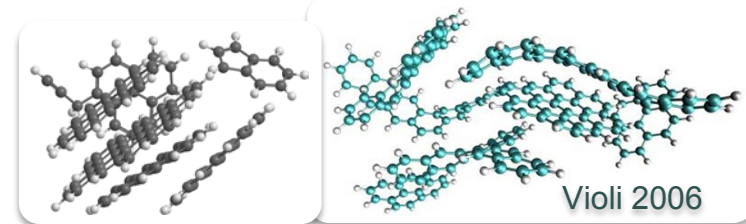
# Critical Issues in Gas Phase Chemical Physics that Impact Combustion

## Soot formation, growth and reaction

**H. Michelsen – Sandia National Laboratories**  
**A. Violi – University of Michigan**

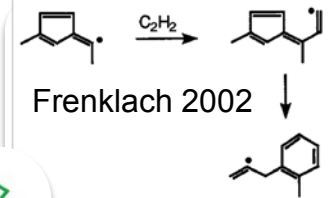
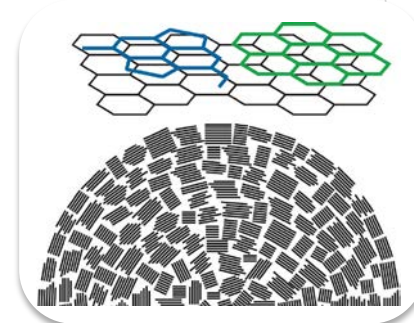
- Soot formation

- What are the mechanisms of inception?
- What are the precursor species involved?
- How do mechanisms depend on conditions?
- How do mechanisms control particle characteristics?



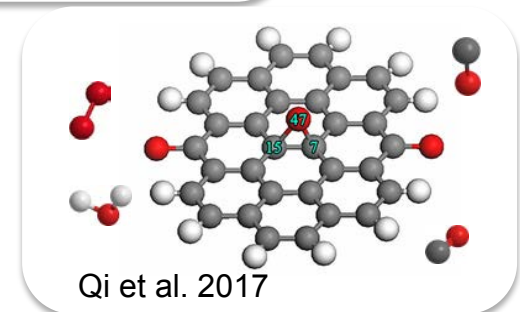
- Soot growth and evolution

- What are the mechanisms of particle growth?
- How does particle fine structure evolve?



- Soot oxidation

- What are the mechanisms of oxidation?
- How do mechanisms depend on particle characteristics and conditions?



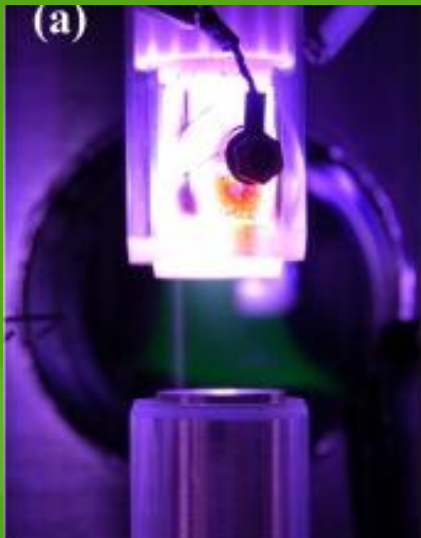
# Critical Issues in Gas Phase Chemical Physics that Impact Combustion

## Soot formation, growth and reaction

- Experimental challenges
  - Incipient particles are hard to detect
  - More mature particles are not spherical – Mie theory inadequate
  - Probes perturb combustion chemistry
  - Lots of interferences for spectroscopic measurements
  - Conditions are extreme – high temperature, high pressure
- Computational challenges
  - Current atoms/molecule/particles interactions are inadequate
  - Multiple timescales involved in soot formation
  - Lack of ergodicity in analyzing soot characteristics
  - Need for better modeling of energy/temperature distribution
  - Current kinetic models need to be augmented

# Gas-Phase Plasma Interactions in Driven Ignition

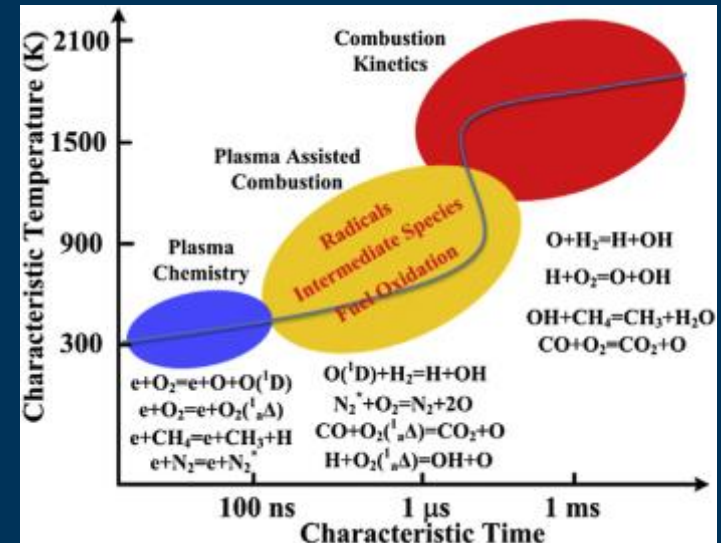
Low-temperature plasmas enhance ignition and flame stabilization  
 Non-equilibrium – different electron and molecular temperatures  
 Discharge can also be used for emission reduction or fuel reforming  
 Kinetics effects and thermal effects



Chemical composition affects discharge characteristics  
 Large kinetic effects on low temperature ignition

Fundamental interactions:

- Electron coupling to molecular degrees of freedom
- Chemical kinetics, including possible non-equilibrium
- Ionic flow and transport within and around the plasma



W. Sun et al., *Combust. Flame* **159**, 221–229 (2012)

Ju and Sun, *Prog. Energy Combust. Sci.* **48** 21-83 (2015)

**PARTITION FUNCTIONS  
IN THERMOCHEMISTRY  
AND KINETICS UNDER  
EXTREME CONDITIONS**

**BRANKO RUSCIC**  
Chemical Sciences and  
Engineering Division  
Argonne National Laboratory

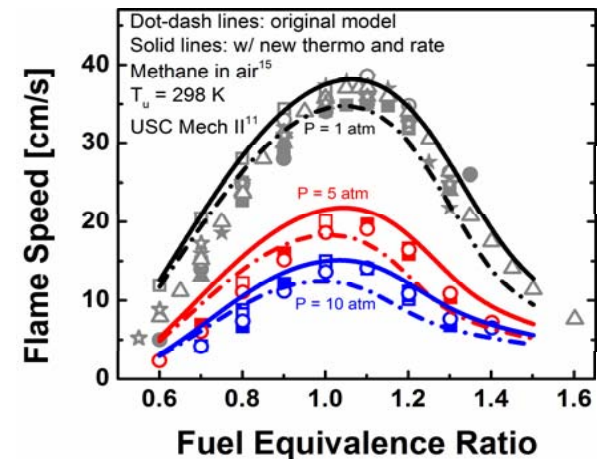
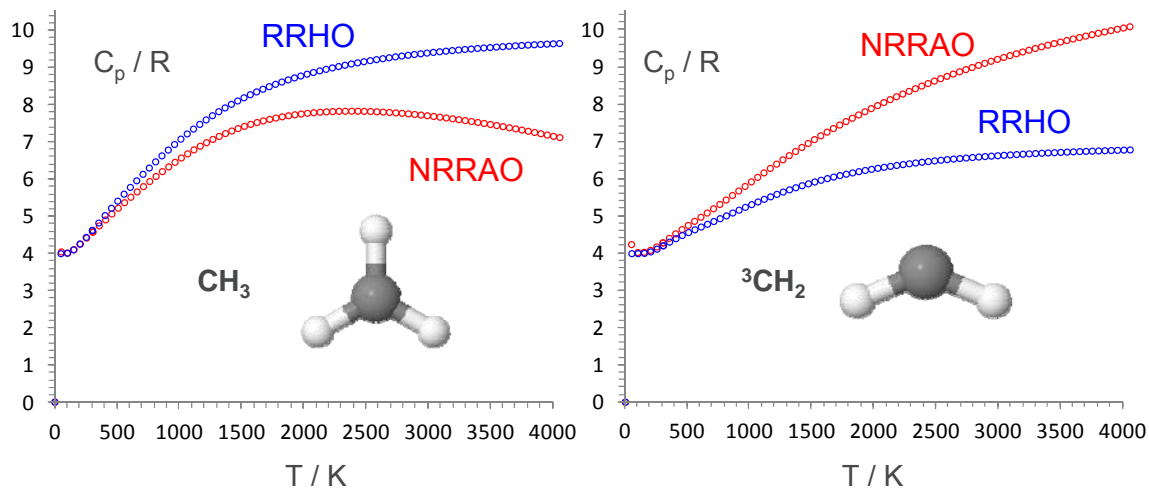
**STEPHEN J. KLIPPENSTEIN**  
Chemical Sciences and  
Engineering Division  
Argonne National Laboratory

June 2, 2017

**ACCURATE PARTITION FUNCTIONS AND THEIR  
ROLES IN THERMOCHEMISTRY AND  
KINETICS, BOTH WITHIN COMBUSTION AND  
OUTSIDE COMBUSTION**

# PARTITION FUNCTIONS

- Partition functions and their derived properties such as  $C_p(T)$ ,  $S(T)$ ,  $H_{\text{incr}}(T)$  are the **next major bottleneck** both in thermochemistry and kinetics
  - we are achieving higher and higher accuracies for  $\Delta_f H_0$  or  $\Delta_f H_{298}$  (ATcT, state-of-the-art electronic structure)
  - it becomes clear that the achieved accuracies will not be preserved at higher  $T$ , unless we have accurate partition functions
- The ubiquitous RRHO partition functions are quite inadequate





# PARTITION FUNCTIONS

- There are essentially three areas of developments with respect to partition functions that are relevant and desperately needed:
  1. A way to systematically improve the current partition functions beyond the ubiquitous rigid-rotor-harmonic-oscillator (RRHO) approximation
    - count of states if PES available?
    - NRRAO corrections to the RRHO partition functions?
    - phase space integrations with direct potential evaluations?
  2. Reexamination of the most fundamental aspects of partition functions (may well lead to entirely new concepts)
    - species identity at higher energies
    - which states of the targeted species should or should not be included
    - how are the actual multiplicities of states (which include nuclear spin statistics) treated in a consistent manner
    - underlying assumption that the chemical species in question is always thermally equilibrated
    - mathematical problems, such as mathematical non-convergence of partition functions in some cases
  3. Real gases vs. ideal gases

# KINETICS - BREAKDOWN OF MODEL AND NORMAL DESCRIPTIONS AT HIGH TEMPERATURES AND PRESSURES

# KINETICS – HIGH T AND P

- High T
  - anharmonic effects are of increasing importance in the TS
  - reactions occur as multistep sequence without thermalization
  - need dynamical theories for reaction of nonthermal species
  - **species are ill-defined** – isomerization and/or dissociation occurs on same time scale as collisional thermalization
  - how do you define rate constants under such conditions?
  - statistical theories less valid – rates faster than IVR
- High P
  - collisions are not isolated
  - how do you define rate constants under such conditions?
  - do weakly bound complexes (van der Waals and hydrogen bonded) modify kinetics

**THANK YOU**

[www.anl.gov](http://www.anl.gov)



## Critical Issues in Gas Phase Chemical Physics that Impact Other Energy Missions of the DOE Basic Energy Sciences Program

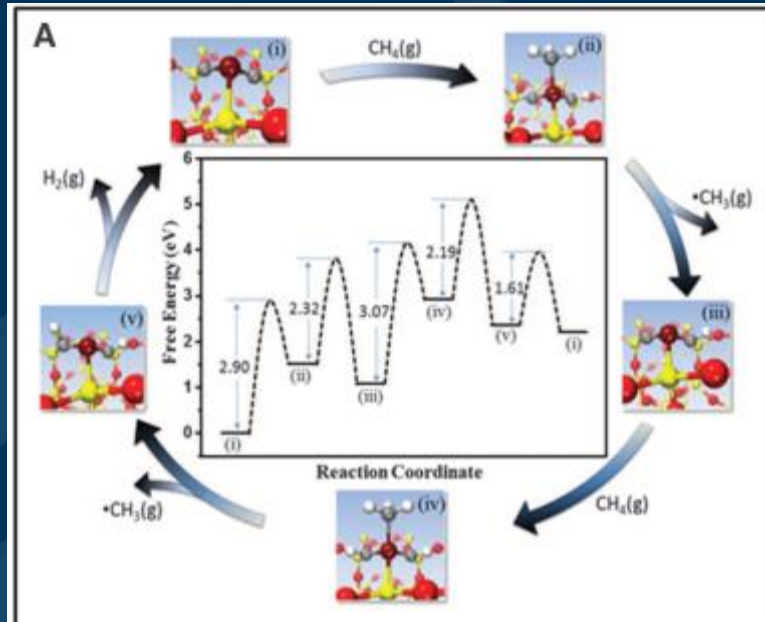
1	<b>Gas-Phase Interactions in Heterogeneous Catalysis</b>	Chandler Taatjes Lester	David Craig Marsha	SNL/CRF SNL/CRF U Penn
2	<b>Characterization and modeling of complex reaction networks</b>	Violi Zwier	Angela Timothy	U Michigan U Purdue
3	<b>Quantitative A Priori Dynamics and Kinetics</b>	Jasper	Ahren	ANL
4	<b>Modern High-Bandwidth Spectroscopy</b>	Field Prozument	Robert Kirill	MIT ANL
5	<b>Phase Changes and Thermal Transport</b>	Ahmed	Musa	LBNL
6	<b>Coupling Experiments and Simulations with Multi-dimensional Data and Uncertainty Quantification.</b>	Frank	Jonathan	SNL/CRF
7	<b>Gas Phase Chemical Physics with Free Electron Lasers</b>	Pratt	Stephen	ANL

# Gas-Phase Interactions in Heterogeneous Catalysis

Direct, Nonoxidative Conversion of Methane to Ethylene, Aromatics, and Hydrogen

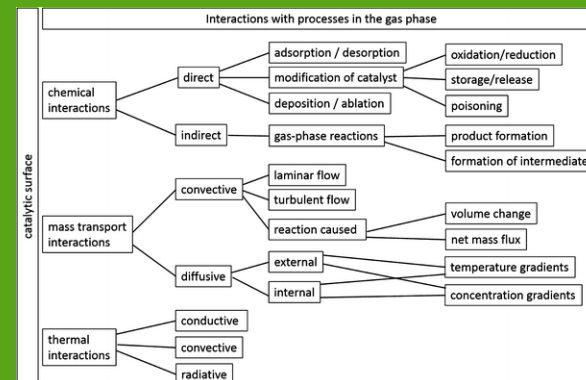
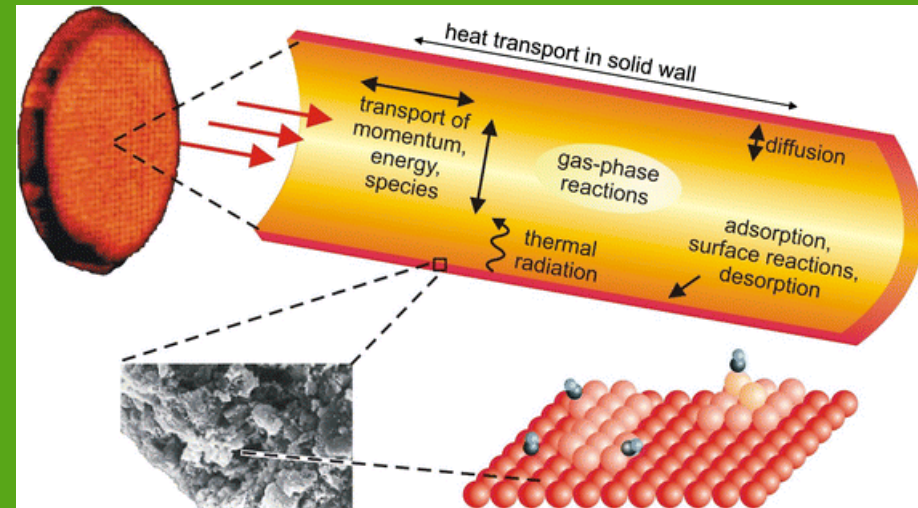
Guo *et al.*, *Science* **344**, 616-619 (2014)

- Demonstrated intermediacy of gas-phase methyl radicals in efficient methane conversion



Modeling of the Interactions Between Catalytic Surfaces and Gas-Phase

Olaf Deutschmann, *Catal. Lett.* **145**, 272–289 (2015)



## BESAC BRN Workshop on Catalysis:

- Develop new compositional characterization and analysis tools
- There is a lack of methodologies for understanding , designing and controlling complex catalytic systems
  - In situ sampling probes with spatial and temporal resolution
  - Rapid analysis methods of complex mixtures
  - Kinetic modeling methods
  - Theoretical tools to understand complex catalysis structures.
  - Accelerated catalyst discovery by leveraging high-throughput screening approaches for data mining with multi-scale models.

## Capabilities in the GPCP program

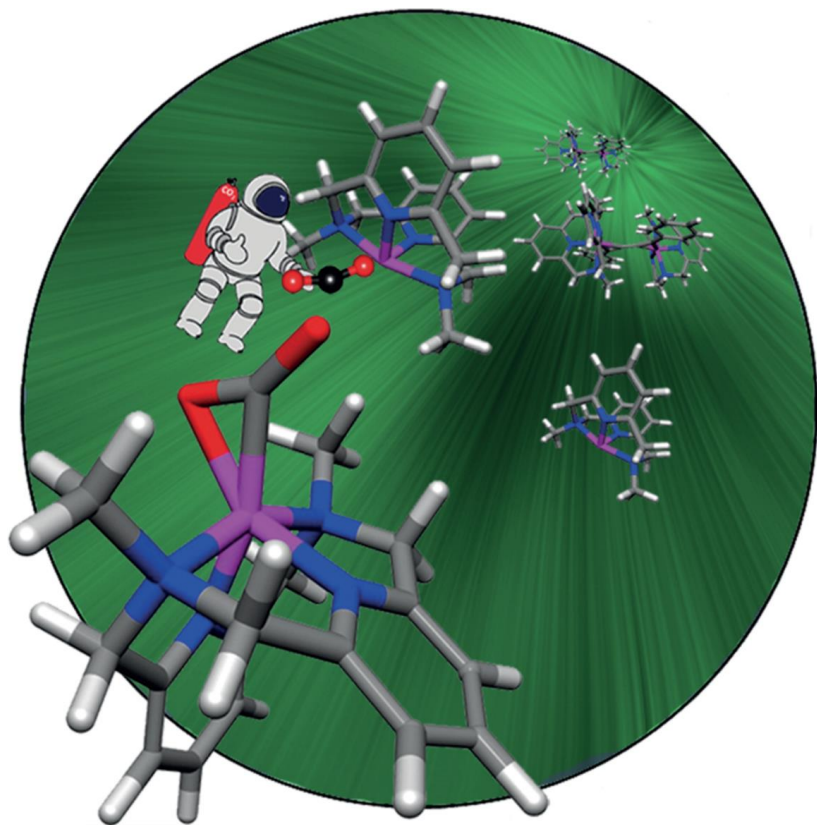
- MPIMS (Multiplexed Photoionization Mass Spectroscopy) provides fast analysis of complex mixtures of hydrocarbons and could be easily modified to monitor catalytic reactors.
- KinBot and other computer tools for understanding complex chemical transformations can be adapted to catalytic environments.
- Chemical kinetic models for molecular growth in flames can be adapted to predict production of high value products from low value feedstock ( $\text{CH}_4$ ,  $\text{H}_2$ ,  $\text{O}_2$ )
- DNS and LES modeling can enhance performance (improved mass and heat transfer) of micro-mixers and reactors used for catalytic conversions.
- Uncertainty Quantification techniques can be applied to complex catalytic systems to improve performance.



## Capture of CO<sub>2</sub> by a Cationic Ni(I) Complex

Characterization of bound, activated CO<sub>2</sub> by vibrational predissociation spectroscopy

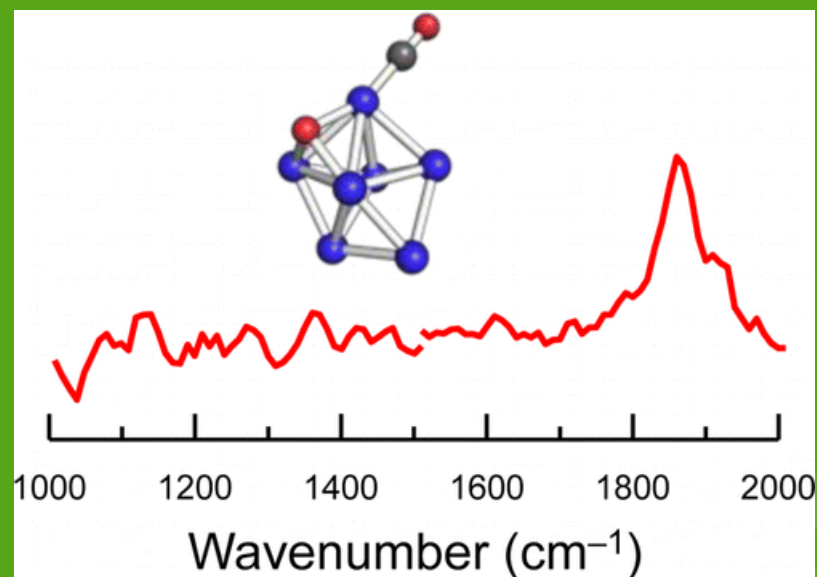
M. A. Johnson and coworkers, *Angew. Chem. Int. Ed.* 55, 1282–1285 (2016)



Highly distorted CO<sub>2</sub> molecule (asym stretch) is bound to the metal center. Ni(I) oxidation state is crucial to the activation of CO<sub>2</sub>.

## Size-Specific, Dissociative Activation of CO<sub>2</sub> by Cobalt Cluster Anions

A. Fielicke and coworkers, *J. Phys. Chem. C* 20, 14209–14215 (2016)

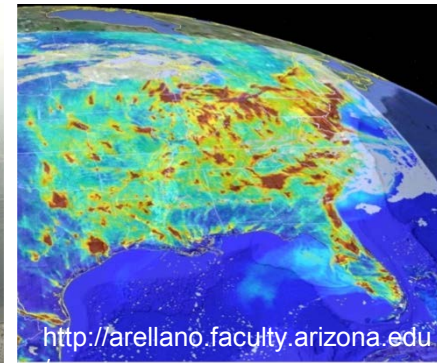
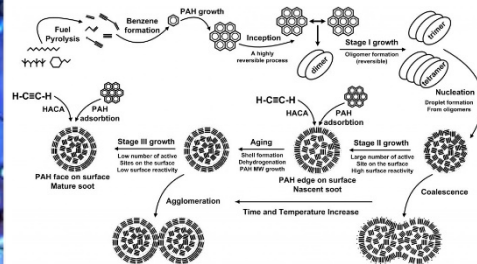
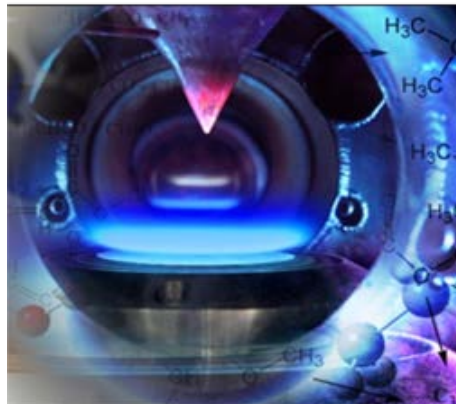


Mass spectrometric measurements show that reactivity depends strongly on cluster size: emerges at  $n = 7$ , peaks at  $n = 8-10$ . Infrared multiple photon dissociation spectra suggest CO<sub>2</sub> is dissociatively adsorbed on Co<sub>*n*</sub><sup>-</sup>. Contrast with metal-bound CO<sub>2</sub><sup>-</sup> on Rh<sub>*n*</sub> clusters.



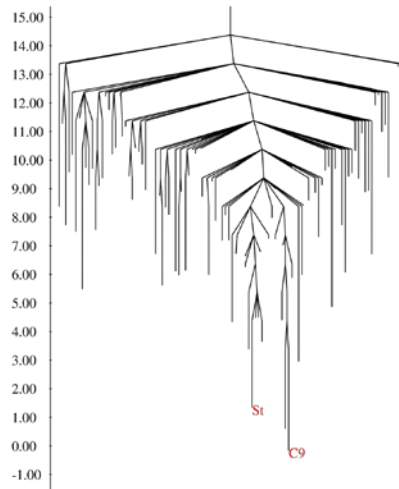
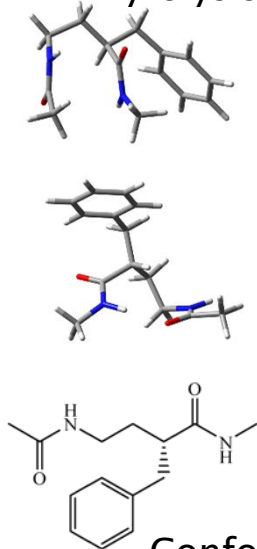
# Critical Issues in GPCP that Impact Other Energy Missions of DOE BES Characterization and Modeling of Complex Reaction Networks

T. Zwiier – Purdue University  
A. Violi – University of Michigan

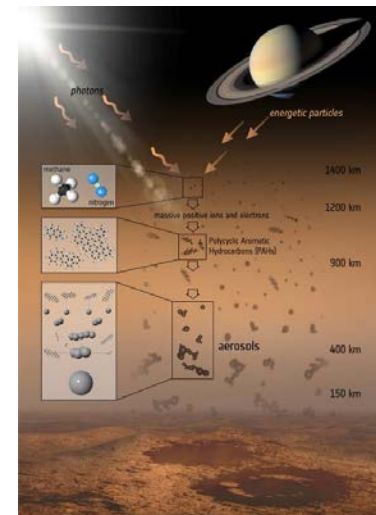


Atmospheric chemistry: Smog formation

Pyrolysis and Combustion of Fuels



Conformational energy landscapes

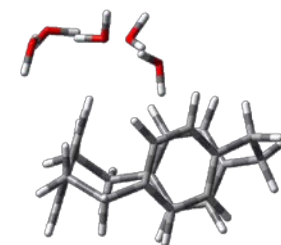
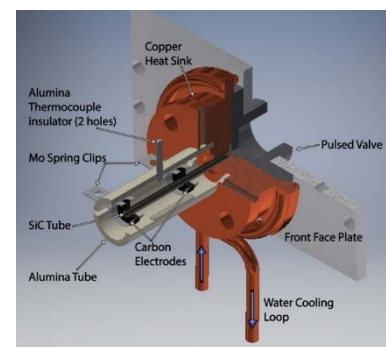
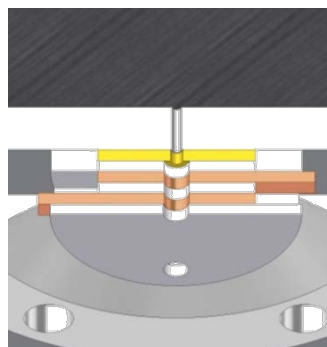
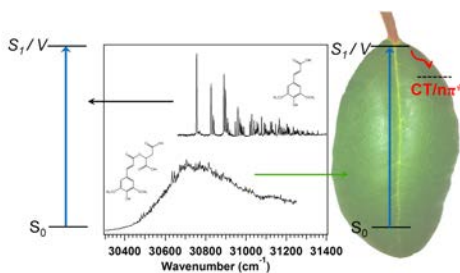
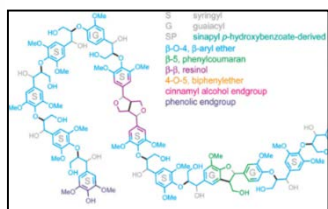


Astrochemistry:  
Photochemistry in Titan's Atmosphere

## Critical Issues in Gas Phase Chemical Physics: Impact on Other Energy Missions of DOE BES Characterization and Modeling of Complex Reaction Networks

- All areas involve a **close partnership** between experiment, theory, and modeling
- As seek to account for larger molecules, aggregates:
  - Strive for **generalizable reactivity patterns**
  - **Heterogeneous reactions** begin to play a role
- Easier identification of **salient characteristics** of process (e.g., bottlenecks, common patterns)
- **Abstraction** from model/experiments that is needed for future deep learning approaches.
- Helps the **identification** of the weaknesses of current models.

# Critical Issues in Gas Phase Chemical Physics: Impact on Other Energy Missions of DOE BES Characterization and Modeling of Complex Mixtures



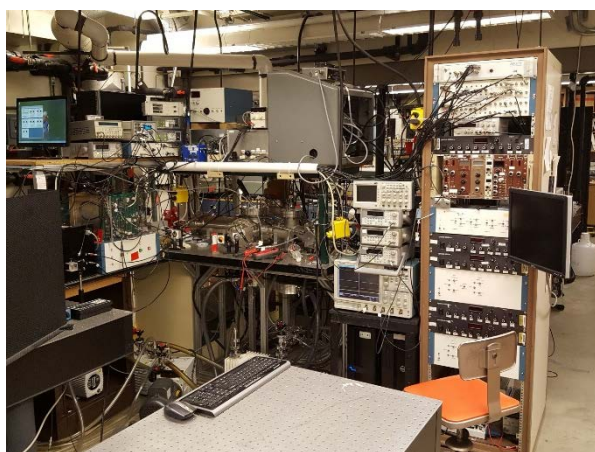
Lignin

Plant sunscreens

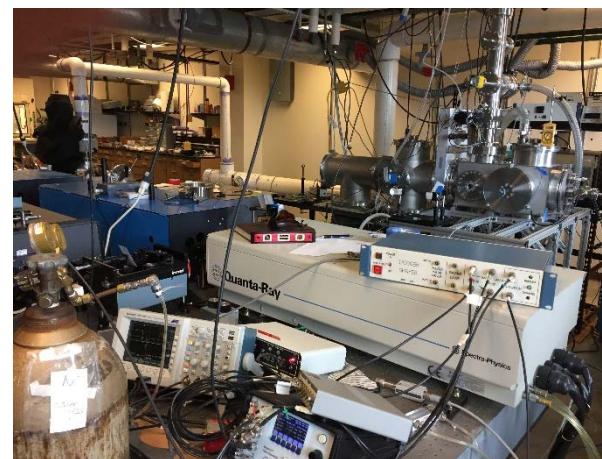
Discharge or  
Photolysis

Flash  
pyrolysis

Molecular  
clusters



Multi-stage mass spec for  
cryocooled ion spectroscopy  
*m/z*, UV, single-conformer IR



CP-FTMW/TOFMS chamber  
Mass-correlated CP-FTMW spectra  
VUV-photoionization MS, microwave

# Critical Issues in Gas Phase Chemical Physics: Impact on Other Energy Missions of DOE BES Characterization and Modeling of Complex Mixtures

## Development of Multiplexed Experimental methods

- Many areas of relevance to DOE Energy Missions (e.g, **biofuels, photosynthesis, plasmas, pyrolysis, solvation effects**) where GPCP can provide incisive experimental tests on model systems
- Often involve the generation of **complex chemical mixtures**
- Analysis via a **single detection** scheme often **incomplete/ambiguous**
- GPCP community is developing powerful **multiplexed methods** that **combine complementary data** on the same mixture
  - More sensitive, selective, comprehensive, faster, cheaper

# Critical Issues in Gas Phase Chemical Physics: Impact on Other Energy Missions of DOE BES Characterization and Modeling of **Complex Mixtures**

## Development of predictive computational methods

- The ability to predict properties of mixture of **several components** (more than 3 or 4) is experimentally challenging due to the the large variable space;
- Interfaces, nano separation, dipole interaction, and polarizability makes the use of standard **ideal models prone to errors** in predicting even the simplest properties (e.g., density compressibility, heat of vaporization, viscosity);
- Computational model, refined with experimental data, can provide fast and cheap **pre-screening** of extremely complex mixtures, allowing for selective experimental validation;
- Computational models enable computation of quantities in ensembles that are **hard to probe experimentally** (e.g., isentropic).
- Applications vary from fuel storage, distribution, injection, and combustion.

# Quantitative *A Priori* Dynamics and Kinetics

## First-principles calculations are a source of fundamental information

- Historically, this role has been filled by experiment, with theory used empirically to extrapolate and/or interpret experiment.
- *A priori* predictions with accuracies comparable to those of experiment are now possible for many classes of systems, thanks to advances in computing power and new theoretical methods—in particular to new electronic structure theory methods and codes.

## Calculating a potential energy surface is always step one of two

- The spectacular advances in electronic structure theory should be matched by corresponding advances in dynamics and kinetics.
- A variety of classical, semiclassical, and quantum mechanical methods should be developed, with varying compromises of computational cost and quantified accuracy.
- A prediction without an error bar is only half of a result.
- Continued progress requires
  - Quantifying the uncertainty in existing approaches for real systems
  - New methods for challenging systems and extreme conditions

# Quantitative *A Priori* Dynamics and Kinetics

*Current needs for a priori theory: More accuracy and broader applicability*

## Questioning fundamental assumptions

- Fast interconversions over low barriers can lead to temperature and pressure dependent definitions of “species” and their associated rates.
- At high pressures, collisions do not occur as isolated binary interactions. At what pressures does this behavior manifest, and how does it relate to supercritical and liquid phases?
- In energetic environments, highly reactive radicals react before they are thermalized, and their reaction rates are typically sensitive functions of their (nonthermal) internal energy distributions.

## Electronically nonadiabatic transitions

- Excited state energies and electronic couplings are still relatively hard to compute.
- They are even harder to represent with analytic forms for efficient use in dynamics.
- Existing dynamical theories lack rigorous treatments of electronic (de)coherence and electronic tunneling.
- Statistical theories for kinetics are even less well developed than dynamical theories.
- The accuracy of these approaches is largely unquantified beyond one-dimensional models.
- Treating more than 2 coupled states is often required but is rarely done.

## Quantum chemistry

- “Gold standard” CCSD(T)/CBS is often not accurate enough.
- Higher level approaches do not take full advantage of HPC.
- Treating complex transition states (or, more generally, geometries away from equilibrium structures) is still a challenge.
- Global multireference descriptions require unfeasible orbital management.

## Vibrational anharmonicity

- Detailed practical methods exist for treating sets of torsions, but few are applicable to other non-harmonic motions.
- The errors in post-RRHO (rigid rotor/harmonic oscillator) methods are not well characterized.
- Anharmonic ZPE errors are not often considered but can be dominant.

## Collisional energy transfer

- The accuracy of classical trajectory-based predictions is unknown at low  $T$ , where comparisons with higher-level dynamics should be possible.
- Energy transfer in van der Waals complexes has not been explored in detail.

# Modern High-Bandwidth Spectroscopy

## Recent Technological Advances

- New laser and microwave sources and detection schemes: high coherence, frequency agile, phase coherent, and almost maintenance-free. Spectral velocity increased by factors from 100x to  $>10^6$ x.
- Broadband pure rotational spectroscopy (chemical specificity, quantitative, direct multiplexed detection of FID – phase and amplitude).
- Ro-vibrational frequency comb spectroscopy (higher pressure samples, quantitative, multiplexed detection).
- Big Data analysis, Machine Learning: mow the grass.

## Potential Breakthrough Areas

### 1. Time-resolved Quantitative Spectroscopy of Complex Reacting Systems

- a. Simultaneous detection of many conformers and species, with capability for time-correlated kinetics.
- b. Tracing time- and quantum state-resolved evolution of multiple reaction intermediates and products will lead to measurement of non-thermal kinetic effects. A powerful tool in combination with accurate kinetic modeling.
- c. Stopped kinetics for laser-initiated reactions in 4K buffer gas cell.
- d. Use of newly developed thermodynamically characterized chemical reactors (e.g. Buffer Gas Cooled and Pulsed Uniform Flow (Laval) reactors, He-cluster, para-H<sub>2</sub> matrix).

### 2. “Standard Model” for Transition States

- a. Access to previously inaccessible or falsely-labeled ergodic regions of state space. Basis for  $H^{\text{eff}}$  models that exploit robust, extrapolatable patterns (polyads). Broken pattern of broken patterns reveals transition state and, in the form of vibronic coupling, the physical reason for the lowest barrier pathway to and through the transition state.

### 3. Spectroscopic Pattern Recognition with Artificial Neural Networks

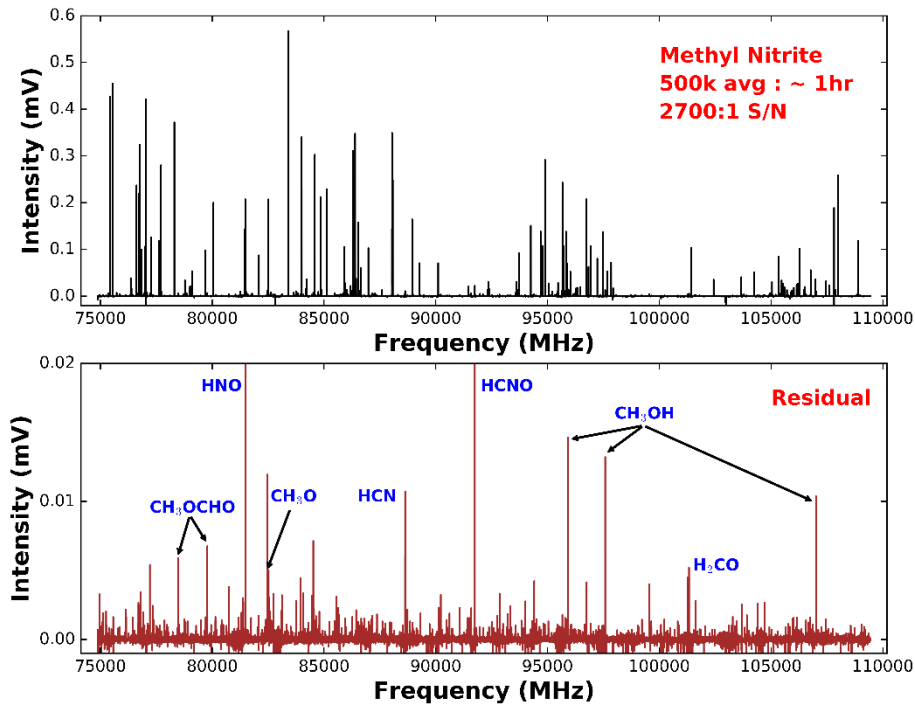
- a. Enormous amounts of useful spectroscopic data are being generated by broadband techniques. New approaches, including use of Artificial Neural Networks, will permit extraction of detailed chemical information: identifying (i) individual species and (ii) signature spectroscopic pattern irregularities that encode transition state properties.



# Quantitative Spectroscopy of Complex Reacting Systems

The pyrolysis of methyl nitrite,  $\text{CH}_3\text{ONO}$ , investigated by the chirped-pulse rotational spectroscopy and kinetic modeling

## 1. 35 GHz-wide rotational spectrum



~1200 lines

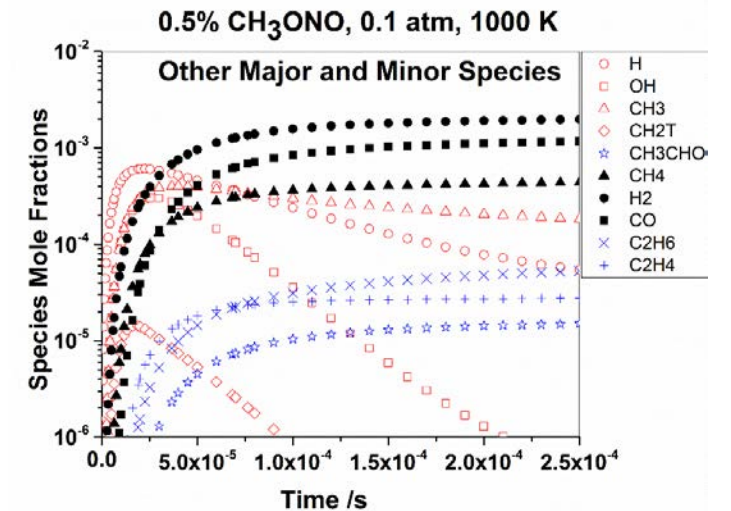
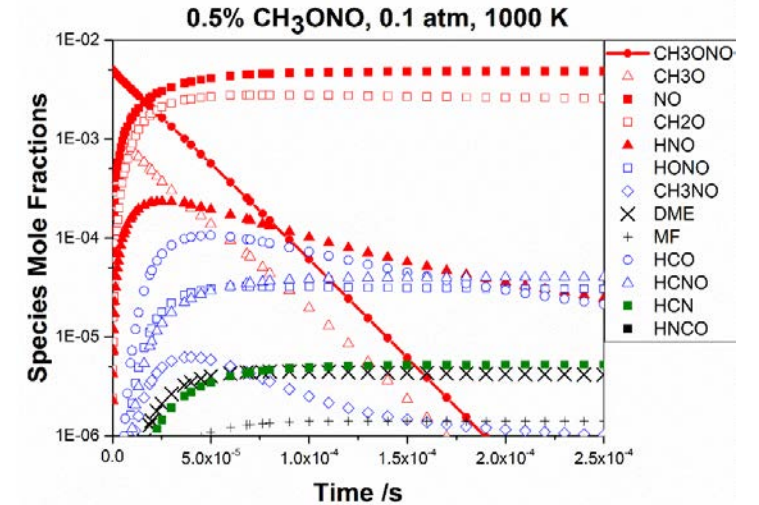
~400 lines assigned

Mow the grass between lines: isotopologues

## 2. 11 pyrolysis products quantified

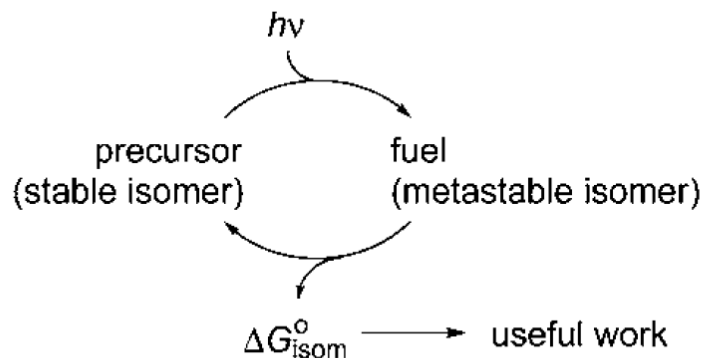
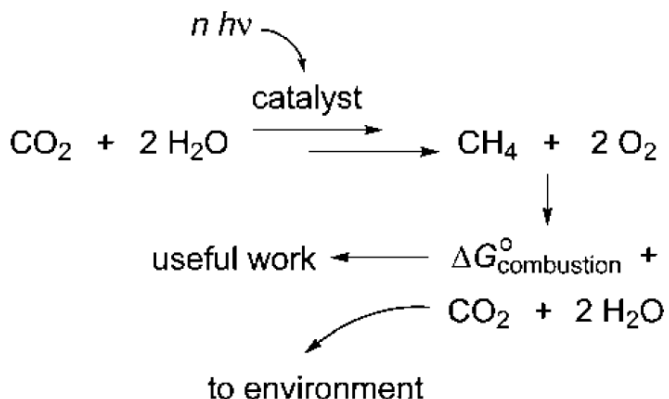
Product	$T_r$ (K)	Rel. Ab.
$\text{H}_2\text{CO}$	150(50)	3000(2000)
HNO	8(2)	160(107)
$\text{CH}_3\text{OCHO}$	8(2)	40(27)
$\text{CH}_3\text{O}$	8(5)	10(7)
$\text{CH}_3\text{OCH}_3$	4(2)	6(4)
$\text{CH}_3\text{NO}$	8(2)	1.2(8)
HCO	8(5)	1.0(3)
<i>trans</i> -HONO	10(2)	0.8(4)
HNCO	[8]	0.2
HCNO	[8]	2.0
HCN	[8]	2.0

## 3. A global model developed



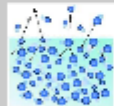

# Phase change and thermal transport

60% of US primary energy use is lost as thermal energy, can we recover %?



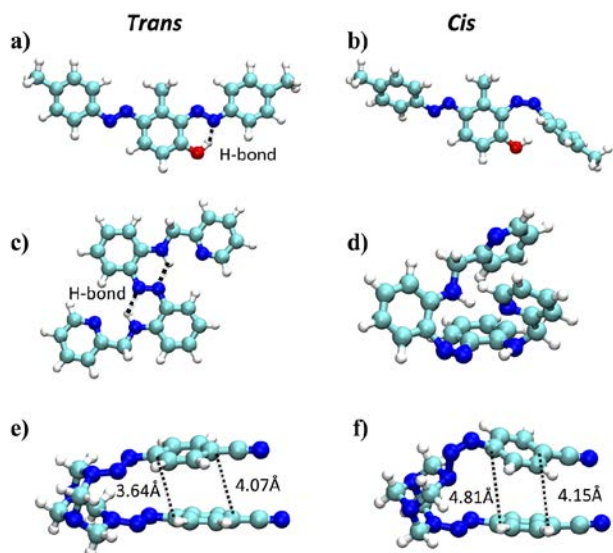
## Aiming for theoretical limits

Thermal Energy Processes are atomic/molecular scale phenomena

	Data	Theoretical limit
Phase change heat transfer 	~5 - 10 MW/m <sup>2</sup>	160 MW/m <sup>2</sup>
Thermal Storage 	< 1 MJ/kg	None (Gasoline ~ 40 MJ/kg)

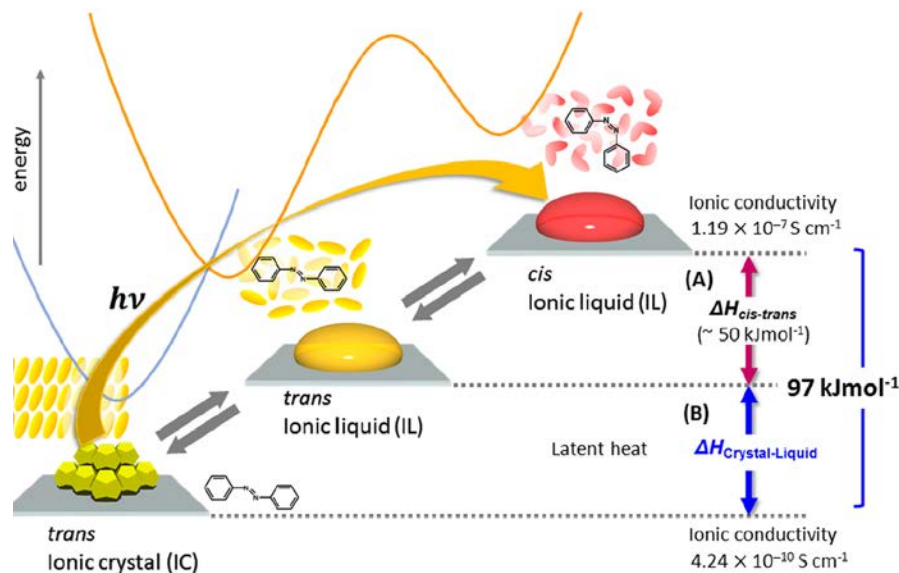
Fresher & Majumdar (to be published)

GPCP has been very good at studying the making and breaking of bonds



Liu et al. DOI/10.1021/nl5034073 | Nano Lett. 2014

Challenge is to store energy in bonds, and transfer them across distance



Kimizuka et al. DOI: 10.1021/acs.Langmuir.6b03363

$$\Delta H = T\Delta S$$

Large entropy change using molecular configurations and chemical bonds

## Liquid Phase Chemical Physics

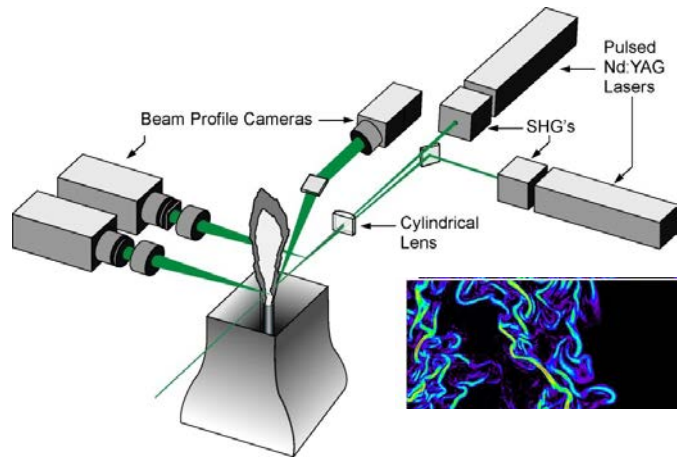
Energy Transfer  
 Phonon Transport  
 Excited States  
 Phase Change  
 Active Thermochemical Tables

# Coupling Experiments and Simulations with Multi-Dimensional Data and Uncertainty Quantification

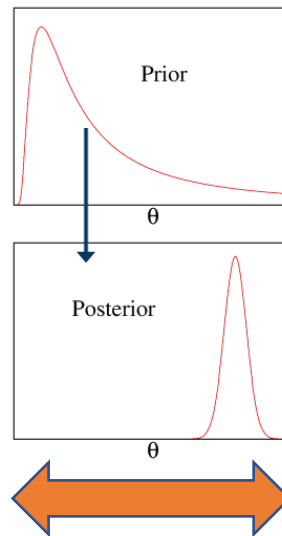
Goal: New scientific understanding and predictive simulation capabilities for complex physical systems (e.g. turbulence-chemistry interactions)

Highly nonlinear 4D (spatio-temporal) problem involving chaotic flow

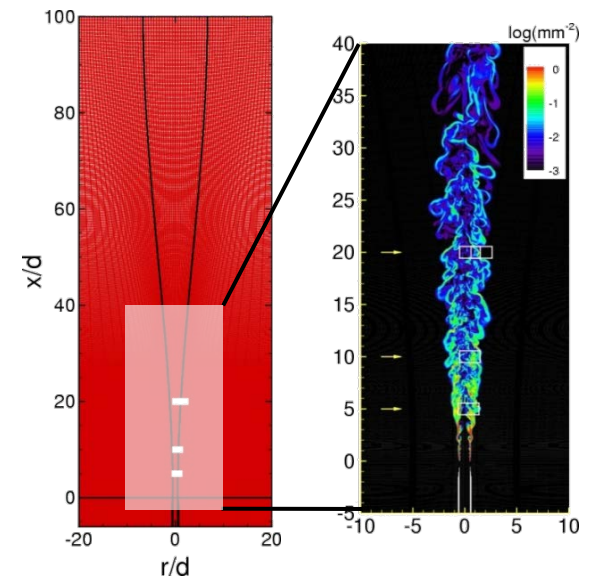
## Experiments



## Uncertainty Quantification



## Simulations



## Challenges

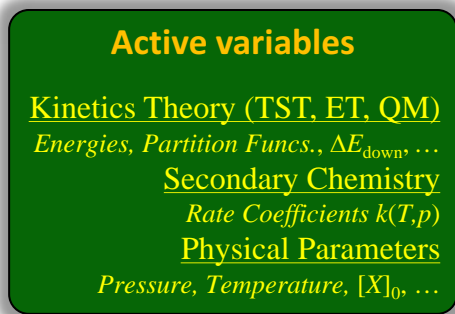
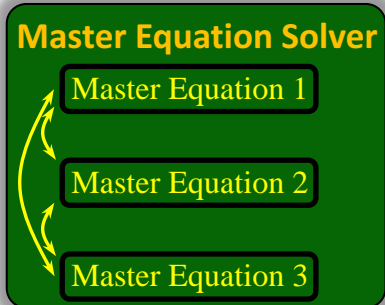
- Large multi-dimensional datasets from diagnostics
- Spatial & temporal resolution, dynamic range
- Number of simultaneously measurable quantities
- Measurement noise, interferences
- High-dimensional random field structure
- Strong non-linearities & chaotic dynamics
- Formulation of appropriate measures of comparison of experimental & computational images
- Large multi-dimensional solutions from modeled simulations
- Interdependence/competition between models and numerics
- Model validation in a sparse, noisy data context
- Sensitivity to boundary conditions

# Multi-Scale Informatics (MSI) Modeling: an Active Approach to Complex Chemistry

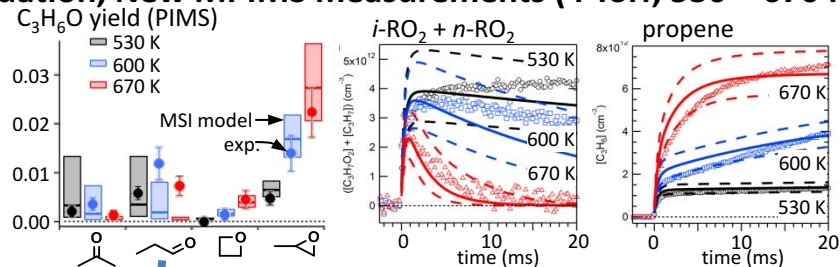
How should we holistically treat diverse information to create robust understanding of chemically reacting systems?

## Advances (propane oxidation):

- combination of multiple coupled MEs and secondary chemistry (assembled by RMG)
- optimization against a diverse set of targets
- proper weighting of uncertainties



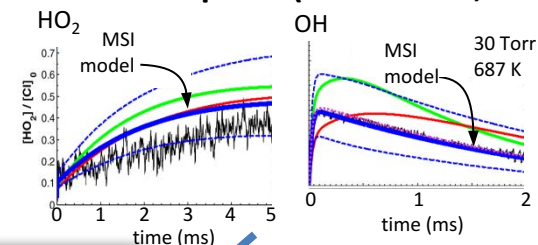
## Propane Oxidation, New MPIMS measurements (4 Torr, 530 – 670 K)



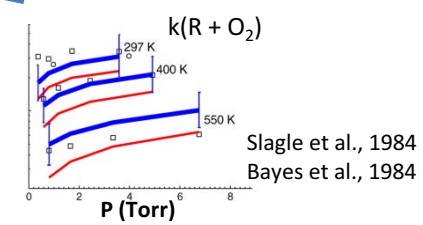
$k_i(T,p)$



## New IR absorption (10 - 60 Torr, 300 - 733 K)



## Literature $C_3H_7 + O_2$ measurements (297 – 550 K)



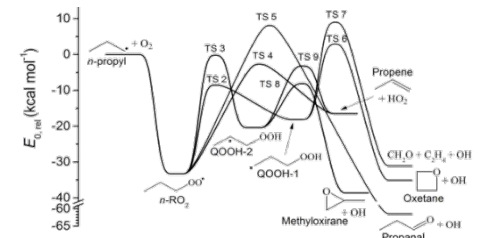
Feedback / Improve



## Future challenges:

- tractable application to complex systems
- better treatment of empirical parameters describing energy transfer, non-Boltzmann energy distributions

## Calculated PES ( $n$ -propyl + $O_2$ )



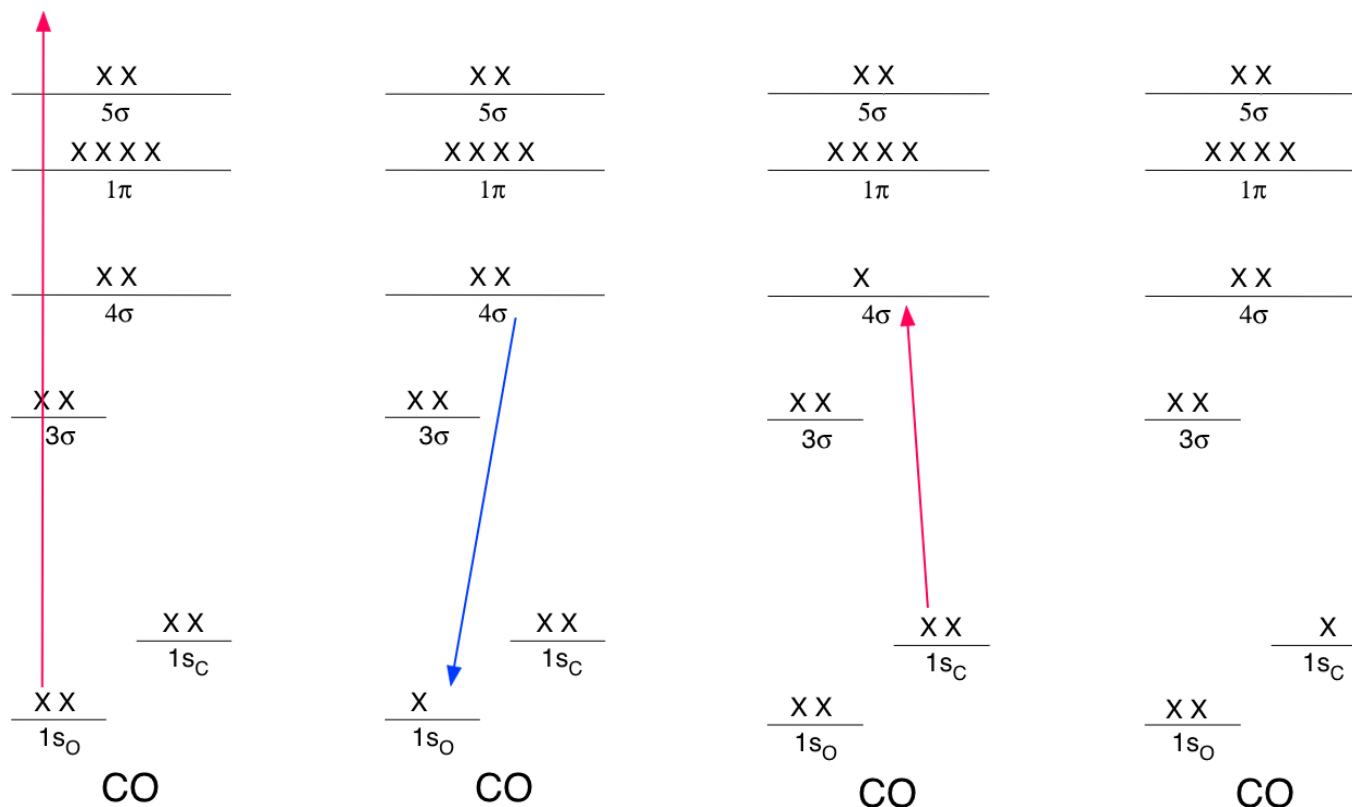
# GAS-PHASE CHEMICAL PHYSICS WITH FREE-ELECTRON LASERS

- DOE-SC-BES is investing substantial funds developing next generation light sources, particularly LCLS II. Regardless of what "use-inspired" justifications there are for GPCP, science using these facilities will likely be supported.
- These sources provide intense (mJ/pulse), ultrafast (3-100 fs), coherent light from the vacuum-ultraviolet (e.g., FERMI, FLASH, etc.) to hard x-rays (LCLS, SACLA, XFEL, etc.) that complement laboratory-based sources based on high-harmonic generation, etc.
- Separately tunable/delayable pulses are available for x-ray/x-ray pump-probe experiments, as well as optical/x-ray pump probe techniques – all the traditional kinds of GPCP experiments, but with localized excitation.
- Most of the CSGB Programs have embraced these sources, but GPCP has not really done so.\*\*
- Opportunities exist in time-resolved electronic and nuclear dynamics, particle/aerosol/cluster imaging, etc.
- X-rays provide the ability to excite or probe molecules in an atomic site-specific manner and thus characterize the flow of excitation throughout the system.

FELs are potentially powerful tools for gas-phase chemical physics

# SITE-SELECTIVE EXCITATION AND DETECTION

*X-ray/x-ray pump probe experiments can create a core hole on one site and then follow how that excitation relaxes across the molecule as a function of delay.*



- ◆ X-ray stimulated Raman scattering can create site-specific, valence shell excitation.
- ◆ Coherent diffraction imaging can visualize individual clusters, aerosols, soot particles, etc.

*There are lots of possibilities*